Investigation into the Effect of Animal Venoms on the Epidermal Growth Factor Receptor and other Receptor Tyrosine Kinases

by

Danielle McCullough

Canterbury Christ Church University

Thesis submitted
for the Degree of Doctor of Philosophy

2020

Contents

List of Figures

List of Tables

List of Abbreviations

1D SDS PAGE:	1-dimension sodium dodecyl sulphate polyacrylamide gel electrophoresis
1º:	Primary
2º:	Secondary
3-FPM:	3-fluorophenylmethoxy
5-FU:	5-fluorouracil
A.aus:	*Androctonus australis*
A.cco:	*Agkistrodon contortrix contortrix*
A.cor:	*Acanthoscurria cordubensis*
A.gen:	*Acanthoscurria geniculata*
A.met:	*Avicularia metallica*
A.sex:	*Anthia sexguttata*
aa:	Amino acid
ab:	Antibody
ADCC:	Antibody-dependent cellular cytotoxicity
ADEPT:	Antibody-dependent enzyme-prodrug therapy
ADP:	Adenosine diphosphate
AECS:	Alcoholic extract of centipede
AFP:	Alpha-fetoprotein
Akt:	Protein kinase B
ALK:	Anaplastic lymphoma kinase
ALT:	Alternative telomere lengthening
AML:	Acute myeloid leukaemia
ANOVA:	Analysis of variance
AO/EtBR:	Acridine Orange/Ethidium Bromide
AP-1:	Activating protein-1
APS:	Ammonium persulphate
AR:	Amphiregulin
ASIC:	Acid sensing ion channel
A-T:	Adenine-thymine
At^{211}:	Astatine-211
ATCC:	American Type Culture Collection
ATP:	Adenosine triphosphate
Axl:	Tyrosine-protein kinase receptor UFO

B.asp:	*Bothrops asper*
B.boe:	*Brachypelma boehmei*
Bad:	BCL2 associated agonist of cell death
Bak:	Bcl-2 homologous antagonist/killer 1
Bax:	Bcl-2 Associated X/ bcl-2-like protein 4
Bcl-2:	B-cell lymphoma 2
bFGF:	Basic fibroblast growth factor
Bi^{212}:	Bismuth-212
Bi^{213}:	Bismuth-213
Bim:	Proapoptotic BH3-only protein/ Bcl-2-like protein 11
BL1:	Basal-like TNBC Subtype 1
BL2:	Basal-like TNBC Subtype 1
BmK:	*Buthus martensi* Karsch
BPF:	Bradykinin-potentiating peptide
bps:	Base pairs
BSA:	Bovine Serum Albumin
BTC:	Betacellulin
BV:	Bee venom
C.atr:	*Crotalus atrox*
C.dve:	*Crotalus durissus vegrandis*
C.gig:	*Colossobolus giganteus*
C.ins:	*Trimeresurus (Cryptelytrops) albolabris insularis*
C.rho:	*Calloselasma rhodostoma*
C.rru:	*Crotalus ruber*
Ca^{2+}:	Calcium
CAM assay:	Chorioallantoic membrane assay
CC-PLA:	*Cerastes cerastes* phospholipase A
CD:	Cluster of differentiation grouping
CD33:	Myeloid cell surface antigen CD33
CD4+:	Cluster of differentiation 4 positive
CD8+:	Cluster of differentiation 8 positive
CDC:	Complement-dependent cytotoxicity
CDRs:	Complementarity determining regions
CEA:	Carcinoembryogenic antigen
CHO:	Chinese hamster ovary
CMC:	Cell membrane chromatography

CO_2:	Carbon dioxide
C-RET/ RET:	Rearranged during transfection proto-oncogene
CTX:	Cytotoxin
Cyt:	Cytoplasmic region
D.pol:	*Dendroaspis polylepis*
D.vir:	*Dendroaspis viridis*
DC:	Dendritic cells
DDRs:	Discoidin domain receptor tyrosine kinases
dH_2O:	Distilled water
DMEM:	Dulbecco's modified eagles medium
DMSO:	Dimethyl sulfoxide
DNA:	Deoxyribonucleic acid
dNTPs:	Deoxyribonucleotide triphosphates
drCT-I:	*Daboia russelii russelli* cytotoxin I
drCT-II:	*Daboia russelii russelli* cytotoxin II
Dtk:	Developmental tyrosine kinase
DTT:	Dithiothreitol
E.foe:	*Eisenia foetida*
EAC:	Ehrlich ascites carcinoma
ECL:	Enhanced Chemiluminescence
EDTA:	Ethylenediaminetetraacetic acid
EGF:	Epidermal Growth Factor
EGFR:	Epidermal Growth Factor Receptor
EGTA:	Ethylene glycol-bis(β-aminoethyl ether)-N,N,N′,N′-tetraacetic acid
EG-VEGF:	Endocrine-gland-derived vascular endothelial growth factor
ELISA:	Enzyme-linked Immunosorbent assay
EMT:	Epithelial-mesenchymal transition
Eph:	Ephrin receptor
ER:	Oestrogen receptor
ER-:	Oestrogen receptor negative
ER+:	Oestrogen receptor positive
ErbB/HER:	Human epidermal growth factor receptor
Erk1:	Mitogen-activated protein kinase 3
Erk2:	Mitogen-activated protein kinase 1
F(ab):	Fragment antigen binding
FADH:	Flavin adenine dinucleotide

FAK:	Focal adhesion kinase
FasL:	Fas Ligand
Fc:	Constant fragment
FCS:	Foetal calf serum
FDA:	Food and Drug Administration
FGFR:	Fibroblast growth factor receptor
FIGO:	Federation of Gynaecology and Obstetrics
Flt-3:	Fms-like tyrosine kinase 3
Ga^{67}:	Gallium-67
G-C:	Guanine-cytosine
H.ari:	*Hadrurus arizonensis*
HER2	Human epidermal growth factor receptor 2
HER3	Human epidermal growth factor receptor 3
HER4	Human epidermal growth factor receptor 4
H.lbo:	*Cyriopagopus (Haplopelma) albostriatum*
H.mac:	*Heteroscodra maculata*
H.swa:	*Heterometrus swammerdami*
H_2O:	Water
H_2O_2:	Hydrogen peroxide
HB-EGF:	Heparin-binding EGF-like growth factor
HCC:	Hepatocellular carcinoma
HCl:	Hydrochloric acid
HGF R/ c-MET:	Hepatocyte growth factor receptor
HGF:	Hepatocyte growth factor
HMECs:	Human mammary epithelial cells
HPLC:	High-performance liquid chromatography
HR-:	Hormone receptor negative
HR+:	Hormone receptor positive
HRP:	Horse radish peroxidase
HSP:	Heat shock protein
HTS:	High throughput screening
HUVEC:	Human umbilical vein endothelial cells
I^{123}:	Iodine-123
I^{125}:	Iodine-125
I^{131}:	Iodine-131
IgA:	Immunoglobulin type A

IgD:	Immunoglobulin type D
IgE:	Immunoglobulin type E
IGF-1R:	Insulin-like growth factor 1 receptor
IgG:	Immunoglobulin type G
IgM:	Immunoglobulin type M
IHC:	Immunohistochemistry
IM:	Immunomodulatory TNBC subtype
IR:	Insulin Receptor
JAK-2:	Janus tyrosine kinase-2
JM:	Juxtamembrane
KCl:	Potassium chloride
KDD:	Kinase domain duplications
Ki67:	HER2 receptor expression and proliferation status
LAAO:	L-amino acid oxidase
LAR	Luminal Androgen Receptor TNBC Subtype
LDH:	Lactate dehydrogenase
LET:	Low energy transfer
LLC:	Lewis lung carcinoma
Lu^{177}:	Lutetium-177
M:	Mesenchymal TNBC Subtype
mAb:	Monoclonal antibody
MACs:	Membrane attack complexes
MALDI-TOF:	Matrix-assisted laser desorption/ionisation- time of flight
MAPK:	Mitogen-activated protein kinase
MCD:	Mass-cell degranulating
M-CSF R:	Macrophage colony-stimulating factor receptor
MDR:	Multiple drug resistant
Mer:	Proto-oncogene tyrosine protein kinase
Met:	Met-proto-oncogene family
MgTx:	Margatoxin
MHC:	Major histocompatibility complex
MMP:	Matrix metalloproteinase
MMP:	Mitochondrial membrane potential
MSL	Mesenchymal-like TNBC Subtype
MSMS:	Mass spectrometry mass spectrometry
MSP R/ Ron:	Macrophage stimulating protein receptor

mTOR:	Mammalian target of rapamycin
MTS:	(3-(4,5-dimethylthiazol-2-yl)-5-(3-carboxymethoxyphenyl)-2-(4-sulfophenyl)-2H-tetrazolium)
MTT:	3-(4,5-Dimethylthiazol-2-yl)-2,5-diphenyltetrazolium bromide
MuSK:	Muscle-specific tyrosine kinase
MVL-PLA2:	*Macrovipera lebetina* phospholipase A2
MW:	Molecular weight
M.xan:	*Montivipera xanthina*
Myc:	MYC Proto-Oncogene protein
N.atr:	*Naja atra*
N.naj:	*Naja naja*
N.nig:	*Naja nigricollis*
N.sia:	*Naja siamensis*
Na^+:	Sodium
NADH:	Nicotinamide adenine dinucleotide + hydrogen
NADPH:	Nicotinamide adenine dinucleotide phosphate
NGF R:	Neurotrophin receptor
NIDDM:	Non-insulin-dependent diabetes mellitus
NLS:	Nuclear localisation signal
NMJs:	Neuromuscular junctions
NP-40:	Tergitol-type NP-40 and nonyl phenoxypolyethoxylethanol
nRTKs:	Non-receptor tyrosine kinases
NSCLC:	Non-small cell lung cancer
O.han:	*Ophiophagus Hannah*
P.cam:	*Psalmopoeus cambridgei*
P.for:	*Poecilotheria formosa*
P.kra:	*Protoiurus kraepelini*
P.lio:	*Parabuthus liosoma*
P.lug:	*Pterinochilus lugardi*
P.map:	*Pachnoda marginata peregrina*
P.wei:	*Pseudechis rossignoli*
p107:	Retinoblastoma-like protein 1
p130:	Retinoblastoma-like protein 2
p38:	p38 mitogen-activated protein kinases
p53:	Cellular tumour antigen p53
PARP:	Poly (ADP-ribose) polymerase

PBMCs:	Human mononuclear cells
PBS:	Phosphate Buffered Saline
PC-12:	Pheochromocytoma cells
PCI:	Percutaneous coronary intervention
PCNA:	Proliferating cell nuclear antigen
PDGFR:	Platelet-derived growth factor receptor
Pen-strep:	Penicillin-streptomycin
PESV:	Polypeptide extracted from scorpion venom
PI3K:	Phosphatidylinositol-3 kinase
PI3Kinase:	Phosphoinositide 3-kinases
PLA2:	Phospholipase A2
PMBCs:	Peripheral blood mononuclear cells
Ponceau S:	3-hydroxy-4-(2-sulfo-4-[4-sulfophenylazo]phenylazo)-2,7-naphthalenedisulfonic acid sodium salt
PR:	Progesterone receptor
PR-:	Progesterone receptor negative
PR+:	Progesterone receptor positive
PSA:	Prostate-specific antigen
PTEN:	Phosphatase and tensin homolog
pTKs:	Protein tyrosine kinases
Puma:	p53-upregulated modulator of apoptosis
PVDF:	Polyoxyethylenersorbitan monolaurate
pY:	Phospho-tyrosine
pY-EGFR:	Phospho-tyrosine EGFR
Rb:	Retinoblastoma
RIPA:	Radioimmunoprecipitation assay
RNA:	Ribose nucleic acid
Ror:	Receptor tyrosine kinase-like orphan receptors
ROS:	Reactive oxygen species
RP HPLC:	Reverse high-performance liquid chromatography
RP:	Reverse Phase
RT:	Room temperature
RTK:	Receptor Tyrosine Kinase
RT-PCR:	Real time polymerase chain reaction
Ryk:	Related to tyrosine kinases
S.har:	*Scolopendra hardwickei*

S.mil:	*Sistrurus miliarus barbouri*
S.sud:	*Scolopendra subspinipes dehaani*
SCF R/ c-Kit:	Stem cell factor receptor
ScFv:	Single-chain variable fragment
SCLC:	Small cell lung cancer
SDS:	Sodium dodecyl sulphate
SEC HPLC:	Size exclusion high performance liquid chromatography
SEC:	Size exclusion
SERMs:	Selective oestrogen receptor modulators
SiRNA:	Small interfering RNA
SM-KIs	Small molecule kinase inhibitors
SM-TKIs:	Small molecule tyrosine kinase inhibitors
SNP:	Single nucleotide polymorphism
Src:	Proto-oncogene tyrosine-protein kinase
STAT:	Signal transducer and activator of transcription
STR:	Short Tandem Repeat
T(reg):	Regulatory T cells
T.cup:	*Tapinauchenius cupreus*
T.pru:	*Thrixopelma pruriens*
T.str:	*Theraphosa stirmi*
TAAs:	Tumour-associated antigens
TACE:	Tumour necrosis factor-α-converting enzyme
TAM:	Tyro3, Axl, Mer
TBS:	Tris buffered saline
TEMED:	N,N,N,N’-tetra-methyl-ethylenediamine
TFA:	Trifluoroacetic acid
TGF-α:	Transforming growth factor alpha
Tie R:	Angiopoietin receptor
TKIs:	Tyrosine kinase inhibitors
TKs:	Tyrosine kinases
TMB:	3,3’,5,5’-tetramethylbenzidine
TNBC:	Triple negative breast cancer
TNF-α:	Tumour necrosis factor alpha
TOF:	Time of flight
TP53:	Cellular tumour antigen p53 gene
Tris:	Tris(hydroxymethyl)aminomethane

Triton x-100:	polyethylene glycol tert-octylphenyl ether
Trk:	Tropomyosin receptor kinase
TSP-1:	Thrombospondin-1
TUNEL:	TdTmediated dUTP-biotin nick-end labeling
Tween20:	Polyethylene glycol sorbitan monolaurate
V.aam:	*Vipera ammodytes ammodytes*
VEGF:	Vascular endothelial growth factor
VEGFR:	Vascular endothelial growth factor receptor
WIF:	Wnt inhibitory factor
Wnt5a:	Wnt Family Member 5A
WW:	Double tryptophan
XTT:	2,3-Bis-(2-Methoxy-4-Nitro-5-Sulfophenyl)-2H-Tetrazolium-5-Carboxanilide
Y^{90}:	Yttrium-90
Z':	Z-factor measure of statistical effect size.
Z score:	Z-score measure of standard deviations from the means
α:	Alpha
β:	Beta
γ:	Gamma

Acknowledgements

I would like to thank my supervisor Carol Trim for all the support and guidance that she has provided me with during the course of my PhD. Your expertise and knowledge, your unwavering patience and belief in me, and your friendship have helped me to explore and overcome new challenges, enabling me to develop into the scientist I am today. I feel truly blessed to have worked alongside and shared this journey with you and could not have asked for a better supervisor. Thanks go to my second supervisor Simon Harvey for his continued support and insight, for encouraging me to push beyond the scope of my understanding, and for providing the support I needed to ensure that my PhD progressed smoothly. Thank you to my panel chair Peter Vujakovic for ensuring that my supervisory meetings proceeded smoothly, that I was on track, and for swiftly and efficiently dealing with any issues which arose. I would sincerely like to thank Professor Michelle Garrett and Dr Edward Rowan for agreeing to examine my thesis.

Thank you to Kent Cancer Trust for your kind donations which supported and funded this project, and to Canterbury Christ Church University for providing me with the opportunity and resources to undertake this PhD. Without both your contributions I would not have been able to undertake and experience such a wide degree of exciting research. Thanks go to Venomtech Ltd for supplying all of the venoms used in this project and for providing me with the opportunity to utilise equipment that would otherwise have been unavailable to me. To Stuart Baker and Sarah Smith, thank you for the time you have both provided in supervising my early endeavours and collecting copious amounts of venom, without which this project could not have proceeded. Special thanks go to Steve Trim, whose continuous support, patience and in-depth knowledge of both venoms and drug discovery enabled me to take this project further than I ever believed was possible. I am grateful for all the time you have provided, both in equipment and technique training and general understanding and writing support. I would like to acknowledge and thank Dr Bill Gullick of the University of Kent for his kind gifts of both the cancer cell lines and a primary antibody that were paramount to the successful advancement of this PhD.

I want to acknowledge the support and friendship of my fellow PhD students and Instructors. Undertaking a thesis is an enormous challenge and it is your friendship, the laughs we have shared through the good times and the guidance and counsel you have provided through the tough times that have made all this truly possible. I honestly would not have gotten here without you. I would like to thank my family, my mum, dad, my brothers Liam and Connor, and Holly, for continually supporting and driving me to excel throughout this process and for providing an ear when I really needed to talk through challenging days. Finally, to my friends Micca, Corinne, Jenny, Emily and Gwen, thank you for believing, supporting and driving me to do this, and for listening to me continually talk science at you for the last 6 years, you really all do deserve enormous thanks!

Abstract

Receptor tyrosine kinases (RTKs), play fundamental roles in the progression of cancer, but also allow for a more targeted approach to cancer treatment. Epidermal growth factor receptor (EGFR) is a key tumour antigen in a variety of difficult to treat cancers. Therapeutics for the treatment of many cancers have improved patient prognosis, however the development of resistance continually drives the need for novel therapeutics. Venoms have evolved over millions of years becoming complex mixtures of biologically active molecules, which elicit a wide range of pathophysiological effects following injection. Recent papers have shown that whole and fractionated venom components can reduce cancer cell viability. However, little research has been undertaken into venom use for direct targeting of tumour-associated antigens. The aim of this thesis was to utilise whole and fractionated venoms to target receptor tyrosine kinases in breast cancer.

Utilising a range of techniques, venomous snake and invertebrate genera were profiled. Treating with whole venoms from six distinct species, a wide range of RTKs in triple negative breast cancer (TNBC) cell line MDA-MB-468, were identified as having their phosphorylation/expression activity affected, including EGFR. Screening of panels identified further venoms, capable of reducing the phosphorylation of EGFR in MDA-MB-468 TNBC cells, and in some instances also in the EGFR-overexpressing squamous carcinoma cell line A431. EGF-competitive binding assays suggested that the mechanism through which the venoms cause reductions to EGFR activity was not through EGF off-competition, however the assay required further optimisation to robustly confirm this. Fractionation of nine whole venoms, using reverse-phase high performance liquid chromatography (RP-HPLC) and rescreening, identified a number of fractions that caused biologically and statistically significant reductions to MDA-MB-468 and A431 cell EGFR phosphorylation. Mass spectrometry of three of these fractions, partially matched two to venom Phospholipase A2 sequences deposited in databases for similar related species.

CHAPTER 1: Cancer and Cancer Therapies

1.1 Cancer

1.1.1 The Hallmarks of Cancer

In 2000 Hanahan and Weinberg published a paper which proposed six essential hallmarks which detailed characteristics cells must acquire to undergo malignant transformation into tumorous cells. These hallmarks describe tumour formation as a multi-step process, with normal cells progressively evolving into a neoplastic state with the acquisition of each of the following subsequent characteristics, 1) the ability to undergo sustained proliferative signalling; 2) the acquired insensitivity to anti-growth signals and ability to evade growth suppression; 3) the development of replicative immortality; 4) resistance to apoptotic cellular death; 5) the implementation of angiogenesis and 6) the capacity to carry out tissue invasion and metastasis (Hanahan and Weinberg, 2000; Gutschner and Diederichs, 2012) (Figure 1.1).

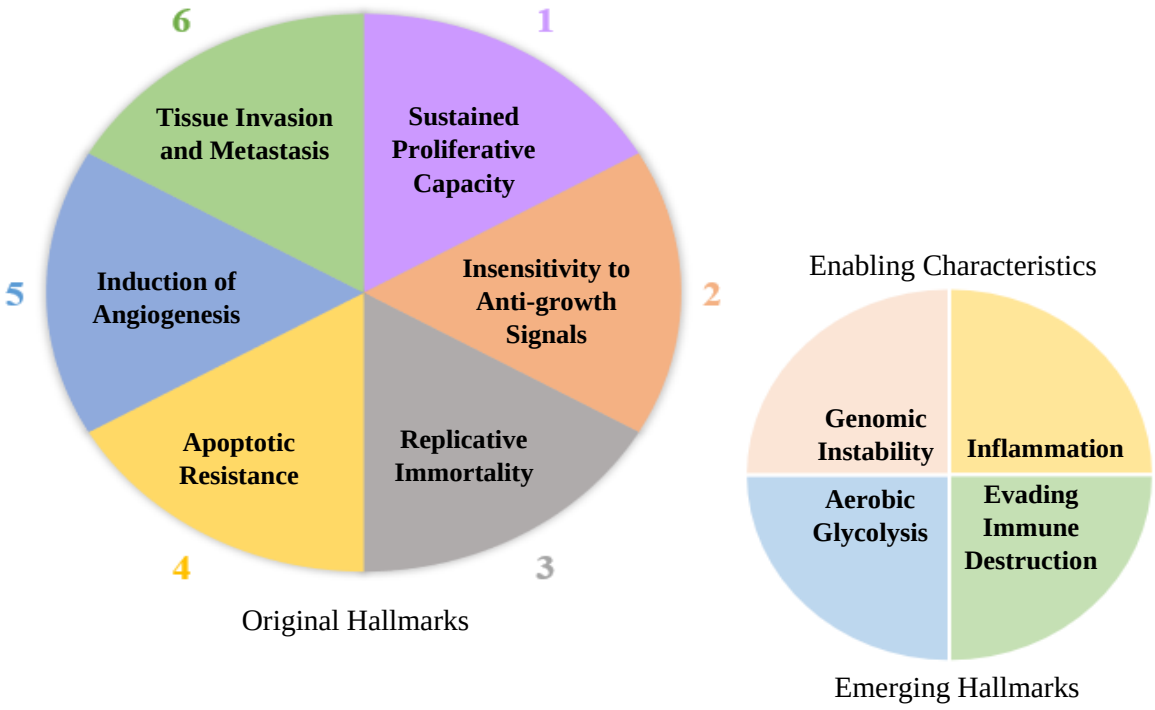

Figure 1.1 The Hallmarks of Cancer

The figure displays the six original and two emerging hallmarks of cancer that are acquired by cells as they progress to a cancerous state. In addition, enabling characteristics which facilitate the development of hallmarks are also displayed. Early hallmarks include sustained proliferative capacity, insensitivity to antigrowth signals and replicative immortality. Later stage hallmarks include apoptotic resistance, angiogenesis and tissue invasion and metastasis. Emerging hallmarks include switching metabolism to aerobic glycolysis and evading immune detection and destruction. Enabling characteristics which facilitate the acquisition of both original and emerging characteristics include increased levels of genomic instability and tumour-associated inflammation (Hanahan and Weinberg, 2000, 2011).

Sustained proliferative capability is an essential and highly prominent characteristic in the progression of tumour development. Tumour cells can show reduced dependency on exogenous growth signal stimulation by the self-production of pro-growth stimulating molecules, the upregulation of cellular growth-factor binding receptors, the partaking in positive autocrine or paracrine signalling loops, hyper-responsive to ambient levels of growth factors, or by forming truncated variants of receptors lacking extracellular domains or mutated downstream secondary signalling molecules which are constitutively active (Hanahan and Weinberg, 2000, 2011; Abbott, Forrest and Pienta, 2006; Gutschner and Diederichs, 2012; Sonnenschein and Soto, 2013).

Tumour cells can become tolerant to antiproliferative signals by undergoing complete loss of the expression of onco-suppressor genes (e.g. *TP53, PTEN, RB*) through the accumulation of mutations within the gene sequence, rendering them functional redundant (Gabriel *et al.*, 2013; Niederst *et al.*, 2015; Liu *et al.*, 2016; Peng *et al.*, 2016). Antiproliferative signals in tumour suppressors, such as retinoblastoma (Rb), p130 and p107 can be disrupted in tumour cells, rendering them insensitive to antigrowth signals and liberating E2F transcription factors to undertake the transcription of genes that promote cellular growth (Hanahan and Weinberg, 2000, 2011; Gutschner and Diederichs, 2012).

Healthy cells display a finite number of replicative divisions they can undertake, known as their replicative potential, before entering into a state of senescence or crisis (Abbott, Forrest and Pienta, 2006). Telomeres, found at both the 3' and 5' ends of chromosomes and consisting of thousands of short hexanucleotide base pair (bp) repeat sequences (TTA GGG), are responsible for protecting coding DNA from degradation and end-to-end fusions over time (Gutschner and Diederichs, 2012). Cellular replication results in the loss of 50-100 bps of telomeric DNA from the end of every cellular chromosome, termed telomere degradation (Hanahan and Weinberg, 2000; Sledge and Miller, 2003). Continuous erosion of telomeres eventually leads to karyotypic disarray associated with crisis (Hanahan and Weinberg, 2000, 2011). 85-90% of cancer cells carry out telomeric maintenance by upregulating the expression of enzyme telomerase, which adds hexanucleotide repeat sequences to the ends of telomeric DNA, replacing those lost during cellular replication cycles (Abbott, Forrest and Pienta, 2006; Low and Tergaonkar, 2013; Macheret and Halazonetis, 2015; Yaswen *et al.*, 2015). The remaining 10-15% of cancer cells activate Alternative Lengthening of Telomeres (ALT) to maintain replicative immortality. ALT is thought to maintain telomeric DNA through a process of recombination-lead inter-chromosomal sequence exchanges (Hanahan and Weinberg, 2000, 2011; Cesare and Reddel, 2010; Heaphy *et al.*, 2011; Castaño and Maurer, 2015).

Cellular death can occur through three distinct, highly regulated pathways, autophagy, necrosis and apoptosis (Gutschner and Diederichs, 2012; Chaabane *et al.*, 2013; Jain *et al.*, 2013; Nikoletopoulou *et al.*, 2013). Cancer cells can acquire both intrinsic and extrinsic apoptotic pathway resistance through mutations in genes that regulate apoptosis, or through alterations to components of cellular signalling pathways. The most common types of apoptotic circumvention include mutations causing the total loss of function of pro-apoptotic regulator genes (e.g. tumour suppressor *TP53*), the reduction in expression of pro-apoptotic factors (e.g. Bim, Bax and Puma) or the upregulated expression of anti-apoptotic factors (e.g. Blc-2) (Sledge and Miller, 2003; Hanahan and Weinberg, 2011; Zhang, Yuan, Zhang, Simayi, *et al.*, 2012; Mohammad *et al.*, 2015).

Tumour cells require a good blood supply to obtain enough nutrients and oxygen to facilitate growth, and so are unable to migrate more than 100 μm in distance from the nearest capillary blood (Hanahan and Weinberg, 2000; Abbott, Forrest and Pienta, 2006). This dependency to be close to vasculature has result in cancer cells developing the ability to undertake sustained angiogenesis, which is the sprouting of new blood vessels from pre-existing vasculature (Hanahan and Weinberg, 2011). Angiogenesis is tightly regulated by the combined activities of both pro-angiogenic signalling molecules (e.g. bFGF and VEGF) and anti-angiogenic, inhibitory signalling molecules (e.g. Thrombospondin-1 (TSP-1)) (Carmeliet and Jain, 2011; Burrell and Zadeh, 2012). Tumour cells can cause a net increase in pro-angiogenic factors through a variety of different mechanisms including altered levels of gene transcription, such as increased or decreased transcription of pro- (e.g. Vascular Endothelial Growth Factors (VEGFs), basic Fibroblast Growth Factors (bFGFs)) and anti- (TSP-1) angiogenic molecules respectively. Genes, such as *RAS*, *MYC*, or *TP53*, which regulate the levels of pro/anti-angiogenic molecules may also have altered levels of gene expression in cancer cells (Hanahan and Weinberg, 2000, 2011)

The transition of tumour cells from a non-invasive state to an invasive one enables cancer cells to undertake local tissue invasion and subsequent metastasis to other distant bodily sites. 90% of all cancer fatalities are the result of secondary cancerous legions that have metastasised from the main tumour bulk and lodged within a new region of the body (Hanahan and Weinberg, 2000; Abbott, Forrest and Pienta, 2006). Tumour cells undertake a variety of morphological alteration processes, including mutations which disrupt cell adhesion molecule and integrin functions (Palmer *et al.*, 2011; Blandin *et al.*, 2015), transcriptional repression of genes preventing metastasis, extracellular matrix degradation by proteolytic enzymes (Kessenbrock, Plaks and Werb, 2010) and epithelial-mesenchymal transition (EMT) (Hanahan and Weinberg, 2000, 2011; Gutschner and Diederichs, 2012; Sonnenschein and Soto, 2013; Diepenbruck and Christofori, 2016; Giannelli *et al.*, 2016; Zhang and Weinberg, 2018). Additionally, secretion of matrix

metalloproteases (MMPs) which degrade the basement membrane and surrounding stroma and disruption of cell adhesion molecules (e.g. E-cadherin and β-catenin) (Kessenbrock, Plaks and Werb, 2010). Both E-cadherin and β-catenin downregulations that confer loss-of-function and upregulations of N-cadherin occur in many highly invasive types of cancer (Abbott, Forrest and Pienta, 2006; Hanahan and Weinberg, 2011; Gutschner and Diederichs, 2012).

Since the first hallmarks were purported in 2000 there has been a variety of emerging hallmarks and enabling characteristics which have been subsequently suggested to also play important roles in tumorigenesis. Novel enabling characteristics, are suggested to facilitate the acquisition of both the classic and emerging hallmarks of cancer. These enabling characteristics include genome instability and tumour-promoting inflammation. Genomic instability endows tumour cells with mutations which feed tumour progression. To orchestrate tumorigenesis, cancer cell increase their rate of mutability by enhancing their sensitive to agents with mutagenic properties and hindering DNA-damage repair mechanisms. Mutations can result in the gain or loss of specific genes which promote or hinder tumour progression respectively (Hanahan and Weinberg, 2011; Fu, Calvo and Samson, 2013; Ferguson *et al.*, 2015; Macheret and Halazonetis, 2015; Lee *et al.*, 2016; Andor, Maley and Ji, 2017; Fouad and Aanei, 2017). Tumour-associated inflammation can enhance tumorigenesis, cancer progression and hallmark development (Cavallo *et al.*, 2011; Hanahan and Weinberg, 2011; Crusz and Balkwill, 2015; Fouad and Aanei, 2017), by flooding the tumour microenvironment with bioactive molecules, such as growth factors, pro-survival and angiogenic factors, ultimately promoting sustained proliferative capability, apoptotic resistance and angiogenic development (Cavallo *et al.*, 2011; Hanahan and Weinberg, 2011).

The switch from oxidative phosphorylation to aerobic glycolysis as an effective method of generating cellular energy is believed to play a role in the progression and development of cancer, despite the fact that this form of glucose metabolism only generates 2 ATPs/glucose compared to the 36 ATPs/glucose produced through oxidative phosphorylation (Fadaka *et al.*, 2017). This emerging hallmark is believed to confer many advantages to developing tumour cells. The switch to an aerobic glycolytic phenotype enables tumour cells to undertake prolonged proliferation, angiogenesis, metastasis and the out-competition for space and resources of surrounding healthy cells. This switch in metabolism is referred to as the Warburg effect (Gatenby and Gillies, 2004; Kaelin and Thompson, 2010; Dang *et al.*, 2011; Hamanaka and Chandel, 2012). Advantageous qualities attributed to the metabolic shift to glycolysis include the generation of glycolytic intermediates, the utilisation of excess glucose and the starving of surrounding healthy cells, lactate generation which causes acidosis of the extracellular matrix, triggering apoptosis and necrosis of healthy surrounding cells and ultimately the creation of greater space for enhanced tumour growth (Gatenby and Gillies, 2004; Kondoh *et al.*, 2005; Kim and Dang, 2006; Kaelin

and Thompson, 2010; Cairns, Harris and Mak, 2011; Hanahan and Weinberg, 2011; Hamanaka and Chandel, 2012).

Through selection pressure during growth and development, cancer cells can develop mechanisms which are beneficial in aiding them to avoid immune destruction or to hijack the immune system into supporting tumoral growth and development (Sukari *et al.*, 2016). Tumour escape mechanisms can be broadly categorised as tolerance inducing or resistance to immune cell killing. Proposed mechanisms include the down-regulation of MHC-I & II expression (Siddle *et al.*, 2013; Paulson *et al.*, 2014; Vinay *et al.*, 2015; Garrido *et al.*, 2016; Tarafdar *et al.*, 2017), loss of function of the β2-microglobulin gene (Challa-Malladi *et al.*, 2011; Bernal *et al.*, 2012), loss of tumour-specific antigens (Van Der Burg *et al.*, 2016), immunodominance shielding of antigen-loss variants (Khong and Restifo, 2002), lack of expression of co-stimulatory factors required for T-cell activation (Seliger, 2005; Crespo *et al.*, 2013; Vinay *et al.*, 2015), triggering of T-cell anergy and apoptosis (Abe and Macian, 2013; Crespo *et al.*, 2013), generation of immunological barrier within the tumour microenvironment (Gajewski *et al.*, 2013; Munn and Bronte, 2016), inhibition of immune cell maturation, activation and function (Woo *et al.*, 2012), expression of death-ligands (e.g. FasL) on their surface (Velcheti *et al.*, 2014; Saigusa *et al.*, 2015) and the generation of regulatory T-cells (Treg) which are capable of suppressing the activity of cytotoxic T-cells against tumours (Nishikawa and Sakaguchi, 2014; Vinay *et al.*, 2015).

1.1.2 Breast Cancer

Breast cancer remains the most common type of cancer in women, with global incidences in 2018 of 2.088 million cases worldwide and global deaths attributed to the disease of 626,679 (Ferlay *et al.*, 2019). It is the most commonly occurring and diagnosed cancer type in women both of menopausal age (Kamińska *et al.*, 2015) and those who are adolescent or young adults (Keegan *et al.*, 2012). Breast cancer can be categorised on the basis of five different biological subtypes, including luminal A, luminal B, basal-like, claudin-low and human epidermal growth factor receptor 2 (HER2) (Al-Mahmood *et al.*, 2018). Standard prognostic factors for breast cancer disease include progesterone receptor (PR) expression, oestrogen receptor expression (ER), HER2 receptor expression and proliferation (Ki67) status (Karlsson *et al.*, 2014; Al-Mahmood *et al.*, 2018). Therapeutic treatment options of breast cancer are dependent open the expression profile of these receptors, with breast cancers classed as hormone-receptor over-expressing (HR+), HER2 over-expressing or triple negative, lacking the expression of all three.

Around 70% of all breast cancers are hormone receptor positive (HR+) (Bae *et al.*, 2015). Oestrogen receptor positive (ER+) breast cancer types are normally also positive for progesterone receptor (PR+), whilst ER- cancers are normally also negative for PR. HR+ breast cancer subtypes

are general indicative of a favourable prognosis, whilst HR- breast cancer subtypes have a poor patient prognosis (Bae *et al.*, 2015). Treatments for oestrogen over-expressing breast cancers include selective oestrogen receptor modulators (SERMs), such as tamoxifen, which bind to oestrogen receptors with high affinity but not to other steroid hormone receptors (Begam, Jubie and Nanjan, 2017). Like oestrogen receptors, progesterone receptor targeted therapies also exist. Selective progesterone receptor modulators (SPRMs), such as mifepristone can be used to target PR (Wagenfeld *et al.*, 2016). HER2 over-expression accounts for around 15-20% of diagnosed breast cancers and until the recent advent of targeted therapies was indicative of poor patient prognosis and an aggressive cancer phenotype (Tolaney *et al.*, 2015; Loibl and Gianni, 2017a). The development of antibody-type HER2 targeted therapies, such as trastuzumab and pertuzumab (Von Minckwitz *et al.*, 2017), and small molecule tyrosine kinases inhibitors, including lapatinib and ibrutinib (Medina and Goodin, 2008; Chen *et al.*, 2016), have changed the landscape for the treatment of HER2 over-expressing breast cancers, making it a more manageable disease (Ahmed, Sami and Xiang, 2015).

However, despite the development of effective therapeutics for the treatment of hormone receptor and HER2 over-expressing breast cancers, there is still a subset of breast cancers which display poor treatability and patient prognosis. These include single hormone receptor expressing breast cancers, such as ER+/PR- or ER-/PR+ (Bae *et al.*, 2015) and more predominantly triple-negative breast cancer (TNBC) (Hudis and Gianni, 2011; Wahba and El-Hadaad, 2015; Bianchini *et al.*, 2016). 10-20% of diagnosed breast cancers are deemed to be triple negative, lacking expression of both hormone receptors (ER & PR) and HER2 (Nakai, Hung and Yamaguchi, 2016). TNBCs present a subset of breast cancers, that are highly diverse, but can be broadly categorised into six subtypes, each displaying unique gene expression profiles and ontologies. These six groups include two basal-like subtypes (BL1 & BL2), an immunomodulatory (IM) subtype, mesenchymal (M) and mesenchymal stem-like (MSL) subtypes and a luminal androgen receptor (LAR) subtype (Lehmann *et al.*, 2011).

Basal-like subtype BL1 has been found to present with higher expression levels of DNA-damage response (e.g., ATR/BRCA) and cell cycle control genes, whilst basal-like subtype BL2 is associated with genes in growth factor signalling (EGF pathway, NGF pathway, MET pathway, Wnt/β-catenin, and IGF1R pathway), glycolysis, and gluconeogenesis (Lehmann *et al.*, 2011; Ahn *et al.*, 2016; Vidal, Paré and Prat, 2016; Yam, Mani and Moulder, 2017). Mesenchymal (M) and mesenchymal stem-like (MSL) subtypes are enriched in gene expression for those key to stem-cell properties and cellular growth factor pathway genes, as well as those genes involved in cell motility (regulation of actin by Rho), extracellular matrix interactions (Wnt pathway, the anaplastic lymphoma kinase [ALK] pathway, and TGF-β signalling) and epithelial-to-

mesenchymal transition (EMT) (Lehmann *et al.*, 2011; Ahn *et al.*, 2016). In addition to those genes involved in cell motility and ECM interaction, the MSL subtype also expresses genes for components and processes linked to growth factor signalling pathways, including inositol phosphate metabolism, EGFR and PDGF expression, calcium signalling, G-protein coupled receptor expression, ERK1/2 signalling, ABC transporter and adipocytokine signalling, as well as genes involved in angiogenesis (VEGFR2 (KDR), TEK, TIE1, and EPAS1) (Lehmann *et al.*, 2011).

The immunomodulatory (IM) or Immune-enriched subtype is highly enriched in immune cell markers and genes involved in immune cell processes (Lehmann *et al.*, 2011; Vidal, Paré and Prat, 2016; Hubalek, Czech and Müller, 2017; Yam, Mani and Moulder, 2017). Enriched gene clusters that are implicated in the IM subtype of TNBC include immune cell signalling associated with B-cells, T-cells, natural killer (NK) cells and dendritic cells. IM subtype is further evidenced by the expression of genes linked to immune cell-surface antigens, cytokine signalling, complement cascade, chemokine receptors and ligands, and antigen processing and presentation. This subtype of TNBC is identifiable by the presence of tumour-infiltrating immune cells. (Lehmann *et al.*, 2011; Ahn *et al.*, 2016). The Luminal androgen receptor subtype (LAR) presents as the most distinct subtype and are considered to be biologically distinct from all other subtypes of TNBC. LAR subtypes are characterised by enhanced androgen receptor signalling, with hormone regulation pathways and oestrogen/androgen metabolism pathways expressed differently when compared to tumours within the other TNBC subtypes (Ahn *et al.*, 2016; Yam, Mani and Moulder, 2017). This subtype presents as ER negative, but gene ontologies are heavily enriched in hormone-regulated pathways including androgen/oestrogen metabolism, porphyrin metabolism and steroid synthesis (Lehmann *et al.*, 2011).

The six different subtypes of TNBC, as well as presenting with very different gene expression ontologies, respond to different therapeutic approaches when treatments are implemented. Due to their changes in expression of genes key to DNA damage response pathways, Basal-like TNBCs have been shown to be receptive to treatment with two groups of therapeutic agent families, chemotherapeutic platinum salts (e.g cisplatin, carboplatin) and poly ADP-ribose polymerase 1 (PARP) (e.g Olaparib, Rucaparib, Veliparib) and cyclin-dependent kinase (CDK) (e.g Dinaciclib) inhibitors, the prior of which show potential in those subtypes carrying BRCA mutations (Du *et al.*, 2015; Ahn *et al.*, 2016; Hubalek, Czech and Müller, 2017). As a group, targeting DNA-repair deficiency appears a promising treatment for BL-TNBC presenting with BRCA-mutations (Du *et al.*, 2015). However, whilst BL1 TNBC tumours have been shown to have pathologic complete responses (pCR) to platinum chemotherapeutic agents (51%), BL2 TNBC subtype in many cases have been shown to be unresponsive, highlighting concerns around whether these two subtypes

should be considered the same entity (Du *et al.*, 2015). Like the mesenchymal-like TNBC (ML-TNBC) subgroup, the BL2 group has been identified as being uniquely enriched in genes with roles in key growth factor signalling pathways, like EGF, MET and IGF1R pathways, as well as other pathways linked to RTK signalling. Suggesting that this subgroup of TNBC may respond well to small molecule tyrosine kinase inhibitors (SM-TKI) or targeted antibody therapeutics (Du *et al.*, 2015; Toy, Rajeshwari R Valiathan, *et al.*, 2015; Chien *et al.*, 2016; Leconet *et al.*, 2017). EGFR, which has been identified as a key player in the BL2 TNBC subtype, has been shown through Immunohistochemistry (IHC)-based interrogation to be expressed in TNBC with a frequency of up to 76% (Guerrab *et al.*, 2016; Nakai, Hung and Yamaguchi, 2016). BL-TNBC subtypes have also been shown to respond well to antimitotic chemotherapeutic agents such as taxanes (e.g paclitaxel or docetaxel) (Lehmann *et al.*, 2011).

Due to their cancer stem cell (CSC) properties, ML and MSL TNBC subtypes can be targeted with compounds that act a CSC regulators. Notch and Wnt/β-catenin signalling pathways have been heavily implemented in the MS and MSL TNBC subtypes, where they are linked to EMT, making both attractive targets for treatment of these particular TNBC subtypes. Wnt pathway inhibitors include vitamin D3, non-steroidal anti-inflammatory drugs and the antibiotic salinomycin, whilst two types of notch inhibitor families have been developed, delta-like ligand 4 monoclonal antibodies (mAbs) and γ-secretase inhibitors (GSIs) (Du *et al.*, 2015). Kinase receptors met tyrosine kinase (c-MET), fibroblast growth factor receptor (FGFR) and mTOR have been identified as other potential targets of interest as therapeutic avenues for the treatment of ML TNBC subtypes, with compounds that inhibit the latter (NVP-BEZ23) already in clinical development. Additionally, preclinical trials have shown that TGFβ tyrosine-kinase inhibitors (TKI) can induced tremendous mesenchymal-to-epithelial transition (MET), thereby offering an avenue for reversing EMT in these TNBC subtypes (Du *et al.*, 2015; Ahn *et al.*, 2016).

Current therapeutic approaches for those cancers which fall into the Immunomodulatory TNBC subgroup, can be categorised as Immune checkpoint blockage inhibitors and tumour vaccines. In immune-associated TNBC, inhibiting immune checkpoints which prevent the excessive activity of T-cells under normal conditions, are used therapeutically to enhance T-cell activity against tumour cells. Programmed-cell-death-1 (PD-1) and its ligand PD-L1 have been found to be over-expressed in 20% of TNBCs, where the interaction of the PD-L1/PD-1 signalling axis is a potent mechanism through which immunogenic tumours can evade immune response and destruction (Mittendorf *et al.*, 2014; Du *et al.*, 2015). Anti-PD-1 (Pembrolizumab) (Schmid *et al.*, 2020) and anti-PD-L1 (Atezolizumab/MPDL3280A) (Powles *et al.*, 2014) monoclonal antibody (mAb) therapies can interrupt this interaction, disrupting the binding of this ligand and receptor, thereby enhancing T-cell immune response against the tumour cells (Du *et al.*, 2015; Hubalek, Czech and

Müller, 2017). Another receptor expressed on the surface of T-cells, cytotoxic T-lymphocyte-associated protein 4 (CTLA4), has also been identified as a therapeutic target of interest in IM TNBC. CTLA4 functions as an immune checkpoint protein, which downregulates the immune system response. When bound to the protein B7, it prevents cytotoxic T-cells from killing other cells. MAb therapeutics which bind CTLA4 (e.g Ipilimumab and Tremelimumab) are under investigation as potential breast cancer therapeutics (McArthur *et al.*, 2016; Jiang *et al.*, 2019) and therapies of this types could have potential applications in the treatment of IM TNBC subtypes, however no trial currently exists to assess their efficacy in the various stratifications of TNBC. Vaccine therapy targeting breast cancer antigens have been under investigation for the past decade, and whilst no TNBC-specific antigen has been elicited and validated, several potential targets in breast-cancer tumour cells have been identified as potential targets for tumour vaccines, including NY-ESO-1, MUC-1 and MAGE-A3 (Curigliano *et al.*, 2011; Du *et al.*, 2015).

In TNBC, the prevalence of AR positivity occurs approximately 10–20% of the time (Hubalek, Czech and Müller, 2017) and as such this subtype requires effective therapeutic treatment options. Currently therapeutic approaches for the treatment of luminal AR TNBC subtypes focus on the administration of androgen receptor blocking compounds. Sensitivity to AR inhibitors, such as bicalutamide, has been shown to be more effective in LAR cell lines, when compared to other subtypes, and a phase II clinical study undertaken into this drug showed a 19% of clinical benefit rate at 24 weeks for ER/PR-negative AR-positive breast cancer patients (Gucalp *et al.*, 2013). Enzalutamide, a new generation, nonsteroidal antiandrogen medication has also been shown in *in vitro* investigation to abrogate AR-mediated proliferation and yielded 42% of clinical benefit rate at 16 weeks in advanced AR-positive TNBC in a 2-stage study (Cochrane *et al.*, 2014; Du *et al.*, 2015). There is data that suggested that non-LAR breast cancer subtypes that express lower levels of AR may also still benefit for AR receptor targeted therapeutics (Barton *et al.*, 2015).

1.2 Non-Targeted Cancer Therapies

Therapeutics are essential for the effect treatment of cancer. Therapeutic treatments can be broadly categorised into targeted and non-targeted therapies. Non-targeted therapies are the mostly commonly employed therapeutic approaches for the treatment of cancer and often include the application of surgery to remove the tumour bulk, followed by either the administration of radiotherapeutic or chemotherapeutic agents to destroy any residual remaining tumour cells. Radiotherapy and chemotherapy are long established methods of cancer treatment, with radiotherapy having been effectively used solely or in conjunction with other treatments for over a 100 years (Gianfaldoni *et al.*, 2017). The use of chemotherapeutic reagents were first properly undertaken as an effective anti-leukaemia therapy in the 1940s, following the discovery of the

anticancer effects of nitrogen mustards (DeVita and Chu, 2008). Both radiotherapeutics and chemotherapeutics will be discussed in more detail in the subsequent sections (Du *et al.*, 2015).

1.2.1 Radiotherapy and Radio-immunoconjugates

Radiotherapy is a common anti-cancer treatment which uses high-energy radiation such as gamma-rays, x-rays or charged chemical isotopes, which emit α-, β-, γ- and auger particles, to shrink tumours and cause cancerous cells to undergo apoptosis (Cornelissen and Vallis, 2010; Wild *et al.*, 2011; Vaidyanathan and R. Zalutsky, 2012; Lee *et al.*, 2013; Aghevlian, Boyle and Reilly, 2017; Müller *et al.*, 2017). Radioactive doses can be delivered to the patient via a variety of different routes including external-beam radiation therapy, internal-radiation therapy or via systemic radiation therapy. External radiation therapy involves the delivery of radiation to the tumour from a machine situated outside of the body, internal-radiation therapy requires the positioning of a radioactive source near the tumour within the patient's body, whilst systemic radiation therapy requires the administration of a radiation-emitting substance directly into the bloodstream. The fundamental principle behind the therapeutic effectiveness of radiotherapy is ionisation. Administration of radiation results in the indirect ionisation of water molecules within cellular cytosols, causing the generation of reactive oxygen species (ROS) such as hydroxyl and superoxide free radicals. Free radical generation results in direct cellular DNA damages in the form of structural abnormalities, such as inter- and intra-strand crosslinks, which if unrepaired prove fatal to affected cell (Lawenda *et al.*, 2008).

Systemic radiotherapies use a range of radioactive isotopes, capable of emitting a variety of radioactive particles such as α-, β- or auger particles, with the greatest extent of nuclides selected for radioimmunotherapy displaying β-particle emitting properties. β-emitters, such as Lu^{177}, I^{131} and Y^{90} have a relatively long, yet sparse emission path, typically 1-10mm in length depending on the physical properties of the selected radioisotope. β-emitters display low linear energy transfer (LET), with the disposition of the β-energy occurring some distance from the actual decay event (Lehenberger *et al.*, 2011). This disposition of energy further than the decay event allows for the additional therapeutic advantage of crossfire killing of other tumour cells beyond those adjacent to the original decay site. Whilst β-emitting radioisotopes prove useful in the treatment of solid tumour masses due to their enhance radiation penetrating properties, their long emission path, low LET and distant energy deposition make them ineffective choices for the treatment of blood cancers, such as leukaemia's, and for metastatic or disseminated diseases (Milenic, Brady and Brechbiel, 2004; Fischer and Kampen, 2012; Lacoeuille, Arlicot and Faivre-Chauvet, 2018). For treatment of these types of cancer α-emitting isotopes prove much more effective.

α-emitters, such as Bi^{212}, At^{211} and Bi^{213}, are high-energy particles with a short decay half-life, relatively short radiation path length and a high LET, around 400 times greater than that of β-emitters. α-particles display a dense emission path, with energy deposition occurring immediately at the decay site. Due to their high LET, α-particles are extremely cytotoxic to the cell directly targeted with the radioisotope and those immediately neighbouring it. Their short-half life and lack of penetrating emission pathlength make α-particle emitting radioisotopes ineffective for the treatment of bulky solid tumours, but perfectly effective for the treatment of leukaemia's, highly vascularised tumours and disseminated or metastatic diseases (Milenic, Brady and Brechbiel, 2004; Couturier *et al.*, 2005; Steiner and Neri, 2011; Aghevlian, Boyle and Reilly, 2017; Zhu *et al.*, 2017; Lacoeuille, Arlicot and Faivre-Chauvet, 2018; Navalkissoor and Grossman, 2019).

Radio-immunoconjugates can make radiation therapy more target-specific by the conjugating of a radioactive isotope to an antibody which is targeted directly to a tumour-specific/tumour-associated antigen expressed upon the cancerous cells' surface (Kraeber-Bodéré *et al.*, 2014). Conjugation of radionuclides to a targeting antibody could confer multiple advantages over the use of either radiotherapy or antibody-therapy alone. Radio-immunoconjugates have the potential to deliver a highly concentrated dose of ionising radiation directly to the tumour site, whilst sparing surrounding healthy cells and tissues or cells on a more systemic level from unintended DNA damage. They also present an interesting possibility for the treatment of cancerous metastatic diseases. (Calvez, Mountzouris and Gramatikoff, 2005; Teicher and Chari, 2011; Choudary, 2012). Both α- and β-emitters can be linked to antibodies to produce therapeutic immunoconjugates, which enables radiotherapeutics to be used in a less systemic and much more tumour targeted way (Dahle *et al.*, 2012). Radio-immunoconjugates could enhance the effectiveness of antibody targeted therapies by-overcoming potential limitations of antibody-only therapies, such as the bypassing of tumour antigen heterogeneity and differential monoclonal antibody penetration in solid tumours (Chames *et al.*, 2009; Pohlmann, Mayer and Mernaugh, 2009; Garrett and Arteaga, 2011; Mukohara, 2011; Vu and Claret, 2012; Wong and Lee, 2012; Arena *et al.*, 2016; Sforza *et al.*, 2016; Zhao *et al.*, 2017). These advantageous characteristics of radio-immunoconjugates could result in the uniform targeting of entire cancerous lesions therefore making them an ideal choice for solid tumoral masses. Simultaneously the conjugation of radioactive isotopes to a tumour-targeted antibody could reduce the potential systemic side-effects experienced by patients receiving radiotherapy, by directly confining the radiation dose specifically to the tumoral micro-environment.

Auger-electron emitters, such as $I^{123/125}$ and Ga^{67} are extremely cytotoxic radioactive particles, with most of their energy deposition occurring within nanometres of the initial decay site. Due to their extremely short decay path, the use of auger emitting isotopes is restricted to conjunction

with internalising antibodies or antigens with a nuclear localisation signal (NLS) (Zereshkian *et al.*, 2014; Bergstrom *et al.*, 2016). Due to their highly toxic nature and the chance for severe damage to surrounding healthy tissues, auger-emitting radioisotopes are internalised allowing the radioactive dose to be delivered within range of the cellular nucleus rather than at a tumour antigen located on the cell surface. It is suggested that auger-emitting isotopes may be most effective in the irradiation of microscopic residual diseases (Milenic, Brady and Brechbiel, 2004; Steiner and Neri, 2011).

Designing an appropriate and effective radioimmunoconjugate is dependent upon the correct selection of a variety of several different components, including the selection of the appropriate type of antibody (e.g. IgG1, IgG4, F(ab), ScFv) and antigen to target (e.g CD33), the type of radionuclide (e.g α-, β- or auger emitter), its half-life, cell clearance behaviour and ultimately its target specificity and bodily elimination via excretory organs (Choudary, 2012).

1.2.2 Chemotherapy

Chemotherapy for the treatment of cancer has become one of the most commonly prescribed treatments over the course of the last 40 years. During this timeframe, a wide variety of chemotherapeutic agents have been developed which can broadly be categorised based on their antitumoral mechanistic activity. To date, commonly used groups of chemotherapeutic agents include the anthracyclines, the antimetabolites, the alkylating agents, platinum-based complexes and the microtubule inhibitors (Peters *et al.*, 2000; Walker *et al.*, 2010; Monsuez *et al.*, 2010; Hatzis *et al.*, 2011; Aparicio *et al.*, 2013; Fu, Calvo and Samson, 2013; Valenzuela, Neidigh and Wall, 2014; Klute *et al.*, 2014; Ranchoux *et al.*, 2015; McGowan *et al.*, 2017; Matera *et al.*, 2018; Oun, Moussa and Wheate, 2018).

Anthracyclines and related compounds comprise a family of intercalating agents, including doxorubicin (Le Cesne *et al.*, 2014), daunorubicin (Lancet *et al.*, 2018), epirubicin (Sun *et al.*, 2011), mitoxantrone (Damiani *et al.*, 2016) and bisantrene (Rothman, 2017) amongst others, which are effectively used in the treatment of many malignant disease types. The antitumoral potential of anthracyclines can be attributed to a combination of interconnected mechanisms, including their ability to utilize multiple drug resistance (MDR) pores to gain entry to tumour cells followed by their subsequent potential to undergo proteasome-mediated trafficking to the nucleus. Once at the nucleus they undergo intercalation into the nuclear DNA which is facilitated by the nature of their multiplanar ring structure. Once integrated into the DNA anthracycline drugs impair DNA transcription, inhibit cellular protein synthesis capabilities and inhibit topoisomerase II, thereby preventing the repair of the cells disrupted DNA strand. Simultaneously anthracyclines promote more cellular DNA, mitochondrial and membrane damage upon their binding by

generating reactive oxygen species (ROS) which eventually lead to the induction of apoptotic pathways through the activation of transcription factor protein (Monsuez *et al.*, 2010; McGowan *et al.*, 2017).

The anti-metabolites comprise a family of cytostatic compounds which prevent DNA replication by blocking either the synthesis or utilisation of nucleic acid bases. The most commonly used type of anti-metabolite for chemotherapeutic affect is 5-fluorouracil (5-FU) (Jover *et al.*, 2011). Anti-metabolites, such as 5-FU and thiopurines resemble co-factors, nucleotide bases or nucleotide precursors, all of which are required for nucleotide biosynthesis and DNA polymerisation processes. Anti-metabolites can use their similarity to nucleotides to either inhibit nucleotide metabolism pathways thereby resulting in the depletion of dNTPs available to the cell, or through the hindrance of replication progression by becoming incorporated into DNA, resulting in termination of the replication process (Helleday *et al.*, 2008; Monsuez *et al.*, 2010).

Alkylating agents, such as cyclophosphamide (Tabchy *et al.*, 2010) and platinum-based drugs including cisplatin (Pagliaro *et al.*, 2010), interfere with DNA replication by altering G-C, A-T base pairings, by generating single and double strand DNA breaks, forming inter- and intra-strand crosslinks as well as forming bulky DNA adducts which distort the double helical structure of the DNA (Fu, Calvo and Samson, 2013). Alkylating agents can be broadly categorised into 2 groups' monofunctional or bifunctional alkylating agents (Lee *et al.*, 2010), the former of which have one active moiety which modifies single DNA bases and the later which have two reactivity sites and as such can cross-link DNA bases from the same strand, from opposite strands or with proteins (Helleday *et al.*, 2008).

The first platinum-based drug was discovered by accident over 40 years ago by Barnett Rosenberg who was interested in applying electromagnetic radiation to bacterial and mammalian cells to ascertain whether electric or magnetic fields play a role in cell division. During the procedure the supposedly inert platinum electrodes generated two compounds upon the activation of the electromagnetic field, one of which was Cisplatin (Kelland, 2007). Since its discovery, Cisplatin and a host of platinum analogues derived from Cisplatin, including carboplatin and oxaliplatin. have been used in the treatment of a variety of tumours, including breast, colon and lung (Chang *et al.*, 2010; Tesniere *et al.*, 2010; de Gramont *et al.*, 2012; Tsao, 2012; Rugo *et al.*, 2016). Platinum anti-tumour compounds promote chemotherapeutic effects by interacting with and binding to cellular DNA, forming a variety of bulky adducts. These DNA lesions block nuclear processes such as DNA replication and transcription and affect a number of transduction pathways inducing either apoptosis or necrosis in the effected cancer cells (Brabec and Kasparkova, 2005).

Finally, microtubule-binding drugs can also be used for effective cancer chemotherapeutics. Compounds which target microtubules exert their inhibitory potential by altering the stability and dynamic capabilities of microtubules, which subsequently prevents mitosis and cellular proliferation (Giannakakou, Sackett and Fojo, 2000; Zhou and Giannakakou, 2005; Balzer *et al.*, 2010). At high concentrations anti-microtubule drugs can alter microtubule dynamics by either inhibiting or promoting microtubule polymerisation, by stabilising or destabilising microtubules or by either increasing or decreasing microtubule polymer mass (Zhou and Giannakakou, 2005). Predominantly microtubule-targeting drugs can be classified into one of two categories, those which are microtubule-destabilising agents like vinca alkaloids (e.g vinblastine and vincristine) or colchicines (Xi *et al.*, 2010; Moudi *et al.*, 2013; Sivakumar, 2013; Ghanbari *et al.*, 2014) and those which are microtubule-stabilising agents like the taxanes (e.g docetaxel and paclitaxel) (Chang *et al.*, 2010; Pagliaro *et al.*, 2010). Vinca alkaloids, colchicines and taxanes bind to 3 specific sites found on β-tubulin, the vinca domain, the colchicines site and the taxane site respectively (Zhou and Giannakakou, 2005; Ganguly and Cabral, 2011). At high concentrations vinca alkaloids can cause microtubule depolymerisation, the dissolution of spindle microtubules, mitotic cell cycle arrest and apoptotic induction whilst colchines promote microtubule depolymerisation. Alternatively, at high concentrations taxanes promote microtubule polymerisation, stabilisation and the production of microtubule bundles. At low concentrations all three groups of anti-microtubule drugs suppress microtubule dynamics, induce mitotic arrest and promote apoptotic induction (Zhou and Giannakakou, 2005).

1.3 Targeted Cancer Therapies

Despite their effective use in as cancer therapeutics, chemotherapeutic drugs, due to their untargeted nature have undesirable and potentially damaging side effects. Platinum anti-tumour drugs have a wide variety of disadvantages. These include their limited treatment potential, both due to the inherent resistance of some tumour types and the inevitable development of acquired resistance during the course of therapy, as well as the severe gastrointestinal, haematological and nephrotoxicities experienced as side-effects by patients (Brabec and Kasparkova, 2005; Ott and Gust, 2007; Oun, Moussa and Wheate, 2018). Anthracycline-type chemotherapeutic agents have been linked to cardiotoxicity (Damiani *et al.*, 2016; McGowan *et al.*, 2017), whilst alkylating agents have been linked to the development of pulmonary hypertension (Ranchoux *et al.*, 2015). Similarly, antimetabolite chemotherapeutics, such as 5-fluoruracil can also cause severe side effects, including cardiac effects, hyperammonemia or encephalopathy and neurologic effects (Thomas *et al.*, 2016). Radiation therapy, due to its very nature can also has undesirable off-target effects on healthy tissue through the damaging of their DNA (Koukourakis, 2012).The identification of the expression of tumour antigens has allowed for the development of a new

generation of increasingly targeted approaches to cancer therapeutics, which have less systemic off-target side effects.

1.3.1 Tumour Antigens

Tumour cells are derived from self-tissues which undergo genetic mutations which result in characteristic developments which promote uncontrolled, rapid cellular growth, changes to differentiation and impaired regulated cell death (apoptosis). As tumours are derived from alterations to normal healthy cells, but have uncontrolled growth characteristics, it makes isolating effective targets for tumour therapies difficult as most antigens expressed on the tumour cells' surfaces are also readily expressed on non-cancerous tissues. The safety and efficacy of oncogenic therapies is highly dependent upon the nature of the tumour antigenic target selected, which ideally should be abundant and easily accessible on the tumour cell surface. The antigen should be expressed consistently and with homogeneity across all tumour cells whilst showing exclusivity and specificity to only cancerous cells, with healthy cells showing no or very little antigen expression (Scott, Wolchok and Old, 2012).

Tumour-associated antigens (TAAs) (Díaz-Zaragoza *et al.*, 2015) can be sub-categorised into 5 classes, mutant antigens, over-expressed antigens, oncofoetal antigens, differentiation/lineage antigens and cancer-testis antigens (Caballero and Chen, 2009; Damelin *et al.*, 2011; Scott, Wolchok and Old, 2012; Hojjat-Farsangi, Moshfegh, Daneshmanesh, Khan, Mikaelsson, Österborg, *et al.*, 2014; Gjerstorff, Andersen and Ditzel, 2015). Mutant antigens can be categorised as those which are expressed solely by tumour cells and are otherwise found unexpressed across other tissue types, such as prostate-specific antigen (PSA) (Nome *et al.*, 2015). Over-expressed antigens are groups of proteins which are found expressed on normal cells, but which have an up-regulated expression in tumour cells, including receptors such as EGFR and HER2 (Hynes and MacDonald, 2009). Oncofoetal antigens are found to be expressed in embryonic or developing foetal tissues, however their expression is not associated with or is seen at very low levels in healthy adult tissues (e.g. carcinoembryogenic antigen (CEA) and α-fetoprotein (AFP) (Mailey *et al.*, 2011; Grunnet and Sorensen, 2012; Kinjo *et al.*, 2012; Zhao and Li, 2013; Bacac *et al.*, 2016). Differentiation or lineage antigens can be further sub-divided into that which stem from haematopoietic differentiations and those from cell surface differentiations. Haematopoietic differentiation antigens are glycoproteins associated with cluster of differentiation (CD) groupings (e.g. CD33 and CD20) (Tettamanti *et al.*, 2013; Pizzitola *et al.*, 2014; Zah *et al.*, 2016) whilst cell surface differentiation antigens are a group of highly diverse glycoproteins and carbohydrates which are expressed on the surface of both cancerous and non-cancerous cells, some of which are involved in growth and differentiation signalling, such as

growth factor receptors (e.g. EGRFR, HER2, MET and IGFR1) (Pollak, 2008; Hynes and MacDonald, 2009; Chen, Tsai and Hung, 2015). Cancer-testis antigens are those found on cancer cells which have shared expression on spermatocyte and spermatogonia cells, located in the testis (Caballero and Chen, 2009; Chiang, Benencia and Coukos, 2010; Scott, Wolchok and Old, 2012; Gjerstorff, Andersen and Ditzel, 2015).

The exploitation of these tumour antigens has allowed for the development of a more targeted approach to patient cancer therapy. Tumour-associated antigens have spawned the generation of a variety of targeted therapies, which include the advent of small molecule inhibitors which disrupt the functioning of these tumour antigens and antibody-type therapeutics which both disrupt the antigen functioning whilst helping to prime the patient immune system against the tumour.

1.3.2 Small Molecule Tyrosine Kinase Inhibitors

Small molecule kinase inhibitors (SM-KIs) are a family of molecules which competitively bind to the ATP-binding pocket of either tyrosine or serine/threonine kinases, thereby preventing their subsequent phosphorylation and the activation of downstream kinase substrates (Steeghs, Nortier and Gelderblom, 2007; Medina and Goodin, 2008; Roy and Perez, 2009; Banerji *et al.*, 2018; Whittaker *et al.*, 2018). This blockage of binding prevents the process of both receptor and substrate phosphorylation, thereby abolishing the potential for the activation of subsequent down-stream cell signalling pathways. Small molecule tyrosine kinase inhibitors (SM-TKIs) can be used to target receptor tyrosine kinases on the surface of cancer cells. Tyrosine kinase inhibitors (TKIs) are often small molecular weight molecules called Tyrphostins (Klein and Levitzki, 2009), which can be further classified on the basis on whether they reversibly or irreversibly inhibit the activity of receptor tyrosine kinases members. (Wu, Nielsen and Clausen, 2015). Reversible TKIs compete with ATP as a substrate for the ATP-binding site of the tyrosine kinase, preventing the phosphoryl transfer of γ-phosphate groups from the ATP-donor to residues within either the tyrosine kinase itself or a secondary messenger protein. Irreversible inhibitors, such as afatinib and neratinib, not only bind to and temporarily block the ATP-binding pocket of the tyrosine kinase but also alkylate a single cysteine residue within the binding cleft, thereby rendering the tyrosine kinase inactive permanently (Zhang *et al.*, 2007). Types I and II tyrosine kinase inhibitors are ATP competitive inhibitors, binding specifically to the ATP-binding pocket of the active or inactive form of the kinase respectively, type III inhibitors bind allosterically to a pocket adjacent to the ATP-binding site, without interacting with it, whilst type IV inhibitors bind allosterically to a site removed from the ATP-binding domain. Type V inhibitors are considered bivalent and are capable of binding to two sites within the receptor simultaneously (Cox, Shomin and Ghosh, 2011; Lamba and Ghosh, 2012; Wu, Nielsen and Clausen, 2015).

Tyrosine kinase inhibitors can also be further sub-categorised as ATP-mimetic tyrphostins, ATP-competitive tyrphostins, substrate-mimetic tyrphostins, allosteric inhibitors and pseudosubstrate inhibitors (Klein and Levitzki, 2009). Most Tyrphostins fall into the category of ATP-mimics or ATP-competitive small molecules and include examples such as the quinazoline derivatives gefitinib and erlotinib which are EGFR-targeted small molecule inhibitors (Cohen *et al.*, 2003; Cohen *et al.*, 2005; Cataldo *et al.*, 2011). Allosteric inhibitors stop kinase activation by preventing allosteric conformational changes within the kinase domain crucial for its effective functioning. Pseudosubstrate inhibitors compete with endogenous substrates by sharing a similar conformational structure to the native substrate. Pseudosubstrates may take the forms of peptide chains derived from the amino acid sequence of the normal receptor substrate (Klein and Levitzki, 2009).

1.3.2.1 First and Second Generation TKIs

With the discovery of receptor tyrosine kinases came the development of first-generation tyrosine kinase inhibitors for the treatment of ErbB over-expressing cancer forms. Two well-known examples of first generation TKIs are Gefitinib (Iressa) and Erlotinib (Tarceva), both approved for the treatment of Non-small cell lung cancers (NSCLC), which carry EGFR mutations (Cohen *et al.*, 2003; Cohen *et al.*, 2005; Cataldo *et al.*, 2011; Roskoski, 2014a) (Figure 1.2). Both Gefitinib and Erlotinib are FDA-approved quinazoline derivatives that reversibly bind to EGFR forming a complex with its ATP-binding pocket (Roskoski, 2014b). Erlotinib contains a quinazoline heterocyclic group which forms a hydrogen bond with the –NH group of amino acid MET793, located within the hinge region of the ATP-binding domain (Roskoski, 2014a). The binding of these TKIs to the adenosine triphosphate binding cleft inhibits the receptor's autophosphorylation and block downstream signalling cascades (Cataldo *et al.*, 2011).

Since the development of first generation TKIs, substantial work has been undertaken to develop more effective second and third generation inhibitors which can overcome the development of cancer resistance to first generation TKIs and ultimately prevent treatment failure. There are a variety of examples of second generation TKIs, which often have the added advantage of blocking multiple members of the ErbB receptor family, unlike their first-generation counterparts. Two examples of currently used second generation TKIs are lapatinib (Konecny *et al.*, 2006) and afatinib (Dungo and Keating, 2013) (Figure 1.2).

Lapatinib is an ATP-competitive inhibitor with dual target kinase sensitivity, which reversibly binds to both ErbB1 (EGFR) and ErbB2 (HER2) (Medina and Goodin, 2008). Lapatinib is approved for the treatment of patients who have advanced/metastatic breast cancer, which

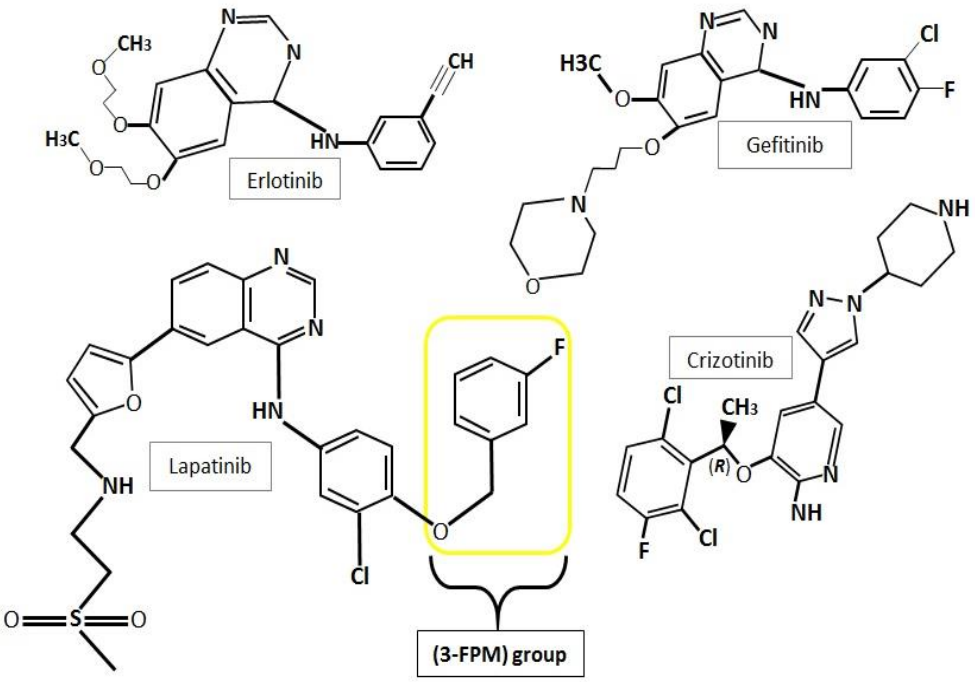

Figure 1.2: Small Molecule Tyrosine Kinase Inhibitor Structures

Displays the chemical structures of the first-generation tyrosine kinase inhibitors, Erlotinib, Gefitinib and Crizotinib and second-generation inhibitor Lapatinib showing their heterocyclic structures and quinazoline rings. Lapatinib also comprises a 3-flourophenylmethoxy (3-FPM) group Images adapted from (Roskoski, 2014a, Cataldo et al 2011)

expresses HER2 at high levels and have undertaken a previous treatment which has failed (Roy and Perez, 2009; Wang *et al.*, 2013). Lapatinib's intracellular activity stems from its ability to reversibly bind to and block the ATP-binding site of the tyrosine kinase, within the receptor cytoplasmic region, thereby preventing receptor phosphorylation, activation and subsequent downstream secondary messenger activation and signalling events (Untch and Lück, 2010). The quinazoline heterocyclic group of Lapatinib binds with the ATP-binding site of the RTK to form a hydrogen bond between itself and MET793 via its –NH group, whilst the anilino group extends into the hydrophobic region found adjacent to the adenine-binding cleft.

The anilino group of Lapatinib comprises a 3-flourophenylmethoxy (3-FPM) group, which displaces the αC-helix to an out-position and forces the hydrophobic pocket to extend to the adenine-binding site's activation segment. Lapatinib, unlike erlotinib which binds to the active conformation of EGFR, binds to the displaced inactive αC-out confirmation of EGFR (Roskoski, 2014a, 2014b). Lapatinib is also used for the treatment of breast cancer with secondary brain metastases, due to its ability to effectively cross the blood-brain barrier (Geuna *et al.*, 2012).

Afatinib, an aniline-quinazoline derivative that is a highly potent, irreversible inhibitor of multiple members of the ErbB family, including EGFR, HER2 and HER4 (Sequist *et al.*, 2013). Afatinib contains an unsaturated acrylamide side chain which functions as a Michael acceptor and can covalently interact with Michael donors, including cysteine residues 797 of EGFR, 805 of HER2 and 803 of HER4, within their ATP-binding sites, to form a covalent adduct which inhibits their enzymatic activities (Geuna *et al.*, 2012; Solca *et al.*, 2012; Mancheril, Aubrey Waddell and Solimando, 2014). Afatinib is approved as a first-line treatment of patients with Non-small cell lung cancers (NSCLCs) which bear either activating exon-19 deletions or Leu858Arg mutations (Roskoski, 2014a, 2014b).

Like with other TKIs, cancers treated with these dual-specific TKI therapies will eventually develop drug resistance. A variety of mechanisms have been proposed to generate resistance to these multi-targeted therapies, including PI3CA mutations, PTEN loss, Src overexpression and AXL over-expression, the last of which is linked particularly with Lapatinib resistance by eliciting PI3Kinase pathway activation (Wang *et al.*, 2013).

1.3.3 Monoclonal Antibodies and Immunotherapy

Immunotherapeutic techniques are currently being investigated as a means of treatment of cancerous cells. The use of monoclonal antibodies is just one such therapeutic agent. Antibodies can be grouped into five classes, IgG (Stockmann *et al.*, 2013), IgD (Gutzeit, Chen and Cerutti, 2018), IgM (Savage and Baumgarth, 2015), IgA (Woof and Russell, 2011) and IgE (Hamilton, MacGlashan and Saini, 2010), based on their heavy chain constant regions sequences. IgGs are the most commonly used class of antibodies in immunotherapies (Weiner, Surana and Wang, 2010). Monoclonal antibodies (mAbs) can act through a number of different mechanisms to bring about therapeutic effects, such as the activation of immunological processes including antibody-dependent cellular cytotoxicity (ADCC) (Seidel, Schlegel and Lang, 2013), complement-dependent cytotoxicity (CDC) (Quast *et al.*, 2015), by balancing the activation or inhibition of Fcγ receptors, by enhancing dendritic cell (DC) uptake (Guilliams *et al.*, 2014) or by triggering the idiotypic cascade (Sarduy *et al.*, 2017). Antibodies can also be used to target specific tumour antigens, such as over-expressed growth factor receptors, where they bind and cause the inhibited functioning of these cancer growth-promoting molecules (Vu and Claret, 2012). Alternatively they can illicit therapeutic effects through their conjugation to a variety of cytotoxic molecules including toxins and radio-ligands, cytokines as well as to enzymes to produce antibody-enzyme conjugates which can then be use to participate in antibody-dependent enzyme-mediated prodrug therapy (ADEPT) (Carter, 2001; Weiner, Dhodapkar and Ferrone, 2009; Weiner, Murray and Shuptrine, 2012).

1.3.3.1 Naked Monoclonal Antibodies

Antibodies are composed of two distinct functional units, the constant fragment (Fc) and the fragment of antigen binding (Fab). The two fab regions which make up the antigen binding portion of the antibody consist of the variable regions which are composed of three highly variable complementarity-determining regions (CDRs) (Polonelli *et al.*, 2008; Dashivets *et al.*, 2016). These CDRs form the highly variable antigen binding sites of the antibody and confer the necessary antigen specificity required for effective antibody function (Weiner, Surana and Wang, 2010). The Fc functional unit of the antibody is essential for naked mAbs to stimulate the immune system by enhancing effector functions through at least three different mechanisms which include antibody-dependent cellular cytotoxic (ADCC), complement-dependent cytotoxicity (CDC) or through triggering immune cell mediated phagocytosis (Seidel, Schlegel and Lang, 2013; Quast *et al.*, 2015; Métayer *et al.*, 2017). ADCC involves the binding of the two Fab regions of the mAb to their target antigen on the tumour cell surface, whilst the Fc region binds to an immune effector cell, such as neutrophils, dendritic, natural killer cell and macrophages, via an Fc receptor on its surface, resulting in the recruitment of adaptor proteins and the activation of immune effector cells (Zhou *et al.*, 1999; DiLillo and Ravetch, 2015; Métayer *et al.*, 2017; Brandsma *et al.*, 2019).

CDC results predominantly as a function of IgG subclasses IgG1 and IgG3, which act as highly potent activators of the complement cascade. Upon the binding of at least two IgG molecules to the cell surface membrane, a high affinity complement component known as C1q is stimulated to bind to the Fc region of the antibody. This results in the activation of the enzymatic capability of complement component C1r and leads to the subsequent downstream activation of the complement cascade proteins, resulting in the formation of membrane-attack-complexes (MACs). MACs form pores in the target tumour cell membrane, leading to subsequent cell lysis (Weiner, Dhodapkar and Ferrone, 2009; Lim *et al.*, 2010; Weiner, Surana and Wang, 2010).

Receptor-targeting antibodies, such as HER2 monoclonal antibody Trastuzumab, have emerged as promising therapeutics for the treatment of over-expressing cancer types. These antibodies can delay cancer progressions and trigger its destruction through immune effector cell binding. Antibodies like trastuzumab are purported to have mechanistic actions linked to internalisation and degradation of the targeted receptor, cytostatic effects, which cause G1 cell cycle arrest via the up-regulation of cell cycle inhibitors and interference of receptor dimerization and signalling through steric hindrance as well as triggering previously discussed ADCC and CDC immune cascades (Pohlmann, Mayer and Mernaugh, 2009; Vu and Claret, 2012).

1.3.3.2 Antibody-Dependent Enzyme-Prodrug Therapy (ADEPT)

Antibody-Dependent Enzyme-Prodrug Therapy (ADEPT) was first proposed in the 1980s as a two-step treatment process which provides therapeutic benefit through the generation of a cytotoxic drug locally within the tumour environment, enabling the delivery of high doses of therapy to tumour cells without a similar corresponding amount of damage being inflicted upon normal healthy cells (Van Rite *et al.*, 2011).

The exceptional potency and specificity of ADEPT can be attributed to the multi-step nature of the therapy, with the treatment occurring in two stages. Primarily, an antibody-enzyme conjugate is administered that selectively binds to a cell surface tumour-associated antigen, which is expressed with high abundance and homogenously across all tumour cells. The antibody-enzyme conjugate localises to the tumour cells' surface and any un-localised conjugate is removed from the body. Once unbound conjugate has been successfully removed a prodrug is administered, which has no cytotoxic activity until it comes into contact with the antibody-enzyme conjugate, localised solely in the tumour environment. The tumour-bound antibody-enzymes conjugate cleaves the non-toxic prodrug into the active cytotoxic form of the drug, which can then destroy tumour cells within the surrounding vicinity (Guo, Hou and Wang, 2011; Sharma and Bagshawe, 2017a, 2017b).

Despite the potential of ADEPT, immunogenicity is a particularly major disadvantage with both the use of non-human enzymes and murine derived antibody fragments eliciting strong immunological responses in patients. Even those undergoing immunosuppression with cyclosporine rapidly develop neutralising antibodies to both the foreign enzymes and antibodies used within this therapy, limiting the therapeutic benefit of the treatment (Sharma and Bagshawe, 2017a).

1.3.3.3 Immunotoxins and Antibody-Drug Conjugates

Like other immuno-based cancer therapies, antibody-drug conjugates use antibody fragments to direct small drug molecules to tumour cells using tumour cell surface antigens. By conjugating the cytotoxic drug to the antibody fragment it renders it non-cytotoxic to cells until it can be internalised into cancer cells and subsequently cleaved under acidic conditions to release it from the antibody (Calvez, Mountzouris and Gramatikoff, 2005; Choudary, 2012). The development of effective antibody-drug conjugates is dependent upon appropriate selection of the antibody or antibody fragment used, the potency and cytotoxic potential of the conjugated drug and the structure and stability of the linker used to combine the antibody to the drug (Choudary, 2012). Currently a variety of small molecule drugs are used for antibody-drug conjugates, including

maytansinoid (Erickson and Lambert, 2012; Maass *et al.*, 2016), auristatin (Sommer *et al.*, 2016), cryptophycin (Verma *et al.*, 2015) and dolastatins (Gianolio *et al.*, 2012), all of which inhibit the enzyme tubulin polymerase, duocarmycin (Black *et al.*, 2016; Menderes *et al.*, 2017) and CC-1065 analogues which are DNA-alkylating agents that bind to A-T rich regions of minor grooves of the double-helix, anthracyclines (Yu *et al.*, 2015; Dal Corso *et al.*, 2017), enediyene (Wang *et al.*, 2018) antibiotics like calicheamin (Ricart, 2011) which catalyse the development of double-strand breaks in cellular DNA and finally taxoid drugs which inhibit microtubule depolymerisation (Payne, 2003; Calvez, Mountzouris and Gramatikoff, 2005; Teicher and Chari, 2011; Choudary, 2012).

The first FDA-approved antibody-drug conjugate developed by Pfizer for the treatment of CD33-positive acute myeloid leukaemia (AML) was Mylotarg (Gemtuzumab ozogamicin). It is composed of a humanised CD33-targeted IgG4 antibody which is conjugated to a highly potent and cytotoxic calicheamicin (N-aceytl-γ-calicheamicin dimethyl hydrazine) antibiotic, via a bifunctional hydrazine linker (Payne, 2003; Govindan and Goldenberg, 2010; Choudary, 2012). Upon the binding of the CD33-positive IgG4 antibody to the CD33 antigen on the surface of tumour cells a complex is formed which results in the internalization of the drug immunoconjugate. Once internalised the calicheamicin derivative is released from the antibody inside a lysosome, transverse the cytosol to the nucleus where it binds to the minor groove of the cellular DNA and generates double strand breaks, ultimately resulting in cellular apoptosis (Govindan and Goldenberg, 2010; Choudary, 2012).

Immunotoxins make for effective anti-cancer therapeutics as they have high specificity; they are extremely potent and lack a mechanism which can induce resistance in tumour cells. Immunotoxins consist of a modified form of either microbial, plant, insect or animal toxin each with diverse biological effects (Pastan *et al.*, 2007; Ochiai *et al.*, 2008). Immunotoxins consist of several domains, including a binding domain, which concentrates the toxin to the target cell surface, a translocation domain, which enables the passage of the toxin across the cell membrane into the cell cytoplasm and an activity domain which interacts with a vital cellular component, resulting in cell death. The use of immunotoxins to target tumour cells requires the coupling of the toxin to a monoclonal antibody specific for a tumour antigen (Pastan *et al.*, 2007; Ochiai *et al.*, 2008). The ability of immunotoxins to reach solid tumour cells results by the slow, inefficient process of diffusion which is influenced by the size of the toxin (Pastan *et al.*, 2007). It has been suggested that the effect of immunotoxin may not be strictly dependent on the cytotoxic effect of the toxin alone but also on its function to enhance antitumor immunity, such as increased functioning of CD4+ and CD8+ T cells (Ochiai *et al.*, 2008).

1.4 Cancer Drug Resistance

Despite its improving therapeutic outlook, continuing high incidences of breast cancer, the existence of highly aggressive and still poorly treatable subtypes, such as TNBC and single-hormone receptor expressing forms, and the continued development of resistance to current therapies make breast cancer a particularly relevant and critically important area for ongoing novel therapeutic research.

Despite the vast array of therapeutic techniques available for the treatment of breast cancer, the development of novel cancer therapies is an ongoing struggle due to resistance. Tumour cells can overcome the cytotoxic effects of both platinum-based chemotherapeutic drugs and targeted cancer therapies by undergoing a process of resistance development. Therapeutic resistance can be classified into two categories, either primary or acquired. Primary resistance is a total lack of response, by the cancer cells, to a targeted therapy even upon its first administration, whilst acquired resistance occurs throughout the period of time when a treatment is being received, eventually rendering the treatment ineffectual. The development of either gene mutations or promiscuous signalling through cell surface receptor interactions (e.g. between EGFR and MET) can result in the primary resistance of tumour cells to antibodies which facilitate tumour killing through the abrogation of cell signalling pathways.

An acquired resistance implies the tumour has developed an 'escape mechanism', enabling it to evade the effects of the drug (Lovly and Shaw, 2014; Fenton *et al.*, 2018). Acquired resistances result from a diverse range of mechanisms including target modifications, histological transformations and mechanisms which bypass drug inhibition. Target modifications can take the form of alterations in the targeted oncogene or receptor, such as gene amplifications and secondary-site mutations. Gene amplifications can mediate drug resistance by up-regulating the expression of the drug target, so the levels are high enough to 'out-compete' the drug (Baselga, 2006). Resistance to antibodies therapies which target cell-surface receptor signalling pathways may result through alterations in the internalization and degradation of a receptor, ultimately leading to a signalling attenuation due to receptor down-regulation. Tumours may escape antibody suppression of signalling pathways by the over-activation of an alternative signalling pathway to compensate for the down-regulation of the pathway being targeted. Up-regulation of downstream secondary messenger proteins such as Src or the over-expression of cell-surface receptor MET are examples of alterations to tumour cell signalling pathways in response to an administered cancer therapy, leading to the development of resistance (Pohlmann, Mayer and Mernaugh, 2009; Garrett and Arteaga, 2011; Scott, Wolchok and Old, 2012; Vu and Claret, 2012; Wong and Lee, 2012; Arena *et al.*, 2016; Sforza *et al.*, 2016; Zhao *et al.*, 2017). Mechanisms of

acquired resistance, that enable the bypass of SM-TKI drug inhibition, occur because oncogenic kinases share common downstream signal mediators. The presence of an inhibitor targeted to a specific kinase can provide an unexpected selective pressure which drives the cancer cell to circumvent the inhibited kinase by utilizing another family member. This circumvention of target inhibition thereby allows for continued signalling along critical downstream signalling pathways ultimately leading to sustained tumour proliferation, even in the continued presence of the inhibiting drug (Lovly and Shaw, 2014; Alexander and Wang, 2015; Costa and Kobayashi, 2015; Huang and Fu, 2015; Stewart *et al.*, 2015; Fenton *et al.*, 2018; Yang *et al.*, 2018).

1.5 Venoms

Despite the overwhelming development of antibody-type and small-molecule kinase inhibiting therapeutic drugs, the hunt for novel receptor kinase targeting compounds is still ongoing. Cancer's inherent ability to acquire mutations, resulting in drug resistances, allows it to circumvent the suppressive effects of these RTK inhibiting drugs. These acquired resistances can lead to structural variance from the standard receptor wild-type, such as truncated forms which confer constitutive receptor activation (Keller *et al.*, 2010). Alternatively, mutations resulting in the up-regulation or constitutive activation of downstream cell-signalling pathway components, or an increased expression of an alternate RTK can render the drug-suppressed kinase redundant and restore downstream-signalling potential (Pohlmann, Mayer and Mernaugh, 2009; Garrett and Arteaga, 2011; Alexander and Wang, 2015; Sforza *et al.*, 2016; Zhao *et al.*, 2017; Yang *et al.*, 2018). As a result, modern pharmacology has turned to the search for novel medicines derived from the natural world (termed biologicals or biologics). Venom is a biological substance, which contains a complex mixture of biologically active compounds, including enzymes and toxins, which are synthesised in the venom glands of a variety of vertebrate and invertebrate species. Venoms have evolved as 'chemical arsenals' to aid the animal in either defence from predation or predatory behaviour (Arbuckle, 2015). To be defined as a venom and not a poisonous secretion, the evolution of the venom must be accompanied by the co-evolution of an active delivery system (such as fangs or stingers) to deliver the venom into the prey, rather than be secreted passively, such as through the skin (Jackson, 2003). A plethora of animal venoms, isolated from members of the classes *Reptilia*, *Amphibia* and the phylum *Arthropoda*, have been identified as potential sources of biologically active compounds that display a variety of antimicrobial, analgesic, anti-coagulant and anti-oncogenic properties (Kong *et al.*, 2013; Trim and Trim, 2013; Da Silva *et al.*, 2014; Mukherjee *et al.*, 2015; Ortiz *et al.*, 2015; Somay Doğan *et al.*, 2018; Dongo, Cardoso and Lewis, 2019; Rita de *et al.*, 2019).

Although therapeutic use of venom for disease treatment seems a fairly novel concept, the administration of small quantities of whole venoms and secretions from toads, spiders and scorpions have been used as ancient traditional remedies for millennia for the treatment of a variety of conditions, including gastrointestinal upset, arthritis and even cancer (Harvey, 2014; Pennington, Czerwinski and Norton, 2018). However, despite their adoption in ancient traditional medicine, there is little evidence to support their efficacy as therapeutic remedies. With modern medicine adopting a more systematic approach to investigating and characterising potential venom components for therapeutic use, there is however emerging evidence already supporting the propensity for them to be used in the targeted treatment of a variety of diseases, including cancer.

Venoms produced by a variety of animals, as a means of predation or defence, are known to contain a complex mixture of toxins and biologically active compounds. These biologically active compounds can promote a diverse array of physiological affects including allergic reaction, pain induction, dermatitis, respiratory arrest, necrosis or coagulation-related disorders such as disseminated intravascular coagulation or alternatively haemorrhage (Heinen and Gorini da Veiga, 2011). Venoms can be broadly categorised as neurotoxic, haemolytic, cardiotoxic, digestive, haemorrhagic or algogenic (pain-inducing) based on their biological activities. Despite the vast array of negative characteristics attributed to venomous exposure, many toxins are under investigation and subject to research projects aimed at the identification and development of new diagnostic or treatment molecule for a multitude of diseases. Most venoms comprise a complex mixture of peptides and proteins, amino acids, alkaloids, salts, biogenic amines (e.g. histamine), terpenes, polysaccharides and organic acids in various quantities; however peptides generally constitute between 90-95% of dry venom weights (Liu *et al.*, 2014). Venom composition is subject to high levels of variation in chemical composition, both inter- and intra-species. Fundamental compositions of protein, toxins and other venom components can vary based on species differences within genera and on the age, sex and geographical location of members from within the same species group (Gomes *et al.*, 2010).

1.5.1 FDA-Approved Venom-Derived Drugs

With the complex nature of venom composition and the diverse range of biological effects they can elicit, it is not surprising that research into identifying new lead compounds for therapeutics is now returning to the natural world for answers. Through previous research, venoms have been shown to possess the propensity to become novel therapeutics for the treatment of chronic and debilitating diseases. Since the first venom-derived therapeutic drug, Captopril, an angiotensin I converting enzyme (ACE) inhibitor derived from bradykinin-potentiating peptides (BPF) was isolated from *Bothrops jararaca* (Brazilian arrowhead viper) venom in 1970 (Ferreira *et al.*, 1970;

Gomes *et al.*, 2010), many more classes of therapeutic drugs derived from venom components have been shown capable of succeeding through clinical trials to become licenced drugs for the treatment of patient diseases (Calderon *et al.*, 2014; Chaisakul *et al.*, 2016; Pennington, Czerwinski and Norton, 2018).

Tirofiban and Eptifibatide, based on echistatin derived from *Echis carinatus* (saw-scale viper) and barbourin from *Sistrurus miliarius barbouri* (south-eastern pygmy rattlesnake) respectively have both been approved for the treatment of patients suffering with unstable angina, at high risk of death or myocardial infarction (Scarborough *et al.*, 1993; Koh and Kini, 2012; Pennington, Czerwinski and Norton, 2018)

Lepirudin and bivalirudin, whose structures are based on hirudin, an extremely potent thrombin, enzyme inhibitor isolated from the saliva of leech *Hirudo medicinalis* (Warkentin, 2004), for the treatment of blood clotting. Lepirudin was withdrawn from market use in 2012 (Beiderlinden *et al.*, 2018) but Bivalrudin, was approved in 2000 for use as an anticoagulant in patients with unstable angina undergoing percutaneous transluminal coronary angioplasty and patients at risk of heparin-induced thrombocytopenia undergoing percutaneous coronary intervention (PCI) (Pennington, Czerwinski and Norton, 2018).

Exenatide (Byetta®), a synthetic exendin-4 utilised for the treatment of type 2 diabetes derived from *Heloderma suspectum* (Gila monster) venom was approved for use in 2005 (Furman, 2012; Calderon *et al.*, 2014). Subsequent improvements in drug stability and delivery systems has resulted in the subsequent development of two further FDA-approved drugs, Bydureon® and Lyxumia®, In 2008, side-effects of Byetta® led to the FDA issuing a mandated warning for possible increases in pancreatitis as a result of taking the medication and in 2010 Bydureon® received a Black Box warning for possible increases in the risk of developing thyroid cancer (Pennington, Czerwinski and Norton, 2018).

Ziconotide, derived from a ω-conotoxin from *Conus magus* (Magical cone snail) venom has been licenced in 2004 for the treatment of chronic pain. However due to dose limiting side effects observed in patient treatment this drug it has been restricted solely for use in patients with intractable pain (Miljanich, 2004). Leconotide, an even more selective ω-conotoxin was under development however this peptide failed at clinical trials as a result of side-effects experienced by patients upon intrathecal administration (Kolosov, Goodchild and Cooke, 2010; Pennington, Czerwinski and Norton, 2018).

1.5.2 Snake Venoms

One of the most highly studied genera of venomous animals is those belonging to the paraphyletic clade Reptilia, infraorder *Serpentes*. Snakes are broadly categorised into three families, the proteroglyphs, solenoglyphs and opistoglyphs, based on the location and structural characteristics of their fangs. The front-fanged proteroglyphs and solenoglyphs (Peichoto *et al.*, 2012) are further sub-classified into two and three sub-families respectively. Proteroglyphs can be sub-classified as *elapinae*, comprising genera including mambas and cobras, and the *hydrophiinae* comprising sea coral snakes. Members of the solenoglyphs are categorised into 3 sub-families comprising the *crotalinae* (pit vipers), the *viperinae* (true vipers) and the monotypic genus *Azemiopinae* (Azemiops) (Smith, Smith and Sawin, 1977). Opistoglyphs, more commonly known as rear-fanged snakes, comprise the largest and most broadly diverse family of snakes categorised into the paraphyletic family the *Colubridae* (Peichoto *et al.*, 2012). Snake venoms comprise a complex mixture of proteins and enzymes groups including cytotoxins, cardiotoxins, hemotoxins, neurotoxins, myotoxins, phospholipase A2s (PLA2s), metalloproteinases, disintegrins, serinoproteases, hyaluronidases, cholinesterases, L-amino acid oxidases, lectins, as well as small peptides, growth factors, such as nerve growth factor, and inorganic cations, such as zinc, calcium, potassium, magnesium and sodium (Jain and Kumar, 2012; Vyas *et al.*, 2013; Shanbhag, 2015; Chaisakul *et al.*, 2016).

1.5.2.1 Snake Venoms and Cancer

As well as displaying a diverse variety of potential biological effects, including anti-microbial, analgesic, anti and pro-coagulant effects, snake venoms have also been shown to display anti-tumoral activities. Use of snake venoms for the treatment of cancer in laboratory animals was first reported in 1933 by Calmette. Elapid, crotalid and viperid venoms were screened for both *in vitro* and *in vivo* effects against chondrosarcoma and B16F10 melanoma cell lines. Findings showed that elapid venoms possessed considerably higher cytotoxicity profiles than either crotalid or viperid venoms (Gomes *et al.*, 2010). Many years later the anticarcinogenic properties of whole *Naja kaouthia* (Indian monocellate cobra) and *Vipera russelli* (Russell's viper) venoms were investigated against sarcoma, carcinoma and leukaemia models. *In vivo* experiments showed that sub-lethal doses of both venoms caused cytotoxicity to Ehrlich ascites carcinoma (EAC) cells and prolonged the lifespan of EAC cell containing mice (Debnath *et al.*, 2007; Gomes *et al.*, 2007). Histopathological analysis of the tumours showed tissue necrosis. Both venoms also displayed strong cytotoxic and apoptotic effects on human lymphoma cell line U937 and K562 leukaemia cells. The venoms were shown to significantly reduce the rate of cell proliferations and produce alterations in morphology indicative of the induction of apoptosis (Debnath *et al.*, 2007). Venom isolated from the elapid *Walterinnesia aegyptia* (Desert black) has been shown both alone and in

combination with silica nanoparticles to cause the growth arrest and apoptosis of breast and prostate cancer cells (Badr *et al.*, 2013).

Many proteins isolated from a variety of snake venoms have been shown to display anti-cancer properties *in vitro* against immortalised human cancer cell lines, including cobra venom factor (Downs-Canner *et al.*, 2016), cytotoxins CTX1, CTX2 and CTX3 (Lin *et al.*, 2010; Ebrahim *et al.*, 2014, 2015), salmosin (Kim *et al.*, 2003, 2016; Arruda Macedo, Fox and Souza Castro, 2015) aggretin (Chang *et al.*, 2014; Chung *et al.*, 2017), obtustatin (Ghazaryan et al., 2015; Ghazaryan et al., 2019), cathelicidin-BF (Wang *et al.*, 2013; Tian *et al.*, 2013), rhodostomin (Huang, Yeh and Wu, 2001; Wojtukiewicz *et al.*, 2017), colombistatin (Sánchez *et al.*, 2009), saxatilin (Jang *et al.*, 2007; Kim *et al.*, 2007a, 2007b; Arruda Macedo, Fox and Souza Castro, 2015) and lebecetin (Jebali *et al.*, 2014; Moga *et al.*, 2018).

1.5.2.1.1 Snake Venom Phospholipase A2s and Cancer

Phospholipase A2 from snake venom have been shown to display many potential anti-cancer effects *in vitro*. Phospholipase A2, isolated from the venom of *Bothrops neuwiedi* was shown to display cytotoxic effects when used in the treatment of B16 F10 melanoma cells (Pal *et al.*, 2002). Three PLA2s isolated from the venom of *Naja naja naja* (Indian cobra), were found to be cytotoxic to EAC cells but devoid of lethality, anticoagulant and haemolytic activities (Rudrammaji and Gowda, 1998). *Naja naja atra* (Chinese/Taiwan cobra) phospholipase A2 activity mediated the death of SK-N-SH neuroblastoma cells, by the induction of Fas and FasL, through Ca^{2+} and ROS-evoked p38 MAPK activation (Chen *et al.*, 2009). Myotoxic phospholipase A2, isolated from the venom of *Bothrops brazili* (Brazil's lancehead) was shown to display cytotoxic activity against human T-cell leukaemia cell line JURKAT (Costa *et al.*, 2008). Two secreted PLA2s, CC-PLA-1 and CC-PLA-2, isolated from the venom of snake *Cerastes cerastes* (Saharan horned viper) were shown to cause dose-dependent inhibition of the adhesion and migration of human brain microvascular endothelial cells and showed antiangiogenic activity when tested *in vivo* in chicken chorioallantoic membrane assays (Kessentini-Zouari *et al.*, 2010). MVL-PLA2, isolated from the venom of *Macrovipera lebetina* (Blunt-nosed viper) exhibited anti-integrin activities through the inhibition of the migration and adhesion of microvascular endothelial and human tumour cells (Bazaa *et al.*, 2009, 2010).

1.5.2.1.2 Snake Venom Cytotoxins and Cancer

Cytotoxins, another class of proteins found in snake venoms have also been shown to display anticancer properties. Cytotoxin P4, isolated from the venom of *Naja nigricollis* (Black-necked spitting cobra) was shown to display cytotoxic effects on melanoma B16 and WEHI-B3

leukaemia cells (Chaim-Matyas, Borkow and Ovadia, 1991; Pal *et al.*, 2002). Cytotoxin III (CTX-3), isolated from the venom of *Naja atra* (Chinese cobra) has been shown to display anticancer activity by inhibiting the growth of bone marrow K562 cells in both a dose and time-dependent manner (Yang *et al.*, 2006). CTX-3 displayed several apoptotic characteristics such as the formation of apoptotic bodies, an increase in the population of sub G1 cells, DNA fragmentation effects and poly (ADP-ribose) polymerase (PARP) cleavage. CTX-3 also appeared to induce apoptosis in K562 cells through both mitochondrial and caspase-dependent mechanisms (Yang, Chien, *et al.*, 2005; Yang, Lu, *et al.*, 2005; Yang *et al.*, 2006; Chien *et al.*, 2008), as well as causing autophagy and apoptosis in human leukaemia cell line U937 (Chiou *et al.*, 2019). A study into CTX-3 also showed that it displayed anti-proliferative properties in HL-60 human leukaemia cells through the activation of apoptosis by increasing populations of cells at the sub G1 cell cycle phase and the activation of c-JUN-N-terminal kinase (Chien *et al.*, 2008).

A toxin drCT-I, isolated from the venom of *Daboia russelii russelii* (Indian Russell's viper), shown to share homology to cytotoxins isolated from *Naja* venoms has been shown to display cytotoxic, anti-proliferative and apoptotic activities against EAC cells *in vivo* and human leukemic cells (U937, K562) *in vitro* (Choudhury *et al.*, 2006; Gomes *et al.*, 2007). Similar protein drCT-II, also isolated from the Indian Russell's viper, has also been found to have antineoplastic properties. Treatment of HepG2 human liver carcinoma cells resulted in an increase in the expression of p53 and moderate expressions of p21 and p27, supporting that it displays cellular apoptotic characteristic (Gomes *et al.*, 2010).

1.5.2.1.3 Snake venom Disintegrins and Cancer

Disintegrins, purified from snake venoms have shown strong anti-angiogenesis effects. Leucurogin, a disintegrin isolated from the venom of *Bothrops leucurus* (white-tail lancehead) showed anticancer properties when used against Ehrlich tumour-implanted mice models, with anti-angiogenesis effects confirmed by sponge-implant model in mice (Higuchi *et al.*, 2011; Li, Huang and Lin, 2018). Obtustatin, a disintegrin isolated from the venom of *Macrovipera lebetina obtuse* (West-Asian blunt-nosed viper) was shown to reduce the size of tumours in Lewis lung syngeneic mouse models by 50% and cause an 84% reduction in angiogenic activities in chick Chorioallantoic Membrane (CAM) assays (Marcinkiewicz *et al.*, 2003; Li, Huang and Lin, 2018). Salmosin, first purified from the venom of *Akistrodon halys brevicaudus* has been shown in studies to significantly suppress the growth of both solid and metastatic forms of Lewis lung carcinoma cells in mouse xenograft models, and displays anti-angiogenetic properties attributed to its ability to actively block $\alpha_v\beta_3$ integrin (Kang *et al.*, 1998). Contortrostatin, derived from the venom of viper *Akistrodon contortrix contortrix* (Southern copperhead) displayed anti-angiogenic activities in mice with primary tumours of human breast cancer MDA-MB-435 (Zhou *et al.*, 1999,

2000; Swenson *et al.*, 2004; Li, Huang and Lin, 2018). In 2012 Thangam *et al* purified a disintegrin from *Naja naja* (Indian cobra) venom which appeared to display anticancer activity against MCF-7 breast cancer cells, A549 lung cancer cells and HepG2 liver cancer cells. Unlike previous disintegrins, which displayed strong anti-angiogenic properties, AO/EtBr staining and DNA fragmentation analysis appear to suggest that this disintegrin was inducing apoptotic cell death in these cell lines (Thangam *et al.*, 2012). Saxatilin, purified from the venom *Gloydius saxatilis* (Rock mamushi) has been shown to inhibit tumour necrosis factor alpha (TNF-α) induced proliferation of ovarian cancer cell line MDAH-2774, by suppressing activating protein-1 (AP-1) and causes a decreases invasion of cancer cells by regulating matrix metalloproteinase-9 (MMP-9) and suppress the angiogenesis capability of human lung cancer cell line NCI-H460 by inhibiting VEGF production and affecting hypoxia induced factor-1α expression via the Akt pathway (Jang *et al.*, 2007; Kim *et al.*, 2007a, 2007b).

1.5.2.1.4 Snake Venoms L-Amino Acid Oxidases (LAAO) and Cancer

L-amino acid oxidases (LAAO), another fundamental group of proteins found in snake venoms have also been shown to possess many potential anticancer properties, many of which are linked to the induction of cancer cell apoptosis. A LAAO, isolated, purified and characterised from the venom of *Akistrodon halys* upon exposure has been shown capable of causing the apoptosis of cultured mouse lymphocytic leukaemia L1210 cells (Suhf and Kim, 1996). Another L amino acid oxidase, AHP-LAAO, isolated from *Akistrodon halys pallas* venom was shown to inhibit the proliferation of HeLa cells and nuclear morphological changes and DNA fragmentation at doses as low as 0.5 μg/ml (Zhang *et al.*, 2004), whilst another LAAO isolated from *Vipera berus berus* venom was found to induce apoptosis in myelogenous leukaemia cell line K562 and HeLa cells (Samel *et al.*, 2006). LAAOs isolated from the venom of *Ophiophagus hannah* (King cobra) were found to be cytotoxic to stomach cancer, fibrosarcoma, murine melanoma, colorectal cancer cells. However this LAAO was also found to display toxic activity against Chinese hamster ovary (CHO) cells, considered a normal immortalised control cell line. Cytotoxicity caused the lost ability of attachment by cells and inhibition of cellular proliferation levels. Reductions of cell proliferation levels of 74% and a reduction in the level of thymidine uptake were observed (Ahn, Lee and Kim, 1997). In another study ACTX-6 treatment, an LAAO isolated from the venom of *Deinagkistrodon (Agkistrodon) acutus* (Sharp-nosed viper), showed an accumulation of tumour cells in the sub G1-phase of the cell cycle and caused apoptosis of A549 lung cancer cells via activation of the Fas pathway and caspase-9 (Zhang and Cui, 2007; Zhang and Wu, 2008). Rusvinoxidase, an LAAO isolated from the venom of *Daboia russelii russelii* (Russell's viper) was also shown to change cellular morphology, membrane integrity and promote cell shrinkage,

apoptosis and DNA fragmentation in human MCF-7 cells through caspase-7 and 8 activation (Mukherjee *et al.*, 2015).

1.5.3 Invertebrate Venoms

As well as the potential for venom components from the paraphyletic clade Reptilia to display anti-cancer properties another highly investigated phyla of venomous creatures is that of the *Arthropoda.* The phylum *Arthropoda* comprises invertebrate animals which show characteristics such as segmented bodies, jointed appendages and a hard chitinous exoskeleton. *Arthropoda* can be categorised into a variety of subphylas and classes with venomous members. These include the scorpions and spiders *(Arachnida)* from subphylum *Chelicerata*, centipedes *(Chilopoda)* and millipedes *(Diplopoda)* from subphylum *Myriapoda* and the Insects *(Insecta)* from subphylum *Hexapoda.*

1.5.3.1 Bee and Wasp Venoms and Cancer

One of the most currently researched orders of the class *Insecta* is that of the *Hymenoptera*, which predominantly comprises bees, wasps, ants and sawflies. The order *Hymenoptera* can be divided into two sub-orders, the *Symphyta* and *Apocrita*, the latter of which demonstrates the first evolutionary step in the development of the hymenopteran venom system. Superfamilies' arising within these suborders include the *Apoidea*, i.e. bees, and the *Vespoidea*, or wasps. Examples of species arising from the *Vespoidea* and *Apoidea* include a diverse variety of cosmopolitan wasps and the common honey bee respectively (Moreno and Giralt, 2015).

Both bee and wasp venoms are composed of complex mixtures of biologically active compounds, which can exert a range of localised and systemic toxic effects such as pain, oedema and localised swelling as well as in a few extreme cases anaphylaxis or a systemic toxic reaction (Moreno and Giralt, 2015). Bee venom (BV) is known to contain at least 18 kinds of biologically active compounds, some of which include melittin, apamin, adolapin, mast-cell degranulating (MCD) peptide as well as a variety of enzymes (e.g. Phospholipases A2/B, Hyaluronidase, Phosphatase and α-Glucosidase) and non-peptide compounds such as dopamine, histamine and norepinephrine (Liu *et al.*, 2014; Premratanachai and Chanchao, 2014; Moreno and Giralt, 2015). Wasp venom, like Bee venom, contains a complex cocktail of biologically active molecules and both share a similar enzymatic composition. Wasp venom, however, shows much more significant variation in venom composition across species. Wasp venom composition varies not just from bee venom composition, but also between those considered social wasp species and solitary wasp species. Significant differences in the composition of BV and wasp venom are predominantly attributed to their differing peptide compositions, with a lack of biologically active peptides such as melittin

and apamin observed in the latter. These peptides appear to be replaced by other active peptides, mastoparan and bradykinins, which are unique to wasp venom (Moreno and Giralt, 2015).

BV components such as melittin, Phospholipase A_2, MCD peptide and apamin, and wasp venom peptides mastoparan (Heinen and Gorini da Veiga, 2011; Moreno and Giralt, 2015) and kinin-related peptides have a diverse range of biomedical potentials attributed to their inherent antimicrobial, antiviral and therapeutic characteristics. However recent investigation has moved into the potential cytotoxic capacities of bee and wasp venom components for development and use as novel oncogenic therapies (Heinen & Gorini da Veiga, 2011; Gajski & Garaj-Vrhovac, 2013; Ahluwalia & Shah, 2014).

Recent research has shown that hymenopteran venom components have the potential to display anti-cancer properties. Several studies have suggested that BV has potential anticancer effects against breast (Jeong *et al.*, 2014), hepatocellular carcinoma (HCC) (Liu *et al.*, 2008), ovarian (Jo *et al.*, 2012), prostate (Park *et al.*, 2011), melanoma (Tu *et al.*, 2008), lung (Choi *et al.*, 2014), leukaemia (Moon *et al.*, 2006) and cervical (Oršolić, 2009) cancers (Rady *et al.*, 2017). A recent study into the effects of whole bee venom and isolated bee venom component melittin on ovarian cancer cell lines found anti-proliferative properties. Bee venom and melittin, at doses of 1-5 μg/ml and 0.5-2 μg/ml respectively, were shown to inhibit the growth of SKOV3 and PA-1 ovarian cancer cell lines in a dose-dependent manner by the induction of the apoptotic cell death pathway. Increases in death receptors DR3 and DR6 were observed in both cell lines in response to treatment, whilst the phosphorylation of JAK2 and STAT3 were inhibited (Jo *et al.*, 2012).

Further studies into the activity of melittin against aggressive, metastatic hepatocellular carcinoma (HCC) found that treatment with melittin reduced tumour cell metastasis by preventing cell migration and motility through the suppression of Rac1-dependent metastasis pathway (Liu *et al.*, 2008). Whilst a study by Jeong *et al.*, found that bee venom component melittin caused reduction in the metastasis and invasion potential of EGFR-expressing breast cancer cell lines MDA-MB-231 and MCF-7. Transwell wound-healing assays demonstrated that whole bee venom and melittin significantly inhibited the EGF-induced migration of breast cancer cells. In addition, it was found that melittin significantly supressed the EGF-induced phosphorylation of FAK through the inhibition of the mTOR/p7056K/4E-BP1 pathway (Jeong *et al.*, 2014).

A further study into the cytotoxic activities of Bee venom components melittin and apamin on normal hepatic cells (L02) and hepatocellular carcinoma cells (HepG2) found no cytotoxic effects to L02 cells but antitumoral effects to HepG2 cells. Both melittin and apamin were found capable of inhibiting HepG2 carcinoma cells in a dose- and time-dependent manner and were found to

markedly increase the onset of early apoptosis in these cells. This specific tumour cell activity suggests the possibility for melittin and apamin as new liver-cancer therapeutics (Zhou *et al.*, 2013).

A recent study into wasp venom component Mastoparan showed the compound capable of displaying strong anti-cancer toxicity against Jurkat and THP-1 leukaemia, HOPC murine myeloma and MDA-MB-231, MDA-MB-468, SKBR3 and T47D breast cancer cells, as well as multi-drug resistant and slow growing cancer types. Mastoparan was found to kill cells through a lytic mechanism. In all cases the study also found that mastoparan was more toxic to cancer cells than normal healthy peripheral blood mononuclear cells (PBMCs), human erythrocytes, and primary human mammary epithelial cells (HMECs) (Hilchie *et al.*, 2016). A further study into mastoparan, published in 2015, investigated potential affects against malignant melanoma murine cell model B16F10-Nex2. *In vitro*, the study found that mastoparan caused melanoma cell death via the induction of caspase-dependent apoptosis through the intrinsic mitochondrial apoptosis pathway, caused loss of mitochondrial-membrane potential, the generation of reactive oxygen species (ROS), caused DNA degradation and cell death signalling. *In vivo*, mastoparan reduced the growth of subcutaneous melanomas in syngeneic mouse models, increasing their overall survival (De Azevedo *et al.*, 2015).

The ongoing extensive research into bee and wasp venom components as novel anti-cancer therapeutics is encouraging and supports the potential for a new class of biologics derived from animal venoms for the treatment of aggressive diseases.

1.5.3.2 Scorpion, Theraphosid and Centipede Venoms

Despite mounting evidence of compounds isolated from venoms for disease treatment there is still little research into a variety of venomous classes of animals, particularly members of the *Arachnida* and *Chelicerata.* Within the *Arachnida*, the families *Theraphosidae* (tarantulas), *Scorpionidae* (Scorpions) and *Buthidae* (Buthids) hold great potential for the discovery of novel tumour-targeted compounds. Despite the limited research currently undertaken into venoms from these classes of animals, there has already been molecules identified from some of these venoms with potential anti-oncogenic properties.

1.5.3.2.1 Scorpion Venom and Cancer

Research into the anticancer properties of scorpion venom has become more apparent over recent years, with scorpion venom and scorpion venom components shown to display potential anticancer properties against a variety of tested cancer types (Ding *et al.*, 2014; Ortiz *et al.*, 2015).

Scorpion venoms have been shown to contain a complex mixture of salts, neurotoxins, low molecular weight peptides and enzymes, and to display biological effects such as immunosuppressive effects, anti-proliferation of cells, cytotoxicity and apoptosis-induction. Scorpion venoms have been shown to prove effective against a variety of human cancers, including leukaemia, gastric, breast, neuroblastoma, brain tumour, glioma, lung, melanoma and prostate (Heinen and Gorini da Veiga, 2011; Mishal *et al.*, 2013; Sarfo-Poku, Eshun and Lee, 2016; Zhang and Zhang, 2016).

Whole venom from buthid scorpion *Androctonus amoreuxi* has been shown to display anti-proliferative properties against prostate cancer cell line PC3 in MTT assay analysis. Treatment with whole venom for 24h at doses of 0.39, 1.56, 6.25, 25 and 100 μg/ml was carried out and a dose-dependent reduction in cell viability was observed with increasing concentrations of venom. An IC50 value of 3.04 μg/ml was determined effective for 24h treatment. Treatment with the IC50 dose resulted in an observable down-regulation in Bcl-2 gene expression compared to untreated cells (Akef *et al.*, 2017). Studies into the effect of whole venoms, isolated from medically significant buthid scorpions *Androctonus crassicauda, Androctonus bicolor* and *Leiurus quinquestriatus* against human breast and colorectal cancer cell lines found the venoms display anticancer properties against human ileocecal adenocarcinoma (HCT-8), colorectal carcinoma (HCT-116) and breast carcinoma (MDA-MB-231). All 3 cell lines showed significant reductions in cell motility and colony formation in response to *Androctonus crassicauda* venom treatment. A complete halting of migration was observed in HCT-8 cells in response to treatment for 24h with 100 μg/ml *Androctonus crassicauda* venom and a marked reduction of ~70-90% in colony formation observed at a concentration of 80-100 μg/ml. Treatment with the same venom resulted also in significant reduction in cell motility and colony formation in HCT-116 at treatment doses of 50 and 100 μg/ml. A similar pattern of cell motility and colony formation were observed in MDA-MB-231 cells treated with *Androctonus crassicauda* venom, confirming effects across multiple tumour cell types. Effects of further scorpion venoms, extracted from *Androctonus bicolor* and *Leiurus quinquestriatus*, were investigated against MDA-MB-231 cells and shown to illicit similar inhibitory effects on cell motility and colony formation to those observed with *Androctonus crassicauda* venom (Al-Asmari, Islam and Al-Zahrani, 2016; Al-Asmari *et al.*, 2017).

Two studies by carried out by Zargan *et al*. in 2011 assessed the ability of scorpion venom from *Odontobuthus doriae* to inhibit the growth of human breast cancer cell line MCF-7 and neuroblastoma cell line SH-SY5Y. The studies showed treatment of SH-SY5Y cells with *Odontobuthus doriae* resulted in antiproliferative and apoptotic effects. Treatment with doses of 10, 25, 50, 100, and 200 μg/ml venom for 24h caused decreases in cell viability to 90.75, 75.53,

55.52, 37.85, and 14.30% respectively, showing a strong dose-dependent effect with increasing dose. Morphological changes to treated cells, including swelling, irregular shape, rupture of membrane, aggregation, inhibition of neurite outgrowth and release of cytosolic components also accompanied the observed changes to viability. Treatment with a dose of 50 μg/ml resulted in Caspase-3 activity increases, DNA fragmentation, increases in lactate dehydrogenase (LDH) level and depolarisation of mitochondrial membranes. A dose of 100 μg/ml resulted did not result in DNA fragmentation but appeared to be killed by acute necrosis (Zargan, Sajad, Umar, Naime, *et al.*, 2011). Treatment of MCF-7 cells resulted in a similar set of observations, with treatment resulting in the induction of apoptosis in MCF-7 cells and the inhibition of DNA synthesis. Cell viability decreased and LDH release increased, in a dose-dependent manner. There was observable depolarisation of mitochondrial membranes, DNA fragmentation and increased activation of caspase-3 in response to *Odontobuthus doriae* venom treatment (Zargan, Umar, *et al.*, 2011).

Another study was carried out in 2013 into the effects of whole scorpion venom from the Cuban scorpion *Rhopalurus junceus* against a panel of human cancer cell lines. The effect of a range of scorpion venom concentrations (0.1, 0.25, 0.5, 0.75 and 1 mg/ml) was tested against various human cancer cell lines, including human cell lines of epithelial origin (Hela, SiHa, Hep-2, NCI-H292, A549, MDA-MB-231, MDA-MB-468, HT-29) and hematopoietic origins (U937, K562, Raji), as well as normal non-malignant cell types (MRC-5, MDCK, Vero) using MTT cell viability assays. Epithelial-derived cancers showed significant reductions in cell viability in response to venom treatment in a dose-dependent manner, with medium cytotoxic concentrations (IC50) ranging from 0.6-1 mg/ml. There was no observable effect in response to venom treatment in either normal human cell lines or cancer cell lines derived from hematopoietic origins, suggesting specificity for solid tumour types. The scorpion venom was identified to induce apoptosis in the least sensitive tumour cell type (HeLa) by causing chromatin condensation, down-regulated expression of Bcl-2 mRNA, increased expression of *TP53* and *BAX* mRNAs and increases in the activity of caspases-3, -8 and -9. In the cell line that displayed the greatest sensitivity (A549), the venom appeared to induce necrosis rather than apoptosis, further evidenced by acridine orange/ethidium bromide fluorescent staining and the down-regulation of pro-apoptosis related genes (Díaz-García *et al.*, 2013). In a follow-up study, treatment of MDA-MB-231 cells with *Rhopalurus junceus* venom resulted in induction of apoptosis in a time-dependent manner, an increase in the expression of p53, p21, Noxa, Bax, Puma and Caspase-3 and a down-regulation in the expression of Bcl-2 and Bcl-xl (Díaz-García *et al.*, 2017).

A study by Zhang *et al*. in 2009 into polypeptide extracted from scorpion venom (PESV), originally isolated from East-Asian buthid scorpion *Buthus martensi Karsch* (BmK) was

investigated for both the prevention and treatment of prostate cancer. DU145 prostate cancer cells were cultured and treated with PESV and the resultant effects on proliferation assessed using MTT assays. The study found that PESV treatment between 10-200 mg/L impaired the proliferative capability of the human prostate cancer cells in a dose-dependent manner. 48h treatment resulted in G1-phase cell cycle arrest at doses of 40μg/ml. PESV treatment caused changes in the expression of several proteins, including strong induced expression of p27 and reductions in cyclin E expression. Treatment triggered high levels of apoptosis at a dose of 40 μg/ml in TdTmediated dUTP-biotin nick-end labeling (TUNEL) assays, which was associated with an increase in pro-apoptotic protein Bax (Zhang *et al.*, 2009).

A 2015 study into the effects of BmK-n2, a peptide isolated from the venom of scorpion *Buthus martensi* (Karsch, 1879) and its derivatives found they displayed anticancer properties against human oral squamous carcinoma cells (HSC-4). BmKn-2 was shown to be most effective against the oral cancer cell line with an IC50 value of 29 μg/ml. The study identified that BmK-n2 killed HSC-4 cells through the induction of cellular apoptosis, confirmed using Real-Time (RT)-PCR and contrast microscopy. Typical morphological characteristics associated with the induction of apoptosis were observed in treated HSC-4 cells, including cell shrinkage and rounding. These observations were further supported by the findings of RT-PCR, which saw the increased expression of pro-apoptosis genes encoding caspases- 3, -7, and -9 and decreases in anti-apoptotic genes such as Bcl-2 (Tong-ngam, Roytrakul and Sritanaudomchai, 2015). A further study by Satitmanwiwat *et al*. in 2016 confirmed that BmKn-2 showed potent cytotoxic effects against HSC-4 and KB oral cancer cell lines through the induction of apoptosis, but did not affect the cell viability or apoptotic pathway initiation in normal human gingival cells (HGC) or dental pulp cells (DPC) (Satitmanwiwat *et al.*, 2016).

The effects of *Buthus matensii Karsch* (BmK) scorpion venom extracts were found result in the inhibition of growth of human breast carcinoma cells MCF-7 and hepatoma cells SMMC7721. The results of a study found the cells to be susceptible to BmK scorpion extracts in both a dose- and time-dependent manner, with MCF-7 breast cells displaying the greater sensitivity both with increasing dose and over time. The treatment of MCF-7 cells with 600 μg/ml of BmK for 24h resulted in changes to the number of cells at each phase of the cell cycle, with the cell number in G0/G1 phase significantly increased compared to untreated controls, those in G2/M phases unchanged and those in S phase significantly decreased. The finding of this research suggest that BmK scorpion venom extract causes an arrest of cell cycle at the G0/G1 phase in MCF-7 breast cancer cells (Li *et al.*, 2014).

Two peptides, neopladin 1 and neopladin 2, isolated from the venom of buthid scorpion *Tityus discrepans* (Venezuelan scorpion) were found to display activity against SKBR3 breast carcinoma cells. The study found that both peptides induced apoptosis in SKBR3 cells following treatment but had negligible effects on a non-malignant monkey kidney cell line MA104 (D'Suze *et al.*, 2010).

Bengalin, a peptide isolated from the venom of the scorpion *Heterometrus bengalensis* (Indian black scorpion) has been shown to display anticancer properties against human leukemic cells. Bengalin caused cell death through the induction of apoptosis, via mitochondrial pathway changes and the inhibition of heat shock proteins. Bengalin was shown to inhibit the proliferations of human leukaemia's U937 (histiocytic lymphoma) and K562 (chronic myelogenous leukaemia) at IC50 values of 3.7 and 4.1 μg/ml respectively but did not show any significant effects against normal human lymphocytes. Inhibition of U937 and K562 cell proliferation appeared to occur via apoptosis, as observed from damaged cell nuclei, augmentation of DNA fragmentation, cell cycle arrest at the G1 phase, reduction in telomerase activity and an increase in the development of early apoptotic cells. Further investigations identified that Bengalin treatment resulted in loss of mitochondrial membrane potential (MMP), cytochrome release into the cytosol, an elevation in the Bax:Bcl2 ratio, a decrease in the expression levels of heat shock proteins (HSP) 70 and 90, activation of caspase-3 and -9 and the induction of poly(ADP-ribose) polymerase (PARP) cleavage (Gupta *et al.*, 2010).

1.5.3.2.2 Spider Venom and Cancer

Spiders comprise the most diverse group of arthropods with over 38,000 species described. Relatively few toxins from the venoms of spiders and theraphosids have been studied, making this an attractive field of research yet to be properly explored (Heinen and Gorini da Veiga, 2011). Studies undertaken into the use of whole spider venoms have shown them to display anti-cancer potentials. A study by Gao *et al*. in 2005 into the venom of *Macrothele raven* (Funnel-web spider) found the whole venom decreased the proliferation of human cervical carcinoma cell HeLa in a dose- and time- dependent manner. The decrease in proliferation was accompanied by an arrest in cell cycle progression and an increase in caspase-3 activation, leading to subsequent cell apoptosis. The *in vivo* effects of *Macrothele raven* venom were assessed in nude mice injected subcutaneously with HeLa cells. Those animals injected with the venom through the tail vein saw a reduction in the overall size of the tumour inside the skin compared to that of the untreated mice (Gao *et al.*, 2005). Gao *et al.* 2005, also investigate the effects of *Macrothele raven* venom on human hepatocellular carcinoma cell line BEL-7402. MTT cytotoxicity assays revealed the venom also inhibited cell proliferation in both a dose- and time-dependent manner. DNA

synthesis was inhibited in the treated cells, which were found to enter into cell cycle arrest at the G0/G1 phase. This arrest in cell cycle progression was linked to an increase in apoptotic cell development (Heinen and Gorini da Veiga, 2011). Another study by Liu *et al*. investigated the effects of *Macrothele raven* venom on myelogenous leukaemia cell line K562. The venom was found to suppress the growth of the leukaemia cells, again in a dose- and time-dependent manner. The venom was shown to have low inhibitory effects against human lymphocytes, showing selectivity specifically towards leukemic cells. The treated cells showed typical morphological changes associated with indicators of apoptosis, including condensation of nuclei and DNA fragmentation. Venom treatment was found to induce caspase-3and caspase-8 activation and promote PARP cleavage (Liu *et al.*, 2012).

Gomensin, an antimicrobial peptide derived from the venom of the Brazilian tarantula *Acanthoscurria gomesiana* has been shown to also display anti-tumoral activities when used in several studies to treat cancer. A study in 2010 into the anti-tumour effects of gomensin identified the venom peptide to display both *in vitro* and *in vivo* anti-tumour activity through an unknown mechanism of action. Treatment of human neuroblastoma (SH-SY5Y) and rat pheochromocytoma (PC12) with gomensin resulted in necrotic cells death and cytotoxicity in both cell lines (Soletti *et al.*, 2010). Another study into gomensin's anti-cancer activities in subcutaneous murine melanoma B16F10-Nex2 again found both *in vitro* and *in vivo* activities. Topical treatment of subcutaneous murine melanoma, using a gomensin-incorporated cream resulted in significant delays to the growth of the tumour. *In vitro*, cytotoxicity assays into the effects of gomensin in murine B16F10-Nex2 melanoma, as well as human breast adenocarcinoma (SKBR3), colon adenocarcinoma (LS180), cervical cancer (HeLa) and melanoma cell lines (SKMel 19 and A2058) were also undertaken. Findings showed that after 12h of incubation with 20 µM gomensin, B16F10-Nex2 melanoma cells lost viability, in a time- and dose-dependent manner that was not reversible after the removal of gomensin. Murine melanoma cells treated for 5h with 10 and 20 µM gomensin and subsequently with complete media in the absence of the peptide did not resume growth. Gomensin was also found to display cytotoxicity against tested human cell cancer lineages *in vitro*, with the most pronounced toxic effects observed in human melanoma A2058 (Rodrigues *et al.*, 2008; Kumar, Sarkar and Jain, 2013).

A 2004 study into Psalmotoxin-1, isolated from the venom of the Trinidad chevron tarantula *Psalmopoeus cambridgei* found that it resulted in inhibition of cation currents mediated by acid-sensing ion channels (ASIC). Electrophysiological experiments in human astrocytoma found that psalmotoxin-1 inhibited Na+ currents and quickly inhibited both inwards and outward currents. The observations of the study suggest the propensity for psalmotoxin-1 to prove useful in both

the diagnosis of specific ASIC-containing glioblastoma multiforme (GMB) tumour cell types and therapeutic treatment of aggressive malignant gliomas (Bubien *et al.*, 2004).

A novel peptide Brachyin, isolated from the venom of the Costa Rican curly-hair tarantula *Brachypelma albopilosum* and identified to display neurotoxic properties was found to also display anti-cancer properties. Zhong *et al*. studied the effects of brachyin against six cancer cell lines, including human T cell lines Molt-4 and C8166, lung cancer cell lines A549 and Calu-6 and bladder cancer cell lines BIU-87 and T24. It was found in the study that brachyin had significant anti-proliferation properties against a six tested cell lines, with human C8166 and Molt-4 T cell lines the most sensitive, respectively. It was found that human tumour cells derived from solid tumour cell lines (Calu-6, T24 and BIU-87) showed lower degrees of sensitivity to brachyin. Phase contrast photomicrographs showed that brachyin did not induce necrosis, toxicity damage or direct lysis in the treated tumour cells (Zhong *et al.*, 2014; Akef, 2018).

A 2013 study by Sun *et al.* investigated the effects of recombinantly produced Chilobrachy jingzhaotoxin (Trxjingzhaotoxin-III), isolated from the venom of the Chinese fawn tarantula *Chilobrachys jingzhao (guangxiensis)* on mouse hepatocellular carcinoma cell line Hepal1-6. The study found that treatment with Trxjingzhaotoxin-III significantly reduced Hepa1-6 cell proliferation and their expression of proliferating cell nuclear antigen (PCNA). It was also found that the peptide inhibited the colony forming and migration potential of the treated malignant cells. Trxjingzhaotoxin-III was also found to induce the cell cycle arrest of Hepa1-6 cells at the G0/G1 phase (Sun *et al.*, 2013).

1.5.3.2.3 Centipede Venom and Cancer

Research into the venoms of giant centipedes is a novel, up and coming area of interest. Whilst centipede venom is not considered to be that of medical significance, centipede bites have been purported to cause extreme pain and local swelling as the result of erythema and induration and necrosis (Bush *et al.*, 2001). Centipedes comprise one of the oldest lineages of terrestrial venomous predators. Despite having been used in traditional medicines for centuries, centipede venoms are poorly studied and the compounds that compose their venoms and their potential pharmacological activities broadly unknown. Recent research has found centipede venoms to be highly complex chemical arsenals, which contain a broad range of disulphide-constrained peptides with novel three-dimensional structures and pharmacology's (Undheim, Jenner and King, 2016). Recent research is beginning to investigate the potential anti-cancer properties of centipede venom in the hunt for novel therapeutic molecules.

A 2014 study was carried out by Ma *et al.*, into the effects of alcoholic extract of centipede (AECS) *Scolopendra subspinipes mutilans* (Chinese red-headed centipede) on the cell viability, apoptosis and cell cycle of malignant melanoma cell line A375. The study found that the AECS resulted in the inhibition of A375 cell proliferation in both a dose- and time-dependent manner. The AECS was found to cause the arrest of A375 cell cycle progression at the S phase, causing an increase in cyclin E protein and a reduction in cyclin D1 protein levels. AECS was shown to cause the induction of apoptosis of A375 cells, found to likely be the result of effects on the Bcl-2 protein family, with reductions in Bcl-2 and increases in Bax, Bak and Bad expression levels observed (Ma *et al.*, 2014).

A further study by Ma *et al.*, undertaken in 2015 investigated the effects of AECS on epidermal growth factor receptor (EGFR) over-expressing cancer types. Treatment of EGFR-overexpressing cancer cell lines A431 and HEK293/EGFR with AECS of *Scolopendra subspinipes mutilans* found a more prominent effect when used to dose highly-expressing EGFR cells when compared to cells which did not express the receptor (HEK293 cells). The study found, through the use of a cell membrane chromatography (CMC) column, that AECS binds to EGFR and competitive binding assays using gefitinib suggested that both may compete for occupation at a single common binding site on the EGFR receptor. SiRNA knockdown of EGFR in A431 cells resulted in the attenuation of the effects of AECS, supporting that EGF receptor was the active target of AECS. As found in the previous study, AECS was found to dramatically induce apoptosis in both HEK293/EGFR and A431 cells, found to be the result of changes to the Bcl-2 family protein expression. Further experiments found that AECS resulted in alterations in EGFR kinase activity, reducing the occurrence of phosphorylation events on both EGFR itself and other downstream protein substrates of the receptor, including AKT and ERK1/2 (Ma *et al.*, 2015).

A 2006 study by Bhagirath *et al.* into the venom of hill centipede *Scolopendra viridicornis* using MTT cytotoxicity assay found no discernible cytotoxic effects when used at selected doses of 7μg and 20μg *in vitro* against 5 human cancer cell lines, hepatocellular carcinoma (Hep 3B), Breast myoepithelial tumour (HBL-100), Neuroblastoma (IMR-32), Leukaemia (HEL 92.1.7/TIB 180) and renal cell adenocarcinoma (CRL-1611). *In vivo* experiments into the inhibition of human breast tumour growth in 15 weeks old inbred female Swiss albino virgin mice using *Scolopendra viridicornis* venom were carried out. The study found that injection of 5μg of the centipede venom directly into the breast tumour resulted in significant reductions in the overall progression of the tumour growth when compared to untreated tumours. The mean growth of the control tumours (n=10) after 7 weeks was 37-times the initial tumour volume whilst venom-treated tumours (n=10) showed only 7-times the initial tumour volume after 7 weeks treatment, an inhibition of tumour growth by the venom of 81.61% (Bhagirath, Chingtham and Mohen, 2006).

A novel peptide isolated from the venom of *Scolopendra subspinipes mutilans* by ultra-filtration and reverse-phase high performance liquid chromatography (HPLC) has been shown in a recent study to display both cytotoxic and anticoagulative properties. The novel peptide was found to display anti-proliferative effects against cancer when used in the treatment of human liver cancer cell line HepG2 and human gastric cancer cell line MGC. Cells were incubated with doses between 16 and 256 μg/ml of the peptide for 72h. The findings showed that the proliferation of both cell lines was inhibited by the peptide in a dose-dependent manner, with the calculated IC50 value of the peptide against HepG2 and MGC cells of 80 and 65 μg/ml, respectively. The survival rate of the cell cells was dramatically reduced to around 10-40% after 72h treatment with the highest tested dose. No observable changes in cell proliferation were observed in either murine prostate cancer cells (RM1) and Human umbilical vein endothelial cells (HUVEC) after treatment with the isolated peptide, suggesting that it displays specificity against human cancer cell types (Kong *et al.*, 2013).

A 2015 study into anti-microbial peptide scolopendrasin VII isolated from the venom of *Scolopendra subspinipes mutilans* showed the peptide also displayed anti-cancer activities against leukaemia cell lines. The effect of scolopendrasin VII on U937 and Jurkat leukaemia cells was assessed using MTS assays. The results found that scolopendrasin VII decreased the viability of both U937 and Jurkat leukaemia cells. Further flow cytometric and acridine orange/ethidium bromide staining revealing that scolopendrasin VII induced necrosis in the leukaemia cells, and that this necrosis was mediated through its interaction with phosphatidylserine in the membrane of the cancer cells (Lee *et al.*, 2015).

Early *in vitro* and *in vivo* evidence from the literature show that venoms could hold great potential for the future treatment of a variety of cancer types. The search for novel therapeutics from the natural world is gaining pace, with scientists turning their attention to new avenues of investigation where therapeutics are concerned. Whilst research into the use of venoms as therapeutics is clearly gaining traction within the scientific community, it should be cautioned that the use of whole venoms for treatment could cause dangerous systemic side-effects due to the toxic nature of many venom components. To be effective options for drug discovery, venoms would need enhanced profiling and characterisation of their effects against a disease-related target and the fractionation and purification of individual active venom component from toxic, undesirable venom constituents. Whilst many of the studies mentioned in this section have indeed isolated single venom components and profiled these for their anti-cancer properties, it is worth mentioning that many of these papers have not compare the potential effects of these venoms and their components against normal immortalised or healthy primary isolated cell types. For this

reason, caution should be employed when interpreting the data presented in these papers, particularly those which show general cytotoxicity data as there is no evidence to suggest that these venom components show any selective effect against cancer cells specifically. However, despite the lack of data on the effects of these whole venoms and venom-derived peptides on normal tissue, the evidence to suggest that they could prove effective avenues of investigation for future anticancer molecules still remains compelling. Some cancers still remain testing in terms of the development of effective therapeutic treatment options, and the use of venom-isolated components for the targeting of tumour-expressed antigens may yet hold the key to unlocking a successful way to overcome the unmet challenges this lack of treatments present.

1.6 Thesis Aims

The aim of this thesis is to investigate the potential for animal venoms, from a diverse range of venomous taxa, to effectively halt growth and inhibit triple negative breast cancer cells. Triple negative breast cancer remains an ongoing problem, with effective treatment options for patients diagnosed with this disease limited or lacking. Venoms are complex mixtures of biologically active compounds which could hold the key to the identification of new therapeutics with novel mechanistic actions. Using EGFR overexpressing breast cancer cell line MDA-MB-468 as a model, venoms will be screened for their use as potential therapeutics. Key aims of the thesis incorporate the use of venoms to profile potentially novel receptor kinome targets for the treatment of this aggressive cancer subtype and the ability of venoms to disrupt the normal activation of these receptor kinase targets. Whole and subsequently fractionated venoms will be screened for their ability to modulate the combined expression/phosphorylation levels of EGFR, which has been identified as a common key oncogenic player in the development and progression of the triple negative breast cancer subtype.

- To assess the ability of snake and invertebrate venoms to cause anti-cancer effects against the TNBC cell line MDA-MB-468
- To determine whether whole venoms, selected based on previous venom and anticancer activity literature, can modulate the combined expression/activity of a panel of receptor tyrosine kinases in TNBC cell line MDA-MB-468 and to attempt to identify novel targetable kinases in TNBC

- To screen a diverse panel of whole snake and invertebrate venoms for cytotoxicity against TNBC cell line MDA-MB-468 and additional epidermal growth factor receptor (EGFR) over-expressing cell line A431

- To investigate the effects of whole snake and invertebrate venoms on the phosphorylation of EGFR in both MDA-MB-468 and A431 cell lines, using Western Blot and ELISA-based techniques

- To assess whether a diverse panel of whole snake and invertebrate venoms are capable of disrupting the binding of epidermal growth factor (EGF) to the EGF-binding pocket of EGFR, using MDA-MB-468 and A431 cell lines as models

- To undertake the fractionation of whole venoms found to modulate EGFR phosphorylation, using reverse phase (RP) high-performance liquid chromatography (HPLC)

- To screen RP HPLC fractions to determine which are responsible for the observed reduction to EGFR phosphorylation levels seen with previously screened whole venoms

- To further fractionate three ‘hit’ fractions using size exclusion HPLC to determine purity

- To send the most relevant fractions for Intact mass and Peptide digest mass spectrometry, to attempt to formally identify the active entity within each selected fraction

- To compare the obtained mass spectrometry data to the existing sequences, deposited in databases, of other venom-derived peptides with similar masses and sequence structure

CHAPTER 2: General Materials and Methods

2.1 Cell Culture Methodology

2.1.1 Cell Lines

This study used the TNBC breast cancer cell line MDA-MB-468 (Cailleau, Olivé and Cruciger, 1978) and epidermal cancer cell line A431 (Giard *et al.*, 1973). All cell lines were derived from ATCC approved human cancers, gifted from Cancer Research UK (London, UK). Both these cell lines were authenticated using STR profiling in March 2018 and were confirmed to be generated from the same source material as the original cell lines profiled on the Cellosaurus database (See Appendix I).

2.1.2 Routine Maintenance and Culture of Cancer Cell lines

All cell lines were cultivated as adherent monolayers using Dulbecco's modified Eagle's medium (DMEM) (Gibco, UK), supplemented with additional L-Glutamine (1%), Foetal Calf Serum (FCS) (10%) and penicillin-streptomycin (pen-strep) (1%) (all Gibco, UK). Cells were cultured at 37 °C in sterile, cell culture treated, 25cm^3 tissue culture flasks (Fisher, UK) in a humidified incubator with an atmosphere of 95% air and 5% CO_2. Trypsin-Ethylene diamine tetra acetic acid (EDTA) (0.05% trypsin, 0.53 mM sodium EDTA) was used to passage the cell lines as required (Gibco, UK). All culture media was removed, and the cells were washed twice with 5ml Phosphate buffered saline (PBS) (Sigma, UK), pre-warmed to 37ºC. Once PBS washing had removed any residual media, cells were incubated with 1ml of trypsin-EDTA at 37ºC, 5% CO_2 until cells began to round and detach from flasks. Before cells completely detached the initial 1ml of trypsin was removed and replaced with 0.2 ml trypsin-EDTA. Flasks were gently rocked to ensure complete trypsin cover of cells and returned to the incubators. Cells were incubated in the fresh trypsin-EDTA at 37°C, 95% air, 5% CO_2 for 1-5 min until the cells had detached from the bottom of the flasks. Flasks of cells were given a gentle tap on the bench to aid the detachment of cells if required. Trypsinised cells were re-suspended in 5ml fresh supplemented DMEM, gently pipetted up and down to disperse cell clumps and re-aliquoted into 25cm^3 flasks, 6 or 96 well-plates according to the experiments undertaken. For routine cell passages, 0.5ml of cells were pipetted into fresh 25cm^3 flasks and re-suspended in 5ml of supplemented DMEM media.

2.1.3 Cell Counting and Cell Plating using a Haemocytometer

MDA-MB-468 and A431 cells were trypsinised as via the standard protocol for routine cell maintenance, laid out in **2.1.2.** Cells were resuspended in a selected volume of media and cell counts undertaken using a haemocytometer. 20µl of resuspended cells were mixed with 12µl of PBS and 8µl of Trypan Blue (Gibco, UK). 20µl of the mixture were pipetted into each side of the Haemocytometer. Using an inverted microscope cell numbers were counted in the four corners of the haemocytometer grid and an average cell number taken.

The total number of cells was calculated using the following equations:

$$\text{Cells/ml} = \text{average cell no. x2 x}10^4$$

$$\text{Total cell number} = \text{Cells/ml x resuspension volume}$$

The volume per well need to be taken from the resuspended cells was calculated using the equation:

$$\text{Volume (µl)} = \frac{\text{Desired Number of Cells/Well}}{\text{Cells/ml}} \text{ x } 1000$$

The final volume was topped up in each well using supplemented DMEM to prevent cell drying due to evaporation. Plated cells were left to settle and adhere overnight, before being used for either Resazurin, ELISA or EGF-Alexa Fluor-488 assays.

2.1.4 Maintaining Frozen Cell Line Stocks

Frozen stocks of the cell lines used in this study were prepared for long term cell culture. Cells were trypsinised as via the protocol described in **2.1.2** (replacing 0.2ml trypsin-EDTA incubation with 0.1ml trypsin-EDTA). Once trypsinised, cells were re-suspended in 10% Dimethyl sulfoxide (DMSO) (Sigma, UK) in 90% FCS. Cells were aliquoted into individual sterile cryotubes (Fisher, UK) and frozen at -20°C for 2h. The cryotubes were transferred to a -80°C freezer for short-term storage or transferred to liquid nitrogen for long-term storage.

Cells were recovered from liquid nitrogen storage as and when required, by thawing a frozen cryotube at room temperature (~22 ºC) and transferring the cells in 10% DMSO/90% FCS into a fresh 25cm^3 flasks containing 5ml supplemented DMEM. Cells were left to settle and adhere to the culture flasks overnight in an incubator at 37°C, 5% CO_2. The following day, once cells had

adhered to the bottom of the flask, the media containing the DMSO was discarded and replaced with 5ml fresh supplemented DMEM.

2.2 Venom Assay

2.2.1 Venom Extraction

Venoms were extracted from both snakes and invertebrates as via Venomtech Ltd's standard proprietary methods. Briefly, snakes were milked using standard bite methods, whilst invertebrates were anaesthetised with CO_2 before venom was extracted with electrical stimulation of the venom glands. Venom protein concentration was quantified via DeNovix DS11 spectrophotometer analysis (**See 2.3.1.3**). Snake venoms were lyophilised whilst invertebrate venoms were frozen. Both were stored at -20ºC until required.

2.2.2 Cell Venom Treatment Protocol

Cells were plated out in 6 well plates (Fisher, UK). 1 flask of cells were trypsinised as via **2.1.2**, resuspended in supplemented DMEM and aliquoted in equal volumes (500 µl/well) across the 6-well plate. All wells were topped up to a total volume of 2ml with supplemented DMEM and grown to at least 70% confluency ($0.84x10^6$ cells/well). Varying venom dilutions were prepared by diluting whole venoms (Venomtech Ltd, UK) in supplemented DMEM, ranging from 1/10-1/10,000,000 (≈10 mg/ml-10 ng/ml) depending upon the experiments undertaken.

All media was removed, and the cells were incubated in the DMEM diluted venoms in a humidified incubator for 2h at 37 ºC, 95% air, 5% CO_2. After 2h, the venom-containing media was removed and replaced with DMEM media containing Epidermal growth factor (EGF) (Sigma, UK) at a final working concentration of $1x10^{-7}$M. The cells were incubated in the EGF containing media at 37 ºC, 95% air, 5% CO_2 for 5 min. After 5 min the media was removed from each well and cell lysis undertaken.

2.2.3 Lysis of Cells

Wells of cells were washed twice with 500µl of 4 ºC 2 mM Ethylene glycol-bis (β-aminoethyl ether) N,N,N',N'-Tetra-acetic acid (EGTA) (Sigma, Poole U.K) in phosphate-buffered saline (PBS) pH 7.4. Radioimmunoprecipitation assay **(**RIPA) lysis buffer (25 mM Tris/HCl pH 7.6, 150 mM NaCl, 1% Tergitol-type NP-40 and nonyl phenoxypolyethoxylethanol (NP-40), 1% sodium deoxycholate, 0.1% Sodium Dodecyl Sulphate (SDS)) was supplemented with 10µl of Halt Protease inhibitor cocktail (100x) (Fisher, UK) (see Table 2.1 for inhibitor cocktail

composition), 10µl of Phosphatase inhibitor cocktail (100x) (Sigma, UK) and 10µl Ethylene diamine tetra-acetic acid (EDTA) (100x) (Fisher, UK) for every ml of lysis buffer.

150µl of supplemented RIPA buffer cocktail was added to each well and the plates were incubated on ice for 5-10 min until all cells had been lysed. Complete cell lysis was confirmed by examining

Inhibitor	Protease Family Targeted	1x Concentration
AEBSF	Serine proteases	1 mM
Aprotinin	Serine proteases	800 nM
Bestatin	Amino-peptidases	50 µM
E64	Cysteine proteases	15 µM
Leupeptin	Serine/Cysteine proteases	20 µM
Pepstatin A	Aspartic acid proteases	10 µM
EDTA	Metalloproteases	5 mM

Table 2.1: Protease inhibitor cocktail components

Final working concentrations of each inhibitor and the family of proteases components they are active against

wells using an inverted microscope. The cell lysates were transferred from each well to new 1ml eppendorf tubes (Fisher, UK) and centrifuged for 10 min, at 4 ^{o}C and 13,300 rpm (17,000 x g) in a benchtop microcentrifuge. Once the lysates had been centrifuged to pellet cell debris and DNA, 100µl of supernatant was transferred from each sample into a clean 1ml microcentrifuge tube containing 25µl of Pierce 5x sample buffer (Fisher, UK). All tubes were mixed and heated at 100 ^{o}C for 10 min in a heating block, before the samples were stored at -20 ^{o}C.

2.3 One Dimensional Sodium Dodecyl Sulphate Polyacrylamide Gel Electrophoresis (1D SDS PAGE) and Western Blotting

2.3.1 Determining Lysate and Venom Protein Concentrations

The protein concentration of whole venoms, fractionated venoms and cell lysates produced for Coomassie analysis and Western blot were determined to enable accurate dosing of cells and protein loading of gels for follow up analysis. Protein concentrations of samples were determined through a combination of Bradford assay analyses (see Appendix II for methodology) and DeNovix DS11 spectrophotometry analysis.

2.3.1.1 Protein Concentration Determination by DeNovix DS11 Spectrophotometer

The protein concentration of whole venom, venom fractions or cell lysates were determined using a DS11 spectrophotometer (DeNovix, UK). Using the built-in software, the DS-11 was blanked using HPLC grade H_2O before being used to read the absorbance at 280nm of 1µl of each sample. Each microliter was read in duplicate to generate replicate readings and two or three microliters of each venom sample were used in total. The average protein concentration was then determined from the replicate readings.

2.3.2 SDS-PAGE Gels

A Mini PROTEAN Tetra Cell (Biorad, UK) was utilised to run 1D SDS-PAGE gels. The glass plates for pouring gels were cleaned with isopropanol and assembled as via the supplier instructions.

2.3.2.1 7%, 9% and 12% Resolving Gel Compositions

Depending upon the molecular weight of the target proteins a 0.75mm, 7%, 9% or 12% resolving gel was utilised. 7%/9%/12% w/v Acrylamide/Bis solution 29:1 (3.3% C) (Bio-Rad, U.K.), 0.37M Tris/HCl pH 8.8, 0.1% w/v SDS were mixed by inverting. 225µl of 10% w/v ammonium persulphate (APS) (Bio-Rad, UK) and 15µl of N,N,N,N'-Tetra-methyl-ethylenediamine (TEMED) (Bio-Rad, UK) were added as catalysts and the mixture thoroughly mixed. The Complete gel solution was pipetted into 0.75mm thick glass gel pouring plates and overlaid with 70% isopropanol to ensure a smooth resolving gel surface. The poured gels were to allowed to stand at room temperature until polymerisation occurred.

2.3.2.2 3.75% Stacking Gel Composition

Once the resolving gel had set, the isopropanol was poured off and the gel surface gently blotted with filter paper to remove any residual alcohol. A 3.75% stacking gel (3.75% w/v Acrylamide/Bis solution 29:1 (3.3% C) (Bio-Rad, U.K.), 0.1M Tris/HCL pH 6.8, 0.1% w/v SDS) was mixed and 10% APS solution (500µl) and TEMED (10µl) added as catalysts. The resolving gel was mixed and swiftly pipetted on top of the resolving gel and a 0.75mm thick comb with either 10 or 15 wells (Biorad, UK) inserted into the unpolymerized gel. Whilst stacking gels were allowed to polymerise at room temperature, Biorad mini-protean tetra cell gel tanks were filled with 1x Tris/Glycine/SDS (TGS) running buffer (0.025M Tris, 0.192M glycine, 0.1% w/v SDS, pH8.3) (Bio-Rad, UK).

2.3.2.3 Running SDS-PAGE Gels

Once the stacking gels had completely set, the combs were carefully removed, and the gel-containing cassettes placed into the Mini Protean gel tank apparatus. Lysate samples were heated for 5 min at 100°C in a heat block before being loaded into separate wells on the gel. 5µls of either a dual colour molecular weight marker (M.W 6,500-250,000) (Bio-Rad, UK) or a wide range colour molecular weight marker (M.W 6,500-205,000) (Sigma-Aldrich, UK) were loaded as reference protein molecular weights. Gels were run at 70V until the dye front had passed through the stacking gel, and at 170V until the dye front reached the bottom of the gel cassette.

2.3.3 Protein Detection and Visualisation

2.3.3.1 Coomassie Gel Protein Visualisation

Gels were carefully removed from glass plates and stained with either Bio-Safe Coomassie G-250 stain (Bio-Rad, UK) or laboratory Coomassie blue reagent (see Table 2.2 for composition) on a Stuart Scientific Gyro-Rocker STR9 (Sigma-Aldrich, UK) for 1h as via the stated instructions. After 1h the Coomassie stain was removed and replaced by destaining solution.

Component	Quantity (for 1L)	Source
Coomassie G250	1g	Fisher, UK
Methanol	500ml	Sigma, UK
Acetic Acid	100ml	Fisher, UK
dH_2O	400ml	

Table 2.2: Laboratory Coomassie Blue Recipe

Gels stained with Bio-Safe Coomassie G-250 stain were subsequently de-stained for 30 min with dH_2O, whilst gels stained with laboratory Coomassie reagent were destained overnight with destaining solution (10% v/v methanol, 10% acetic acid v/v, 80% dH_2O), both of which were gently agitated on the Stuart gyrorocker (Fisher, UK). Gels were imaged after sufficient destaining using a Gel Doc (Biorad, UK) or ChemiDoc (Biorad, UK).

2.3.3.2 Semi-Dry Western Blotting

Amersham Protran 0.22 µm pore nitrocellulose (GE Healthcare, UK) or PVDF membrane (Fisher, UK), 6 pieces of 3MM Whatman filter paper (Maidstone, UK) and the polyacrylamide gel were soaked in semi-dry blotting buffer (0.24% w/v Tris, 1.13% v/v glycine, 20% v/v methanol). Polyvinylidene difluoride (PVDF) Membranes were briefly activated for 10-20s using 100% methanol (Fisher, UK) prior to soaking in semi-dry blotting buffer. The soaked filter paper, selected membrane and gel were sandwiched together into a semi-dry Western blotter (Invitrogen, UK) or a Trans-blot Turbo Transfer System (Biorad, UK). Proteins were transferred in the

Invitrogen system for 45-60 min at 15V. Alternatively proteins were transferred in the Trans-blot Turbo system at 25V, 1A for 60 min. Proteins were visualised on the nitrocellulose to confirm complete transfer by staining for 20-30s with 3-hydroxy-4-(2-sulfo-4-[4-sulfophenylazo]phenylazo)-2,7-naphthalenedisulfonic acid sodium salt (Ponceau S solution) (0.1% w/v in 5% acetic acid) (Sigma, UK) followed by rinsing with H_2O to destain.

2.3.3.3 Immuno-detection

After semi-dry transfer, nitrocellulose or PVDF membranes were transferred onto a gyrorocker and shaken in blocking buffer (5% w/v Marvel non-fat milk powder solution (Premier Brands, UK) in phosphate-buffered saline (PBS) 0.1% v/v Polyoxyethylenersorbitan monolaurate (Tween 20) (Sigma, UK)) for 1h. Blots were washed on the Stuart gyrorocker (Fisher, UK) in PBS/0.1% Tween 20 (5 x 5 min washes) and probed overnight at 4°C with primary antibody made up in PBS/0.1% Tween 20 (Table 2.3).

Blots were washed in PBS/0.1% Tween 20 (5 x 5 min washes) and probed with Rabbit-anti-mouse secondary antibody conjugated to horse radish peroxidase (HRP) for 1h (Table 2.3).

Antibody	**Species and Clonality**	**Directed Against**	**Working Dilution**	**Stock Antibody Conc.**	**Working Antibody Conc.**
PY20 *(Sigma, UK)*	Mouse Monoclonal	Phospho-tyrosine	1/2000	1 mg/ml	0.5 µg/ml
F4 (Gullick *et al.*, 1986)	Mouse Monoclonal	EGFR	1/1000	1 mg/ml	1 µg/ml
Anti-β-actin antibody (AC-15 Clone) *(Sigma, UK)*	Mouse Monoclonal	β-actin	1/20,000	2-2.5 mg/ml	0.1 µg/ml
Anti-α-Tubulin antibody (DM1A clone) *(Sigma, UK)*	Mouse Monoclonal	α-tubulin	1/5,000	1-1.2 mg/ml	0.2 µg/ml
Secondary Antibodies	**Species and Clonality**	**Directed Against**	**Working Dilution**	**Stock Antibody Conc.**	**Working Antibody Conc.**
Rabbit-α-mouse-Horse Radish Peroxidase (HRP-Tagged) *(Sigma, UK)*	Rabbit Monoclonal	Anti-mouse	1/20,000	0.8 mg/ml	0.04 µg/ml

Table 2.3: Primary and Secondary antibodies used for Western Blots. Table contains details on antibody species, clonality, target, selected dilution and working concentration

After 1h blots were washed 5 final times in PBS/0.1% Tween 20 (5 x 5 min washes) and the signal developed using enhanced chemiluminescence (ECL) and a Bio-Rad ChemiDoc. Laboratory-made ECL reagents were prepared as via Table 2.4 and stored in the dark at 4°C for up to 3 weeks. 1ml of each reagent were mixed together, applied to each blot and the signal developed.

Blots were exposed for varying times depending upon the visible band signal. All blots contained a positive (phosphorylated EGFR) and negative (unphosphorylated EGFR) samples to ensure all venom treated samples could be directly compared to controls exposed for the same time duration.

ECL Reagent 1		**ECL Reagent 2**	
Luminol (250 mM in DMSO)	*500µl*	30% Hydrogen Peroxide (H_2O_2)	*32µl*
Coumaric acid (90 mM in DMSO)	*220µl*	Tris/HCl pH 8.5 (1M)	*5 ml*
Tris/HCl pH 8.5 (1M)	*5 ml*	dH_2O	*Make up to 50 ml*
dH_2O	*Make up to 50 ml*		

Table 2.4: Composition of ECL reagents 1 and 2

2.3.4 1D Image Analysis

1D image analysis of Biorad ChemiDoc generated Western blot images was undertaken using LabVIEW software (Bio-Rad, UK). Lane and band detection were created using the automated software and manually edited. Once pixel intensity reports were obtained for all bands, graphs of sample vs. EGFR phosphorylation levels were plotted.

2.4 Cell-Based, 96 Well Plate Assay Protocol

2.4.1 Cell Fixing

The appropriate number of cells for each experimental assay undertaken were plated out and incubated overnight to settle and adhere. Cells were washed twice with 100µl of PBS to remove residual media, before being fixed for 20 min at 37ºC with 50µl per well of 4% paraformaldehyde solution (4% paraformaldehyde in 1x PBS, pH 6.9). After fixed, cells were washed twice with 100µl of PBS to remove any residual paraformaldehyde solution.

2.4.2 PY20 ELISA Protocol

MDA-MB-468 and A431 cells were trypsinised and counted as via standard protocol in **2.1.2** and **2.1.3.** Both cell lines were plated out into clear 96 well Biolite plates (Fisher, UK) at a concentration of $5x10^4$ and $1x10^5$ cells/well respectively. Cells were treated in quadruplicate with a panel of lyophilised whole or fractionated venoms. All whole venoms were diluted in supplemented DMEM media to a working concentration of 20 µg/ml, and a volume of 50µl was

added to each of the quadruplicate wells. Fractionated venoms were resuspended from lyophilised in 100µl of sterile distilled H_2O, before being diluted further in 900µl of supplemented DMEM media. 50µl of diluted fraction was added to each of the quadruplicate wells.

Cells were incubated in the appropriate whole venom or venom fraction for 2h to allow for potential binding of venom compounds to EGF receptors expressed on the cells' surface. All venom was removed after incubation and the cells stimulated with 50µl of $1x10^{-7}$ M EGF (excluding –EGF controls) for 5 min. Cells were washed with 200 µl/well PBS and then fixed at 37ºC) with 4% paraformaldehyde/PBS pH 6.9 as via **2.4.1**. After fixation, all paraformaldehyde was removed from all wells and the fixed cells washed with PBS (0.2%) polyethylene glycol tert-octylphenyl ether (Triton x-100) to permeabilise them (3x 10 min, 200 µl/well) on a rocker. After permeabilization, endogenous cellular peroxides were quenched with quenching buffer (18.8ml PBS (0.2%) Triton x-100 (Fisher, UK), 2.11ml 30% Hydrogen Peroxide (H_2O_2) (Sigma, UK), 211µl 10% Sodium Azide) (Fisher, UK) for 20 min at RT on a rocker. After quenching, cells were washed again with PBS (0.2%) Triton x-100 (3x 10 min, 200 µl/well), before being blocked with filtered 2% w/v Bovine Serum Albumin (BSA)/PBS (0.2%) Triton x-100 for 1.5h at room temperature (RT) on a rocker. After the blocking period, blocking buffer was removed and 50µl of PY20 1º antibody (1/1000) in filtered 2% BSA/PBS (0.2%) Triton x-100 was added to all wells (excluding 2º antibody only controls). 2º antibody only controls were incubated in 50µl 2% BSA/ PBS (0.2%) Triton x-100. All cells were incubated overnight at 4ºC. All 2% BSA/PBS (0.2%) Triton x-100 solutions were filter sterilised using a 0.2 µm syringe filter to remove undissolved particulates. After overnight incubation, all 1º antibody was removed and cells were washed again with PBS (0.2%) Triton x-100 (3 x 10 min, 200 µl/well). Cells were then incubated in 2º antibody in PBS (0.2%) Triton x-100 (1/50,000) for 1h at RT on a rocker (excluding 1º antibody only controls). 1º antibody only controls were incubated in 50µl PBS (0.2%) Triton x-100. After 1h cells were washed with PBS (0.2%) Triton x-100 (6x 10 min, 200 µl/well) and the plate was blotted dry using blue roll to remove residual PBS (0.2%) Triton x-100 from the wells. 100µl of 3,3',5,5'-Tetramethylbenzidine (TMB) substrate, pre-warmed to RT, was added to each well. The plate was stored in the dark at RT and the TMB colour change was allowed to develop for 30-60 min, depending on the speed of TMB colour development. Once TMB had developed to a mid-blue colour, 100µl of 0.2M sulphuric acid was added to each well to halt the colour change reaction. The absorbance of the plate was read at an absorbance of 450nm within 10 min of the reaction completion, using a BMG Labtech Fluostar plate reader. Reference reads were also taken at 550nm and 655nm respectively.

2.4.2.1 Crystal Violet Cell Staining for Cell Number Control (PY20 ELISA Protocol)

After the plate absorbance was read, cell crystal violet staining was undertaken to ensure a consistent number of cells were still present in each well. All coloured TMB substrate was removed from the wells and the cells were washed 2x10 min with PBS (0.2%) Triton x-100, followed by 2x10 min washes with PBS. Plates were blotted to remove residual PBS and left to air dry for 5 min before the addition of 30µl of crystal violet (0.5% aqueous) stain to each well (0.5g crystal violet (Fisher, UK) in 100ml dH_2O). Wells were incubated in crystal violet stain for 30 min at RT (≈25^{o}C) on a rocker. After 30 min all excess crystal violet stain was removed, and the wells were washed repeatedly with 200µl of PBS (10 min intervals) on a rocker until all excess unbound crystal violet stain was removed. After washing was complete 100µl of 1% SDS solution was added to each well and the plates incubated for 1h at RT on a rocker to release crystal violet stain trapped within the cells. After 1h the sample absorbance was measured at 595nm using the Fluostar (BMG Labtech, UK) plate reader.

CHAPTER 3: Effect of Snake and Invertebrate Venoms on Cancer Cell Cytotoxicity

3.1 Introduction

Venoms, a complex mixture of toxins and biologically active compounds, have been shown to display a wide array of physiological effects, including coagulation (Núñez *et al.*, 2004), anticoagulation (Wadood *et al.*, 2012), neurotoxicity and myotoxicity (Zamunér *et al.*, 2004), cardiotoxicity (Debnath *et al.*, 2010), haemolysis (Johnston *et al.*, 2013), algogenesis (Trim and Trim, 2013), haemorrhage (Leonardi, Gubenšek and Križaj, 2002) and cytotoxicity (Abdel-Rahman *et al.*, 2010; Naumann *et al.*, 2011).

Venoms have been shown through previous scientific research to be capable of displaying oncogenic cytotoxicity (Jain and Kumar, 2012; Mishal *et al.*, 2013; Liu *et al.*, 2014; Shanbhag, 2015). Treatment with whole venoms and venom-derived peptides from a range of snakes and invertebrates have been shown capable of reducing cancer cell viability. A study evaluating panels of snake venoms, including 61 taxa from the families Viperidae, Elapidae and Colubridae, found some are capable of inhibiting the viability of breast cancer (MCF-7) and skin cancer (A-375) cell lines (Bradshaw *et al.*, 2016). 3-(4,5-Dimethylthiazol-2-yl)-2,5-diphenyltetrazolium bromide (MTT) cellular metabolic assays identified viper venoms to be potently cytotoxic, showing greater levels of cell inhibition in the breast cancer than skin cancer cell line. Elapid and colubrid venoms were found to be overall much less toxic, with the exception of elapid genera *Naja*, *Pseudechis* and *Micrurus*, which were found to be toxic to both cancer cell types and *Agkistrodon* and *Bothrops*, which were found to be toxic to breast cancer cells only (Bradshaw *et al.*, 2016).

A study which screened a panel of 31 theraphosid and other spider venoms, from 23 distinct genera identified venoms capable of causing the death of breast cancer cells. Clonogenic survival assays showed substantial cytotoxicity was observed in breast cancer cell line MCF-7 in response to 5 days treatment with 17 of the 31 tested venoms, including venoms collected from a broad range of genera, such as *Acanthoscurria*, *Chilobrachys*, *Nhandu*, *Psalmopoeus* and *Hadronyche* amongst others. (Wilson *et al.*, 2017).

MTT assays were used to analyse whole scorpion venoms from *Androctonus crassicaud*a, *Androctonus bicolor* and *Leiurus quinquestriatus*, which were shown to exert cytotoxic effects on MDA-MB-231 breast and HCT-8 colorectal cancer cell lines in both a dose- (500-1000 µg/ml) and time-dependent manners (24 or 48h) (Al-Asmari *et al.*, 2016; Al-Asmari, Riyasdeen and Islam, 2018). MTT assay analysis of KYSE-510 (human oesophageal cancer cells) treated with

increasing doses (12.5, 25, 50, and 100 µg/ml) of *Heterometrus liangi* venoms showed cellular cytotoxicity in time- and dose-dependent manners, with IC50 for 24 h of 50 µg/mL and 34.5 µg/mL for 48 h (Li, Xiao and Wang, 2015). Cytotoxicity of whole *Centruroides tecomanus* venom was assessed by MTT assay against mouse lymphoma (L5178Y) cell line. MTT assay analysis showed that the soluble venom had a significant effect on cell viability at 10-100 µg/mL concentrations with respect to control murine splenocytes (Valdez-Velazquéz *et al.*, 2016).

Oncology cytotoxicity assays have been used throughout the literature to assay the ability of whole venoms from snakes and invertebrates to inhibit cancer cell metabolism and viability. MTT assays and clonogenic survival assays are commonly used biological techniques to assess the efficacy of venom anti-oncogenic effects. The MTT analysis is a colorimetric cell-based assay used for the assessment of cellular metabolism, which utilises the activity of NAD(P)H-dependent cellular oxidoreductase enzymes to reflect the number of viable cells present within a well (Stockert *et al.*, 2018). As a colorimetric technique, MTT assays utilise the change in absorbance, following the conversion of a tetrazolium dye to insoluble formazan, which is blue-purple in colour (Sánchez and Königsberg, 2006). Whilst tried and tested techniques, MTT assays have technical limitations, one of which is that MTT is an end-point detection assay, in which a single detection measurement can be performed after a fixed incubation period. Additionally, as an assay that works using absorbance as its detection method, MTT assays have a smaller window for detectable differences than those seen in fluorescence-based assays (Stockert *et al.*, 2018).

Resazurin salt, sold commercially as a solubilised detection dye under the commercial name AlamarBlue, is a cell viability reagent that, unlike MTT, allows for the development of a fluorescent and colorimetric kinetic assay. The assay incorporates an oxidation-reduction (REDOX) indicator that both fluoresces and changes colour in response to biological reduction of Resazurin by cellular metabolism. Resazurin, a blue non-fluorescent compound readily undergoes reduction to form resorufin, a pink, highly fluorescent compound that can be detected using either fluorescence or absorbance filters on a suitable plate-reader. Over prolonged periods of time, further reduction of resorufin occurs to produce a clear non-fluorescent compound, dihydroresorufin (O'Brien *et al.*, 2000; Bonnier *et al.*, 2015). The dye acts as an intermediate electron acceptor in the electron transport chain, without interfering with the normal transport of electrons within the chain. Resazurin can be reduced by cellular NADPH, NADH, FADH, and cytochromes (Rampersad, 2012). The conversion of resazurin by cells can be used as an indicator of normal cellular metabolism and so changes in metabolism or cell viability can be detected by a lack of conversion of the dye to its fluorescent form. This enables resazurin dye to be used effectively to measure levels of cytotoxicity in cellular viability assays.

Changes in the dye from an oxidised to reduced state allows for flexibility in detection. Measurements can be collected quantitatively using colorimetric and/or fluorometric readings, with fluorescence providing greater assay sensitivity. Simultaneously data can be collected qualitatively by observing if there is a visible change in colour, which indicates the presence or absence of viable cells (Rampersad, 2012). Conversion of Resazurin results in the development of resorufin, which can be detected without the need for cellular lysis and so allows for the development of a kinetic assay that can be monitored for changes over a prolonged period of time, rather than the single end-point detection method observed with methods such as MTT assays (O'Brien *et al.*, 2000; Bonnier *et al.*, 2015). This allows the monitoring of changes in real-time and the collection of a larger body of data from a single assay.

With the advantages of Resazurin detection over the MTT assay, it was decided that the development of a Resazurin-based cytotoxicity assay would be undertaken for profiling venoms for their cytotoxic potential against cancer cell lines MDA-MB-468 and A431. A panel of snake and a panel of invertebrate venoms will be screened for their potential cytotoxicity against both cancer cell lines. The rationale applied for the investigation of the two panels is differences in venom composition. Whole snake venoms contain a mixture of large proteins and small peptide components. Snake venoms have been shown to have an 80% venom composition of peptides with molecular weights 10 kDa or smaller, and to contain classes of toxin peptides including cardiotoxins, neurotoxins and cytotoxins (Binh, Thanh and Chi, 2010). They are also heavily composed of enzymatic peptides, such as PLA2s, proteases and metalloproteases which can cause disruption to cellular surface proteins. Invertebrate venoms are more heavily composed of small peptide components, with a study into the venom of theraphosid *Chilobrachys jingzhao* (Chinese Fawn Tarantula) showing that more than 70% of the detected venom peptides fell into the 3-5 kDa mass range, an additional 10% in the 5-8 kDa range, and with 130 peptides in total of mass 2-8 kDa identified (Liao *et al.*, 2007).

3.1.1 Chapter Aims

- To develop, optimise and statistically validate a robust Resazurin-based fluorescent cell viability assay for determining cell cytotoxicity in cancer cell lines

- To screen a panel of diverse snake venoms for cytotoxicity using the optimised Resazurin assay against MDA-MB-468 and A431 cancer cells at 3 selected doses

- To screen a panel of invertebrate venoms for cytotoxicity using the optimised Resazurin assay against MDA-MB-468 and A431 cancer cells at 2 selected doses

3.2 Materials and Methods

3.2.1 Optimisation of the Resazurin Assay to Determine Cellular Toxicities of Snake and Invertebrate Panels

3.2.1.1 Selection of Optimal A431 and MDA-MB-468 Cell Plating Numbers for Resazurin Toxicity Assay

To determine the appropriate number of cells to utilise for each cell line in the final Resazurin whole venom toxicity screens, MDA-MB-468 and A431 cells were trypsinised, counted as via section **2.1.3** and plated into 96 well plates at four different cell concentrations: $2x10^5$, $1x10^5$, $5x10^4$ and $2.5x10^4$ cells/well (See Appendix III).

Each cell number was plated out in 2 rows of 6 replicates and were returned to a humidified incubator at 37°C, 5% CO_2 overnight to resettle and adhere. To determine which cell number gave the greatest fold-change in fluorescence in the best timeframe, one row of each cell number were treated for 2h with a toxic dose of whole *Naja Nigricollis* (N.nig) venom, diluted to a final concentration of 100 µg/ml in supplemented DMEM. The plate was incubated at 37°C, 5% CO_2 for the duration of the 2h treatment.

After 2h all media was removed from all wells of cells and replaced with 50µl of media containing Resazurin at a final concentration of 160 µM. Changes in fluorescence intensity were monitored over time using a Fluostar plate reader (excitation 544 nm, emission 590 nm) (BMG Labtech) every 15 min for the first hour and every 30 min thereafter until 5h had elapsed. A graph of fold-change over time was plotted for each cell line to determine which cell number gave the greatest fold-change in fluorescence.

3.2.1.2 Z' Analysis of Cell Number to Confirm a Robust Assay

A431 and MDA-MB-468 cells were trypsinised and counted as via the standard protocols laid out in **2.1.2** and **2.1.3.** A431 cells were plated out in 96 well plates at a concentration of $1x10^5$ cells/well and MDA-MB-468 cells at $2x10^5$ cells/well. Optimal cell numbers for both cell lines were ascertained from previous optimisation experiments laid out in **3.2.2.1.** Cells were plated out as via the layout in Appendix IV and returned to the incubator at 37ºC, 5% CO_2, 95% air overnight to resettle and adhere to well bottoms.

Once settled, all media was removed from the cells and the plate divided into positive and negative control replicates as displayed in figure 4.2. To all positive control wells 50µl of 100µg/ml *N.nig* venom was applied and to all negative control wells 50µl of DMEM media was applied. Both plates of cells were returned to the incubator at 37°C, 5% CO_2 for 2h.

After 2h the media and *N. nigricollis* venom was removed from all wells and replaced with 50µl of Resazurin (final concentration 160 µM) in supplemented DMEM (10% FCS, 1% L-glutamine, 1% Pen-strep). Fluorescent readings were taken using the BMG Fluostar plate reader (excitation 544 nm, emission 590 nm) every 15 min for the first hour and every 30 min thereafter until 5h had elapsed.

A z' value was calculated, using the following equation for each cell line at each of the selected time point.

$$Z\text{-}factor = 1 - \frac{3(\sigma p + \sigma n)}{|\mu p - \mu n|}$$

σp = standard deviation of positive control replicates

μp = mean of positive control replicates

σn = standard deviation of negative control replicates

μn = mean of negative control replicates

3 = measure of normal distribution, for which more than 99% of values occur within *3* standard deviations of the mean

A Z' value is a measure of how statistically robust an assay is, taking into consideration the mean value of your positive and negative control samples and the standard deviation of both sets of replicates across the plate. The higher the z' value the higher the likelihood that experimental replicates will yield the same results. Z' values of above 0.5 consider the assay to be robust, whilst z' values above 0.7 consider the assay to be excellent. A z' value of below 0.5, suggests the assay is not as statistically robust as would be liked and may need further optimisation to become so.

3.2.2 Determination of the Toxic Properties of a Panel of Snake and Invertebrate Venoms Using an Optimised Resazurin Assay Protocol

3.2.2.1 Preparation of Working Concentrations of Snake and Invertebrate Panel Venoms

A panel of 18 whole snake venoms (Table 3.1) and 23 invertebrate venoms (Tables 3.2 & 3.3) were collected, and the protein concentration of each venom determined by DeNovix DS11 analysis as via **2.3.1.3**. All venoms were diluted using sterile RNAse/DNAse free water to produce a 20mg/ml stock from which further dilutions for Resazurin assays could be undertaken.

20 mg/ml stock concentrations of each snake venom were diluted in supplemented DMEM media to produce working concentrations of each venom at 2 mg/ml, 200 µg/ml and 20 µg/ml. The 20 mg/ml stocks of invert venoms were diluted in DMEM media to produce a working concentration of each venom at 20 µg/ml and 200 µg/ml.

Code	Name	Family	Common Name
P.wei	*Pseudechis rossignoli*	Elapinae	Papuan Pygmy Mulga
N.sia	*Naja siamensis*	Elapinae	Indochinese Spitting Cobra
N.nig	*Naja nigricollis*	Elapinae	Black-Necked Spitting Cobra
N.atr	*Naja atra*	Elapinae	Chinese Cobra
N.naj	*Naja naja*	Elapinae	Indian Cobra
O.han	*Ophiophagus Hannah*	Elapinae	King Cobra
D.pol	*Dendroaspis polylepis*	Elapinae	Black Mamba
D.vir	*Dendroaspis viridis*	Elapinae	Western Green Mamba
C.rho	*Calloselasma rhodostoma*	Crotalinae	Malayan ground pit viper
C.atr	*Crotalus atrox*	Crotalinae	Western Diamondback Rattlesnake
C.rru	*Crotalus ruber*	Crotalinae	Red Diamond Rattlesnake
C.dve	*Crotalus durissus vegrandis*	Crotalinae	Uracoan Rattlesnake
S.mil	*Sistrurus miliarus barbouri*	Crotalinae	Barbour's Pygmy Rattlesnake
C.ins	*Trimeresurus (Cryptelytrops) albolabris insularis*	Crotalinae	White-Lipped Island Pit Viper
M.xan	*Montivipera xanthina*	Viperinae	Ottoman Viper
V.aam	*Vipera ammodytes ammodytes*	Viperinae	Nose-Horned Viper
A.cco	*Agkistrodon contortrix contortrix*	Crotalinae	Northern Copperhead
B.asp	*Bothrops asper*	Crotalinae	Fer-de-lance

Table 3.1: Panel of Snake Venoms

Panel includes venoms extracted from a variety of species, including many families of cobra, mamba, vipers and pit vipers. All snake venoms were diluted to working concentrations of 2 mg/ml, 200 µg/ml and 20 µg/ml).

Code	Name	Family	Common Name
A.aus	*Androctonus australis*	Buthidae	Fat Tailed Scorpion
H.ari	*Hadrurus arizonensis*	Caraboctonidae	Giant Hairy Desert Scorpion
H.swa	*Heterometrus swammerdami*	Scorpionidae	Giant Forest Scorpion
P.kra	*Protoiurus kraepelini*	Luridae	Kraepelin's Scorpion
P.lio	*Parabuthus liosoma*	Buthidae	African Black Tailed Scorpion
A.cor	*Acanthoscurria cordubensis*	Theraphosinae	Argentinian Bird Eating Tarantula
A.gen	*Acanthoscurria geniculata*	Theraphosinae	Brazilian Whit Knee Tarantula
A.met	*Avicularia metallica*	Aviculariinae	Metallic Pink Toed Tarantula
B.boe	*Brachypelma boehmei*	Theraphosinae	Mexican Fire Leg Tarantula
H.lbo	*Cyriopagopus (Haplopelma) albostriatum*	Ornithoctoninae	Thailand Zebra Leg Tarantula
H.mac	*Heteroscodra maculata*	Stromatopelminae	Togo Starburst Baboon Tarantula
P.cam	*Psalmopoeus cambridgei*	Selenocosmiinae	Trinidad Chevron Tarantula
P.for	*Poecilotheria formosa*	Poecilotheriinae	Salem Ornamental Tarantula
P.lug	*Pterinochilus lugardi*	Harpactirinae	Dodoma Baboon Tarantula
T.cup	*Tapinauchenius cupreus*	Aviculariinae	Violet Tree Tarantula
T.pru	*Thrixopelma pruriens*	Theraphosinae	Peruvian Green Velvet Tarantula
T.str	*Theraphosa stirmi*	Theraphosinae	Goliath Bird Eating Tarantula

Table 3.2: Panel of Theraphosid and Scorpion venoms

Panel includes venoms extracted from a variety of species, including individuals from a variety of families of scorpion and theraphosids.

Code	Name	Family/Subfamily	Common Name
S.har	*Scolopendra hardwickei*	Scolopendridae	Indian Tiger Centipede
S.sud	*Scolopendra subspinipes dehaani*	Scolopendridae	Thai Centipede
C.gig	*Colossobolus giganteus*	Pachybolidae	Super Giant Madagascar Millipede
E.foe	*Eisenia foetida*	Lumbricidae	Redworm
P.map	*Pachnoda marginata Peregrina*	Cetoniinae	Sun Beetle
A.sex	*Anthia sexguttata*	Carabidae	Six-Spot Ground Beetle

Table 3.3: Panel of Centipede venoms and Millipede, beetle and worm secretions

Panel includes venoms extracted from 2 species of centipedes and secretions collected from a millipede, 2 species of beetle and from one species of worm

3.2.2.2 Execution of Resazurin Assays for the Snake Venom Panel at Three Selected Concentrations

A431 and MDA-MB-468 cells were trypsinised and counted as via the standard protocol laid out in **2.1.3.** A431 cells were plated out in 96 well plates at a concentration of $1x10^5$ cells/well and MDA-MB-468 cells at $2x10^5$ cells/well, previously established as the optimal cell number per/well in **3.2.2.1.** Cells were returned to the incubator overnight to resettle and adhere to well bottoms. All media was removed from the cells and the appropriate dilution (2 mg/ml, 200 µg/ml or 20 µg/ml) for each snake venom added to wells of cells in triplicate. All plates of MDA-MB-468 and A431 cells were treated with venoms, as via the organised plate layout in Appendix V.

All plates of venom treated cells were returned to the incubator at 37°C, 5% CO_2 for 2h. After 2h all venom and media was removed from all wells of cells and replaced with 50µl of a 160 µM Resazurin/complete DMEM solution.

Fluorescent readings were taken using the BMG Fluostar plate reader (excitation 544 nm, emission 590 nm) every 15 min for the first hour and every 30 min thereafter until 5h had elapsed. The average fluorescence of each venom at the 3 different concentrations was plotted on graphs to determine whether any venom was displaying cytotoxic properties.

3.2.2.3 Execution of Resazurin Assays for the Invertebrate Venom Panel at Two Selected Concentration

A431 and MDA-MB-468 cells were trypsinised, counted and plated as via **2.1.2** and **2.1.3** and plated at seeding densities already ascertained in **3.2.1.1.** Cells were allowed to settle and adhere overnight. The following day all media was removed from the cells and a dilution of 20 µg/ml or 200 µg/ml for each invertebrate venom added to wells of cells in triplicate. Due to small quantities of invertebrate venom obtained during each extraction, it was decided that a dose no greater than 200 µg/ml would likely be used for live cell plate-based assays.

MDA-MB-468 and A431 cells were treated with venoms as via the organised plate layout in Appendix VI. The Resazurin assay was carried out in the same way as those previously described in **3.2.2.2.**

3.3 Results and Discussion

3.3.1 Selection of the Ideal Cell Number to Ensure an Efficient Plate-Based Assay

The selection of an appropriate number of both A431 and MDA-MB-468 cells was essential to ensure the development of an optimal and statistically robust assay. Both cell lines were plated at 4 cell/well concentrations, either treated with or without a lethal dose of venom and monitored over the course of 5h to determine which cell number gave the greatest fold-change in fluorescence between living and dead cells over time (Figure 3.1).

A **MDA-MB-468**

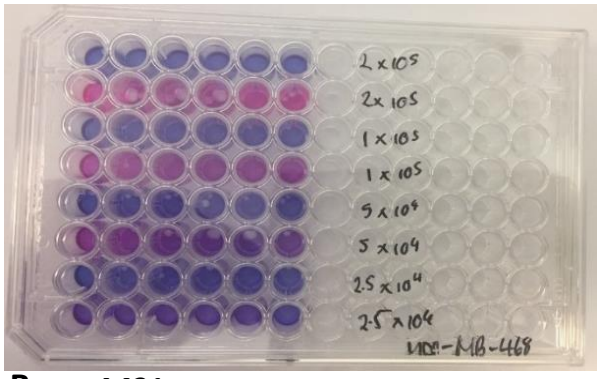

	1	2	3	4	5	6
A	5695	5406	5390	5353	5411	5485
B	147382	107448	113680	119294	145292	148563
C	5147	5232	5219	5139	5849	5152
D	125178	117060	114831	113676	116268	112933
E	5158	5062	5031	5028	5742	5243
F	108503	103255	87150	66268	55439	76024
G	5069	5292	5372	4981	4889	5158
H	55762	56952	50685	47328	44202	24284

B **A431**

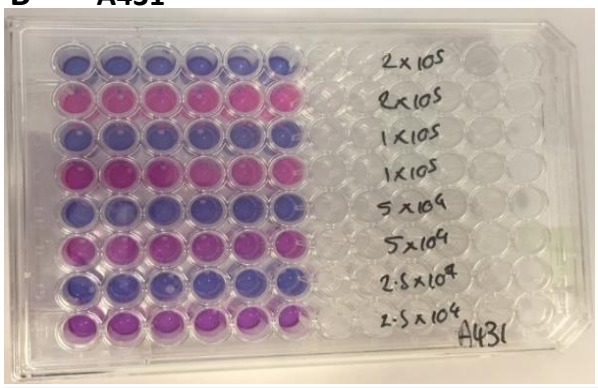

	1	2	3	4	5	6
A	5854	5830	5753	5711	5833	5882
B	144928	145185	143417	143899	143039	143788
C	5445	5872	5284	5421	5348	5531
D	135758	139701	137089	138186	138335	136114
E	5617	4264	5361	5115	5153	5127
F	123903	126129	119410	115115	112560	115596
G	5327	5112	4980	5078	5077	5237
H	103459	102171	101242	102208	99396	93540

Figure 3.1: Resazurin Cell Number Analysis Data

Figure A and B show example plate and plate reader images of the changes in Resazurin colour and fluorescence at 2 ½h of the 4 selected concentrations of MDA-MB-468 and A431 cells respectively. Cells treated with a toxic dose of *N. nigricollis* venom (rows A, C, E, G) show no change in fluorescence at any cell concentration whilst cells untreated with venom (rows B, D, F, H) show massive increases in fluorescence, with greater fluorescence observed at higher cell numbers. Green colour-coded rows indicate low levels of resazurin fluorescence (no/low resazurin metabolism-cellular toxicty), whilst red colour-coded rows indicate high levels of resazurin fluorescence indicative of continued cellular viability. Biological replicates/cell line = N2, Technical replicates/biological replicate = N6

Fold-changes in fluorescence were calculated for each cell concentration at each selected timepoint throughout the course of the assay and the subsequent fold changes were plotted

graphically to show the progression of Resazurin conversion to fluorescent resorufin over time (Figure 3.2).

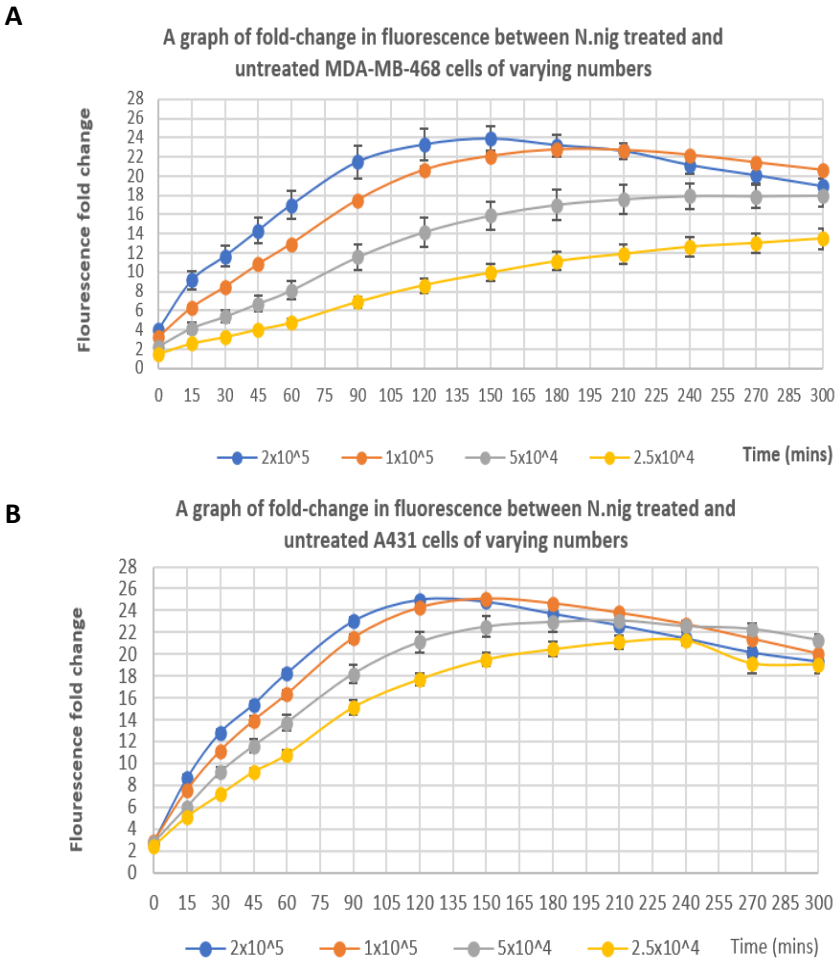

Figure 3.2: Cell number analysis for Resazurin Assay

Figs A. displays the fluorescent fold change between +VE Control **(**100 µg/ml toxic dose of *N. nigricollis* venom: **Minimum fluorescence**) and –VE Control (No venom, DMEM media only: **Max Fluorescence**) treated MDA-MB-468 cells. Data is displayed graphically. 4 different concentrations of MDA-MB-468 cells/well ($2x10^5$, $1x10^5$, $5x10^4$, $2.5x10^4$) were monitored over a 5h time period.

Figs B. displays the fluorescent fold change between +VE Control **(**100 µg/ml toxic dose of *N. nigricollis* venom: **Minimum fluorescence**) and –VE Control (No venom, DMEM media only: **Max Fluorescence**) treated A431 cells. Data is displayed graphically. 4 different concentrations of MDA-MB-468 cells/well ($2x10^5$, $1x10^5$, $5x10^4$, $2.5x10^4$) were monitored over a 5h time period. Biological replicates/cell line = N2, Technical replicates/biological replicate = N6

Analysis of the 4 investigated cell concentrations for MDA-MB-468 showed that the maximum observed fold-change in Resazurin assay fluorescence peaked around 24-fold and was observed in conjunction with the highest investigated cell number, $2x10^5$cells/well (Figure 3.2A). Maximum fluorescence was reached within 2½h, with fluorescent fold-change slowly decreasing

further overtime as the cells exhausted the available Resazurin resources. None of the other investigated cell number ($1x10^5$cells/well, $5x10^4$cells/well, $2.5x10^4$cells/well) were capable of reaching the same fold change in fluorescence over the course of the 5h time frame, and so a concentration of $2x10^5$ cell/well was determined to be the optimal number of MDA-MB-468 cell to take forward to z' assay analysis.

Similar analysis of A431 cells, plated out at the same cell/well concentrations as MDA-MB-468 cells, were conducted over the same 5h time period and the resulting fold-changes in fluorescence plotted graphically. Unlike with MDA-MB-468 cells there was little observable difference in the fluorescent fold-changes observed with the 2 highest selected cell concentrations, with the $1x10^5$ cell/well concentration reaching the same level of maximum fluorescent fold change, 25-fold, just 30 min after the higher $2x10^5$ cell/well concentration. After maximum fluorescence was reached (around 2½-3h) there was a much more rapid drop off in the fluorescent fold-change observed with the higher cell number than $1x10^5$ cell, which showed a more gradual decrease over the following 2h. With these details in mind, it was decided that there was little incentive to pick the highest number of cells when a $1x10^5$ (half the concentration of plated cells) elicited the same fluorescent response in almost the same time frame. A cell concentration of $1x10^5$ A431 cells/well was selected to be taken forward for z' assay analysis (Figures 3.2B).

3.3.2 Z' Analysis of Selected Cell Numbers to Ensure a Robust Assay

$2x10^5$ and $1x10^5$ concentrations of MDA-MB-468 and A431 cells, respectively, were selected to take forward for future Resazurin cell viability assays. In order to determine that the selected cell concentrations were sufficient for a statistically robust assay, z' assay analysis was carried out for both cell lines (Figure. 3.3). Z' assay analysis was also carried out over the course of a 5h time period to determine the most robust time point to select for subsequent Resazurin assays. Z' analysis of both cell lines showed the selected cell concentration and developed assay to be statistically robust at all investigated timepoints, except from timepoint 0. In both cases the assays were statistically robust at the first investigated timepoint (15min), showing changes in cell viability to be rapidly detectable using this assay method. The greatest z' values, and so the most optimal timepoint for taking assay readings, were determined to be 2h and 1 ½h for A431 and MDA-MB-468 cells, respectively. Maximum z' assay values peaked at 0.914 (Fig 3.3A) and 0.888 (Fig 3.3B) for A431 and MDA-MB-468 cells, respectively. Z' analysis at all timepoints (except timepoint 0) generated a z' value greater than 0.7 for both cell lines, suggesting the assay to be extremely robust.

A

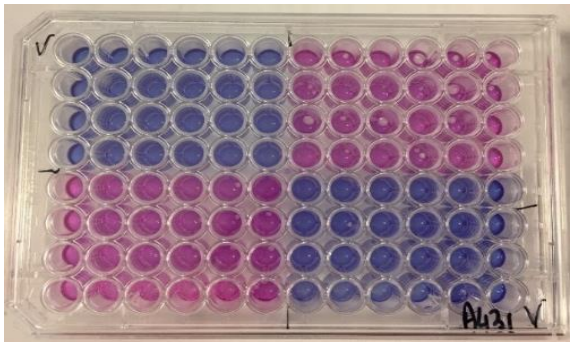

	1	2	3	4	5	6	7	8	9	10	11	12
A	5804	5855	5760	5767	5732	5777	114019	116986	114461	98020	116784	115386
B	5840	5789	5859	5950	5950	5820	114765	112771	111198	112547	109302	112248
C	5746	5677	5642	5769	5693	5813	105836	113015	112623	114374	112733	112648
D	5909	5636	5710	5690	5646	5707	113262	113924	112876	112901	114084	113080
E	112494	111998	111880	110278	108879	110856	5760	5774	5751	5755	5928	5955
F	109665	111150	111743	111288	110859	112048	5712	5875	5824	5852	5943	5921
G	111840	111193	111158	110521	109771	109819	6130	5846	6205	5997	6109	6009
H	110487	110713	111661	108581	112137	114659	5632	5456	5372	5524	6339	6010

A431

time point	z' assay
0	-0.0089
15	0.773455
30	0.719829
45	0.750444
60	0.775108
90	0.851902
120	0.91371
150	0.91138
180	0.881762
210	0.864996
240	0.84295
270	0.832619
300	0.823219

B

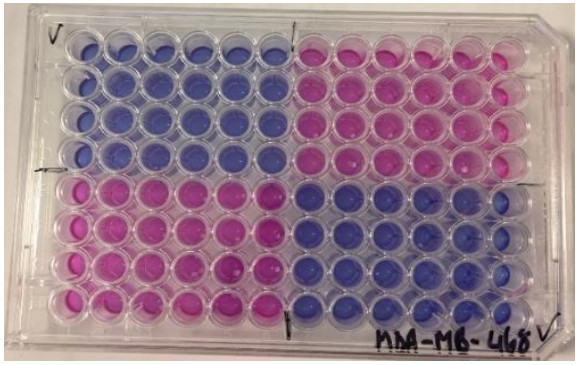

	1	2	3	4	5	6	7	8	9	10	11	12
A	5953	5796	5781	5623	6173	5970	116579	116693	118080	116506	116525	103444
B	5817	5743	5674	6024	5572	5609	119677	116816	117049	123154	117388	114642
C	5759	5692	5582	5787	5612	5620	123406	123140	122971	118807	119167	112772
D	6030	5552	6067	5550	5545	5648	118972	122754	118741	117774	118893	109705
E	121353	121501	125399	121216	128135	119166	5652	5685	5595	5574	6531	5218
F	124973	121750	122841	121487	120502	123587	5654	5694	5830	5820	5638	5646
G	122143	116762	120479	121671	113593	117049	5796	5628	5742	5578	5877	5035
H	122856	120078	114170	119280	114818	115674	5745	5733	5782	5621	5958	5928

MDA-MB-468

time point	z' assay
0	-0.47077
15	0.848864
30	0.867824
45	0.875999
60	0.880956
90	0.8879
120	0.88185
150	0.86403
180	0.851318
210	0.845155
240	0.837088
270	0.830535
300	0.828234

Figure 3.3: Z' Analysis for Resazurin Assay

Figure A shows the z' analysis of A431 cells. The Plate and plate reader images show an example of the colour and fluorescent changes respectively (2h timepoint). The table of z' assay values for $1x10^5$ A431 cells show the assay to be robust at all timepoints, excluding timepoint 0, with the best timepoint being 120 min. Figure B shows the z' analysis of MDA-MB-468 cells. The Plate and plate reader images show an example of the colour and fluorescent changes respectively (2h timepoint). The table of z' assay values for $2x10^5$ MDA-MB-468 cells show the assay to be robust at all timepoints, excluding timepoint 0, with the best timepoint being 90 min. Green colour-coded wells indicate low levels of resazurin fluorescence (no/low resazurin metabolism-cellular toxicity), whilst red colour-coded wells indicate high levels of resazurin fluorescence indicative of continued cellular viability. Biological replicates/cell line = N2, Technical replicates/biological replicate = N48

With z' analysis in mind it was determined that the assay was robust enough to proceed to assess both the snake and invertebrate venom panels for cytotoxicity against both the investigated cell lines.

3.3.3 Determination of the Toxic Properties of a Panel of Snake Venoms Using an Optimised Resazurin Assay Protocol

Cytotoxic analysis of eighteen whole snake venoms, investigated in the panel, were assessed to determine whether they could be potentially viable options to take forward for further investigation. Each venom was diluted to 3 concentrations in an attempt to ascertain their cytotoxic range of action. Venoms were diluted to concentrations of 2 mg/ml, 200 µg/ml and 20 µg/ml. Each well of cells was treated with 50µl of the venom concentration, giving both A431 and MDA-MB-468 cells either a total protein dose of 100 µg, 10 µg, or 1 µg, respectively. A percentage inhibition of 50% or greater was set as a biological significance threshold. Whole venoms causing reductions of 50% or greater at any of the tested doses were considered significant (See Appendix VII).

Graphical analysis (Figures. 3.4C and 3.5C) shows that most of the snake venoms tested showed no or negligible cytotoxicity in either cell line at the lowest tested concentration of 20 µg/ml (1µg protein dose). With the exception of *Naja siamensis* (N.sia: Indochinese spitting cobra) which still caused a significant reduction in cell viability (61%) in MDA-MB-468 cells. At doses of 200 µg/ml and 2 mg/ml, cell line specific toxicities were observed after treatment with the snake venom panel. The overall cellular inhibition results clearly show a pattern, with MDA-MB-468 breast cancer cells appearing to display a greater susceptibility to cytotoxicity at lower whole snake venom doses when directly compared with the inhibition levels observed in treated A431 cells (Figures 3.4 and 3.5). These differences in toxic effect against the two investigated cell lines can likely be attributed to differences in tissue origins between the two lines, and differences in their gene mutations and protein expression profiles. One proposed suggestion which could attribute to the differences observed in toxic effect could be due to the expression levels of growth promoting tumour antigen EGFR, which is known to be over-expressed in both these cell lines. EGFR has been shown to be expressed at $\approx 3x10^6$ EGFR/cell in A431 cells compared to around $\approx 1.3 - 2x10^6$ EGFR/cell in MDA-MB-468 cells (Merlino *et al.*, 1984; Armstrong *et al.*, 1994; Jackson and Ceresa, 2016). This increased number in EGFR could be conferring a beneficial survival effect to A431 over MDA-MB-468 cells. However, without further in-depth profiling of the genes and proteins expressed by both cell lines, and the possible changes to these in response to venom treatment, it is impossible to propose the exact reasons for the observed cell line specific toxicity.

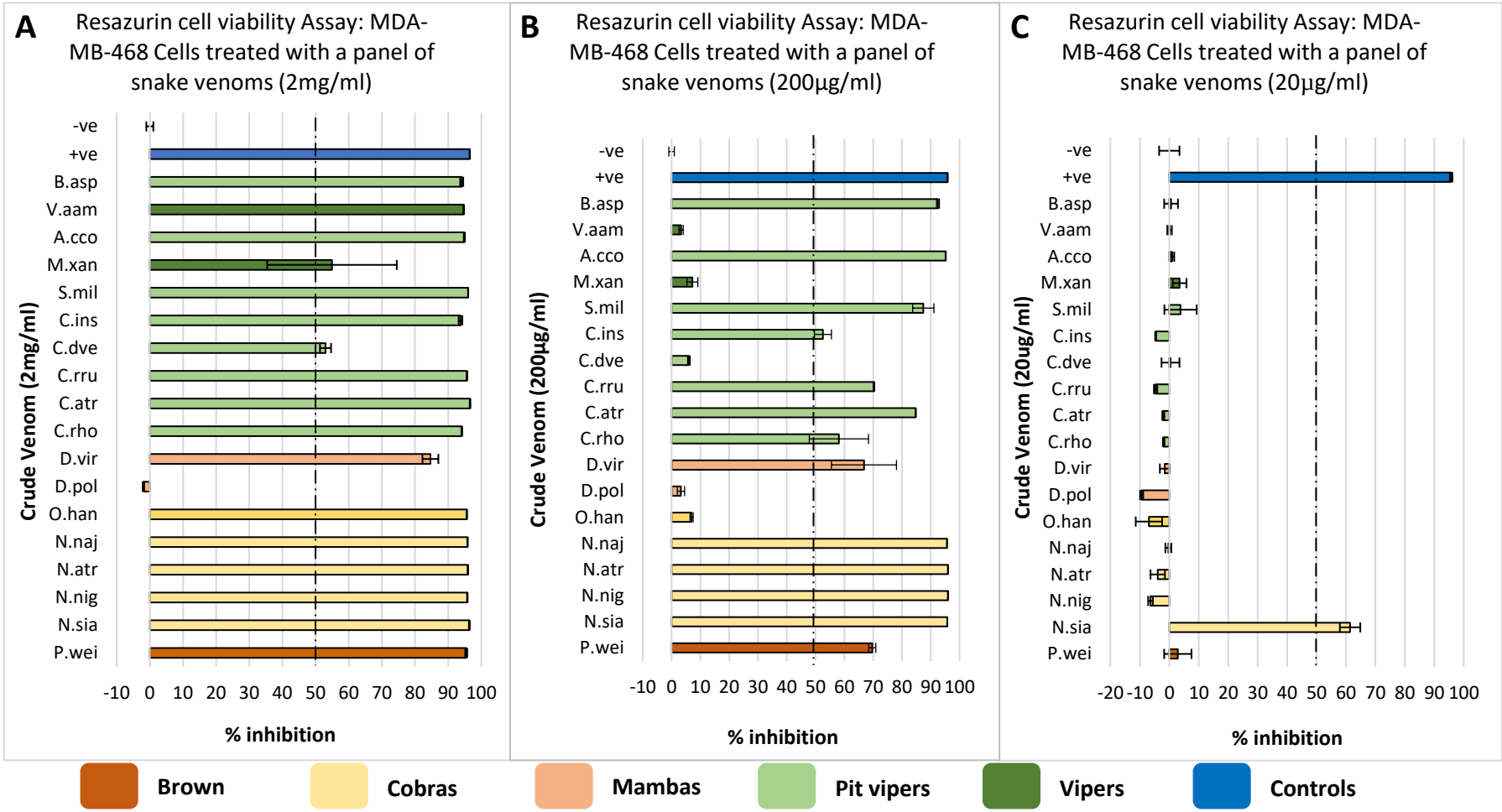

Figure 3.4: Graphical Analysis of Resazurin Snake Toxicology Panel in MDA-MB-468 cells

Shows the % inhibition of MDA-MB-468 cells treated with whole snake venoms at concentrations of 2 mg/ml **(A)**, 200 µg/ml **(B)**, & 20 µg/ml **(C)** respectively. % Standard Error calculated and used for error bars of each graph. A percentage inhibition of 50% or greater was set as a biological significance threshold. Dotted line represents 50% inhibition threshold. Biological replicates/cell line = N1, Technical replicates/Biological replicate = N3

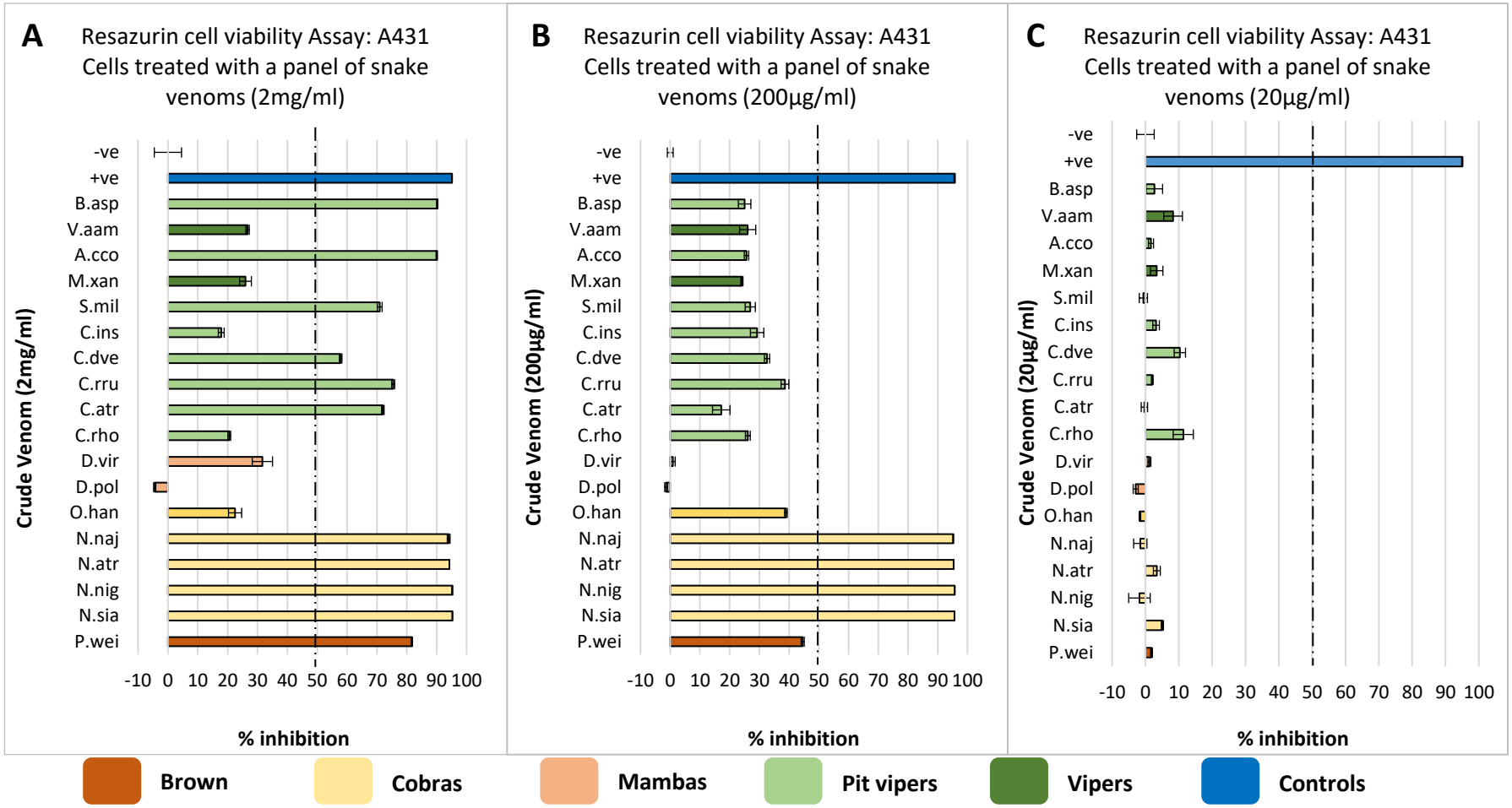

Figure 3.5: Graphical Analysis of Resazurin Snake Toxicology Panel in A431 cells

Shows the percentage inhibition of A431 cells treated with whole snake venoms at concentrations of 2 mg/ml **(A)**, 200 µg/ml **(B)**, & 20 µg/ml **(C)** respectively. % Standard Error calculated and used for error bars of each graph. A percentage inhibition of 50% or greater was set as a biological significance threshold. Dotted line represents 50% inhibition threshold. Biological replicates/cell line = N1, Technical replicates/biological replicate = N3

The Resazurin assay analysis revealed differences in toxicity profiles in response to treatment with venoms collected from different snake families. Venoms collected from true cobras (*Naja* spp) from the Elapidae family of snakes showed consistently the highest levels of significant cellular cytotoxicity, with 94% or greater cytotoxicity observed in both cell lines in response to treatment with doses of both 2 mg/ml and 200 µg/ml (N.sia: Indochinese spitting cobra; N.nig: Black-necked spitting cobra; N.atr: Chinese cobra; N.naj: Indian cobra) (Table 3.4). True cobra venoms have been shown to be capable of causing cancer cell death in a variety of tumour types including breast and skin-derived cancer cell lines (Bradshaw *et al.*, 2016; Attarde and Pandit, 2017; Bhowmik *et al.*, 2017). The high levels of cytotoxicity observed in both cancer cell lines following treatment with all the investigated true cobra venoms can likely be attributed to the composition of cobra venoms specifically. Venoms isolated from individuals belonging to the genus *Naja* have been shown to predominantly consist of a large number of cytotoxins/cardiotoxins with highly conserved amino acid sequences and overall three-finger toxin peptide structures (Dubovskii and Utkin, 2015). Cytotoxins have been shown capable of exhibiting a wide range of distinct biological activities such as muscular cell depolarisation and contraction and lysis of a wide variety of cells including healthy erythrocytes and epithelial cells, as well as selective destruction of certain tumour cell types (Panda, Kumari and Panda, 2016). *Ophiophagus hannah* (O.han: King cobra) venom, arising from a snake belonging to a separate monotypic genus, displayed a distinctly differing cellular inhibitory profile to those of the true cobras. *O. hannah* venom was found to cause significant reductions to MDA-MB-468 cells at a dose of 2mg/ml, similar to the reductions observed with true cobra venoms (Figure 3.4A). However, the venom was found not to be causing biologically significant reductions in MDA-MB-468 cells at 200 µg/ml, or in A431 cells at either of these doses (Figure 3.4B and 3.5). *O. hannah* venom has been found in previous literature to display cytotoxic activities against cancer cells, reducing their viability and backing up the findings found in the Resazurin assay. L-amino acid oxidases (LAAO) isolated from *O. hannah* venom have been consistently shown in the literature to promote reductions in cell viability against SNU-1 (gastric), MCF-7 (breast), A549 (lung) and PC-3 (prostate) cancer cell lines, with IC_{50} values following 72- 96h dosing of 0.1-0.15 µg/ml, 0.04 µg/ml, 0.05 µg/ml and 0.05 µg/ml respectively (Ahn, Lee and Kim, 1997; Li Lee *et al.*, 2014; Lee *et al.*, 2014). With the literature pointing to LAAOs as the main candidate within *O. hannah* venom responsible for mammalian cell cytotoxicity, it is likely that a similar component may be responsible here. The differences in the dose needed for 50% inhibition in previous studies and these Resazurin assays are likely the result of differing exposure times, with cells in the literature exposed to LAAO from *O. hannah* venom for 3-4 days as opposed to the 2h incubation time adopted for this study.

Whilst venoms isolated from the true cobras showed consistent toxicity levels across both cell lines and all tested species, elapid snakes belonging to other genera, including those from *Dendroaspis* (mamba) and *Pseudechis* (P.wei: Brown snake), did not show such consistent levels of cellular inhibition. Treatment with the venom of *Dendroaspis viridis* (D.vir: Western green mamba) caused significant inhibitions to MDA-MB-468 cell viability in response to doses of both 2 mg/ml (88.8%) and 200 μg/ml (66.8%) (Table 3.4), whilst no significant reductions were observed to A431 cell viability with this venom at either doses (Figure 3.5A & B). Whilst *D. viridis* venom was shown to cause significant reductions to MDA-MB-468 cell viability at the higher tested doses, indicating the presence of cytotoxic peptide components, venom from *Dendroaspis polylepis* (D.pol: Black mamba) caused no biologically significant reductions in either cell line at any of the tested doses (Figures 3.4 & 3.5). The toxicity observed with *D. viridis* venom treatment and thereof lack of it with *D. polylepis* venom is likely the result of differing venom mechanistic actions. Venom from *D. viridis* has not been well characterised, with only one report published into the effects experienced by a bite patient, which did not appear to display local cytotoxic symptoms (Fuchs, Weiler and Meier, 2019). However, treatment of breast cancer cells with three-finger toxin peptides isolated from the venom of eastern green mamba, *D. angusticeps* resulted in the cytotoxicity of MDA-MB-231 (breast), A549 (lung) and HT-29 (colon) cancer cell lines (Conlon *et al.*, 2014), suggesting mamba venoms can contain cancer cytotoxic molecules. Whilst *Conlon et al*. do not elaborate on the mechanism for this observed cancer cell cytotoxicity, a large number of the three-finger toxin family exhibit general cytolytic effects through the forming of ion pores within cell lipid membranes, and are therefore referred to as cytolysins (Kini and Doley, 2010). Whilst venom from *D. polylepis* has been characterised to displays strong neurotoxic properties, envenomation's are not associated with haemolysis or local signs of cytotoxicity, such as swelling, haemorrhage, or necrosis (Závada *et al.*, 2011; Laustsen *et al.*, 2015). Treatment of MDA-MB-468 and A431 cells with *Pseudechis rossignoli* (P.wei: Papuan Pygmy Mulga) venom at 2 mg/ml and 200 μg/ml doses resulted in significant reductions at both of the highest doses respectively (Figures 3.4 & 3.5). Cells saw reductions in viability of 95.5% and 84% in MDA-MB-468 and A431 cell lines respectively at 2 mg/ml, with additional reductions of 69.7% observed in MDA-MB-468 cells at a dose of 200 μg/ml (Table 4.4). A previous study, investigating the cytotoxicity of venoms from the *Pseudechis* genera found that 11 of the 13 tested species, including *P. rossignoli* resulted in significant reductions to MM96L melanoma cells in a dose-dependent manner and showed significantly higher toxicity at lower tested doses to MM96L cancer cells than to NFF (normal foetal fibroblasts) (Goldenberg *et al.*, 2018).

Treatment with the 2 selected viper venoms on the snake panel, *Montivipera xanthina* (M.xan: Ottoman Viper) and *Vipera ammodytes ammodytes* (V.aam: Nose-horned viper) resulted in no

significant reductions to A431 cell viability at any of the three tested doses (Figure 3.5), whilst biologically significant reductions were observed in MDA-MB-468 cells in response to both venoms at 2 mg/ml but not 200 µg/ml (Figure 3.4). Whilst significant reductions occurred in MDA-MB-468 cells in response to both viper venoms, the venom from *Vipera ammodytes ammodytes* resulted in a larger significant reduction (81.6%) in cell viability than the venom collected from *Montivipera xanthina* (55%) (Table 3.4). Treatment with M.xan venom at a dose of 2mg/ml resulted in mixed toxicity results across the three replicate readings, which resulted in an average that passed the biological threshold but with a large error bar. These differences in toxicity across the replicates could be the result of the selected dose falling upon the cusp of toxic effect, and so any slight variations in cell numbers could have shifted the balance from a toxic to non-toxic dose. Venoms from the genera Montivipera have been found in previous literature to cause the reduction in cell viability of a large and broadly diverse group of cancers, with 48h dosing of *V. bulgardaghica* and *V. raddei* venoms found to inhibit the viability of CaCo-2 (colon), MCF-7 (breast), HeLa (cervical), U87MG (glioblastoma), MPanc-96 (Pancreatic) and A549 lung cancer cell lines, with IC_{50} values between 0.65- 9.07 µg/ml (Nalbantsoy *et al.*, 2017). Another study by Sawan *et al*. 2017, saw a dose-dependent reduction in the cell viability of both benign (A5) and low grade malignant (II4) keratinocyte cancer cell lines following 24h treatment with *M. bornmuelleri* venom (Sawan *et al.*, 2017). Whilst additional studies also identified *M. bulgardaghica* venom as causing toxicities to HeLa and A549 cells (Erzurumlu *et al.*, 2017) and *M. xanthina* venom causing reductions to A549 cells in XTT cell proliferation and clonogenic assays at IC_{50} doses between 1.5- 2.2mg/ml (Huriyet *et al.*, 2017).

Venoms from the genus *Vipera* have also been shown in the literature to display anti-oncogenic characteristics. *Vipera ammodytes* venom and purified components of its venom have been identified in 2 separate studies to inhibit the viability of several cancer cell lines. Whole *V. ammodytes* venom caused reductions to CaCo-2 (colon), MCF-7 (breast), U-87 MG (glioma) and PC3 (prostate) cancer cell lines in a dose dependent manner, with the most potent activities observed against CaCo-2 cells (İğci *et al.*, 2016). A dimeric disintegrin, isolated from the venom of *V. ammodytes ammodytes* has also been shown in previous literature to result in the loss of cell viability of MDA-MB-231 (breast) cancer cells and prevent their cell migration (Latinović *et al.*, 2017). The presence of a disintegrin in *V. ammodytes ammodytes* venom that reduces breast cancer viability is interesting as treatment with this same venom only resulted in significant reductions to cell viability in MDA-MB-468 breast cancer cells in the Resazurin assay analysis undertaken in this chapter.

Treatment with the eight selected pit viper venoms resulted in a mixture of significant reductions

A431 (Percentage Reduction in Cell Viability ± % SE)			
	2mg/ml	200µg/ml	20µg/ml
Pseudechis rossignoli	84.02 (± 0.20)	44.56 (± 0.52)	1.81 (± 0.26)
Naja siamensis	95.25 (± 0.03)	95.63 (± 0.06)	5.08 (± 0.33)
Naja nigricollis	95.21 (± 0.13)	95.73 (± 0.02)	-1.81 (± 3.22)
Naja atra	94.25 (± 0.06)	95.35 (± 0.07)	3.41 (± 1.04)
Naja naja	94.00 (± 0.47)	95.21 (± 0.10)	-1.55 (± 2.00)
Ophiophagus Hannah	22.47 (± 2.19)	34.17 (± 0.45)	-1.66 (± 0.23)
Dendroaspis polylepis	-4.41 (± 0.35)	-1.38 (± 0.49)	-2.93 (± 0.77)
Dendroaspis viridis	31.63 (± 3.39)	0.87 (± 0.78)	1.19 (± 0.45)
Calloselasma rhodostoma	20.54 (± 0.45)	26.10 (± 0.82)	11.34 (± 3.02)
Crotalus atrox	71.96 (± 0.43)	17.16 (± 2.94)	-0.32 (± 0.96)
Crotalus ruber	75.43 (± 0.51)	38.59 (± 1.32)	2.04 (± 0.25)
Crotalus durissus vegrandis	57.83 (± 0.44)	32.56 (± 0.88)	10.31 (± 1.70)
Trimeresurus albolabris insularis	17.86 (± 0.98)	29.22 (± 2.25)	3.18 (± 0.99)
Sistrurus miliarus barbouri	70.91 (± 0.81)	26.91 (± 1.71)	-0.62 (± 1.23)
Montivipera xanthina	25.97 (± 1.98)	24.10 (± 0.36)	3.37 (± 1.87)
Agkistrodon contortrix contortrix	90.01 (± 0.22)	25.65 (± 0.75)	1.66 (± 0.76)
Vipera ammodytes ammodytes	26.66 (± 0.56)	26.05 (± 2.72)	8.28 (± 2.80)
Bothrops asper	90.18 (± 0.20)	25.02 (± 2.11)	2.68 (± 2.46)
MDA-MB-468 (Percentage Reduction in Cell Viability ± % SE)			
	2mg/ml	200µg/ml	20µg/ml
Pseudechis rossignoli	95.45 (± 0.29)	69.71 (± 1.22)	2.90 (± 4.64)
Naja siamensis	96.37 (± 0.12)	96.98 (± 0.08)	61.41 (± 3.47)
Naja nigricollis	95.78 (± 0.08)	95.99 (± 0.05)	-6.39 (± 0.79)
Naja atra	95.96 (± 0.03)	95.65 (± 0.03)	-3.93 (± 2.45)
Naja naja	95.84 (± 0.05)	95.78 (± 0.03)	-0.32 (± 1.01)
Ophiophagus Hannah	64.37 (± 0.04)	6.96 (± 0.54)	-6.92 (± 4.49)
Dendroaspis polylepis	-1.92 (± 0.22)	3.25 (± 1.26)	-9.39 (± 0.52)
Dendroaspis viridis	88.79 (± 2.39)	66.83 (± 11.29)	-1.54 (± 1.67)
Calloselasma rhodostoma	92.22 (± 0.11)	58.12 (± 10.29)	-1.91 (± 0.24)
Crotalus atrox	96.60 (± 0.09)	88.09 (± 0.12)	-2.04 (± 0.34)
Crotalus ruber	95.67 (± 0.09)	76.61 (± 0.21)	-4.65 (± 0.57)
Crotalus durissus vegrandis	52.99 (± 1.67)	6.01 (± 0.43)	0.40 (± 3.05)
Trimeresurus albolabris insularis	93.72 (± 0.55)	52.57 (± 2.95)	-4.63 (± 0.15)
Sistrurus miliarus barbouri	94.48 (± 0.01)	87.43 (± 3.68)	3.82 (± 5.48)
Montivipera xanthina	54.95 (± 19.55)	7.22 (± 1.89)	3.50 (± 2.35)
Agkistrodon contortrix contortrix	94.88 (± 0.17)	95.21 (± 0.13)	0.99 (± 0.68)
Vipera ammodytes ammodytes	81.65 (± 0.10)	3.31 (± 0.74)	0.08 (± 0.78)
Bothrops asper	94.09 (± 0.46)	92.53 (± 0.49)	0.59 (± 2.34)

Table 3.4: Snake Venom Panel % Reductions in MDA-MB-468 and A431 Cell Viability

Displays the percentage reductions ± % SE in MDA-MB-468 and A431 cancer cell lines in response to 20 µg/ml, 200 µg/ml and 2 mg/ml doses of snake venoms. Table colour coding separates snake panel into families Elapinae (orange, yellow, peach), Crotalinae (light green), Viperinae (dark green). Elapinae are further subdivided by genera into *Pseudechis* (orange), *Naja* (light yellow), *Ophiophagus* (dark yellow) and *Dendroaspis* (peach). The same colour coding has been used in this table as in Figures 3.4 & 3.5.

to both A431 and MDA-MB-468 cells. Overall, MDA-MB-468 cells showed a greater susceptibility to the pit viper venom panel than A431 cells, with greater percentage reductions in cell viabilities observed in the breast cancer cell line when compared to the squamous carcinoma (Figures 3.4 & 3.5). A431 carcinoma cells showed no biologically significant reductions following treatments with all eight pit viper venoms at a dose of 200 μg/ml (Figure 3.5B).

Treatment with 2mg/ml doses of *Crotalus* venoms *Crotalus atrox* (C.atr: Western diamond back rattlesnake), *Crotalus ruber* (C.rru: Red diamond rattlesnake) and *Crotalus durissus vegrandis* (C.dve: Uracoan rattlesnake) resulted in significant reductions of 72%, 75.4% and 57.8% respectively in A431 cells (Figure 3.5A & Table 3.4). Significant reductions were not observed in A431 cells in response to 2 mg/ml treatments of either *Calloselasma rhodostoma* (C.rho: Malayan ground pit viper) or *Trimeresurus albolabris insularis* (C.ins: White-lipped island pit viper), however significant biological reductions were observed following treatment with *Sistrurus miliarus barbouri* (S.mil: Barbour's pygmy rattlesnake) of 70.9%, *Agkistrodon contortrix contortrix* (A.cco: Northern copperhead) of 90% and *Bothrops asper* (B.asp: Fer-de-lance) of 90.2% at the same dose (Figure 3.5A & Table 3.4).

Treatment with the panel of pit viper venoms also resulted in significant reductions in MDA-MB-468 breast cancer cells. Significant biological reductions were observed in response to all the pit viper venoms when cells were dosed with 2 mg/ml, with all venoms apart from *C. durissus vegrandis* resulting in reductions in cell viability of 90% or greater (Figure 3.4A). Interestingly, *C. durissus vegrandis* venom caused the lowest observed cytotoxicity of all the tested pit vipers in MDA-MB-468 cells, with a % reduction in viability of 52% (Table 3.4). At a dose of 200 μg/ml, MDA-MB-468 cells showed a greater susceptibility to pit viper venoms than A431 cells, with significant reductions still observed in cell viability in response to seven of the eight pit viper venoms, compared to none in A431 cells at the same concentration (Figure 3.4B). 200 μg/ml doses of both *Agkistrodon contortrix contortrix* and *Bothrops asper* caused greater than 90% reduction in cancer cell viability, with *Sistrurus miliarus barbouri* causing reduction just short of that at 87.4%. Despite all belonging to the genus *Crotalus*, significant differences in cell cytotoxicity were observed in MDA-MB-468 cells in response to 200 μg/ml of *Crotalus atrox* (88%), *Crotalus ruber* (76.6%) and *Crotalus durissus vegrandis* (6%) venoms (Table 3.4). Finally, treatment with *Calloselasma rhodostoma* and *Trimeresurus albolabris insularis* at 200 μg/ml caused reductions in MDA-MB-468 cell viability of 58.1% and 52.5% respectively, lower than the % inhibitions to viability observed with all other pit viper venoms (excluding *C. durissus vegrandis*), but still biologically significant (Table 3.4). *Calloselasma rhodostoma* venom has been shown in the literature to cause reductions to the viability of cancer cells, including against metastatic breast cancer types such as MDA-MB-231 (Ling, Sikarwar and Yi, 2015). Studies has

linked the cancer cell cytotoxicity to L-amino acid oxidases (LAAOs), which have subsequently been isolated from the venom and their anti-cancer activities assessed. LAAO, isolated from *C. rhodostoma* venom (CR-LAAO) has been shown to demonstrate cytotoxic activity against human colon cancer cell lines SW480 and SW620, in both dose- and time-dependent manners. Treatment with the LAAO for 48h was found to result in EC_{50} values of 6 μg/ml and 7 μg/ml for SW480 and SW620 respectively (Zainal Abidin *et al.,* 2018). Another study into the cytotoxic effects of *C. rhodostoma* LAAO also showed that the venom component caused high levels of HepG2 liver (IC_{50} 10.78 μg/ml) and HL-60 leukaemia (IC_{50} 1.7 μg/ml) tumour cells, whilst causing lower levels of toxicity to human mononuclear cells (PBMCs) (Costa *et al.,* 2015). A third study into CR-LAAO also found the venom component to have anticancer properties, with reductions observed to the viability of erythroleukemia HEL 92.1.7 (IC_{50} 0.15 μg/ml) and leukaemia SET-2 (IC_{50} 1.5 μg/ml) cancer cells in a concentration dependent manner (Tavares *et al.*, 2016).

The venoms of the genus *Crotalus,* and in particular the venom of *Crotalus durissus terrificus,* have been shown to display anticancer properties against a variety of different cancer types, including breast, glioma, pancreatic, cervical, oesophageal and prostate cells (Hayashi *et al.,* 2008; Teixeira *et al.*, 2016; Gimenes *et al.*, 2017; Tan *et al.*, 2017; Muller *et al.*, 2018). The cytotoxic activities associated with these venoms have been linked to the actions of a variety of venom proteins, including LAAOs and phospholipase A2s, such as crotoxin. Despite the research into certain Crotalus species, there is a lack of research into others including *Crotalus atrox* and *Crotalus ruber*. Interestingly, a screen of Crotalus venoms carried out by Bradshaw *et al.* 2016 saw significant reductions in MCF-7 breast cancer cell viability in response to *C. ruber ruber* venom but not in response to *Crotalus durissus terrificus* venom (Bradshaw *et al.*, 2016). This supports the findings of the screens in this chapter, which showed sub-species *C. durissus vegrandis* venom causing the lowest levels of cytotoxicity of all the tested Crotalus venoms, with *C. ruber* venom causing significantly larger cytotoxicity in MDA-MB-468 breast cancer cells.

Agkistrodon contortrix contortrix and *Bothrops asper* venoms were shown in the Resazurin assay toxicity panels to be consistently cytotoxic, causing significant reductions to both investigated cell lines. The venom of Agkistrodon species has been found to display anticancer properties against cervical (Zhang and Wei, 2007), lung (Zhang and Cui, 2007) and breast (Zhou *et al.*, 2000) cancer cell lines, with the venom activity attributed to LAAOs, including isolated peptides ACTX-6 and ACTX-8. Similarly, extensive research has found that the venom of Bothrops species can cause cytotoxicity to a variety of cancer types. *Bothrops leucurus* venom has been shown to cause cell viability reductions against K562 (leukaemia), NCI-H292 (lung), Hep-2 (epidermoid carcinoma), T98, U87 and RT2 (glioblastoma), MCF7 (breast), EAC (Ehrlich ascites carcinoma) and UACC (melanoma) (Gabriel *et al.*, 2012; Nunes *et al.*, 2012). BJcuL, a lectin

isolated from the venom of *Bothrops jararacussu* has also been shown to cause reductions to cancer cell survival, when used to treat OVCAR-5 (ovarian), MDA-MB-435 (breast), A-172 and U87 (glioblastomas), T24 (bladder), K-562 (leukaemia) and MKN45 and AGS (gastric) (De Carvalho *et al.*, 2001; Nolte *et al.*, 2012). 5 Bothrops venoms were found to cause significant reductions to A-375 skin cancer cell line, including *B. asper* venom which was used in the panel screens in this chapter and was found to cause reductions to both cell lines (Bradshaw *et al.*, 2016). *Bothrops pirajai, B. diporus and B. pauloensis* venoms were observed to cause reductions in a variety of cancer cell lines following 24h of dosing, including HL-60 (leukaemia), HCT-8 (colon), MDA-MB-435 (breast) and SF-295 (nervous system), where effective doses ranged between 6- 19 μg/ml (Jorge *et al.*, 2011).

Sistrurus miliarius barbouri and *Trimeresurus albolabris insularis* venoms resulted in mixed reductions to the tested cell lines, with the venom from the prior causing more extensive cytotoxicity to both tested cell lines than the latter. However, both venoms caused significant reductions, with *S. miliarius barbouri* resulting in reductions to both cell lines, whilst *T. albolabris insularis* showed toxicity specifically to MDA-MB-468 breast cancer cells. Whilst venoms from both these genera have been poorly investigated for their cytotoxic potential against cancer cells, previous research has shown that venoms from the genera *Trimeresurus* and *Sistrurus* have the potential to display cytotoxic effect against both cancer and normal cells. Treatment of MCF-7 and A-375 with venoms from 4 different *Sistrurus* species were found to result in four (MCF-7) and three (A-375) significant reductions to cell viability, with around 80% and 50-60% reductions observed in the breast and skin cell lines respectively (Bradshaw *et al.*, 2016). 72h treatment with *T. albolabris* venom was found to cause significant reductions to the viability of normal human skin fibroblast between doses of 3-5μg/well (Phaopongthai *et al.*, 2015), whilst *T. malabaricus* venom was found to result in significant reductions to HT1080 (fibrosarcoma), MCF-7 (breast), DU-145 (prostate) and MIA PaCa-2 (pancreatic) cells following 24h doses of between 6-10 μg/ml, whilst proving non-toxic to 3T3-L1 fibroblast cells at the same dose range (Vanuopadath *et al.*, 2020). A further study into *T. malabaricus identified* fractions which display toxicity to MCF-7 breast cancer cells (Satose *et al.*, 2018), whilst a fraction isolated from the venom of *T. flavoviridis*, OHAP-1, showed significant reductions in the viability of C6, RBR17T and U251 glioma cancer cell lines from 48h treatment at doses as low as 2.5 μg/ml (Sun *et al.*, 2003).

3.3.4 Determination of the Toxic Properties of a Panel of Invertebrate Venoms Using an Optimised Resazurin Assay Protocol

Treatment of MDA-MB-468 and A431 cells with a panel of invertebrate venoms and secretions resulted in significant reductions to cell viability in response to a few of the tested candidates. Theraphosid venoms were selected for the greatest possible geographical and family diversity. Species were selected that spanned the 4 larger theraphosid categories, including representative venoms from new-world terrestrial (*Acanthoscurria cordubensis* (A.cor), *Acanthoscurria geniculata* (A.gen), *Brachypelma boehmei* (B.boe), *Thrixopelma pruriens* (T.pru), *Theraphosa stirmi* (T.str)), new-world arboreal (*Avicularia metallica* (A.met), *Tapinauchenius cupreus* (T.cup), *Psalmopoeus cambridgei* (P.cam)), old-world terrestrial (*Cyriopagopus albostriatum* (H.lbo), *Pterinochilus lugardi* (P.lug)) and old-world arboreal species (*Poecilotheria formosa* (P.for), *Heteroscodra maculata* (H.mac)), 8 different families and 11 distinct genera. Treatment of both cell lines with all the selected theraphosid venoms at doses of 200 μg/ml and 20 μg/ml resulted in no biologically significant reduction to cellular viability (Figures 3.6 & 3.7). This lack of observable toxicity suggests that theraphosid venoms appear to lack cytotoxic peptide compositions, and that this lack of cancer cell cytotoxic peptides appears to be a conserved feature of theraphosid venoms across a large number of distinct representative species. However previously published literature has suggested that theraphosid venoms can show cytotoxic activities against MCF-7 breast cancer cells, with the study identifying seventeen whole venoms that caused significant reductions in cell viability using clonogenic survival assays (Wilson *et al.*, 2017). Whilst the study by Wilson *et al*. found toxicity using some of the same venoms used for these Resazurin toxicity screens (*Acanthoscurria geniculata* and *Theraphosa stirmi*), it is worth noting that the MCF-7 cells used in their study were exposed to each theraphosid venom in the clonogenic survival assay for a duration of 5 days. This exposure time is significantly longer than the 2h exposure time used for the Resazurin assays in this chapter, and so may account for the observed differences in breast cancer cell toxicity. Also worth noting, is that whilst both breast cancer cell lines, MCF-7 cells are ER and PR receptor positive, whilst MDA-MB-468 cells are triple negative breast cancer cells, that over-express EGFR (Dai *et al.*, 2017) and so with different phenotypic make ups this could potentially impact the type of response observed from both cell lines following venom treatment. Research into *in vivo* toxicity in mice, suggests that the main biological effects observed following theraphosid envenomation are the result of neurotoxicity (Escoubas and Rash, 2004), which may account for the lack of cytotoxicity observed with this particular screen.

Treatment with venoms from a selection of scorpions resulted in only one clearly significant reduction in cell viability in one of the 2 tested cancer cell lines. 5 scorpion venoms, from 4 diverse families (Buthidae, Caraboctonidae, Scorpionidae and Luridae) and 5 distinct genera (*Androctonus, Hadrurus*, *Heterometrus, Protoiurus* and *Parabuthus*) were selected for cytotoxic

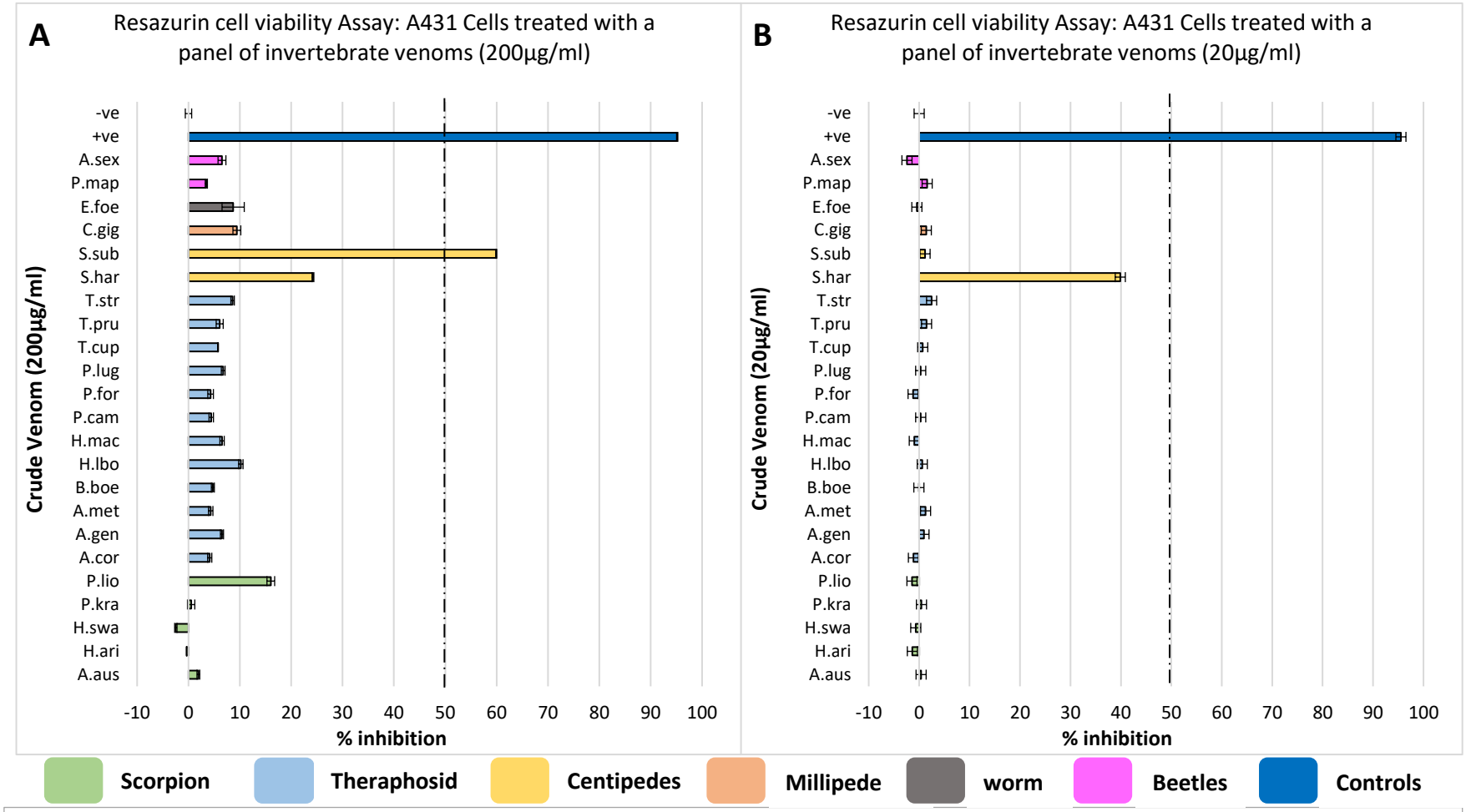

Figure 3.6: Graphical Analysis of Resazurin Invertebrate Toxicology Panel in A431 cells

Shows the % inhibition of MDA-MB-468 cells treated with whole invertebrate venoms at concentrations of 200 µg/ml **(A)** and 20 µg/ml **(B)** respectively. % Standard Error calculated and used for error bars of each graph. A percentage inhibition of 50% or greater was set as a biological significance threshold. Dotted line represents 50% inhibition threshold. Biological replicates/cell line = N1, Technical replicates/biological replicate = N3

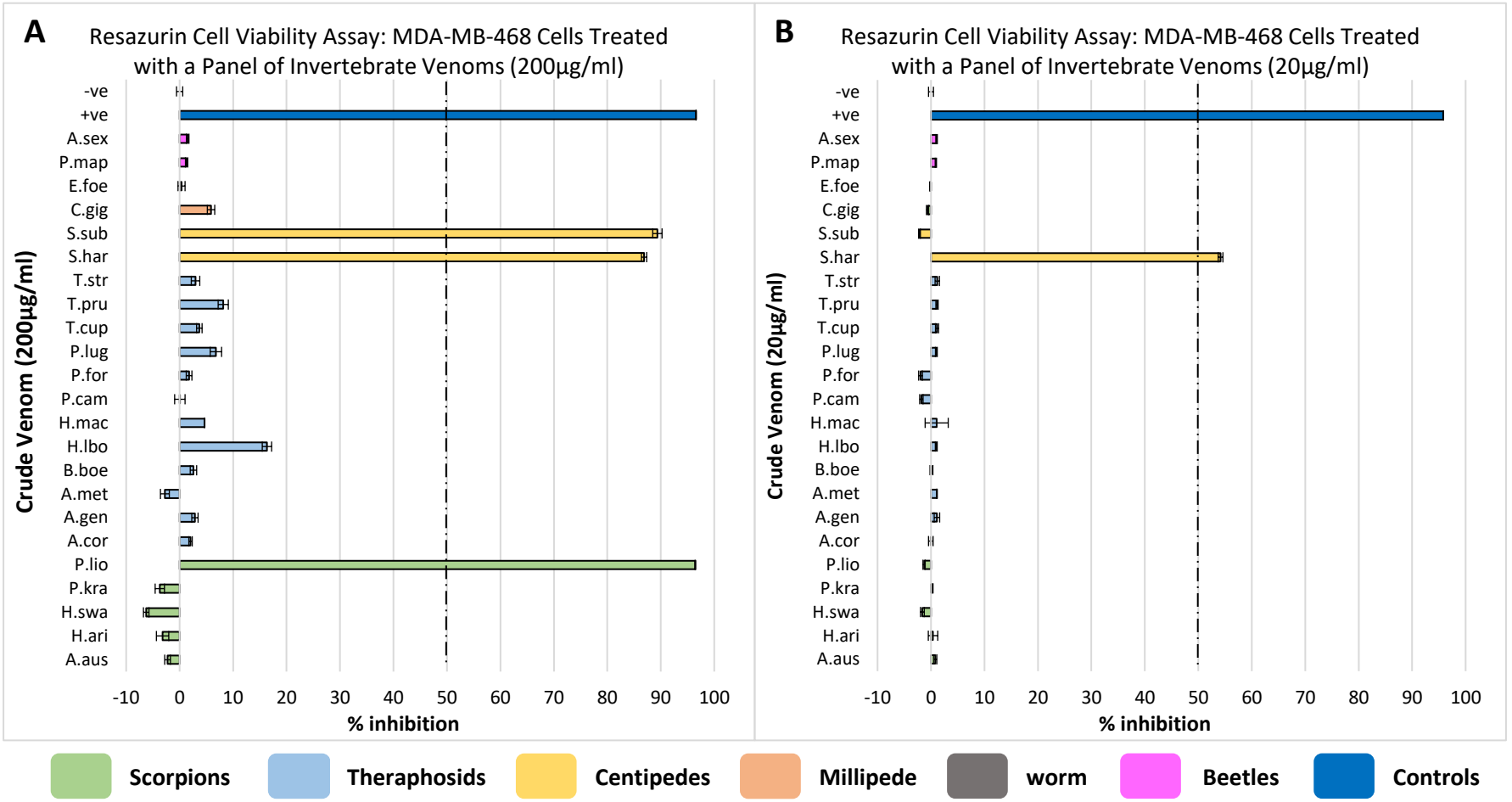

Figure 3.7: Graphical Analysis of Resazurin Invertebrate Toxicology Panel in MDA-MB-468 cells

Shows the % inhibition of MDA-MB-468 cells treated with whole invertebrate venoms at concentrations of 200 µg/ml **(A)** and 20 µg/ml **(B)** respectively. % Standard Error calculated and used for error bars of each graph. A percentage inhibition of 50% or greater was set as a biological significance threshold. Dotted line represents 50% inhibition threshold. Biological replicates/cell line = N1, Technical replicates/biological replicate = N3

A431 (Percentage Reduction in Cell Viability ± % SE)			MDA-MB-468 (Percentage Reduction in Cell Viability ± % SE)		
	200 µg/ml	20 µg/ml		200 µg/ml	20 µg/ml
Androctonus australis	1.92 (± 0.27)	0.39 (± 0.23)	*Androctonus australis*	-2.26 (± 0.53)	0.80 (± 0.29)
Hadrurus arizonensis	-0.36 (± 0.03)	-1.35 (± 0.00)	*Hadrurus arizonensis*	-3.19 (± 1.16)	0.38 (± 0.88)
Heterometrus swammerdami	-2.46 (± 0.23)	-0.67 (± 0.35)	*Heterometrus swammerdami*	-6.25 (± 0.51)	-1.61 (± 0.36)
Protoiurus kraepelini	0.52 (± 0.71)	0.46 (± 0.13)	*Protoiurus kraepelini*	-3.71 (± 0.87)	0.24 (± 0.14)
Parabuthus liosoma	16.03 (± 0.75)	-1.42 (± 0.18)	*Parabuthus liosoma*	96.45 (± 0.06)	-1.30 (± 0.21)
Acanthoscurria cordubensis	4.14 (± 0.40)	-1.14 (± 0.35)	*Acanthoscurria cordubensis*	2.04 (± 0.32)	-0.04 (± 0.43)
Acanthoscurria geniculata	6.52 (± 0.30)	0.96 (± 0.15)	*Acanthoscurria geniculata*	2.86 (± 0.59)	1.11 (± 0.52)
Avicularia metallica	4.32 (± 0.44)	1.27 (± 0.23)	*Avicularia metallica*	-2.76 (± 0.83)	1.09 (± 0.06)
Brachypelma Boehmei	4.74 (± 0.29)	-0.05 (± 0.38)	*Brachypelma Boehmei*	2.58 (± 0.60)	0.08 (± 0.27)
Cyriopagopus albostriatum	10.19 (± 0.43)	0.62 (± 0.18)	*Cyriopagopus albostriatum*	16.33 (± 0.87)	0.99 (± 0.17)
Heteroscodra maculate	6.54 (± 0.42)	-0.96 (± 0.61)	*Heteroscodra maculata*	4.66 (± 0.04)	1.06 (± 2.16)
Psalmopoeus cambridgei	4.43 (± 0.43)	0.31 (± 0.32)	*Psalmopoeus cambridgei*	0.04 (± 0.97)	-1.80 (± 0.32)
Poecilotheria Formosa	4.31 (± 0.54)	-1.20 (± 0.35)	*Poecilotheria formosa*	1.77 (± 0.53)	-1.95 (± 0.35)
Pterinochilus lugardi	6.75 (± 0.36)	0.31 (± 0.42)	*Pterinochilus lugardi*	6.78 (± 1.06)	1.00 (± 0.17)
Tapinauchenius cupreus	5.75 (± 0.05)	0.71 (± 0.64)	*Tapinauchenius cupreus*	3.69 (± 0.51)	1.13 (± 0.29)
Thrixopelma pruriens	6.08 (± 0.68)	1.47 (± 0.13)	*Thrixopelma pruriens*	8.15 (± 0.95)	1.12 (± 0.21)
Theraphosa stirmi	8.59 (± 0.34)	2.47 (± 1.87)	*Theraphosa stirmi*	2.97 (± 0.79)	1.17 (± 0.41)
Scolopendra hardwickei	24.24 (± 0.17)	39.88 (± 1.09)	*Scolopendra hardwickei*	86.87 (± 0.49)	54.16 (± 0.44)
Scolopendra subspinipes dehaani	59.92 (± 0.08)	1.17 (± 0.32)	*Scolopendra subspinipes dehaani*	89.37 (± 0.87)	-2.15 (± 0.17)
Colossobolus giganteus	9.42 (± 0.76)	1.42 (± 0.34)	*Colossobolus giganteus*	5.87 (± 0.69)	-0.65 (± 0.20)
Eisenia foetida	8.70 (± 2.16)	-0.45 (± 0.23)	*Eisenia foetida*	0.36 (± 0.66)	-0.16 (± 0.07)
Pachnoda marginata peregrina	3.47 (± 0.21)	1.58 (± 0.29)	*Pachnoda marginata peregrina*	1.31 (± 0.22)	0.91 (± 0.12)
Anthia Sexguttata	6.52 (± 0.77)	-2.42 (± 0.58)	*Anthia Sexguttata*	1.51 (± 0.23)	1.04 (± 0.14)

Table 3.5: Invertebrate Venom Panel % Reductions in MDA-MB-468 and A431 Cell Viability

Displays the % reductions ± % SE in MDA-MB-468 and A431 cancer cell lines in response to 20 µg/ml and 200 µg/ml doses of invertebrate venoms. Table colour coding separates invertebrate panel into scorpions (green), tarantulas (blue), centipedes (yellow), millipede (peach), worm (grey) and beetles (purple).The same colour coding has been used in this table as in Figures 3.6 & 3.7.

analysis against the 2 cancer cell lines. Significant biological reductions were only observed in MDA-MB-468 cells in response to *Parabuthus liosoma* (P.lio) venom at the higher tested dose of 200 µg/ml (Figure 3.7A). Reductions in cell viability were substantial, with around 95% cell loss observed following treatment at this particular dose (Table 3.5). Reduction in dose of *P. liosoma* venom resulted in a loss of this observed toxicity in MDA-MB-468 cells (Figure 3.7B). A431 cells showed no significant reductions to cell viability in response to treatment with *P. liosoma* venom or any of the other 4 selected scorpion venoms at either investigated dose (Figure 3.6). Whilst there is limited literature into the cytotoxic effects of *Parabuthus* venom, a study by Dyason *et al*. in 2002 identified pore-forming peptides in the venoms of some, but not all the *Parabuthus* species they tested. These peptides, identified by matrix-assisted laser desorption time-of-flight mass spectrometry, were hypothesised to be responsible for cell membrane disruption, which ultimately leads to cardiomyocyte cytotoxicity and cell death (Dyason *et al.*, 2002). The presence of these pore-forming peptides could potentially explain the MDA-MB-468 cell cytotoxicity observed with *P. liosoma* venom at the 200 µg/ml dose.

Whilst literature has indicated that venom from the genera *Hadrurus* has been found to contain peptides which display strong antimicrobial activity (Torres-Larios *et al.*, 2000; Trentini *et al.*, 2017), there is a lack of literature with regards to whether the venom contains peptides that are cytotoxic to eukaryotic cells. This supports the findings of the Resazurin assays, which showed no detectable cytotoxicity to either cancer cell line. Whilst the Resazurin assay data in this chapter identified no observable cytotoxicity against either cancer cell line, a paper published by Somay Dogan *et al*. in 2018 into the venom of *Protoiurus kraepelini* (P.kra), identified the venom to display cytotoxicity against Jurkat human T-cell leukaemia cell line. Doses of 0.5 and 1 mg/ml for 24h resulted in reductions in Jurkat cell viability of greater than 80%. Interestingly a dose of 250 µg/ml resulted in minimal reductions to cell viability (Somay Doğan *et al.*, 2018). This could explain why reductions in cell viability were observed in this study but not in the work carried out in this chapter. The maximum dose used for the invertebrate Resazurin panels in this study was 200 µg/ml with a dosing time of 2h only, and so a combination of both higher dose and longer exposure period to *P. kraepelini* venom may well result in toxicity to the cell lines investigated in this thesis.

Interestingly, it was surprising to see a lack of cytotoxicity following treatment with *Androctonus australis* (A.aus) venom, as cancer cell cytotoxicity has been demonstrated in previous literature to occur in response to this venom and the venoms derived from other individuals from the same genus. Treatment with whole *A. australis* venom has been shown to cause reductions in both lung (NCI-H358) and breast (MCF-7) cancer cell viability, with the venom found to cause significant

decreases, in a dose dependent manner (Béchohra, Laraba-Djebari and Hammoudi-Triki, 2016a; Nafie *et al.*, 2020). Mauriporin, isolated from the venom of related scorpion *Androctonus mauritanicus*, has been found to exert potent and selective cytotoxicity against prostate cancer cell lines (PC-3, LNCaP, DU145) (Almaaytah *et al.*, 2013), whilst *Androctonus amoreuxi* venom was shown to cause significant reductions to MCF-7 cell viability (Salem *et al.*, 2016). *Androctonus crassicauda* venom has also been shown to cause cytotoxicity in SH-SY5Y (neuroblastoma) and MCF-7 (breast) cancer cells (Zargan, Sajad, Umar, Naime, *et al.*, 2011), *Androctonus bicolor in* MDA-MB-231 (breast) and HCT-8 (colon) cells (Al-Asmari *et al.*, 2016) and *Androctonus crassicauda* venom to reduce the viability of BC3H1 (mouse brain tumour) following doses of 50-250 μg/ml (Caliskan *et al.*, 2013). Given that the dosing ranges selected for these venoms overlap with the highest tested doses in this study, differences in observed toxicity levels can likely be attributed again to differences in dosing durations, with all of these studies dosing cells for a minimum of 24h, in some cases for as long as 48-72h, before MTT or clonogenic survival assays were undertaken. It can be hypothesised based on the available literature that dosing MDA-MB-468 and A431 cells with *Androctonus australis* venom for an extended period of time, beyond the original 2h dosing timeframe, has the potential to result in observable levels of cellular cytotoxicity, similar to those found in these previous studies.

Similarly, whilst there is a lack of literature specifically for *Heterometrus swammerdami* (H.swa) venom, there is previous literature that has suggested that venoms from the genus *Heterometrus* can display cytotoxicity and anticancer properties. Venom, collected from *Heterometrus bengalensis* has been found to display cytotoxicity against human leukaemia cell lines U937 and K562, where IC50 values were determined to be 41.5 μg/ml and 88.3 μg/ml (Das Gupta *et al.*, 2007). Another study which looked at the proteomic and transcriptome analysis of venom from *Heterometrus petersii* identified 4 families of antimicrobial and cytolytic peptides within the venom, with cytolytic peptides identified as the most abundantly expressed toxin family in the venom gland transcriptome, where they accounted for approximately 14.4% of the expression sequence tags (ESTs) in the cDNA library (Ma *et al.*, 2010). A final study identified peptides Heterin-1 and -2, isolated from the venom *Heterometrus spinifer*, which were found to display haemolytic activity in a dose dependent manner (Wu *et al.*, 2014). The lack of cytotoxicity seen with *H. swammerdami* venom in the Resazurin screens, may be the result of differing cell sensitivities, with erythrocytes used in the Wu *et al*. study being naturally more sensitive to cell lysis. Alternatively, differences could be due to differing dosing times, with venom dosing in MTT assay carried out by Gupta *et al*. being undertaken for 48h, or simply due to differences in composition between the venoms investigated in the other literature and in the one specifically investigated in this chapter's toxicity screen.

Treatment of cancer cells wither venoms and secretions from other classes of invertebrates, including centipedes, millipede, worm and beetles resulted in a mixture of reductions and non-reductions in cancer cell viability. Treatment with two tested beetles (*Pachnoda peregrina* (P.map) & *Anthia sexguttata* (A.sex)) and one worm *(Eisenia foetida* (E.foe)) secretions resulted in no observable reductions to the viability of either cancer cell line at either of the tested doses. Treatment with secretions collected from millipede *Colossobolus giganteus* also resulted in no significant differences in cancer cell viability at either dose (Figures 3.6 & 3.7).

Treatment with the venom from two investigated centipede species (*Scolopendra hardwickei* (S.har) and *Scolopendra subspinipes dehaani* (S.sud)) both resulted in significant reductions to cancer cell viability in the cancer cell lines. MDA-MB-468 showed significant reductions (>90%) to both *Scolopendra* venoms when dosed with a concentration of 200 µg/ml (Figure 3.7A, Table 3.5), with significant reductions of ≈55% still observed in these cells when dosed with 20 µg/ml of *S. hardwickei* venom (Figure 3.7B, Table 3.5). A significant reduction of 60% was observed in A431 cells following treatment with *S. subspinipes dehanni* venom at 200 µg/ml (Figure 3.6A), however significant reductions were not observed at the lower tested dose (Figure 4.6B). Whilst reductions in cell viability were observed in A431 cells in response to *S. hardwickei* venom, they were below the previously set 50% viability reduction threshold and so they were considered to not be biologically significant (Figure 3.6).

There is mounting literature to suggest that centipede venoms display strong cytotoxic effects against cancerous mammalian cells. The venom of *Scolopendra subspinipes mutilans* has been identified to contain cytotoxic peptides which displayed specific inhibitory effects on the proliferation of human liver cancer (HepG2) and human gastric cancer cells (MGC) after 72h of treatment in a dose dependent manner (Kong *et al.*, 2013) and in mouse fibroblast cell line NIH3T3 after 24h of treatment (He *et al.*, 2019). Peptide scolopendrasin VII, isolated from the venom of *Scolopendra subspinipes mutilans* has been shown to decrease the viability of leukaemia cell lines U937 and Jurkat in MTS assay analysis, with acridine orange/ethidium bromide staining identifying the venom as causing this cell death via necrosis (Lee *et al.*, 2015). A similar study into *S. subspinipes mutilans* venom identified 2 further peptides, isoquinoline alkaloids -1 and -2 as having good cytotoxicity against a panel of five human cancer cell lines (HT-29, A549, U87, HeLa, Bel-7402, MGC-803), with IC_{50} values ranging from 1.19-31.28 µM and the lowest levels of cytotoxicity observed in normal human liver cell line L-02 (Ding *et al.*, 2016).

3.4 Conclusions

Cytotoxicity analysis, utilising the Resazurin assay to analyse whole snake and invertebrate venom panels, identified a large number of venoms that caused reductions to the viability of both MDA-MB-468 and A431 cancer cell lines. Cell line specific difference were observed following panel treatments, with the TNBC cell line MDA-MB-468 cells routinely displaying increased sensitivity to venom toxicity. True cobra venoms (Naja spp) proved consistently cytotoxic to both cell lines at the two highest tested doses, with one proving toxic to MDA-MB-468 cells at the lowest tested dose of 20 µg/ml. Other elapid venoms displayed varying levels of toxicity in both cell lines, with *Ophiophagus hannah, Dendroaspis viridis* and *Pseudechis rossignoli* venoms causing significant reductions to MDA-MB-468 cells, with only the latter causing significant reductions in A431 cells at the highest tested dose. The venom of *Dendroaspis polylepis* proved to be non-cytotoxic to both cell lines at doses as high as 2 mg/ml.

Overall, selected viper venoms *Vipera ammodytes ammodytes* and *Montivipera xanthina* proved less toxic to both cell lines than the tested pit viper and elapid venoms selected for the screen. Pit viper venoms proved more toxic to MDA-MB-468 cells, showing significant reductions to cell viability not seen in A431 cells at a dose of 200 µg/ml. Of all the screened pit viper venoms, *C. durissus vegrandis* venom appeared the least cytotoxic, providing the lowest reductions in MDA-MB-468 cell viabilities at doses of both 200 µg/ml and 2 mg/ml. Overall, invertebrate venoms proved less cytotoxic to cancer cells than snake venoms at the same tested doses, with the exception of venom extracted from *Scolopendra hardwickei*, which still caused substantial levels of cytotoxicity to MDA-MB-468 cells at a dose of 20 µg/ml. Whilst no theraphosid venoms proved significantly cytotoxic to either cancer cell line, one scorpion venom, *Parabuthus liosoma* was found to cause significant reductions to MDA-MB-468 cells only at a 200 µg/ml dose.

Substantial levels of literature back up the findings of the Resazurin screens, however IC_{50} levels and toxic doses observed between this data and the data in the literature vary substantially due to significant difference between dosing timeframes; with 24-72h dose periods commonly observed in the literature. The differences in dose time are the result of differing techniques, with MTT toxicity assays commonly run for extended periods of time before detection. Whilst whole venoms have been shown capable of toxicity against multiple cancer cell types, both in the literature and in the data of this chapter, the mechanisms of these toxicities are still unclear. A more targeted approach using venoms to cause cancer cell inhibition would prove more effective and reduce the chances of toxicity occurring to normal healthy mammalian cells. With this in mind, the selection of a cancer-specific or cancer-associated antigen to target with venoms would be a more appropriate progression. Previous experimentation, carried out in Chapter 3 into

receptor tyrosine kinases, identified whole venoms as causing changes to the combined phosphorylation/expression levels of many cellular surface receptors important for normal cell signalling cascades, including commonly TNBC over-expressed receptor EGFR. Given its prevalence as a hallmark antigen of TNBC, that it is well established as an important therapeutic target for the treatment of many different cancer types and that it would provide a more targeted approach than general cytotoxicity, it was determined that the venom panels screened in this chapter would be screened to see if the mechanism of action for the cytotoxicity could be inhibition of EGFR Phosphorylation specifically.

CHAPTER 4: Kinome Array Analysis for Identification of phosphorylation Changes in Receptor Tyrosine Kinase Family Members in Response to Whole Candidate Venoms

4.1 Introduction

4.1.1 Protein Tyrosine Kinases

The healthy functioning of all cells of the body is dependent upon the tightly controlled activation and deactivation of cellular signalling cascades (Ersahin, Tuncbag and Cetin-Atalay, 2015; Lake, Corrêa and Müller, 2016). The binding of ligands to receptors, followed by their subsequent activation leads to the induction of a variety of interconnected down-stream signalling cascades, which ultimately initiate the transcription of a variety of genes. These activated genes encode for proteins which play fundamental roles in many cell survival and death processes, such as cellular growth, differentiation, division, motility and apoptosis (Ersahin, Tuncbag and Cetin-Atalay, 2015; Lake, Corrêa and Müller, 2016). Activation of receptors on the cell membrane can be linked to the triggering of signalling cascades throughout the cytosol in many downstream interconnected pathways including the Ras/Raf/MAPKinase pathway (Pohlmann, Mayer and Mernaugh, 2009; Shin *et al.*, 2009; Lemmon and Schlessinger, 2010; Brand, Iida and Wheeler, 2011), PI3Kinase pathway (Yuan and Cantley, 2008; Chalhoub and Baker, 2009; Hynes and MacDonald, 2009; Pohlmann, Mayer and Mernaugh, 2009; Wong, Engelman and Cantley, 2010; Brand, Iida and Wheeler, 2011), PLCγ/PKC (Steinberg, 2008; Newton, 2010; Brand, Iida and Wheeler, 2011) and STATS (Quesnelle, Boehm and Grandis, 2007; Li, 2008; Mohr *et al.*, 2012) pathways, and Nuclear EGFR pathway (Wang and Hung, 2009; Wang *et al.*, 2010; Brand, Iida and Wheeler, 2011) amongst others.

Protein tyrosine kinases (pTKs) are a group of signalling proteins, responsible for propagating signalling cascades and initiating gene transcription. which can be categorised into 2 families based on whether they are membrane-bound or cytosol-free. pTKs can be broadly categorised into two families, consisting of 58 membrane-bound receptor tyrosine kinases and 32 cytosol-free non-receptor tyrosine kinases (Hubbard and Miller, 2007). Receptor tyrosine kinases are further classified into a variety of sub-families, which link them based on the compositional structure of their extra-cellular domain and the fundamental functional roles they play in continuing cell functionality. Receptor tyrosine kinases are broadly categorised into 20 sub-families (Zwick, Bange and Ullrich, 2002; Lemmon and Schlessinger, 2010) (Figure 4.1). Some of the more

characterised and functionally understood sub-families include EGFRs, platelet-derived growth factor receptors (PDGFR), Eph (ephrin receptors), insulin receptors, fibroblast growth factor receptors (FGFRs), vascular endothelial growth factor receptors (VEGFRs) and Met receptors (hepatocyte growth factor/scatter factor [HGF/SF]) (Hubbard & Miller 2007; Schlessinger, 2014).

Despite the overall conformational and structural homogeneity observed in tyrosine kinases, they display a diverse range of operational functions. Signalling mediated through members of this receptor group has been linked to the formation of new vascular tissue via angiogenesis (Shibuya, 2014), and interactions between cells and their extracellular matrix proteins (Fu *et al.*, 2013; Leitinger, 2014) amongst many other functions. Intracellular kinases are responsible for the continued propagation of downstream signalling cascades, ensuring subsequent gene activations beneficial to continued cellular viability. Ligand binding to RTKs or protein-protein interactions between nRTKs result in the activation of the receptor's intrinsic protein kinase domain, triggering enzymatic activity. This activation of enzymatic activity leads to the subsequent catalysis and phosphoryl transfer of γ-phosphate groups, from ATP donor molecules, onto tyrosine residues within the receptor's own polypeptide chain or within other protein substrates.

Despite belonging to a variety of sub-families with diverse biological activities RTKs share a highly conserved receptor structure, including components such as a large, highly glycosylated extracellular domain containing a ligand binding region, a transmembrane domain and an intracellular cytoplasmic region. The cytoplasmic region comprises a juxtamembrane domain, a catalytic tyrosine kinase domain and a terminal carboxyl tail. The characteristic structure of different receptors' extracellular domains influences the classification of each receptor into its relevant sub-group, with receptor extracellular domains including cysteine-rich motifs, fibronectin type III or immunoglobulin-like repeats amongst others (Figures 4.1 & 4.2) (Hubbard, 2000; Bazley & Gullick 2005; Hunter 2009; Li, 2010; Du 2018)

The transmembrane domain functions to anchor the receptors securely within the plane of the cell plasma membrane, thereby allowing the receptors to interact with both the intracellular and extracellular environments of the cell. The juxtamembrane region plays an active role in RTK dimerisation, ensure proper alignment between the pair of receptors, engage in the process of receptor transmodulation, and involved in downregulation and ligand-dependent internalisation. Juxtamembrane domains are highly conserved between members of the same RTKs family but show divergence between members of separate sub-families (Jorissen *et al.*, 2003).

The tyrosine kinase domain is essential for efficient receptor signalling and is the most conserved region across all the different RTK sub-families. Kinase domains contain kinase insertion regions

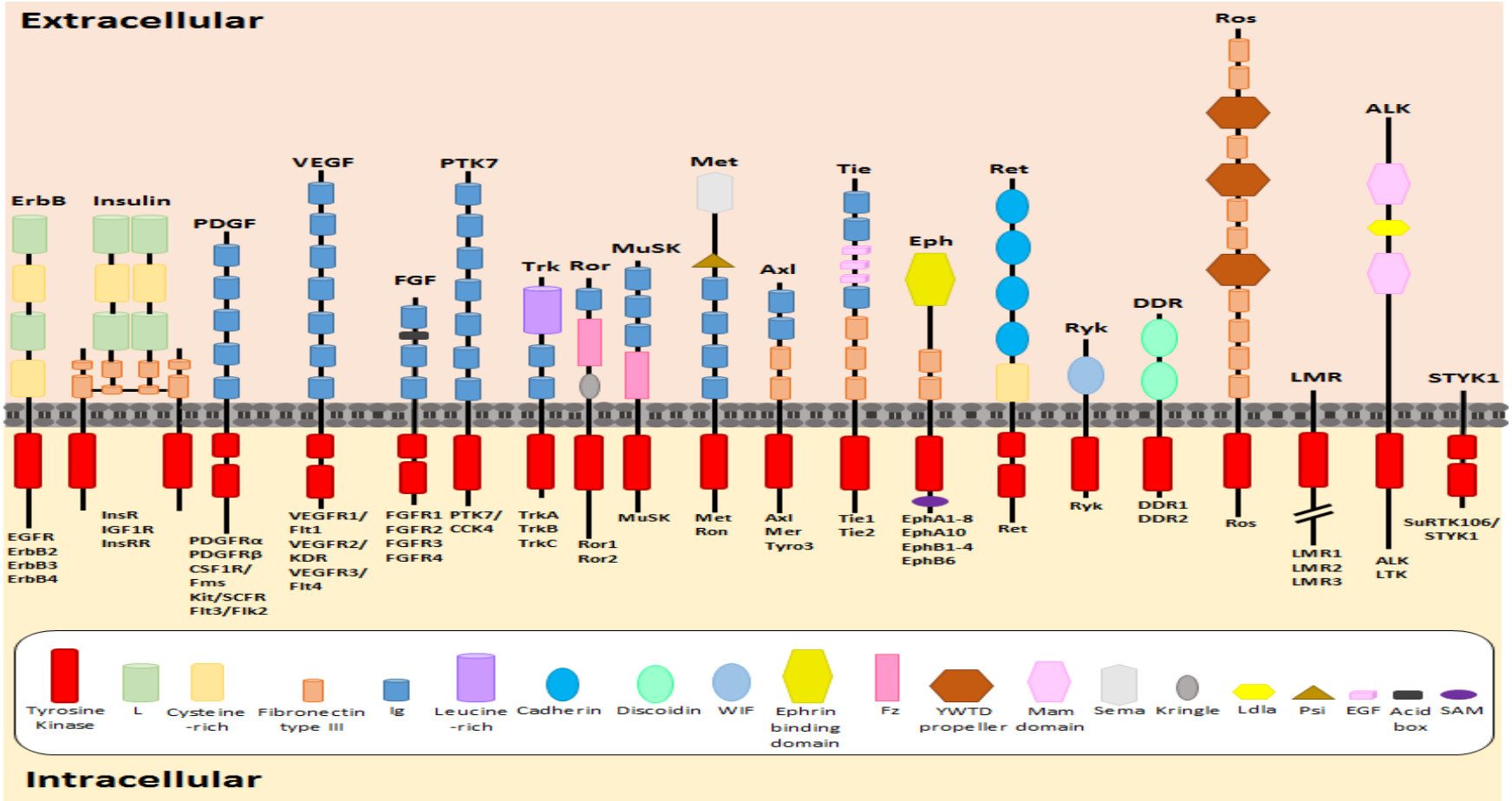

Figure 4.1: Receptor Tyrosine Kinase Subfamily Categorisation

Displays the highly conserved structure of all 58 RTKs but shows the individual extracellular characteristic subgroups and overall domain structures. The composition of each RTK's extracellular domain dictates its classification into its relevant sub-family. Figure adapted from (Lemmon, 2010)

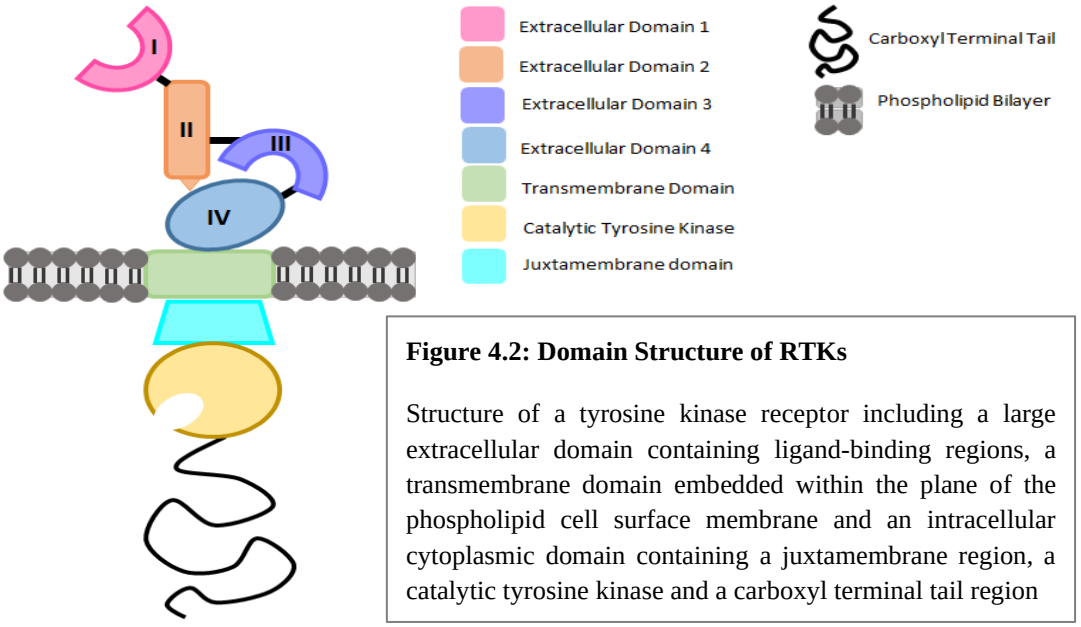

Figure 4.2: Domain Structure of RTKs

Structure of a tyrosine kinase receptor including a large extracellular domain containing ligand-binding regions, a transmembrane domain embedded within the plane of the phospholipid cell surface membrane and an intracellular cytoplasmic domain containing a juxtamembrane region, a catalytic tyrosine kinase and a carboxyl terminal tail region

(composed of up to 100 amino acid residues) which mediate interactions of secondary messengers with the TK receptor and auto-phosphorylation sites. Autophosphorylation sites undergo phosphorylation when the kinase becomes active, further enhancing receptor activity (Ullrich and Schlessinger, 1990; Wilden *et al.*, 1992; Bae and Schlessinger, 2010; Endres *et al.*, 2014). The carboxyl-tail region of the receptor regulates kinase activity by also undergoing phosphorylation. Carboxyl-terminal tail regions are extremely diverse between RTKs and the subsequent number and location of specific tyrosine residues within the carboxyl tail region of each different RTK is essential for the activation of specific signalling cascades. The absence of certain tyrosine residues within specific loci in the carboxyl tail may render a RTK incapable of activating certain signalling cascades (Schulze, Deng and Mann, 2005; Linggi and Carpenter, 2006; Burgess, 2008).

Tyrosine Kinases (TKs), comprise a large family of cellular surface receptors and intracellular catalytic proteins, whose activation and signalling are fundamental to the subsequent triggering of many downstream signalling cascades (Hunter, 2009b). Many types of human cancers display some kind of aberrant expression profile or functional mutation of key players of cell signalling pathways. There is strong evidence suggesting causative association between dysfunctional behaviours in tyrosine kinases and cancer. Changes in tyrosine kinases such as constitutive activation through kinase domain duplications (KDD) (Gallant *et al.*, 2015; Gay *et al.*, 2017), somatic mutations (Robertson *et al.*, 1998; Wu *et al.*, 2000; Heinrich *et al.*, 2003; Marchetti *et al.*, 2005; Sharma *et al.*, 2007; Brewer *et al.*, 2013; Ou *et al.*, 2017), gene amplification and receptor over-expression (Menard *et al.*, 2001; Selvaggi *et al.*, 2004; Hanawa *et al.*, 2006; Lopez-Gines *et al.*, 2010; Ha *et al.*, 2013) and chromosomal rearrangement or gene fusions (Huang *et al.*, 2011; Medves and Demoulin, 2012; Takeuchi *et al.*, 2012; Dacic *et al.*, 2014; Lovly, Gupta, *et al.*, 2014;

Stransky *et al.*, 2014; Wiesner *et al.*, 2014; Chmielecki *et al.*, 2015; Konduri *et al.*, 2016) have been linked to cancer development and progression (Du and Lovly, 2018). Yet despite the mounting evidence for the key role tyrosine kinases play in cancer development, the full range of members that may be linked to the progression of oncogenic development is still not completely understood (Valiathan *et al.*, 2012).

4.1.2 Venom Components and Poisonous Secretions Targeting RTKs

Despite the extensive role receptor tyrosine kinases have been shown to play in the development and progression of many types of cancer and despite the large amount of emerging evidence showing the potential for whole and venom-isolated compounds to display anti-oncogenic properties, very little research has been carried out into the ability of venoms to regulate the expression or phosphorylation of RTK family members. Venoms components isolated from a handful of highly diverse species, including cobras, vipers, toads and centipedes have been shown capable of modulating the activity of members of the RTK superfamily, some of which are known to often play key roles in aggressive cancers subtypes.

Cardiotoxin III (CTX3), a basic 60aa polypeptide derived from the venom of *Naja atra* (Chinese cobra/Taiwan cobra) from the family *Elapidae*, has been shown to display cytotoxicity to A549 lung cancer cells through the inhibition of EGFR phosphorylation (Su *et al.*, 2010). A similar study by Tsai et al. 2012 into CTX3 found it suppressed cell metastasis in MDA-MB-231 TNBC cells by blocking EGFR phosphorylation. This led to ERK1/2 and PI3K/Akt downstream signal-pathways blockage, and ultimately decreased matrix metalloproteinase-9 expression (Tsai *et al.*, 2012). Su et al. 2010 showed EGFR-phosphorylation blockage led to reduced activation of downstream signal proteins PI3K/Akt, Janus tyrosine kinase-2 (JAK2) and activator of transcription STAT3 (Su *et al.*, 2010). CTX3 was also shown to display anti-metastatic and anti-invasive properties in MDA-MB-231 cells via the suppression of hepatocyte growth factor (HGF) induced c-MET phosphorylation (Tsai *et al.*, 2014). A follow up study published by the same group also found that CTX3 from *Naja naja atra* inhibited EGFR phosphorylation in triple-negative MDA-MB-231 breast cancer cells, resulting in a loss of activation of downstream signal cascade proteins phosphatidylinositol 3-kinase (PI3K)/Akt and ERK1/2. CTX3 was also found to inhibit the migration and invasion potential of these cells through the suppression of both EGF/EGFR activation and epithelial-mesenchymal transition (EMT) (Tsai *et al.*, 2016).

Crotoxin, a phospholipase A2 isolated from the venom of *Crotalus durissus terrificus* (South American Rattlesnake) has been reported to display anti-proliferative properties against squamous carcinoma cell lines, A431 and ME-180. Anti-proliferative properties of crotoxin were attributed

to its ability to regulate EGFR. The results of the study suggested an association between high level EGFR expression and enhanced cellular sensitivity to the phospholipase A2 activity of crotoxin. The study also found that crotoxin appeared to cause increased EGFR phosphorylation levels in both cells lines (Donato *et al.*, 1996). A more recent study investigating crotoxin from the same snake also showed stimulation of EGFR phosphorylation, however they were unable to establish the significance of this observation (Wang *et al.*, 2012).

A study into the effects of alcoholic extracts from the centipede Scolopendra (AECS) by Ma *et al.* in 2015 demonstrated its potential use in the inhibition of EGFR-dependent cancers. Experimental data showed that AECS inhibited cellular proliferation in high-EGFR expressing cell lines A431, HEK293 and HEK293/EGFR. Proposed mechanisms for this observation included the induction of apoptosis and the regulation of EGFR-dependent signalling cascades by altering EGFR-kinase phosphorylation and activity levels (Ma *et al.*, 2015).

A study by Li *et al*. in 2012 investigated the potential of arenobufagin to inhibit angiogenic processes by targeting the VEGF/VEGFR-2 signalling pathways. Arenobufagin is a bufadienolide, secreted from the postauricular and skin glands of the toads *Bufo bufo gargarizans Cantor* (Asiatic toad) or *Bufo melanostictus Schneider* (Asian common toad). Experimental data showed that arenobufagin inhibited human umbilical vein endothelial cells' (HUVECs) viability, cell migration and invasion. Similarly, it prevented the angiogenic process of VEGF-induced vascular vessel sprout formation by inhibiting VEGFR-2 kinase activation. Arenobufagin inhibited VEGFR-2 phosphorylation and subsequently the downstream phosphorylation of Akt and mTOR without affecting their overall expression levels. Computational docking simulations suggested interactions between arenobufagin and the ATP-binding domain of VEGFR-2 kinase are responsible for these observations (Li *et al.*, 2012). The inhibition of VEGFRs through the administration of arenobufagin is a potentially interesting find as the over-expression or aberrant signalling of VEGFRs has been linked heavily to the developmental progression of cancer, where it aids both angiogenesis and metastasis (Guo *et al.*, 2010; Rodríguez-Antona *et al.*, 2010; Rapisarda and Melillo, 2012; Kopparapu *et al.*, 2013; Ning *et al.*, 2013).

A study by Huh *et al*. in 2010 showed the potential of bee venom in the inhibition of angiogenesis and metastasis in lung cancer, through the downregulation of the expression of VEGF and VEGFR-2. Their study found that treatment with bee venom inhibited the cellular viability of cancer cells without exhibiting direct cytotoxicity, downregulated the expression of VEGFR-2 in Lewis lung carcinoma (LLC) and Human umbilical vein endothelial cell (HUVECs) cells, blocked the VEGFR-2 signalling pathway by interfering with AKT and p42/44MAPK activation

and inhibited the VEGF-induced migration, proliferation and capillary formation of endothelial cells (Huh *et al.*, 2010).

Whilst venoms have been shown in previous literature to hold great potential for the targeted treatment of cancer, the field of research is still relatively novel and there is a large number of venoms from unexplored genera still to be characterised. The investigation into whether they could be used in a more target-specific manner, rather than for direct cell cytotoxicity, is still relatively under-explored. The move to more targeted patient therapies, such a small molecules and antibodies, over more systemic treatments is gaining pace. These targeted therapies have been shown to provide therapeutic benefit with less undesirable of-target side-effects then conventionally used treatments. There is very little in the literature with regards to the investigation of venoms, particularly those from invertebrate classes, displaying receptor targeting effects in cancer cells. Whilst, there has been more interest in snake venoms, research confirming effects which target RTKs are still limited. With this in mind it was decided that the screening of 49 RTKs with whole venoms, from the widest possible range of genera, could enable the identification of novel lead venoms for alteration of RTKs shown to be over or under-expressed in cancer, as well as those previously shown to be difficult to drug using existing therapies.

4.1.3 Venom Selection

Venoms were selected from a diverse range of species to enable the greatest versatility in venom composition. Published research literature was consulted to enable the selection of novel venoms or previously investigated venoms, displaying anti-cancer potential. Selected venoms were chosen for novel research into their effects against a panel of RTKs. Human RTK arrays, with representative members from most receptor tyrosine kinase sub-families were obtained to allow for a wide range of potential novel targets to be investigated. Venoms selected for this investigation included those extracted from the Indian cobra *Naja naja*, the Uracoan rattlesnake *Crotalus durissus vegrandis*, the Western green mamba *Dendroaspis viridis*, the Giant forest scorpion *Heterometrus swammerdami*, the African black tail scorpion *Parabuthus liosoma* and the Brazilian white-knee tarantula *Acanthoscurria geniculata* (See Table 4.1). The TNBC cell line, MDA-MB-468 was selected to be screened for potential changes to RTK expression/phosphorylation in response to venom treatments. Triple negative breast cancers have poor patient prognosis due to a lack of expression of the three main receptors upregulated in breast cancer, oestrogen, progesterone and RTK HER2, making this type of breast cancer an attractive target for novel therapy development. Whilst MDA-MB-468 cells do not over-express HER2, the cell line does however over-express EGF RTK (Simon *et al.*, 2016).

Extensive research into the effects of venom from a wide variety of cobras, including *Naja naja* and many of its classified sub-species, have shown its propensity for cancer inhibition and apoptosis (Gomes *et al.*, 2010; Lin *et al.*, 2010; Das *et al.*, 2011, 2013; Tsai *et al.*, 2012, 2014; Yen *et al.*, 2013; Ebrahim *et al.*, 2016; Attarde and Pandit, 2017; Fakhri *et al.*, 2017). The continued evidence of cancer inhibition and apoptosis inducing effects make venom from this family of venomous snakes interesting to investigate for possible RTK altering molecules, and so *Naja naja* venom was selected to take forward for further investigation.

Whilst less extensive research has been carried out into the inhibitory effects of mamba venom on cancer, mambas form a distinct group of four species that (like the cobras) belong to the larger family Elapinae. Two toxin peptides which are members of the three-finger superfamily, isolated from the venom of eastern green mamba *Dendroaspis angusticeps* have been found to display anti-tumour activities against non-small cell lung cancer adenocarcinoma A549, an EGFR-over-expressing lung cancer type (Conlon *et al.*, 2014). Prokineticins, identified in the venom of black mamba *Dendroaspis polylepis* have been shown to inhibit angiogenesis in cancer cells through alterations in prokineticin receptors, known to play roles in angiogenesis in many cancer types (Monnier and Samson, 2010). Despite the limited research, evidence does suggest the potential for mamba venoms to display anti-oncogenic properties. Due to the potential novel molecules that could be contained with mamba venoms it was decided that Dendroaspis viridis venom would be selected for investigation.

Research into venoms derived from *Crotalinae* pit vipers have shown extensive inhibition of cancer cell proliferation, migration and survival by both whole and components purified from their venoms. In particular, extensive research has been carried out into the anticancer effects of venom derived from pit viper species *C. durissus terrificus*, including research that has shown isolated components effective against highly aggressive triple negative breast cancer cell line MDA-MB-231 (Donato *et al.*, 1996; Marcussi *et al.*, 2011; Wang *et al.*, 2012; Calderon *et al.*, 2014; Araújo *et al.*, 2016; Teixeira *et al.*, 2016; Gimenes *et al.*, 2017; Muller *et al.*, 2018; Oliveira *et al.*, 2018). Whilst Venomtech Ltd does not house this particular sub-species of *Crotalus durissus* they do house closely related species *Crotalus durissus vegrandis* and so it was decided that venom from this sub-species may prove interesting to investigate further.

Two scorpion species were selected to take forward for the RTK panel screen, one belonging to the family *Scorpionidae* and one from the family *Buthidae*. Research into the scorpion genus Heterometrus has identified venom components that have been shown to actively inhibit cancer progression and survival. Bengalin, a peptide isolated from the venom of *Heterometrus Bengalensis* has been shown to display anti-proliferative and apoptotic effects against two human

leukaemia cell lines, U937 and K562 (Das Gupta *et al.*, 2007; Gupta *et al.*, 2010; Moradi *et al.*, 2018). Research published in 2015 into the effects of whole venom from *Heterometrus liangi* on the proliferation of human oesophageal cancer cell line KYSE-510, found marked morphological changes in cell appearance post-treatment, dose-dependent inhibition of cell proliferation, the induction of apoptosis and necrosis and an increase in the protein expression levels of p21 and caspase-3 (Xiao *et al.*, 2012; Li, Xiao and Wang, 2015). Due to scorpion availability and a lack of research undertaken into this scorpion genus it was decided that venom from *Heterometrus swammerdami* would be selected.

Extensive research has been carried out into the effects of buthid family scorpion venom on cancer. The family Buthidae broadly consists of the genera *Androctonus, Buthus, Buthotus, Leirus, Mesobuthus* and *Parabuthus* found within Africa and Asia and *Centruroides* and *Tityus* found in America (Gómez Rave *et al.*, 2019). Research into the effects of venom isolated from buthid scorpions *Androctonus crassicauda, Androctonus bicolor* and *Leiurus quinquestriatus* has shown its propensity to inhibit breast and colorectal cancer cell lines, HCT-8, HCT-116 and MDA-MB-231. Two studies have shown that treatment with these scorpion venoms resulted in cytotoxicity in a dose- and time-dependent manner, cell cycle arrest, enhanced apoptotic cell presence, increased levels of reactive oxygen species (ROS) and inhibition of matrix metalloproteases leading to loss of metastatic potential in these cell lines (Al-Asmari *et al.*, 2016; Al-Asmari, Islam and Al-Zahrani, 2016; Al-Asmari, Riyasdeen and Islam, 2018). Whole Androctonus species venom and components isolated from it, have been shown capable of cytotoxic effects against a variety of cancer types including lung (NCI-H358) (Béchohra, Laraba-Djebari and Hammoudi-Triki, 2016b), Prostate (PC-3, LNCaP, DU145) (Almaaytah *et al.*, 2013), breast cancer and neuroblastoma (MCF-7, SH-SY5Y) (Zargan, Sajad, Umar, Naime, *et al.*, 2011). Similar effects have been seen following treatment with American buthid venoms, with cytotoxic effects seen in breast cancer (SKBR3) following treatment with peptides isolated from *Tityus discrepans* venom (D'Suze *et al.*, 2010; Olvera *et al.*, 2016) and cervical cancer (SiHa, HPV-16 and HeLa-18) following *Tityus serrulatus* venom treatment (Bernardes-Oliveira *et al.*, 2019). Treatment with margatoxin (MgTX), isolated from the venom of *Centruroides margartatus* resulted in inhibition of proliferation of lung adenocarcinoma cells A549 (Jang *et al.*, 2011). Whilst some sub-families of buthid venoms have been properly characterised for their anti-cancer properties, others such as *Parabuthus* species are still poorly researched. Due to this lack of current research, it was decided that venom from *Parabuthus liosoma* would be selected to take forward for investigation.

Finally, a theraphosid venom was to be selected for investigation to add another level of diversity. Very little research has been undertaken into the venom composition and effects of theraphosid venoms, and their potential anti-cancer properties are poorly investigated, making this a highly novel and diverse field for investigation. Gomensin, an antimicrobial peptide isolated from the venom of *Acanthoscurria gomesiana* has been shown to display anticancer properties, *in vitro* against human neuroblastoma cells SH-SY5Y and rat pheochromocytoma cells (PC-12) (Soletti *et al.*, 2010), and both *in vitro* and *in vivo* against murine melanoma cell line B16F10-Nex2 (Rodrigues *et al.*, 2008). As there is very little research into the anticancer properties of many genera and species of theraphosids, it was decided that a species from a similar genus would be selected for investigation and so venom from *Acanthoscurria geniculata* was chosen.

Code	Name	Family	Common Name
A.gen	*Acanthoscurria geniculata*	Theraphosidae	Brazilian White-Knee Tarantula
H.swa	*Heterometrus swammerdami*	Scorpionidae	Giant Forest Scorpion
P.lio	*Parabuthus liosoma*	Buthidae	African Black Tailed Scorpion
C.dve	*Crotalus durissus vegrandis*	Crotalinae	Uracoan Rattlesnake
N.naj	*Naja naja*	Elapinae	Indian Cobra
D.vir	*Dendroaspis viridis*	Elapinae	Western Green Mamba

Table 4.1: Panel of Venoms Selected for Kinome Array Analysis

Panel includes venoms extracted from a variety of venomous genera, including Brazilian white-knee tarantula *A. geniculata*, Giant forest scorpion *H. swammerdami*, African black tailed scorpion *P. liosoma*, Uracoan rattlesnake *Crotalus durissus vegrandis*, Indian cobra *Naja naja* and Western green mamba *Dendroaspis viridis*

4.1.4 Chapter Aims

- To optimise the concentration of venoms to take forward for kinome profiling using Coomassie gel analysis of venom treated MDA-MB-468 cell lysates at a series of dilutions.

- To screen MDA-MB-468 cell lysates, treated with the optimal concentration of each selected venom for effects against the combined expression/phosphorylation levels of a panel of 49 Receptor tyrosine kinases (RTKs)

- To analyse the data obtained from kinome RTK arrays to determine where significant increases or reductions in phosphorylation are occurring in response to venom treatment

- To confirm potential changes in EGFR phosphorylation/expression levels in response to venom treatment using phosphor-tyrosine and pan-EGFR Western blots

<u>Disclaimer</u>: The experimental work in this chapter was undertaken in conjunction with a master's by research student. Whilst the raw data has already been submitted for her master's by research degree, the data analysis, interpretation and its discussion within the context of the wider scientific literature carried out in this thesis chapter is novel and was carried out solely by me.

4.2 Methods

4.2.1 Determining the Protein Concentration of Each Venom via DS-11 Analysis

The protein concentration of all the whole venoms of interest were determined using a DeNovix DS11 spectrophotometer as via the standard protocol in **2.3.1.1**. Lyophilised venoms were reconstituted in RNAse/DNAse free distilled H_2O. Venoms used in these experiments were *Acanthoscurria geniculata* (A.gen), *Crotalus durissus vegrandis* (C.dve), *Dendroaspis viridis* (D.vir), *Heterometrus swammerdami* (H.swa), *Parabuthus liosoma* (P.lio) and *Naja naja* (N.naj) (See Appendix VIII).

4.2.2 Determining the Ideal Concentration of Each Venom to Use for Kinome Arrays, Using Coomassie Stained Polyacrylamide Gels

7%, 9% and 12% SDS PAGE were utilised as via the protocol laid out in **2.3.2.** Once gels were sufficiently run, they were stained for protein visualisation with Coomassie blue dye as via protocol **2.3.3.1**.

4.2.3 Kinome Array

MDA-MB-468 cells were grown in flasks with a $25cm^2$ surface area to 90% confluency in supplemented DMEM via standard procedures laid out in **2.1.2**, before being treated with the selected concentrations of each of the following venoms; *A. geniculata*, *C. durissus vegrandis*, *D. viridis*, *H. swammerdami*, *P. liosoma* and *N .naja*. Cells were incubated at 37ºC, 5% CO_2 for 2h to allow the venom to take effect. Cells were stimulated with $1x10^{-7}$M EGF for 5 min and lysed using 1ml of lysis buffer, containing protease and phosphatase inhibitors, per flask. The lysis was carried out as via the standard protocol laid out in **2.2.2** and **2.2.3**. 100µl of each lysate was collected and mixed with 25µl of 5x sample buffer. These samples were heated to 100ºC for 10 min before being stored at -20ºC until Coomassie and Western blot analyses was undertaken.

Remaining lysates were collected and diluted using buffer provided in the Human Phospho-RTK Array Kinome Kit (R&D systems). Kinome blot membranes were pre-blocked and washed using the reagents and protocol provided with the kit. Diluted lysate samples were loaded onto the blots and incubated overnight at room temperature on a rocker (~25ºC). Lysate samples were removed, the blots rewashed and probed with primary and secondary antibodies provided with and according to the kit protocol. Array membranes were developed using a Biorad ChemiDoc and provided chemiluminescent reagents. All arrays were imaged simultaneously for a series of

different exposure times to obtain the optimal exposure timepoint. Antibodies for each receptor were laid out as via the Phospho-Array template in Appendix IX.

4.2.4 ImageLab Analysis of Kinome Arrays

Kinome Array images were analysed using Biorad's ImageLab software. Lanes and pairs of dots were identified, allowing for the production of a pixel intensity from each duplicate pair of receptor dots (See Appendix X). A fold change in intensity was created by dividing the intensity of each venom treated receptor by the intensity generated from the positive control of each receptor (No venom, +EGF). Changes in receptor phosphorylation/expression were then displayed graphically as a fold-change in intensity, relative to the positive control receptor intensity levels. Receptors with a 2-fold or greater increase or decrease, relative to the positive control receptor intensity were considered further (see Appendix XI).

4.2.5 Coomassie Gel Analysis of Total Protein in MDA-MB-468 Cell Lysates After 2h Treatment with Venoms.

15µl (≈40µg) of each cell lysates previously produced in **4.2.3** were loaded on a 12% polyacrylamide gel and ran through SDS PAGE as via the protocol laid out in **2.3.2.** Once gels were sufficiently run, they were stained for protein visualisation with Coomassie blue dye as via protocol **2.3.3.1**. Gels were imaged using a Biorad gel doc and the overall proteome level compared for consistency.

4.2.6 Western Blot Analysis of EGFR Phosphorylation Levels in MDA-MB-468 Cell Lysates After 2h Treatment with Venoms.

15µl of each cell lysates previously produced in **4.2.3** were loaded on a 9% polyacrylamide gels and ran through SDS PAGE as via the protocol laid out in **2.3.2.** Once gels were sufficiently run proteins were transferred to nitrocellulose and probed with PY20, F4 and anti-β actin primary antibodies as via protocol **2.3.3.2** and **2.3.3.3**. Blots were imaged as standard using ECL reagents and Biorad ChemiDoc. Western blot bands were analysed using ImageLab software.

4.3 Results and Discussion

4.3.1 Determining the Ideal Dilution of Each Venom to Use for Kinome Arrays, via Coomassie Gel

Coomassie stained SDS PAGE gels of MDA-MB-468 cell lysates from cells treated with a dilution of (1/50-1/1,000,000) the 6 venoms to be investigated for RTK phosphorylation effects, showed varying degrees of cytotoxicity towards the cells. Slight reductions in total protein amount were observed in the lysates of MDA-MB-468 cells treated with the highest three doses of *A. geniculata* (A.gen) venom. However, these discrepancies in total protein could be the result of slightly uneven protein loading in the samples rather than cytotoxicity (Figure 4.3A). As there was still plenty of detectable protein at all of these doses it was decided that a concentration of 1/100 (2.5 mg/ml) would be selected as most appropriate.

Dosing with both *Dendroaspis viridis* (D.vir) and *Naja naja* (N.naj) venoms at the selected dose range resulted in significant cytotoxicity at the highest two and three concentrations respectively (Figure 4.3B and 4.3C). Complete degradation and or loss of the cellular proteome were observed at all these doses, and so these higher doses were not considered appropriate for taking forward to kinome array analysis. Both snake venoms displayed very similar total protein concentrations and cellular cytotoxicity profiles despite originating from different genera, *Naja* (cobra) and *Dendroaspis* (mamba), however this is not entirely surprising as both snakes belong to the larger family Elapidae. It is likely that both venoms contain some conserved families of proteins and peptides with similar mechanistic actions, as well as having protein differences specific to their genera variations. With that in mind, it was decided that for a better contrast and comparison of effects that both venoms would be taken forward for kinome array analysis at the same dose of 1/10,000 (25 µg/ml).

Dosing MDA-MB-468 cells with *Crotalus durissus vegrandis* (C.dve) venom resulted in no observable cellular toxicity as shown by a lack of loss of cellular proteome in the undertaken Coomassie gel analysis (Figure 4.3D). Analysis of this venom showed it had a much lower whole concentration than either of the elapid snake venoms, which may account for the lack of some of the cytotoxicity observed by treatment of the other two. However, *Crotalus durissus vegrandis* belongs to a completely different family of snakes, the crotalinae (pit vipers) and so its venom concentration and activity cannot be directly compared to the activity of the other 2 snake venoms. Despite the lack of cytotoxicity up to doses as high as 1/50, it was decided that a dose of 1/1000 (65 µg/ml) be taken forward for kinome array analysis.

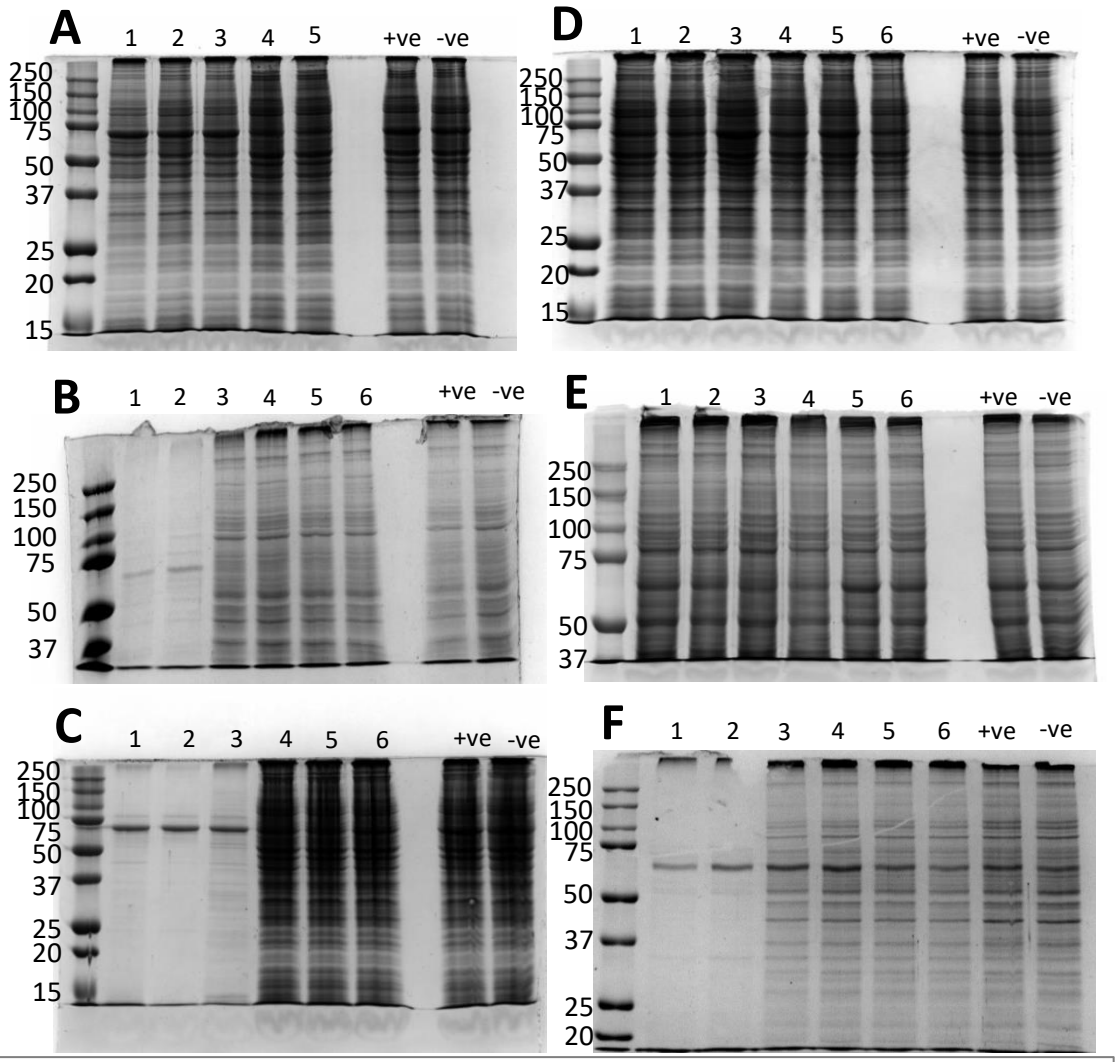

Figure 4.3: Coomassie Gel Analysis of Venom Toxicities

A. MDA-MB-468 cell lysates from cells treated with a serial dilution of whole *A. geniculata* venom lanes **1-5 (1:**1/50, **2:**1/100, **3:**1/1000, **4:**1/10,000, **5:**1/100,000, respectively). **B.** MDA-MB-468 lysates from cells treated with a serial dilution of whole *D. viridis* venom lanes **1-6 (1:**1/50, **2:**1/100, **3:**1/1000, **4:**1/10,000, **5:**1/100,000, **6:**1/1,000,000 respectively). **C.** MDA-MB-468 lysates from cells treated with a serial dilution of whole *N. naja* venom **1-6 (1:**1/50, **2:**1/100, **3:**1/1000, **4:**1/10,000, **5:**1/100,000, **6:**1/1,000,000 respectively). **D.** MDA-MB-468 lysates from cells treated with a serial dilution of whole *C .durissus vegrandis* venom **1-6 (1:**1/50, **2:**1/100, **3:**1/1000, **4:**1/10,000, **5:**1/100,000, **6:**1/1,000,000 respectively). **E.** Displays the Coomassie gel analyses of MDA-MB-468 lysates from cells treated with a serial dilution of whole *H. swammerdami* venom **1-6 (1:**1/50, **2:**1/100, **3:**1/1000, **4:**1/10,000, **5:**1/100,000, **6:**1/1,000,000 respectively). **F.** MDA-MB-468 lysates from cells treated with a serial dilution of whole *P. liosoma* venom lanes **1-6 (1:**1/50, **2:**1/100, **3:**1/1000, **4:**1/10,000, **5:**1/100,000, **6:**1/1,000,000 respectively)

All positive controls were produced from MDA-MB-468 cells treated with $1x10^{-7}$M EGF (No venom, +EGF). All negative controls were produced from untreated MDA-MB-468 cells (No venom, -EGF). No discernible difference in protein concentration was distinguishable between the +ve and -ve controls, as lysates are derived from the same cell type but due to differing EGF stimulation will present with different phosphorylation profiles (not observable by Coomassie gel analysis) Biological replicates/whole venom = N2

Analysis of treatment with *Heterometrus swammerdami* (H.swa) venom at the selected range showed no observable cytotoxicity or loss of cellular proteome and so it was determined that doses as high as 1/50 (2 mg/ml) would be suitable to take forward for subsequent kinome array analysis (Figure 4.3E). However, dosing with *Parabuthus liosoma* (P.lio) venom resulted in cellular cytotoxicity at the 2 highest selected doses of 1/50 and 1/100 (Figure 4.3F). Complete loss of proteins in the cell lysate was observed with both these doses, whilst doses of 1/1000 or less resulted in no cellular cytotoxicity. Analysis of venom concentration showed that *P. liosoma* venom had a concentration of around 217 mg/ml. Given this is just over twice the concentration of the venom extracted from *H. swammerdami*, but that a dose of 1/100 was still cytotoxic for the cells, for comparison it was decided that a concentration of 1/150 (1.5 mg/ml) would be taken forward for analysis. Whilst this concentration had not been specifically tested for cytotoxicity, a concentration of 1/1000, shown by Coomassie analysis to cause no cytotoxicity, would be too low to directly compare the effects of the venoms from the 2 scorpion genera.

4.3.2 Changes in Receptor Kinome Phosphorylation and Expression Profiles in Response to Whole Venom Treatment

Changes in the phosphorylation and/or expression of 49 members of the receptor tyrosine kinase family, in response to 2h treatment with whole snake, scorpion and theraphosid venoms, were analysed using kinome array membranes. The arrays assess the changes in the combined expression/phosphorylation levels of representative members from most of the diverse sub-families of RTKs. Changes in receptor expression/phosphorylation that showed at least a two-fold increase or reduction in response to the venom were considered significant, with both increases and decreases observed. (Figure 4.4).

Initial observable changes in receptor expression/phosphorylation profiles showed a biologically significant reduction in most of the 49 detectable RTKs in response to treatment with *C. durissus vegrandis* venom, excluding just 4 of the screened RTKs (Figure 4.4G, Appendix XI). Whilst it is possible that this particular whole venom may be having a pan-targeting effect against multiple RTK subfamily members, it is worth considering that viper venoms can be high in protease components (Bottrall *et al.*, 2010) and this could be leading to proteolytic cleavage and an overall degradation effect to the cell surface receptors.

Large amounts of reductions were observed in response to treatment with *P. liosoma* venom (Figure 4.4D). However, upon further follow up investigations with Coomassie gel analysis of the treated cell lysates produced for the kinome arrays, it was determined that the selected dose

of *P. liosoma* venom appeared to have caused a large degree of cytotoxicity (Figure 4.5). Due to these high levels of observed cytotoxicity, all changes in the expression/phosphorylation of the

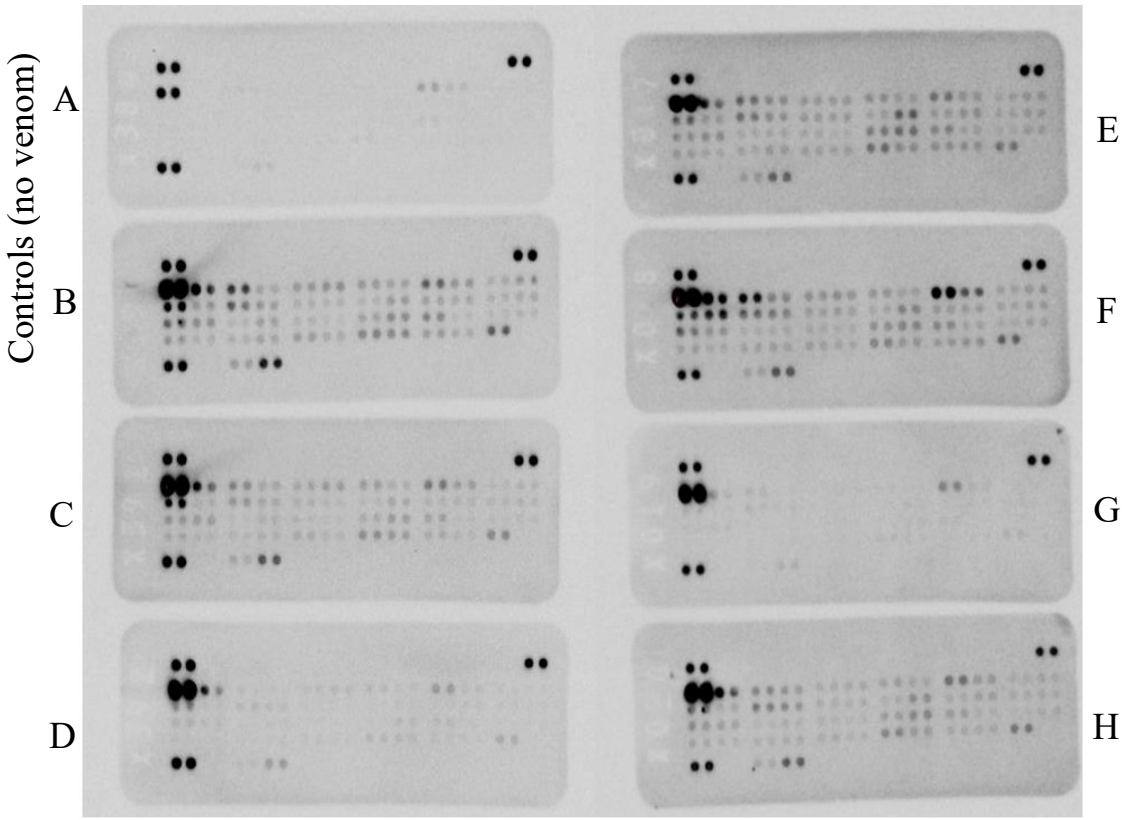

Figure 4.4: Kinome Array Analyses of MDA-MB-468 Cells Treated with Whole Venoms

The kinome arrays show changes in the expression and activity of 47 receptor tyrosine kinases in MDA-MB-468 cells in response to the application of the 6 venoms of interest. All cells were treated with the venoms for 2h and subsequently stimulated with $1x10^{-7}$M EGF for 5 min except for the positive and negative controls **Fig 4A.** Shows receptor expression and activity levels in untreated MDA-MB-468 cells which have not been stimulated with $1x10^{-7}$M EGF (Negative control). **Fig 4B.** Shows receptor expression and activity levels in untreated MDA-MB-468 cells which have been stimulated with $1x10^{-7}$M EGF for 5 min (positive control). **Fig 4C.** Shows receptor expression and activity levels of MDA-MB-468 cells which have been treated with a 1/10,000 dilution (0.025 mg/ml) of *N. naja* venom. **Fig 4D.** Shows receptor expression and activity levels of MDA-MB-468 cells which have been treated with a 1/150 dilution (1.5 mg/ml) of *P. liosoma* venom. **Fig 4E.** Shows receptor expression and activity levels of MDA-MB-468 cells which have been treated with a 1/50 dilution (2 mg/ml) *of H. swammerdami* venom. **Fig 4F.** Shows receptor expression and activity levels of MDA-MB-468 cells which have been treated with a 1/10,000 dilution (0.025 mg/ml) of *D. viridis* venom. **Fig 4G.** Shows receptor expression and activity levels of MDA-MB-468 cells which have been treated with a 1/1,000 dilution (0.065 mg/ml) of *C. durissus vegrandis* venom. **Fig 4H.** Shows receptor expression and activity levels of MDA-MB-468 cells which have been treated with a 1/100 dilution (2.5 mg/ml) of *A. geniculata* venom. Biological replicates/whole venom = N1, Technical replicates/biological replicate = N2

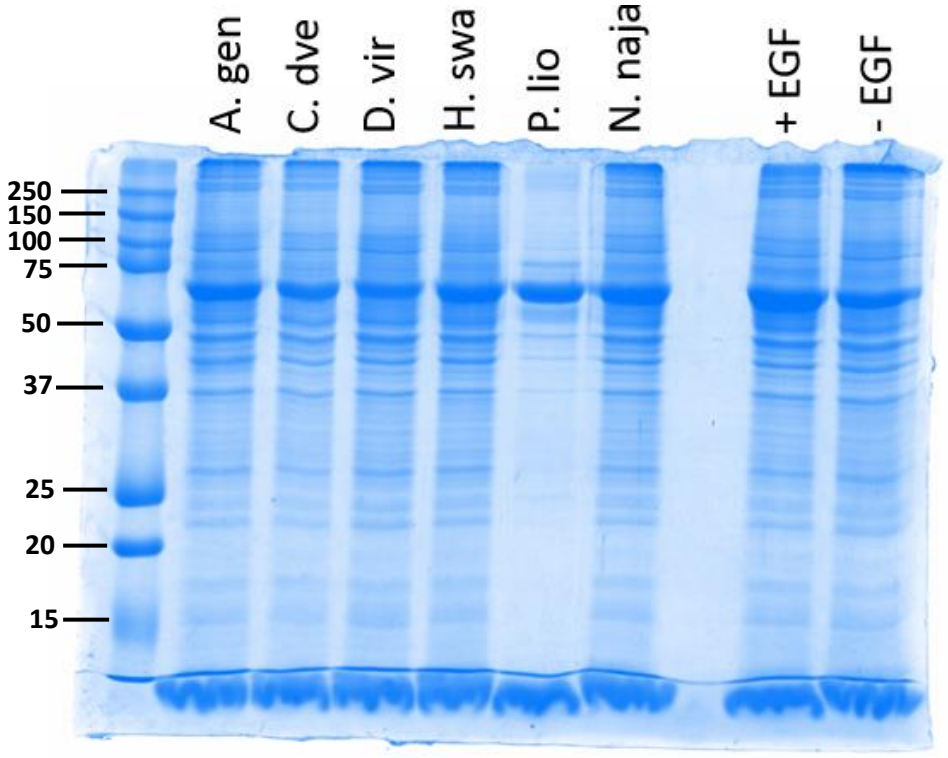

Figure 4.5: Coomassie Gel Analysis of Total Protein in MDA-MB-468 Cell Lysates After 2h Treatment with Venoms.

The Coomassie gel analysis of venom-treated MDA-MB-468 cell lysates shows that all cell lysates appear to have consistent levels of total protein, with the exception of the lysate produced from MDA-MB-468 cells treated with *P. liosoma* venom for 2h. This lack of total protein can be attributed to cytotoxic at the dose of this venom selected for cell treatment. Biological replicates = N1, Technical replicates/biological replicate = N3

RTKs treated with this venom were deemed inconclusive and subsequently disregarded. There is still the possibility that *P. liosoma* venom may potentially still have an effect on some of the 49 members of the RTKs provided on the array membranes at an appropriately selected sub-lethal dose, but this cannot be confirmed from these results.

The consistency seen in overall protein level in all other lysates (Figure 4.5) supports that any changes to the expression/phosphorylation levels of specific RTKs within these lysates are real affects resulting from venom treatment, and not due to differing levels of protein loading. As changes can be deemed a real venom affect further in-depth discussion of some of the observe changes in RTK sub-family members and the implications of these changes in response to cancer therapy will be further discussed.

Intensities for each pair of replicate receptor dots (Appendix X & Figure 4.4) were calculated using Biorad ImageLab lab software and fold change in average dot intensities were calculated in

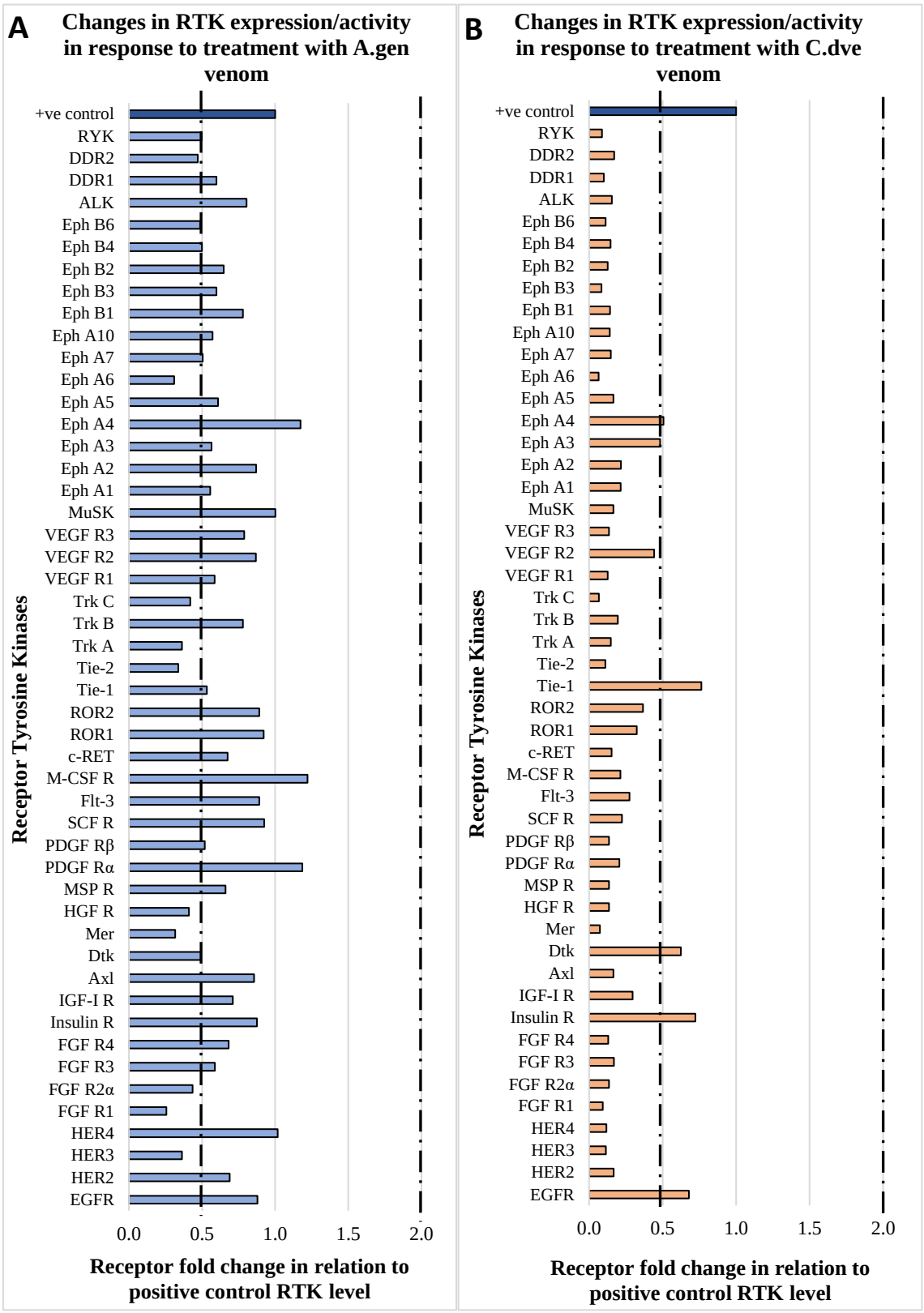

Figure 4.6: Kinome Array Analysis Graphs of MDA-MB-468 Cells Treated with *A. geniculata* and *C. durissus vegrandis* Venom

Graphs display the fold-changes in combined receptor expression/phosphorylation in response to treatment with each venom compared to levels in venom untreated cells. Dotted lines represent 2-fold reduction/increase thresholds

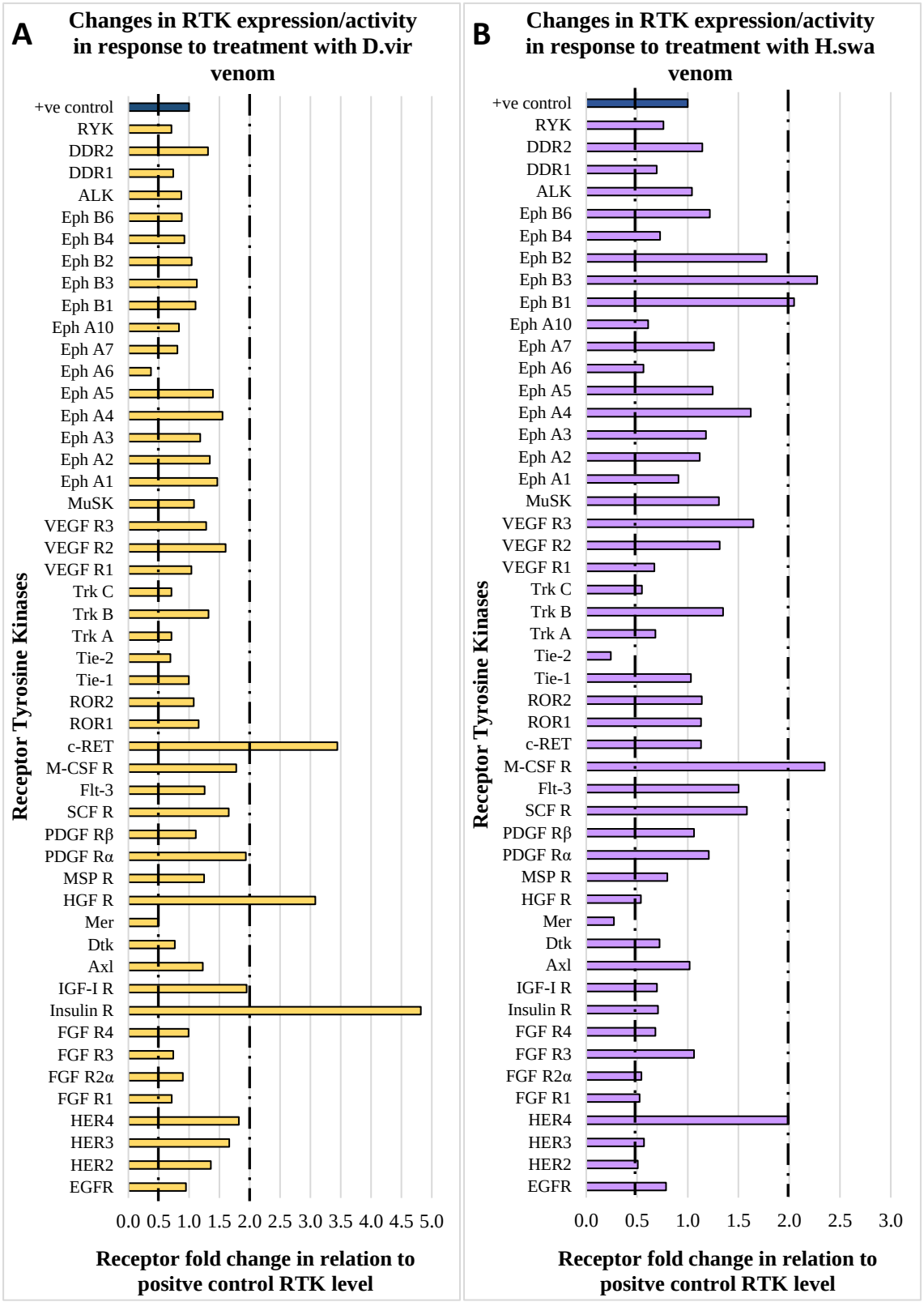

Figure 4.7: Kinome Array Analysis Graphs of MDA-MB-468 Cells Treated with *D. viridis* and *H. swammerdami* Venom

Graphs display the fold-changes in combined receptor expression/phosphorylation in response to treatment with each venom compared to levels in venom untreated cells. Dotted lines represent 2-fold reduction/increase thresholds

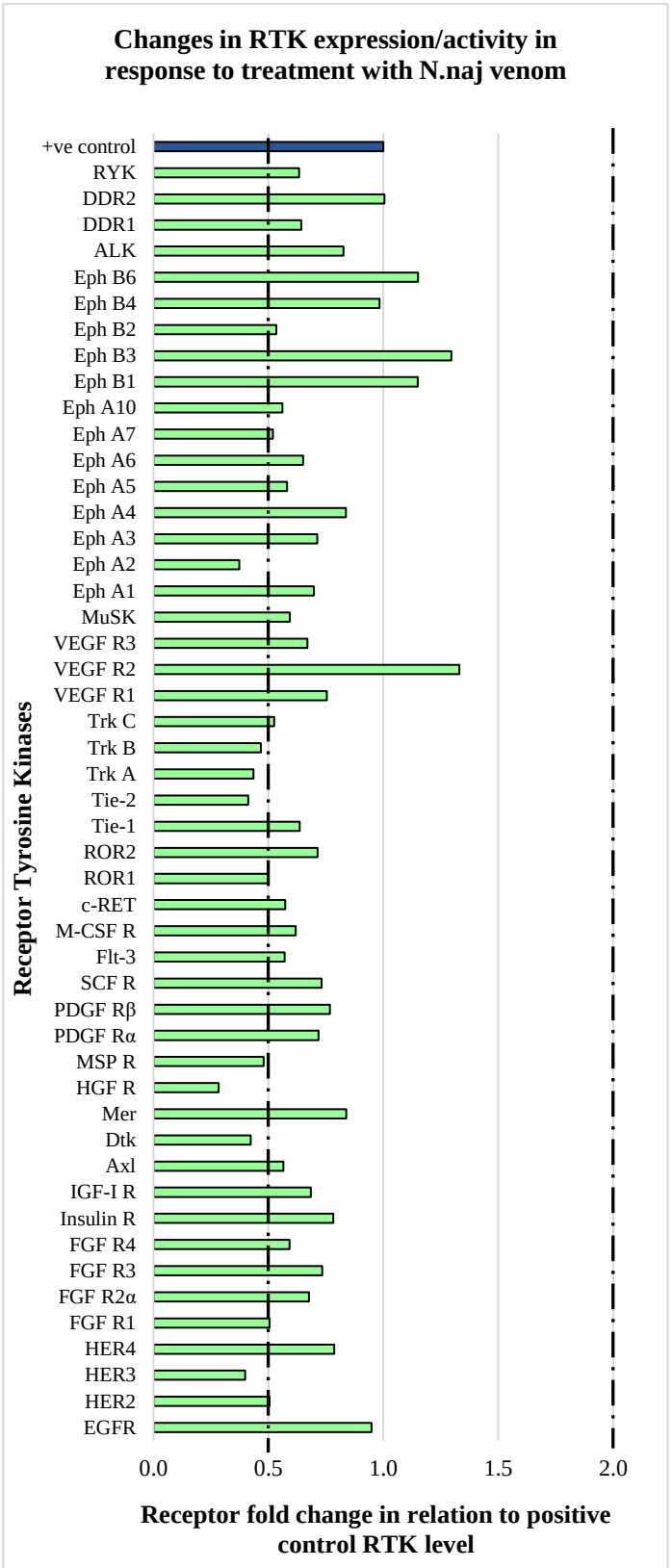

Figure 4.8: Kinome Array Analysis Graph of MDA-MB-468 Cells Treated with *N. naja* Venom

Graphs display the fold-changes in combined receptor expression/phosphorylation in response to treatment with each venom compared to levels in venom untreated cells. Dotted lines represent 2-fold reduction/increase thresholds

relation to +EGF (no venom) treated control cells. Graphs were plotted to display fold-changes in all 49 receptors in response to treatment with a particular venom (Figures 4.6-4.8). Minimum 2-fold reductions or increases in phosphorylation/expression limits were set to determine what would be considered a significant change in each receptor in relation to expression/phosphorylation levels of $1x10^{-7}$M EGF stimulated cell receptor levels. All receptor changes were displayed in a table for ease, with greater than 2-fold up/down-regulations highlighted (See Appendix XI).

4.3.2.1 Changes in the Phosphorylation/Expression of ErbB Receptors in Response to Venom Treatment

ErbB family members showed some two-fold reductions in phosphorylation in response to 2h treatment with some, but not all, of the investigated venoms. Interestingly, from the changes observed in the ErbB receptor family members, there appears to be both venoms that display specificity for certain sub-family, sister receptor members and some that display multiple targeting of like-receptor types. This could possibly hint at either the presence of single molecules which are capable of binding multiple members of the same subfamily, in similar mechanisms to second-generation small molecule inhibitors, or multiple molecules that bind each receptor independently.

No significant reductions were seen in EGFR expression/phosphorylation in response to treatment with any of the selected venoms using the kinome arrays (Figures 4.6-4.8). However due to the massive over-expression of EGFR in the MDA-MB-468 cells used as a model for these experiments, it was considered possible that changes may be occurring but are undetectable due to saturation of the EGFR antibody binding capacity of the blots. Follow up Western blot analysis was undertaken on lysates previously produced for kinome array analysis to determine if changes to EGFR expression or phosphorylation could be observed using an alternative/less sensitive method (Figure 4.9). Anti-β actin analysis was used to confirm consistent protein loading of all lysate samples. Anti-β actin analysis confirmed that all samples were loaded with a similar amount of total protein, with the exception of the *P. liosoma* treated cell lysate, previously shown in Coomassie gel analysis to be lacking protein due to toxicity. Western blot analysis of EGFR phosphorylation (pY) and expression levels (EGFR) show that there were significant differences in phosphorylation in response to the different venoms, previously undiscernible in kinome arrays because of oversaturation (Figure 4.9A).

A potential cause for the differences in EGFR expression/phosphorylation level observed between the kinome blots and the Western blots may be the degree of sensitivity of the two analyses.

Kinome arrays are highly sensitive to low levels of receptors or small changes in their expression level. MDA-MB-468 cells express EGFR in such high numbers that there is a very strong probability that even in low levels (like with the *P. liosoma* lysate) there was enough receptor present to saturate the preloaded antibody available on the blot for binding.

The Western blot analysis revealed that reductions in EGFR receptor phosphorylation levels of nearly 70% occurred in response to treatment with both *A. geniculata* and *N. naja* venom. A combination of changes in the overall expression and phosphorylation level of EGFR were seen in response to treatment with *C. durissus vegrandis* venom, with calculated reduction in expression of 60% and reductions in the detectable phosphorylation levels of nearly 95%. Western blot analyses looking at EGFR expression and phosphorylation levels post-dosing with *H. swammerdami* venom revealed that there appears to be what looks like EGF receptor breakdown in response to treatment. A detectable phosphorylated band of around 75 kDa can be observed when looking at phosphorylation levels of EGFR on the Western blot, with reductions in detectable EGFR phosphorylation of 75% also observed. Overall EGFR expression levels are also considerably lower compared to the untreated EGFR expression level controls, with around 55% reductions in total EGFR protein. There appears to be a slight EGFR expression reduction of 15% in response to *D. viridis* treatment, however despite this, treatment with this venom still appears to have resulted in nearly a 30% increase in EGFR phosphorylation levels (Figures 4.9B & 4.9C).

Reductions in EGFR expression and phosphorylation or receptor in response to treatment with 4 of the selected venoms, including two distinctly diverse snake species, one scorpion and a theraphosid venom is an exciting find. EGFR over-expression and signalling have been shown to be important in the development, progression and metastasis of a large number of cancer types including triple-negative breast cancer (Foley *et al.*, 2010; Ueno and Zhang, 2011; Davis *et al.*, 2014; Park *et al.*, 2014; Nakai, Hung and Yamaguchi, 2016; Ali and Wendt, 2017; Liang *et al.*, 2017), colorectal cancer (Huang *et al.*, 2017, 2018; Koustas *et al.*, 2017; Zhao *et al.*, 2017) and lung cancer (Nukaga *et al.*, 2017; X. Liu *et al.*, 2017; Singh and Jadhav, 2018) amongst many others. EGFR is now well established as a target for treatment in a wide variety of cancers, with high-level EGFR in primary tumours correlating with highly aggressive basal-like phenotypes and poor patient prognosis. Due to its over-expression in many cancer types, the inhibition of EGFR phosphorylation has been shown to be a successful strategy in the fight against cancer (Ono and Kuwano, 2006). However, development of resistance to current cancer therapies through further EGFR mutation or EGFR-pathway circumvention is a common occurrence (Pietrantonio *et al.*, 2017; Yu *et al.*, 2018; Lim *et al.*, 2018; Liu *et al.*, 2018), often linked to patient relapse. Reduction in EGFR expression and phosphorylation levels seen in response to *C.*

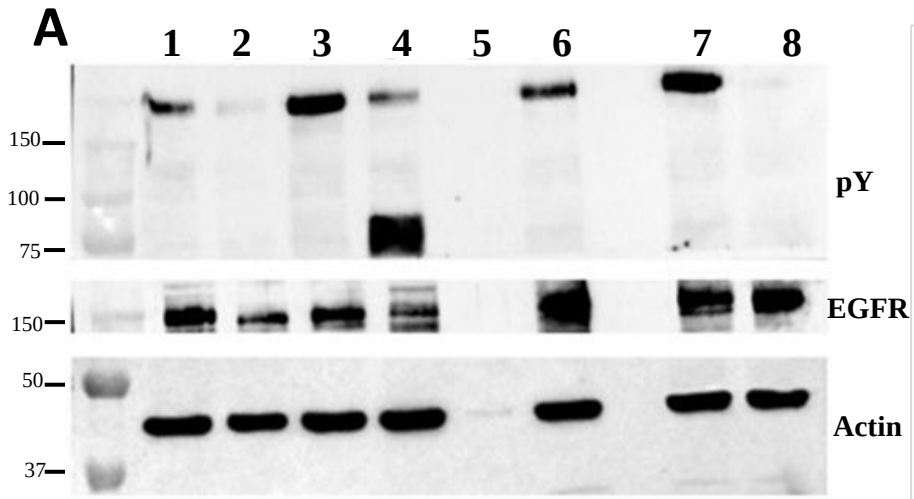

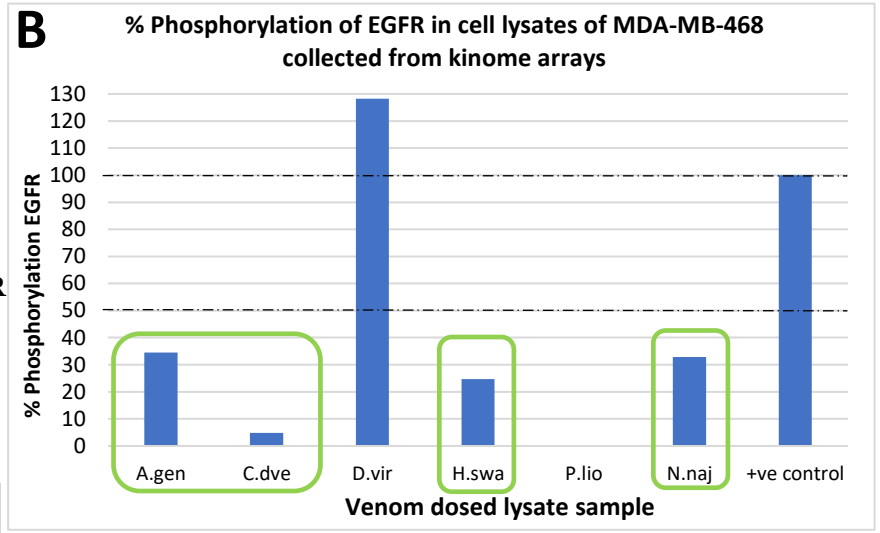

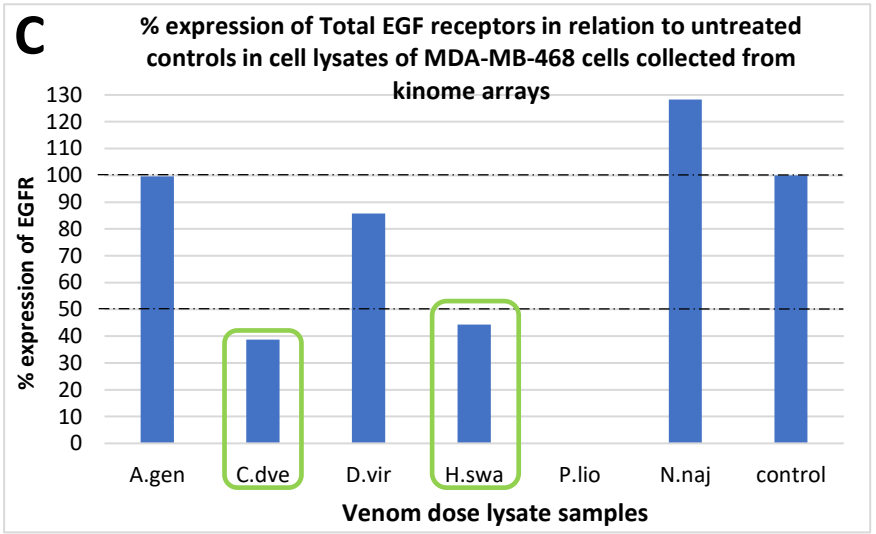

Figure 4.9: Western Blot Analysis of EGFR Phosphorylation and Expression Levels in MDA-MB-468 Cells Post Whole Venom Treatment.

Lysates produced for kinome array analysis were analysed via western blot to determine changes in expression (EGFR) and phosphorylation (pY) (A). Anti-β actin was used as a loading control to validate any observable changes. All pY and EGFR bands were normalised against actin bands before % phosphorylation/expression was calculated relative to the +ve control band for each blot. Graphs represent changes in either EGFR phosphorylation (B) or expression (C) levels in response to venom treatment. 50 & 100% EGFR phosphorylation/expression levels are marked on the graphs with lines, whilst venoms that caused greater than 50% reductions are highlighted in green

1: *A. geniculata*, 2: *C. durissus vegrandis*, 3: *D. viridis*, 4: *H. swammerdami*, 5: *P. liosoma*, 6: *N. naja*, 7: *+EGF only* (+ve Control), 8: *-Venom, -EGF* (-ve Control). Biological replicates = N1, Technical replicates/biological replicate = N3

durissus vegrandis, *N. naja* as well as scorpion *H. swammerdami* and theraphosid *A. geniculata* venoms could open up a large pool of venom-derived biological molecules, from a large diverse population of species, which may possess novel mechanisms for the targeted suppression of EGFR and treatment of EGFR-expressing cancers where prior treatment has failed due to therapy resistance.

HER2 over-expression has been shown to be linked to the induction and progression of a variety of cancer types including, prostate (Day *et al.*, 2017), colon and colorectal (Takegawa and Yonesaka, 2017; Pirpour Tazehkand *et al.*, 2018; Siena *et al.*, 2018), gastric and oesophageal (Gerson *et al.*, 2017; Wu *et al.*, 2017), ovarian (Luo *et al.*, 2018) and predominantly occurring in the HER2+ breast cancer subtypes (Baselga *et al.*, 2017; Loibl and Gianni, 2017a; Pondé *et al.*, 2018). A 2-fold reduction was observed in HER2 phosphorylation in response to treatment with *N. naja* and *H. swammerdami* venoms (Figures 4.7B & 4.8), with over a 2-fold reduction in phosphorylation/expression observed in response to treatment with *C. durissus vegrandis* venom. Whilst prognosis for patients presenting with HER2-positive breast cancers has greatly improved thanks to improvements in targeted therapies, resistance through HER3 up-regulation is a common problem. Oncogenic HER3 mutations have emerged as new therapeutic targets for the treatment of ovarian, breast, lung, prostate and other cancer subtypes (Jaiswal *et al.*, 2013; Schardt *et al.*, 2017). Targeting of HER3 has also been shown to sensitize head and neck squamous cell carcinomas by increasing tumour sensitivities to Cetuximab, reducing HER3 activity and preventing HER2/HER3 Dimerisation occurrence (Wang *et al.*, 2017). HER3 has been shown to play fundamental roles in cancer, both independently and in conjunction with other RTKs to circumvent therapeutic suppression, making it, like other ErbB receptor kinases a key target for therapeutic development. Reductions in combined HER3 phosphorylation/expression levels were observed in response to *A. geniculata*, *C. durissus vegrandis* and *N. naja* (Figures 4.6A & 4.8), suggesting that these venoms could be interesting for the treatment of HER3 over-expressing cancers. Activating mutations in HER3 have been identified in both HER2+ and ER+ breast cancer types, with HER2 and HER3 co-expression in breast cancer commonly observed (Mishra, Alanazi, *et al.*, 2018; Mishra, Patel, *et al.*, 2018). Studies have shown upregulations in HER3 expression by HER2 as a mechanism to circumvent therapeutic suppression and to induce therapy-resistance (Yang *et al.*, 2017; Li *et al.*, 2018; Lyu *et al.*, 2018). Treatment with both *C. durissus vegrandis* and *N. naja* venoms resulted in the suppression of both HER2 and HER3, suggesting the propensity for these venoms to be used in the treatment of these HER2/HER3 co-expressing cancers and HER2+ breast cancer subtypes which have upregulated HER3 to overcome therapeutic suppression.

HER4 was the only member of the EGFR sub-family to show both a venom that caused a reduction in its phosphorylation/expression state and one that showed an increase. Treatment with *C. durissus vegrandis* venom showed greater than 2-fold reduction in receptor intensity (Figure 4.6B), whilst treatment with *H. swammerdami* venom appears to have caused a two-fold increase in HER4 intensity (Figure 4.7B). Given that both up-regulations and down-regulations in HER4 expression and signalling have been linked to the development and progression of cancer, both increases and decreases pose potential changes of interest in relation to possible cancer therapeutic effects. The observed increase in expression of HER4 following treatment with H.swa venom could have useful implications in restoring normal receptor levels in cancers known to down-regulate HER 4 expression, such as renal (Thomasson *et al.*, 2004), papillary carcinoma (Kato *et al.*, 2004) high-grade gliomas (Andersson *et al.*, 2004) and invasive breast cancer. Whilst *C.dve* venom would not be useful as a treatment in HER4 downregulating cancers, including forms of breast cancer, due to its potential to cause further receptor downregulations, it could still prove useful in the treatment of HER4 over-expressing cancer types, such as head and neck cancers (Bei *et al.*, 2004). HER4 expression levels have been shown to be both down- and up-regulated in triple-negative and non-triple-negative breast cancer types respectively (Ansarin, Bagheri and Sharifi, 2018).

Pan-HER treatments, targeting EGFR, HER2 and HER3 simultaneously have been developed in recent years in an attempt to overcome the development of resistance to antibody-based therapies through target circumventing (Iida *et al.*, 2016) and small molecules tyrosine kinase inhibitors (Geuna *et al.*, 2012; Solca *et al.*, 2012; Mancheril, Aubrey Waddell and Solimando, 2014). Aptamer based therapies that also target the three receptors in breast cancer are also being used in an attempt to eliminated the problem of resistance development and therapy failure (Yu *et al.*, 2018). Treatment with both *C. durissus vegrandis* and *N. naja* venoms displayed this same Pan-HER targeting ability, causing reductions in the combined phosphorylation/expression levels of EGFR, HER2 and HER3, with *C. durissus vegrandis* also causing reductions in HER4. *A. geniculata* venom, whilst not targeting all HER receptors showed dual targeting of EGFR receptor and HER3.

Whilst all other tested venoms resulted in a change in at least one of the ErbB receptor family members expression/phosphorylation, *D. viridis* venom resulted in no significant changes in the detectable levels of any of the members of this receptor sub-family. Therefore, this venom would not be useful in the treatment of ErbB expressing cancers and so appears to be of no further interest in the targeting of these four receptors.

4.3.2.2 Changes in the Phosphorylation/Expression of FGF Receptors in Response to Venom Treatment

FGFRs are a sub-family of receptor tyrosine kinases, whose signalling is thought to have functions in many normal and aberrant cellular and biological processes, including embryogenesis, angiogenesis, tissue homeostasis, wound repair and cancer development. FGF gene abnormalities, predominantly in the form of amplifications, have been identified in approximately 14% of human malignancies, whilst a screen of 210 human cancers for possible somatic mutations in 518 protein kinase genes revealed that genes encoding for FGF/FGFR components are frequently affected by non-synonymous mutations (Presta *et al.*, 2017). Significant changes were observed in the 4 members of the fibroblast growth factor receptor (FGFR) tyrosine kinases, FGF R1, FGF R2α, FGF R3 and FGF R4 in response to treatment with some of the tested venoms (Appendix XI).

FGF R1 activity/expression has been significantly downregulated in response to 3 of the venoms tested. The greatest reductions, (greater than 2-fold) were seen with treatment of *C. durissus vegrandis* and *A. geniculata* (Figure 4.6) whilst a 2-fold reduction was seen upon treatment with *N. naja* venom (Figure 4.8). FGFR1 is involved in cancer, with its amplification linked to 21% of lung adenocarcinomas (Dutt *et al.*, 2011), as well as being observed in prostate (Devilard *et al.*, 2006), ovarian (Cole *et al.*, 2010), lung (Heist *et al.*, 2012; Jiang *et al.*, 2015) and oral squamous cell carcinomas (Freier *et al.*, 2007). FGFR1 upregulation has been found to occur in 10% of cases in oestrogen-dependent breast cancer (Gru and Allred, 2012), where it is linked to the promotion of cell proliferation. Gene amplification of FGFR1 have been shown to occur in breast cancer (Turner *et al.*, 2010). It is interesting that FGFR1 receptor amplifications were reported in oestrogen-dependent breast cancers, where its upregulation is linked to increased cellular proliferation. Whilst MDA-MB-468 cells are not an oestrogen over-expressing cancer, reductions in FGFR1 expression/phosphorylation levels were observed in response to treatment with three of the selected venoms tested, suggesting the potential for these venoms to be used in the treatment of other breast cancer types that do over-express FGFR1. Research supports the important role for FGFR1 in the progression of several cancer types, suggesting the possibility for these venoms to be used in the treatment of cancers from multiple tissue origins.

Similar reductions were seen in FGF R2α receptor expression/phosphorylation in response to treatment with 2 of the venoms shown to cause reductions in FGFR1, *C. durissus vegrandis* and *A. geniculata* (Figure 4.6). 12% of endometrial cancers have been identified as positive for FGFR2 gene mutations (Dutt *et al.*, 2008) as well as cases of lung squamous cell and cervical cancers (Liang *et al.*, 2013). FGFR2 gene amplifications or missense mutations are more

commonly occurring than FGFR1 mutations in cancer, with amplifications found in 10% of gastric cancers (Katoh and Katoh, 2009) and 2% of breast cancers (Heiskanen *et al.*, 2001; Bai *et al.*, 2010). Whilst FGFR2 mutations do not commonly occur in breast cancer, detectable reductions in FGFR2 using MDA-MB-468 breast cancer cells purely as a model, highlight the propensity for some of these venoms to be used for the inhibition of FGFR2 in other over-expressing cancer types.

Studies have shown that around 15-20% of bladder cancers are positive for somatic mutations in the region of the FGFR3 gene that encodes the extracellular domain of the receptor, whilst other mutations affecting both the intra- and extracellular domains of FGFR3 have been identified in cervical, prostate and squamous carcinomas, amongst others (van Rhijn *et al.*, 2002; Tomlinson *et al.*, 2007; Liang *et al.*, 2013; Presta *et al.*, 2017). Around 42% of patient bladder cancer samples were found to display FGFR3 over-expression profiles (van Rhijn *et al.*, 2002; Tomlinson *et al.*, 2007; Liang *et al.*, 2013). Significant reductions in FGFR3 expression/phosphorylation were observed following treatment with *C. durissus vegrandis* venom only (Figure 4.6B), and while FGFR3 does not seem to be a commonly occurring mutation or amplification in breast cancer cells, the reductions observed still offer a potential avenue of further investigation for cancer types that do display amplifications in FGFR3 expression.

In MDA-MB-453 breast cancer model, the analysis of single nucleotide polymorphisms (SNPs) revealed that mutation in FGFR4 (G388R) resulted in the promotion of metastasis and resistance of the breast cancer cells to chemotherapy (Bange *et al.*, 2002). In FGFR4 over-expressing breast cancer cells, interference with FGFR4 functioning was shown to re-establish the efficiency of chemotherapy significantly (Roidl *et al.*, 2009). Reduction in FGFR4 was only observed in response to treatment with *C. durissus vegrandis* venom (Figure 4.6B). With FGFR4 over-expression linked to breast cancer cell metastasis and chemotherapy resistance, reduction of its combined phosphorylation/expression by *C. durissus vegrandis* or other crotalid venoms could prove useful in the treatment of these cancer types, where other therapies such as chemotherapy have failed.

4.3.2.3 Changes in the Phosphorylation/Expression of Insulin Receptors in Response to Venom Treatment

Whilst the role of insulin Receptor (IR) tyrosine kinase in the development and progression of cancer is still unclear, it is becoming more apparent that like other RTKs, IR could have a potential role to play in the propagation of cancer. Some studies have hinted at the implication of IR receptor in breast cancer pathogenesis, through its activation by ligand IGF-II and its elevated

levels of expression (Sciacca *et al.*, 1999). In a study of 8 human breast cancer cell lines high affinity IGF-II binding to the IR-A isoform of insulin receptor, followed by its subsequent activation was observed. In breast cancer cell lines, IGF-II was found to have a high affinity for IR-A of 63% of that compared to insulin its native ligand. However, in non-malignant human breast cancer cells this affinity was found to be less than 1% of insulin, suggesting that there is increased sensitisation of breast cancer cells to IGF-II stimulation in breast cancer development. IGF-II activation of IR-A has been linked to mitogenic rather than metabolic effects and in breast cancer cell lines was shown to correlate with increased levels of cellular growth (Frasca *et al.*, 1999; Sciacca *et al.*, 1999).

Treatment with the selected venoms resulted in no observable significant reductions in Insulin receptor (IR) expression/phosphorylation levels, suggesting that venoms may not be particularly useful for targeting IR-over-expression in breast cancer. Surprisingly, treatment with *D. viridis* venom actually resulted in greater than a 4.5-fold increase in combined IR expression/phosphorylation levels (Figure 4.7A). Whilst an increase in IR expression/phosphorylation levels at this point may prove ineffective as a cancer therapeutic, there has been research suggesting that defective adipocyte-derived IR kinase activity may play a role in non-insulin-dependent diabetes mellitus (NIDDM), with these patients displaying reduced IR-kinase activity than the normal levels observed in obese non-diabetics (Freidenberg *et al.*, 1988). Reduced IR activity of around 40% was found in the skeletal muscle of obese individuals with NIDDM compared to lean individuals (Arner *et al.*, 1987). The acquirement of Insulin resistance has been linked to mutations in the IR gene, leading to extreme forms of resistance including leprechaunism, Rabson-Mendenhall syndrome, or the type-A syndrome. Patients with these syndromes often require a hundredfold more insulin than typical diabetic patients and often present with nonsense or missense mutations in the extracellular domain, ligand binding domain or intracellular kinase domain of IR. These mutations cause reduced insulin binding and reduced kinase activity (Boucher, Kleinridders and Kahn, 2014).

An increase in the combined expression/phosphorylation levels of IR in response to *D. viridis* venom could potentially provide a novel mechanism to overcome the loss of receptor function observed with all of these conditions, by increasing receptor expression levels or increasing its functional activity.

Type I insulin-like growth factor receptor (IGF-1R) has been considered an interesting target for cancer therapeutics, (Hofmann and García-Echeverría, 2005; Larsson, Girnita and Girnita, 2005; Hartog *et al.*, 2007; Pollak, 2008) with more than 10 inhibitors against this particular receptor, including small molecule inhibitors and antibodies, shown to have entered into clinical trials (B.

Cohen *et al.*, 2005; Mulvihill *et al.*, 2009; Gao *et al.*, 2011; Chen and Sharon, 2013). Clinical trials with IGF-1R inhibitors have been undertaken into patients presenting with non-small cell lung cancer, breast cancer and pancreatic cancer (Chen and Sharon, 2013), however despite the large number of potential IGF-1R targeted therapies currently entering clinical trials, many of these failed to show any clinical benefit in the overall patient population. A greater than 2-fold reduction in IGF-1R receptor was observed in response to *C. durissus vegrandis* treatment (Figure 4.6B). IGF-1R has been found to play important roles in the progression of human breast cancers (Milazzo *et al.*, 1992; Hua Zhang *et al.*, 2007), with a loss of IGF-1R or aberrations to its normal signalling linked to tumour progression and drug resistance (Fagan *et al.*, 2012). Upregulation of IGF-1R in breast cancer during neoadjuvant therapy has been shown to be a predictor of poor outcome in patient treatment and recovery (Heskamp *et al.*, 2015). Reductions in IGF-1R levels in a breast cancer cell line in response to *C. durissus vegrandis* venom is an encouraging find, which could offer a potential to overcome the challenges faced by currently used IGF-1R-targeted therapies. Due to the highly conserved nature of both sister receptors' structures, current therapies have been shown to display inhibitory affects against both IGF-1R and Insulin receptor simultaneously. This dual-targeting capability is potentially an undesirable off-target effect due to the import role played by IR in cell metabolism and signalling. Treatment with *C. durissus vegrandis* venom resulted in a reduction in IGF-1R receptor expression/phosphorylation levels without effecting Insulin receptor levels (Figure 4.6B), suggesting a degree of specificity not seen with many of the antibody or small molecule therapies that have currently entered the clinic (Cohen *et al.*, 2005; Mulvihill *et al.*, 2009; Gao *et al.*, 2011; Chen and Sharon, 2013). With the subsequent failure of many small molecule and antibody therapies to show benefit to patients in clinical trials, this could provide the possibility of a new peptide group with a potentially novel mechanism of action to those employed by either therapy types currently entering the clinic. Treatment with venoms capable of targeting IGF-1R could provide a potentially interesting avenue of investigation for IGF-1R over-expressing or aberrantly functioning cancers, including breast cancer.

A single greater than 2-fold reduction in ALK receptor tyrosine kinase phosphorylation/expression was observed in response to treatment with *C. durissus vegrandis* venom (Figure 4.6B). No other significant reductions or increases were observed in response to treatment with any of the other tested venoms. Anaplastic lymphoma kinase (ALK) has been shown to play an important role in cancer progression and pathogenesis, particularly in ALK-fusion and ALK-rearranged lung cancers, making it an attractive target for small-molecule inhibitor therapies (Webb *et al.*, 2009; Holla *et al.*, 2017). Recent research has suggested that the dual targeting of ALK, in conjunction with other receptor tyrosine kinases such as IGF-1R and

EGFR in lung cancer, can over-come the problem of developed resistance to tyrosine kinase inhibitor drugs such as crizotonib (Lovly *et al.*, 2014; Yamaguchi *et al.*, 2014). Interestingly, treatment with *C. durissus vegrandis* venom resulted in greater than 2-fold reduction in EGFR, IGF-1R and ALK, suggesting the potential to target all these receptors simultaneously using either a single venom component or a combination of venom components isolated from this particular venom. Whilst ALK-inhibitors such as crizotonib have been developed, acquired resistance in lung cancer to these inhibitor types often occurs by signal-suppression bypass through other RTKs, such as EGFR. This required resistance drives the need for novel drugs with different mechanisms to small-molecule inhibitors, which venoms such as *C. durissus vegrandis* may be able to provide (Yamaguchi *et al.*, 2014; Miyawaki *et al.*, 2017).

4.3.2.4 Changes in the Phosphorylation/Expression of Axl Receptors in Response to Venom Treatment

Axl family member receptor tyrosine kinases are becoming emerging targets for potential cancer therapy, with the roles they play in tumour growth, metastasis and angiogenesis becoming more apparent (Li *et al.*, 2009; Verma *et al.*, 2011; Wu *et al.*, 2014). Axl expression or upregulation has been linked to the development and progression of a diverse variety of cancer types including breast cancer (Gay, Balaji and Byers, 2017), pancreatic ductal cancers (Koorstra *et al.*, 2009; Song *et al.*, 2011), colorectal cancer (Martinelli *et al.*, 2015), prostate cancer (Paccez *et al.*, 2013), ovarian cancer (Rankin *et al.*, 2010) and lung cancer (Shieh *et al.*, 2005). The upregulation of Axl in certain cancers has been linked to the failure of treatment therapies, with Axl expression attributed to facilitating resistance to small-molecule inhibitor and chemotherapies in myeloid leukaemia (Hong *et al.*, 2008; Dufies *et al.*, 2011) and where its activation has been shown to confer resistance to EGFR-targeted therapies in lung cancer (Zhang, Jae Cheol Lee, Lin, Olivas, *et al.*, 2012; Ghiso *et al.*, 2017). Axl has been identified as a key player in breast cancer (Berclaz *et al.*, 2001; Meric *et al.*, 2002), where it has been identified as an essential regulator of metastasis induced through the process of epithelial-to-mesenchymal transition (Gjerdrum *et al.*, 2010; Asiedu *et al.*, 2014) and has been found to play a role in circumventing lapatinib-suppression of HER2+ cancer subtypes (Liu *et al.*, 2009; Gay, Balaji and Byers, 2017). Axl is expressed in highly aggressive breast cancer types, where it is a mediator of breast cancer cellular motility and invasiveness, however, it does not appear to be expressed in those with low invasiveness (Zhang *et al.*, 2008), suggesting the increased ability to invade surround tissue is a characteristic strongly attributed to Axl over-expressing.

Proto-oncogene tyrosine-protein kinase (Mer) receptor, like Axl, has been shown to play roles in the development of cancer. Mer is overexpressed in many human cancers, including various

leukaemia's and numerous solid tumours, including breast cancer (Linger *et al.*, 2010). Mer upregulation has been linked to increased cancer cell aggression, where like Axl, it has been found over-expressed in metastatic breast cancer cells, relative to non-metastatic breast cancer cells (Tavazoie *et al.*, 2008; Linger *et al.*, 2010). Frequent over-expression of Mer receptor has been found to occur in human non-small cell lung cancer (NSCLC), where it has been shown to attribute to erlotinib small molecule resistance, in EGFR mutated cancer types (Xie *et al.*, 2015). A study, evaluating 88 human NSCLC tumours found that Mer and Axl receptor tyrosine kinases were over-expressed in 69% and 93% of the tumours tested respectively, when compared to the levels of these receptors in normal surrounding lung tissue. The study also found that Mer and Axl were frequently over-expressed and activated in NSCLC cell lines. They showed that inhibition of Axl and Mer receptor activities promoted apoptosis, prevented proliferation and enhanced the chemosensitivity of the cells (Linger *et al.*, 2013). A similar study in astrocytoma found that inhibition of these receptors resulted in increased apoptosis and chemosensitivity (Keating *et al.*, 2010).

Axl was found to only be downregulated by *C. durissus vegrandis* venom (Figure 4.6B), and whilst Axl receptors do not seem to be expressed in particularly abundant level in MDA-MB-468 cells (Meric *et al.*, 2002) it has been reported to be overexpressed in other more invasive and aggressive MDA breast cancer cell lines including MDA-MB-435, MDA-MB-157, MDA-MB-436 and MDA-MB-231(Shen *et al.*, 2018). Treatment with the selected venoms resulted in a mixture of 2-fold or greater reductions in Mer expression/phosphorylation levels. Greater than 2-fold reductions were observed in Mer receptor in response to all of the treatment venoms, with the exception of *N. naja* venom, with the most pronounced reductions seen in response to *C. durissus vegrandis* venom (Figures 4.6-4.8).

Given that both Axl and Mer receptor over-expression developments have been linked to the failure of EGFR and HER2-targeting cancer treatments (Liu *et al.*, 2009; Xie *et al.*, 2015; Gay, Balaji and Byers, 2017), potential therapies with the capacity to target both ErbB receptor members and Axl receptor members simultaneously could prove beneficial in preventing therapy failure and patient treatment-relapses. Treatment with *C. durissus vegrandis* venom resulted in significant reductions in all four receptors (Figure 4.6B), suggesting the potential for targeting of all simultaneously or the potential ability to exploit certain venom components to dual target EGFR/Axl, EGFR/Mer or HER2/Axl specifically. Treatment with *H. swammerdami* venom and *A. geniculata* venom resulted in down-regulation of EGFR and Mer (Figures 4.6A, 4.7B & 4.9) without suppression of Axl and so could potentially provide a more targeted approach for

treatment of cancer types that express these two receptors simultaneously, without Axl upregulation.

Reductions in the expression/phosphorylation of developmental tyrosine kinase (Dtk) Receptor were observed in response to treatment with *A. geniculata* and *N. naja* venoms (Figures 4.6A & 4.8). Unlike with the previous two Axl family receptors, no reductions in Dtk were observed in response to *C. durissus vegrandis* venom (Figure 4.6B), suggesting that this receptor may be structurally and conformationally distinct in some way from its sister receptors. Very little is known about the aberrant functioning of Dtk and very little evidence to suggest that like its sister receptors it plays a substantiated role in cancer development of progression. A paper, published in 1995 by Crosier highlighted Dtk as a potentially novel tyrosine kinase expressed in acute myeloid leukemic blasts (Crosier *et al.*, 1995; Hamilton *et al.*, 2015). Another study carried out in 2014 into tyrosine kinase expression changes in a long-term oestrogen deprived (LTED) ER+ breast cancer cell line, found that Dtk expression/phosphorylation levels increased compared to parental cells, however the implications of this increase in the oestrogen-deprived cell does not appear to have been investigated further (Liu *et al.*, 2014). Whilst reductions were seen in the expression/phosphorylation of Dtk in response to treatment with 2 of the tested venoms, compared to untreated cells, the implications for what these changes could mean for the functioning of the MDA-MB-468 cells still remains unclear.

4.3.2.5 Changes in the Phosphorylation/Expression of MET Receptors in Response to Venom Treatment

The Met-proto-oncogene family comprises 2 sister receptors, hepatocyte growth factor receptor (HGF R/c-MET) and macrophage stimulating protein receptor (MSP R/Ron). Both c-MET and Ron receptor expressions have been linked to cancer, with their roles in its progression becoming more studied and understood. MET and RON receptor binding to their ligands have been found to induce complex gene activation program, that results in invasive growth, cell dissociation, migration, and extracellular matrix invasion (Lee *et al.*, 2005).

C-MET receptor tyrosine kinase has been identified as a key player in many cancers including breast (Yan *et al.*, 2015), lung (Zucali *et al.*, 2008), melanoma (Cheng *et al.*, 2017), myeloma, (Moschetta *et al.*, 2013) adrenocortical Carcinoma (Phan *et al.*, 2015), pancreatic cancer (Brandes *et al.*, 2015) and gastric cancer (Ha *et al.*, 2013), with its over-expression indicative of poor patient prognosis and highly invasive tumour types (Cazet *et al.*, 2010; Goetsch, Caussanel and Corvaia, 2013; Ho-Yen *et al.*, 2014; Ho-Yen, Jones and Kermorgant, 2015; Yan *et al.*, 2015; Zhang *et al.*, 2018). Within breast cancer subtypes high levels of c-MET protein in hormone-receptor (HR)+

breast cancers and phosphor-c-MET in HER2+ breast cancers were indicative of worse relapse-free survival and overall survival rates in patients. High levels of c-MET and phosphor-c-MET were identified in all breast cancer types are were indicative of poor patient prognosis (Raghav *et al.*, 2012), with c-MET over-expressions also having been identified in triple-negative breast cancer cell lines, MDA-MB-468, HCC-1395, and MDA-MB-231, where it has been linked to EGFR-therapy resistance (Sohn *et al.*, 2014). The use of independent c-MET inhibitors that target its expression or activity (Hyuga *et al.*, 2013; Fu *et al.*, 2014) or in conjunction with other RTK targeting therapies have been shown to reduce breast cancer metastasis (Previdi *et al.*, 2012), inhibit the proliferation of constitutively active c-MET over-expressing cancer cell line and induce caspase-dependent apoptosis (Munshi *et al.*, 2010; Stanley *et al.*, 2017). Treatment with *A, geniculata, C. durissus vegrandis* and *N. naja* venoms resulted in greater than 2-fold reductions in c-MET (HGF) receptor expression/phosphorylation levels (Figures 4.6 & 4.8), suggesting that these venoms could prove useful in the treatment of c-MET overexpressing cancer types. Treatment with *D. viridis* venom resulted in a greater than 2-fold increase in combined c-MET expression/phosphorylation (Figure 4.7A), making this venom unsuitable for the treatment of c-MET over-expressing cancers, including breast cancer. Current research suggests that c-MET amplification is often in response to therapeutic suppression of other tyrosine kinase receptors such as EGFR, HER2 and IGF-1R (Mehta *et al.*, 2013; Sohn *et al.*, 2014; Stanley *et al.*, 2017) and so combination therapies targeting multiple RTKs is desirable. *C. durissus vegrandis* venom was found to be capable of causing reductions in EGFR, HER2, IGF-1R and c-MET simultaneously (Figure 4.6B), potentially making this a good candidate venom for investigation into simultaneous targeting of c-MET and other key TKRs.

RON (MSP R), like its sister c-MET has been shown to play fundamental roles in cancer progression. RON receptor expression has been linked to the progression of many cancer types, including pancreatic (Thomas *et al.*, 2007), thyroid (Wang *et al.*, 2007), prostate (Thobe *et al.*, 2010) and breast cancer (Maggiora *et al.*, 1998; Peace *et al.*, 2005; Vinnedge *et al.*, 2015). Like c-MET, RON expression correlates with the development of small molecule inhibitor (Wang *et al.*, 2013a) and tamoxifen (McClaine *et al.*, 2010) resistance in HER2+ and ER+ breast cancers respectively, ultimately leading to treatment failure. Silencing of RON receptor signalling has been shown to promote apoptosis and restore Gemcitabine susceptibility in pancreatic cancer cells (Logan-Collins *et al.*, 2010). Direct antibody targeting of RON in triple negative breast cancer cell lines, including MDA-MB-468, has been shown to result in rapid RON receptor internalisation, cell cycle arrest and massive cell death (Suthe *et al.*, 2018). Treatment with the whole venoms showed significant reductions of greater than 2-fold in response to *C. durissus vegrandis* and *N. naja* only (Figures 4.6B & 4.8), hinting at the potential for novel compounds

within these venoms capable of silencing RON signalling. Both these venoms caused significant reductions in both c-MET and Ron, lending the potential for the option of dual targeting of both sister receptors simultaneously. A study into samples from node-negative breast cancer patients has shown that breast cancer can co-express both Ron and c-MET concurrently and that this combination is indicative of an exceptionally poor patient prognosis. 10-year disease-free survival for patients with RON-/cMET- tumours was found to be 79.3%, whilst this was only 11.8% in patients with RON+/cMET+ cancers. 10-year disease-free survival in patients presenting with either RON or c-MET upregulations but not both (RON+/cMet- or RON-/cMET+), were found to be 55.6% and 43.9% respectively (Lee *et al.*, 2005).

4.3.2.6 Changes in the Phosphorylation/Expression of PDGF Receptors in Response to Venom Treatment

The expression of platelet-derived growth factor (PDGF R) family members in cancer has been well established. Platelet-derived growth factor receptor (PDGF R) family members include PDGF Rα, PDGF Rβ, stem cell factor receptor (SCF R/c-kit), Fms-like tyrosine kinase 3 (Flt-3) and macrophage colony-stimulating factor receptor (M-CSF R). Changes in the expression of these receptors or their ligands have been linked to proliferation, angiogenesis and metastasis of many cancer types, with defects including deletions, mutations and copy number aberrations in genes encoding for PDGF A/B/C/D and PDGF Rα/β commonly occurring. Defects in the PDGFR/PDGF signalling axis have been determined to be present in melanoma (10-30%), glioblastoma (15-20%), bladder cancer (15-20%), lung cancer (10-20%), ovarian cancer (10-20%), colorectal cancer (10-15%) and breast, renal, liver and myeloid leukaemia (<10%) (Farooqi and Siddik, 2015).

The activation of PDGF Rs has been shown to promote metastasis in mammary tumours through autocrine signalling (Jechlinger *et al.*, 2006), and autocrine activation of PDGF Rα has been shown to promote the progression of ovarian cancer (Matei *et al.*, 2006). The blockage of PDGFR signalling has been shown to impair the metastasis of lung cancer to bone, indicating the role PDGFRs play in cancer cell metastasis (Catena *et al.*, 2011) and the PDGF Rβ/PDGF-D signalling axis have been found to be active in prostate cancer (Ustach *et al.*, 2010). M-CSF is overexpressed in many tumours (Chockalingam and Ghosh, 2014) and its increased expression in breast cancer (Templeton *et al.*, 2014) is linked with a poor outcome, making it a potentially effective target for therapeutic agents (Kluger *et al.*, 2004). Inhibition of M-CSFR signalling has been utilised to stop differentiation of tumour associated macrophages (Bonelli *et al.*, 2018). Like PDGF R α/β and M-CSF receptor, aberrations in SCF R/c-Kit receptor tyrosine kinase have been linked to cancer development and progression, where it's signalling is particularly prevalent in reproductive tissue

tumours, including prostate and testicular cancer (Cardoso, Figueira and Socorro, 2017), breast (Pillai *et al.*, 2012; Regan *et al.*, 2012; Kashiwagi *et al.*, 2013; Zhu *et al.*, 2014), ovarian (Schmandt *et al.*, 2003; Chau *et al.*, 2013) and endometrial (Yilmaz *et al.*, 2012). Unlike the other PDGFR family members, flt3 does not appear to be mutated in a wide range of cancers, however it is among one of the most frequently mutated protein in acute myeloid leukaemia (AML) (Singh *et al.*, 2010; Garg *et al.*, 2015; Park *et al.*, 2015; Zhi *et al.*, 2018).

Inhibition of PDGFR family members using microRNAs have been shown to inhibit tumorigenesis and induce apoptosis in lung cancer (Garofalo *et al.*, 2013) and combinations of small molecule therapies have been shown to inhibit breast cancer cell growth by blocking PDGF Rβ signalling (Weigel *et al.*, 2009). Significant reductions in PDGF Rα, PDGF Rβ, SCF R, Flt-3 and M-CSF receptors were observed in response to treatment with *C. durissus vegrandis* venom (Figure. 4.6B). Currently used therapies have shown the benefit of inhibiting PDGFR family member signalling in terms of limiting cancer progression, and so treatment with *C. durissus vegrandis* venom has the potential to provide novel avenues for targeting PDGFR over-expressing cancers. Over-expression of Axl RTK in Flt-3 over-expressing leukemic cells has been shown to confer resistance to Flt-3 supressing therapies (Park *et al.*, 2015). *C. durissus vegrandis* venom caused significant reductions in the activity of both Flt-3 and Axl receptors, suggesting the potential for the use of this venom to prevent Axl-related therapy failure, seen with Flt-3-only targeted therapies, by inhibiting both receptors simultaneously. Interestingly there was a greater than 2-fold observable increase in the combined expression/activation of M-CSF receptor in response to treatment with *H. swammerdami* venom (Figure 4.7B), which was not seen in any of the other PDGF family members or following treatment with any of the other selected venoms. The fact that M-CSF was downregulated by *C. durissus vegrandis* suggests that this venom warrants further investigation, however as *H. swammerdami* upregulated this receptor it would not be useful as a potential therapeutic. Though *H. swammerdami* venom would not be useful as a therapeutic treatment of M-CSF receptor expressing cancers, it could still be useful as a tool to understand the effects of the overexpression of this receptor.

4.3.2.7 Changes in the Phosphorylation/Expression of Tie and VEGF Receptors in Response to Venom Treatment

Both Tie and VEGF receptor tyrosine kinases have been shown to play roles in angiogenesis and vascular development, making them attractive targets of down-regulation or inhibition in the progression of cancer development. Effective cancer growth and metastasis is dependent upon the induction of angiogenesis and new vascular development, and as a result, aberrant expression in VEGFR and Tie receptors often occur in cancer. VEGFR-1 and R2 are expressed in highly

invasive bladder cancer (Kopparapu *et al.*, 2013) and breast cancer (Guo *et al.*, 2010; Mezquita *et al.*, 2010; Sezgintürk, 2011; Ning *et al.*, 2013; Thielemann *et al.*, 2013), VEGFR-1-3 and Tie-2 receptors in ovarian cancer (Sallinen *et al.*, 2011; Skirnisdottir, Seidal and Akerud, 2016; Avril *et al.*, 2017) and Tie-2 in prostate (Tang *et al.*, 2016) and colorectal cancer (Zhang *et al.*, 2014). A soluble form of VEGFR1 (sVEGFR1) is overexpressed in breast and other cancers. Activation of VEGFR1 in breast cancer cells supports their survival and growth (Rapisarda and Melillo, 2012).

Greater than 2-fold reductions in expression/phosphorylation were observed in Tie-2 receptor in response to all treatment venoms, apart from *D. viridis* (Figures 4.6-4.8), with the greatest reductions observed after treatment with *C. durissus vegrandis* (Figure 4.6B) and *H. swammerdami* (Figure 4.7B) venoms, respectively. Interestingly, no significant increases or reductions were observed in Tie-1 receptor in response to treatment with any of the 5 selected venoms (Figures 4.6-4.8). Given Tie-1 is an orphan receptor and depends on dimerisation with Tie-2 to promote its activation (Savant *et al.*, 2015; Mueller and Kontos, 2016), it is possible that its expression and activity levels were unaffected by treatment with the venoms as there were no compatible binding molecules. Tie-2 mutation and upregulation has been linked to the development and progression of cancer, with increased expressions promoting the onset of angiogenesis in tumour microenvironments. Decreases in the expression or activation of this receptors in response to venoms, may prove beneficial in over-expressing tumour types, by delaying the triggering of angiogenesis. The lack of reduction in Tie-1 receptor expression/activity may also be beneficial, as Tie-1 is thought to play a role as a tumour suppressor in Tie-2 over-expressing cancers cells, by reducing Tie-2 signalling activity upon their dimerisation together (Singh *et al.*, 2012).

Changes in VEGFRs 1-3 were only observed in response to treatment with 1 of the selected venoms. Greater than 2-fold reductions were observed in all 3 receptors in response to treatment with *C. durissus vegrandis* venom alone (Figure 4.6B). Similar degrees of reduction were observed in both VEGFR1 and VEGFR3 in response to C.dve venom treatment, however considerably smaller reductions in combined expression/phosphorylation levels were observed in VEGFR2. Over-expressions of all VEGFRs have been shown to be linked to the development of cancer, with many cancers showing the ability to over-express multiple members of the VEGFR family to promote growth and angiogenesis. Reductions in all 3 VEGFRs following *C. durissus vegrandis* treatment could prove useful in the inhibition of angiogenesis induction in multiple cancer types, including breast cancer (Valtola *et al.*, 1999; Yan *et al.*, 2015; Zhu and Zhou, 2015). The inhibition of all 3 VEGFRs by *C. durissus vegrandis* venom could offer the potential for a

pan-VEGFR targeting therapy (Kieran *et al.*, 2015), that could be used to suppress angiogenic induction by downregulating the levels of all 3 VEGFRs, simultaneously, thus limiting the potential for late-stage cancer hallmarks, angiogenesis and metastasis.

4.3.2.8 Changes in the Phosphorylation/Expression of NGF Receptors in Response to Venom Treatment

Neurotrophin receptor signalling through tropomyosin receptors kinases (Trk) A, B and C has been linked to the development of certain types of cancer. Whilst rare in most cancers, Trk fusions with other proteins are well-established oncogenic-driver events in papillary thyroid carcinoma, glioblastomas and secretory breast carcinomas. As well as Trk fusions, amplifications and alternative splicing events have been described as drivers in cancer pathogenesis (Lange and Lo, 2018). Trk A over-expression has been linked to enhanced growth and metastatic propensity of breast cancer cells (Lagadec *et al.*, 2009; Demont *et al.*, 2012), with downregulation of Trk A expression by small interference RNAs (siRNAs) shown to abolish metastatic potential and increase chemosensitivity in them (Zhang *et al.*, 2015). In neuroblastoma tumours, variable expression of Trk B in conjunction with brain-derived neurotrophic factor (BDNF) are indicative of poor patient prognosis, whilst high-level expression of Trk A and Trk C are associated with a good prognosis (Lucarelli, Kaplan and Thiele, 1997; Yamashiro *et al.*, 1997; Sugimoto *et al.*, 2001; Thiele, Li and McKee, 2009; Tanaka *et al.*, 2014). Trk B over-expression has also been identified in highly aggressive metastatic human pancreatic cancers (Sclabas *et al.*, 2005). Crosstalk between EGFR and Trk B has been shown to enhance cell migration and proliferation in ovarian cancer cells (Qiu *et al.*, 2006), whilst Trk B has been found to be a key regulator of PI3K and JAK/STAT signalling pathway activated metastasis and epithelial-mesenchymal transition in breast cancer cells (Kim *et al.*, 2015).

Downregulations in the combined expression/phosphorylation levels of Trk receptor tyrosine kinases were observed in response to treatment with three of the whole venoms investigated. At least 2-fold reductions were observed in all three Trk receptors in response to treatment with *C. durissus vegrandis* (Figure 4.6B) venom, whilst significant reductions were only observed in Trk A and Trk C in response to treatment with *A. geniculata* venom (Figure 4.6A). Reductions were also observed in both Trk A and Trk B, but not in Trk C in response to *N. naja* venom (Figure 4.8). Treatment of Trk Receptors in cancer with these venoms, will be highly dependent on the cancer type to be treated. Both Trk A and B over-expressions and truncations have been linked to the progression and metastasis of breast cancer, making *C. durissus vegrandis* and *N. naja* interesting venoms to follow up for potential therapeutics. In other cancer types, high expression of Trk A and Trk C are indicative of good patient prognosis and so these whole venoms would

not be best suited for therapies due to their ability to downregulate multiple Trk receptors simultaneously. Whilst *A. geniculata* venom does not inhibit Trk A and B, but rather A and C, it could still prove effective for the treatment of Trk A over-expressing cancers, with the potential for venom fractionation to result in a Trk A-only targeted compound being isolated from the venom. A Pan-Trk inhibitor, Entrectinib, is currently in clinical trials with studies into its effectiveness for the treatment of colorectal, neuroblastoma, non–small cell lung cancer, mammary analogue secretory carcinoma, melanoma, and renal cell carcinoma currently being assessed (Ardini *et al.*, 2016; Iyer *et al.*, 2016; Russo *et al.*, 2016; Drilon *et al.*, 2017). The development of a pan-Trk small molecule, currently in clinical trials, highlights the potential for *C. durissus vegrandis* venom to potentially provide a similar type of pan-Trk inhibiting therapy.

4.3.2.9 Changes in the Phosphorylation/Expression of Eph Receptors in Response to Venom Treatment

Eph receptors and their binding ligands, ephrins, constitute the largest sub-family of receptor tyrosine kinases. Eph receptors play a fundamental role in cell signalling pathways involved in animal development (Castaño *et al.*, 2008). Binding of ephrins, to Eph receptors results in the bi-directional stimulation of the eph/ephrin signalling axis. Over-expression of ephrins and eph receptors in can result in tumorigenesis, promoting tumour growth, survival, angiogenesis and metastasis (Surawska, Ma and Salgia, 2004; Pasquale, 2010). Eph receptors can act as both suppressors and promotors of tumours in different contexts (Genander and Frisén, 2010). Many of the family members are clinically relevant and tractable targets for intervention in human breast cancer (Brantley-Sieders *et al.*, 2011; Kaenel, Mosimann and Andres, 2012). Receptors of this subfamily are attractive targets for antiangiogenic therapy (Mosch *et al.*, 2010). This families signalling activities in cancer appear to be complex (Pasquale, 2010) and therefore since some of the venoms target members of this subfamily they could be used to understand these pathways further.

EphA1 over-expression has been identified in gastric cancer (Yuan *et al.*, 2009), prostate cancer and a sub-set of colon, liver, lung, melanoma and mammary carcinomas (Robinson *et al.*, 1996; Kao *et al.*, 2003; Herath *et al.*, 2006). EphA2 receptor over-expression has been identified in oesophageal, gastric, prostate and breast cancer (Easty *et al.*, 1999; Zelinski *et al.*, 2001; Miyazaki *et al.*, 2003; Nakamura *et al.*, 2005; Xu *et al.*, 2005; Yuan *et al.*, 2009; Gökmen-Polar *et al.*, 2011; Petty *et al.*, 2012; Huang *et al.*, 2014; Tsouko *et al.*, 2015) as well as lung cancer, where high EphA2 levels predicts metastatic outcome (Kinch, Moore and Harpole, 2003). EphA3 mutations are the most commonly occurring Eph receptor change, identified in lung, hepatocellular, colorectal, glioblastoma and melanoma (Balakrishnan *et al.*, 2007; Bae *et al.*, 2009). These

mutations appear to confer impaired kinase function, suggesting that EphA3 may function as a kinase-dependent tumour suppressor, which is disrupted by somatic cancer cell mutations (Lisabeth, Fernandez and Pasquale, 2012). High levels of EphA4 expression have been linked to poor patient survival in gastric cancers (Miyazaki *et al.*, 2013) promotes cell proliferation and migration of human glioma cells (Fukai *et al.*, 2008) promotes cell growth in human pancreatic ductal adenocarcinoma (Iiizumi *et al.*, 2006) and increased levels of metastasis in colorectal cancer (Oshima *et al.*, 2008). EphA5 receptor has been shown to be downregulated in breast cancer (Fu *et al.*, 2010) and EphA6, whilst shown to be downregulated in colorectal and kidney cancer (Hafner *et al.*, 2004), has been shown to be upregulated in breast cancer (Zhou *et al.*, 2018). EphA7 has been shown to have an increased expression in breast and glioblastoma cancers (Wang *et al.*, 2008; Brantley-Sieders *et al.*, 2011) and a reduced expression level in colorectal and prostate cancer (Wang *et al.*, 2005; Guan *et al.*, 2009). EphA10 receptor has been shown to be upregulated in breast cancer including triple negative types, prostate and colorectal cancer (Nagano, Maeda, *et al.*, 2014; Nagano, Yamashita, *et al.*, 2014; Li *et al.*, 2017).

Downregulations were observed in all tested EphA receptors in response to *C. durissus vegrandis* venom (Figure 4.6B), with additional reductions in EphA2 observed in response to *N. naja* venom (Figure 4.8), EphA6 in response to *A. geniculata* and *D. viridis* venoms (Figures 4.6A & 4.7A), and EphA7 in response to *A. geniculata* venom (Figure 4.6A). Over-expressions of EphA1 and A2 have been identified in a variety of cancers, including breast cancer, making *C. durissus vegrandis* and *N. naja* venoms attractive for further investigation. Reductions in EphA3 receptor in response to *C. durissus vegrandis* venom are less interesting from a therapeutic point of view as mutations in this receptor often confer down-regulations and loss of functions, making this receptor a target for therapeutic upregulation. Whilst EphA4 receptor does not appear to be commonly upregulated in breast cancer, its upregulation in gastric, pancreatic, colorectal and glioma cancers are indicative of metastasis and poor patient prognosis, making *C. durissus vegrandis* venom potentially interesting for follow up work into its affects in these cancer types. *C. durissus vegrandis* venom caused down-regulations in EphA5 receptors, which would not be beneficial for the treatment of breast cancer, which has been shown to actively down-regulate the expression of EphA5. *C. durissus vegrandis*, *A. geniculata* and *D. viridis* venoms would however be interesting to follow up for down-regulation of EphA6, which has been shown to be over-expressed in breast cancer, where it is indicative of poor patient prognosis (Zhou *et al.*, 2018). Similarly *A. geniculata* and *C. durissus vegrandis* venom show potential for interesting targeting molecule for EphA7 receptor, which has also been shown to be overexpressed in breast cancer and glioblastoma (Wang *et al.*, 2008; Brantley-Sieders *et al.*, 2011). Down-regulations in EphA10 receptor were also observed following *C. durissus vegrandis*, which is particularly interesting due

to this receptor's expression in triple-negative breast cancer subtypes. The search for novel targets for triple negative breast cancer makes EphA10 a viable target for novel therapies.

Loss of EphB1 receptor tyrosine kinase has been linked to the progression of aggressive cancer types including acute myeloid leukaemia (Kampen *et al.*, 2015), gastric, colorectal and ovarian cancer (Sheng *et al.*, 2008; Wang *et al.*, 2014) and renal cell carcinoma (Zhou *et al.*, 2014). Both upregulations and downregulations in the expression of EphB2 have been linked to the progression of cancer. EphB2 has been shown to be over-expressed in highly aggressive breast cancer types, where it has been shown to regulate multiple functions including autophagy, apoptosis and invasion (Chukkapalli *et al.*, 2014) and to result in poor survival in patients with ovarian cancers presenting with high levels of EphB2 (Wu *et al.*, 2006). Whilst reduced EphB2 expression has been linked to liver metastasis in colorectal cancer (Oshima *et al.*, 2008). Like EphB2, EphB3 has been found to be both upregulated and downregulated in the progression of cancer. EphB3 has been shown to be both up and downregulated in non-small cell lung cancers (Ji *et al.*, 2011; Li *et al.*, 2012). Over-expression of EphB3 has been linked to the suppression of colon cancer tumour growth (Chiu *et al.*, 2009) and alternatively has been linked to stimulation of cell migration and metastasis in papillary thyroid cancer (Li *et al.*, 2017). EphB4 receptor increases and decreases have both been linked to breast cancer progression (Xiao *et al.*, 2012). EphB4 has been shown to supress breast cancer tumorigenicity through an Abl/crk pathway (Noren *et al.*, 2006) and to acts as a survival factor in breast cancers (Kumar *et al.*, 2006). The extracellular domain of EphB4 has also been shown to induce angiogenic responses in endothelial cells and its expression on the surface of breast cancer cells has been shown to promote angiogenesis by activating EphB2 reverse signalling, increasing tumour growth (Noren *et al.*, 2004; Noren and Pasquale, 2007). EphB4 has been shown to be expressed in other cancers, with its upregulation shown in colon cancer (Stephenson *et al.*, 2001), bladder cancer (Xia *et al.*, 2006) and ovarian cancer (Kumar *et al.*, 2007). Finally, the expression levels of EphB6 in cancer cells has been linked to their progression and development, with losses in EphB6 expression often indicative of a more aggressive cancer type. Downregulations in EphB6 receptor have been seen in breast cancer cells, where it has been found to interact with c-Cbl to function as a tumour suppressor and to prevent tumour cell invasiveness (Fox and Kandpal, 2004, 2006, 2009; Truitt *et al.*, 2010). EphB6 expression has been shown to partially supress epithelial-to-mesenchymal transition in triple negative breast cancer cells and to reduce tumour drug-resistance to DNA-damaging drugs, resulting in better chances for recurrence-free survival in patients with higher EphB6 expressing tumours (Toosi *et al.*, 2018). Silencing or mutations of EphB6 expression in early stage non-small cell lung cancer has been found to be associated with the development distant metastases and a more aggressive cancer type. It is thought, like with breast cancer, that

EphB6 confers tumour suppression in NSCLCs (Yu *et al.*, 2010; Bulk *et al.*, 2012). Reduced gene expression of EphB6 in neuroblastoma, melanoma and prostate cancer are indicative of poor patient prognosis, amongst other cancer types (Tang *et al.*, 2000, 2004; Mohamed *et al.*, 2015). Alternatively, EphB6 receptor over-expression in colorectal cancer has been linked to the promotion of tumour cell proliferation, migration and invasion (Xu *et al.*, 2016).

All EphB type receptors saw significant reductions in combined expression/phosphorylation in response to treatment with *C. durissus vegrandis* venom, with additional reductions observed in EphB4 and B6, following *A. geniculata* venom treatment (Figure 4.6). Greater than 2-fold increases in EphB1 and B3 were observed in response to treatment with *H. swammerdami* venom (Figure 4.7B). Losses of EphB1 receptor have been shown in literature to be indicative of highly aggressive cancer types and poor patient prognosis. Whilst treatment with *C. durissus vegrandis* is unlike to be useful as it caused further reductions in receptor expression, treatment with *H. swammerdami* venom could prove interesting. Treatment with this venom resulted in a 2-fold increase in EphB1 combined expression/phosphorylation levels, which could be useful for restoring EphB1 expression levels in cancers where, EphB1 acts as a tumour suppressor and had been downregulated. Both up and downregulations in EphB2 expression levels have been observed in cancer. Only treatment with *C. durissus vegrandis* venom result in any observable changes in EphB2 expression/phosphorylation levels, with greater than 2-fold reductions observed. This venom would be interesting to investigate further for compounds capable of causing reduced expressions for the treatment of EphB2 over-expression cancer types, such as highly aggressive breast cancer and ovarian cancer. Like EphB2, both increases and decreases in the expression of EphB3 have been linked to cancer progression. Treatment with *C. durissus vegrandis* venom resulted in a greater than 2-fold reduction in the expression/phosphorylation of EphB3 receptor, which could provide a potentially interesting avenue of investigation for EphB3 over-expressing cancer types such as papillary thyroid cancer. Alternatively, treatment with *H. swammerdami* venom resulted in a greater than 2-fold increase in the combined expression/phosphorylation of ErbB3. This could have potentially interesting implications for the treatment of cancers where EphB3 is a known tumour suppressor and has been downregulated in expression to circumvent this, such as has been shown to be the case in colon cancer (Chiu *et al.*, 2009) tumours. Both EphB4 and EphB6 receptors showed 2-fold or greater downregulation in response to treatment with both *A. geniculata* and *C. durissus vegrandis* venoms (Figure 4.6). Whilst both receptors have been shown to be up and downregulated in cancer types, EphB4 upregulations are more commonly implicated in poor cancer prognosis, whilst EphB6 downregulations are more indicative of poor patient outcome. Treatment with both these venoms resulted in downregulations in both receptors expression/phosphorylation levels. These changes

could prove beneficial for the treatment of ErbB4 over-expressing cancers, including breast, bladder, ovarian and colon cancer. Whilst EphB6 downregulations are less likely to be useful in a therapeutic capacity for the treatment of cancer as loss of EphB6 expression appears more common in tumorigenesis, there are cases of cancer that do appear to express over-expression of EphB6, such as colorectal cancer.

4.3.2.10 Changes in the Phosphorylation/Expression of DD Receptors in Response to Venom Treatment

Discoidin-domain receptor tyrosine kinases (DDRs) are a subfamily with distinctive activating ligands and signalling cascades to other members of the larger receptor tyrosine kinase family. The extracellular domain of DDRs contains discoidin homology domain which include specific collagen binding sites (Borza and Pozzi, 2014). Sister receptors DDR1 and DDR2 comprise the subfamily, however, whilst DDR2 exists in only one isoform, DDR1 can be alternatively spliced in 5 (DDR1a-e) (Borza and Pozzi, 2014). DDR1 receptor is predominantly activated by collagen types, I and IV, whilst DDR2 is activated by types I and III. As well as being unique as the only RTKs capable of binding collagen, their activation through phosphorylation appears to be more delayed, with a more sustained effect when compared to the rapid and transient phosphorylation that is observed with other RTK activation (Rammal *et al.*, 2016).

Cancer cells hijack DDRs to disrupt the normal balance in cell to extracellular matrix communication and subsequently can use this to initiate the pro-migratory and pro-invasive programs necessary for the progression of tumour tissue invasion and metastasis (Valiathan *et al.*, 2012). Upregulation, mutation, constitutive activation and even loss of function of DDR have all been suggested to play a role in the progression of many types of cancer. There have been reports of mutations to DDRs in many cancer types (Valiathan *et al.*, 2012; Rammal *et al.*, 2016), including lung (Ford *et al.*, 2007; Yang *et al.*, 2010; Valencia *et al.*, 2012), ovarian (Quan *et al.*, 2011), bladder (Xie *et al.*, 2017), gastric (Hur *et al.*, 2017), colorectal cancer (Badiola *et al.*, 2012), melanoma (Badiola *et al.*, 2011), breast (Dejmek *et al.*, 2005; Toy *et al.*, 2015; Corsa *et al.*, 2016; Takai *et al.*, 2018) and head and neck cancers (Chua *et al.*, 2008).

Over-expression of DDR2 levels in breast cancer correlated with high tumour grade, worse survival rates and triple-negative breast cancer subtypes (Toy *et al.*, 2015). Greater than 2-fold reductions in the expression/phosphorylation of both DDR1 and DDR2 were observed in response to treatment with *C. durissus vegrandis* venom, with a further 2-fold reduction also observed in DDR2 receptor in response *A. geniculata* venom (Figure 4.6). With the over-expression of both DDR1 and DDR2 linked to the development of many types of cancer, including breast cancer,

reductions in the combined expression/phosphorylation profiles of these receptors could provide interesting avenues for investigation. Interestingly, DDR1 receptor has been shown to modulate the expression of Insulin receptor-A isoforms in breast cancer cells (Vella *et al.*, 2017), a target previously shown through the kinome array analysis to be unaffected by any of the tested venoms. As well as the potential for direct DDR-targeting in overexpressing cancers using *A. geniculata* and *C. durissus vegrandis* venoms, the targeting of IR through the suppression of DDR2 signalling could prove an interesting alternative for IR receptor silencing in breast cancer.

4.3.2.11 Changes in the Phosphorylation/Expression of Ret, ROR, MuSK and Ryk Receptors in Response to Venom Treatment

Receptor tyrosine kinase-like orphan receptors (Ror) 1 and 2 are a sub-family of receptor tyrosine kinases that were considered orphan receptors, as no definitive binding and activating ligands had yet to be confirmed, however emerging evidence suggests that Ror receptors are actually activators and suppressors of Wnt genes (Green, Kuntz and Sternberg, 2008; Solt and Burris, 2012). However, despite the controversy still surrounding their orphan receptor status and signalling roles, it has become clear that changes in Ror receptor tyrosine kinases expression patterns have been implicated in cancer progression and poor patient prognosis. Ror1 receptor over-expression has been identified in a wide variety of cancers including leukaemia's and lymphomas, ovarian cancer, triple negative breast cancer, pancreatic cancer, gastric carcinomas and lung adenocarcinomas (Gentile *et al.*, 2011; Zhang, Chen, Cui, *et al.*, 2012; Zhang, Chen, Wang-Rodriguez, *et al.*, 2012; Borcherding *et al.*, 2014; Hojjat-Farsangi, Moshfegh, Daneshmanesh, Khan, Mikaelsson, Osterborg, *et al.*, 2014; Zhang *et al.*, 2014; Balakrishnan *et al.*, 2017). Ror1 over-expression has been linked to enhanced tumour growth in primary human breast cancers, with triple negative breast cancer types expressing highly elevated levels of Ror1 (Zhang, Chen, Cui, *et al.*, 2012). Breast adenocarcinomas, shown to express high levels of Ror1, were more likely to present with gene expression signatures associated with epithelial-mesenchymal transition (EMT) and to have higher relapse and metastasis rates then low Ror1 expressing breast adenocarcinomas (Cui *et al.*, 2013). High Ror1 expression was identified in 55% of ovarian cancer samples compared with just 12% of normal ovary tissue samples, where a correlation between Ror1 expression and disease-free patient survival was observed. Patient ovarian cancers, presenting with High Ror1 expression and advanced FIGO stage showed unfavourable disease-free and overall survival times (Zhang *et al.*, 2014).

Like Ror1, High expressions of Ror2 orphan receptor tyrosine kinase have been found in a wide variety of cancers, where its over-expression is considered indicative of a poor prognosis, However, there is evidence also suggesting that loss of Ror2 expression in some cancer can be an

undesirable effect that fuels the progression of these particular cancer types. Many types of cancer, including colorectal, osteosarcoma, renal, melanoma, head and neck squamous cell carcinoma, breast cancer, ovarian cancer, non-small cell lung cancer (Morioka *et al.*, 2009; Oconnell *et al.*, 2010; Rasmussen *et al.*, 2013; Henry *et al.*, 2014, 2015; Mei *et al.*, 2014; Debebe and Rathmell, 2015; Lu *et al.*, 2015; Bayerlová *et al.*, 2017) have been shown to carry increased Ror2 expressions, which have been linked with more aggressive disease states. Interestingly, despite the numerous cancers carrying Ror2 over-expression, downregulation of Ror2 mRNA was found in 63% of hepatocellular carcinoma compared to adjacent non-tumorous tissues. Survival analysis identified that Ror2 downregulation in conjunction with Wnt5a downregulation in these tumours was indicative of poorer patient prognosis, compared to patients presenting with elevated Wnt5a and Ror2 expressing hepatocellular carcinomas (Geng *et al.*, 2012).

Significant reductions were observed in both Ror1 and Ror2 expression/phosphorylation levels in response to treatment with *C. durissus vegrandis* venom (Figure 4.6B), with a further reduction observed in just Ror1 in response to *N. naja* venom (Figure 4.8). Given both Ror1 and Ror2 over-expression are highly implicated in the development of aggressive cancer types and given that attempts to therapeutically target Wnt-signalling pathways in cancer have proved disappointing (Ford *et al.*, 2013), down-regulation in the expressions of Ror1 and Ror2 could open up potential avenues of investigation. The findings suggest that snake venoms, including crotalid and cobra venoms, could hold the potential to target Wnt signalling pathways through the downregulation of Ror receptor tyrosine kinases, with both *C. durissus vegrandis* and *N. naja* venoms shown to cause significant reduction in these sister receptors.

Gain-of-function mutations and upregulation in the expression of Ret (REarranged during Transfection) proto-oncogene (c-RET) receptor tyrosine kinase have been linked to the development of several cancer types. C-Ret expression is often observed in oestrogen receptor positive (ER+) breast cancer subtypes, where RET expression is induced by oestrogens and RET signalling enhances oestrogen-driven proliferation of the breast cancer cells. RET expression has been detected in primary breast cancer samples, with higher RET expression levels identified in ER+ tumours (Boulay *et al.*, 2008; Morandi, Plaza-Menacho and Isacke, 2011). RET mutations in the form of chromosomal rearrangements (inversion of balanced-translocation) involving the RET catalytic domain and leading to the creation of fusion RET/PTC oncogenes have been linked to papillary thyroid carcinoma (PTC) development (Mologni, 2011). Gain-of-function mutations in RET have also been linked to the development of medullary thyroid carcinoma (MTC) (Phay and Shah, 2010; Carlomagno, 2012; Hedayati *et al.*, 2016). Both small molecule (Andreucci *et al.*, 2016) and antibody-drug conjugate (Nguyen *et al.*, 2015) therapies have been developed as

potential therapies for the treatment of RET over-expressing breast cancer, with treatments proving effective against these RET over-expressing cancers. However, despite the evidence for RET as an oncogene promoting cancer development in thyroid cancer and pheochromocytoma, RET has been identified to potentially have a tumour suppressive role in colon cancer. RET methylation was found in 27% of colon adenomas and 63% of colorectal cancers, where these aberrant methylation events were found to correlate with decreased RET expression. Subsequent restoration of RET expression in these instances was found to result in apoptosis of colorectal cancer cells (Luo *et al.*, 2013).

Changes in RET expression/phosphorylation were observed following treatment with 2 venoms, with *C. durissus vegrandis* venom resulting in a greater than 2-fold reduction in c-RET (Figure 4.6B) whilst *D. viridis* venom resulted in nearly a 3-fold increase in detectable RET levels (Figure 4.7A). Reductions in RET expression could prove beneficial in the treatment of many cancer types, including breast and thyroid cancers, with therapies shown to target this receptor proving effective in cancer treatment. *C. durissus vegrandis* venom has been shown capable of causing significant reductions in the combined expression/phosphorylation levels of RET, making this venom and the venom of other crotalid pit vipers of interest for the search of potential RET-targeting therapeutics. Interestingly down-regulation of RET in colorectal cancer, appears to confer advantageous characteristics to colon cancer cells, which contradicts the over-expression of this receptor seen with other RET-expressing cancers. *D. viridis* venom caused a greater than 3-fold increase in RET expression levels following treatment, offering mamba venoms as a potential avenue of follow up for the treatment of RET-downregulating cancers. Whilst not cancer, mutations in RET receptor that prevent activation have been associated with the development and progression of Hirschsprung's disease, a disorder characterized by the absence of ganglion cells along variable lengths of the distal gastrointestinal tract (Ruiz-Ferrer *et al.*, 2011). *D. viridis* and mamba venoms could also provide a potential avenue of investigation for novel molecules that may present an opportunity to re-establish RET-activity or normal RET-functioning in this disorder.

Muscle-specific tyrosine kinase (MuSK) is a receptor tyrosine kinase that belongs to its own subfamily with its own unique extracellular domain structure. MuSK, though titled muscle-specific tyrosine kinase has since been found to be expressed in a variety of mammalian tissues, including skeletal muscle, excitatory neurons and sperm (Garcia-Osta *et al.*, 2006; Kumar, Ferns and Meizel, 2006; Hubbard and Gnanasambandan, 2013). MuSK has been found to play central signalling roles in the formation of neuromuscular junctions (NMJs) activated via a complex spatio-temporal manner by promoting the cluster of acetylcholine receptors on the postsynaptic

(muscle) side of a synapse and inducing differentiation of the nerve terminal on the presynaptic side (Burden, 2002; Hubbard and Gnanasambandan, 2013). Whilst there is no evidence to suggest that aberrant signalling through MuSK receptor is linked to cancer development and progression, changes to MuSK receptor kinase have been linked to the development of the rare but severe autoimmune disease MuSK Myasthenia gravis (Koneczny, Cossins and Vincent, 2014). Antibodies incorrectly targeted by the immune system against MuSK receptor result in the pathology associated with this disease (Hoch *et al.*, 2001). Treatment with *C. durissus vegrandis* venom resulted in greater than 2-fold reductions in the expression/phosphorylation of MuSK (Figure 4.6B). Whilst down-regulations in MuSK in response to this venom would not prove a valuable therapeutic option for disease treatment, it could prove a valuable tool to enable further investigation into what is occurring during MuSK Myasthenia gravis disease development and progression, by simulating loss of MuSK receptor expression. This study has also shown the propensity for venom components to be capable of causing changes to the expression pattern of MuSK, and so other venoms could potentially hold the key to increasing MuSK receptor signalling in patients suffering from MuSK Myasthenia gravis.

Ryk (related to tyrosine kinases) receptor is an atypical member of the larger RTK family, differing from all other members at a number of normally highly conserved residues, found within the activation and nucleotide binding domains of other RTKs. The fact that Ryk receptor appears to contain some unusual and idiosyncratic variations at these highly conserved resides and is a catalytically inactive, suggests that it may play a highly specialised role in signal transduction within the cells (Hovens *et al.*, 1992; Halford and Stacker, 2001). Very little is known about the function of Ryk receptor and there is limited evidence to suggest that aberrations in its expression or activation profile are frequently linked to the development and progression of cancer. Normal Ryk expression has been linked to biological processes including, cell polarity and differentiation, migration, skeletal development and neurite and axon outgrowth through its high affinity binding response to Wnt family ligands (through a Wnt inhibitory factor (WIF) domain) (Halford *et al.*, 2013; Green, Nusse and van Amerongen, 2014). H-Ryk, the human homolog of Ryk receptor has been linked to the development of epithelial ovarian cancer. Overexpression of H-Ryk in both malignant epithelium and blood vessel was found to be linked with a significant reduction in overall survival rates. H-Ryk blood vessel overexpression was found to confer a significantly shorter progression-free survival (Wang *et al.*, 1996; Katso, Russell and Ganesan, 1999; Katso *et al.*, 2000).

Significant reductions were observed in Ryk in response to treatment with both *A. geniculata* venoms and *C. durissus vegrandis*, with greater than 2-fold reductions observed with the latter

(Figure 4.6). Reductions in Ryk receptor in response to these venoms could prove useful for the treatment of H-Ryk over-expressing ovarian cancers, by blocking Wnt signalling cascades. However, what is more interesting about the venoms that target Ryk is the propensity for them to be used as an investigative tool to enable greater understanding of how Ryk functions both in normal physiology and its potential role in disease and pathophysiology.

4.4 Conclusion

The data collected in this chapter has shown the propensity for venoms, from a selection of distinctly diverse species, including snakes, scorpion and theraphosids, to be used as therapeutic tools for the targeting of receptor tyrosine kinase-driven cell signalling pathways. The RTK kinome analysis has shown that whole animal venoms have the potential to reduce the expression/phosphorylation profiles of a number of members of thirteen RTK subfamilies, potentially opening up a large pool of candidate druggable receptors for the treatment of diseases, such as cancer. The complex, inter-linked nature of cell signalling cascades, means that aberrations to receptor functionality or signalling can lead to both gains and losses of functions, both of which are highly linked to the development of pathophysiological diseases.

The experiments undertaken in this chapter and the data they generated have identified both detectable increases and decreases to the expression/phosphorylation profiles of many RTK subfamily members, expressed at both high and low levels in triple negative breast cancer cell line MDA-MB-468. Interestingly the experiments revealed both significant increases and decreases in the expression of RTK receptors in response to treatment with specific selected venoms but not others, displaying venom specific receptor effects. Due to the complex nature of their composition, venoms could contain potential candidate molecules for the treatments of both RTK upregulating and downregulating cancer subtypes or even prove useful in the treatment of diseases where an RTK's expression has been lost. The observability of selective receptor effects when using whole venoms is an encouraging sign and hints that, with the possibility of fractionation, these whole venoms could yield an array of molecules with specific individual receptor targeting capabilities

Changes in the expression or activity of these receptors in response to venoms has interesting implications, not just as potential avenues of interest for novel therapeutic options, but also as tools for enabling us to better understand the complex and inter-linked nature of these receptor mediated cell signalling pathways. Many of the receptors that have been shown to be affected by the venoms tested in this chapter, including DDRs and Ryk are still poorly understood, with their roles in both normal cellular signalling events and their aberrant effects in disease only beginning

to become more clear. Changes to these receptors within the model of a triple negative breast cancer cell line, could help to identify novel receptor tyrosine kinases as targetable antigens for the treatment of this notoriously aggressive and difficult to treat form of breast cancer. It is also possible, due to their complex nature and their heavy protein and small peptide composition, that treatment with the selected venoms may have resulted in detectable changes to RTKs that have previously been identified as interesting novel tumour-associated antigens, but have proved challenging to target with the current routinely used forms of targeted therapy.

The kinome array analysis identified that some RTKs were more susceptible to venom treatment than others, with multiple tested venoms shown to cause similar levels of changes to their signalling potential. These similarly observed effects, from multiple venoms from genetically diverse genera, could be attributed to the likelihood that they contain similar active components or component with similar conformational structures whose evolution have been conserved. Conversely, the data also revealed that certain RTKs proved difficult to target, with only one or in some cases none of the selected venoms causing any significant effects. It is possible that those receptors that were shown to be unchanged by all of the tested whole venoms may be un-targetable or simply that the venoms selected did not contain the necessary components to actively and effectively inhibit these particular individual receptors.

Amongst the whole venoms tested, some were shown capable of simultaneously targeting multiple sister RTKs from the same subfamily, as well as RTKs from separate subfamilies. The observation of multiple RTK targeting simultaneously could indicate the presence of single component within these venoms which display non-selective inhibition of a variety of RTK subfamily members, or could in turn be indicative of multiple active molecules within the venom, each which target a specific RTK family member independently from each other. This multi-targeting could potentially open up the option for the pan-targeting of a particular RTK subfamily or the simultaneous targeting of RTKs from different sub-families that are co-expressed together in particular cancer types, such as HER2 and Axl in breast cancer. This observed multitargeting effect holds interesting potential, as the development of current second and third generation small molecule and antibody-based therapies are now exploiting the simultaneous targeting of multiple RTKs in an attempt to pre-empt the development of cancer therapy resistance and subsequent patient relapse.

As venoms have been shown capable of causing effects to the combined signalling/expression of a range of highly cancer relevant RTKs, the use of venoms for the targeting of these receptors warrants further investigation. Whilst initial kinome array data did not suggest any changes to the expression/phosphorylation of EGFR in response to the treatment venoms, follow up western blot

analysis determined effects to be occurring to the receptor. Western blot analysis suggested that the lack of changes observed in the kinome arrays may be the result of saturation due to the high levels of EGFR expression. Due to the prevalence of its increased expression in triple negative breast cancer subtypes and the observance of detectable changes to its expression in response to whole venom treatment, EGFR makes for an attractive target to follow up for subsequent venom targeted therapy.

In subsequent chapters, an increased panel of whole snake and invertebrate venoms will be screened for their potential to reduce the phosphorylation of EGFR in both TNBC cell line MDA-MB-468 and EGFR over-expressing squamous carcinoma model cell line A431. Venoms will be assessed for their non-targeted cancer cytotoxicity and will be fractionated and rescreened to identify specific venom actives.

CHAPTER 5: Identification of Whole Venoms that reduce the Phosphorylation of EGF Receptor Tyrosine Kinase

5.1 Introduction

5.1.1 The ErbB Receptor Tyrosine Kinase family

The ErbB receptor tyrosine kinases are probably one of the most characterised and well understood sub-families of RTKs. The family consists of 4 members which include EGFR and its three sister receptors HER2 (ErbB-2), HER3 (ErbB-3) and HER4 (ErbB-4). All members of the EGFR family have an extracellular domain consisting of four sub-domains designated I, II, III and IV or L1, S1, L2 and S2. Regions I and III interact to form the ligand binding domain of the receptor, whilst regions II and IV are homologous cysteine-rich regions which participate in the facilitation of receptor dimerisation (Figure 5.1) (Bazley and Gullick, 2005; Hongtao Zhang *et al.*, 2007; Kovacs *et al.*, 2015).

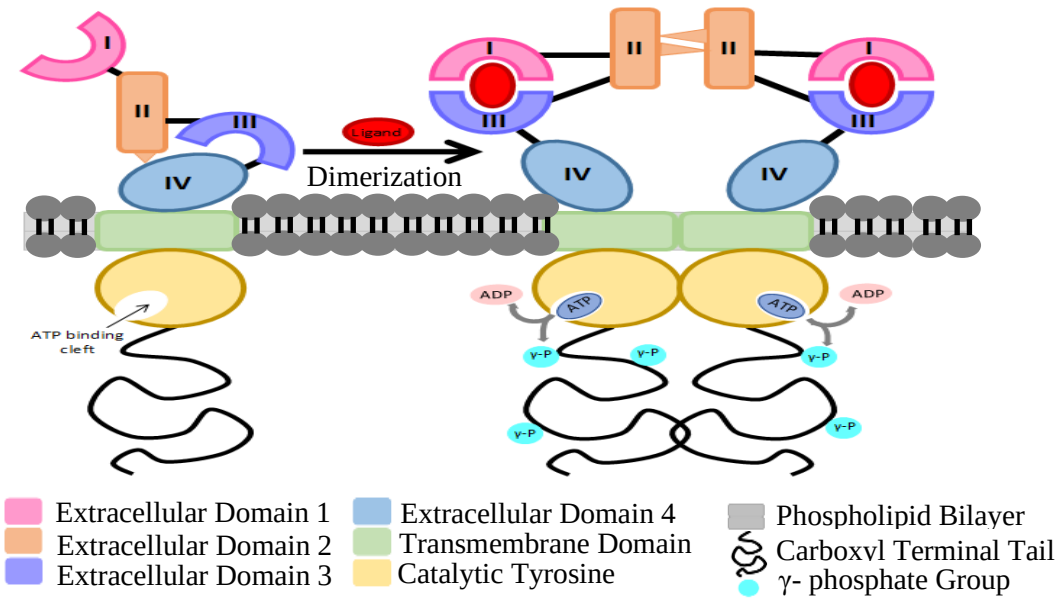

Figure 5.1: Receptor Tyrosine Kinase Dimerization Diagram

Upon Ligand binding to extracellular domain I, a conformational change occurs in the RTK. Dimerization can then be mediated by a protrusion in extracellular domain II that interacts with certain regions of a similar adjoining receptor. This interaction facilitates receptor-receptor interactions and activation of catalytic tyrosine kinases domains

over-expressed, mutated or constitutively active in many different types of cancers, (Arteaga and Engelman, 2014; Lee *et al.*, 2015; Sequist *et al.*, 2015; Hsu and Hung, 2016; Lucas and Cristovam, 2016; Morgillo *et al.*, 2016; Nakai, Hung and Yamaguchi, 2016; Chan *et al.*, 2017; Liu *et al.*, 2017; Loibl and Gianni, 2017) making them interesting targets for potential targeted therapies.

Despite their similarities in extracellular domain composition, HER2 is unique amongst the EGFR sister receptors as it is considered an 'orphan receptor' (Dittrich *et al.*, 2014). As an 'orphan receptor', HER2 is not known to have a high-affinity binding ligand capable of stimulating the receptor and activating its intrinsic kinase domain, therefore HER2 is considered unable to signal independently (Arteaga and Engelman, 2014; Hsu and Hung, 2016). Homo-dimerisation of HER2 to HER2 receptor would not result in a functioning dimerization partnership, and so HER2 has to undergo receptor dimerisation with another member of the ErbB family and function as a co-receptor to illicit its kinase response (Burgess, 2008; Dittrich *et al.*, 2014; Weitsman *et al.*, 2016). HER3 is similarly unique in that it displays characteristics not seen in other EGF Receptor family members. HER3 lacks an active kinase domain, caused by the mutation of multiple residues within the catalytic site of the kinase domain, essential for efficient kinase activity (Shi *et al.*, 2010). Like HER2, HER3 must undergo dimerization with and activate the receptor tyrosine kinase domain of another ErbB receptor family member in order to confer downstream signal transductions. The preferred dimerisation partner of HER3 is HER2, and the HER3/HER2 receptor dimerization combination generates the strongest proliferation signals of any ErbB receptor dimerization pairing (Weitsman *et al.*, 2016). With HER2 lacking a ligand and the inability of HER3 to generate intrinsic kinase activity in response to suitable ligand stimulation, these ErbB receptors have been referred to as the ''deaf and dumb receptors'' (Figure 5.2) (Citri, Skaria and Yarden, 2003; Leahy, 2004).

Members of the EGFR receptor family are activated by a variety of ligands collectively termed the EGF-related peptide growth factors. Seven of the ErbB ligands are produced as single gene products which contain both a transmembrane domain and an EGF motif. These ligands initially reside in anchored, transmembrane precursor states which undergo processing via proteolytic cleavage, subsequently leading to their release from the plasma membrane (Olayioye *et al.*, 2000; Gullick, 2009).The first ErbB family ligand was discovered in the late 1950s by Cohen and Levi-Montalcini as a side-fraction obtained during the purification of extracts of bovine hypothalami. Cohen and Levi-Montalcini, whilst trying to isolate nerve growth factor from the bovine hypothalami extracts, fractionated out Epidermal Growth Factor (EGF), the first of the ligands which actively binds to EGFR (Gullick, 2009). Since the discovery of EGF, the family of ErbB ligands has expanded to include 11 members, each which specifically bind to certain members of the ErbB family.

The 11 ligands can be subdivided into two categories: those which are unspliced such as EGF, Transforming Growth Factor-α (TGF-α), Epigen, Epiregulin, Amphiregulin (AR), Heparin-binding EGF-like Growth Factor (HB-EGF) and Betacellulin (BTC) and those which are spliced, such as neuregulins 1-4 (Gullick, 2009). Two other genes, tomoregulin and epiglycan C have

been suggested to encode for 2 additional ErbB ligands, Neuregulins 5 and 6 respectively (Bazley and Gullick, 2005). The 11 ErbB ligands can also be divided into further categorises based on the receptors they bind, with (i) EGF, TGF-α, AR and Epigen binding to EGFR, (ii) HB-EGF, Epiregulin and Betacellulin which bind dual-specifically to both EGFR and ErbB4 and (iii) the neuregulins, with NRG1 and NRG2 binding both ErbB3 and ErbB4, whilst NRG3 and NRG4 bind solely to ErbB4 (Olayioye *et al.*, 2000; Gullick, 2009; Tsujioka *et al.*, 2010; Cooper *et al.*, 2011).

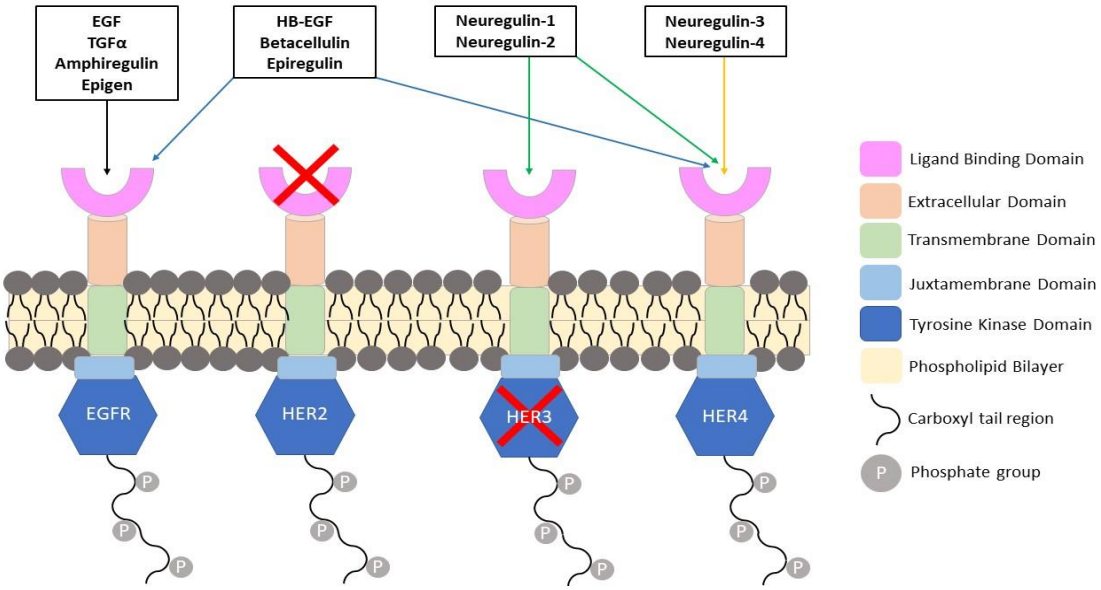

Figure 5.2: The variety of ligands that bind to ErbB Receptor Family Members

The diagram illustrates the conserved structure of all RTKs, previously shown in figure 5.2. The figure illustrates that family of ligands capable of binding to ErbB receptor family members. The figure displays the lack of a high-affinity binding ligand for HER2 receptor and the lack of intrinsic tyrosine kinase activity associated with HER3 receptor.

HER4, unlike other members of the EGF receptor family, can be expressed in 4 different isoforms which result as a consequence of alternative tissue-specific splicing. HER4 contains 2 spliceable regions, the intracellular cytoplasmic region (Cyt) and the extracellular juxtamembrane (JM) region (Burgess, 2008). A process of alternative exon splicing in the JM region results in 2 different isoforms, JM-a and JM-b. These isoforms differ in their two-step proteolytic cleavage susceptibility, with the JM-a isoform containing a tumour necrosis factor-α converting enzyme (TACE) cleavage site, which is absent from the JM-b isoform. As a result of this TACE cleavage site the JM-a isoform can release a shed ectodomain. Ectodomain shedding is essential to produce a proteolytically truncated receptor which can then undergo a further secondary cleavage by γ-secretase. γ-secretase cleavage, also referred to as regulated intra-membrane proteolysis (RIP), generates a cleavage event within the ErbB-4 transmembrane domain resulting in the release of the soluble intracellular domain of the JM-a HER4 isoform from the cell membrane The JM-a

intracellular domain of HER4 can then undergo translocation to the nucleus, where it may be involved in the regulation of gene expression (Muraoka-Cook, 2008; Veikkolainen *et al.*, 2011; Hoesl *et al.*, 2018). Alternatively an exon containing 16 amino acids, which encodes a PI3-K binding motif and a WW domain binding motif, is either present or absent from within the cytoplasmic region of the mature ErbB4 mRNA, resulting in 2 different isoforms of the HER4 receptor Cyt-1 and Cyt-2 respectively (Figure 5.3) (Paatero and Elenius, 2008; Veikkolainen *et al.*, 2011; Hoesl *et al.*, 2018). The WW domain comprises a short, conserved region of 40 amino

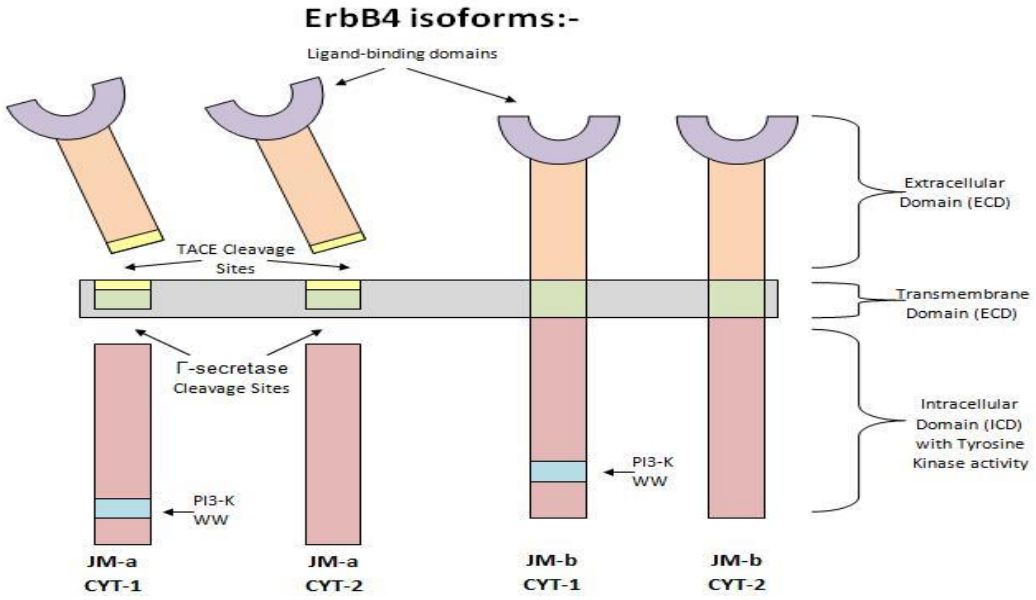

Figure 5.3: The four different isoforms of ErbB4

Isoform JM-a contains an extracellular TACE cleavage site and a transmembrane γ-secretase cleavage site, resulting in the release of both an ectodomain and a soluble intracellular region, whilst isoform JM-b does not. Isoform CYT-1 contains both PI3-K and WW binding motifs within the cytoplasmic receptor region whilst CYT-2 does not.

acids which can fold to form a stable triple-stranded beta sheet in several unrelated proteins (Sudol *et al.*, 1995). This domain receives its name from the presence of two signature tryptophan residues, found 20-23 amino acids apart and binds to proline-rich polypeptides or proteins containing phosphoserine-phosphothreonine motifs (Chen and Sudol, 1995; Macias, Wiesner and Sudol, 2002). The presence of a WW domain is frequently associated with the presence of other domains typical for proteins found to play a role in signal transduction processes.

5.1.2 The role of ErbB RTKs in cancer

The up-regulation or mutation of RTKs, particularly those members of the ErbB family are commonly observed in a variety of tumour types and are often diagnostic of a poorer patient prognosis or a more aggressive tumour form. Mutations and up-regulation can occur at many

stages of receptor signalling cascades, with the up-regulation of secondary messenger signals or alternative RTKs often compensating for the therapeutic repression of upstream RTKs. Several of the most prevalently observed tumour types globally have been found to contain ErbB receptor mutations or upregulation, including lung cancer, breast cancer, gastric cancer, colorectal cancer, pancreatic cancer and glioblastomas (Sergina and Moasser, 2007; Liu *et al.*, 2009; Foley *et al.*, 2010; Koutras *et al.*, 2010; Jaiswal *et al.*, 2013; Lee *et al.*, 2014; Roskoski, 2014b; Gallant *et al.*, 2015; Sequist *et al.*, 2015; Morgillo *et al.*, 2016; Takegawa and Yonesaka, 2017; Gerson *et al.*, 2017; Ansarin, Bagheri and Sharifi, 2018).

Lung cancer is currently the most prevalent cancer form worldwide with incidences of between 1.6-1.8 million cases globally every year and with overall mortality rates of 1.4-1.6 million, demonstrating that lung cancer is a disease attributed with high rates of mortality and poor treatment prognosis (Roskoski, 2014b; Hirsch *et al.*, 2017). Lung cancers are generally categorised into one of two categories: non-small cells lung cancer (NSCLC) types which account for around 85% of diagnosed lung cancers, including squamous cell carcinomas (35% of total lung carcinomas), adenocarcinomas (45%) and large cell carcinomas (10%), and small-cell lung cancer (SCLC) types which account for the remaining 15%. ErbB1/EGFR mutation or up-regulation plays important roles in the pathogenesis of lung carcinomas. EGFR kinase-domain mutations occur in around 10% of Caucasian lung cancer samples and 30-40% of Asian samples, with overexpression of EGFR occurring in around 60% of NSCLCs (Roskoski, 2014b). Increased EGFR expression as the result of gene amplification, increased receptor biosynthesis or decreased levels or receptor degradation have all been identified in large percentages of NSCLCs prompting the use of EGFR targeted therapies for the treatment of many lung carcinomas (Cataldo *et al.*, 2011; Roskoski, 2014b; Russo *et al.*, 2015, 2017; Morgillo *et al.*, 2016; Miyawaki *et al.*, 2017; T.Liu *et al.*, 2017). HER2 amplifications and over-expression have also been identified in lung cancer, with HER2 protein overexpression observed in 6% to 30% of patients with lung cancers and gene amplification present in 2% to 20% (Pillai *et al.*, 2017). HER2 protein over-expression has been identified in up to 35% of NSCLCs, with strong over-expression identified in 2-6% of cases. HER2 gene amplifications were observed in 10-20% of NSCLC patients and HER2 gene mutations found in 2-4% of cases (Mar, Vredenburgh and Wasser, 2015).

Both breast cancer and gastric cancer, two of the most commonly occurring cancer forms have been found to at times contain ErbB2 receptor mutations. In 2008 the estimated global incidence of breast cancer was 1.4 million, with around 460,000 deaths recorded for the malignancy making it the leading cause of cancer mortality for women worldwide (Roskoski, 2014b). Breast cancers can typically be grouped into three categories: hormone-receptor positive tumours, tumours with gene amplifications in or the over-expression of ErbB2/HER2 and triple-negative breast cancer

which lack both hormone receptor expression and HER2 overexpression or amplification status (Karlsson *et al.*, 2014; Al-Mahmood *et al.*, 2018). The overexpression or gene amplification of HER2 receptors occurs in around 20-30% of breast cancers, with high levels of HER2 expression linked with a poor patient prognosis before the advent of ErbB2 targeted therapies, such as Trastuzumab (Wang *et al.*, 2013b; Roskoski, 2014b; Ahmed, Sami and Xiang, 2015; Baselga *et al.*, 2017; Loibl and Gianni, 2017a). Triple negative breast cancer subtypes are often found to carry increased expression profiles of EGFR in place of the lack of hormone receptor and HER2 expression (Foley *et al.*, 2010; Ueno and Zhang, 2011; Pillai *et al.*, 2012; Park *et al.*, 2014; Sohn *et al.*, 2014; Simon *et al.*, 2016; Al-Mahmood *et al.*, 2018).

Gastric cancer is currently the second leading cause of total male and female cancer deaths globally, with incidence of around 1 million recorded stomach cancers each year and a mortality rate of 720,000-730,000 and accounting for around 20% of the total diagnosed cancers (Roskoski, 2014b; Van Cutsem *et al.*, 2016). Gastric cancers typically fall into two categories: the intestinal subtypes consisting of bulky tumours derived from glandular structures which account for 70-80% of gastric tumours and the diffuse subtype, which make up the remaining 20-30% and consist of infiltrative tumours comprising signet-ring morphologies (Roskoski, 2014b). Around 22% of gastric tumour patients present with HER2 overexpressing cancer types, with HER2 over-expression more likely to occur in the intestinal tumour group than the diffuse subtype. As with breast cancer HER2 overexpression was indicative of a poor patient prognosis before the use of HER2 targeted therapy Trastuzumab (Roskoski, 2014b; Ha *et al.*, 2015; Matsuoka, 2015; Fuse *et al.*, 2016; Kelly and Janjigian, 2016; Lucas and Cristovam, 2016). The over-expression of EGFR has also been identified in gastric cancers (Nagatsuma *et al.*, 2015; Fuse *et al.*, 2016; Junxiong Wang *et al.*, 2016). A study into gastric adenocarcinomas, which screened patient tumours for HER2, EGFR, MET and FGFR2, identified EGFR over-expressions in 23.5% of those investigated, and where its strong expression was indicative of poor patient outcome (Nagatsuma *et al.*, 2015).

5.1.2 Chapter Aims

- To assess a panel of snake and invertebrate venoms for their ability to cause reductions to EGFR phosphorylation levels in MDA-MB-468 and A431 cell lines using in-cell EGFR ELISAs

- To undertake dose responses of selected venoms from the ELISA screens in MDA-MB-468 cells using Western Blot analysis

5.2 Materials and Methods

5.2.1 Development of 96 well plate ELISA assays for the identification of changes in EGFR Phosphorylation state: Optimisation of the ELISA protocol

5.2.1.1 Determination of the Ideal Cell Number to Ensure an Appropriate Absorbance Window and Efficient Plate-Based Assay

MDA-MB-468 and A431 cells were trypsinised and counted as via standard protocol laid out in **2.1.3**. Cells were plated out at 6 different concentration in 96 well plates as via the plate layout in Appendix XII and returned to the incubator to settle and adhere overnight at 37ºC, 5% CO_2, 95% air.

Cells were treated (excluding the –ve EGF wells) with 50 µl/well of $1x10^{-7}$M EGF for 5 min. After 5 min all EGF was removed and cells were washed with PBS (2x 10 min, 100 µl/well). All PBS was removed, and the cells were fixed as via **2.4.1**. Subsequent ELISA steps were carried out as via the standard PY20 ELISA protocol laid out in **2.4.2,** with the exception of the following changes. PY20 1º antibody was used at a final working concentration of 1/2000, secondary antibody was used at a final working concentration of 1/40,000 and washes after the removal of secondary-HRP antibody were undertaken for 3x 10 min.

5.2.1.2 Adjustment of 1º antibody concentrations and wash steps to reduce background and optimise absorbance window

Due to a plateau in +EGF absorbance levels at the 2 highest cell concentrations in the previous optimisation it was decide that changes to 1º antibody concentrations may help to optimise the window of absorbance between +EGF and –EGF treated wells. The protocol was carried out as before in **5.2.1.1** with the following changes to antibodies implemented. Cells were plated out as before at the same 6 concentrations and the protocol adhered to as before until the 1º antibody incubation step. Each well was treated with 50µl of 1/1000 PY20 in 2% BSA/PBS (0.2%)Triton x-100 and left to incubate at 4 ºC overnight. Cells were washed 3x10 min with 200µl of PBS (0.2%)Triton x-100 before 100µl of diluted 2º antibody was added to each well (excluding 1º ab only control wells). Cells were incubated in the 2º antibody (rabbit-a-mouse-HRP in in 2% BSA/PBS (0.2%)Triton x-100, 1/40000 dilution) for 1h at RT on a rocker. After 1h, wells were washed 6x10 min with 200µl of PBS (0.2%)Triton x-100. The plate was then blotted and developed with TMB as via the previous methodology.

5.2.1.3 Adjustment of 2° antibody concentrations and determination of the best combination of 2° antibody and cell number

MDA-MB-468 and A431 cells were trypsinised and counted as via standard protocols laid out in **2.1.2** and **2.1.3**. MDA-MB-468 cells were plated at concentrations of $2x10^5$ and $5x10^4$ cells/well and A431 cells were plated at $2x10^5$ and $1x10^5$ cells/well. Cells were left to settle and ahead to plates overnight. Plate layout for combinations of cell number and 2° ab concentrations were laid out as via Appendix XIII.

Cells were treated in duplicates in different ways, with some receiving stimulation with EGF and some without (Appendix XIII B). All cells were fixed, permeabilised and quenched as via previous protocol laid out in **5.2.1.2**, and treated with PY20 antibody overnight at a concentration of 1/1000, previously ascertained in **5.2.1.2** (excluding 2°ab only controls) (Appendix XIII C). The following day, cells were rewashed and treated for 1h with 2° ab at concentrations of either 1/10,000, 1/20,000 or 1/40,000 (Appendix XIII D).

Cells were washed and TMB substrate signal developed for 30 min as via previous methodology determined in **2.4.2.** The absorbance of the plate was read within 10 mins of reaction completion at 450nm using a BMG Labtech Fluostar plate reader.

5.2.1.4 Z' Analysis of Optimised PY20 ELISA

MDA-MB-468 cells were trypsinised and counted as via the standard protocols laid out in **2.1.2** and **2.1.3**. Z' assay analysis was carried out to determine the robustness of the optimised PY20 ELISA assay. Cells were plated at the optimal cell number determined in **5.2.2.3** left to settle and adhere overnight. Cells were treated with either supplemented DMEM (-ve control) or $1x10^{-7}$M EGF (+ve control) for 5 min as via the plate layout in Appendix XIV.

After 5 min, cells were fixed using paraformaldehyde and the optimised PY20 ELISA protocol carried out as via **2.4.2**. Absorbance of TMB at 450nm was collected using a Fluostar plate reader (BMG Labtech) and the data analysed to produce a z' prime value for the assay for each cell line.

5.2.2 PY20 ELISA Screening of a Panel of Diverse Snake Venoms

MDA-MB-468 and A431 cells were trypsinised and counted as via standard protocol in **2.1.2** and **2.1.3**. Both cell lines were plated out into clear 96 well plates (Fisher, UK) at a concentration of $5x10^4$ and $1x10^5$ cells/well respectively. Cells were treated in quadruplicate with a panel of previously investigated snake venoms (See Table 4.1). All venoms were diluted in supplemented DMEM media to a working concentration of 20µg/ml, and a volume of 50µl (1µg total protein)

was added to each of the quadruplicate wells as via the plate layout in Appendix XV. Cells were incubated in the appropriate venom for 2h. After 2h, all venom was removed and the cells were stimulated with $1x10^{-7}$M EGF for 5min. PY20 ELISA protocol was undertaken as via the optimised protocol laid out in **2.4.2**.

Absorbance was recorded at 450nm using a Fluostar plate reader (BMG Labtech). Data was analysed, the % reduction in EGFR phosphorylation calculated and plotted graphically.

5.2.3 PY20 ELISA Screening of a Panel of Diverse Invertebrate Venoms

MDA-MB-468 and A431 cells were trypsinised and counted as via standard protocol in **2.1.2** and **2.1.3**. Both cell lines were plated out into clear 96 well (Fisher, UK) plates at a concentration of $5x10^4$ and $1x10^5$ cells/well respectively. Cells were treated in quadruplicate with a panel of previously investigated invertebrate venoms (See Tables 4.2 & 4.3). All venoms were diluted in supplemented DMEM media to a working concentration of 100 µg/ml, and a volume of 50µl (5µg total protein) was added to each of the quadruplicate wells as via the plate layout in Appendix XVI.

Cells were incubated in the appropriate venom for 2h. After 2h all venom was removed and the cells were stimulated with $1x10^{-7}$M EGF for 5 min. PY20 ELISA protocol was undertaken as via the optimised protocol laid out in **2.4.2**. Absorbance was recorded at 450nm using a Fluostar plate reader (BMG Labtech). Data was analysed, the % reduction in EGFR phosphorylation calculated and plotted graphically.

5.2.4 PY20 Analysis of Whole Snake and Invertebrate PY20 ELISA Data to produce % reduction in EGFR Phosphorylation Graphs

TMB absorbance data collected at 450nm for both cell lines treated with a panel of whole snake and whole invertebrate venoms was analysed. The absorbance of TMB at 450nm for each well was corrected for potential cell number variations upon assay completion by dividing the TMB absorbance value for each well by the corresponding absorbance of the crystal violet stain data collected at 595nm. An average of the corrected absorbances for each group of treatment or control replicates was calculated, excluding any obvious outlier values. Background phosphorylation levels were removed from each average value for each treatment group by subtracting the average absorbance of -EGF treated controls. The percentage phosphorylation of EGFR receptors for each treatment group was calculated, relative to the average +EGF absorbance group. Average corrected absorbance (-background) for each treatment group was divided by the average value for +EGF treatment and multiplied by 100 to produce a percentage

phosphorylation value. These percentage phosphorylation values for each treatment were then subtracted from 100 to produce a percentage reduction in phosphorylation value. Percentage reduction in EGFR phosphorylation was plotted graphically against whole venom treatment. Percentage standard error was calculated from crystal violet corrected replicates for each venom treatment group and plotted on the graphs as error bars.

Using Minitab statistical analysis software, normality and equal variance tests were performed on each data set (See Appendix XVII), followed by ANOVA analyses with post hoc Tukey comparisons.

5.2.5 Western Blot Analysis of Changes in EGFR Phosphotyrosine Levels

Western blot analysis was carried out to determine whether treatment with both a panel of whole snake venoms at a set dose or serial dilutions of selected whole venoms could result in changes in EGFR phosphorylation state.

5.2.5.1 Whole Snake Venom Panel Western Blots at a dose of 20 µg/ml

MDA-MB-468 cells were plated as via **2.2.2** and allowed to grow to at least 70% confluency. Cells were incubated in a panel of snake venoms, diluted to a final concentration of 20 µg/ml for 2h at 37^{o}C, 5% CO_2 (see Table 4.1). After 2h cells were stimulated with 1x10^{-7}M EGF for 5 min and cell lysis undertaken as via standard protocol in **2.2.3**. 10µl of each sample were loaded into 9% polyacrylamide gels and semi-dry Western Blotting and immunodetection undertaken as via protocols laid out in **2.3.2** and **2.3.3**. Blots were analysed as via **2.3.4** (See Appendix XVIII for analysis report)

5.2.5.2 Whole Venom Dose Response Western Blots

MDA-MB-468 cells were incubated in serial dilutions (within the range of 5 mg/ml-20 ng/ml) of whole venoms from a diverse range of species for 2h, before receptors were stimulated with EGF at a working concentration of 1x10^{-7}M and cell lysis undertaken as via standard protocol in **2.2.3**. 10-20µl of each sample were loaded into 9% polyacrylamide gels, to ensure equal protein loading of all samples and semi-dry Western Blotting and immunodetection undertaken as via protocols laid out in **2.3.2** and **2.3.3**. Blots were analysed as via **2.3.4** (See Appendix XIX for analysis reports)

5.3 Results and Discussion

5.3.1 Optimisation of the ELISA protocol

5.3.1.1 Determination of the ideal cell number to ensure an appropriate absorbance window and efficient plate-based assay

Cells were plated out at 6 different concentrations with the aim of identifying which cell number gave the largest window in TMB absorbance between EGF stimulated cells and the natural background phosphorylation levels observed in non-EGF stimulated cells. Development of the ELISA plate showed increased cells resulted in both an increase in the absorbance seen with EGF treated and non-treated cells. However lower cell numbers result in a smaller window as background levels do not appear to increase at the same rate as the absorbance levels of the cells treated with EGF. Both the primary and secondary antibody controls showed slight absorbance readings, suggesting the potential for a degree of non-specific antibody binding, with the secondary antibody contributing to a larger degree of non-specific binding than the primary (Figures 5.4A & B). There was the potential that some of the background observed in the –EGF treated cells could be attributed to non-specific antibody binding, as well as ambient levels of phosphorylation. With this in mind it was decided, in an attempt to further reduce non-specific antibody binding, that the wells of cells would be blocked with 200µl of 2% BSA/PBS (0.2%)Triton x-100 rather than the previously used 100µl. Interestingly after 30 min TMB incubation it was observable that the max absorbance was plateauing out at the highest 2 cell concentrations picked, despite the highest cell number containing twice the number of cells/well (Figures 5.4A & B). This was suggestive that this plateau effect could be the result of an exhaustion of the available primary antibody being added into each well, and that maybe an increase in primary antibody concentration could cause a boost in the absorbance window further by allowing more antibody binding to phosphotyrosine residues within the EGF receptors. Given that the max absorbance the plate reader can detect and still be accurate at is around 2 there was the potential to increase the absorbance window further by making adjustments to the primary antibody concentration.

It was also observable that the max absorbance obtainable in A431 cells at each of the different cell numbers was higher than that observed in MDA-MB-468 cells (Figures 5.4A & B). This is likely the result of the number of EGF receptors expressed per cell, with A431 cells known to express more EGF receptors per cell (≈$3x10^6$ EGFR/cell) than MDA-MB-468 cells (≈$1.3 - 2x10^6$ EGFR/cell) (Merlino *et al.*, 1984; Armstrong *et al.*, 1994; Jackson and Ceresa, 2016). This difference in EGFR number/cell is likely to result in differences in optimum cell number and the

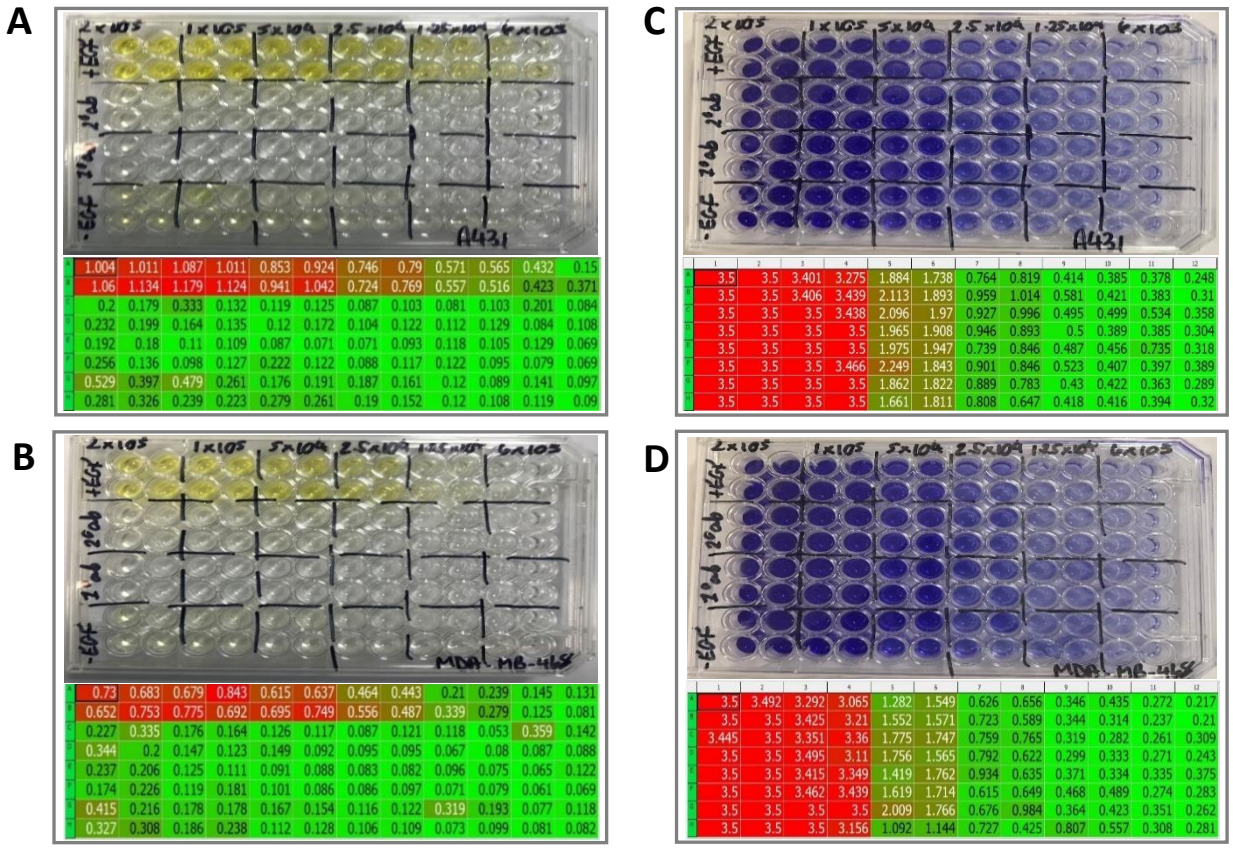

Figure 5.4: TMB and Crystal Violet Plate Images and Plate Reader Data

Figures A and B display the finished ELISA TMB Colour changes and plate reader data. The figures show higher levels of TMB absorption in the EGF stimulated cell wells compared with EGF-untreated wells and the wells treated with EGF but only one of the two required antibodies (antibody background controls). The data shows reductions to the obtained TMB absorbance with decreasing cell numbers (from left to right), showing higher cell numbers improve the obtainable signal. Figures C and D display the crystal violet detection of cells. Crystal violet staining showed that top cell numbers ($2x10^5$ cells, $1x10^5$ cells) are causing the 595nm absorption signal to max out, and so a dilution step is required to bring the absorbance back to within an accurate detectable range. Biological replicates/cell line = N1, Technical replicates/biological replicate = N4

obtainable max absorbance between the two investigated cell lines. Crystal violet staining of the cells showed an expected reduction in absorbance as the cell numbers decrease across the plates. Crystal violet absorbances appear fairly consistent across all the replicates for each of the investigated cell numbers (Figures 5.4C & D). Variations in crystal violet absorbance can be used to correct for differences in cell number from well to well. The absorbances obtained at the two highest cells numbers are well above the accuracy threshold of the plate reader used and so if either of these cell numbers were selected for the final ELISA a consistent dilution would need to be applied across the plate to bring the 595nm absorbance values back to within the accurate detectable range of the plate reader (Figures 5.4C & D).

5.3.1.2 Adjustment of 1º antibody concentrations and wash steps to reduce background and optimise absorbance window

To increase the absorbance window between wells treated with or without EGF, adjustments were made to the concentration of primary antibody used in the assay and the number and frequency of wash steps carried out after the completion of the secondary antibody binding step. Data obtained from the previously tested protocol showed a plateau effect in maximum obtainable absorbancy at the 2 highest cell numbers tested (Figure 5.4). With twice the number of cells plated at the highest tested cell seeding there should have been the potential for twice the absorbancy window. As available receptors for antibody binding can not be considered the limiting cause for no change in absorbance window, then the availability of primary antibody, capable of initial binding to those receptors colud not be ruled out. Increasing the concentration of primary antibody from 1/2000 to 1/1000 resulted in increases to the achievable maximum fluorescence in EGF-treated cells of almost double (Figures 5.5) that the values previously obtained for 1/200 PY20 antibody (Figures 5.4). Increasing the concentration of primary anitbody did not appear to cause dramatic increases to the levels of detectable background phosphorylation (-EGF treated wells) suggesting that increasing the concentration of primary antibody does not result in an increase to background through non-specific binding.

Statistical analysis of the six selected cell numbers was undertaken using Minitab Statistical Analysis software. Total background signal was calculated from each cell number group of -EGF-treated samples and this average subtracted from each replica of the EGF-treated samples of the same cell number. Normality and equal variance tests were performed on each data set, which confirmed that the data conformed to the patrameteres exprected for that of normally distributed data. A one-way ANOVA, with posthoc Tukey's pairways comparison was performed on the data sets from both cell lines, to determine the optimal cell number to take forward for future ELISA assays. ANOVA of both A431 and MDA-MB-468 cells resuted in p-values of 0.00, showing that

A

Analysis of Variance

Source	DF	Adj SS	Adj MS	F-Value	P-Value
Subscripts	5	2.7598	0.551960	69.25	0.000
Error	16	0.1275	0.007971		
Total	21	2.8873			

Model Summary

S	R-sq	R-sq(adj)	R-sq(pred)
0.0892777	95.58%	94.20%	91.50%

Grouping Information Using the Tukey Method and 95% Confidence

Subscripts	N	Mean	Grouping
2x105	3	1.4873	A
1x105	3	1.4697	A
5x104	4	1.2757	A B
2.5x104	4	1.0955	B C
1.25x104	4	0.9958	C
6x103	4	0.4417	D

Means that do not share a letter are significantly different.

B

Analysis of Variance

Source	DF	Adj SS	Adj MS	F-Value	P-Value
Subscripts	5	1.3569	0.27138	19.62	0.000
Error	18	0.2490	0.01383		
Total	23	1.6059			

Model Summary

S	R-sq	R-sq(adj)	R-sq(pred)
0.117621	84.49%	80.19%	72.43%

Grouping Information Using the Tukey Method and 95% Confidence

Subscripts	N	Mean	Grouping
5x104	4	1.0148	A
2x105	4	1.0097	A
2.5x104	4	1.0078	A
1x105	4	0.9792	A B
1.25x104	4	0.7225	B
6x103	4	0.3718	C

Means that do not share a letter are significantly different.

Figure 5.5: ANOVA Analysis of Maximum TMB Absorbance at Different Cell Plating Numbers

ANOVA analysis of TMB absorption in A431 (A) and MDA-MB-468 (B) at 6 different cell plating numbers ($2x10^5$, $1x10^5$, $5x10^4$, $2.5x10^4$, $1.25x10^4$ & $6x10^3$). Tukey's Grouping method identified no statistical differences between the absorbance widow in the three highest tested cell numbers for MDA-MB-468 and the 4 highest tested cell numbers in A431 cells.

there are significant differences between the obtainable window at different cell concentrations (Figure 5.5E & F). Tukey's comparision identified there as being no statistical difference in achievable window of the three highest cell numbers investigated for A431 (Figure 5.5E) and the four highest tested cell numbers for MDA-MB-468 cells (Figure 5.5F). Despite the statistical analysis deeming there to be no statistically significant difference between the three highest cell numbers tested for A431 cells, there was a difference in maximum absorbance window between the top two highest cell numbers ($2x10^5$, $1x10^5$) and the third highest cell concentration ($5x10^4$) of around 1.48 in the previous two and 1.27 in the latter. It was decided that as there was no difference in window between the top two cell concentrations that $1x10^5$ cells/well would be selected to take forward for future A431 cell assay ELISAs. Similarly, whilst statistically analysis identified the top four MDA-MB-468 cell concentrations as being statistically the same, there was a slight reduction to the window of absorbance between the fourth cell ($2.5x10^4$) concentration and the three higher cell concentrations ($2x10^5$, $1x10^5$, $5x10^4$). Therefore, it was decided that a cell concentration of $5x10^4$ cells/well seemed the most appropriate to take forward for future MDA-MB-468 cell ELISAs. Crystal violet cell staining of both the A431 and MDA-MB-468 optimal cell numbers identified that both cause absorbance readings greater than the accurate absorbance threshold of the plate reader (Figure 5.5C & D). Therefore, a dilution step will be implemented to all wells to bring the absorption values for each well back within the workable range of the plate reader.

5.3.1.3 Determination of correct 2° antibody concentrations and cell number combination

Analysis of A431 and MDA-MB-468 cells at the two selected cell numbers and the three selected secondary antibody concentrations identified that increasing the secondary antibody concentration further increased the maximum achievable TMB absorption values for EGF-stimulated cells (Figure 5.6). However, with the increases to +EGF treated cells signals also came an increases to the -EGF and background absorbance values, most likely the result of increased incidences of non-specific secondary antibody binding. Combinations of higher cell number and higher antibody concentrations resulted in absorbance figures above two, which increases the likelihood of error within the absorbance values. Analysis of the values obtained for A431 cell and antibody concentrations identified that increasing the secondary antibody concentration seems to have more of an effect than increasing the number of cells, with both the cell numbers ($2x10^5$, $1x10^5$) at the highest antibody concentration yielding the same absorption window value of around 1.7 (Figure 5.6C). It was therefore decided that selected the higher antibody concentration of 1/10,000 and the lower cell number ($1x10^5$) would be the most logical choice to take forward to future ELISA assays. For consistency it was decided that the same secondary antibody concentration should be considered for both A431 and MDA-MB-468 cell ELISAs, to

A

	1	2	3	4	5	6	7	8	9	10	11	12
A	0.157	0.197	2.826	1.562	0.115	0.114	0.225	0.229	2.774	2.626	0.146	0.138
B	0.645	0.656	2.885	1.776	0.446	0.461	0.669	0.726	2.826	2.663	0.696	0.715
C	0.428	0.46	2.545	1.15	0.308	0.307	0.478	0.487	2.321	2.011	0.351	0.396
D	0.295	0.301	2.501	1.092	0.201	0.211	0.358	0.349	2.583	2.015	0.284	0.276
E	0.158	0.213	1.814	0.666	0.103	0.114	0.221	0.207	1.465	1.285	0.14	0.127
F	0.708	0.717	1.928	0.696	0.539	0.543	1.076	1.049	1.424	1.309	0.882	0.885
G	0.505	0.499	0.158	0.098	0.333	0.326	0.672	0.65	0.234	0.147	0.544	0.541
H	0.337	0.346	0.14	0.095	0.265	0.244	0.493	0.475	0.151	0.111	0.411	0.517

B

MDA-MB-468 cells								
	$2x10^5$ cells (+EGF)		$2x10^5$ cells (-EGF)		$5x10^4$ cells (+EGF)		$5x10^4$ cells (-EGF)	
	Average	St. Dev	Average	St. Dev	Average	St. Dev	Average	St. Dev
1/10,000	2.8555	0.0295	0.7125	0.0045	1.669	0.107	0.541	0.002
1/20,000	2.523	0.022	0.502	0.003	1.121	0.029	0.3295	0.0035
1/40,000	1.871	0.057	0.3415	0.0045	0.681	0.015	0.2545	0.0105

window:-		
	$2x10^5$ cells (+EGF - -EGF)	$5x10^4$ cells (+EGF - -EGF)
1/10,000	2.143	1.128
1/20,000	2.021	0.7915
1/40,000	1.5295	0.4265

C

A431 cells								
	$2x10^5$ cells (+EGF)		$2x10^5$ cells (-EGF)		$1x10^5$ cells (+EGF)		$1x10^5$ cells (-EGF)	
	Average	St. Dev	Average	St. Dev	Average	St. Dev	Average	St. Dev
1/10,000	2.8	0.026	1.0625	0.0135	2.6445	0.0185	0.8835	0.0015
1/20,000	2.452	0.131	0.661	0.011	2.013	0.002	0.5425	0.0015
1/40,000	1.4445	0.0205	0.484	0.009	1.297	0.012	0.464	0.053

window:-		
	$2x10^5$ cells (+EGF - -EGF)	$1x10^5$ cells (+EGF - -EGF)
1/10,000	1.7375	1.761
1/20,000	1.791	1.4705
1/40,000	0.9605	0.833

Figure 5.6: Analysis of Combined Cell Number and Secondary Antibody Concentrations on Achievable TMB Absorption

Figure A displays the raw data generated from the plate reader for TMB absorptions. Plate layout contained MDA-MB-468 and A431 cells at concentrations of $2x10^5$ (maximum tested cell number/well) and $5x10^4$ and $1x10^5$ cells respectively (previously selected optimal cell number). The plate contains controls for all three secondary antibody concentrations, +EGF treated samples and -EFG treated samples at all three secondary antibody concentrations (1/10,000, 1/20,000, 1/40,000). Figure B shows the average and standard deviation (St. Dev) values for the MDA-MB-468 data and the resultant absorbance values when the background absorbance is subtracted at each secondary antibody and cell number concentration. Figure C shows the average and standard deviation (St. Dev) values for the A431 data and the resultant absorbance values when the background absorbance is subtracted at each secondary antibody and cell number concentration. Biological replicates/cell line = N1, Technical replicates/biological replicate = N2

minimise the potential for variation as a result of differing assay parameters. MDA-MB-468 cell numbers of $2x10^5$ and $1x10^5$ in combination with a secondary antibody concertation of 1/10,000 resulted in TMB absorbance values of 2.143 and 1.128, respectively. Whilst increasing the cell number does appeared to have caused increases to the obtainable cell values for MDA-MB-468, the higher cell number of $2x10^5$ cells caused an absorbance value greater than 2 and so it was decided that a cell number of $5x10^4$ would allow for both an absorbance value within the accuracy range of the plate reader and allow for cells to go further in future screening assays.

5.3.2 Z' Analysis of Optimised PY20 ELISA to Determine Assay Robustness

Z' analysis of the optimised ELISA protocol was undertaken to determine whether the assay is statistically robust. Z' analysis generated z' values for the A431 assay of 0.465 and for the MDA-MB-468 assay of 0.486 (Figure 5.7). In order for an assay to be considered good and statistically robust it should pass with a z' value of greater than 0.5. Both of these z' values fall just below this 0.5 z' value threshold, suggesting that the assay could require further optimisation to make it even more statistically robust. Standard deviations of the +EGF positive values for both the A431 and MDA-MB-468 assays show an error of around 10% of the average absorbance values. Whilst a smaller percentage error would be better, there also appears to be around 10% standard deviation in the -EGF replica readings, suggesting that this could be error associated with equipment rather than experiment error associated with differences in replica treatments. Despite optimisation, the window between the absorbance values obtained for EGF-stimulated vs normal background EGF levels (unstimulated) are still relatively small in comparison to the windows obtainable with some fluorescent substrates. The use of TMB, a commonly used ELISA substrate in combination with fixed cells which have ambient levels of receptor phosphorylation could be the reason why the z' assay for both cell lines fell below the 0.5 threshold.

Whilst further optimisation may have improved the potential window further, it was decided that the z' values were close enough to the 0.5 threshold to proceed to the whole venom screening assays.

5.3.3 PY20 ELISA screening of a panel of 18 diverse snake venoms

Treatment with whole snake venoms at a dose of 20 µg/ml resulted in several reductions to the phosphorylation levels of EGFR in either one or both of the investigated cancer cells lines (Figure 5.8). Of the venoms selected from members of the elapid family (Cobras, mambas, brown snakes), true cobras (Naja spp) showed little effect on the phosphorylation levels of EGFR in either cell line (Figure 5.8). Both Brown snake *P. rossignoli* and King cobra *O. hannah* resulted in reductions

A

A431 Cells

	1	2	3	4	5	6	7	8	9	10	11	12
A	1.343	1.333	1.38	1.458	1.434	1.485	0.58	0.565	0.6	0.563	0.577	0.576
B	1.395	1.497	1.506	1.384	1.528	1.584	0.687	0.632	0.628	0.57	0.622	0.667
C	1.428	1.528	1.514	1.455	1.415	1.527	0.687	0.738	0.689	0.68	0.623	0.629
D	1.461	1.526	1.524	1.501	1.287	1.58	0.634	0.636	0.683	0.596	0.634	0.638
E	0.643	0.683	0.712	0.686	0.687	0.648	1.599	1.58	1.575	1.67	1.615	1.589
F	0.608	0.645	0.672	0.671	0.716	0.696	1.591	1.647	1.642	1.634	1.756	1.663
G	0.538	0.606	0.59	0.616	0.64	0.627	1.638	1.641	1.679	1.764	1.814	1.7
H	0.622	0.599	0.597	0.592	0.63	0.634	1.512	1.537	1.699	1.716	1.698	1.535

μp	1.553479
μn	0.63525
σp	0.118892
σn	0.04488
Z' value	0.46493

B

MDA-MB-468 Cells

	1	2	3	4	5	6	7	8	9	10	11	12
A	0.317	0.328	0.305	0.316	0.333	0.353	1.521	1.393	1.379	1.276	1.167	0.93
B	0.269	0.348	0.309	0.326	0.345	0.359	1.519	1.435	1.325	1.326	1.341	1.078
C	0.276	0.34	0.313	0.326	0.348	0.364	1.524	1.491	1.366	1.273	1.204	0.917
D	0.276	0.303	0.34	0.309	0.339	0.379	1.54	1.422	1.347	1.346	1.25	1.215
E	1.279	1.391	1.509	1.457	1.625	1.532	0.374	0.36	0.35	0.36	0.332	0.29
F	1.292	1.434	1.422	1.454	1.428	1.516	0.342	0.345	0.353	0.339	0.305	0.277
G	1.252	1.492	1.461	1.423	1.534	1.5	0.379	0.373	0.448	0.351	0.319	0.291
H	1.255	1.32	1.38	1.357	1.428	1.425	0.331	0.356	0.329	0.327	0.31	0.309

μp	1.369813
μn	0.332729
σp	0.145259
σn	0.032323
Z' value	0.486304

Figure 5.7: Z' Assay Analysis of PY20 ELISA Protocol

Figure shows the plate reader outputs and z' statistical analyses of A431 **(A)** and MDA-MB-468 **(B)** Cells stimulated with $1x10^{-7}$ M EGF (max EGFR phosphorylation) or untreated (min EGFR phosphorylation). Biological replicates/cell line = N2, Technical replicates/biological replicate = N48

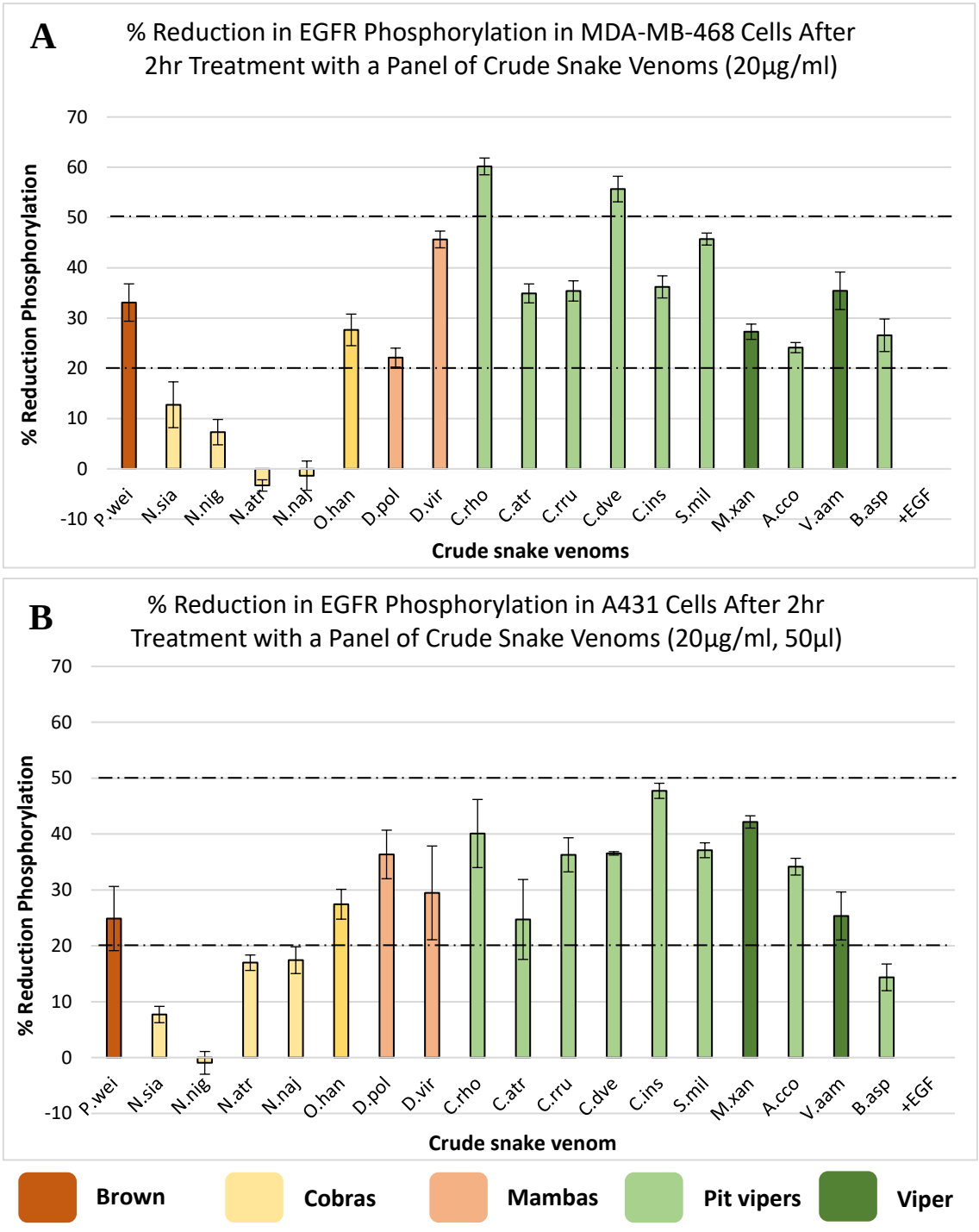

Figure 5.8: PY20 Assay Graphs of MDA-MB-468 and A431 cells treated with 20µg/ml Snake Panel

Graphical analysis of MDA-MB-468 **(A)** and A431 **(B)** cells treated in PY20 ELISAs with a panel of whole snake venoms. % Standard error of the mean was calculated for each group of treatment replicates and plotted on the graphs as error bars. Threshold lines of 20% and 50% EGFR phosphorylation reduction were added to the graphs to enable easy identification of venoms that caused reductions greater than these thresholds. Biological replicates/cell line = N1, Technical replicates/biological replicate = N4

A

Analysis of Variance

Source	DF	Adj SS	Adj MS	F-Value	P-Value
Subscripts	18	0.18052	0.010029	22.32	0.000
Error	49	0.02201	0.000449		
Total	67	0.20254			

Model Summary

S	R-sq	R-sq(adj)	R-sq(pred)
0.0211952	89.13%	85.14%	79.68%

Grouping Information Using the Tukey Method and 95% Confidence

Subscripts	N	Mean	Grouping
N.atr	4	0.29865	A
N.naj	3	0.2930	A
+EGF	3	0.2891	A B
N.nig	4	0.2680	A B C
N.sia	3	0.22817	B C D
D.pol	4	0.22511	C D
A.cco	3	0.21936	C D
P.wei	3	0.21273	C D E
M.xan	4	0.21023	D E
O.han	4	0.2092	D E
B.asp	3	0.19530	D E
C.atr	4	0.18820	D E
V.aam	4	0.1867	D E
C.ins	4	0.1844	D E
C.rru	3	0.17624	D E F
D.vir	4	0.15716	E F G
S.mil	4	0.15694	E F G
C.dve	3	0.1168	F G
C.rho	4	0.11516	G

Means that do not share a letter are significantly different.

B

Analysis of Variance

Source	DF	Adj SS	Adj MS	F-Value	P-Value
Subscripts	18	0.3973	0.022073	5.11	0.000
Error	49	0.2117	0.004320		
Total	67	0.6090			

Model Summary

S	R-sq	R-sq(adj)	R-sq(pred)
0.0657230	65.24%	52.48%	30.02%

Grouping Information Using the Tukey Method and 95% Confidence

Subscripts	N	Mean	Grouping
N.nig	4	0.6084	A
+EGF	3	0.5324	A B C
N.sia	4	0.5241	A B
B.asp	4	0.5162	A B C
P.wei	3	0.5040	A B C D
N.atr	4	0.5004	A B C D
N.naj	4	0.4977	A B C D
V.aam	4	0.4500	A B C D
O.han	4	0.4374	A B C D
C.dve	3	0.4178	B C D
A.cco	4	0.3968	B C D
C.atr	3	0.3966	B C D
C.rru	3	0.3841	B C D
D.pol	3	0.3837	B C D
S.mil	4	0.3791	B C D
D.vir	3	0.3749	B C D
C.rho	4	0.3611	B C D
M.xan	4	0.3486	C D
C.ins	3	0.3150	D

Means that do not share a letter are significantly different.

Figure 5.9: Statistical Analysis of MDA-MB-468 and A431 Whole Snake Venom PY20 ELISA Assays

ANOVA Statistical analysis of MDA-MB-468 **(A)** and A431 **(B)** PY20 ELISAs. Normality and equal variance tests confirmed data sets were normal and so ANOVA analysis was undertaken. ANOVA statistical analysis generated a P value and R-sq value for level of significance. Post Hoc Tukey's Test analysis identified whole venoms causing significant reductions from +EGF-only treated cells. Results of significant differences are highlighted in yellow boxes. Red boxes highlight the EGF-only treated Tukey Grouping letters.

of between 25-35% in EGFR phosphorylation in both MDA-MB-468 and A431 cells in the undertaken ELISAs. Treatment with mamba venom *D. viridis* resulted in reductions to EGFR phosphotyrosine levels of around 45% and 30% in MDA-MB-468 and A431 cells respectively, whilst treatment with *D. polylepis* caused reductions in the two cell lines of 22% and 35% (Figure 5.8). Overall, larger degrees of reductions were observed in EGFR phosphotyrosine levels in response to treatment with the panel of pit viper venoms than the elapid venoms. Treatment with two whole pit viper venoms, *C. durissus vegrandis* and *C. rhodostoma*, resulted in reductions of greater than 50% to EGFR phosphotyrosine levels in MDA-MB-468 cells. Treatment with S. miliarius barbouri venom saw reductions of greater than 45%, whilst treatment with three other pit viper venoms and one viper venom (*C. atrox, C. ruber*, *T. albolabris insularis* and *V. ammodytes ammodytes*) saw reductions of around 35% (Figure 5.8A).

No reductions of 50% or greater were observed in EGFR phosphotyrosine levels in A431 cells, with the largest observed reductions in this cell line between 40-50% and in response to pit viper venoms *C. rhodostoma, T. albolabris insularis* and viper venom *Montivipera xanthina*. Whilst reductions in phosphotyrosine levels in this cell line were smaller than some of the reductions observed in MDA-MB-468 cells, there was a similar pattern to the venoms causing reductions, with no or small reductions observed in response to true cobra venoms but reductions following *P. rossignoli, D. viridis, D. polylepis* and *O. hannah,* and the bulk of the reductions observed in response to treatment with the screened pit viper and viper venoms (Figure 5.8B). The lower reductions to EGFR phosphotyrosine levels observed in A431 cells are likely the result of a combination of both the selected dose of 20 µg/ml and the higher expression levels of EGFR in A431 cells over MDA-MB-468 cells.

Minitab statistical analysis was undertaken to determine whether the snake venoms in the PY20 ELISA screens were causing statistically significant reductions to EGFR phosphotyrosine levels in either cell line. Normality and equal variance tests were performed on each data set for both cell lines. The data sets were confirmed to both be normally distributed and to have equal variance (See appendix XVII) and so one-way ANOVA analysis with post hoc Tukey comparisons were performed (Figure 5.9). Analysis of the MDA-MB-468 data generated a p-value of 0.00, with Tukey's analysis identifying 14/18 of the tested whole venoms as being statistically significant. Statistical analysis identified that the 4 tested true cobra venoms (*N. atra, N. naja, N. siamensis* and *N. nigricollis*) were the only 4 venoms that did not cause statistically significant reductions to EGFR phosphotyrosine levels in MDA-MB-468 cells (Figure 5.9A). Most statistically significant reductions were identified as being the result of *C. rhodostoma, S. miliarius barbouri, D. viridis* and *C. durissus vegrandis* pit viper venoms. ANOVA analysis of A431 cell ELISA data sets generated a p-value of 0.000, with the Tukey's comparison test identifying only one of the

screened venoms as being statistically significant from the EGF-only treated data set (*T. albolabris insularis*) (Figure 5.9B). As seen with the MDA-MB-468 the smallest differences from the EGF-only treated data set was those treated with true cobra venoms (*Naja* spp), brown snake (*P. rossignoli*) and pit viper *B. asper*. Despite not being considered statistically significant, other venoms which caused the greatest reductions in EGFR phosphotyrosine levels in A431 cells when compared to EGF-only treated levels also included *C. rhodostoma, S. miliarius barbouri, D. viridis* and *M. xanthina*. Interestingly, *C. rhodostoma, S. miliarius barbouri* and *D. viridis* venoms were found to be amongst those venoms causing the greatest reductions to EGFR phosphorylation in both of the screened cell lines.

5.3.4 PY20 ELISA screening of a panel of diverse invertebrate venoms venom

Treatment with whole invertebrate venoms at a dose of 100 µg/ml resulted in slight reductions to the phosphorylation levels of EGFR in response to a few of the venom panel (Figure 5.10). Unlike with the previously screened snake panel, reductions to EGFR phosphotyrosine levels were significantly smaller in response to treatment with the invertebrate panel. The largest reductions observed were seen in A431 cells in response to scorpion venom *H. swammerdami* and theraphosid venom *P. cambridgei*, with reductions of just over 30% seen following treatment with the 100 µg/ml doses of these two venoms. Reductions were observed in both MDA-MB-468 and A431 cell EGFR phosphotyrosine levels following treatments with some the same venoms, which included *H. swammerdami, P. kraepelini, P. liosoma* (scorpions), *A. geniculata, A. metallica, P. cambridgei, T. pruriens* (theraphosids) and *C. giganteus* (millipede). Additional reductions were observed in A431 cells following treatment with *A. australis, H. arizonensis, A. cordubensis* and *P. lugardi*, with additional reductions observed in MDA-MB-468 cells in response to *B. boehmei* and *C. albostriatum*. Interestingly, the theraphosid venoms which were found to cause reductions to EGFR phosphotyrosine levels in both cell lines were all new world tarantulas and included both arboreal (*A. metallica, P. cambridgei*) and terrestrial (*A. geniculata, T. pruriens*) members.

Minitab statistical analysis was undertaken to determine whether the invertebrate venoms in the PY20 ELISA screens were causing statistically significant reductions to EGFR phosphotyrosine levels in either cell line. Normality and equal variance tests were performed on each data set for both cell lines. The data sets were confirmed to both be normally distributed and to have equal variances (see appendix XVII), and so one-way ANOVA analysis with post hoc Tukey comparisons were performed (Figure 5.11). Analysis of the MDA-MB-468 data generated a p-value of 0.00. However, Tukey's testing identified that there was no statistically significant differences between any of the whole venoms treated ELISA data sets and the EGF-treated data

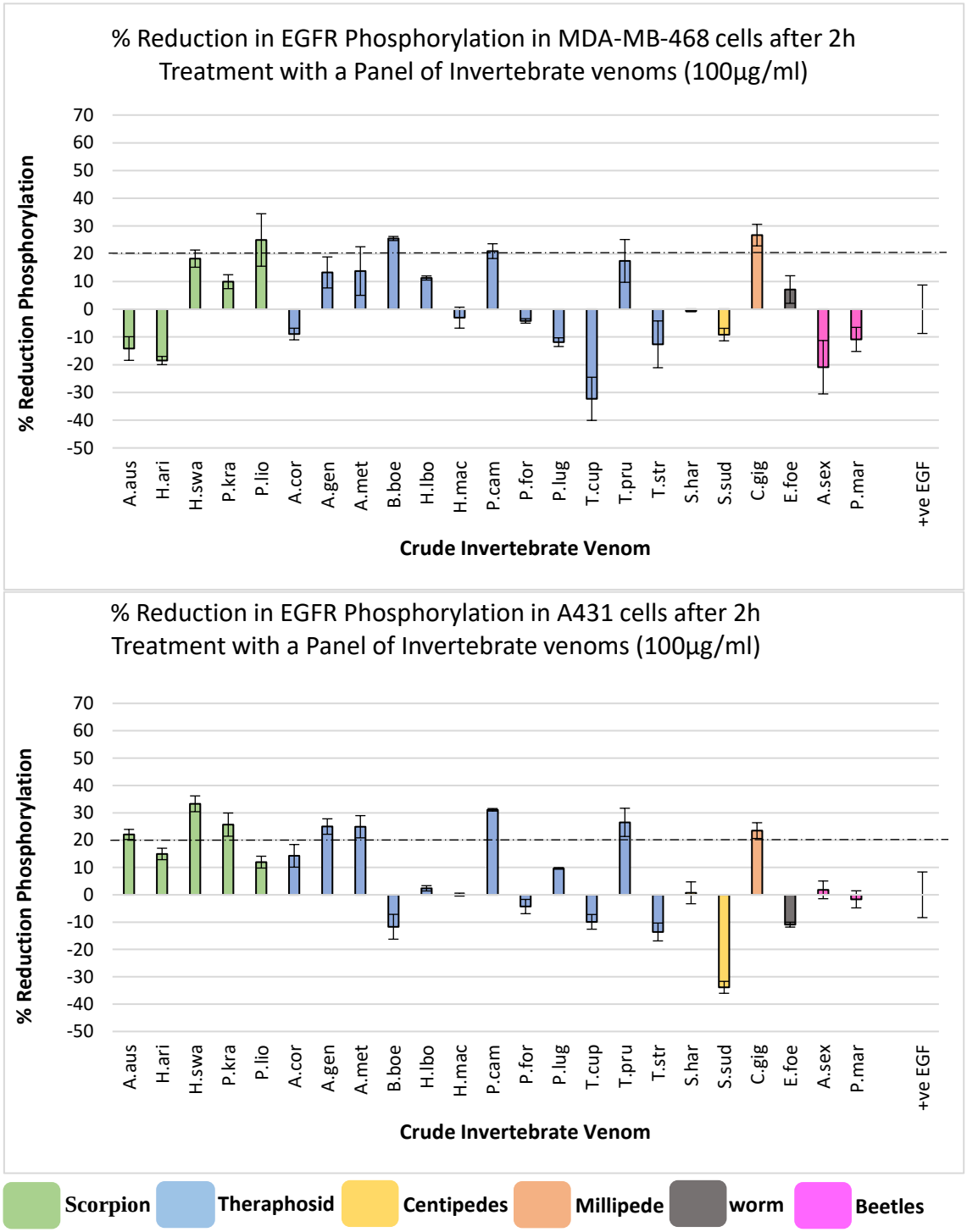

Figure 5.10: Graphical Analysis of PY20 ELISA Data from MDA-MB-468 and A431 Cells Treated with a Panel of Invertebrate Venoms at 100µg/ml

Shows the % Reduction in Phosphorylation on EGF receptors in MDA-MB-468 (A) and A431 (B) cells treated with whole invertebrate venoms at concentrations of 100µg/ml for 2h. Error bars were calculated as % standard error across the repeat readings. Biological replicates/cell line = N1, Technical replicates/biological replicate = N3

A

Analysis of Variance

Source	DF	Adj SS	Adj MS	F-Value	P-Value
Subscripts	23	2.958	0.12859	3.41	0.000
Error	41	1.548	0.03775		
Total	64	4.505			

Model Summary

S	R-sq	R-sq(adj)	R-sq(pred)
0.194290	65.65%	46.38%	15.42%

Tukey Pairwise Comparisons

Grouping Information Using the Tukey Method and 95% Confidence

Subscripts	N	Mean	Grouping
T.cup	3	1.894	A
H.ari	3	1.7757	A B
A.sex	2	1.731	A B C
T.str	2	1.613	A B C
P.lug	3	1.6018	A B C
P.mar	3	1.5877	A B C
S.sud	3	1.5627	A B C
A.cor	2	1.5600	A B C
H.mac	3	1.4754	A B C
S.har	2	1.44141	A B C
A.aus	3	1.441	A B C
+ve EGF	5	1.432	A B C
P.for	3	1.4059	A B C
A.gen	3	1.380	A B C
H.lbo	3	1.3423	A B C
E.foe	3	1.3302	A B C
P.kra	3	1.2897	A B C
H.swa	3	1.271	B C
A.met	2	1.235	A B C
T.pru	2	1.182	B C
P.cam	2	1.1321	B C
B.boe	3	1.0969	C
P.lio	2	1.074	C
C.gig	2	1.0492	C

Means that do not share a letter are significantly different.

B

Analysis of Variance

Source	DF	Adj SS	Adj MS	F-Value	P-Value
Subscripts	23	2.6694	0.11606	7.14	0.000
Error	51	0.8296	0.01627		
Total	74	3.4990			

Model Summary

S	R-sq	R-sq(adj)	R-sq(pred)
0.127538	76.29%	65.60%	51.45%

Tukey Pairwise Comparisons

Grouping Information Using the Tukey Method and 95% Confidence

Subscripts	N	Mean	Grouping
S.sud	3	1.6949	A
B.boe	3	1.4144	A B
E.foe	3	1.4045	A B
T.cup	3	1.3916	A B C
T.str	3	1.3737	A B C
H.lbo	3	1.3327	A B C D
P.for	3	1.3207	A B C D
P.mar	3	1.2874	B C D
+ve EGF	7	1.2672	B C D
H.mac	3	1.26538	B C D
S.har	3	1.2571	B C D
A.sex	3	1.2434	B C D E
A.cor	3	1.1622	B C D E
P.lug	3	1.14403	B C D E
C.gig	3	1.125	B C D E
P.lio	3	1.1150	B C D E
A.aus	3	1.101	B C D E
H.ari	3	1.0771	B C D E
T.pru	3	1.037	B C D E
A.met	3	0.9511	D E
A.gen	2	0.9502	C D E
P.cam	3	0.9452	D E
P.kra	3	0.9412	D E
H.swa	3	0.8449	E

Means that do not share a letter are significantly different.

Figure 5.11: Statistical Analysis of MDA-MB-468 and A431 Whole Invertebrate Venom PY20 ELISA Assays

ANOVA Statistical analysis of MDA-MB-468 **(A)** and A431 **(B)** PY20 ELISAs. Normality and equal variance tests confirmed data sets were normal and so ANOVA analysis was undertaken. ANOVA statistical analysis generated a P value and R-sq value for level of significance. Post Hoc Tukey's Test analysis identified whole venoms causing significant reductions from +EGF-only treated cells. Results of significant differences are highlighted in yellow boxes. Red boxes highlight the EGF-only treated Tukey Grouping letters.

set. Statistically significant differences were detected between different venom-treated sets, with some of the whole venoms causing increases to EGFR phosphotyrosine levels, whilst others caused reductions (Figure 5.11A).

ANOVA analysis of A431 cell ELISA data sets generated a p-value of 0.000, with the Tukey's comparison test identifying two of the screened venoms as being statistically significant from the EGF-only treated data set, one which caused a significant decrease to EGFR phosphorylation (*H. swammerdami*) and the other which caused a significant increase (*S. subspinipes dehaani*) (Figure 5.11B). Increasing the dose of some of the whole invertebrate venoms which caused slight reductions to EGFR phosphotyrosine levels from the 100 µg/ml could increase the reductions, making them statistically significant.

5.3.5 Western Blot analysis of MDA-MB-468 cells treated with a 20 µg/ml panel of snake venoms

Western Blot analysis of EGFR phosphotyrosine profiles in breast cancer cell line MDA-MB-468 treated with a panel of snake venoms at a dose of 20 µg/ml for 2h identified a variety of venoms that appear to cause a reduction in EGF receptor phosphorylation levels. There appeared to be family specific affects, with several members of the tested pit vipers and the mambas causing the largest reductions in phosphorylation levels (Figure 5.12).

Treatment with selected venoms from the elapid family, comprising 1 brown snake, 4 true cobras, 1 king cobra and 2 mambas, resulted in a mixed degree of changes to EGFR phosphorylation levels post-treatment at the selected dose. Treatment with the true cobras (*Naja siamensis, Naja nigricollis, Naja atra* and *Naja naja*) resulted in a mixture of small reductions to EGFR phosphorylation levels and increases to overall phosphorylation levels. Treatment with 20 µg/ml of *N. siamensis* and *N. naja* venoms resulted in reductions in EGFR phosphorylation levels of 20% and 30% respectively. Treatment with *N. nigricollis* venom resulted in around 10% increases in receptor phosphorylation levels, whilst treatment with *N. atra* venom resulted in increases in receptor phosphorylation level greater than 70% (Figure 5.12). The findings of these Western Blots appear to be fairly consistent with the previous findings of the PY20 ELISAs, that found that treatment with true cobra family members caused no statistically significant changes to EGFR phosphotyrosine levels when used at a dose of 20 µg/ml, with the exception of the increases seen in response to *N. atra* venom in these Western blots (Figures 5.8 & 5.12). Treatment with a 20 µg/ml dose of king cobra venom (*Ophiophagus hannah*) and Western Blot analysis identified slight reductions to EGFR phosphotyrosine levels of around 20% (Figure 5.12). The reductions observed in response to *O. hannah* venom are consistent with the previous reductions seen in both

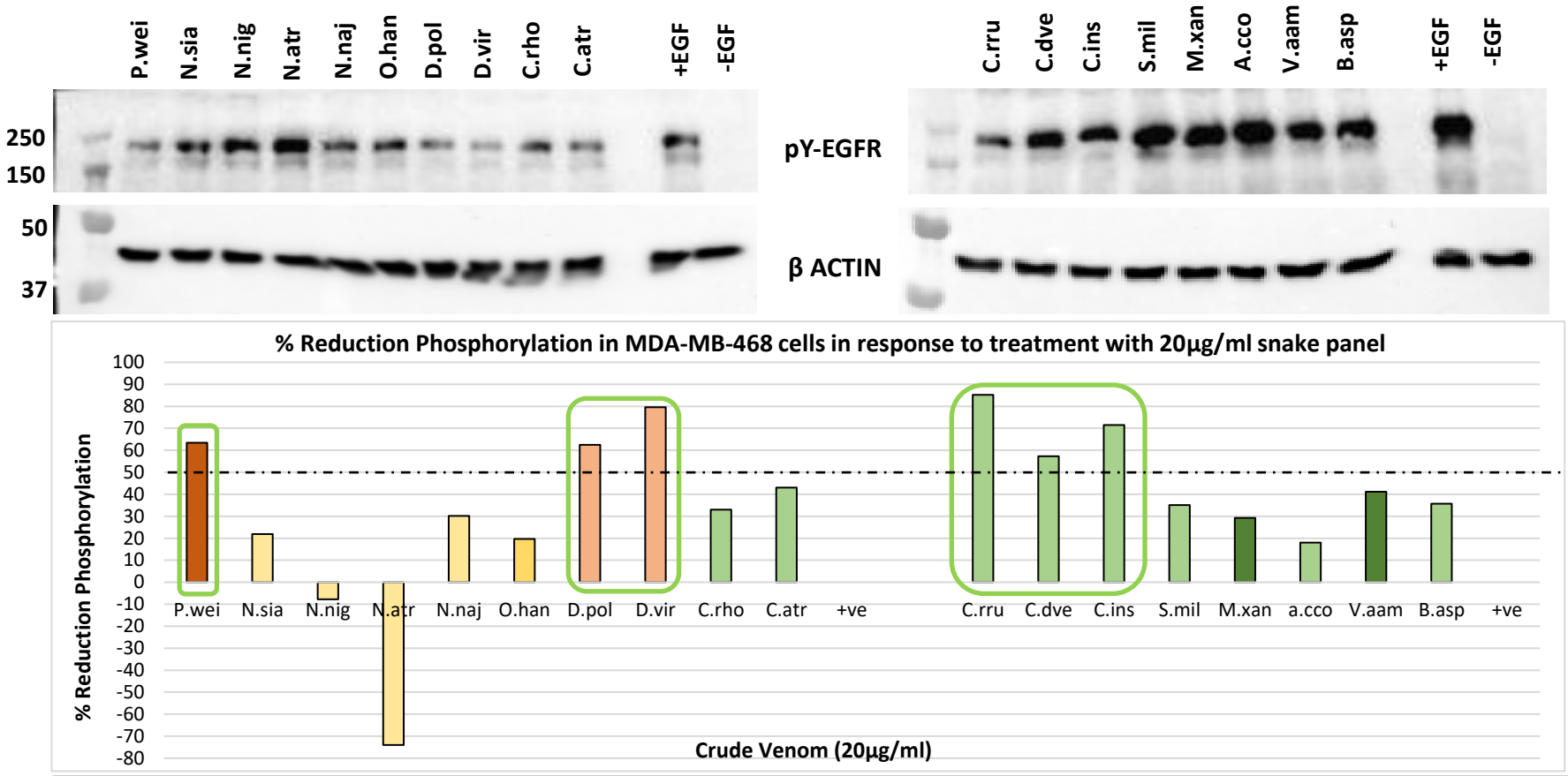

Figure 5.12: Western Blot Analysis of EGFR Phosphorylation levels in MDA-MB-468 Breast Cancer Cells After 2h Dosing with 20 µg/ml of a Panel of Whole Snake Venoms

Displays Western Blot EGFR phosphotyrosine band intensities of cell lysates harvested from cells treated for 2h with 20µg/ml of each of the labelled whole snake venoms. Western band intensities for β-actin are also displayed in the figure to display equal sample loading for each lysate. Graphs display the percentage reduction in phosphotyrosine in response to venom treatment. pY intensities were generated using ImageLab software, normalised using actin control band intensities, then phosphotyrosine levels calculated as a percentage of venom-untreated, EGF-stimulated controls. A 50% reduction line was added to the graph. Biological replicates= N1, Technical replicates = N2

the MDA-MB-468 and A431 cell ELISAs, where both saw reductions of around 25% in response to treatment with the whole venom (Figure 5.8).

Western Blot analysis of the cell lysates generated from the mamba venom-treated cells (*D. polylepis* (D.pol) and *D. viridis* (D.vir)) and brown snake venom-treated cells (*P. rossignoli* (P.wei)) all resulted in more substantial reductions to EGFR phosphotyrosine levels. Reductions in phosphorylation of greater than 60% and 65% were observed following treatment with *D. polylepis* and *P. rossignoli* venom respectively and a massive reduction of 80% was observed in response to treatment with *D. viridis* venom (Figure 5.12). These reductions are higher than those seen in the previous MDA-MB-468 ELISA analysis that was undertaken (Figure 5.8A), however the fact that both techniques using independent venom treated samples generated detectable reductions, supports that these venoms are causing real reductions to EGFR phosphotyrosine levels.

Treatment with a panel of crotalid venoms all resulted in reductions in EGFR phosphorylation levels post-dosing, however the degree of reduction in phosphorylation was variable depending upon the venom used to treat. The greatest reductions in phosphorylation were particularly observed in response to treatment with venoms derived from the south American Crotalus sub-family of pit vipers (*C. atrox, C. ruber* and *C. durissus vegrandis*), as well as Indonesian pit viper *Trimeresurus albolabris insularis* (C.ins) (Figure 5.12). Treatment with *C. durissus vegrandis* venom resulted in lysate samples with reductions of around 60% in EGFR phosphotyrosine levels, consistent with the 55% reductions observed in the previous MDA-MB-468 ELISAs (Figure 5.8) and to the reductions observed in the Western Blot analysis undertaken with this venom in chapter 4 (Figure 4.9). Similarly, *Crotalus ruber* (C.rru) venom resulted in reductions in EGFR phosphotyrosine of around 85%, whilst treatment with *Crotalus atrox* (C.atr) venom still caused an observable reduction in EGFR phosphotyrosine levels of just over 40%. Both venoms have been previously shown in ELISA analysis to cause reductions to EGFR phosphotyrosine levels of around 35%, further supporting that the reducing effects of these venoms are also real results.

Treatment with *Trimeresurus albolabris insularis* (C.ins) venom resulted in reductions in EGFR phosphorylation levels of greater than 70%, suggesting that similarly to the Crotalus family, venoms from the Trimeresurus family may display strong inhibitory effects of EGFR phosphorylation. However, as *T. albolabris insularis* was the only member from this family investigated this cannot be confirmed. The Western Blot is also backed up again by the previous ELISA data which also showed reductions to EGFR phosphorylation in both MDA-MB-468 and A431 cells following treatment with this venom (Figure 5.8). Reductions in phosphorylation of around 35% were seen in MDA-MB-468 cell EGFR phosphorylation levels in response to

treatment with both *Sistrurus miliarus barbouri* (S.mil) and *Bothrops asper* (B.asp), whilst reductions of less than 20% were observed after treatment with *Agkistrodon contortrix contortrix* (A.cco) venom (Figure 5.12), again all of which remain pretty consistent with the reductions observed in the ELISA undertaken in MDA-MB-468 cells (Figure 5.8). Treatment with the two selected vipers *Montivipera xanthina* (M.xan) and *Vipera ammodytes ammodytes* (V.aam) both resulted in reductions to MDA-MB-468 EGFR phosphotyrosine levels of around 30% and 40% respectively (Figure 5.12), which match to the levels obtained using the ELISA technique, where reductions were observed to be around 30% and 35% respectively (Figure 5.8).

The undertaking of Western Blot analysis of MDA-MB-468 cell lysates, produced from venom treated samples at the same dose of 20 µg/ml, supports the initial findings of the ELISA panels carried out at the same venom concentrations. Venoms that had been previously shown to cause reductions to EGFR phosphotyrosine levels in the ELISAs were still shown to cause reductions following Western Blot analysis. A similar lack of activity against EGFR was observed follow true cobra venom treatment in the Western Blot analysis as was seen in the ELISAs. Whilst many venoms showed venom similar levels of reductions to EGFR phosphorylation using both techniques, there were some venoms that appeared to show greater reductions using the Western Blotting technique than the ELISAs. Suggestable reasons for the variability in the reductions observed with the two techniques is that they are both only semi-quantitative techniques. Additionally, the ELISA technique requires the permeabilization of cells to allow the antibodies access to the phosphotyrosine residues of EGFR, and so this need for antibody permeability into cells could result in reduced antibody-binding capabilities than those seen using the Western Blot technique. Alternatively, difference in available antibody and amount of EGFR available to bind it in both techniques may influence the levels of phosphorylation that are detectable. However, despite variations to the amount of EGFR phosphotyrosine reduction observed between the two techniques, what was consistent was that the reductions were being detected in both techniques.

5.3.6 Western Blot Analysis of MDA-MB-468 Cells Treated with Dose Responses of Selected Whole Snake and Invertebrate Venoms

To further investigate the potential effects of whole snake and invertebrate venoms on EGFR phosphorylation levels in breast cancer, MDA-MB-468 cells were treated with dose responses of whole venoms previously shown in Figures 4.9, 5.8, 5.10 and 5.12 to cause reductions in EGFR phosphotyrosine levels. MDA-MB-468 cells were treated with serial dilutions of a variety of whole venoms from a diverse set of species, including theraphosids *Acanthoscurria geniculata* (Figure 5.13A) and *Brachypelma boehmei* (Figure 5.13B) scorpion *Heterometrus swammerdami* (Figure 5.13C), rattlesnake *Crotalus durissus vegrandis* (Figure 5.13D) and Mamba *Dendroaspis*

viridis (Figure 5.13E). Additional venoms were selected from those previously shown to have not caused reductions to EGFR phosphorylation to determine whether the lack of observable effect is the result of differing venom compositions or purely the result of the previously selected concentrations being too low to bring about effects. Cobra *Naja naja* (Figure 5.13F) and centipedes *Scolopendra hardwickei* and *Scolopendra subspinipes dehaani* (Figures 5.13G & H) were also investigated. Analysis of EGFR phosphotyrosine Western Blots, normalised against β-actin blot loading controls, showed that some of the investigated whole venoms displayed dose-dependent effects on EGFR phosphorylation levels post dosing. 50% reductions or greater in EGFR phosphorylation levels were considered biologically significant.

Treatment with a dose response of *A. geniculata* venom showed reductions of 75% in receptor phosphorylation at a dose of 2.5mg total venom protein (5 mg/ml), however there appears to be a decrease in ability to inhibit EGFR phosphorylation at doses of *A. geniculata* (A.gen) venom between 1.25mg-12.5µg (2.5 mg/ml-25 µg/ml) (Figures 5.13 & 5.14). Interestingly, Western Blot analysis appears to suggest a second reduction in EGFR phosphorylation at the lowest tested dose of *A. geniculata* venom (1.25 µg/ml). As we are dealing with whole venoms, which are a complex mixture of molecules and peptides, it is possible that there are a combination of effects occurring simultaneously from several different venom components. In this instance it is possible that there are multiple molecules within the venom capable of causing EGFR phosphorylation reductions, with greatest activities at widely different concentrations. Alternatively, there could be an antagonistic molecule, which is attenuating the effects of EGFR phosphorylation blockage. At the highest tested dose of 2.5mg it is possible that there is a larger amount of pro-inhibitory molecule, and so it is capable of outcompeting, however at lower doses the molecules are balanced, resulting in no or little change to phosphorylation levels. It is also worth noting that, Western Blotting is only a semi-quantitative analysis technique, and so some of the slight reductions or increases in phosphorylation, may be the result of limitations in the technique applied. As the reduction in phosphorylation for the dose of 12.5µg falls just above the 50% significance threshold, it is possible that affects at this dose may be breaching the significance threshold as a result of the semi-quantitative nature of the technique. Previous Western blot analysis of MDA-MB-468 cells treated with 2.5 mg/ml (2.5mg total protein) of *A. geniculata* venom, carried out in Chapter 4, identified the venom to cause similar levels of reductions to EGFR phosphorylation (≈65%) at the same selected dose, which further supports the findings of this dose-response western blot (Figure 4.9B).

The dose response Western Blot for *B. boehmei* (B.boe) venom showed strong reductions to EGFR phosphorylation capabilities at all tested doses. Reductions of around 70% or greater were observed with all tested doses, including as low as 0.2 µg/ml (0.1µg total venom protein), with

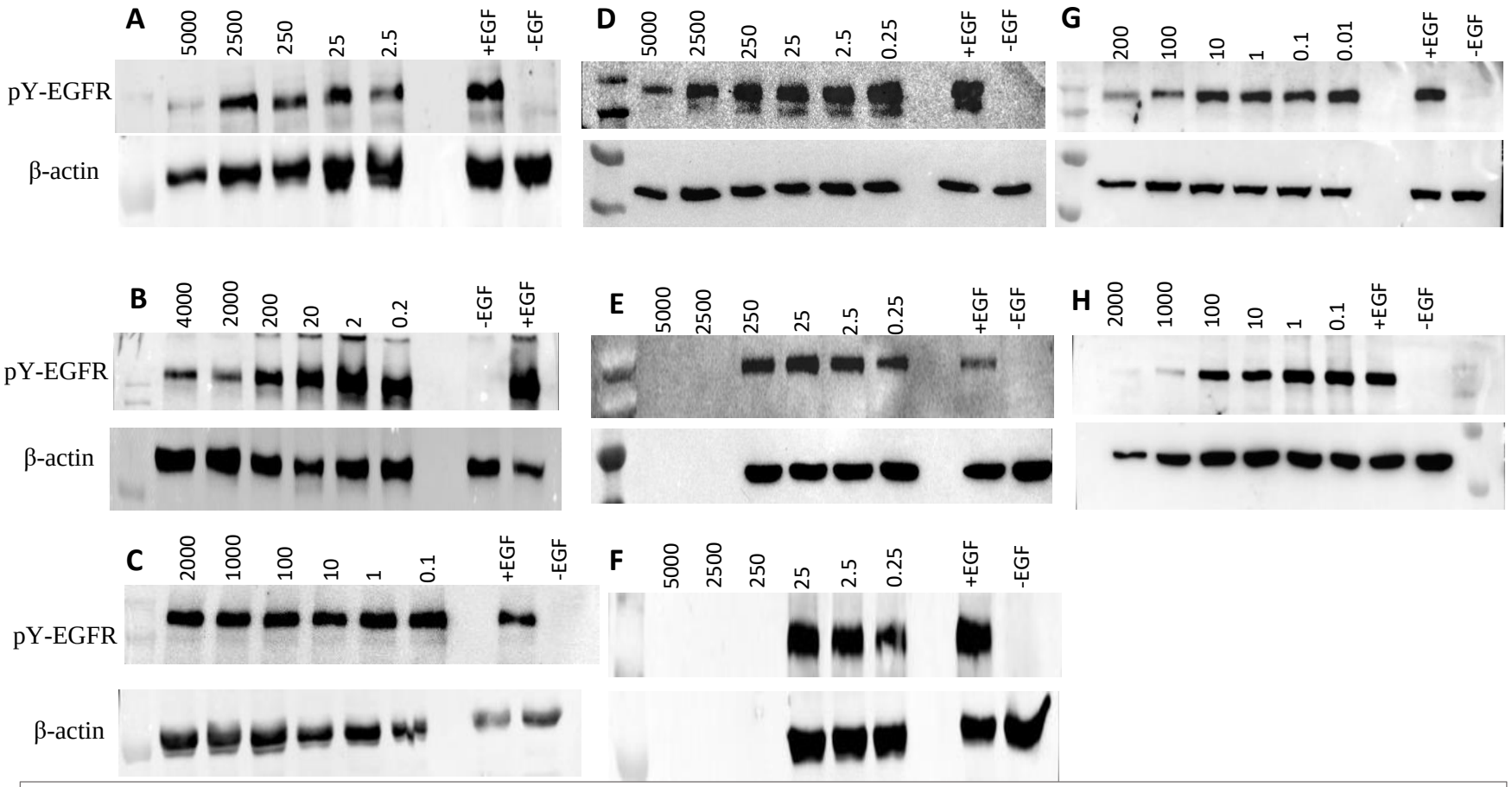

Figure 5.13: Western Blot Analyses of MDA-MB-468 Cells Treated with Venom Dose Responses

Western blots display both the phosphorylation of tyrosine residues with EGFR (pY-EGFR) and the expression of control protein β-actin at decreasing concentrations of *A. geniculata* venom (A), *B. boehmei* venom (B), *H. swammerdami* venom (C), *C. durissus vegrandis* venom (D), *D. viridis* venom (E), *N. naja* venom (F), *S. subspinipes dehaani* (G) and *S. hardwickei* venom (H). Concentrations in µg/ml. Biological replicates/whole venom = N1

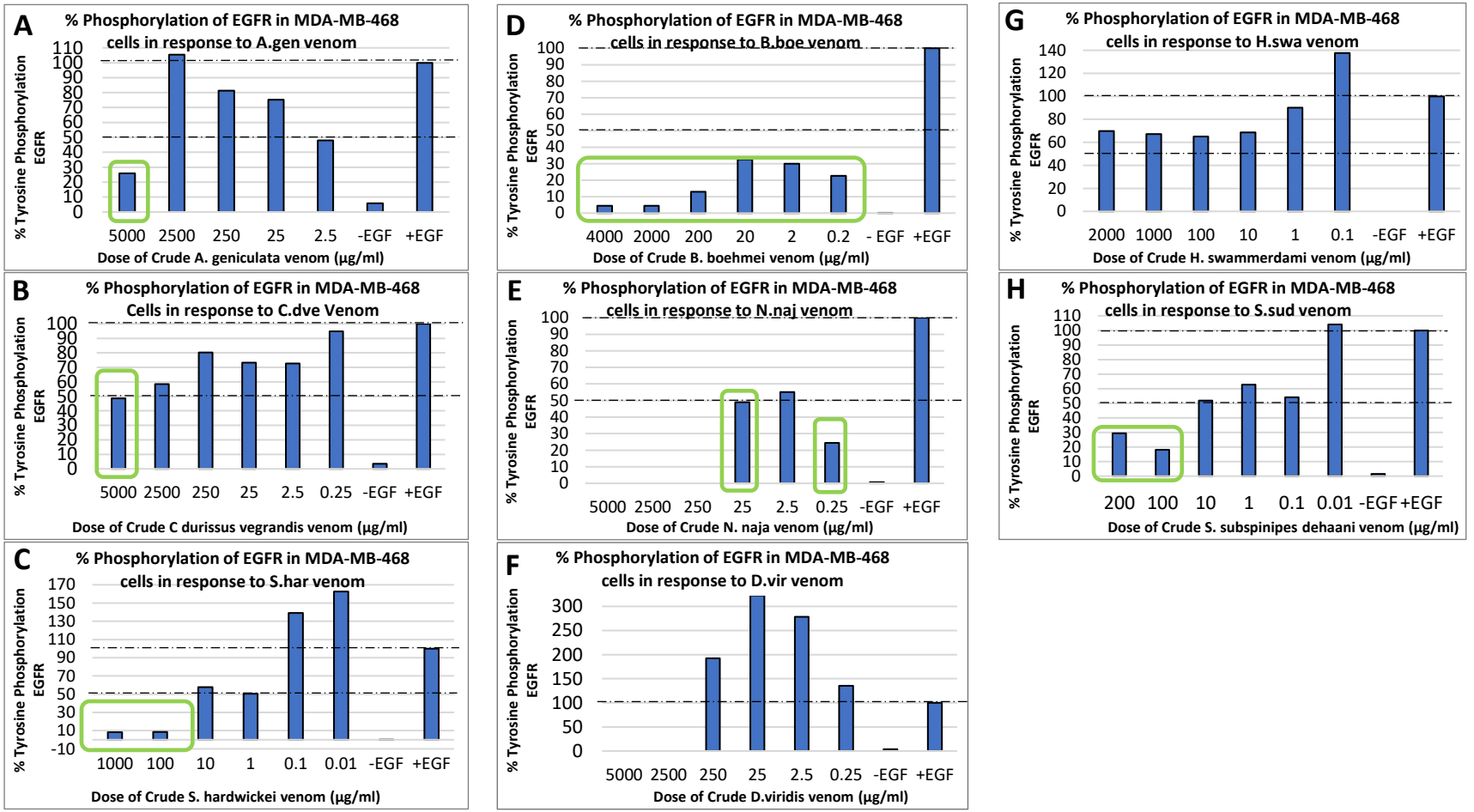

Figure 5.14: Graphical Representation of % Tyrosine Phosphorylation of EGFR in MDA-MB-468 Cells Treated with Venom Dose Responses

% pTyr EGFR in venom-treated MDA-MB-468 cells. Venom treated p-Tyr EGFR bands were normalised against actin bands and the the percentage of pTyr EGFR calculated relative to EGF-treated only control bands (+EGF). +EGF controls display the max achieved phosphorylation in non-venom treated, EGF-stimulated cells. Graphs display percent EGFR phosphorylation in response to *A. geniculata* venom (A), *C. durissus vegrandis* venom (B), *S. hardwickei* venom (C), *B. boehmei* venom (D), *N. naja* venom (E), *D. viridis* venom (F), *H. swammerdami* venom (G) and *S. subspinipes dehaani* (H). Dotted lines represent 50% and 100% EGFR phosphorylation. Doses showing ≤50% pTyr EGFR (≥50% reductions) are highlighted in green boxes

greater than 90% reductions observed in response to treatment with the two highest tested doses of 4 mg/ml (2mg total protein) and 2 mg/ml (1mg total protein). The findings of this dose response suggest that this venom may contain potent inhibitors of EGFR phosphorylation. Previous ELISA analysis identified that this venoms caused reductions of around 25% in MDA-MB-468 cells treated with a dose of 100 µg/ml. This is considerably lower that the reductions observed in in response to the dose response Western Blot carried out for this venom. It is worth noting that this particular Western Blot appeared to suggest lower sample loading of the EGF-only treated control lysate (+EGF) and so when all samples were corrected using β-actin loading control, it made the effects at each concentration more pronounced (Figure 5.13B & 5.14D). Despite this, it is observable just from looking at the pY-EGFR Western Blot for *B. boehmei* venom that there is an obvious dose-dependent reduction occurring in EGFR phosphotyrosine levels, with the higher doses of venom causing smaller bands and therefore more substantial reductions to phosphorylation levels (Figure 5.13B).

Similarly, the dose response Western Blot for *H. swammerdami* (H.swa) venom showed reductions to EGFR phosphorylation capabilities at all tested doses, with the exception of 0.1 µg/ml. No reductions of greater than 50% were observed in response to treatment with any of the selected doses of *H. swammerdami* venom (Figure 5.13C). Doses of between 2 mg/ml-10 µg/ml resulted in reductions of between 30-40% (Figure 5.14F). As seen with the Western Blot for *B. boehmei*, this particular Western Blot appeared to suggest lower sample loading of the EGF-only treated control lysate (+EGF) and so when all samples were corrected using β-actin loading control, it made the effects at each concentration more pronounced (Figure 5.13C & 5.14F). Previous investigations into this whole venom in Chapter 3 identified significant reductions to both EGFR phosphotyrosine (≈80%) and expression (≈55%) levels at a dose of 2 mg/ml (total protein: 2mg) (Figure 4.9). Whilst a concentration of 2 mg/ml was used for the maximum dose of *H. swammerdami* venom in the Western blot analysis the total venom protein load was lower (1mg) and so this may account for the difference observed in combined EGFR phosphorylation and expressions level reductions observed between this Western Blot and the one in Chapter 3.

Whilst there are no papers showing effects of theraphosid or scorpion venoms and their components specifically against EGFR, as discussed in previous chapters they have been shown to display anti-cancer effects. Whilst there are no papers into the effects of *A. geniculata* venom on EGFR phosphorylation/expression or cancer cell cytotoxicity, Gomensin an antimicrobial peptide derived from the venom of the Brazilian tarantula *Acanthoscurria gomesiana* has been shown to also display anti-tumoral activities when used in several studies to treat cancers including human breast adenocarcinoma (SKBR3) and human melanoma A2058 cell lines (Rodrigues *et al.*, 2008; Soletti *et al.*, 2010; Kumar, Sarkar and Jain, 2013). Similarly, there are

no papers identifying *B. boehmei* venom, or the venom of any other *Brachypelma* species as causing reductions to EGFR phosphorylation/expression. However, antimicrobial peptide Brachyin, has been shown to display anticancer effects against many cancer types, including human T cell lines Molt-4 and C8166, lung cancer cell lines A549 and Calu-6 and bladder cancer cell lines BIU-87 and T24 (Zhong *et al.*, 2014; Akef, 2018). Similarly, whilst the venoms of *Heterometrus* scorpions have not been published as effecting EGFR phosphotyrosine levels of receptor expression, venoms from *Heterometrus* species have also been found to display anticancer properties. Bengalin, isolated from the venom of *Heterometrus bengalensis* (Indian black scorpion) displayed anticancer properties against human leukemic cells, with the attributed cell death caused by Bengalin identified as apoptosis, via mitochondrial pathway changes and the inhibition of heat shock proteins (Gupta *et al.*, 2010).

Reductions were also observed in response to treatment with *C. durissus vegrandis* venom at several of the tested doses (Figures 5.13D & 5.14B). As with other previously discussed venom dose-responses treatment with *C. durissus vegrandis* venom appears to have resulted in an observable dose-dependent reduction in EGFR phosphotyrosine levels, with higher doses of venom causing greater reductions. The highest dose of *C. durissus vegrandis* venom caused reductions to EGFR phosphotyrosine levels of greater than 50%, however the other tested doses did not. This is different from the findings of both previous Western Blot (Figure 4.9) and ELISA analysis (Figure 5.8) which showed that lower doses of this venom caused significant reductions to EGFR phosphotyrosine levels. One suggestion for the differences could be that as venoms are a whole biological mixture, differences in venom composition may vary between extraction cycles, and this may account for the differences in potency observed between the multiple experimental techniques. However, despite the differences in potency the venom still showed reductions to EGFR phosphotyrosine levels, supporting the findings of the previous experimental work which highlighted this venom as containing potentially interesting active molecules. Whilst papers specifically identifying venom from this Crotalid species have not been published, several studies have been performed into venom-isolated peptide Crotoxin. Crotoxin, a phospholipase A2 (PLA2) isolated from the venom of *Crotalus durissus terrificus* (South American Rattlesnake) has been reported to display anti-proliferative properties against squamous carcinoma cell lines, A431 and ME-180. Anti-proliferative properties of crotoxin were attributed to its ability to regulate EGFR, The results of the study suggested an association between high level EGFR expression and enhanced cellular sensitivity to the PLA2 activity of crotoxin (Donato *et al.*, 1996). Conversely to findings of the Western Blots and ELISAs in this study, Crotoxin was found to cause increased EGFR phosphorylation levels in both cells lines (Donato *et al.*, 1996). A more recent study investigating crotoxin from the same snake also showed stimulation of EGFR

phosphorylation, however they were unable to establish the significance of this observation (Wang *et al.*, 2012).

Treatment with *D. viridis* venom at a dose response did not appear to cause any reductions to EGFR phosphorylation levels, with greater band intensities obtained for the venom treated samples (Figure 5.13E, pY blot). Whilst both this Western Blot (Figure 5.13E) and the one carried out in Chapter 4 (Figure 4.9) suggest this venom does not cause reductions to EGFR Phosphorylation, both ELISAs (Figures 5.8) and the 20 µg/ml snake panel Western Blot suggest that it does cause reductions (Figure 5.12). These conflicting results make this venom difficult to interpret. Higher doses of venom do not enhance the effect of the venom on EGFR phosphotyrosine levels, and due to its cellular cytotoxicity, doses above 200 µg/ml are impossible to profile using either of these techniques. The development of an ELISA which uses purified EGFR, isolated from cells using immunoprecipitation, may allow for more in-depth profiling of this venom at higher concentrations whilst eliminating the complication of potential cellular cytotoxicity. Treatment with *N. naja* venom at a dose response caused high levels of cellular cytotoxicity at doses between 5 mg/ml-250 µg/ml). Doses of 25 µg/ml (12.5µg protein) and below appear to cause reductions to EGFR phosphotyrosine levels, with significant reductions observed at all doses (Figure 5.13F & 5.14E). As previously discussed with *D. viridis*, the findings for *N. naja* venom appear to be quite variable. No reductions were observed in EGFR phosphorylation levels in the undertaken ELISAs (dose of 1µg total protein) (Figures 5.8), however the dose response Western Blot suggest that effects can be seen as low as 0.25 µg/ml) (Figure 5.14E). Previous Western Blot analysis in Chapter 3 identified the venom as causing reductions to Phosphotyrosine levels of around 70% at a dose of 25 µg/ml (25µg total protein) (Figure 4.9). This venom could also benefit from similar further investigations using an alternative ELISA technique. It is possible that as both venoms are derived from *Elapidae* that they may contain components with EGFR phosphorylation antagonistic effects, and so fractionation of these venoms may help to further understand and interpret what is actually occurring following treatment with them.

Whilst the Western Blot and ELISA data for *N. naja* venom appears to be inconclusive, there is published evidence that suggests that components of cobra venoms are capable of influencing EGFR expression and phosphorylation in cancer. Cardiotoxin III (CTX3), a basic 60aa polypeptide derived from the venom of *Naja atra* (Chinese cobra/Taiwan cobra), has been shown to display preferential cytotoxicity to A549 lung cancer cells through the inhibition of EGFR phosphorylation (Su *et al.*, 2010), whilst a similar study into CTX3 found it suppressed cell metastasis in MDA-MB-231 breast cancer cells by blocking EGFR phosphorylation (Tsai *et al.*, 2012). Interestingly, a follow up study published by the same group also found that CTX3 from

Naja naja atra inhibited EGFR phosphorylation in another triple-negative breast cancer cell line, MDA-MB-231, where its effects were found to result in a loss of activation of downstream signal cascade proteins phosphatidylinositol 3-kinase (PI3K)/Akt and ERK1/2. Inhibition of EGFR phosphorylation by CTX3 were also found to inhibit the migration and invasion potential of these cells through the suppression of both EGF/EGFR activation and epithelial-mesenchymal transition (EMT) (Tsai *et al.*, 2016). Whilst significantly less well characterised and with no papers supporting EGFR modulation by *Dendroaspis* venoms, there have been two toxin peptides which are members of the three-finger superfamily, isolated from the venom of eastern green mamba *Dendroaspis angusticeps*. Both these venom peptides were found to display anti-tumour activities against non-small cell lung cancer adenocarcinoma A549, an EGFR-over-expressing lung cancer type, whilst one of the two peptides was also effective against EGFR-over-expressing TNBC cell line MDA-MB-231. However, whilst both cells line are EGFR over-expressing the paper did not suggest a proposed mechanism through which the toxicity may be occurring (Conlon *et al.*, 2014).

Treatment with both the venoms of centipedes *S. hardwickei* and *S. subspinipes dehaani* appear to cause obvious dose-dependent effects to EGFR phosphotyrosine levels in MDA-MB-468 cells (Figures 5.13G & H). Cytotoxic effects were observed with higher doses of 1 mg/ml (500µg total protein), which can be seen through the reduction to β-actin loading control, despite additional sample loading to attempt to correct for this (Figure 5.13H, β-actin blot). Doses of 0.2 and 0.1 µg/ml *S. subspinipes dehaani* and 0.1 µg/ml *S. hardwickei* venoms (50-100µg total protein) caused strong reductions to EGFR phosphotyrosine levels which could be easily observed by just looking at the bands on the Western Blots (Figures 5.13G & H, pY blots). Analyses of band intensities identified biological reductions of greater than 50% in response to doses as low as 1 µg/ml (0.5µg protein) and 0.1 µg/ml (0.05µg protein) of *S. subspinipes dehaani* and *S. hardwickei* venoms respectively (Figures 5.14C & G). These effects at doses this low are the opposite of the finds of the ELISAs which showed no effects at doses of 100 µg/ml (5µg total protein) (Figure 5.10). Despite the discrepancies in effect at lower concentrations, the observable effects at higher concentrations are harder to dispute, suggesting that these venoms also contain dose-dependent EGFR effecting compounds. A paper into the effects of alcoholic extract of centipede (AECs) identified it capable of causing reductions to EGFR phosphorylation levels in high EGFR-expressing cancers. Experimental data showed that AECS inhibited cellular proliferation in A431, HEK293 and HEK293/EGFR cell lines. Proposed mechanisms for this observation included the induction of apoptosis and the regulation of EGFR-dependent signalling cascades by altering EGFR-kinase phosphorylation and activity levels. The study found, that AECS bound to EGFR and competitive binding assays using gefitinib suggested that both may compete for occupation at a single common binding site on the EGFR receptor, suggesting AECS works through a similar

inhibitory mechanism seen with SM-TKIs (Ma *et al.*, 2015). A further study into Centipede Scolopendra extract (CSE) identified that it inhibited A431 cell proliferation through by targeting EGFR and by inhibiting EGF secretion from A431 cells (Zheng *et al.*, 2017). Whilst these studies do support the findings of the two Scolopendra venoms assessed by Western Blot analysis in this chapter, it is worth noting the composition and collection methods of the venom used in this chapter and the extracts used in these papers are very different. The venom used for this study was an aqueous prep, with the venom collected directly from the animals and diluted to desired concentrations in RNAse-free water. The extracts collected for these papers were whole crushed centipedes, not just venom, suspended in a 3/2 v/v ethanol/water solution, and so cautions must be taken when drawing direct comparisons between these studies and the work presented in this thesis.

5.4 Conclusions

The results of this chapter identify the successful optimisation of a self-developed in cell ELISA assay for the effective profiling of whole venom effects against EGFR phosphotyrosine activity in EGFR over-expressing cancer cells. Both ELISAs and Western Blot analysis identified that whole snake and invertebrate venoms are capable of causing reductions to the phosphotyrosine levels of EGFR in MDA-MB-468 and A431 cell lines. ELISAs of the snake whole venom panel of venoms at a dose of 20 µg/ml identified that greater reductions in EGFR phosphotyrosine levels in both cell lines were identified following treatment with pit viper and mamba venoms. True cobra venoms were identified to not cause particularly large reductions to the EGFR phosphotyrosine levels in either of the two cell lines. Of the eighteen whole snake venoms screened, *P. rossignoli, O. hannah, D. polylepis, D. viridis, C. rhodostoma, C. atrox, C. ruber, C. durissus vegrandis, T. albolabris insularis, S. miliarius barbouri, M. xanthina, A. contortrix contortrix* and *V. ammodytes ammodytes* were identified to cause greater than 20% reductions in MDA-MB-468 and A431 cells, with *B. asper* additionally causing greater than 20% reductions to MDA-MB-468 cells only. Two venoms were identified to cause greater than 50% reductions in MDA-MB-468 cells (*C. durissus vegrandis* & *C. rhodostoma*).

Screening of the invertebrate whole venom panel at 100 µg/ml resulted in significantly smaller reductions to EGFR phosphotyrosine levels overall than those seen with the screening of the snake panel, with the largest percentage reduction of around 30% only. Reductions of greater than 20% to EGFR phosphorylation were observed in MDA-MB-468 cell in response to invertebrate venoms *H. swammerdami, P. liosoma, B. boehmei, T. pruriens* and *C. giganteus*, whilst reductions were observed in A431 cells in response to *A. australis, H. swammerdami, P. kraepelini, A. geniculata, A. metallica, T .pruriens* and *C. giganteus*. However, the composition

of snake and invertebrate venoms are likely to be highly different, with invertebrate venoms more heavily composed of small peptide components and so the reductions cannot be directly compared. Reductions were observed in both MDA-MB-468 and A431 cell lines in response to scorpion venoms, both arboreal and terrestrial new world theraphosids and secretions from millipede *C. giganteus*.

Further investigation of the whole snake panel at 20 µg/ml in MDA-MB-468 cells using alternative technique Western Blotting further supported the findings of the ELISAs, identifying a similar pattern of effects across the panel. Pit viper and mamba venoms were shown to cause the greatest reductions to detectable EGFR phosphotyrosine levels, whilst true cobra venoms caused smaller reductions. This correlation between the results observed in the ELISAs and the reductions observed using the alternative Western Blot technique support that the changes observed are genuine venom effects. Further profiling of a set of selected venoms at multiple different doses identified greater achievable reductions to EGFR phosphorylation in response to invertebrate venoms. *A. geniculata* and *H. swammerdami* venoms were found to cause greater reductions to EGFR phosphotyrosine levels at higher doses (5 mg/ml), with *B. boehmei* venom identified to cause biologically significant reductions at most of the tested doses. Further investigations into *Scolopendra* venoms, shown not to cause reductions in the ELISAs, showed strong dose-dependent effects on EGFR phosphorylation, with higher doses than those used in the invertebrate panel ELISAs causing significant reductions to phosphorylation. Highest tested (1 mg/ml) doses of *Scolopendra* venoms ultimately resulted in MDA-MB-468 cellular cytotoxicity and cell death within the 2-hour dosing timeframe.

As with previous ELISAs and Western Blots, dose response blots identified *C. durissus vegrandis* venom as capable of causing biologically significant reductions to EGFR phosphotyrosine levels at the highest tested dose (5 mg/ml). However, there was some inconsistency between the potency of the venom in this last dose response Western Blot and all the previous Western Blot and ELISA analyses carried out in Chapters 3 and 5, which showed more significant reductions at considerably lower doses. However, despite the inconsistent potencies at the tested dose the venom has been consistently shown to reduce EGFR phosphotyrosine levels in all of the ELISA and Western Blot analyses carried out throughout this thesis.

Dose response analysis of *D. viridis* venom seemed to cause no reductions to EGFR phosphorylation, which is supported by the findings of Western Blot analysis in Chapter 3 but in contradiction to the findings of the ELISAs and single dose snake panel Western Blot. The dose response Western Blot of *N. naja* caused biology significant reductions to EGFR phosphorylation at the three lowest tested doses, which is supports the findings of the Western Blot in Chapter 3

and the snake panel Western Blot in Chapter 5, however is contradictory to the findings of the ELISA screens. Both *D. viridis* and *N. naja* venoms caused high levels of cellular cytotoxicity at doses of 250 µg/ml and above, resulting in no detectable EGFR levels. The contradictory findings of these venoms could be the result of multiple venom components which display antagonistic effects against EGFR. ELISAs which do not rely on intact cells, could enable the profiling of this venoms at higher doses without encountering the issue of cellular cytotoxicity. Immunoprecipitation and purification of EGFR from cell lysates and the development of an ELISA where it can be directly applied to the wells of plates rather than the fixing of cells should overcome cytotoxicity issues.

Further investigations into individual components, isolated from the whole venoms shown to have effects on EGFR phosphorylation in this and previous thesis chapters, would help to identify the specific venom component that is responsible for the observed changes to EGFR. By fractionating the venoms into constitutive components, it should eliminate the potential complications of the antagonistic and opposing effects that have made interpreting the effects of some of these venoms more complicated.

CHAPTER 6: Development of an EGF Alexa Fluor-488 Competitive Binding Assay to Assess Venoms for EGF Antagonistic Effects

6.1 Introduction

Western Blot and ELISA analyses of whole venoms from both invertebrates and snakes have been shown in Chapters 3 & 5 to be capable of causing reductions to EGFR phosphorylation levels. However, both techniques are unable to identify the mechanism through which these observed reductions are occurring.

With the advent of small-molecule and antibody type therapeutics, the employment of targeted cancer therapies for the treatment of EGFR over-expressing cancers are becoming more commonly used. Small-molecule EGFR-targeting therapies function by binding to the ATP binding pocket of EGFR's kinase domain, thereby inhibiting its ability to auto-phosphorylate (Berardi *et al.*, 2013). However, those patients with activating mutations in EGFR who show initial responsiveness to SM-TKIs eventually develop acquired resistance (Jun Wang *et al.*, 2016). Mutations, over-expression of native ligands, or amplifications/suppressions of alternative RTKs or downstream signalling proteins can confer resistance to SM-TKIs (Alexander and Wang, 2015; Costa and Kobayashi, 2015; Huang and Fu, 2015; Bae *et al.*, 2015; Stewart *et al.*, 2015; Yang *et al.*, 2018). Antibody-type therapies bind extracellularly to RTKs and bring about cancer death through multiple mechanisms, such as by eliciting the destructive activity of the immune system, by binding and causing steric hinderance to receptor dimerisation, by causing receptor internalisation and through cytostatic effects which cause G1 cell cycle arrest (Pohlmann, Mayer and Mernaugh, 2009; Vu and Claret, 2012). However, resistance to antibody therapies can occur through obstacles which hinder the binding of the antibody to the receptor, the up-regulation of downstream signalling pathway members, the activation of alternative signal transduction pathways to compensate for the antibody suppression, or through mechanisms which fail to trigger effective immune-mediated responses (Pohlmann, Mayer and Mernaugh, 2009; Garrett and Arteaga, 2011; Mukohara, 2011; Vu and Claret, 2012; Wong and Lee, 2012; Arena *et al.*, 2016; Sforza *et al.*, 2016; Zhao *et al.*, 2017).

Whilst antibody-based therapies, such as chimeric cetuximab antibody (Erbitux) and Fab11F8, are able to disrupt the binding of ligand EGF to EGFR by the direct overlap of their binding with the EGF-binding site on domain III of EGFR (Li *et al.*, 2005; Li, Kussie and Ferguson, 2008), there is limited research into the ability of small-molecule type compounds and peptides to occupy

this binding space. Venoms are uniquely poised to potentially antagonists to EGF binding. Venoms, particularly those of invertebrate species (Liao *et al.*, 2007; Escoubas and King, 2009; Morgenstern and King, 2013), have a composition heavily comprised of small peptides, that are readily found to naturally act on a variety of receptor types and ion channels to illicit their pathology (Bringans *et al.*, 2008; Wingerd *et al.*, 2017; Doğan *et al.*, 2018; Grashof *et al.*, 2019).

Epidermal growth factor, is a ligand of 53 amino acids with a molecular weight of around 6 kDa (Cohen and Carpenter, 1975). Many classes of venom derived peptides have molecular weights of 10kDa or below (Liao *et al.*, 2007; Wagstaff *et al.*, 2008; Escoubas and King, 2009; Binh, Thanh and Chi, 2010). A study into the venom of theraphosid *Chilobrachys jingzhao* (Chinese Fawn Tarantula) identified that more than 70% of the detected venom peptides fell into the 3-5 kDa mass range, with an additional 10% in the 5-8 kDa range, and with 130 peptides in total of mass 2-8 kDa identified by matrix-assisted laser desorption/ionization-time of flight (MALDI-TOF) mass spectrometry analysis of the venom (Liao *et al.*, 2007). Similarly, analysis of *Naja naja* venom identified 80% of the venom composition to be of molecular weights 10 kDa or smaller, and to contain classes of toxin peptides including cardiotoxins, neurotoxins and cytotoxins (Binh, Thanh and Chi, 2010). The abundant presence of these small molecular weight peptides in venoms increases the likelihood of naturally derived biological molecules, with sequences and sizes that could be capable of effectively disrupting EGF binding to the EGF-binding pocket of EGFR.

Previous venoms, screened for their effects on EGFR phosphorylation may be acting through mechanisms similar to those seen with SM-TKIs and antibodies, however they could just as easily be competitively inhibiting EGF binding to EGFR. The development of a competitive binding assay, utilising fluorescently labelled EGF and whole venoms, may allow for either the conformation or dismissal of EGF off-competition as a viable mechanism of action for receptor activity disruption. The use of fluorophores or fluorescent compounds has become a powerful tool for the development of biological binding assays and for the visualisation of biological events in living cells and organisms (Terai and Nagano, 2013). The tagging of peptides and proteins using fluorescence-emitting molecules allows for the rapid and effective studying of proteins of interest, and can be readily detected using equipment such as fluorescence microscopes and plate readers with fluorescent filters (Sheff and Thorn, 2004; Stadler *et al.*, 2013). Bioconjugates, produced from dyes with emission maxima beyond the 550nm wavelengths and into the near infrared range have become highly valuable tools, which have expanded the range of options for multicolour fluorescence detection (Berlier *et al.*, 2003). Alexa Fluor dyes are a group of fluorescent probes who are considered to be superior to Cy dyes of similar wavelengths, through their resistance to fluorescence quenching and absorption spectral artefacts following protein

conjugations. They are believed to undergo lower self-quenching and are capable of retaining their fluorescent-intensity when conjugates are heavily labelled (Berlier *et al.*, 2003).

The use of EGF, conjugated to an Alexa Fluor dye, would potentially allow for observable disruptions to EGF:EGFR binding following whole venom treatment, in MDA-MB-468 and A431 cells, should they be occurring. Competitive disruption of EGF binding by venoms would result in detectable reductions to fluorescence levels, indicating that venom components are binding extracellularly and to EGFR. It was decided that the development of a competitive binding assay, using a fluorescently labelled form of EGF would be developed and undertaken. This assay would be used to determine whether venoms, including those previously identified to be capable of causing reductions to EGFR phosphorylation, could be bringing about these reductions through the inhibition of the EGF-binding event.

6.1.1 Chapter Aims

- To develop and optimise a Fluorescent EGF competitive binding assay

- To screen a panel of whole snake and invertebrate venoms, including those previously shown to inhibit EGFR phosphorylation, for their potential ability to antagonistically off-compete EGF from EGFR

6.2 Materials and Methods

6.2.1 Confirming the Detectable Fluorescence of EGF Alexa Fluor-488

EGF Alexa Fluor-488 (Fisher Molecular probes, E-13345) was resuspended from lyophilised powder in 1.65ml of molecular RNAse-free water, to produce a 1 $x10^{-5}$ M (100µg/1.65 ml) stock solution from which dilutions could be prepared. 1 $x10^{-7}$ M, 1 $x10^{-8}$M and a 1 $x10^{-9}$M working concentrations were produced from the stock in PBS buffer. 100µl of each diluted EGF Alexa Fluor-488 concentration was added to 6 replica wells of a clear 96 well Nunclon Delta Surface plate (Thermo Scientific). The fluorescence of each EGF Alexa Fluor-488 concentration were read using a Fluostar plate reader (BMG Labtech) at excitation/emission wavelengths 485/520nm. Averages were calculated from replica reading and plotted graphically. Standard deviations were calculated for all replica readings and plotted as error bars.

6.2.2 Selecting the Optimal Wash Buffer to Reduce Background Fluorescence Intensity

6 different wash buffers were tested for levels of background fluorescence, in an attempt to maximise the overall fluorescent window. PBS, PBS 0.1% Tween20, Tris buffered saline (TBS), TBS 0.1% Tween20, 0.9% Potassium chloride (KCl) and KCl 0.1% Tween20 were directly compared. 100µl of each potential wash buffer were loaded in replicates of 12 into a clear 96 well Nunclon Delta Surface plate (Thermo Scientific) and the plate fluorescence read using a Fluostar plate reader (BMG Labtech) (exc. 485nm, em. 520nm). Average were calculated from replica reading and plotted graphically. Standard deviations were calculated for all replica readings and plotted as error bars. Normality and equal variance tests were run on all replica treatment readings, before a one-way ANOVA with post-hoc Tukey's comparison test was undertaken to determine whether treatment groups were statistically different.

6.2.3 Identification of Optimal Plate Type and Cell Number Combination Using A431 and MDA-MB-468 Cells

3 plates were selected to determine which gave the optimal window in fluorescence between EGF Alexa-Fluor-488 and PBS only treated cells, in combination with 3 different cell numbers for each cell line. Plates and cell number combination was also investigated for their effect on fluorescence in samples that have the added step of treatment with a labelled-EGF antagonist (unlabelled EGF). Black clear bottom 96 well plates (Corning), white clear bottom 96 well plates (Greiner) and clear 96 well Nunclon Delta Surface plates (Thermo Scientific) were used for this investigation. MDA-MB-468 and A431 cells were, trypsinised, counted, plated at concentrations of $2x10^5$, $1x10^5$ and $5x10^4$ cells/well and fixed as via **2.1.2, 2.1.3** and **2.4.1** (Appendix XX)**.**

The different concentrations of MDA-MB-468 and A431 cells were also treated on all plates with 3 different unlabelled EGF concentrations ($1x10^{-6}$ M, $1x10^{-8}$ M, $1x10^{-11}$ M) for 5 min (50 µl/well) to act as binding antagonists. After 5 min the unlabelled-EGF was removed from all treated wells and the plates washed 3x PBS (100 µl/well), before being treated with 50µl of EGF Alexa Fluor-488 ($1x10^{-7}$ M) for 5 min (excluding -ve control wells). After 5 min the EGF Alexa Fluor-488 was removed from all wells of all plates and the wash step repeated. Positive control wells were treated with $1x10^{-7}$ M EGF Alexa Fluor-488 only for 5 min. Negative control wells were treated with neither normal EGF nor EGF Alexa Flour-488. Where EGF or EGF Alexa Fluor-488 were omitted from the controls, cells were instead incubated with 50µl of PBS for 5 min. % window between maximum and minimum achievable fluorescence was calculated for each cell and plate combination to determine which gave the biggest window between background and maximum fluorescent signal for both MDA-MB-468 and A431 cell lines.

6.2.4 EGF vs EGF Alexa Fluor-488 Dose Responses

MDA-MB-468 and A431 cells were trypsinised, counted and plated out in Black clear bottom 96 well plates (Corning) at a concentration of $2x10^5$ cells/well as via protocols **2.1.2 & 2.1.3** and as pre-determined to be the optimal plate/cell number combination in **6.2.3.** Cells were returned to the incubator at 37ºC, 5% CO_2, 95% atmosphere overnight to allow cells to resettle and adhere. EGF (Sigma), resuspended from lyophilised powder in 1.65ml of molecular RNAse-free water to produce a stock concentration of $1 x10^{-5}$ M (100µg/1.65 ml) was used to produce a serial dilution of EGF ($1 x10^{-6}$ M - $1 x10^{-13}$ M) in PBS buffer. Cells were fixed with 4% paraformaldehyde as in **2.4.1**, washed 3x 100µl with PBS and treated in triplicate for 5 min with 100µl per well of the serial dilutions of EGF/PBS. After 5 min the EGF/PBS dilutions were removed and each well of cells were washed 3 times with 100µl of PBS. All wells of cells were treated with $1x10^{-7}$M concentration of EGF Alexa Fluor-488/PBS for 5 min. After 5 min the EGF Alexa Fluor-488 was removed from all wells of cells and rewashed again 3 times with 100µl of PBS. 50µl of PBS was added to all wells and the fluorescence measured using a Fluostar plate reader (BMG Labtech, exc. 485nm, em. 520nm). Both positive ($1x10^{-7}$ M EGF Alexa Fluor-488 only) and negative (PBS only) controls were run in triplicate. Averages were calculated for all replicates from each treatment group. Average background (minimum fluorescence) was subtracted from all EGF dose treatment groups. Remaining fluorescent signal was plotted vs dose of unlabelled EGF to produce dose response curves. Standard deviation of each treatment group was calculated and plotted as error bars on the dose response curves.

6.2.5 Execution of EGF Alexa Fluor-488 Competition Assays

6.2.5.1 EGF Alexa Fluor-488 Competition Assay of a Panel of 18 Diverse Snake Venoms

MDA-MB-468 and A431 cells were trypsinised and counted as via the standard protocol in **2.1.2 & 2.1.3**. Both cell lines were plated out into black, clear bottom 96 well plates (Corning) at a concentration of $2x10^5$ cells/well. Cells were incubated and left to settle and adhere overnight at 37ºC, 5% CO_2. Cells were fixed using a 4% paraformaldehyde solution as via **2.4.1** and washed 3x 100µl with PBS. Cells were treated in triplicate with 50µl of each snake venom, at a concentration of 2 mg/ml (100µg protein/well) (Appendix XXI). One plate of MDA-MB-468 and A431 cells were incubated for 2h in each venom, whilst another plate of each cells was incubated for 10 min at 37oC, 5% CO2. After each allocated time point, all venoms were removed, and the cells washed with PBS (3x 100 µl/well). 50µl of $1x10^{-7}$ M EGF Alexa Fluor-488/PBS was added to all wells except the –ve control wells (PBS only) for 5 min. After 5 min all EGF Alexa Fluor-488 was removed and all cells were washed again with PBS (3x 100 µl/well). After 3 washes all wells were filled with 50µl of PBS and the plate fluorescence was read using a Fluostar plate reader (BMG Labtech, exc. 485nm, em.520nm).

6.2.5.2 EGF Alexa Fluor-488 Competition Assay of a Panel of 23 Diverse Invertebrate Venoms

MDA-MB-468 cells were trypsinised and counted as via the standard protocol in **2.1.2** and **2.1.3.** The cells were plated out into black, clear bottom 96 well plates (Corning) at a concentration of $2x10^5$ cells/well. Cells were returned to the incubator and left to settle and adhere overnight at 37ºC, 5% CO_2. A panel of invertebrate venoms (Appendix XXII) were diluted in PBS to working concentrations of 2 mg/ml. The protocol was carried out as via the steps laid out in **6.2.5.1**.

6.2.5.3 Z Score Analysis of EGF Alexa Fluor-488 Competitive Snake and Invertebrate Panel Screens

Averages and standard deviations were calculated from all the collected fluorescence readings of each venom screen panel (excluding control samples). Each individual replica for venom treated samples was then generated a Z score of ranking by subtracting the calculated average plate fluorescence and dividing by the standard deviation. Averages of the generated Z scores from each treatment group (N=3) were calculated and plotted graphically. Standard deviations of each treatment group were also calculated from the Z scores and plotted as error bars. Z score thresholds of ±3 were selected to allow for the identification of venoms that appear to be causing a real detectable difference in fluorescently-labelled EGF binding to EGFR (Brideau *et al.*, 2003; Malo *et al.*, 2006).

6.3 Results and Discussion

6.3.1 Confirming the Detectability of EGF Alexa Fluor-488 Fluorescence Using the Fluostar Plate Reader

EGF Alexa Fluor-488 was detectable by a Fluostar plate reader (BMG Labtech) using fluorescence excitation and emissions filters of 485nm and 520nm, respectively. EGF Alexa Fluor-488 at three different concentrations, 10-fold difference apart, showed an obvious dose-dependent increase in fluorescence when read using a Fluostar Plate reader (BMG Labtech) (Figure 6.1). Despite there being detectable levels of fluorescence still observable at EGF Alexa

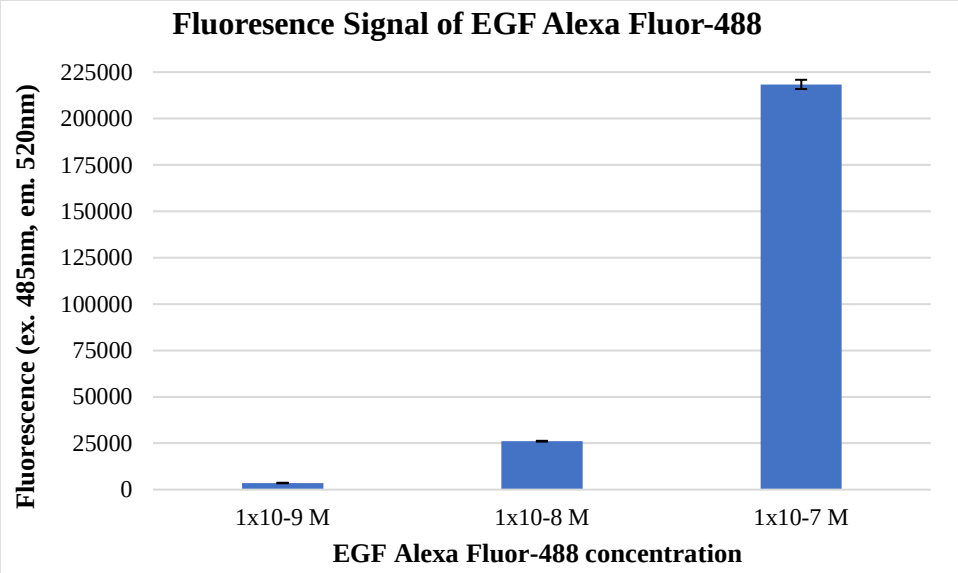

Figure 6.1: Detectable Fluorescent Intensity of EGF Alexa Fluor-488

Figure shows the fluorescence intensity obtained from EGF Alexa Fluor-488 at concentrations of $1x10^{-7}$ M, $1x10^{-8}$ M and $1x10^{-9}$ M. Averages were calculated from replicated readings and the standard deviation of the replicates calculated and plotted as error bars. Biological replicates = N1, Technical replicates/biological replicate = N6

Fluor-488 concentrations of $1x10^{-8}$ M and $1x10^{-9}$ M, a concentration of $1x10^{-7}$ M EGF Alexa fluor-488 was selected for cell treatment to remain in-line with the concentration of un-labelled EGF normally used for cell stimulation in previous Western Blot and ELISA analyses. Cell numbers to be investigated for this assay will be around the same cell seeding densities as previous plate-based assays, and so a similar concentration will allow for enough fluorescent-EGF to ensure effective levels of binding to EGFR.

6.3.2 Selecting the Appropriate Wash Buffer to Reduce Background Fluorescence Intensity

Analysis of the 6 wash buffers showed a visual difference in background fluorescence levels between those buffers that contained 0.1% Tween20 and those which did not, with those containing Tween20 showing elevated levels of background fluorescence when compared to their non-Tween20 containing counterparts (Figure 6.2A). The mean fluorescence for each buffer was calculated and displayed graphically, with error bars derived from the standard deviation of the

A

	1	2	3	4	5	6	7	8	9	10	11	12
PBS	232264	236533	237796	243356	243113	241897	242082	240170	238725	237029	234627	234266
PBST	246004	248818	250985	258038	254583	255120	253661	254760	253987	253348	251409	249897
dH_2O	231127	238709	241725	240796	238825	241809	238194	240195	240417	238628	237787	233903
TBS	237162	237782	241746	239727	239012	237946	235951	239433	243070	242462	240580	240206
TBST	248396	253640	254830	255545	254267	253511	251590	253621	255182	255697	252360	251140
dH_2O	231263	235328	237586	240193	244461	240988	241767	241952	239609	238858	238608	234739
KCl	231549	236986	239656	241438	241554	242186	242883	239034	244410	238849	236259	233627
KClT	245766	250816	254803	256247	254321	256230	256865	254046	254466	254158	259961	251096

B

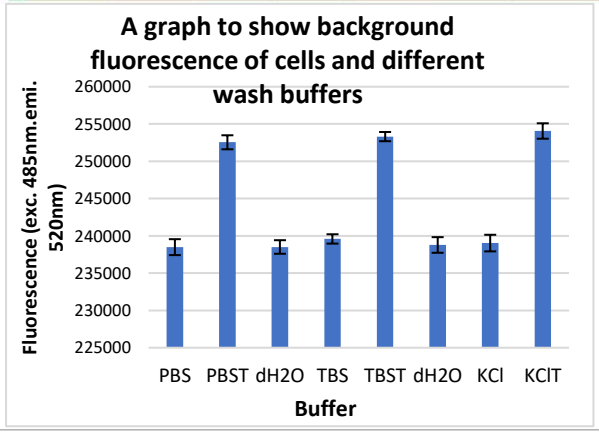

Grouping information using the Tukey Method

Subscripts	N	Mean	Grouping
KCIT	12	254065	A
TBST	12	253315	A
PBST	12	252551	A
TBS	12	239590	B
KCl	12	239036	B
dH2O.	12	238779	B
PBS	12	238488	B

Figure 6.2: Results of EFG Competitive Bind Assay Buffer Trial

Fig A shows the fluorescence levels of the 6 wash buffers tested. Each well contained 100µl of the desired buffer only.

Fig. B shows the subsequent analysis of the plate read out shown in Fig 7A. Graphical representation shows that the 3 buffers containing 0.1% Tween20 caused a higher level of background fluorescence compared to the buffers in which tween20 were omitted. ANOVA analysis of the data shows there to be a statistically significant difference between the buffers containing or lacking 0.1% Tween20. There is however no observable difference between in background fluorescence levels between PBS, TBS or KCl. As PBS has the overall lowest background fluorescence it was taken forward for subsequent assay development. Buffers are grouped into coloured boxes displaying those identified as the same by Tukey's comparison. Red and Green colour coding represent increasing levels of detectable buffer autofluorescence, with lower levels of auto-fluorescent signal assigned a green colour and higher, red. Biological replicates = N1, Technical replicates/biological replicate = N12

12 replicates. The greatest standard deviation across the 12 replicates was observed with the KCl containing buffers (1112.5 and 1033.8) with the lowest standard deviation observed for the TBS containing buffers (626.8 and 617.8). Analysis of the 6 buffers was undertaken to determine whether there was a detectable and statistically significant difference between the background fluorescent levels of the different buffers. Normality and equal variance tests confirmed that the data followed a normal distribution pattern, and so an ANOVA was selected as the appropriate statistical test. ANOVA analysis confirmed that there was a statistically significant difference between those buffers containing Tween20 and those without, with Tukey's post hoc testing categorising the buffers into 2 groups on the basis of Tween20 presence/absence (Figure 6.2B). The ANOVA and Tukey's analysis revealed there was no statistically significant difference in the intrinsic fluorescent levels of Tween20-free buffers PBS, TBS, KCl or dH2O (Figure 6.2B). With the statistical analysis in mind, it was decided that PBS would be selected to take forward and used for subsequent assay development, as of the 3 buffers it gave a marginally lower average background fluorescence then either TBS or KCl.

6.3.3 Identification of Optimal Plate Type and Cell Number Combination Using A431 and MDA-MB-468 Cells

Analysis of plate and cell number combinations, using both MDA-MB-468 and A431 cells were carried out, and the subsequent window between the maximum and minimum levels of achievable fluorescence were calculated (Figure 6.3A and 6.3B). Fluorescent readouts for both cell lines showed that the white, clear bottom Greiner plates closed the obtainable fluorescent window by increasing the levels of auto-fluorescence in the PBS only treated wells (min. fluorescence), whilst not causing an increase to the observable fluorescence in the EGF Alexa Fluor-488 only treated wells (max. fluorescence) (Figure 6.3). Increasing the cell number seemed to have little effect on the fluorescent window observed with MDA-MB-468 cells, however the higher two cell numbers seemed to give a greater percentage difference between max and min fluorescence in A431 cells (Table 6.1). Analysis of the % window in fluorescence was calculated for each plate and cell number combination. This analysis revealed that the different cell lines required different plate types to achieve their maximum fluorescent window, with MDA-MB-468 achieving the best window with the black clear bottom corning plates (19.1%) and A431 (26%) in the clear Nunc plates (Table 6.1). However, for consistency it was decided that the plates used needed to be directly comparable and having 2 different plate types would complicate the experiment. Given the smaller % window in fluorescence in MDA-MB-468 cells it was decided that the plate and cell number combination to use for follow-up assays, for both cell lines, would be selected on the basis of optimising the fluorescent window of this cell line.

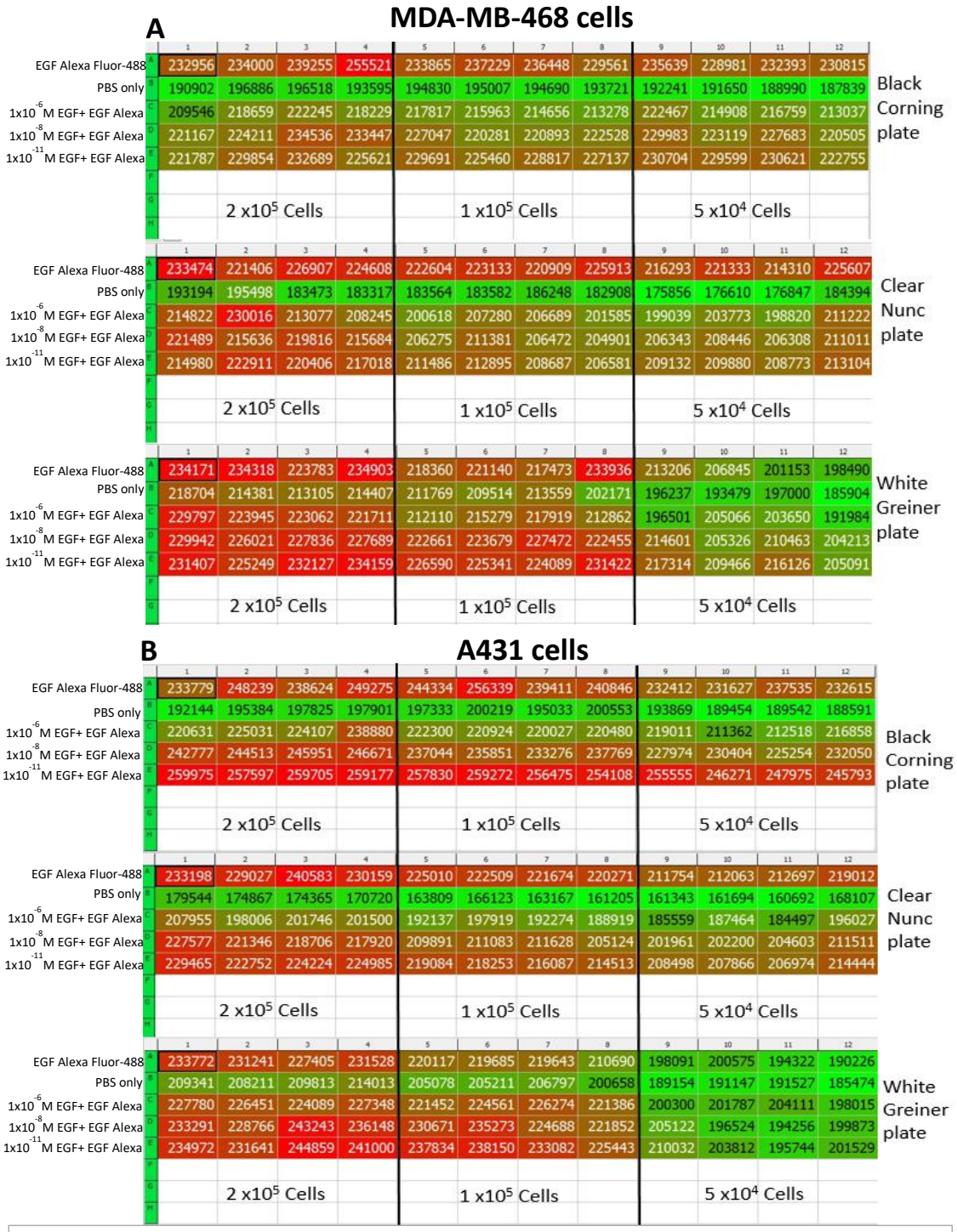

Figure 6.3: Results of EGF Competitive Binding Assay Plate and Cell No. Trial

Fig. A shows the fluorescence levels of MDA-MB-468 cells plated out at 3 different concentration of cells/well ($2x10^5$, $1x10^5$, $5x10^4$) in 3 different plate types. **Fig. B** shows the fluorescence levels of A431 cells plated out at 3 different concentration of cells/well ($2x10^5$, $1x10^5$, $5x10^4$) in 3 different plate types. Cells were treated with varying concentrations of non-fluorescent EGF ($1x10^{-6}$M, $1x10^{-8}$M, $1x10^{-11}$M) for 10 mins. Cells were then treated with either $1x10^{-7}$M EGF Alexa Fluor or PBS for 5 mins). Fluorescence of each plate and cell no. was read using BMG Fluostar plate reader (ex. 485nm, em.520nm). Red and Green colour coding represent increasing levels of detectable fluorescence (greater EGF-Alexa Flour-488 binding to EGFR), with lower levels of fluorescent signal assigned a green colour and higher, red. Biological replicates = N1, Technical replicates/biological replicate = N4

Cell Type	Plate Type	Cell No.	% Fluorescent Window
MDA-MB-468	Black Corning	$2x10^5$	19.11
MDA-MB-468	Black Corning	$1x10^5$	16.95
MDA-MB-468	Black Corning	$5x10^4$	18.01
MDA-MB-468	Clear Nunc	$2x10^5$	16.64
MDA-MB-468	Clear Nunc	$1x10^5$	17.50
MDA-MB-468	Clear Nunc	$5x10^4$	18.67
MDA-MB-468	White Greiner	$2x10^5$	7.18
MDA-MB-468	White Greiner	$1x10^5$	6.05
MDA-MB-468	White Greiner	$5x10^4$	5.74
A431	Black Corning	$2x10^5$	19.24
A431	Black Corning	$1x10^5$	19.14
A431	Black Corning	$5x10^4$	18.49
A431	Clear Nunc	$2x10^5$	25.02
A431	Clear Nunc	$1x10^5$	26.43
A431	Clear Nunc	$5x10^4$	23.80
A431	White Greiner	$2x10^5$	8.93
A431	White Greiner	$1x10^5$	6.02
A431	White Greiner	$5x10^4$	3.30

Table 6.1: Determining the Ideal Cell Number and Plate Combination for EGF Alexa Fluor Competition Assay

MDA-MB-468 and A431 cells were plated at 3 cell concentrations ($2x10^5$, $1x10^5$and $5x10^4$). Cells were treated with varying concentrations of non-fluorescent EGF ($1x10^{-6}$M, $1x10^{-8}$M, $1x10^{-11}$M) for 10 mins. Cells were then treated with either $1x10^{-7}$M EGF Alexa Fluor or PBS for 5 mins). Fluorescence of each plate and cell no. was read using BMG Fluostar plate reader (ex. 485nm, em.520nm). The percentage difference (percentage fluorescent window) between max (Alexa Fluor treated only) and min fluorescence (PBS treated only) was calculated to enable selection of the optimal plate and cell number combination. Yellow boxes highlight the selected cell number and plate type combination selected for both cell lines.

Observation of the fluorescent window in MDA-MB-468 cells showed that the greatest window between maximum and minimum achievable fluorescence was obtained using a combination of black clear bottom Corning plates and a cell seeding density of $2x10^5$ cells/well. Analysis determined that this combination gave an achievable fluorescent window of around 19.1%. Investigation of A431cell fluorescent window in the same plates and at the same cell seeding density revealed that this combination also resulted in an achievable fluorescent window of around 19.2% (Table 6.1). Given that this cell and plate combination resulted in a directly

comparable fluorescent window between both cell lines, it was selected to take forward for further assay analysis.

6.3.4 EGF vs EGF Alexa Fluor-488 Dose Responses

MDA-MB-468 and A431 cells were plated out and treated with a serial dilution of unlabelled EGF ($1x10^{-6}$ M - $1x10^{-13}$ M), before being treated with $1x10^{-7}$M EGF Alexa Fluor-488. Pre-incubation with increasing concentrations of EGF resulted in a dose-dependent inhibition in the binding of fluorescent EGF Alexa Fluor-488 to EGFR. The highest tested two concentrations of EGF ($1x10^{-6}$ M and $1x10^{-7}$ M) caused reductions of EGF Alexa Fluor-488 binding to EGFR in both cell lines (Figure 6.4). Reductions to EGF Alexa Fluor-488 binding at the two highest doses of EGF, but not at lower doses, are not surprising, as the two highest doses represent a 10:1 and 1:1 molar ratio of unlabelled to fluorescently tagged EGF respectively, and so equimolar concentrations or an excess of unlabelled EGF resulted in the off competition of EGF Alexa Fluor-

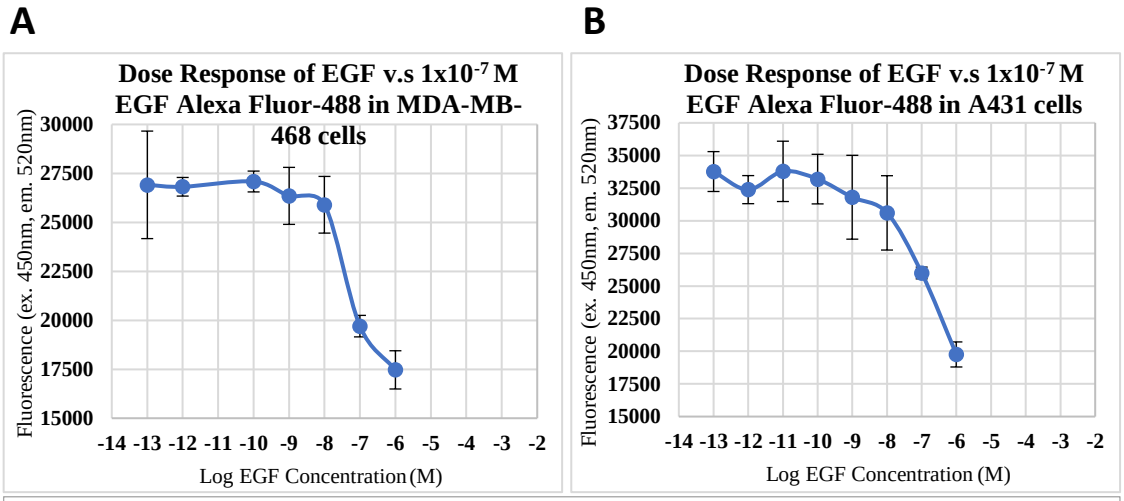

Figure 6.4: Dose Response Curves of EGF vs. EGF Alexa Fluor-488

Dose response curves of a serial dilution of EGF ($1x10^{-6}$ - $1x10^{-13}$ M) vs EGF Alexa Fluor-488 ($1x10^{-7}$ M) in $2x10^{5}$ MDA-MB-468 (A) and A431 (B) cells. Standard error was calculated from the repeat readings and plotted as error bars for each EGF concentration. An outlier value was observed for MDA-MB-468 cells at an unlabelled EGF dose of $1x10^{-11}$M, and so this point was omitted from the dose response curves. Biological replicates = N1, Technical replicates/biological replicate = N3

488 from the EGFR on the surface of the cell lines. Lower concentrations of unlabelled EGF ($1x10^{-8}$ - $1x10^{-13}$M) are not effectively able to off-compete the fluorescent Alexa-tagged EGF, due to an excess of the fluorescently labelled form, and so reductions to fluorescent signal from binding were unobserved. Higher doses of unlabelled-EGF appear to be needed to further off-compete the Alexa Fluor-labelled EGF, however higher doses than $1x10^{-6}$ M EGF were not feasible to test. It is also worth noting that even if it were possible to have investigated higher concentrations of the unlabelled-EGF for these dose response curves, that some of the residual

binding signalling can likely be attributed to the non-specific binding of the Alexa-fluor labelled EGF-form to both the plastic wear and potentially other cellular components other than EGFR. Despite the lack of complete EGF Alexa Fluor-488 off-competition, the dose response curves still confirm the ability of an appropriate antagonist to effectively off-compete the fluorescent EGF and that this reduction is detectable using the developed optimised assay method.

6.3.5 EGF Alexa Fluor-488 Competition Assay of a Panel of 18 Diverse Snake and 22 Diverse Invertebrate Venoms

MDA-MB-468 and A431 cells were treated with a panel of 18 snake venoms for an incubation period of 2h or 10 min to determine whether any of the venoms in the panel could effectively off-compete the binding of Alexa Fluor-488 tagged-EGF to EGFR on the surface of the cancer cells. The average fluorescence of each of the venom-treated triplicate was calculated, along with the maximum (EGF Alexa Fluor-488 treated) and background (PBS only treated) fluorescence control triplicates. All averages were plotted graphically, and error bars were produced from the standard deviations of each triplicate of venom treated wells (Figures 6.5 & 6.6).

After treatment with a dose of 2 mg/ml (100µg protein/well) for 2h it appeared that *Agkistrodon contortrix contortrix* (A.cco) and *Bothrops asper* (B.asp) venoms were causing reductions in each Alexa Fluor-488 signal, and therefore thought to be disrupting the binding of the labelled-EGF to EGFR in both cell lines (Figure 6.5). Additional smaller reductions to fluorescence were also observed in MDA-MB-468 cells following 2h treatment with *Sistrurus miliarus barbouri* (S.mil) and *Montivipera xanthina* (M.xan) venoms (Figure 6.5B). However, upon inspection of these particular wells under an inverted microscope there was evidence of substantial cell shredding and degradation with these particular venoms, despite the cells being pre-fixed with 4% paraformaldehyde prior to venom treatment. It is possible that a combination of a concentration of 2 mg/ml and a 2h treatment period caused a cellular-shredding response to be viable. No reductions were observed in EGF Alexa Fluor-488 fluorescence in response to any of the other treatment venoms in either cell line.

Due to the cell degradation observed with some of the snake panel venoms at previous treatment conditions and a lack of reduction in fluorescence in response to the rest of the panel, it was decided that a 2 mg/ml dose of each venom would be tested again, but at a shorter dose interval. It was inferred that this change in incubation time may both eliminate the cell shredding observed with some of the panel venoms and also potentially allow for the identification of venoms that may contain components which bind rapidly to EGFR but dissociating from it over a longer incubation time period. It was hypothesised that incubation of the cells in each venom for a shorter

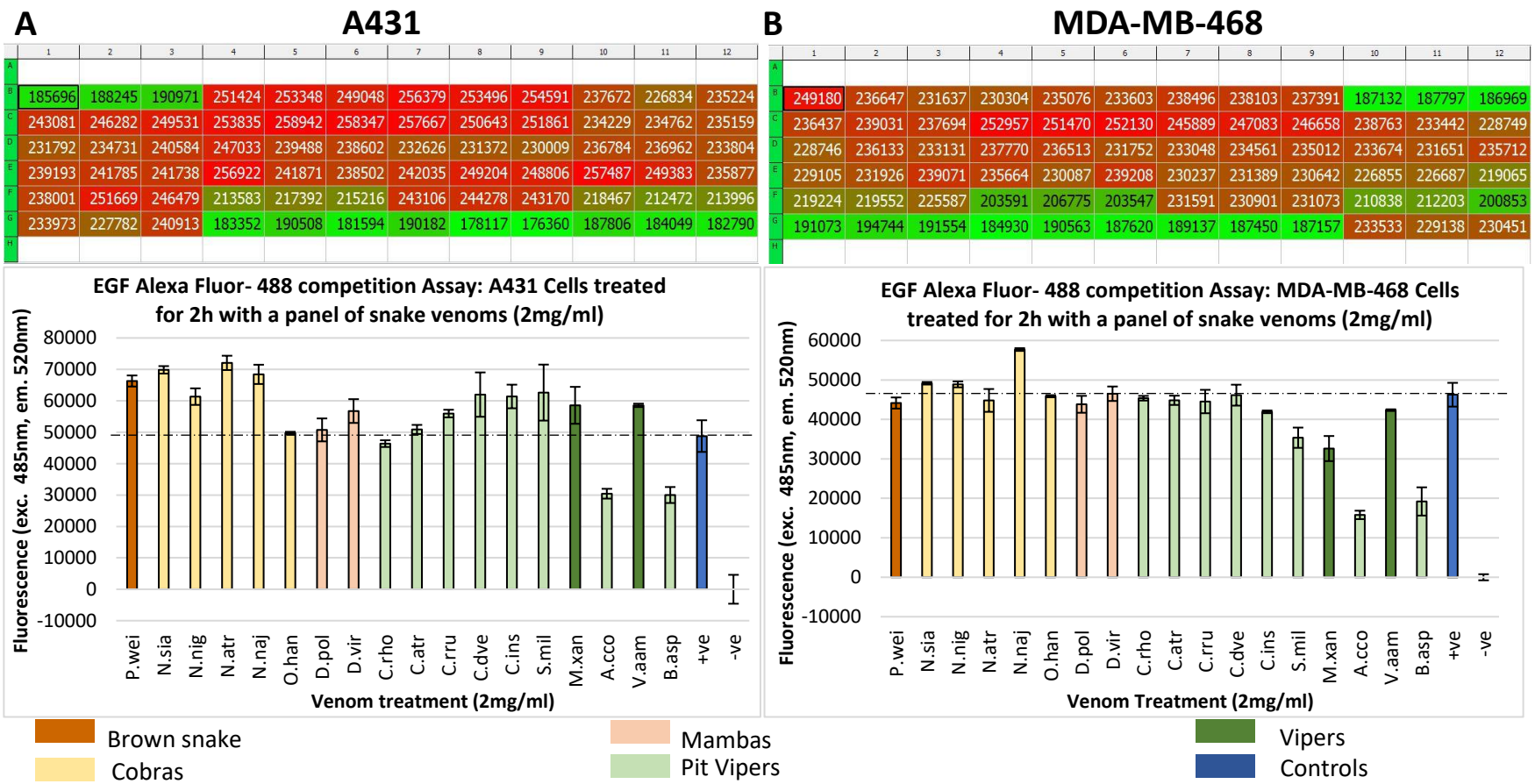

Figure 6.5: EGF Alexa Fluor-488 Competition Assay: Snake Panel Data (2h Incubation)

Graphical representation of EGF Alexa Fluor-488 fluorescence in A431 (A) and MDA-MB-468 (B) following 2h treatment with a panel of 18 snake venoms (50 µl/well, conc. 2 mg/ml). Average fluorescence readings were calculated, and standard deviation plotted as error bars for each group of triplicate values. Fluorescence was read on a BMG Fluostar plate reader (ex. 485nm, em.520nm). Threshold lines were set to the level of the EGF Alexa Fluor-488 only treated control. Red and Green colour coding represent increasing levels of detectable fluorescence (greater EGF-Alexa Flour-488 binding to EGFR), with lower levels of fluorescent signal assigned a green colour and higher, red. **+ve control** = treatment with $1x10^{-7}$M EGF Alexa Flour-488 only. Biological replicates = N1, Technical replicates/biological replicate = N3

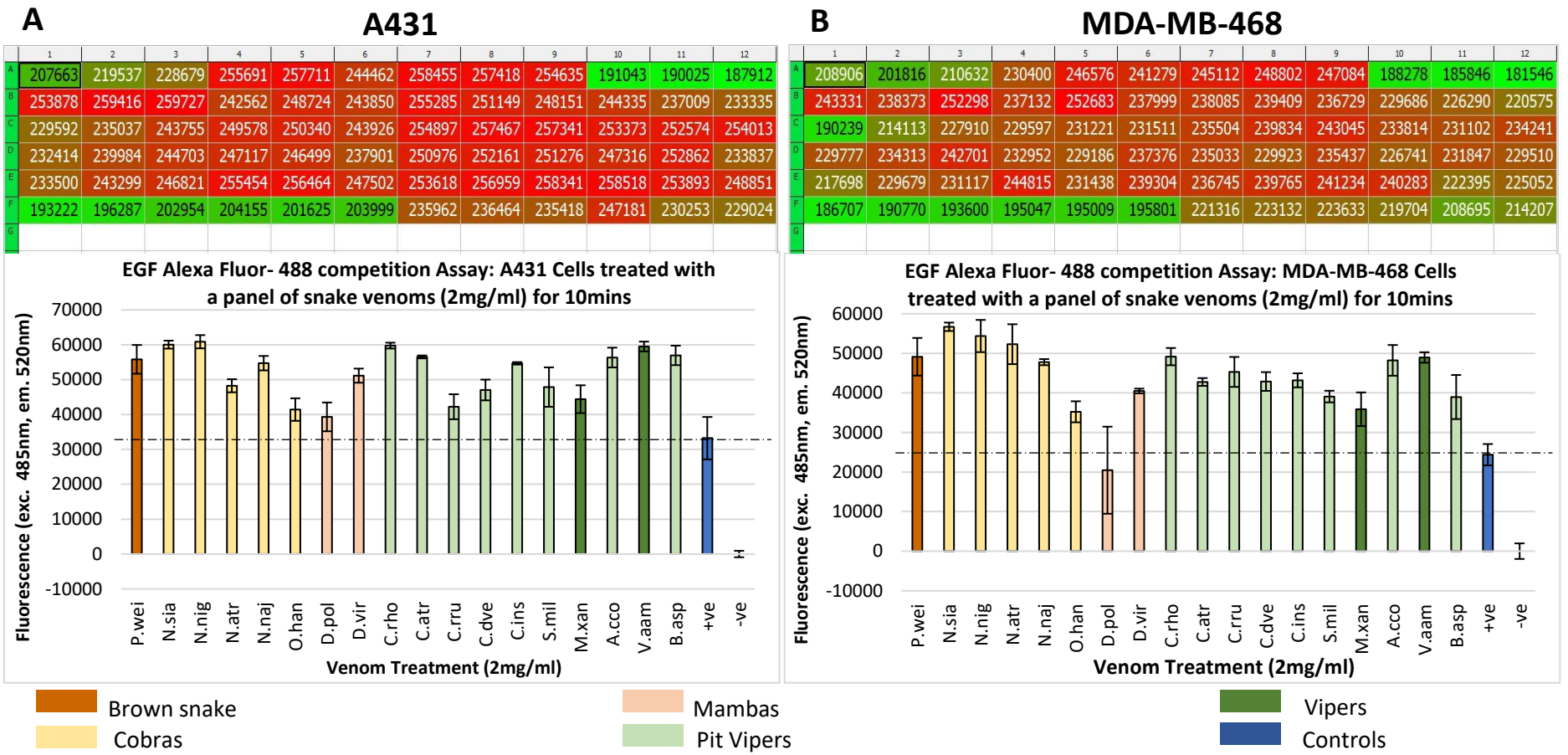

Figure 6.6: EGF Alexa Fluor-488 Competition Assay: Snake Panel Data (10 min Incubation)

Graphical representation of EGF Alexa Fluor-488 fluorescence in A431 (A) and MDA-MB-468 (B) following 10mins treatment with a panel of 18 snake venoms (50 µl/well, conc. 2 mg/ml). Average fluorescence readings were calculated, and standard deviation plotted as error bars for each group of triplicate values. Fluorescence was read on a BMG Fluostar plate reader (ex. 485nm, em.520nm). Threshold lines were set to the level of the EGF Alexa Fluor-488 only treated control. Red and Green colour coding represent increasing levels of detectable fluorescence (greater EGF-Alexa Flour-488 binding to EGFR), with lower levels of fluorescent signal assigned a green colour and higher, red. **+ve control** = treatment with $1x10^{-7}$M EGF Alexa Flour-488 only. Biological replicates = N1, Technical replicates/biological replicate = N3

time period before fixing may allow for binding events to be seen that may have been undetectable in the 2h treatment group due to the process of EGFR receptor recycling, a process which could be masking binding in the longer incubation group. MDA-MB-468 and A431 cells treated with the snake panel for 10 min showed no detectable reductions to EGF Alexa Fluor-488 binding to EGFR (Figure 6.6), with the exception of *Dendroaspis polylepis* (D.pol) in MDA-MB-468 cells (Figure 6.6B). However, analysis of the replicate readings identified that there was a larger degree of variation between the values obtained for these particular triplicate readings, with the error bar for *D. polylepis* overlapping with the average maximum fluorescence error bar. Variations in the observed replicate readings could suggest a potential effect, but that the dose of 2 mg/ml utilised is not sufficiently high enough to effectively off-compete all of the fluorescent EGF. Variations across the triplicate results could also be the result of, or further exacerbated by, limitations of the assay design itself including the high degree of non-specific binding of the EGF Alexa-fluor-488 and the very narrow dynamic range of the assay. It is worth noting that whilst a dose of 2 mg/ml seems high, it is the complete venom protein concentration and so it is likely that any component displaying EGF-antagonistic effects would be at a considerably lower concentration. This could also explain the lack of effect observed with this venom when treating A431 cells. A431 cells express a larger number of EGF receptors/cell compared to MDA-MB-468 cells, and so would require a larger dose of the potentially antagonistic component in the *D. polylepis* venom to bring about the same level of observable binding inhibition. As with the results seen following 2h of venom treatment, no reductions were observed in the binding of EGF Alexa Fluor-488 to EGFR in A431 cells following 10 min venom incubation (Figure 6.6A). Whilst EGF has not been specifically identified in the venom of *D. polylepis*, it is worth noting that venoms, including those from the family *Elapidae*, have been found to contain growth factors, including VEGF, NGF, and non-toxic proteins with high sequence homology to human growth factors, such as endocrine-gland-derived vascular endothelial growth factors (EG-VEGF) (LeCouter and Ferrara, 2002; Warrell, 2010), and so it is possible that a molecule of this type could be present and causing a reduction to Fluorescently-labelled EGF binding ability.

Whilst the graphical data appeared to show no observable off-competing of EGF Alexa Fluor-488 by the screened panel of snake venoms, Z score analysis was undertaken to further validate the findings of the assays. Z score analysis was selected as it is calculated without the need to use control samples, which appeared in all screens to be continually lower than all other wells on the plates; potentially the result of the placement of the controls within each plate layout and plate edging effects (Figures 6.5 & 6.6). Z scores are calculated by comparing each individual treated value to the overall plate mean and standard deviation values thereby eliminating the need to use controls, and is a common statistical scoring method used in high through-put screening (HTS)

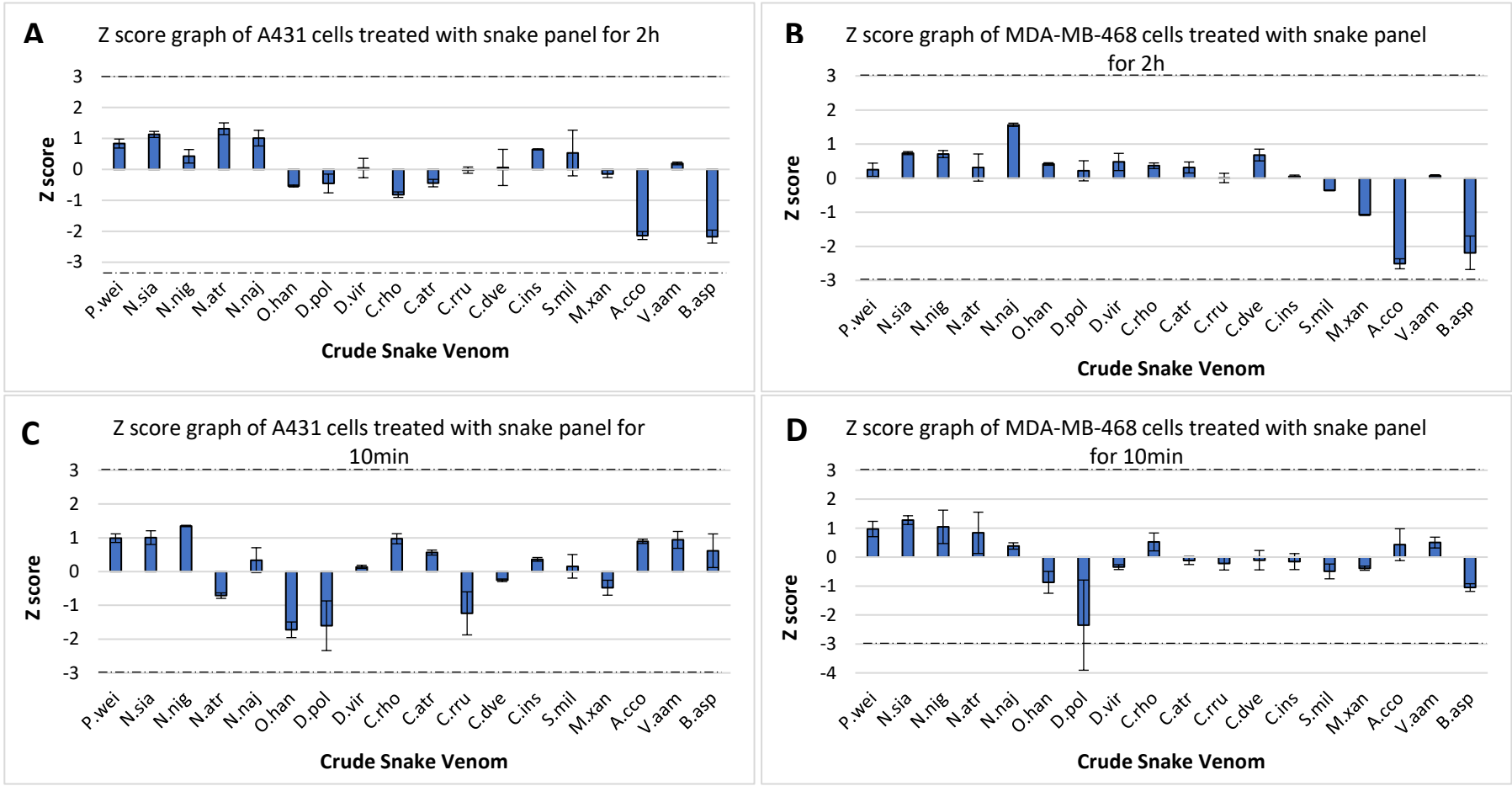

Figure 6.7: Z Score Graphs of MDA-MB-468 and A431 Cell Snake Panel Screens

Z score graphs of A431 cells treated with the snake panel for 2h (A), MDA-MB-468 cells treated with the snake panel for 2h (B), A431 cells treated with the snake panel for 10 min (C) and MDA-MB-468 cells treated with the snake panel for 10 min (D). Standard deviation was calculated from replicate Z scores and plotted as error bars. Dotted lines represent the ±3 threshold required to be considered a real effect.

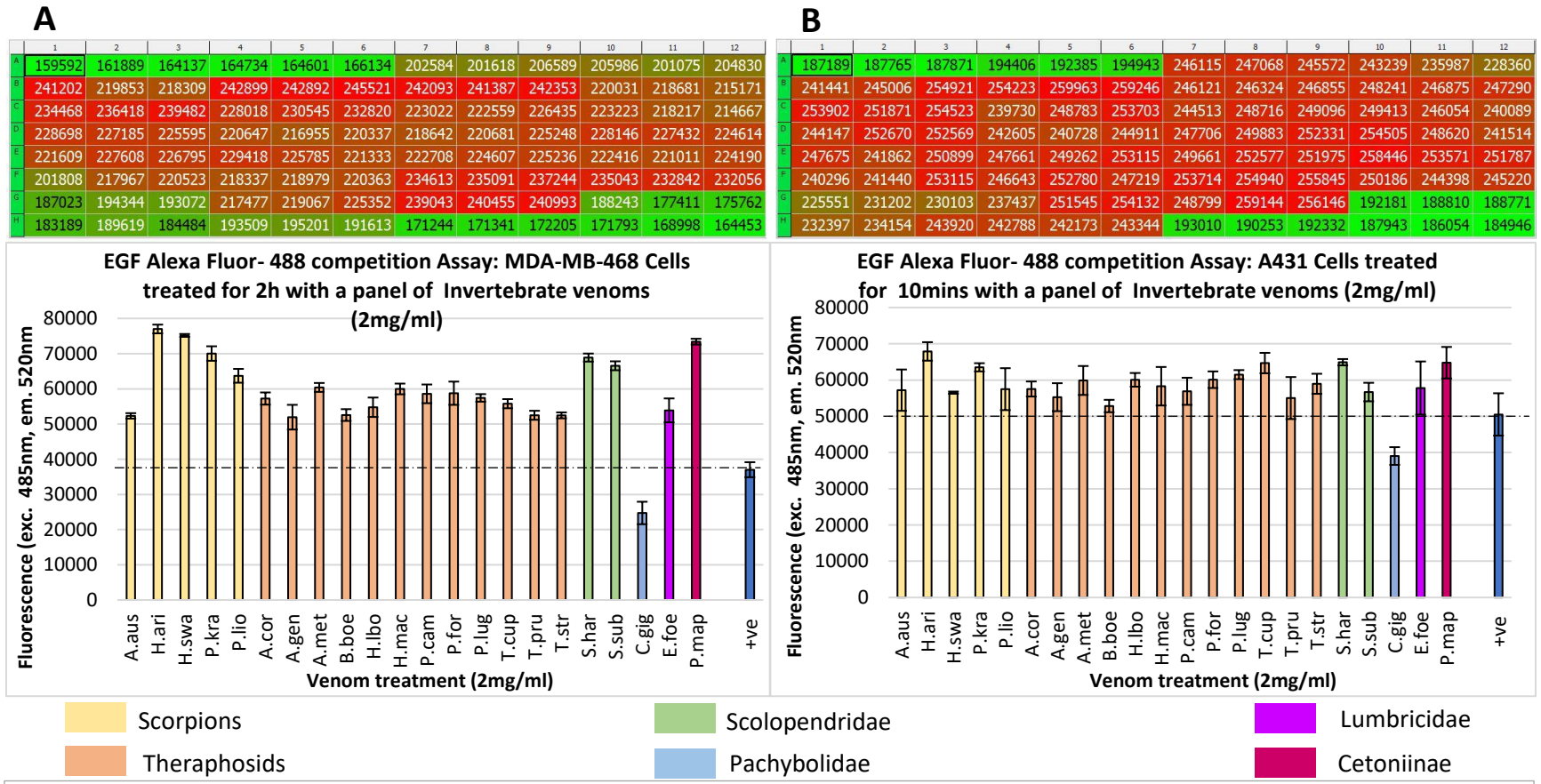

	1	2	3	4	5	6	7	8	9	10	11	12
A	159592	161889	164137	164734	164601	166134	202584	201618	206589	205986	201075	204830
B	241202	219853	218309	242899	242892	245521	242093	241387	242353	220031	218681	215171
C	234468	236418	239482	228018	230545	232820	223022	222559	226435	223223	218217	214667
D	228698	227185	225595	220647	216955	220337	218642	220681	225248	228146	227432	224614
E	221609	227608	226795	229418	225785	221333	222708	224607	225236	222416	221011	224190
F	201808	217967	220523	218337	218979	220363	234613	235091	237244	235043	232842	232056
G	187023	194344	193072	217477	219067	225352	239043	240455	240993	188243	177411	175762
H	183189	189619	184484	193509	195201	191613	171244	171341	172205	171793	168998	164453

	1	2	3	4	5	6	7	8	9	10	11	12
A	187189	187765	187871	194406	192385	194943	246115	247068	245572	243239	235987	228360
B	241441	245006	254921	254223	259963	259246	246121	246324	246855	248241	246875	247290
C	253902	251871	254523	239730	248783	253703	244513	248716	249096	249413	246054	240089
D	244147	252670	252569	242605	240728	244911	247706	249883	252331	254505	248620	241514
E	247675	241862	250899	247661	249262	253115	249661	252577	251975	258446	253571	251787
F	240296	241440	253115	246643	252780	247219	253714	254940	255845	250186	244398	245220
G	225551	231202	230103	237437	251545	254132	248799	259144	256146	192181	188810	188771
H	232397	234154	243920	242788	242173	243344	193010	190253	192332	187943	186054	184946

Figure 6.8: MDA-MB-468 EGF Alexa Fluor-488 Competition Assay: Invertebrate Panel

Graphical representation of EGF Alexa Fluor-488 fluorescence in A431 MDA-MB-468 following 2h (A) and 10 mins (B) of treatment with a panel of 22 invertebrate venoms (50 µl/well, conc. 2 mg/ml). Average fluorescence readings were calculated, and standard deviation plotted as error bars for each group of triplicate values. Fluorescence was read on a BMG Fluostar plate reader (ex. 485nm, em.520nm). Threshold lines were set to the level of the EGF Alexa Fluor-488 only treated control. Red and Green colour coding represent increasing levels of detectable fluorescence (greater EGF-Alexa Flour-488 binding to EGFR), with lower levels of fluorescent signal assigned a green colour and higher, red**. +ve control** = treatment with $1x10^{-7}$M EGF Alexa Flour-488 only. Biological replicates = N1, Technical replicates/biological replicate = N3

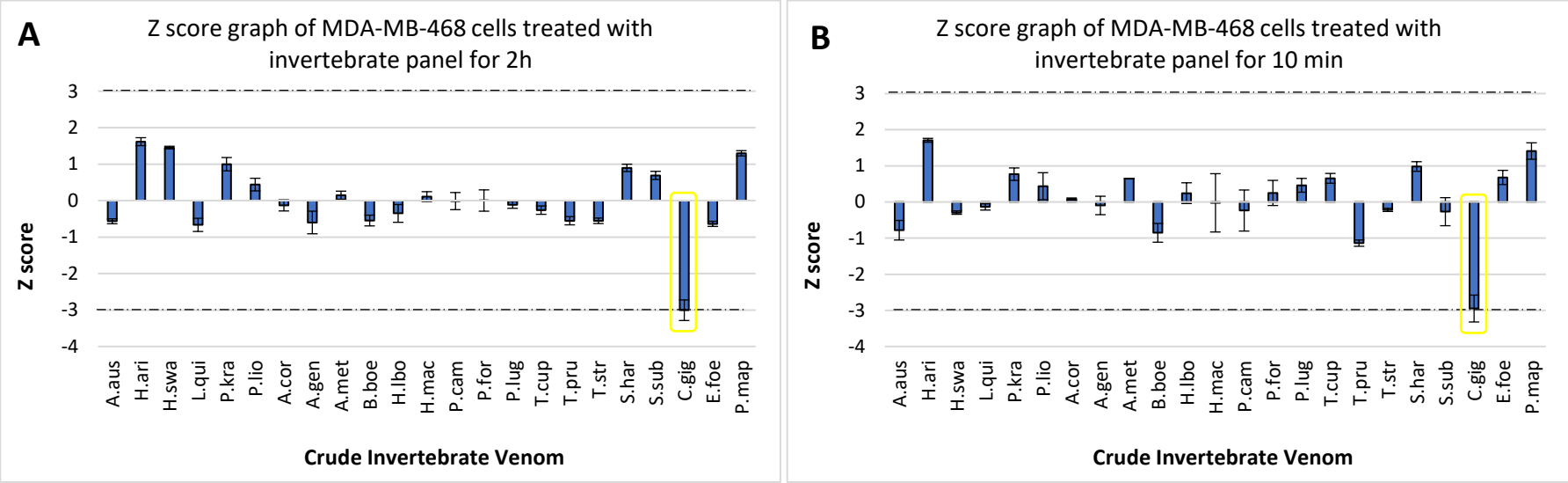

Figure 6.9: Z Score Graphs of MDA-MB-468 Cell Invertebrate Panel Screens

Z score graphs of MDA-MB-468 cells treated with the invertebrate panel for 2h (A) and 10 mins (B). Standard deviation was calculated from replicate Z scores and plotted as error bars. Dotted lines represent the ±3 threshold require to be considered a real effect. Bars highlighted in yellow boxes represent those which passed the selected Z score significance threshold

techniques (Brideau et al., 2003; Malo et al., 2006). Z score ranking did not identify any of the tested snake venoms as passing the selected scoring thresholds (Figure 6.7), and so the findings of these screens suggest that none of the snake venoms from the 18 selected for the panel appear to contain EGF antagonists, capable of specifically off-competing its binding to EGFR.

MDA-MB-468 cells were treated with a panel of 22 invertebrate venoms for 2h (Figure 6.8A) and 10 min (Figure 6.8B) respectively, to determine whether any of the venoms in the panel could effectively off-compete the binding of fluorescent EGF to EGF receptors on the cancer cells' surfaces. Due to the availability of venoms generated by many of the invertebrate species, it was determined that observing one cell line at two different dosing times may generate more useful data (both fast and slow binding events) than both cell lines at the same timepoint. It was decided that the MDA-MB-468 breast cancer cell line would be a more relevant model to undertake this work in, as triple-negative breast cancers (TNBCs) account for around 10-15% of all breast cancer cases and still have extremely poor patient prognosis due to lack of effective therapies (Brewster, Chavez-MacGregor and Brown, 2014). EGFR has been found to be commonly up-regulated in many TNBCs, making it an attractive target for therapeutic suppression (Chacón and Costanzo, 2010).

As with the previously investigated snake panel, the average fluorescence of each venom triplicate was calculated along with the +VE and –VE control triplicates. All averages were plotted graphically, and error bars were produced from the standard deviations of each triplicate of venom treated wells (Figure 6.8). After treatment with a dose of 2 mg/ml (100µg protein/well) of each venom for both 10 min and 2h the only detectable reductions observed in EGF Alexa Fluor-488 binding were observed in response to treatment with *Colossobolus giganteus* (C.gig) secretion (Figure 6.8) Similar levels of reductions appeared to have occurred in response to *C. giganteus* secretion at both the tested time points, suggesting that active molecules in this secretion could be continually rapidly binding and dissociating from EGFR or that they are quickly and irreversibly binding. Z score analysis was undertaken to further validate the findings of the assays and the subsequent ranking data confirmed that *C. giganteus* secretions alone passed the selected reduction threshold of -3 at both of the selected timepoints (Figure 6.9). Z score ranking identified no other tested invertebrate venoms as causing biologically different effects to EGF: EGFR binding.

Previous reductions of between 20-30% were observed in response to treatment with *C. giganteus* secretion in both MDA-MB-468 and A431 ELISA analyses (Figure 5.10). These combined finding suggest that *C. giganteus* secretion is could be capable of competitively binding to the EGF-binding domain of EGFR. However, it is also worth noting that the secretions from millipede

are predominantly formed of alkaloids, phenols, benzoquinones, fatty acid esters, cyanogenic compounds and terpenoids, rather than peptidyl components, which tend to act as topical irritants (Arab *et al.*, 2003; Shear, 2015). It is possible that these compounds, rather than binding specifically to EGFR in the EGF binding domain are actually causing more of a generic barrier to EGF binding and thus resulting in a lower degree of EGF binding to EGFR just by the very nature of their presence. This type of barrier would not prove useful as a therapeutic treatment as it could potentially disrupt the effective binding of multiple ligands to cellular surface receptors, not just EGF to EGFR, ultimately causing multiple unintended off-target effects.

Interestingly, there are venoms tested within both these panels which have previously been shown in PY20 ELISAs and Western blot analyses to cause detectable reductions in EGFR phosphorylation following 2h of treatment, including *P. rossignoli* (P.wei), *C. durissus vegrandis* (C.dve), *C. rhodostoma* (C.rho), *T. albolabris insularis* (C.ins), *N. naja* (N.naj), *B. boehmei* (B.boe), *H. swammerdami* (H.swa) and *A .geniculata* (A.gen) amongst others (Figures 4.9, 5.8, 5.10, 5.12 & 5.13). This inhibition in EGFR phosphorylation events, coupled with the subsequent information that these venoms cannot antagonistically off-compete EGF binding to EGFR, suggest that these venoms may be working through a different mechanism to bring about changes to EGFR activity. Given that the inhibition of EGF binding is not causing the observed changes to EGFR activity, perhaps the active component in these venoms may be binding intrinsically to the receptor's internal kinase domain, preventing activation of the receptor via a similar mechanism used by small molecule kinase inhibitors (SM-TKIs) (Wu, Nielsen and Clausen, 2015). Components in venoms and secretions have been found capable of disrupting the normal functioning of RTK kinase domains, however the literature evidence detailing this is still fairly scarce. Arenobufagin, a toxin isolated from the secretion of toad *Bufo bufo gargarizans Cantor* has been shown to inhibit the activation of RTK VEGFR-2. It has been suggested through computational modelling that this inhibition is the result of the blockage of the ATP-binding pocket of the receptor tyrosine kinase domain, ultimately leading to inhibited VEGFR-2 auto-phosphorylation and the suppression of VEGFR-2-mediated signalling cascades (Li *et al.*, 2012).

Alternatively, it is entirely possible that these venoms may be binding to neither the EGF binding site nor to the tyrosine kinase domain, but rather be binding allosterically to EGFR. This binding could be causing a change to the receptors structure and/or forming some kind of structural hindrance or conformational change in the receptor, ultimately leading to a disruption of receptor dimerisation and activation, in a similar mechanism observed with antibody-targeted therapies (Pohlmann, Mayer and Mernaugh, 2009; Vu and Claret, 2012). However, there is no evidence in the literature of venom components that have been specifically identified as causing reduced activation in RTKs by binding allosterically or to novel regions of their extracellular domains.

Whilst the assay does appear to have generated a potentially interesting hit for EGF off-competition, it is worth noting that despite previous optimisation the assay itself still possessed several limitations. These limitations appear to have included potential issue with plate edging effects and plate layouts, leading to queries surrounding the validity of the maximum fluorescence controls, and a very small workable window between maximum and minimum achievable fluorescence. This could have led to the identification of false negatives in the Z scoring. Further optimisation could be undertaken to attempt to improve the fluorescent window, by the potential addition of a blocking step which may aid to bring non-specific EGF Alexa Fluor-488 binding background down. Alternatively, the isolation of EGFR directly from the cells through immunoprecipitation and the subsequent coating of plates directly with it, rather than the fixing of cells, may also improve the window by removing potential cell autofluorescence and increasing the overall number of available EGF receptors to which EGF Alexa Fluor-488 can bind. Both of these could ultimately open up the window between maximum and minimum fluorescence. Plate layouts which resulted in the spread of replicate wells across the 96 well plate may have helped to eliminate the possibility of edging effects by better allowing for the identification of edge outlier data points. There is also the possibility that the selection of EGF conjugated to a different fluorophore, with different excitation and emission wavelengths, may have allowed for more sensitivity and a larger fluorescent window. If optimisation failed to further enhance the workable window of the assay, the potential to acquire a commercially available fluorescent EGF-competitive binding assay, such as the EGF/EGFR AlphaLISA Binding Kit (PerkinElmer) could also be considered.

6.4 Conclusion

The work undertaken in this chapter identified only one invertebrate secretion, *C. giganteus*, as causing interesting reductions to EGF Alexa Fluor-488 binding. However, due to the nature of the composition of this venom the work raises questions as to whether EGF off-competition or the formation of a general barrier by this venom may be occurring. The lack of EGF off-competition by many of the other tested venoms, potentially rule out this as a particular mechanism of action for the reductions in EGFR phosphorylation observed in previous work carried out in Chapters 3 & 5. Whilst the data in this chapter does not positively identify the exact mechanistic action of the venoms shown to have positive effect on EGFR reduction, it does appear to suggest that antagonism of EGF binding as a possible mechanism of action is unlikely. However, in order to effectively confirm this, further investigative work and assay development would have to be undertaken. Similarly, whilst the assay generated a potential venom of interest, it is worth noting that the assay could undergo addition optimisation to further enhance and

validate the data. However, given that the outcome of this assay does not directly impact the decisions of the work to be undertaken in Chapter 7, and the difficulty experienced in obtaining a workable fluorescent window in the initial assay optimisation stages, it was decided that this further optimisation would not be undertaken.

CHAPTER 7: Fractionation and Identification of Venom Components Responsible for Observed Reductions in EGFR phosphorylation

7.1 Introduction

7.1.1 HPLC and Mass Spectrometry Analytical Techniques

Whole venoms from a variety of diverse species have been shown in previous chapters to be capable of causing both inhibitory and excitatory effects on the phosphorylation potential of EGFR. However, as previously shown in Chapter 3, due to their incredibly complex biological composition, whole venoms are capable of interacting and causing changes to multiple proteins simultaneously. Complex mixtures of compounds are unlikely to be suitable as potential future therapeutics due to the propensity for an increased chance for undesirable off-target side effects.

Venoms are a complex mixture of many types of biological molecules, including peptides, proteins, amines and polysaccharides, amongst others. The dry weight of venom consists of between 90-95% peptide and protein (Liu *et al.*, 2014). Fractionation of whole venom by high-performance liquid chromatography (HPLC) allows for the separation of individual biological molecules on the basis of specific characteristics they display, such as type of biological molecule, size, charge or hydrophobicity. Using HPLC and the fact that venoms have a peptide/protein composition of over 90%, whole venoms from a diverse range of genera including cobras (Malih *et al.*, 2014; Lauridsen *et al.*, 2017), crotalids (Wang *et al.*, 2010; Moore *et al.*, 2015), scorpions (Asmari, Khan and Manthiri, 2012; Xu *et al.*, 2014) and theraphosids (Cherki *et al.*, 2014; Ikonomopoulou *et al.*, 2016) have been shown to be successfully fractionated into a large number of potential biologically active compounds, that can then be screened like component libraries to assess their possible target specificity.

HPLC separation of complex mixtures exploits the binding capabilities of a column (stationary phase) with the changing composition of a mobile liquid phase. Reverse phase (RP) HPLC is a method used to separate complex mixtures of proteins and peptides on the basis of the hydrophobicity of each peptide component. A column with a hydrophobic stationary phase is used, capable of binding peptides and proteins which display strong hydrophobic characteristics with a greater affinity than those which display hydrophilic properties. A mobile phase, normally in the form of buffers, is passed through the stationary phase column (Figure 7.1). During RP HPLC, proteins with high hydrophilicity elute quickly from the column in highly polar buffers.

Proteins which display high hydrophobicity require buffers with an increasing concentration of a non-polar organic solvent to cause their eventual eluting from the column.

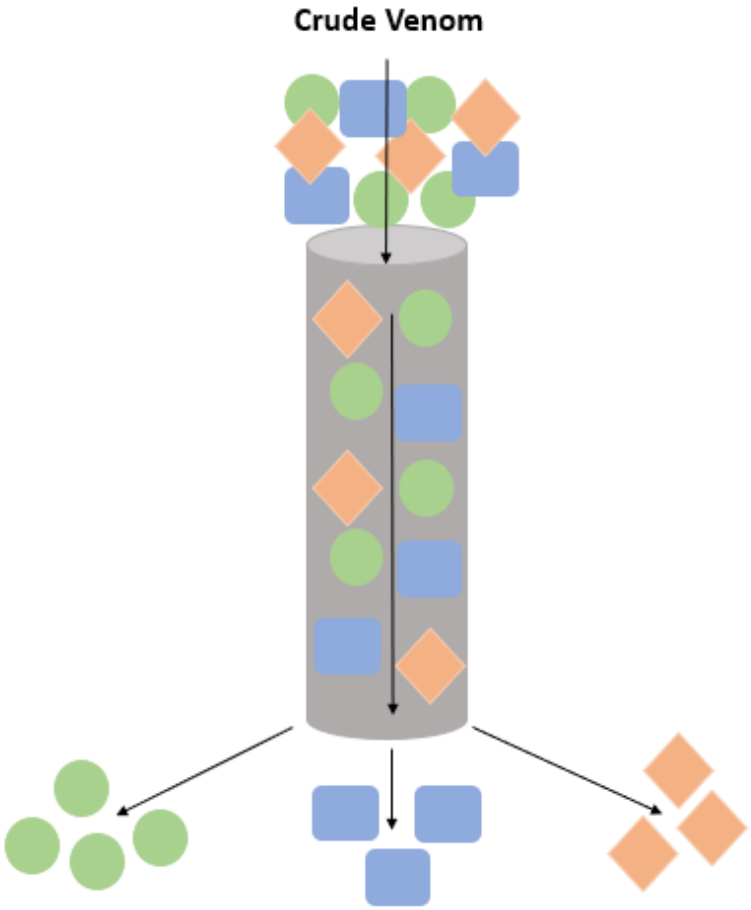

Figure 7.1: Diagram of HPLC Fractionation

Whole mixtures of proteins and peptides are separated through the column. Samples bind to the column (stationary phase) and buffers of differing compositions are passed through the column (mobile phase) to elute proteins/peptides based on their compositional characteristics, such as size, charge or hydrophilicity. Individual components that elute at certain buffer compositions are collected independently, allowing for a complex mixture to be purified into individual components

The degree of hydrophobicity with which peptides bind to the hydrophobic stationary phase, and the gradual shift from a polar to a non-polar mobile phase through increasing solvent levels, results in the separation of peptides and proteins with slightly different amino acid compositions (Dong, 2006). Size exclusion (SEC) HPLC exploits a column which contains beads with various size pores. An isocratic mobile phase is used to move mixture components through the column. Larger mixture components elute from the column first, as they are too large to pass through the pores of the beads and instead migrate around them, traveling the shortest distance. Small components pass through the beads and so take a longer, more convoluted route to eventually elute from the column (Dong, 2006).

HPLC fractionation has been shown to be an effective method for the isolation and subsequent identification of venom components. These subsequent fractions, that have been isolated using HPLC have been shown to have effects both *in vitro* against immortalised cancer cell lines and in *in vivo* models. Fractions, isolated using RP-HPLC from the pit viper venom *Pseudocerastes persicus* were shown to display cytotoxic effects against A549 lung cancer cells (Shahbazi *et al.*, 2019), whilst the disintegrin Crotatroxin 2, isolated through HPLC from *Crotalus atrox* venom has been shown to inhibit lung tumour cell colonisation in BALB/c mice (Galán *et al.*, 2008). The fraction NN-32 isolated through ion exchange HPLC from *Naja naja* venom has been found to display cytotoxic and antioxidant effects against Ehrlich ascites carcinomas cells in BALB/c mice (Das *et al.*, 2011). Peptides have also been successfully isolated from scorpion venoms using HPLC methods, with those fractionated from *Androctonus crassicauda* venom shown to be growth modulating against PC-3 prostate cancer and NCI-H460 lung carcinoma cells (Du *et al.*, 2014). Peptides isolated from *Tityus discrepans* scorpion venom utilising gel affinity and reverse phase HPLC fractionation have also been shown to display apoptogenic effects against SKBR3 breast cancer cells (D'Suze *et al.*, 2010).

Mass spectrometry has become a well-accepted and increasingly important technique in proteomics (Aebersold and Mann, 2003; Heck and Van Den Heuvel, 2004; Choudhary and Mann, 2010; Chambers *et al.*, 2012; Li, Wang and Chen, 2017), thanks to its unparalleled ability to achieve high-quality information about biological samples of enormous complexity (Cravatt, Simon and Yates, 2007). Proteomics-based mass spectrometry techniques can provide information on both the complete molecular masses of peptides or on their primary sequence, through the utilisation of site-specific proteases such as trypsin which digest larger proteins into peptide fragments (Olsen, Ong and Mann, 2004; Ong and Mann, 2005). Peptide fragments, generated and detected in the mass spectrometer, are utilised to obtain the corresponding peptide sequence data by using both the molecular mass of each peptide fragment and searches of existing database entries.

7.1.2 Venoms Selected for RP Fractionation and Mass Spectrometry Identification

Venoms were selected for HPLC fractionation and mass spectrometry identification on the basis of previous experimental work undertaken in Chapters 3, 4 and 5. Venoms were selected from those previously shown in Western blot and ELISA analyses to display EGFR phosphorylation/expression reducing properties and with the aim of providing the greatest diversity in investigated genera. Three crotalid venoms, three elapid venoms and three invertebrate venoms were selected for RP HPLC fractionation.

The venoms from Venezuelan rattlesnake *C. durissus vegrandis*, South-eastern USA rattlesnake *Sistrurus miliarius barbouri* and Asian pit viper *Calloselasma rhodostoma* were selected to take forward for HPLC fractionation and further investigation, The three snakes provide a large degree of genetic diversity by belonging to three distinct genera, a good degree of geographical distinction by being endemic to three separate continents, and have been shown through Western Blot and ELISA assays, undertaken in this thesis, to routinely cause reductions in EGFR phosphorylation to both the EGFR-over expressing immortalised cell lines used as models in this thesis. The geographically distinct dispersions of these crotalid species across multiple continents and the reductions in both cancer cell lines caused by their venoms makes them robust and interesting candidates for fractionation and individual component rescreening.

As with the three crotalid venoms selected for HPLC fractionation and further screening, the Elapid venoms were selected to allow for an equal degree of genera and geographical diversity. Selection of a representative from the genera *Naja* (cobras), *Ophiophagus* (king cobra) and *Pseudechis* (brown snakes) allows for the greatest potential variations in venom composition and allows for the inclusion of a venom from a phylogenetically distinct monotypic taxon, and so *Naja naja, Ophiophagus hannah* and *Pseudechis rossignoli* venoms were selected. By selecting one candidate from each of these genera it also allows for investigations again of three species from two different continents, Asia and Australia. Whilst these venoms did not show as pronounced effects in EGFR phosphorylation reductions in the work carried out in previous chapters, there was some instances where reductions occurred, particularly following treatment with the *Pseudechis* venom and in some instances with *Naja naja* venom, however this has not been consistently seen. Despite the lack of consistency in the findings when this venom has been used, it still makes it an interesting selection for fractionated investigation rather than just into its effects when used straight from the animal, and it may also add a degree of clarity around the contradictory findings of earlier chapters.

A large number of invertebrate venoms were investigated from a large number of genera in earlier chapters, and so it was decided that the selection of just three venoms to take forward for further investigation should be predominantly dependent on those shown in previous work to cause the greatest reductions routinely to EGFR phosphorylation. It was also hypothesised that a representative from both theraphosid and scorpion genera would be good to take forward to allow for greater diversity. Previous ELISA data identified that venoms from new world tarantulas appeared to be causing the greatest reductions to EGFR phosphorylation, and previous Western Blot and Kinome analysis in Chapters 4 & 5 identified the venoms of *Acanthoscurria geniculata* and *Brachypelma boehmei* as reproducibly causing reductions to EGFR phosphorylation. And so, these venoms were considered the best to take forward for fractionation. They also have the

additional benefit of belonging to different genera and being endemic to different countries, Brazil and Mexico respectively, making them geographically distinct. Finally, the whole venom from scorpion *Heterometrus swammerdami* has been shown in previous Western blot analysis to cause reductions to EGFR receptor phosphorylation in MDA-MB-468 cells, with possible receptor degradation also observed in response to treatment with this venom, making it potentially interesting for follow up against cancers with high EGFR over-expression profiles. ELISA analysis of *H. swammerdami* venom also identified reductions to both MDA-MB-468 and A431 EGFR expression levels in the two model cell lines.

So in summary the best nine venom options to take forward for further investigation in this chapter, based from previous experimental findings and allowing for the potential for the greatest genetic and geographical-driven venom diversity, were determined to be *C. durissus vegrandis* (Venezuelan Uracoan Rattlesnake), *S. miliarius barbouri* (American pygmy rattlesnake), *Calloselasma rhodostoma* (Malayan ground pit viper), *Naja naja* (Indian cobra), *O. hannah* (King cobra), *Pseudechis rossignoli* (Papuan pygmy mulga), *A. geniculata* (Brazilian white-knee tarantula), *B. boehmei* (Mexican fire-leg tarantula) and *H. swammerdami* (Giant forest scorpion).

7.1.3 Chapter Aims

- Fractionate the nine whole venoms, selected from those which caused reductions to EGFR phosphorylation in previous chapters, using first dimension Reverse Phase (RP) high-performance liquid chromatography (HPLC)

- Screen RP fractions for EGFR-reducing activity using ELISA-based detection

- Analyse ELISA data to determine fractions which cause both statistically and biologically significant reductions to EGFR phosphorylation levels

- Select three fractions to take forward for second dimension Size Exclusion (SEC) HPLC and Mass Spectrometry analysis (Intact mass and peptide mapping)

- Assess the data obtained from Mass spectrometry of fractions using databases and literature to propose the likely components of each venom fraction

7.2 Methods

7.2.1 1st Dimension Fractionation: Reverse Phase (RP) High Performance Liquid Chromatography

1st dimension fractionation of whole venoms was carried out using Reverse Phase high-performance liquid chromatography. Fractionations were undertaken using an Agilent 1100 HPLC system with sample injector, degasser, changeable HPLC columns, UV detector and an automated fraction collector. All whole venoms previously identified as of interest were analysed using the DS11 spectrophotometer (DeNovix, USA) to obtain whole protein concentrations and then diluted in reverse phase buffer A to a concentration of 100 mg/ml. Diluted venoms were centrifuged in a benchtop microcentrifuge (Fisher, UK) for 10 min to sediment undissolved particulates and proteins. Supernatant was pipetted from all centrifuged tubes and transferred to fresh HPLC injection vials. HPLC column Vydac 218TP54 5 µm 250x4.6mm (JayTee part number GP-STD-125) was inserted into the HPLC and 5mg of each whole venom was injected on to the column. Reverse Phase (RP) buffers A and B were used for the duration of the protocol; **Buffer A:** 0.05% TFA, 99.95% HPLC-Grade H_2O, **Buffer B:** 0.045% TFA, 80% ACN, 19.95% HPLC-Grade H_2O

Proteins and peptides were separated from the whole venom using a gradient mode, with a high-pressure limit of 275 bar and a low limit of 3 bar. The change in HPLC buffer gradient overtime was performed via Venomtech Ltd's optimised propriety methodology for RP HPLC fractionation. Fractions were collected using a peak based detection method, with detection wavelengths of 215nm and 280nm. Fractions exceeding 5U (1unit - mAU) were collected into vials. Collection of fractions from whole snake venoms were collected at 280nm, whilst fractions collected from whole invertebrate venoms were collected at 215nm. Other collection parameters were set up as Appendix XXIII. Selected whole venoms, previously shown to have displayed potential reductions in EGFR phosphorylation by either Western Blot or ELISA analysis, were fractionated via this method.

7.2.2 The Production of Lyophilised Venom Fractions

Venom fractions were generated from extracted whole venom using RP High Performance Liquid Chromatography (HPLC). Vials containing fractions were removed from the HPLC and frozen at -20°C. Fractions were lyophilised using a freeze drier. Initial freeze-drier temperature was set to -55°C and the pre-frozen fraction vials transferred to equilibrate to this temperature. Once frozen to -55°C a vacuum was set. The temperature was gradually increased from -55°C to 4°C over 4

days to evaporate off both acetonitrile and water. Lyophilised fractions were stored in a freezer at -20^{o}C until used.

7.2.3 Determining the Effect of 1st Dimension Venom Fractions on EGFR Phosphorylation State by PY20 ELISA

A431 cells and MDA-MB-468 cells were counted and plated as via standard protocols **2.1.2** & **2.13** in 96 well plates at a concentration of 1x10^{5} and 5x10^{4} respectively and left overnight to resettle and adhere. Fractions previously produced in **7.2.1** were resuspended in 100µl of dH_2O. 50µl of resuspended fractions were further diluted in 450µl of supplemented DMEM media. Cells were treated in either triplicate or quadruplicate with each venom fraction (50 µl/well) for 2h. Positive, negative and antibody controls (1^{o} and 2^{o}) were also run in replicates. After 2h venom incubation the ELISA protocol was carried out as via the standard optimised protocol laid out previously in **2.4.2**.

7.2.3.1 Analysis and Graphical Representation of EGFR Phosphorylation State Following Venom Fraction Treatment

ELISA data, generated from MDA-MB-468 and A431 cells treated with fractionated venoms, were analysed to determine whether there were any observable reductions in EGFR phosphorylation in either cell line in response to treatment. Absorbance data of TMB at 450nm for each well was corrected for well to well cell number differences by dividing by the collected absorbance of crystal violet cell staining at 595nm for the same well. Averages of replicate-treated wells were calculated, excluding any obvious outlier wells. Average background phosphorylation (EGF untreated absorbance) was subtracted from all average corrected absorbance readings to give the change (increase/decrease) in phosphorylation levels in response to EGF/venom fraction treatment. Percentage increases/decreases in EGFR phosphorylation levels for each fraction were calculated by dividing the average corrected absorbance (minus background) by the average corrected absorbance (minus background) of EGF only stimulated cells (control phosphorylation level increase). Percentage changes in EGFR phosphorylation levels were plotted graphically. Standard error of each triplicate/quadruplicate of corrected absorbances was calculated and converted to percentage standard error. These were plotted as error bars on all graphs to display the degree of variation between replicate treated wells. 20% and 50% reduction lines were added to all graphs to enable the quick identification of fractions which display levels of EGFR phosphorylation reduction greater than these thresholds. Fractions causing 50% or greater reductions in EGFR phosphorylation were highlighted in green boxes for easy identification. Fractions which appeared to display any cytotoxic properties at the cell dosing stage, prior to EGF

stimulation and cell fixing, were identified as potential sources of false positives. Whilst crystal violet staining was used to correct for uneven cell numbers it is not capable of accurately correcting for complete cell death, and so these fractions were subsequently highlighted in red on graphical analysis.

7.2.3.2 Minitab Statistical Analysis of EGFR Phosphorylation State Following Venom Fraction Treatment

TMB Absorbance readings generated from ELISAs were analysed for statistically significant differences. Venom fraction-treated data sets, shown through analysis carried out in **7.2.3.1**, to result in 20% or greater reductions in EGFR phosphorylation in either cell line were selected for further statistical analysis. Average background phosphorylation absorbances were calculated from the replicates on each ELISA and the average background level subtracted from all other selected absorbance readings, including venom fraction-treated and EGF-treated samples. Obvious outliers were removed from each data set, with the remaining corrected absorbances imported into Minitab 19 Statistical analysis software. Normality tests and equal variance tests were performed on all data sets to confirm the normality of the data. Normally distributed data with equal variance underwent subsequent ANOVA analysis with post hoc Tukey's testing, to enable direct comparison of all data sets simultaneously. Data sets shown not to have normally distributed data underwent Kruskal-Wallis comparisons. Normality tests were performed on all residuals generated from statistical modelling tests to ensure that the analysis performed was correct and robust. The direct comparison of 2 normally distributed data sets with equal variance was carried out using a 2-Sample T-Test, whilst a Mann-Whitney test was carried out for the direct comparison of 2 data sets which had a non-normal distribution or had unequal variance. Data sets with a P value below 0.05 were considered to be showing statistical significance between the sets tested, with the Tukey's comparison identifying where the statistical differences were occurring.

7.2.4 2nd Dimension Fractionation: Size Exclusion High Performance Liquid Chromatography of Fractions Shown to Cause Reductions in EGFR Phosphorylation

Three first dimension RP fractions shown to cause greater than 50% reduction in EGFR phosphorylation in at least one of the tested cell lines were selected to take forward for further analysis. The fractions (C.dve_R7, B.boe_R6, H.swa_R30) were subjected to a second dimension HPLC to determine whether the effects observed in the previously carried out ELISAS were the result of a pure venom compound, or a possible mixture. Fractions underwent further DS11 analysis prior to 2nd Dimension HPLC to determine concentration and fraction yield, with some

triaged due to lack of sufficient sample for further work. Selected fractions were passed through a second dimension Size Exclusion (SEC) column chromatography to further fractionate out potential components, using Ion Exchange Buffers A and B. SEC HPLC was used as an analytical tool further fractionate 'hit' fractions out on the basis of size rather than previously used hydrophilicity. Up to 10µg of each fraction were injected onto a size exclusion column and an isocratic HPLC performed with a mobile phase buffer composition of 80% Ion Exchange Buffer A, 20% Ion Exchange Buffer B, with samples run at a flow rate of 1ml/min for 15 min.

7.2.5 Mass Spectrometry Analysis of Fractions Shown to Display Inhibition of EGFR Phosphorylation Potential

10µg of two fractions shown to cause greater than 50% inhibition in EGFR phosphorylation in both MDA-MB-468 and A431 cell lines (C.dve_R7 & H.swa_R30) and one fraction shown to only be specific to MDA-MB-468 cells (B.boe_R7) were sent to Peak Proteins Ltd (Alderley Park, Macclesfield) for Intact Mass and Peptide Mapping mass spectrometry analysis. Samples were analysed by Peak Proteins and the collected data returned for analysis.

Briefly the methodology used for intact mass spectrometry by Peak Proteins was as follows. 5µg of each lyophilised fraction sample was reconstituted in 40µl of 0.1% formic acid/5% acetonitrile. 10µl of the sample was loaded onto a Sciex Exion liquid chromatography and a 5 min reverse phase gradient run, using a 0.1% formic acid Buffer A and a 0.1% formic acid/100% acetonitrile Buffer B. RP HPLC was performed with a flow of 500ul over a gradient, starting with 5% Buffer B increasing to 45% B over 3min, followed by a 95% B wash and an equilibration of 5% B. The column used was a Phenomenex Jupiter 5um, C4, 300A 50x2.1mm. Flow from the column was passed into the Sciex X500B mass spectrometer, set to collect data in positive ion mode. To enable ionisation of the eluate the source was set to 400°C, 5500V with gas at 50psi. A TOF mass window of 500-3000Da was collected, scanning at 0.5s. The X500B mass spectrometer was calibrated with a positive calibration mix and the error for the experiment was estimated to 0.5Da. The resultant total ion chromatogram (TIC) was deconvoluted using BioToolKit software (Sciex).

For Peptide Mapping mass spectrometry 5µg of each lyophilised sample was reconstituted in 50µl of 100 mM ammonium bicarbonate. 5µl of 100 mM DTT in 100 mM ammonium bicarbonate was added to each sample and the sample heated at 65 °C for 30 min. 5µl of 500 mM iodoacetamide in 100 mM ammonium bicarbonate was added to all samples and the samples re-incubated in the dark at room temperature for 30 min. 10µl of 25 ng/µl trypsin in 50 mM ammonium bicarbonate was added to each sample and they were incubated overnight at 37°C. 10µl of the complete digest

was taken and mixed with 10µl of 0.1% trifluoroacetic acid (TFA). 10µl of mixed sample was loaded onto the Sciex Exion liquid chromatography and a 10 min reverse phase gradient run. A Phenomenex Lunar 1.6 µm, PS C18, 100A 150x2.1mm column was used. Buffer compositions were as intact mass MS (0.1% formic acid Buffer A and a 0.1% formic acid/100% acetonitrile Buffer B). Flow was set to 300µl and a gradient performed, starting with 5% buffer B, increasing to 45% B over a 15 min duration, before a 95% buffer B wash and an equilibration at 5% B. Flow from the column was passed into the Sciex X500B mass spectrometer set to collect data in positive ion mode. To enable ionisation of the eluate the source was set to 400°C, 5500V with gas at 30psi. A TOF mass window of 300-1800Da was collected, scanning at 1.2s. Mass spec mass spec (MSMS) data was collected using an information Dependent Acquisition method, where up to 10 MSMS were collected per scan. The X500B was calibrated with positive calibration mix, the error for the experiment was estimated at 1ppm. The resultant data from the MSMS was analysed using Mascot (Matrix Science) using the Swissprot database.

7.2.6 Alignments of Sequence Fragment Data Obtained from Intact Mass and Peptide Digest Mass Spectrometry

Amino acid sequence fragments, obtained by peptide digest mass spectrometry from Peak Proteins, were entered into the UniProt database to search for the closest existing matches to venom peptides already deposited within the database. Resultant sequence matches were ranked on the basis of percentage match to the amino acid sequence fragments generated from the fractions sent for peptide digestion mass spectrometry analysis, and also on the basis of the similarity of genera from which these venom peptide sequences were derived. Alignments were undertaken on the complete deposited sequences from the top matching identified venom peptide sequences, using the UniProt sequence alignment tool. Using the alignment tool, regions of high similarity, implying conserved regions across all of the selected deposited sequences, were identified and highlighted. These regions were considered to be conserved and critical to the overall structure and functioning of the classes of venom peptide molecules. Sequence data generated from the mass spectrometry of the samples sent in this chapter were compared to the aligned sequences, with both conserved regions and the obtained sequence data used to try to determine the most likely overall amino acid sequence of the venom fraction component. In regions which showed high variability and a lack of peptide sequence data, all possible amino acid combinations from the top selected hits were considered to be plausible at these loci. Intact mass analysis of each fraction was used to determine the overall molecular weight of the venom fraction component, and this overall mass was in turn used to propose the most like amino acids at the unknown variable loci, by narrowing down those combinations which allowed for a perfect match to the overall obtained molecular weight.

7.3 Results and Discussion

7.3.1 1st Dimension Fractionation: Reverse Phase High Performance Liquid Chromatography

Whole venoms from a variety of species including, cobras, theraphosids and scorpions were fractionated via RP HPLC to produce a collection of fractions corresponding to the elution of particular peptides and proteins from the HPLC column. Snake venom fractionations were carried out with a detection wavelength of 280nm (proteins) and resulted in the collection of 15-20 fractions on average, with the exception of elapid *Pseudechis rossignoli* (P.wei) in which only 12 fractions were collected. Fractionations of invertebrate venoms, including theraphosid and scorpion venoms were carried out with a collection wavelength of 215nm (peptides), which resulted in a larger number of collected fractions, ranging from 26-42 (Table 7.1).

Each elution profile for a particular venom was distinct from others from similar species in its unique peptide/protein elution pattern. Traces from similar genera however did displayed some similarities in fractionation profiles, with peaks of similar sizes and shapes eluting from the column at similar timepoints and % buffer B. Reverse Phase fractionation of Pit viper venoms resulted in the elution of proteins and peptides with very similar looking profiles. All 3 venoms displayed the elution of most components 60 min or later into the fractionation protocol, with the exception of one or two large peaks eluting around 20-30 min into the protocol (Figure. 7.2, see arrows). The late elution of most components of these venoms indicates a composition of proteins and peptides predominantly hydrophobic in nature. Fractionation of *Calloselasma rhodostoma* (C.rho) and *Sistrurus miliarius* (S.mil) venoms resulted in very similar looking elution profiles. The lack of clearly defined peaks, not returning to baseline between 60-120 min suggests a large number of proteins and peptide eluting simultaneously. Fractionation of *Crotalus durissus vegrandis* venom resulted in some sharper peaks eluting around 60-80 min and returning to baseline in-between.

Interestingly, venoms from the elapid family seems to display opposing elution profiles, with most of the abundant protein and peptide components of the venom eluting before 60-70 min into the protocol. The three elapid venoms displayed similar looking profiles, with a large number of components eluting simultaneously in a large multi-peak, with lack of returning to baseline in-between around 30-60 min into the fractionation protocol (Figure 7.3, see arrows).

Like with the elapid family venoms, fractionation of invertebrate venoms resulted in elution profiles were most of the peptides and proteins eluted within the first 60 min of the separation

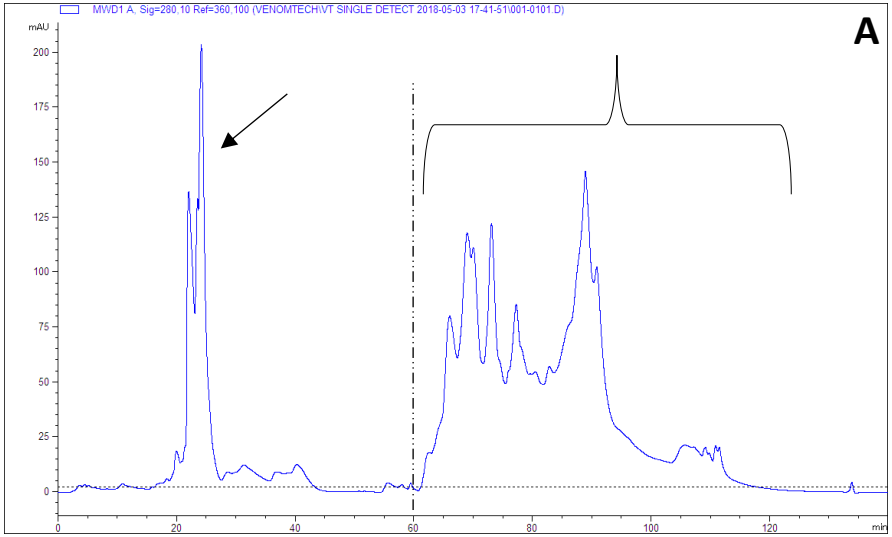

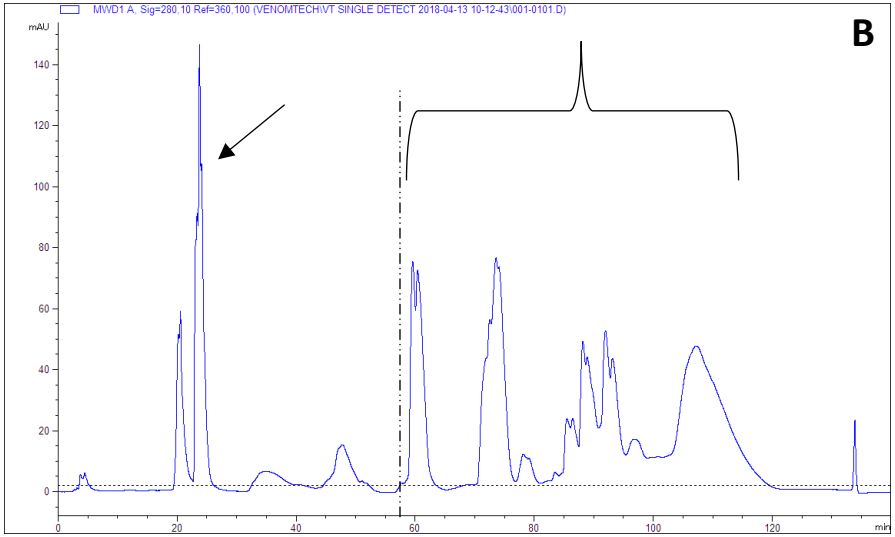

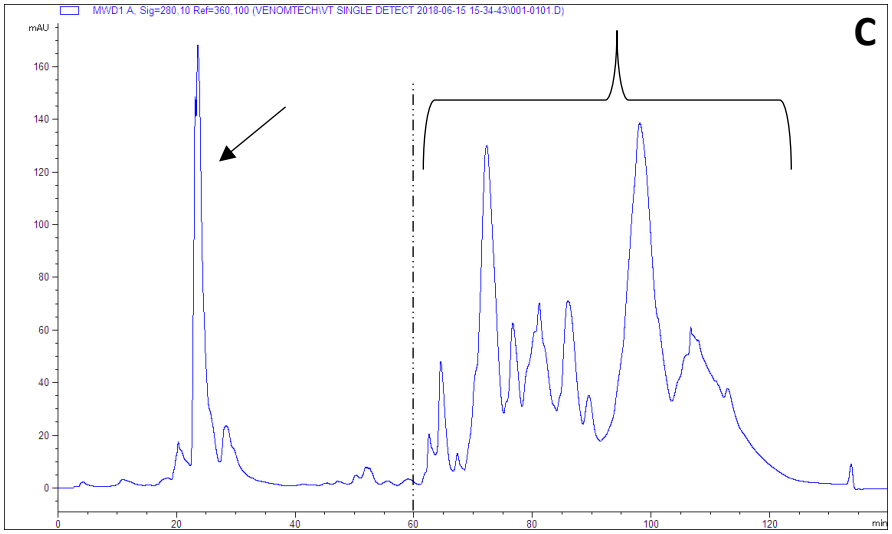

Figure 7.2: Reverse Phase HPLC Traces of Crotalid Venoms

(A): *Calloselasma rhodostoma*, (B): *Crotalus durissus vegrandis* and (C): *Sistrurus miliarius* traces displaying collected peaks. X-axis displays the time of elution of peaks in minutes, whilst Y-axis displayed the intensity of each eluted peak in milli-absorbance unit (mAU). The dotted line indicates around 60 mins into the fractionation protocol and shows a clear time-dependent element to the elution of venom components, with most components eluting after this timepoint, indicating venoms heavy in hydrophobic peptide components (see bracket). Arrows indicate the elution of two (A & B) and one (C) peak of similar profiles and elution times before the bulk of the rest of the venom peptide components (around 20-30 min times point). These similar peak profiles suggest the likely presence of similar molecules with the same hydrophilicity across the venoms of the three fractionated Crotalid venoms, despite the isolation of the whole venom from three genetically and geographically distinct genera.

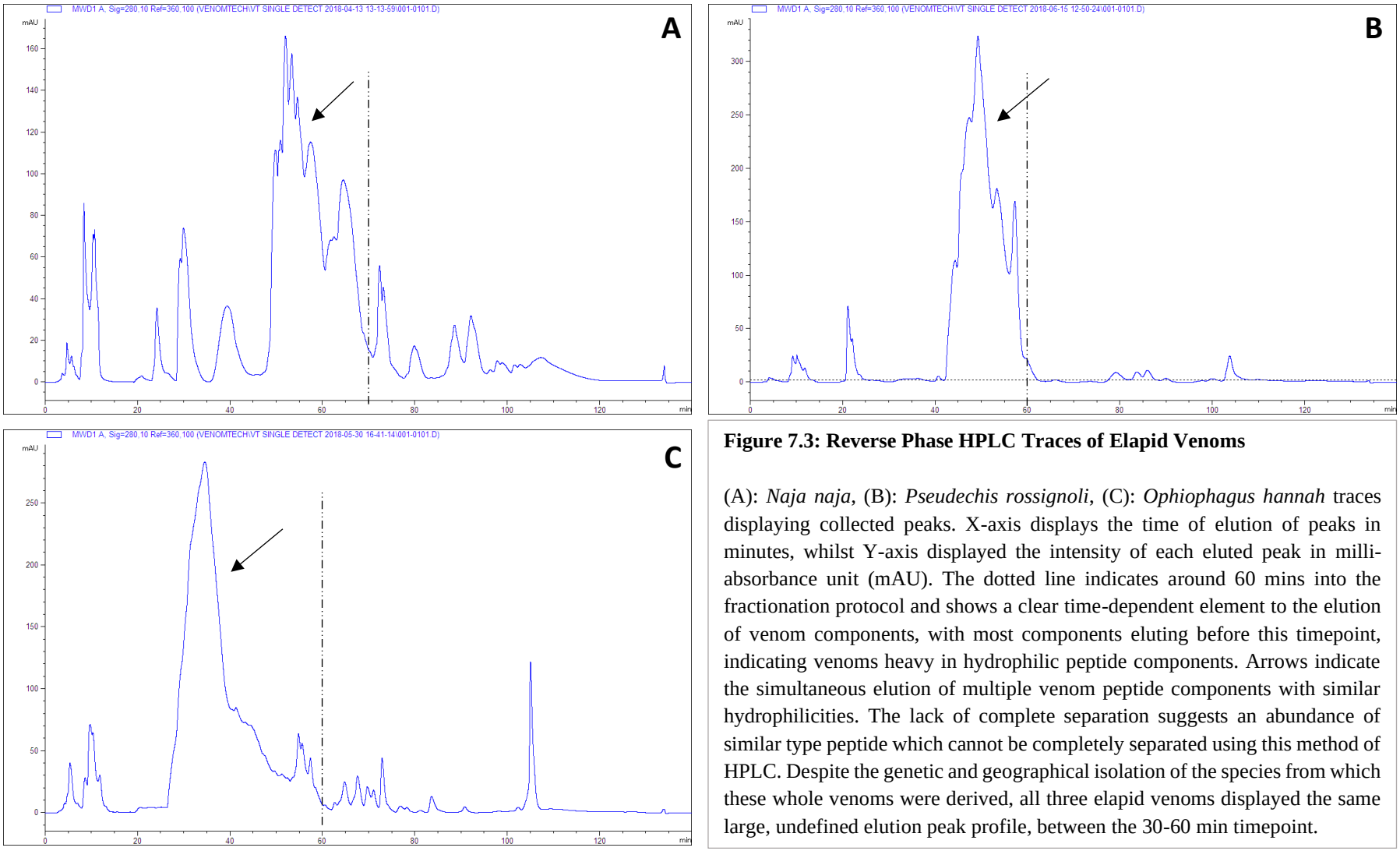

Figure 7.3: Reverse Phase HPLC Traces of Elapid Venoms

(A): *Naja naja*, (B): *Pseudechis rossignoli*, (C): *Ophiophagus hannah* traces displaying collected peaks. X-axis displays the time of elution of peaks in minutes, whilst Y-axis displayed the intensity of each eluted peak in milli-absorbance unit (mAU). The dotted line indicates around 60 mins into the fractionation protocol and shows a clear time-dependent element to the elution of venom components, with most components eluting before this timepoint, indicating venoms heavy in hydrophilic peptide components. Arrows indicate the simultaneous elution of multiple venom peptide components with similar hydrophilicities. The lack of complete separation suggests an abundance of similar type peptide which cannot be completely separated using this method of HPLC. Despite the genetic and geographical isolation of the species from which these whole venoms were derived, all three elapid venoms displayed the same large, undefined elution peak profile, between the 30-60 min timepoint.

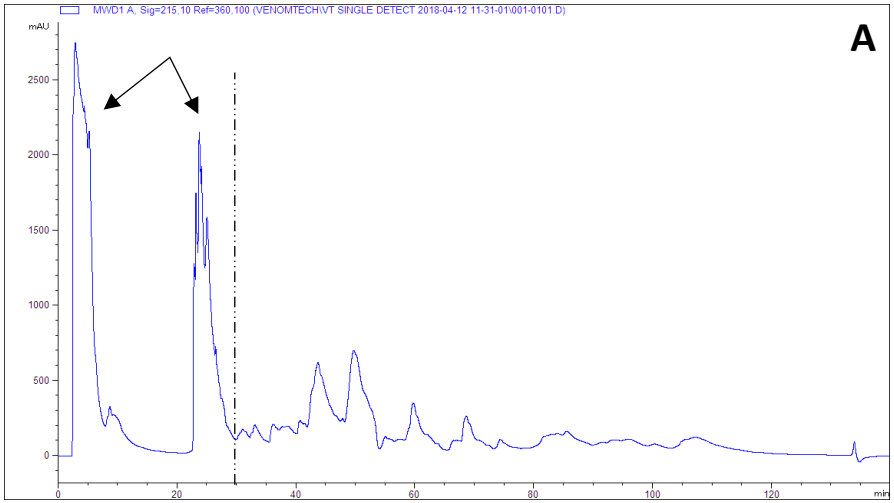

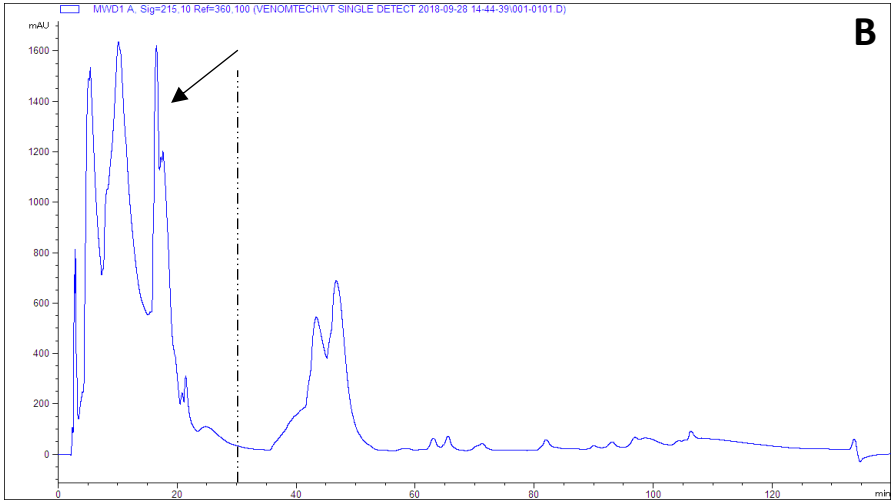

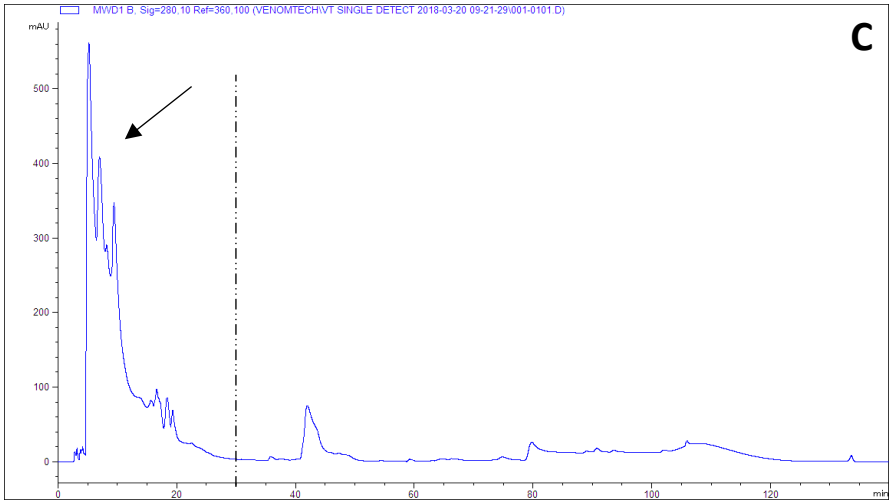

Figure 7.4: Reverse Phase HPLC Traces of Invertebrate Venoms

RP HPLC traces of Scorpionidae venom (A): *Heterometrus swammerdami*, and Theraphosidae venoms (B): *Brachypelma boehmei* and (C): *Acanthoscurria geniculata*. X-axis displays the time of elution of peaks in minutes, whilst Y-axis displayed the intensity of each eluted peak in milli-absorbance unit (mAU). The dotted line indicates around 30 mins into the fractionation protocol and shows a clear time-dependent element to the elution of venom components, with most components eluting before this timepoint, indicating venoms that are heavy abundant in hydrophilic peptide components. Arrows indicate the elution of two (A) and one (B & C) regions of simultaneously eluting peaks suggesting an abundance of similar type peptides which cannot be completely separated using this method of HPLC. There appears to be extremely limited peptide elution with increasing acetonitrile concentrations (after the 20 min line), suggesting invertebrate venoms are rich in hydrophilic and lacking in hydrophobic components.

Whole Venom	Generic Genus	HPLC Collection Wavelength (nm)	Number of Fractions Obtained
Crotalus durissus vegrandis	Crotalid (Pit viper)	280	16
Calloselasma rhodostoma	Crotalid (Pit viper)	280	20
Sistrurus miliarius	Crotalid (Pit viper)	280	17
Naja naja	Elapid (Cobra)	280	20
Ophiophagus Hannah	Elapid (King Cobra)	280	19
Pseudechis rossignoli	Elapid (brown snake)	280	12
Acanthoscurria geniculate	Theraphosidae	215	37
Brachypelma boehmei	Theraphosidae	215	26
Heterometrus swammerdami	Scorpionidae	215	42
			TOTAL: 209

Table 7.1: Fractions Collected from the RP Fractionation of Whole Venoms

Displays the whole snake and invertebrate venoms taken forward for fractionation following whole venom ELISA and Western Blot findings. Table shows the animal genus and species, the concentration of the whole venom stock pre-dilution, the HPLC collection wavelength employed, and the number of fractions obtained from the complete fractionation of the whole venom. Peaks were determined by the Agilent 1100 software, set up with detection parameters as follows: The peak must have had a detectible signal at a wavelength of 280nm (snake venom) and 215nm (invertebrate venoms). Peaks were collected in threshold/slope mode and had to display an up-slope threshold of at least 0.1 U/s, and down-slope threshold of 0.5 U/s, a minimum collection threshold of of at least 5U detection and an upper collection threshold of no greater than 3000U. Column flow rate was 1ml/min and maximum peak collection duration was set to a maximum of 4 minutes.

protocol. The elution of the main bulk of venom peptides in all three invertebrate venoms (*Acanthoscurria geniculata*, *Brachypelma boehmei* and *Heterometrus swammerdami*) was observed in the first 30 min of the protocol, suggesting that the main components of these venoms are hydrophilic peptides (Figure 7.4).

Fractionation of three pit viper, three elapid and three invertebrate venoms resulted in 209 fractions to be tested for their potential to reduce phosphorylation of EGFR in MDA-MB-468 and A31 cell lines.

7.3.2 Analysis of Venom Fractions

7.3.2.1 Analysis of Crotalinae (pit viper) Fractions: (*Crotalus durissus vegrandis, Calloselasma rhodostoma* and *Sistrurus miliarius*)

A431 and MDA-MB-468 cells were treated with fractions from a selection of pit viper venoms, previously shown in work carried out in Chapters 3-5 to display potential inhibitory effects on EGF receptor phosphorylation. Treatment with 53 fractions collected from the HPLC of 3 whole venoms yielded 7 fractions which displayed a greater than 50% reduction in EGFR phosphorylation levels in at least one of the two tested cells lines (Figures 7.5A and B).

Statistical analysis using Minitab 19 software identified several *Crotalus durissus vegrandis* fractions that appear to be causing significant reductions in EGFR Phosphorylation levels in both MDA-MB-468 and A431 cell lines. Fractions shown through excel analysis and graphical representation (Fig 7.5A and B) to cause 20% or greater reductions in EGFR phosphorylation were analysed using Minitab 19 statistical software. Fractions shown to cause less than 20% reductions or to cause increases in phosphorylation were not analysed further. Normality and equal variance tests on all treatment groups confirmed that data sets were normally distributed and displayed equal variance (See Appendix tables XXIV & XXV) and an ANOVA analysis with post hoc Tukey's test was performed. ANOVA analysis generated p-values of 0.000 for both MDA-MB-468 and A431 data sets confirming that fractions of C.dve venom had caused significant reductions in EGFR phosphorylation in both cell lines. Tukey's post hoc testing identified all fractions causing 20% or greater reduction of EGFR phosphorylation in MDA-MB-468 cells as being statistically significant (See Appendix XXVI), whilst only fractions R7, R8, R12 and R13 were shown to be causing significant reductions in EGFR phosphorylation levels in A431 treated cells (See Appendix XXVI). Normality testing of the residuals generated from the ANOVAs of both data sets confirmed normal distributions, supporting ANOVA test results are robust.

Treatment with *C. durissus vegrandis* fractions resulted in 3 fractions which displayed greater than 50% reduction in EGFR phosphorylation in both tested cell lines (fractions R7, R8 and R13), with a further fraction identified to cause a greater than 50% reduction in just MDA-MB-468 cells (R14). All these fractions were shown by ANOVA analysis to be causing significant reductions in EGFR phosphorylation levels. Whilst Fractions R6 and R12 were shown by ANOVA analysis to be causing significant reductions in EGFR phosphorylation levels of MDA-MB-468 and both cell lines respectively, they were observed at the cell dosing stage to display cellular cytotoxicity effects and so were disregarded as potential fractions of interest for follow up work at a later stage.

Analysis of the HPLC trace for *C. durissus vegrandis* shows that fractions R7 and R8 are shouldered peaks (Figure 7.2B), eluting from the column in quick succession without returning to baseline in-between collection. This collection could indicate that the 2 peptides/proteins are eluting from the column simultaneously, and so both fractions R7 and R8 may contain the same active peptide, thus explaining the similar levels of EGFR phosphorylation inhibitory activity observed with both these fractions. Alternatively, the rapid succession of elution of these two fractions could be indicative of 2 distinct peptide/proteins with very similar amino acid sequences, structures and hydrophilicities. In this instance these peptides are likely to belong to a similar class of molecules, thus displaying similar activities and inhibitory affects due to their inherent structural and pharmacological properties.

Statistical analysis using Minitab 19 software identified several *Sistrurus miliarius* fractions that appear to be causing significant reductions in EGFR Phosphorylation levels in both MDA-MB-468 and A431 cell lines. % reductions in EGFR phosphorylation found to be 20% or greater (Figures 7.5C and D) were analysed using Minitab 19 statistical software. Normality and equal variance tests on all treatment groups confirmed that data sets were normally distributed and displayed equal variance (See Appendix tables XXIV & XXV) and an ANOVA analysis with post hoc Tukey's test was performed. ANOVA analysis generated p-values of 0.000 for both MDA-MB-468 and A431 data sets confirming that fractions of *S. miliarius* venom had caused significant reductions in EGFR phosphorylation in both cell lines. Tukey's post hoc testing identified 7 fractions of *S. miliarius* venom (R3, R6-9, R13 and R15) that caused significant reductions in EGFR phosphorylation in MDA-MB-468 cells (See Appendix XXVI) and 6 fractions (R5-R9, R13) that caused significant reductions to EGFR phosphorylation in A431 cells (See Appendix XXVI). Normality testing of the residuals generated from the ANOVAs of both data sets confirmed normal distributions, supporting ANOVA test results are robust.

Treatment with fractions from *Sistrurus miliarius* venom identified 1 fraction for each cell line that resulted in reductions of greater than 50% in EGFR phosphorylation. A 60% reduction was

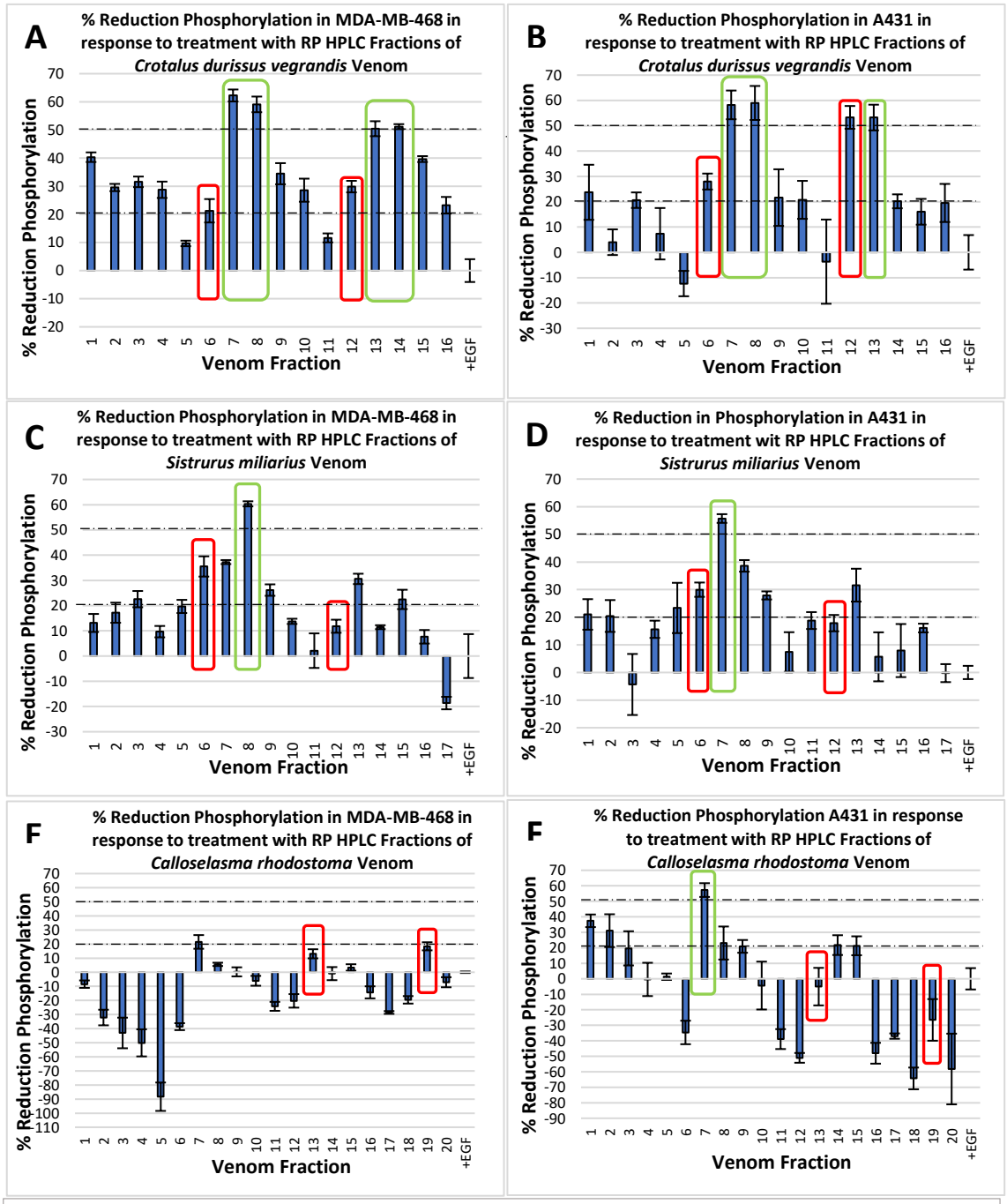

Figure 7.5: Percentage Reduction in EGFR Phosphorylation in MDA-MB-468 and A431 Cells Treated with Crotalid Venom Fractions

Graphical representation of data generated from venom fraction treated EGFR ELISAs. Graphs display % reduction in EGFR phosphorylation levels in response to treatment with *C. durissus vegrandis* venom fractions in MDA-MB-468 (A) and A431 (B) cells, *S. miliarius* venom fractions in MDA-MB-468 (C) and A431 (D) cells and *C. rhodostoma* venom fractions in MDA_MB-468 (E) and A431 (F) cells. % standard error was calculated and added to each bar as error bars. 20% and 50% reduction thresholds were added as dotted lines for easy identification of effective fractions. Fractions shown to display cytotoxicity were highlighted in red, whilst fractions causing greater than 50% reductions were highlighted in green. Negative values equate to % increases to EGFR phosphorylation in response to venom fraction treatment. Toxicity was determined through visual inspection of wells following completion of dosing window. Biological replicates = N1, Technical replicates/biological replicate = N4

observed in MDA-MB-468 cells in response to treatment with fraction R8, whilst a 55% reduction was observed in A431 cells in response to fraction R7. Whilst Fraction R6 was shown by ANOVA analysis to be causing significant reductions in EGFR phosphorylation levels of both cell lines, it was observed at the cell dosing stage to display cellular cytotoxicity effects and so was disregarded as a potential fraction of interest for follow up work at a later stage (Figures 7.5C & D).

Whilst the cell lines appear to be affected differently by 2 different fractions, upon inspection of the HPLC trace for the fractionation of *S. miliarius* venom, it became apparent that fraction R7 is again a shoulder peak of a much larger fraction R8 (Figure 7.2C). This would suggest that both fractions R7 and R8 and likely to contain the same active molecule, with fraction R8 beginning to elute at the same time as fraction R7 is being collected. Both cells lines still saw nearly a 40% reduction in phosphorylation in response to treatment with the fractions causing greater than 50% reduction in the other.

Unlike with previously tested pit viper venoms from *C. durissus vegrandis* and *S. miliarius*, excel and graphical analysis of the effects of *C. rhodostoma* fractions suggested that these fractions caused minimal changes to EGFR phosphorylation levels in either cell line, with fraction R7 the only one shown to cause a greater than 50% reduction in EGFR phosphorylation in A431 but not MDA-MB-468 cells (Figures. 7.5E & F). Statistical analysis using Minitab 19 software was undertaken to determine whether fractions from *C. rhodostoma* venom were causing statistically significant reductions in EGFR Phosphorylation levels in either cell lines. MDA-MB-468 cells only displayed one fraction that appeared to be causing a 20% reduction in EGFR phosphorylation levels. Normality and equal variance tests were carried out on MDA-MB-468 data sets for this fraction and for venom untreated, EGF stimulated phosphorylation levels. Both data sets were shown to have normal distribution, however Levene's test for equal variance identified that the data sets did not have equal variance (See Appendix tables XXIV & XXV). As the data did not have equal variance, a non-parametric Mann-Whitney U test was carried out to compare the 2 data sets for significant differences. Mann-Whitney U testing generated a P value of 0.030. As this P value is lower than the 0.05 significance threshold the test confirms that despite only causing a 20% reduction in EGFR phosphorylation levels, this reduction is still statistically significant (See Appendix XXVI).

8 fractions from *C. rhodostoma* venom were identified as causing 20% or greater reductions in EGFR phosphorylation in A431 cells, and so these fractions were taken forward for further statistical analysis. Normality and equal variance tests on all these treatment groups confirmed that data sets were normally distributed and displayed equal variance (See Appendix tables XXIV

& XXV) so an ANOVA analysis with post hoc Tukey's test was performed. ANOVA analysis generated a P value of 0.061, suggesting that there are not significant differences between any of the *C. rhodostoma* treated or EGF-only treated data sets. However, Tukey's post hoc testing identified fraction R7 as being statistically distinct from all other data sets, including the venom-untreated control data set. Normality testing of the residuals generated from the ANOVA confirmed normal distributions, supporting ANOVA test results as robust. To confirm that fraction C.rho_R7 was definitely causing a statistically significant reduction in EGFR phosphorylation levels when compared to the EGF-only control data set, a 2-sample t-test was perform on these data set specifically, which generated a P value of 0.003. As this P value is considerably below the 0.05 statistics significance threshold, the 2-sample T-test confirms that there is a statistically significant reduction in EGFR phosphorylation levels in A431 cells treated with fraction C.rho_R7. All other fractions that caused 20% or greater reductions in phosphorylation levels in A431 cells were found in Tukey's ad hoc testing to not be significant (See Appendix XXVI)

7.3.2.2 Analysis of Elapidae Fractions: (*Naja naja, Ophiophagus Hannah* and *Pseudechis rossignoli*)

A431 and MDA-MB-468 cells were treated with fractions from a selection of elapid venoms, previously shown in work carried out in Chapter 4 to display potential inhibitory effects on EGFR phosphorylation, including venoms from cobras, brown snake and king cobra. Treatment with 51 fractions collected from the HPLC of 3 whole venoms yielded 5 fractions which displayed a greater than 50% reduction in EGFR phosphorylation levels in at least one of the two tested cells lines (Figure 7.6).

Analysis of the Treatment of A431 cells with *Naja naja* fractions identified 3 which displayed greater than 50% reduction in EGFR phosphorylation (fractions R7, R8 and R14). No fractions were identified to causing a greater than 50% reduction in EGFR phosphorylation in MDA-MB-468 cells. Fractions R9 to R12 were identified at the cell dosing stage as displaying cellular cytotoxicity in both cell lines, with cytotoxicity also observed in MDA-MB-468 cells following treatment with fraction R8. Due to the high levels of cellular toxicity caused at the cell dosing stage of the assay, changes in these fractions were disregarded as potentials for follow up work at a later stage.

Statistical analysis using Minitab 19 software was undertaken to determine whether fractions from N.naj venom were causing statistically significant reductions in EGFR Phosphorylation levels in

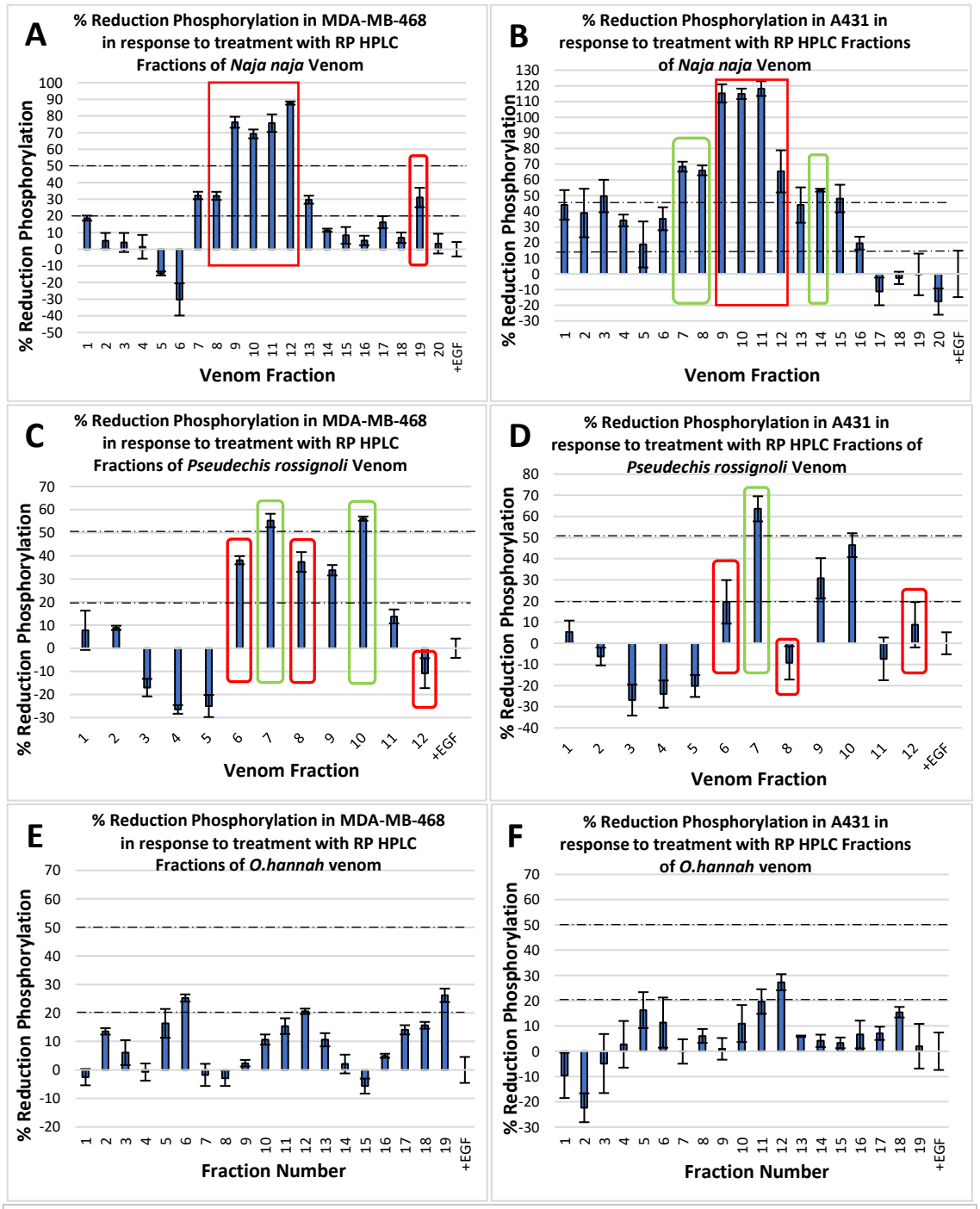

Figure 7.6: Percentage Reduction in EGFR Phosphorylation of MDA-MB-468 and A431 Cells Treated with Elapid Venom Fractions

Graphical representation of data generated from venom fraction treated EGFR ELISAs. Graphs displays % reduction in EGFR phosphorylation levels in response to treatment with *N. naja* venom fractions in MDA-MB-468 (A) and A431 (B) cells, *P. rossignoli* venom fractions in MDA-MB-468 (C) and A431 (D) cells and *O. hannah* fractions in MDA_MB-468 (E) and A431 (F) cells. % standard error was calculated and added to each bar as error bars. 20% and 50% reduction thresholds were added for easy identification of effective fractions. Fractions shown to display cytotoxicity were highlighted in red, whilst fractions causing greater than 50% reductions were highlighted in green. Negative values equate to % increases to EGFR phosphorylation in response to venom fraction treatment. Toxicity was determined through visual inspection of wells following completion of dosing window. Biological replicates = N1, Technical replicates/biological replicate = N4

either cell lines. Fractions seen to be causing high levels of toxicity at the cell dosing stage were not further analysed using statistical software. Two fractions, R7 and R13 caused greater than 20% reductions in EGFR phosphorylation in MDA-MB-468 cells, without displaying cellular toxicity. Normality and equal variance tests on these treatment groups confirmed that the data sets were normally distributed and displayed equal variance (See Appendix tables XXIV & XXV). ANOVA analysis with post hoc Tukey's test was performed, which generated a p-value of 0.000 confirming that a significant difference was observed between the tested data sets. Tukey's post hoc testing identified that both fractions R7 and R13 caused significant reductions to EGFR phosphorylation in MDA-MB-468 cells (See Appendix XXVI). Greater than 20% reductions were observed in EGFR phosphorylation levels of A431 cells in response to treatment with 11 other fractions (R1-4, R6-8, R13-16), not including those shown to display high cytotoxicity. Normality and equal variance tests on these treatment groups confirmed that the data sets were normally distributed and displayed equal variance (See Appendix tables XXIV & XXV). An ANOVA analysis with post hoc Tukey's test was performed, which generated a p-value of 0.044. A P value of 0.044 is below that of the 0.05 statistical significance threshold and so indicates that a statistically significant reduction in EGFR phosphorylation level occurred. Tukey's post hoc testing identified that fraction R7 alone caused significant reductions to EGFR phosphorylation in A431 cells, all other fraction changes were insignificant from each other and from +EGF maximum phosphorylation control data set (See Appendix XXVI). Normality testing of the residuals generated from the ANOVAs of both data sets confirmed normal distributions, supporting ANOVA test results as robust.

Analysis of MDA-MB-468 and A431 cells treated with fractionated *Pseudechis rossignoli* venom identified 2 (R7 and R10) and 1 (R7) fractions respectively that caused greater than 50% reduction in EGFR phosphorylation levels. Statistical analysis using Minitab 19 software was undertaken to determine whether fractions from *P. rossignoli* venom were causing statistically significant reductions in EGFR Phosphorylation levels in either cell lines. Five fractions (R6-R10) were shown through excel and graphical analysis to caused greater than 20% reductions in EGFR phosphorylation in MDA-MB-468 cells. Normality and equal variance tests on the data from these fractions confirmed normal distributed and equal variances (See Appendix tables XXIV & XXV). ANOVA analysis with post hoc Tukey's test was performed, which generated a p-value of 0.000, confirming that a significant difference was observed between the tested data sets. Tukey's post hoc testing identified that all 5 fractions did cause statistically significant reductions to EGFR phosphorylation in MDA-MB-468 cells, with fractions R7 and R10 causing the greatest reductions to phosphorylation (See Appendix XXVI).

Greater than 20% reductions were observed in EGFR phosphorylation levels of A431 cells in response to treatment with 4 fractions (R6, 7, 9, 10). Normality and equal variance tests on these treatment groups confirmed that the data sets were normally distributed and displayed equal variance (See Appendix tables XXIV & XXV). An ANOVA analysis with post hoc Tukey's test was performed, which generated a p-value of 0.003. A P value of 0.003 is below that of the 0.05 statistical significance threshold and so indicates that a statistically significant reduction in EGFR phosphorylation level occurred. The Tukey's post hoc test identified fractions R7 and R10 as having caused statistically significant reductions in EGFR phosphorylation levels, whilst fractions R6 and R9 did not (See Appendix XXVI).

Fractions R6, R8 and R12 were identified at the cell dosing stage to display cellular cytotoxicity in both cell lines, and so significant changes observed with these fractions in either cell lines were regarded as potentially inconclusive and the fractions disregarded for further follow up analysis work. No tested fractions of *O. hannah* venom were shown to cause greater than 50% reduction in EGFR phosphorylation in either MDA-MB-468 or A431 cells, however graphical and excel analysis of the ELISA data identified 3 (R6, 12 and 19) and 2 (R11 and 12) fractions respectively that caused 20% or greater reductions in EGFR phosphorylation levels. Statistical analysis using Minitab 19 software was undertaken to determine whether these fractions from *O. hannah* venom were causing statistically significant reductions in EGFR Phosphorylation levels in either cell lines. Normality and equal variance tests on the data from these fractions confirmed normal distribution and equal variances (See Appendix tables XXIV & XXV). ANOVA analyses with post hoc Tukey's tests were performed, which generated p-values of 0.008 and 0.040 for MDA-MB-468 and A431 data sets, respectively. Both these P values are smaller than the 0.05 statistical significance threshold, confirming that a statistically significant difference was observed between the tested data sets. Tukey's post hoc testing confirmed that all 3 fractions (R6, 12 and 19) did cause significant reductions to EGFR phosphorylation in MDA-MB-468 cells, whilst only fraction R12 caused significant reductions in A431 cells (See Appendix XXVI). Normality tests performed on the residual from both these ANOVAs confirmed normal distribution, supporting the statistical significance of the result shown in the Tukey's and ANOVA analyses.

7.3.2.3 Analysis of Theraphosid Fractions: (*Acanthoscurria geniculata* and *Brachypelma Boehmei*)

Graphical and excel analysis of MDA-MB-468 and A431 cells treated with fractions separated from the venom of *Brachypelma boehmei* resulted in very different observable changes in the phosphorylation levels of EGFR in the 2 cell lines. Treatment of MDA-MB-468 cells resulted in the identification of 5 fractions that caused 50% or greater reductions in EGFR phosphorylation

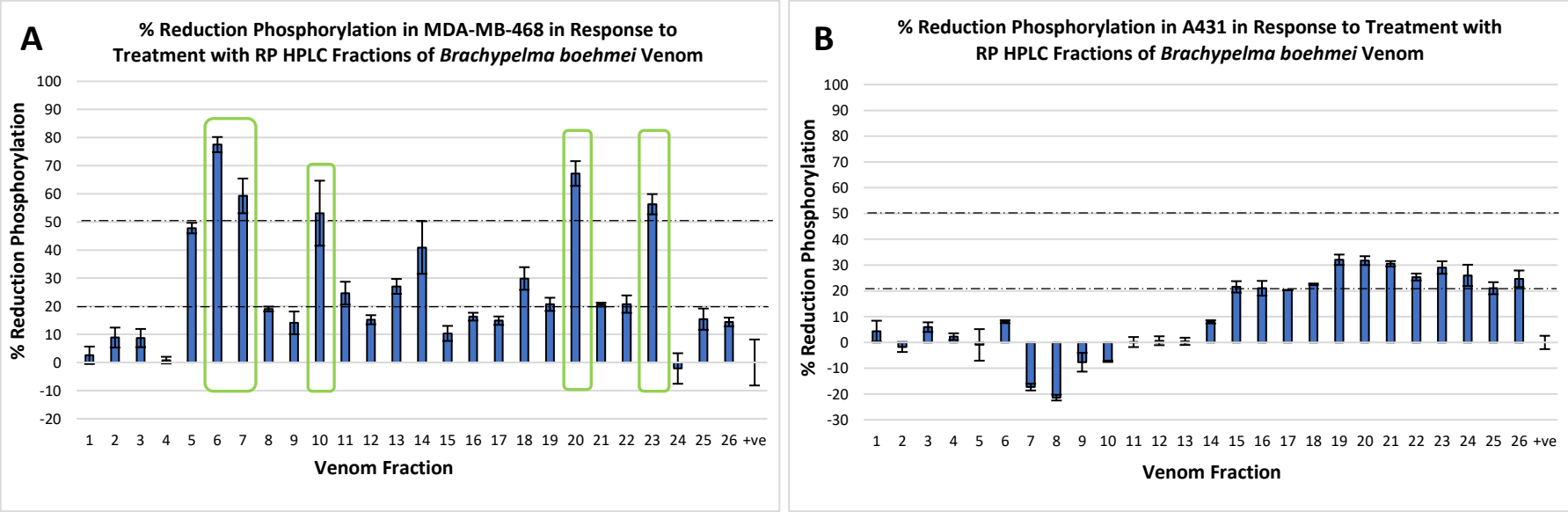

Figure 7.7: Percentage Reduction in EGFR Phosphorylation of MDA-MB-468 and A431 Cells Treated with *Brachypelma boehmei* Venom Fractions

Graphical representation of data generated from venom fraction treated EGFR ELISAs. Graphs displays % reduction in EGFR phosphorylation levels in response to treatment with *B. boehmei* venom fractions in MDA-MB-468 (A) and A431 (B) cells. % standard error was calculated and added to each bar as error bars. 20% and 50% reduction thresholds were added for easy identification of effective fractions. Fractions shown to display cytotoxicity were highlighted in red, whilst fractions causing greater than 50% reductions were highlighted in green. Negative values equate to % increases to EGFR phosphorylation in response to venom fraction treatment. Toxicity was determined through visual inspection of wells following completion of dosing window. Biological replicates = N1, Technical replicates/biological replicate = N4

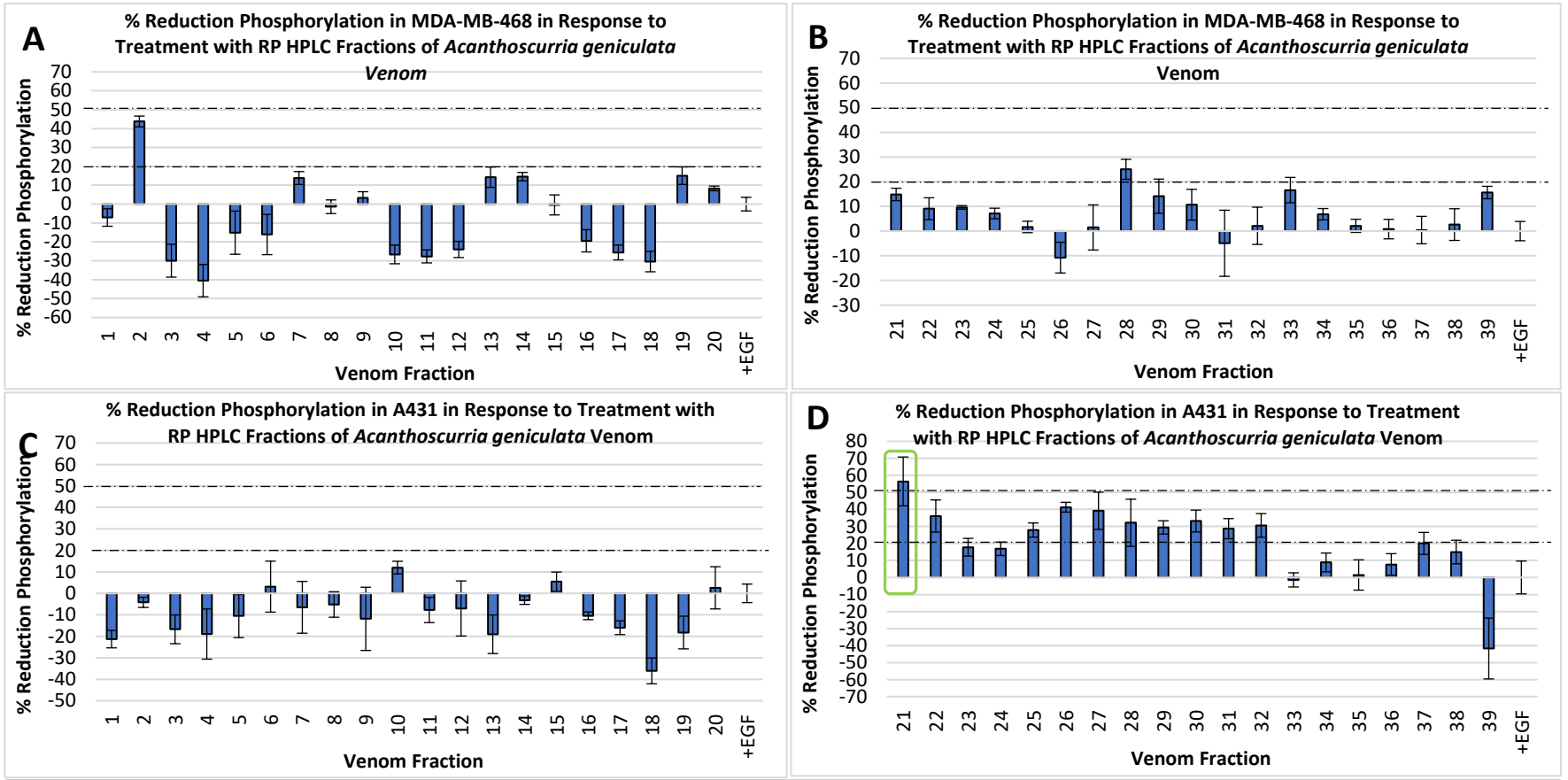

Figure 7.8: Percentage Reduction in EGFR Phosphorylation of MDA-MB-468 and A431 Cells Treated with *Acanthoscurria geniculata* Venom Fractions

Graphical representation of data generated from venom fraction treated EGFR ELISAs. Graphs displays % reduction in EGFR phosphorylation levels in response to treatment with *A. geniculata* venom fractions in MDA-MB-468 (A & B) and A431 (C & D) cells. % standard error was calculated and added to each bar as error bars. 20% and 50% reduction threshold lines were added for easy identification of effective fractions. Fractions shown to display cytotoxicity were highlighted in red, whilst fractions causing greater than 50% reductions were highlighted in green. Negative values equate to % increases to EGFR phosphorylation in response to venom fraction treatment. Toxicity was determined through visual inspection of wells following completion of dosing window. Biological replicates = N1, Technical replicates/biological replicate = N4

levels. However, treatment of A431 cells with the same fractions did not result in any reductions of 50% or greater (Figures 7.7 & 7.8). 13 fractions (R5-7, R10-11, R13-14 and R18-23) were identified to cause 20% or greater reductions in EGFR phosphorylation in MDA-MB-468 cells. Minitab 19 statistical analysis of these 13 fractions was undertaken. Normality and equal variance tests on the data from these fractions confirmed normal distribution and equal variances (See Appendix tables XXIV & XXV). ANOVA analyses with post hoc Tukey's tests were performed, which generated a p-value of 0.000. All but two of the tested fractions (R19 & 22) were identified by ANOVA and Tukey's analysis to be causing statistically significant reductions in EGFR phosphorylation in this cell line (See Appendix XXVI). 12 fractions (R15-R26) were identified to cause 20% or greater reductions in EGFR in A431 cells. Normality and equal variance tests on the data from these fractions confirmed normal distribution and equal variances (See Appendix tables XXIV & XXV) for all data sets. ANOVA analyses with post hoc Tukey's tests were performed, which generated a p-value of 0.002. 7 fractions of the 13 tested were identified by Tukey's analysis to be causing statistically significant reductions in EGFR phosphorylation in A431 cells (R19-24, R26) (See Appendix XXVI). Normality tests performed on the residuals from both these ANOVAs confirmed normal distribution, supporting the statistical significance of the result shown in the Tukey's and ANOVA analyses.

Graphical and excel analysis of MDA-MB-468 and A431 cells treated with fractions separated from the venom of *Acanthoscurria geniculata* resulted in different observable changes in the phosphorylation levels of EGFR in the 2 cell lines. Treatment of MDA-MB-468 cells resulted in the identification of no fractions that caused 50% or greater reductions in EGFR phosphorylation levels, however fraction R2 was shown to cause nearly a 45% reduction. Treatment of A431 cells with the same fractions resulted in one fraction (R21) that caused greater than 50% reduction in EGFR phosphorylation (Figure 7.8). 2 fractions (R2 and R28) were identified to cause 20% or greater reductions in EGFR phosphorylation in MDA-MB-468 cells. Minitab 19 statistical analysis of these fractions was undertaken. Normality and equal variance tests on the data from these fractions confirmed normal distribution and equal variances (See Appendix tables XXIV & XXV). 2-sample T-tests were undertaken to directly compare each fraction to the +EGF-treated control data sets. The 2-sample T-test comparing R2 to +EGF generated a P value of 0.000, whilst the T-test comparing R28 to +EGF generated a P value of 0.008 (See Appendix XXVI). Both these P values are lower than the 0.05 statistical significance threshold and so these fractions are causing statistically significant reductions to EGFR phosphorylation in MDA-MB-468 cells.

11 fractions (R21-R32, R37) were identified to cause 20% or greater reductions in EGFR in A431 cells. Normality and equal variance tests on the data from these fractions confirmed normal distribution and equal variances (See Appendix tables XXIV & XXV) for all data sets. ANOVA

analyses with post hoc Tukey's tests were performed, which generated a p-value of 0.215. ANOVA and Tukey's analysis determined that none of the 11 fractions shown to be causing greater than 20% reduction in EGFR phosphorylation in A431 cells were significant (See Appendix XXVI). The normality test performed on the residual from the A431 ANOVA statistical analysis confirmed normal distribution, supporting the statistical significance of the result shown in the Tukey's and ANOVA analyses.

7.3.2.4 Analysis of Scorpionidae Fractions: (*Heterometrus swammerdami*)

A431 and MDA-MB-468 cells were treated with fractions from *Heterometrus swammerdami* venom, previously shown in work carried out in chapters 3-5 to display potential inhibitory effects on EGF receptor phosphorylation (Figure 7.9).

Statistical analysis using Minitab 19 software identified several *H. swammerdami* fractions that appear to be causing significant reductions in EGFR Phosphorylation levels in either MDA-MB-468 or A431 cell lines. Fractions shown through excel analysis and graphical representation to cause 20% or greater reductions in EGFR phosphorylation only were analysed using Minitab 19 statistical software. Normality and equal variance test on all treatment groups confirmed that data sets were normally distributed and displayed equal variance (See Appendix tables XXIV & XXV) and an ANOVA analysis with ad hoc Tukey's test was performed. ANOVA analysis generated p-values of 0.001 and 0.000 for MDA-MB-468 data sets (See Appendix XXVI) 0.004 and 0.019 for A431 data sets (See Appendix XXVI), confirming that fractions of *H. swammerdami* venom had caused significant reductions in EGFR phosphorylation in both cell lines.

Tukey's ad hoc testing identified 8 fractions that caused significant reduction in EGFR phosphorylation in MDA-MB-468 cells (H.swa_R7, R8, R9, R23, R29, R30, R36 and R37) (See Appendix XXVI), whilst only fractions R8 and R30 were shown to be causing significant reductions in EGFR phosphorylation levels in A431 treated cells (See Appendix XXVI). Normality testing of the residuals generated from the ANOVAs of both data sets confirmed normal distributions, supporting ANOVA test results are robust. Treatment with the 42 fractions, collected from the HPLC of the whole venom, yielded 2 fractions which displayed a greater than 50% reduction in EGFR phosphorylation levels in both MDA-MB-468 and A431 cells lines. All these fractions were shown by ANOVA analysis to be causing significant reductions in EGFR phosphorylation levels.

Analysis of the HPLC trace for *H. swammerdami* showed that fractions R7 and R8 are shouldered peaks, eluting from the column in quick succession without returning to baseline in-between collection (Figure 7.4). This collection could indicate that the 2 peptides/proteins are eluting from

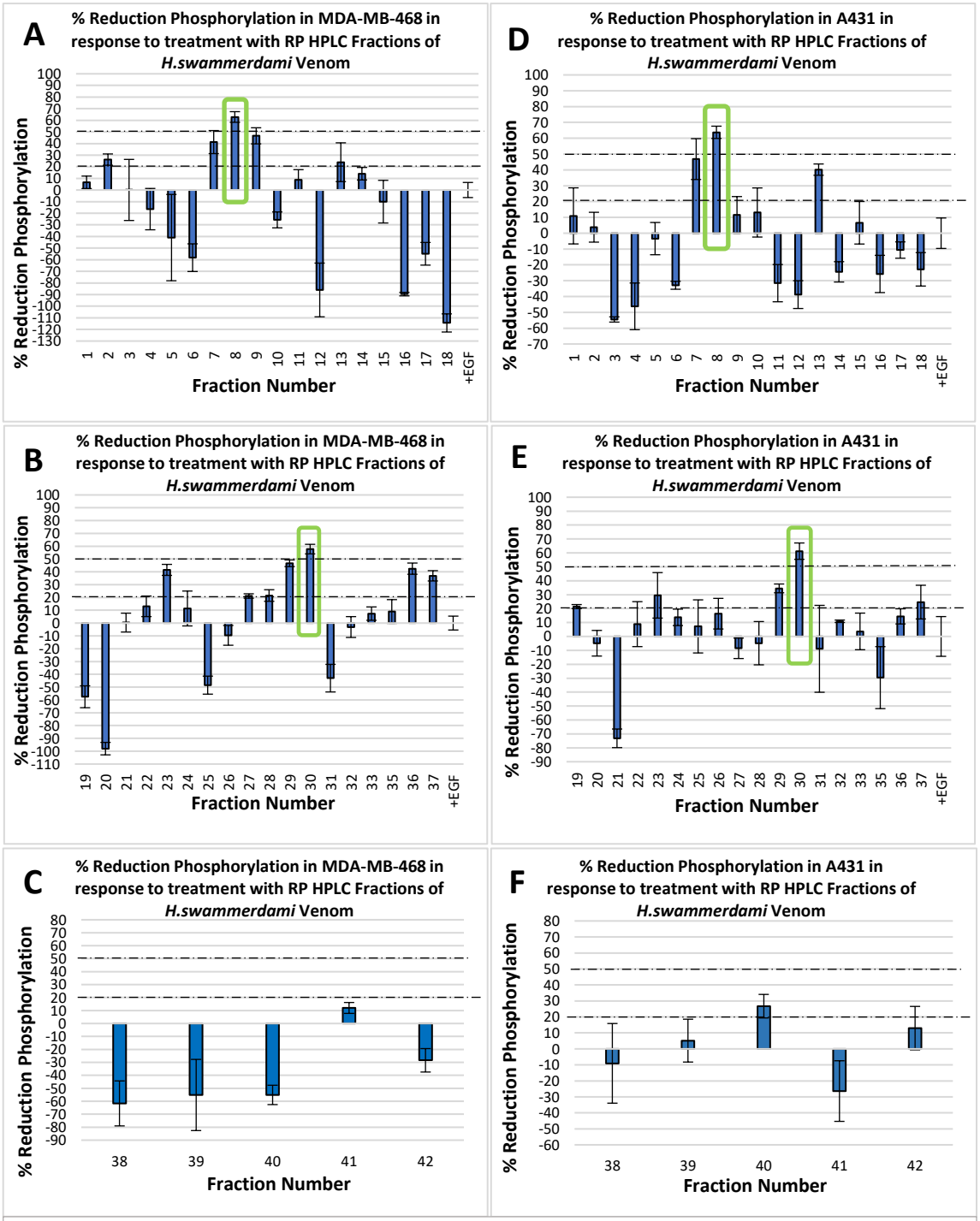

Figure 7.9: Percentage Reduction in EGFR Phosphorylation of MDA-MB-468 and A431 Cells Treated with *Heterometrus swammerdami* Venom Fractions

Graphical representation of data generated from venom fraction treated EGFR ELISAs. Graphs displays % reduction in EGFR phosphorylation levels in response to treatment with *H. swammerdami* venom fractions in MDA-MB-468 (A, B & C) and A431 (D, E & F) cells. % standard error was calculated and added to each bar as error bars. 20% and 50% reduction thresholds were added for easy identification of effective fractions. Fractions shown to display cytotoxicity were highlighted in red, whilst fractions causing greater than 50% reductions were highlighted in green. Negative values equate to % increases to EGFR phosphorylation in response to venom fraction treatment. Toxicity was determined through visual inspection of wells following completion of dosing window. Biological replicates = N1, Technical replicates/biological replicate = N4

the column simultaneously, and so both fractions R7 and R8 may contain the same active peptide, thus explaining the similar levels of EGFR phosphorylation inhibitory activity observed with both these fractions. Alternatively, the rapid succession of elution of these two fractions could be indicative of 2 distinct peptide/proteins with very similar amino acid sequences, structures and hydrophilicities. In this instance these peptides are likely to belong to a similar class of molecules, thus displaying similar activities and inhibitory affects due to their inherent structural and pharmacological properties.

Testing of all fractions identified a total of 53 and 24 fractions that were found to be causing statistically significant reductions to EGFR phosphorylation levels in MDA-MB-468 and A431 cells, respectively. However, as well as statistical significance, a biological significance threshold of 50% or greater reductions to EGFR phosphorylation levels was assigned. Fractions that were also found to display strong levels of cytotoxicity within the 2h dosing period were disregarded as viable fractions for follow up, as the effects of these fractions were determined to likely rely less on EGFR-targeting and more on general cytotoxic effects.

Number of Fractions			
	MDA-MB-468	**A431**	**Fractions affecting both cell lines**
C. durissus vegrandis	4	3	R7, R8, R13
S. miliarius barbouri	1	1	
C. rhodostoma	0	1	
N. naja	0	1	
P. rossignoli	2	1	R7
O. hannah	0	0	
B. boehmei	5	0	
A. geniculata	0	0	
H. swammerdami	2	2	R8, R30
Total:	**14**	**9**	**6**

Table 7.2: Fractions identified as causing significant reductions to EGFR phosphorylation

Fractions that were identified to cause both significant biological and statistical reductions to EGFR phosphorylation when analysis was undertaken, without causing high levels of observed cellular cytotoxicity following 2h of cellular dosing. Venoms which contained fractions causing reductions in either cell line have been highlighted

Following the application of these criteria, the 53 and 24 fractions previously identified as causing statistically significant reductions were triaged based on their biological significance and cytotoxicity, leading to the identification of 14 fractions for MDA-MB-468 and 9 for A431 which

fulfilled all three selected criteria. Application of these criteria resulted in the elimination of 4 venoms for MDA-MB-468 and 3 venoms for A431 as providing viable candidate fractions for follow up work or identification. Of the 14 and 9 fractions identified to cause significant reductions to EGFR phosphorylation, 6 were identified to cause significant reductions to both cell lines (Table 7.2), whilst the others were found to only effect one of the cells lines.

3 fractions were to be selected to take forward for mass spec identification. To allow for the greatest possible diversity, it was decided that fractions would be selected from differing species and families and would include fractions from snake and invertebrate venoms. Fractions S.mil_R7 and S.mil_R8 were identified as causing significant reductions to MDA-MB-468 and A431 cell lines respectively, whilst not causing significant reductions to the other. Whole *S. miliarius barbouri* venom has been shown in previous experimental work to cause reductions to MDA-MB-468 and A431, with reductions in phosphorylation of between 35-45% observed (See Figures 5.8 & 5.12). Similarly, Western blot and ELISA analysis of fellow pit viper *C. durissus vegrandis* whole venom has been shown to reduce the phosphorylation levels of both MDA-MB-468 and A431 cells (See Figures 4.9, 5.8, 5.12 & 5.13), with 3 fractions identified from this venom as causing significant reductions to EGFR phosphorylation in both cell lines (Table 7.2). Whole *C. durissus vegrandis* venom has been routinely shown to cause reduction to EGFR phosphorylation in MDA-MB-468 cells of between 55-95%, depending on dose (Figures 4.9, 5.8, 5.12 & 5.13), with reductions of around 35% observed in A431 cells (Figure 5.8). Fractions C.dve_R7 and C.dve_R8 were identified to cause reductions to EGFR phosphorylation of 62.2 and 59.1% respectively in MDA-MB-468, whilst causing 58.2 and 59% reductions in A431 cells. Fraction C.dve_R30, whilst also causing significant reductions to EGFR phosphorylation in both cell lines, resulted in slightly lower overall reductions of 50.44 and 53.3% respectively. Treatment with fractions from *Elapid* venom *P. rossignoli* also resulted in significant reductions to both MDA-MB-468 and A431 cell lines. Fraction P.wei_R7 affected both cell lines, causing reductions of 63.6% and 55.3% to A431 and MDA-MB-468 cells, respectively. Fraction P.wei_R10 also caused significant reductions of 56.1% in MDA-MB-468, but not in A431 cells. Whole *P. rossignoli* venom has been shown in previous Western Blots and ELISAs to cause reductions to MDA-MB-468 cells of between 30-65% and A431 cells of 25% at doses of 20 μg/ml (See Figures 5.8 & 5.12).

Given that fractions from *C. durissus vegrandis* caused similar levels of EGFR phosphorylation reduction in both cell lines, and that whole *C. durissus vegrandis* venom has been routinely shown to cause greater reductions to EGFR phosphorylation than *S. miliarius barbouri* and *P. rossignoli* venoms, it was decided that a fraction from *C. durissus vegrandis* venom would be selected for further investigation. Given that fractions R7 and R8 are shoulder peaks eluting around the same

time and % buffer B, and so are likely to be similar types of peptides, fraction C.dve_R7 which caused marginally higher reductions to EGFR receptor in MDA-MB-468 cells than fraction R8 was selected to be taken forward for further size exclusion (SEC) HPLC.

Fractions H.swa_R8 and H.swa_R30 were identified from *H. swammerdami* venom as causing significant reductions to both MDA-MB-468 and A431 cells. Despite eluting from the venom at distinct timepoints and % buffer B, both fractions caused similar levels of reduction to EGFR phosphorylation levels in both cell lines. Fraction H.swa_R8 was shown to cause reductions of 62.8 and 63.8% and fraction H.swa_R30 to cause 57.7 and 61.3% reductions to MDA-MB-468 and A431 cells, respectively. Whole *H. swammerdami* venom has been found in previous chapters to cause reductions to EGFR phosphorylation and potentially its expression (See Figures 4.9, 5.10, 5.13). As *H. swammerdami* venom was the only scorpion representative that was fractionated, that the whole venom continually appears to cause significant reductions to EGFR phosphorylation, and that 2 fractions that caused ≈60% reduction in both cell lines have been identified, it was decided that one fraction would be selected to take forward for further SEC HPLC. Fraction H.swa_R30 was selected to take forward, as fraction H.swa_R8 was a significantly smaller collected peak and so the overall protein collected for further follow up work, including mass spec analysis was lower.

Treatment with fractions of *B. boehmei* venom resulted in very different outcomes for the 2 cell lines. Analysis identified 5 fractions that caused significant reductions to EGFR phosphorylation in MDA-MB-468 cells. However interestingly, no fractions were identified to cause significant reductions to EGFR phosphorylation in A431 cells. This lack of effect against A431 cells, whilst high levels of effectiveness against MDA-MB-468 cells appears to suggest cell line specific effects against EGFR receptor phosphorylation. MDA-MB-468 and A431 cells originate from differing source tissues, but both present as EGFR over-expressing cancer cell lines. It is an interesting find to identify potential venom molecules which strongly target one but not the other cell line, particularly given other whole venoms and venom fractions have been shown to effect both cell lines in a similar manner. Fractions R6, R7, R10, R20 and R23 caused reductions to EGFR phosphorylation levels in MDA-MB-468 cells of 77.5, 59.3, 53.1, 67.2 and 56.3% respectively. Due to the differences in observed cell line effects, a fraction from *B. boehmei* venom was selected as an interesting avenue for follow up. It was decided that fraction R6 would be selected to take forward as it caused reductions to EGFR phosphorylation of 77.5%, the greatest reductions observed in response to treatment with any of the tested 209 fractions.

7.3.3 2nd Dimension Size Exclusion High Performance Liquid Chromatography (SEC), Intact Mass and Peptide Mapping Mass Spectrometry of 1st Dimension Hits

Fractions B.boe_R6, H.swa_R30 and C.dve_R7 were selected to take forward for subsequent 2nd dimension size exclusion chromatography (SEC) and Intact mass and peptide mapping mass spectrometry. SEC HPLC of B.boe_R6, H.swa_R30 and C.dve_R7 were undertaken to ascertain

A C.dve_R7 SEC

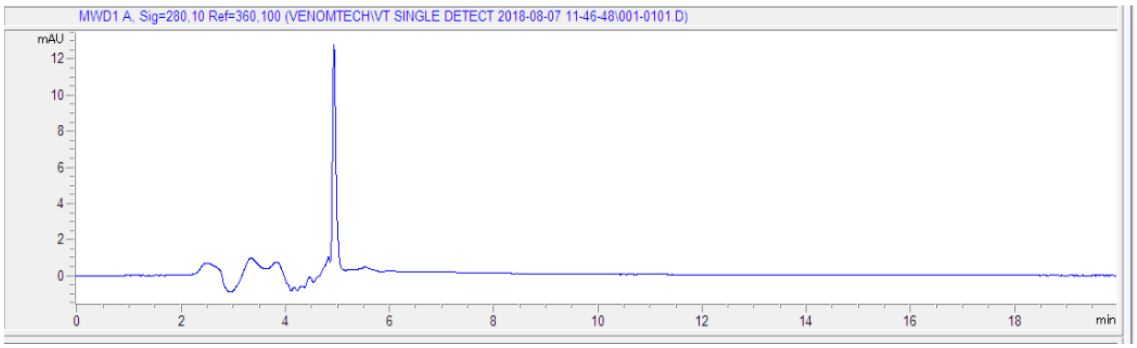

B H.swa_R30 SEC

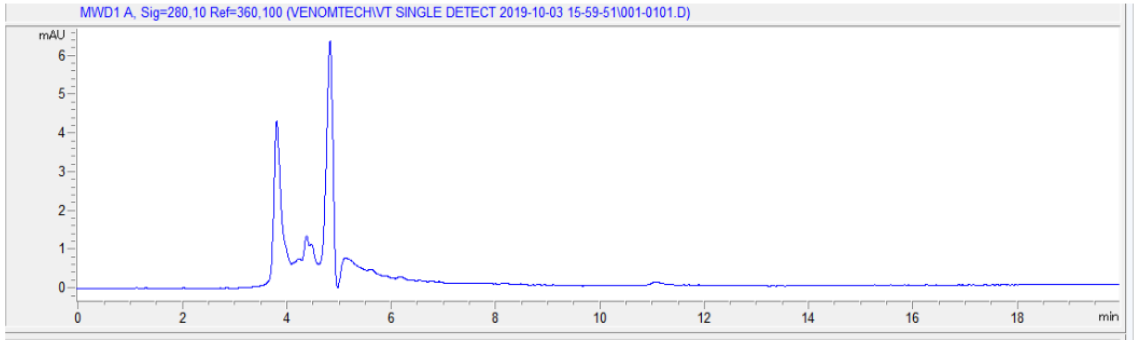

C B.boe_R6 SEC

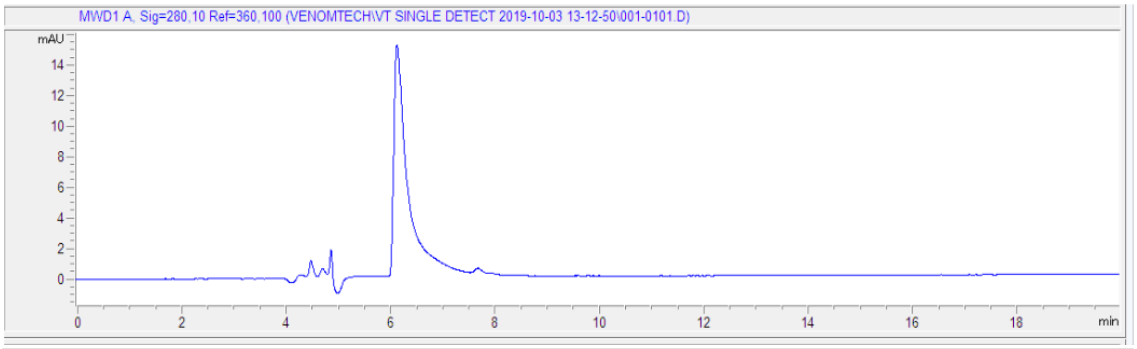

Figure 7.10: SEC HPLC Traces of Fractions Shown to Reduce EGFR Phosphorylation

(A) shows the Size Exclusion HPLC trace of fraction C.dve_R7, (B) shows the Size Exclusion HPLC trace of fraction H.swa_R30 and (C) shows the Size Exclusion HPLC trace of fraction B.boe_R6. X-axis displays the time of elution of peaks in minutes, whilst Y-axis displayed the intensity of each eluted peak in milli-absorbance unit (mAU).

whether the tested fractions contained individual pure venom components or whether they still contained a mixture of multiple. Fractionation of both B.boe_R6 and C.dve_R7 fractions using SEC HPLC, resulted in the elution of single dominant peaks, eluting from the column around 6-8 min and 5 min, respectively. The elution of a single dominant peak in both of these fractions indicates that these fractions are composed of a single venom component that is likely the cause of the reductions observed to EGFR phosphorylation. Elution of the B.boe_R6 peak later than the peak in C.dve_R7 indicates that the venom components differ in size, with the component in B.boe_R6 likely to have a peptide mass smaller than that of the venom component in C.dve_R7. Whilst these 2 venom fractions appear to be single entities, SEC HPLC of H.swa_R30 revealed that this fraction still contains multiple peptide components of varying sizes. Two dominant peaks were identified from H.swa_R30, with the first eluting from the column around 3 min and the second eluting at 5 min into fractionation. The elution time and profile of the peak detected at 5 min is similar to that of the peak detected in C.dve_R7, possibly suggesting that these venom fraction peptides could be similar in molecular mass and function. The second peptide identified in fraction H.swa_R30 was the earliest of all the venom components detected by SEC HPLC to elute and so is likely to be the largest in molecular mass.

Samples of fractions B.boe_R6, H.swa_R30 and C.dve_R7 were sent to Peak Proteins for both intact mass and peptide mapping mass spectrometry. Mass spec. analysis resulted in both intact masses and some peptide mapping sequence data in two of the three selected fractions (See Appendix XXVII). Both intact mass and peptide mapping mass spec analysis of fraction B.boe_R6 resulted in the detection of no significant data for either technique. The lack of achieved data for fraction B.boe_R6 from either mass spec technique could indicate that the molecule causing the observed effect to EGFR phosphorylation in MDA-MB-468 is not a peptide component of *B. boehmei* venom. However, SEC HPLC of fraction B.boe_R6 did detect peaks within the fraction at wavelengths that correspond to both peptide and protein detection (215nm, 280nm). Alternatively, as the peak in B.boe_R6 appears to indicate that this peptide is the smallest in size of the compounds detected by SEC (Figure. 7.10), a larger amount of peptide sample may have been required for accurate MS detection, with the failure to detect peptides in this fraction the result of it falling below the threshold of detection (Ong and Mann, 2005).

Mass spec. analysis of fraction C.dve_R7 identified both sequence fragments, using peptide mapping, and an intact mass for the fraction component. Mass spec. analysis identified the peptide component as having a complete mass of 14198Da, whilst peptide mapping identified several fragments of consecutive sequence. Blast and database searches matched the peptide fragments obtained from C.dve_R7 to phospholipase A2 (PLA2) peptides in the database from a number of members of the same genus *Crotalus*. Whilst there was not an exact match *to C. durissus*

vegrandis specifically, this was not entirely surprising as there is a lack of entries for this specific subspecies in the UniProt database, with only a fragment of a PLA2 deposited. However, the presence of PLA2 peptides in pit viper venoms appears to be common, with many identified for *Crotalus durissus* subspecies including *C. durissus terrificus* (Muller *et al.*, 2018), *C. durissus ruruima* (Diz Filho et al., 2009), *C. durissus collilineatus* (Toyama et al., 2009), *C. durissus cumanensis* (Pereañez et al., 2009). The sequence fragments from C.dve_R7 were identified in Blast searches to match sequences from PLA2s, derived from all of these subspecies, as well as PLA2s from different species from the same genera, including *Crotalus scutulatus scutulatus* and different genera, such as *Sistrurus* and *Gloydius (Agkistrodon).*

Sequence alignments from the top 11 PLA2s derived from *Crotalus* species, with the highest percentage matches to the mass spec sequence data, were directly compared to determine conserved regions of peptide sequence. In addition to the 11 selected *Crotalus* sequences, additional PLA2 sequences with similar percentage matches, from 2 distinct genera *Sistrurus* and *Gloydius* (*Agkistrodon*) were also included to determine whether sequence conservation occurs across several diverse snake genera (Figure 7.11). Although not a complete sequence, the only sequence fragment of PLA2 from *C. durissus vegrandis* was also included in a separate alignment for cross-comparison to other *Crotalus* species (Figure 7.12). Alignment of the 13 sequences identified that all the PLA2s shared a highly conserved sequence structure, with large regions of the peptide structure conserved not just between members of the same species, but also across different genera (Figure 7.11). Alignments demonstrated that PLA2s from pit viper venoms come in both long (≈138aa) and short (≈122aa) forms, with three of the analysed sequences displaying an additional sequence of 16 amino acids at the c-terminal end of the peptide. These additional amino acids were shown to be unshared by the rest of the assessed sequences, however the 16 amino acids appear to all share a highly conserved sequence structure, with all three displaying the exact same additional c-terminal sequence (Figure 7.11).

Long PLA2s have been routinely shown in the database to have molecular masses between 15-16,000Da, with short PLA2s around 14-14,500Da. With an intact mass of 14184Da and peptide fragment matches to multiple database entries, it is likely that the peptide identified in fraction C.dve_R7 is a short-form PLA2. The closest sequence match to the peptide fragment data obtained was to a PLA2 from the venom of *Crotalus durissus ruruima* with an intact mass size mismatch of only 1Da, however large fragments of the sequence were still undetected via the mass spec technique. However, using the sequence fragments obtained from peptide mapping mass spec and regions of the PLA2 sequence that are highly conserved across multiple *Crotalus* species, it was possible to account for around 87.7% of the potential amino acid sequence of the peptide component in fraction C.dve_R7 (See figure 7.12).

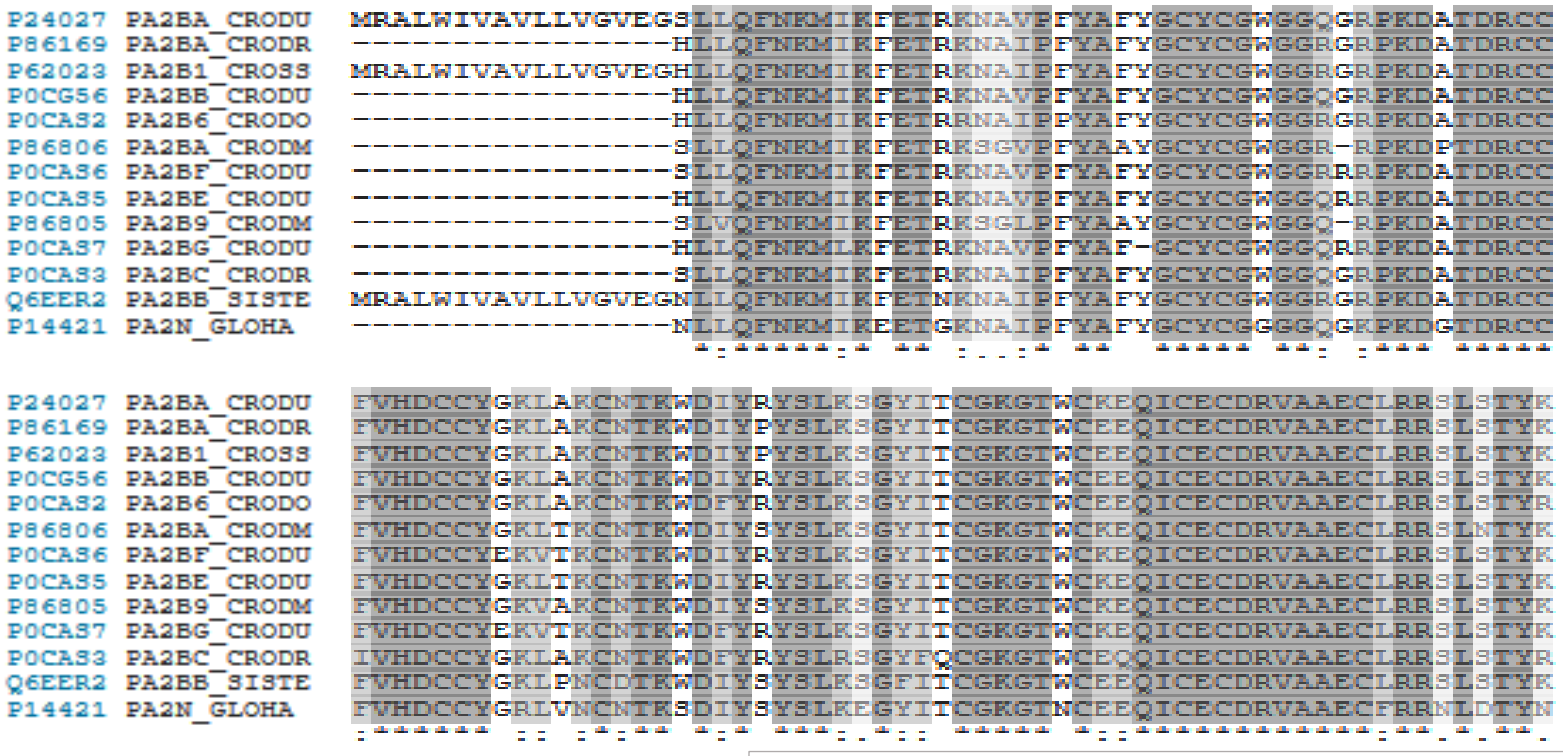

Figure 7.11: Full Sequence Alignments of top 13 UniProt Phospholipase A2 sequence matches to C.dve_R7

Displays the complete sequences of the top 13 closet UniProt matches to the amino acid sequence fragments obtained from the peptide digest mass spec of fraction C.dve_R7. The UniProt sequences of the top 13 matches all belong to the same peptide class, phospholipase A2s. The alignments display conserved regions of similarity (grey) in amino acid sequences amongst the top highlighted phospholipase A2 sequences. 11 sequences matched to PLA2s from other Crotalus species, whilst an additional 2 PLA2s from outlier genera *Sistrurus* and Gloydius were also highlighted as matches. Due to a lack of complete sequence and only fragment data for fraction C.dve_R7 (isolated from *Crotalus durissus vegrandis* venom) the fraction itself is not directly included in this alignment (See Appendix XXV)

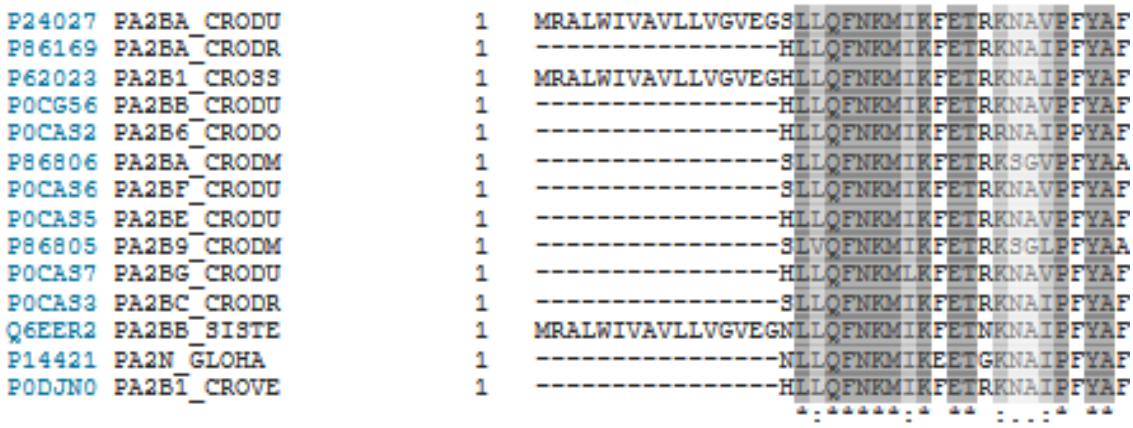

Figure 7.12: Partial Sequence Alignments of the top 14 UniProt Phospholipase A2 sequence matches to C.dve_R7

Displays the first 39 amino acids, from the top 14 closet UniProt sequence matches to the amino acid sequence fragments obtained from the peptide digest mass spec of fraction C.dve_R7. This alignment includes the addition of the only identified UniProt deposited, partial peptide sequence fragment of a PLA2 from the venom of *Crotalus durissus vegrandis* (PA2B1_CROVE), the same Crotalus species from which fraction C.dve_R7 is derived. The alignments display conserved regions of similarity (grey) in amino acid sequences amongst the top highlighted matching PLA2 sequences. Due to a lack of complete sequence and only fragment data for fraction C.dve_R7 (isolated from *Crotalus durissus vegrandis* venom) the fraction itself is not directly included in this alignment (See Appendix XXV)

Despite such a close intact mass match to the *Crotalus durissus ruruima* PLA2 *(PA2BA_CRODR)*, there is still a mass mismatch of 1Da. Excluding the amino acid residues confirmed by mass spec sequence data and those that are completely conserved across all the investigated *C. durissus* PLA2 sequences taken from UniProt, that potentially left 14 amino acid residue which could be responsible for the observed discrepancies in mass (Figure 7.13).

Assessing the possible changes each amino acid substitution causes to the mass of the peptide in Da (Figure 7.13) it is possible to identify 5 amino acids (aa16, aa33, aa39, aa55 & aa101), whose combined substitutions could result in an overall change in the intact mass of UniProt PLA2 (PA2BA_CRODR) by 1Da, bringing the mass to be in line with the intact mass determined for fraction C.dve_R7 (Figure 7.14). Starting with the complete sequence for *C. durissus ruruima* PLA2 (PA2BA_CRODR), a substitution of aa16 from asparagine (N) to serine (S) in combination with the substitution of either aa39 or 55 from alanine (A) to proline (P), results in the loss of 1Da to the molecular mass, bringing it to match the mass of C.dve_R7. The analysis of the sequences of PLA2s from the 11 aligned *Crotalus* species identified that these sequence substitutions already do occur in other PLA2s, with S occurring at loci 16 in 2 PLA2s from *C. durissus cumanensis*, with P also occurring at loci aa39 in one of these PLA2s (PA2BA_CROMD). The identification of a P at aa55 was not seen to occur in the PLA2 sequences assessed from *Crotalus* species, however it was observed to occur in a phospholipase sequence identified from *Sistrurus tergeminus* (PA2BB_SISTE) (figure 7.11).

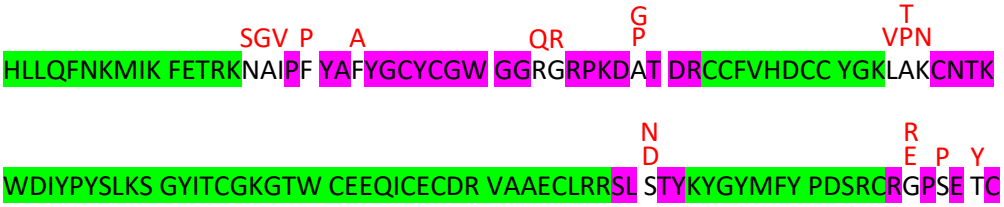

Figure 7.13: Proposed sequence of peptide in Fraction C.dve_R7

Displays the closest sequence match from the UniProt database *(*PA2BA_CRODR), with highlighted sequences for conserved regions, mass spec match data from C.dve_R7 and amino acids (aa) which show variations.

Sequence obtained from peptide mapping. Conserved amino acids between Crotalus species' phospholipase A2s. Red letters represent variable amino acids, identified across the 13 selected UniProt sequences at these aa loci, which lack peptide mapping sequence data

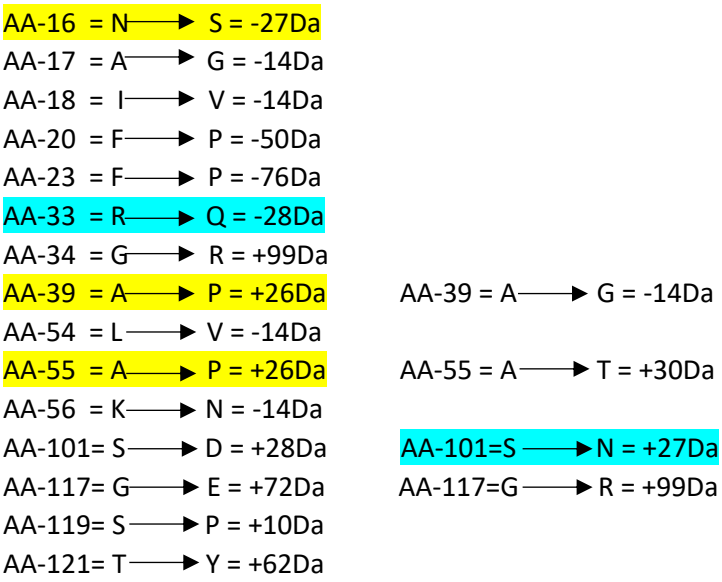

Figure 7.14: Amino Acids in *Crotalus durissus ruruima* phospholipase A2 sequence that could be substituted to Mass Match to C.dve_R7

Shows where variations to aa sequences occur between different phospholipase A2s from multiple Crotalus species (excluding where mass spec sequence data was obtained). Changes to molecular weight in Da of each amino acid that can be substituted in relation to the amino acid in that position for *Crotalus durissus ruruima* phospholipase A2 sequence (UniProt: PA2BA_CRODR). Highlighted amino acids indicate where substitutions could occur to fix the mismatch in intact mass (-1Da) between fraction C.dve_R7 and PA2BA_CRODR (See Appendix XXVI for table of amino acids)

Alternatively, the substitution of aa33 in *C. durissus ruruima* PLA2 (PA2BA_CRODR) from arginine (R) to glutamine (Q) in conjunction with the substitution of aa101 from serine (S) to asparagine (N), also results in the loss of 1Da to the molecular mass, bringing it to match the mass

of C.dve_R7 (Figure 7.14). The combination of glutamine at aa33 and asparagine at aa101 appears to be fairly common in pit viper PLA2s with 6 of the aligned sequences presenting with this amino acid combination, including 4 PLA2s from *C. durissus terrificus*, 1 from *C. durissus cumanensis* and one from outlier genus *Gloydius halys* (Figure 7.11). Interestingly, this particular combination would result in the correct mass for the peptide whilst allowing for sequence match to the only fragment of sequence deposited in UniProt for a *C. durissus vegrandis* PLA2 (Figure 7.12).

PLA2s, identified from the venoms from many snakes, including pit vipers from the genus *Crotalus* have been identified to display anticancer properties (Pal *et al.*, 2002; Costa *et al.*, 2008; Bazaa *et al.*, 2009, 2010; Kessentini-Zouari *et al.*, 2010; Muller *et al.*, 2018). Crotoxin, a neurotoxic peptide isolated from the venom of *Crotalus durissus terrificus*, one of the most highly investigated venom PLA2s has been long studied for its ability to elicit anticancer properties through many avenues. Crotoxin has been found to inhibit cell proliferation in A549 cells both *in vitro* and *in vivo*, where it was found to effect the levels of VEGF growth factor and inhibit angiogenesis (Ye *et al.*, 2011). Crotoxin has also been suggested to prove effective against EGFR-over-expressing cancers, where its effectiveness has been linked to alterations in the signalling dynamics of the receptor. A paper by Donato *et al.*, 1996, first purported findings that Crotoxin caused A431 cell inhibition through EGFR-directed means, with increases to the levels of phosphorylation of EGFR linked to Crotoxin treatment (Donato *et al.*, 1996). Subsequent research into the effects of crotoxin have shown treatment with the PLA2 to enhance the effectiveness of EGFR-targeting small molecule kinase inhibitor gefitinib in SK-MES-1 human lung cancer cells (Wang *et al.*, 2012). Interestingly, whilst studies of Crotoxin seem to attribute the PLA2 with EGFR stimulatory effects, another study into a basic secretory PLA2 (sPLA2), identified from the venom of an un-named snake, was reported to cause inhibitory effects to A431 cell proliferation and to block EGF-stimulated EGFR phosphorylation and the subsequent phosphorylation of downstream signalling proteins (Zhao *et al.*, 2002). The findings of this paper in conjunction with the mass spec data and PLA2 sequence analyses support the suggestion that fraction C.dve_R7 could feasibly contain a novel PLA2 from the venom of *C. durissus vegrandis*. This PLA2 would appear to be functioning to reduce EGFR phosphorylation levels in over-expressing cancer cell lines.

Mass spec analysis of fraction H.swa_R30, identified both intact mass and fragments of sequence data for the fraction component. Mass spec analysis identified the venom fraction as having a mixture of peptides with varying masses, which is not entirely surprising given that SEC HPLC identified the fraction as containing at least 2 dominant peaks (Fig. 7.20). Peptides ranged in mass from around 7900-9000Da, with the most abundant detectable component presenting with an intact mass of 8896Da. Peptide mapping identified several fragments of consecutive sequence,

with Blast and database searches matching some of the peptide fragments to PLA2s in the database from a variety of scorpions and other fragments to cytotoxins in the database from cobra venoms. Whilst sequence data that matched cobra cytotoxins was identified from the fraction H.swa_R30, the likelihood of this being a viable comparison molecule is fairly low, given that whole *H. swammerdami* venom and the fraction alike have both proven in previous experiments to not display direct cellular cytotoxicity against cancer cells at doses as high as 4 mg/ml (Figure 5.13). Tested cobra venoms and their fractions have been routinely shown both in the literature (Feofanov *et al.*, 2005; Debnath *et al.*, 2010; Ebrahim *et al.*, 2014, 2016) and in previous experiments to cause high levels of cytotoxicity at doses as low as 20 μg/ml (Figures 4.5 & 4.6), and so if fraction H.swa_R30 contained a similar type of compound to cobra cytotoxins a similar level of cytotoxicity would be expected to be observed.

Whilst there was not an exact match *to H. swammerdami* venom components specifically, this was not entirely surprising as there is a lack of entries for this specific species in the UniProt database. However, there were successful matches of partial sequence to PLA2s from other scorpion species and genera, including *Heterometrus fulvipes* (Hariprasad *et al.*, 2007), *Heterometrus laoticus* (Incamnoi *et al.*, 2013; Jridi *et al.*, 2015), *Hottentotta tamulus* (Hariprasad *et al.*, 2009), *Pandinus imperator* (Conde *et al.*, 1999), *Anuroctonus phaiodactylus* (Valdez-Cruz, Batista and Possani, 2004) and *Hadrurus gertschi*. However, despite matching sequences to PLA2s from other scorpion species, the intact mass obtained for the dominant component and all the other detected components of fraction H.swa_R30 are significantly smaller (7000-8896Da) than the masses of PLA2s deposited for these other scorpions (11487-18664Da). The closest size match was to the large subunit of a PLA2 derived from the venom of *H. fulvipes.* Sequence entries for 7 scorpion PLA2 peptides were aligned to determine regions of conserved sequence and matches to the mass spec sequence data obtained for H.swa_R30 (Figure 7.15).

The mass spec. data obtained from fraction H.swa_R30, matches to a highly conserved region within the centre of all 7 of the aligned scorpion PLA2 sequences (Figure 7.15, yellow box), however given that the molecular mass for the region of sequence obtained by peptide mapping MS is 3609Da and the total intact mass was recorded as 8896Da, there is still large portions of the sequence for H.swa_R30 that are unaccounted for. Taking into consideration the lack of sequence generated for this fraction, the larger degree of variation between the possible amino acids at both the c- and n-terminal regions of the 7 aligned sequences and the fact that the intact

Figure 7.15: Alignments of Top 7 UniProt Phospholipase A2 sequence matches to peptide fragments obtained from the Mass Spectrometry of fraction H.swa_R30

UniProt sequence alignments of Scorpion phospholipase A2s, in the database, with the closest sequence matches to H.swa_R30 mass spec sequence fragments. The alignments display the regions of similarity (grey) in amino acid sequences amongst all the selected phospholipase A2 sequences. The figure shows the complete sequences for all PLA2s selected for alignment. Yellow highlighted region identifies region of obtained mass spec data from Peak Proteins (See Appendix XXVII), green highlighted region matches to purported PLA2 active site

mass for H.swa_R30 is significantly smaller than that of the sequences for scorpion PLA2s already deposited in the database, makes it almost impossible to predict likely additional sequence. Interestingly, a paper investigating group III phospholipase A2s, looked into the sequence of a PLA2 identified from the venom of *Mesobuthus (Hottentotta) tamulus*. The paper identified a region of the sequence as the active site for both this PLA2 and other type III PLA2s from differing genera (Hariprasad *et al.*, 2009). This region for the proposed active site of type III PLA2s overlaps with obtained sequence data from fraction H.swa_R30 (Figure 7.24, green box). The fact that part of the active site for type III PLA2s has been detected in sequence fragments from the mass spec data for H.swa_R30 adds more robustness to the hypothesis that the component identified in H.swa_R30 may be a short or truncated form of a yet unidentified Phospholipase A2.

Given the similar reductions to EGFR phosphorylation seen with both fractions C.dve_R7 and H.swa_R30, plus the partial match to scorpion PLA2s in the database, and the SEC HPLC traces which identified peaks in both fractions with similar profiles and elution times, adds support to the suggestion that the latter could contain a similar type of peptide to C.dve_R7. However, in order to confirm these suggestions additional lab experimentation would need to be undertaken, including possible enzymatic assays such as a PLA2 activity screen of both fractions. Edman degradation of the three selected samples could be undertaken in the future to attempt to obtain the complete amino acid sequence for each fraction, not just the fragments generated through the undertaken peptide digest mass spectrometry.

7.4 Conclusions

HPLC fractionation of 9 selected whole venoms and subsequent EGFR phosphorylation ELISAs identified 14 and 9 fractions that caused both statistically and biologically significant reductions to EGFR phosphorylation levels in MDA-MB-468 and A431 cells, respectively. These fractions were identified across a wide range of venomous genera, including venoms from snake, scorpion and theraphosid representatives. Snake venoms from both genetically and geographically distinct taxa were shown to cause reductions in EGFR phosphorylation in similar manner. All statistically and biologically significant fractions were shown through analysis to be causing reductions to EGFR phosphorylation of 50% (2-fold) or greater after 2h treatment. Three fractions (B.boe_R6, C.dve_R7 and H.swa_R30), collected via the reverse phase HPLC, which were found to cause both statistically and biologically significant reductions to EGFR phosphorylation and whose whole venoms (*Brachypelma boehmei*, *Crotalus durissus vegrandis* and *Heterometrus swammerdami*) had routinely cause EGFR phosphorylation reductions in previous chapters, were selected to take forward for further investigation, including attempted mass spectrometry

identification. Two of the selected fractions were shown to cause similar significant reductions to both EGFR over-expressing cell lines, whilst the third (B.boe_R6) showed strong EGFR phosphorylation reducing properties against MDA-MB-468 TNBC cell line whilst unaffecting A431 cells, suggesting the potential for a cancer-specific venom component.

Second dimension analytical SEC HPLC of the three fractions selected (B.boe_R6, C.dve_R7 and H.swa_R30), identified the prior two as appearing to comprise of one clear dominant peptide component, which was hypothesised to be the likely cause of the EGFR phosphorylation reductions observed with these fractions. SEC HPLC of H.swa_R30 however identified a mixture of venom components, with at least 2 dominant peaks composing the fraction. Intact mass and peptide mapping mass spectrometry was employed in an attempt to identify potential venom components in the 3 selected fractions. Both mass spec techniques yielded no useful peptide information for fraction B.boe_R6, suggesting that either the fraction comprises some other non-peptidyl venom entity or that the fraction sample may have fallen below the threshold of detection employed for the analysis. Samples C.dve_R7 and H.swa_R30 both returned mass spec aa sequence and molecular weight data, matching peptide fragments from both to phospholipase A2 sequences deposited for other closely related species and taxa in the UniProt database. Whilst sequence data was incomplete for both, aa fragments in conjunction with intact mass and sequence alignments of the top 14 hits for fraction C.dve_R7 strongly hint at the possibility that the component in the fraction may be a phospholipase A2. Due to a lack of peptide size match to existing deposited sequences, and a larger degree of variation between the top aa sequences matches identified in UniProt for H.swa_R30, the identification of the fraction component is more inconclusive. However, a paper into PLA2s matched aa sequence obtained for fraction H.swa_R30 to amino acid sequences from the active sites of type III scorpion PLA2s. The presence of sequence that matches to the active sites of already identified scorpion PLA2s, increases the potential for a peptide which displays PLA2 activity in fraction H.swa_R30. In addition, the SEC HPLC traces for both fractions C.dve_R7 and H.swa_R30 identified peaks of similar shape, size and elution times, which may further support the presence of peptide components with similar structures and mechanisms of actions.

Despite the suggestion that both C.dve_R7 and H.swa_R30 may contain venom phospholipase A2s, further follow up work would be a necessity to confirm this. The undertaking of a phospholipase A2 activity detection assays could help to confirm the likelihood that these fraction components could be PLA2s, as well as the undertaking of Edman degradation to determine the complete amino acid sequence of the venom peptide components. Fraction B.boe_R6 also requires follow up investigations, which could include a second attempt at mass spec., supplying a larger quantity of the fraction to attempt to overcome any threshold limitations. Alternatively,

if the fraction is not peptidyl in composition, then the implication of tests for other common venom components, such as amides could be undertaken. In terms of follow up work for all the fractions, additional experiments including fraction dose response ELISAs, kinome array analyses to assess any potential phosphorylation effects on other RTK family members and effects to EGFR phosphorylation levels in normal, non-cancerous EGFR expressing cell lines, would all add further useful information for the characterisation and profiling of the effects of these venom fractions.

CHAPTER 8: Final Discussion

8.1 Discussion

The aim of this thesis was to evaluate whether whole animal venoms and venom isolated components could be used to modulate the expression or phosphorylated activity of RTKs identified as key players in cancer development and progression. A selection of whole snake and invertebrate venoms were profiled for their ability to target Receptor tyrosine kinases, within the model of the TNBC cell line MDA-MB-488.

Whole venoms were screened for their toxicity to the TNBC cell line MDA-MB-468 and squamous carcinoma cell line A431. Venoms were screened using a Resazurin-based cell viability assay, optimised for this study. The data obtained in Chapter 3 identified that overall the MDA-MB-468 cell line appeared to be more susceptible to the cytotoxic effects of the venom panels, with toxicity passing the 50% reduction threshold at lower doses than those needed to cause similar effects in A431 cells. True cobra venoms (Naja spp) were found to be more cytotoxic than pit viper, mamba, viper and invertebrate venoms, unanimously causing cytotoxicity to both cell lines at the two highest tested doses. However, this finding was not entirely surprising, as cobra venoms have been identified as being rich in three-finger cytotoxins (Dubovskii and Utkin, 2015). Overall snake venoms proved more cytotoxic to both cell lines, with the venoms from Scolopendra species *S. hardwickei* and *S. subspinipes dehaani* and buthid scorpion *P. liosoma* the only invertebrate venoms identified to cause cytotoxic effects to either cell line. The findings of this data are backed up by extensive literature which has shown that whole venoms are capable of reducing cancer cell viability in both time- and dose-dependent manners. However, whilst this toxicity data is interesting and highlights the ability of venoms to kill cancer cells, with different cancer types responding with differing sensitivities, the work does not highlight the mechanism through which these venoms are causing the observed anti-oncogenic effects. This data opens up the potential for further investigation into the mechanistic action through which these venoms are causing cellular death. Further work into whether the induced cell death is apoptotic or necrotic would give a better understanding of how these venoms are working, and if the death is occurring through an untargeted cell membrane disrupting mechanism or whether it is brought about through a more targeted effect. The observation of cell line specific effects opens up the opportunity to explore the toxicity of these venoms further in a variety of other different cancer cell types and more importantly in non-cancerous cell lines. The investigation of effects into non-cancerous cell types would help us to better understand and determine whether there is a natural inherent targeting of cancer cell specifically over normal healthy tissue.

In Chapter 4, whole venoms were selected from those genera highlighted to display antineoplastic effects *in vitro* in previously published literature. Whilst venoms were selected, using data published in previous peer-reviewed literature, from those shown to previously have displayed anti-cancer activities, there is little research that has actually been carried out into the effects of venoms for cancer therapeutic effects in *in vivo* experiments. The six selected whole venoms were chosen to allow for the broadest possible degree of variation between venom composition, and comprised venoms selected from cobra (*N. naja*), mamba (*D. viridis*), Pit viper (*C. durissus vegrandis*), scorpion (*H. swammerdami*), buthid (*P. liosoma*) and theraphosid (*A. geniculata*) lineages. Venoms were profiled for their ability to influence the combined expression/phosphorylation of TNBC MDA-MB-468's RTK profile. The results found that the six selected venoms were capable of causing biologically significant (≥2-fold increases/reductions) to the expression/phosphorylation of almost all of the 49 investigated RTKs (with the exception of Tie-1), with both increases and decreases in the expression/phosphorylation profiles of some RTKs observed in response to different venom treatments. Venom from *C. durissus vegrandis* appeared to be having almost a pan-reducing effect against the kinome panel, with 46/49 receptors showing biological reductions. However, it is worth noting that whilst this effect may be true, pit viper venoms contain high levels of protease activity and so this cannot be ruled out for the observed complete reduction to almost all of the surface expressed RTKs. The profiling of these receptor tyrosine kinases implies that venoms have the propensity to be used in a more targeted manor, in this instance to target RTKs from a broad variety of subfamilies, and that specific venoms are capable of causing both increases and decreases to their signalling capability. This could have wider potential implications for the future study of many of these RTK members. Venoms could prove useful tools in enabling us to better understand the mechanisms behind how some of the more poorly investigated and understood RTKs work, both within the context of normally functioning healthy cells, but also in the aberrant functioning of a diseased cell state. This work could also open up potential avenues for further investigation in terms of the identification of novel RTK targets for some of the more notoriously difficult to treat cancer subtypes, such as TNBC. The identification of under-investigated kinases as novel druggable options for the treatment of TNBC could open up new therapeutic avenues of investigation for the advent of drugs with different mechanistic effects.

Treatment with the six venoms highlighted that reductions to Epidermal growth factor receptor (EGFR), commonly identified as a key player in the progression of TNBC (Guerrab *et al.*, 2016; Nakai, Hung and Yamaguchi, 2016), were possible in response to venoms, opening up avenues of investigation for potential EGFR-targeting venom-derived peptides which could have novel mechanistic actions. Whilst the differences in observed cytotoxicity were interesting, it was difficult from this data to ascertain whether the toxicity was occurring through a targeted

approach, or whether a general cellular cytotoxic effect was occurring. Untargeted toxicity would be more undesirable than a targeted inhibition as it would be more likely to increase the chances of more systemic toxic side-effects. Due to its levels of over-expression in both cell lines, it was hypothesised that if a targeted-cell cytotoxicity effect was occurring, it maybe as the result of changes to the phosphotyrosine activity of EGFR. Venoms, that had been previously screened for cytotoxicity were rescreened using a developed in-cell ELISA for their ability to specifically reduce EGFR phosphotyrosine levels. MDA-MB-468 and A431 cells were screened using a self-developed and optimised ELISA. Viable cells were dosed with whole snake and invertebrate venom panels for 2h at doses of 20 µg/ml and 100 µg/ml respectively, before being stimulated with natural ligand EGF. Cells were then fixed with paraformaldehyde to preserve the phosphorylation state and probed with an anti-phosphotyrosine antibody. The data generated from these whole venom ELISAs (Chapter 5), identified nine snake venoms which caused 30% or greater reductions to EGFR phosphotyrosine levels in MDA-MB-468 cells, including six pit viper venoms, one mamba, one viper and one brown snake. Greater than 50% reductions were observed in response to two whole pit viper venoms, isolated from *C. durissus vegrandis* (previously shown to modulate EGFR phosphorylation in Chapter 4) and *C. rhodostoma*. Eight whole snake venoms were found to cause 30% or greater reductions in A431 cell phosphotyrosine levels, including six pit vipers, one mamba and one viper. It is worth noting, that unlike MDA-MB-468 cells, none of the venoms caused greater than 50% reductions to the phosphorylation levels. Interestingly the majority of the venoms that caused reduction greater than 50% at this dose were pit viper venoms, suggesting that perhaps these venoms have a similar composition or contain components of a similar mechanistic action. Minimal reductions were observed in response to treatment with true cobra (Naja spp) venoms at this selected dose.

Smaller reductions to EGFR phosphotyrosine levels were observed in response to treatment with the invertebrate venom panel, with no venoms found to be causing reductions greater than 50% in either cell line. No whole invertebrate venoms were found to cause 30% or greater reductions in MDA-MB-468 cells, with only two identified in A431 cells. However, it is worth noting that this could be an effect of differences in the composition of invertebrate venoms compared to that of snakes and also a limitation of the selected dose. Further investigation into both panels at a variety of different doses would allow for the potential identification of venoms which cause reductions greater than these thresholds. A selection of whole venoms, both shown to cause detectable reduction and non-detectable reductions to EGFR phosphotyrosine levels at the doses used in the ELISAs were selected to be further profiled at a range of doses using the Western Blotting technique. *A. geniculata, B. boehmei, H. swammerdami, C. durissus vegrandis, D. viridis, N. naja, S. hardwickei and S. subspinipes dehanni* whole venoms were all profiled against TNBC cell line MDA-MB-468 at doses ranging between 5 mg/ml-20 ng/ml. The western blots

identified reductions to EGFR phosphotyrosine levels in MDA-MB-468 cells in response to all of the tested venoms, with the exception of *D. viridis*. Greater than 50% reductions were observed in response to *A. geniculata, B. boehmei, C. durissus vegrandis, N. naja, S, hardwickei* and *S. subspinipes dehaani* venoms at at least some of the tested doses.

The findings of chapter 5 highlight that venoms can cause detectable reductions to EGFR phosphotyrosine levels and that these can be determined using two distinctly different techniques. This data opens up avenues for further dose response investigations into some of the other venoms highlighted as causing reductions to EGFR phosphorylation in the single dose ELISAs. The identification of venoms which can reduce EGFR activity levels holds interesting potential for further investigation into novel EGFR targeting venom components. The data is interesting as there is limited research published suggesting the propensity for animal venoms to specifically modulate the phosphotyrosine levels of EGFR and so these findings appear to be relatively novel in the context of the wider scientific community.

In an attempt to try and elicit a mechanism through which the previously screened snake and invertebrate venoms could be causing EGFR phosphotyrosine reductions, an EGF-competitive binding assay was developed, optimised and employed. MDA-MB-468 and A431 cells were fixed with paraformaldehyde and treated with 2 mg/ml of snake and invertebrate venoms for either 2h or 10 min to determine whether the venoms contained components that demonstrated either slow- or fast-binding to the EGF-binding pocket. Cells were then treated with EGF conjugated to an Alexa fluor fluorescent dye. Reductions to fluorescent signal were deemed to be indicative of venom component binding to the EGFR binding pocket. The data generated in Chapter 6 suggested that venoms did not appear to be competitively binding to the EGF binding pocket, with almost none of the tested venoms showing reductions to fluorescence signal. The only detectable reduction deemed to be significant using Z score analysis was in response to millipede *C. giganteus* secretion. However, it is worth noting that despite attempts to optimise the assay, the achievable fluorescent window was still small and there appeared to be plate edging effects which caused routinely lower fluorescent levels in the plate controls. Further optimisation of this assay could yield more robust data and enable the definitive determination of whether EGF-competitive binding could be ruled out as the mechanistic action causing the observed reductions to EGFR phosphotyrosine levels. Future work, including the potential addition of a blocking step to attempt to reduce non-specific EGF Alexa Fluor-488 binding or the isolation of EGFR directly from the cells through immunoprecipitation and the subsequent coating of plates directly with it, rather than the fixing of cells, may also improve the window. Both of these optimisations could reduce potential cell autofluorescence or background fluorescence and increase the overall number of available EGF receptors to which EGF Alexa Fluor-488 can bind, increasing the

maximum achievable fluorescence levels. Plate layouts which accommodated the spread of replicate wells across the 96 well plate may have helped to eliminate the possibility of edging effects by better allowing for the identification of edge outlier data points. There is also the possibility that the selection of EGF conjugated to a different fluorophore, with different excitation and emission wavelengths, may allow for more sensitivity and a larger fluorescent window. If optimisation failed to further enhance the workable window of the assay, the potential to acquire a commercially available fluorescent EGF-competitive binding assay, such as the EGF/EGFR AlphaLISA Binding Kit (PerkinElmer) could also be considered.

The identification of small peptide venom components which can either competitively bind to the EGF binding pocket or bind to the tyrosine kinase domain could present novel options for cancer therapeutic development, as current targeted cancer therapies generally fall into small molecule tyrosine kinase inhibitors (SM-TKIs) (Roy and Perez, 2009; Geuna *et al.*, 2012; Wu, Nielsen and Clausen, 2015) or antibody therapies (Chames *et al.*, 2009; Guo, Hou and Wang, 2011; Scott, Wolchok and Old, 2012), which bind allosterically or overlap the EGF binding domain, with peptide inhibitors not routinely investigated as potential therapeutics.

Nine venoms, previously shown to cause reductions to EGFR phosphotyrosine levels in Chapters 4 and 5 were selected to undergo reverse phase high performance liquid chromatography (RP-HPLC). Venoms were fractionated and the resulting obtained fractions screened using the previously optimised in-cell ELISA to determine which fractions were responsible for the observed reductions. Screening of 209 fractions identified 14 and 9 fraction which caused both biological (≥50% reduction) and statistically significant reductions to EGFR phosphotyrosine levels in MDA-MB-468 and A431 cells, respectively. Six of the identified fractions caused significant reductions in both of the investigated cell lines. Three fractions shown to cause the greatest reductions to phosphotyrosine levels (B.boe_R6, C.dve_R7 and H.swa_R30) was selected to undergo Intact Mass and Peptide Digestion mass spectrometry. Two of the fractions (C.dve_R7 and H.swa_R30) returned usable peptide mass spectrometry data, and subsequent searches of the existing venom peptide database deposited sequences partially matched the peptide fragments from both fractions to venom phospholipase A2 (PLA2) peptides from closely related genera and species. Interestingly a paper published in 1996 identified, crotoxin, a phospholipase A2 from the venom of *Crotalus durissus terrificus* as altering the phosphorylation of EGFR, however in this instance it was found to be causing increases rather than the decreases observed in this thesis (Donato *et al.*, 1996). Whilst mass spec data hints that these fractions are phospholipase A2s, additional work would need to be undertaken to confirm this implicitly. Additional mass spectrometry in the form of Edman degradation could achieve complete amino acid sequences for the fraction components, rather than fragments, allowing for better matching

to existing sequences from closely related species and the possibility for the depositing of our own new venom sequences for novel venom species. The undertaking of a PLA2 activity assay could be used to determine whether the fractions contain catalytically active PLA2s, however this would not be useful in the identification of non-catalytically functional PLA2 venom components.

For future direction and project progression, additional profiling of the effects of the PLA2s isolated from the crude venoms on both a larger panel of cancer cell lines, as well as patient-derived samples and normal non-cancerous cells would help further our understanding of whether these peptides show true selectivity for cancer cells. In order to enable the screening of the PLA2 compounds against a bank of cell lines, bulk up of the peptides would need to be undertaken and at that scale, venom extraction and HPLC fractionation of venom components from whole venom is both time consuming, labour-intensive and not cost-effective. Synthetic bulk up could be achieved through either Edman degradation, generating complete amino acid sequence profiles, followed by structure activity relationship (SARs) analysis and subsequent synthetic production of the peptide. Alternatively, through the expression of the peptides of interest, using either a mammalian cell or bacterial expression system, the process could be taken through transfection, colony culture, selection of the greatest producing colonies and bulk up culturing in bioreactors.

Further investigation into any potential off target effects against other RTKs or protein kinases should be investigated and if there are effects against more family members than EGFR, it should be ascertained whether they can be considered beneficial or detrimental targets to effect. Investigation into the effects of the venom-derived PLA2 peptides in *in vivo* animal cancer models would add further support to the data of real anticancer therapeutic properties or identify that the compounds do not work effectively when scaled from *in vitro* plate-based cellular assays to whole organism *in vivo* trials. The switch to animal model testing would also enable the undertaking of safety testing when administered *in vivo*, highlighting any potential side effects when the venom fractions are administered within a whole organism and not just a monolayer of cells. If all proceeded well with animal trials, then there would be the potential to pass the compounds over or join collaboratively to undertake clinical trials.

8.2 Concluding Remarks

The profiling of whole venoms for both their general cancer cytotoxic effect and their ability to modulate the combined expression/activity of receptor tyrosine kinases in this thesis has generated a large degree of novel work, with the potential to inspire a wide degree of areas for further scientific research. Whilst whole snake venoms have been investigated for their anti-cancer potential, there has been limited large scale profiling of invertebrate venoms for cancer treatment. Whilst several papers have focused on the anticancer cytotoxicity of a selected few

whole venoms, the large-scale profiling of the effects of whole venoms against forty-nine cancer expressed receptor tyrosine kinases carried out in this thesis is novel, previously un-investigated work. The investigation into the EGFR modulating potential of a panel of 41 snake and invertebrate venoms and secretions, presents new data for EGFR-modulating molecules from naturally derived biological sources. The successful fractionation of whole venoms into a usable screening library for EGFR, the generation of observable reductions to EGFR phosphotyrosine levels from specific fraction components, and the collection of usable mass spec data which has led to the possible identification of the venom component responsible for an observed biological effect highlight that venoms can be utilised as an effective source of molecules for selected cancer-specific targets. These findings could have wider implications for the way in which the wider scientific community view venom-derived peptides and could lead to venoms being perceived as more than just complex mixtures of toxins which cause harmful pathophysiological effects, and could potentially lead to their use in future scientific investigations against not just cancer, but a wider variety of clinically relevant diseases.

References

Abbott, R. G., Forrest, S. and Pienta, K. J. (2006) 'Simulating the hallmarks of cancer.', *Artificial life*, 12, pp. 617–634. doi: 10.1162/artl.2006.12.4.617.

Abdel-Rahman, M. A., Omran, M. A. A., Abdel-Nabi, I. M., Nassier, O. A. and Schemerhorn, B. J. (2010) 'Neurotoxic and cytotoxic effects of venom from different populations of the Egyptian Scorpio maurus palmatus', *Toxicon*, 55(2–3), pp. 298–306. doi: 10.1016/j.toxicon.2009.08.003.

Abe, B. T. and Macian, F. (2013) 'Uncovering the mechanisms that regulate tumor-induced T-cell anergy', *OncoImmunology*, 2(2), pp. 1–3. doi: 10.4161/onci.22679.

Aebersold, R. and Mann, M. (2003) 'Mass spectrometry-based proteomics', *Nature*, 422, pp. 198–207. doi: 10.1016/j.ics.2004.02.087.

Aghevlian, S., Boyle, A. J. and Reilly, R. M. (2017) 'Radioimmunotherapy of cancer with high linear energy transfer (LET) radiation delivered by radionuclides emitting α-particles or Auger electrons', *Advanced Drug Delivery Reviews*. Elsevier B.V., 109, pp. 102–118. doi: 10.1016/j.addr.2015.12.003.

Ahluwalia, S. and Shah, N. (2014) 'Animal Venom for treating breast cancer', *International Journal of Pharmacy and Pharmaceutical Sciences*, 6(9), pp. 24–30.

Ahmed, S., Sami, A. and Xiang, J. (2015) 'HER2-directed therapy: current treatment options for HER2-positive breast cancer', *Breast Cancer*, 22(2), pp. 101–116. doi: 10.1007/s12282-015-0587-x.

Ahn, M. Y., Lee, B. M. and Kim, Y. S. (1997) 'Characterization and cytotoxicity of L-amino acid oxidase from the venom of king cobra (Ophiophagus hannah)', *International Journal of Biochemistry and Cell Biology*, 29(6), pp. 911–919. doi: 10.1016/S1357-2725(97)00024-1.

Ahn, S. G., Kim, S. J., Kim, C. and Jeong, J. (2016) 'Molecular classification of triple-negative breast cancer', *Journal of Breast Cancer*, 19(3), pp. 223–230. doi: 10.4048/jbc.2016.19.3.223.

Akef, H., Kotb, N., Abo-Elmatty, D. and Salem, S. (2017) 'Anti-proliferative Effects of Androctonus amoreuxi Scorpion and Cerastes cerastes Snake Venoms on Human Prostate Cancer Cells', *Journal of Cancer Prevention*, 22(1), pp. 40–46. doi: 10.15430/jcp.2017.22.1.40.

Akef, H. M. (2018) 'Anticancer, antimicrobial, and analgesic activities of spider venoms', *Toxicology Research*. Royal Society of Chemistry, 7(3), pp. 381–395. doi: 10.1039/c8tx00022k.

Al-Asmari, A. K., Islam, M. and Al-Zahrani, A. M. (2016) 'In vitro analysis of the anticancer properties of scorpion venom in colorectal and breast cancer cell lines', *Oncology Letters*, 11(2), pp. 1256–1262. doi: 10.3892/ol.2015.4036.

Al-Asmari, A. K., Riyasdeen, A. and Islam, M. (2018) 'Scorpion Venom Causes Apoptosis by Increasing Reactive Oxygen Species and Cell Cycle Arrest in MDA-MB-231 and HCT-8 Cancer Cell Lines', *Journal of Evidence-Based Integrative Medicine*, 23, pp. 1–8. doi: 10.1177/2156587217751796.

Al-Asmari, A. K., Ullah, Z., Balowi, A. Al and Islam, M. (2017) 'In vitro determination of the efficacy of scorpion venoms as anti-cancer agents against colorectal cancer cells: A nano-liposomal delivery approach', *International Journal of Nanomedicine*, 12, pp. 559–574. doi: 10.2147/IJN.S123514.

Al-Asmari, A., Riyasdeen, A., Abbasmanthiri, R., Arshaduddin, M. and Al-Harthi, F. (2016) 'Scorpion (Androctonus bicolor) venom exhibits cytotoxicity and induces cell cycle arrest and apoptosis in breast and colorectal cancer cell lines', *Indian Journal of Pharmacology*, 48(5), pp. 537–543. doi: 10.4103/0253-7613.190742.

Al-Mahmood, S., Sapiezynski, J., Garbuzenko, O. B. and Minko, T. (2018) 'Metastatic and triple-negative breast cancer: challenges and treatment options', *Drug Delivery and Translational Research*. Drug Delivery and Translational Research, 8(5), pp. 1483–1507. doi: 10.1007/s13346-018-0551-3.

Alexander, P. B. and Wang, X. F. (2015) 'Resistance to receptor tyrosine kinase inhibition in cancer: molecular mechanisms and therapeutic strategies', *Frontiers of medicine*, 9(2), pp. 134–138. doi: 10.1007/s11684-015-0396-9.Resistance.

Ali, R. and Wendt, M. K. (2017) 'The paradoxical functions of EGFR during breast cancer progression', *Signal Transduction and Targeted Therapy*. The Author(s), 2(December 2016), pp. 1–7. doi: 10.1038/sigtrans.2016.42.

Almaaytah, A., Tarazi, S., Mhaidat, N., Al-Balas, Q. and Mukattash, T. L. (2013) 'Mauriporin, a novel cationic α-helical peptide with selective cytotoxic activity against prostate cancer cell lines from the venom of the scorpion androctonus mauritanicus', *International Journal of Peptide Research and Therapeutics*, 19(4), pp. 281–293. doi: 10.1007/s10989-013-9350-3.

Andersson, U., Guo, D., Malmer, B., Bergenheim, A. T., Brannstrom, T., Hedman, H. and Henriksson, R. (2004) 'Epidermal growth factor receptor family (EGFR, ErbB2-4) in gliomas and meningiomas.', *Acta neuropathologica*. Germany, 108(2), pp. 135–142. doi: 10.1007/s00401-004-0875-6.

Andor, N., Maley, C. C. and Ji, H. P. (2017) 'Genomic instability in cancer: Teetering on the limit of tolerance', *Cancer Research*, 77(9), pp. 2179–2185. doi: 10.1158/0008-5472.CAN-16-1553.

Andreucci, E., Francica, P., Fearns, A., Martin, L. A., Chiarugi, P., Isacke, C. M. and Morandi, A. (2016) 'Targeting the receptor tyrosine kinase RET in combination with aromatase inhibitors in ER positive breast cancer xenografts', *Oncotarget*, 7(49), pp. 80543–80553. doi: 10.18632/oncotarget.11826.

Ansarin, A., Bagheri, F. and Sharifi, A. (2018) 'Opposite Pattern of ERBB4 / HER4 Gene Expression in Triple- Negative and Non-Triple Negative Breast Cancer', Special Is(2), pp. 149–154.

Aparicio, A. M., Harzstark, A. L., Corn, P. G., Wen, S., Araujo, J. C., Tu, S. M., Pagliaro, L. C., Kim, J., Millikan, R. E., Ryan, C., Tannir, N. M., Zurita, A. J., Mathew, P., Arap, W., Troncoso, P., Thall, P. F. and Logothetis, C. J. (2013) 'Platinum-based chemotherapy for variant castrate-resistant prostate cancer', *Clinical Cancer Research*, 19(13), pp. 3621–3630. doi: 10.1158/1078-0432.CCR-12-3791.

Arab, A., Zacarin, G. G., Fontanetti, C. S., Camargo-Mathias, M. I., Santos, M. G. and Cabrera, A. C. (2003) 'Composition of the defensive secretion of the Neotropical millipede Rhinocricus padbergi Verhoeff 1938 (Diplopoda : Spirobolida : Rhinocricidae)', *Entomotropica*, 18(2), pp. 79–82.

Araújo, L. da S., Conceição, A. S. M. M., Cunha, D. M. de S., Morais, G. B. de, Silveira, J. A. de M., Xavier Júnior, F. A. F., Macambira, K. D. da S., Araújo, S. L., Pessoa, N. O. and Evangelista, J. S. A. M. (2016) 'Crotalus durissus venom: biological effects and relevant applications. A Review', *Revista Brasileira de Higiene e Sanidade Animal*, 10(1), pp. 9–21. doi: 10.5935/1981-2965.20160002.

Arbuckle, K. (2015) 'Evolution of Venomous Animals and Their Toxins', *Evolution of Venomous Animals and Their Toxins*, (2006), pp. 1–23. doi: 10.1007/978-94-007-6727-0.

Ardini, E., Menichincheri, M., Banfi, P., Bosotti, R., De Ponti, C., Pulci, R., Ballinari, D., Ciomei, M., Texido, G., Degrassi, A., Avanzi, N., Amboldi, N., Saccardo, M. B., Casero, D., Orsini, P., Bandiera, T., Mologni, L., Anderson, D., Wei, G., *et al.* (2016) 'Entrectinib, a Pan-TRK, ROS1, and ALK inhibitor with activity in multiple molecularly defined cancer indications', *Molecular*

Cancer Therapeutics, 15(4), pp. 628–639. doi: 10.1158/1535-7163.MCT-15-0758.

Arena, S., Siravegna, G., Mussolin, B., Kearns, J. D., Wolf, B. B., Misale, S., Lazzari, L., Bertotti, A., Truslino, L., Adjei, A. A., Montagut, C., Nicolantonio, F. Di, Nering, R. and Bardelli, A. (2016) 'MM-151 overcomes acquired resistance to cetuximab and panitumumab in colorectal cancers harboring EGFR extracellular domain mutations Authors':, *Science Translational Medicine*, 8(324), pp. 1–41.

Armstrong, D. K., Kaufmann, S. H., Ottaviano, Y. L., Furuya, Y., Buckley, J. A., Isaacs, J. T. and Davidson, N. E. (1994) 'Epidermal Growth Factor-mediated Apoptosis of MDA-MB-468 Human Breast Cancer Cells', *Cancer Research*, 54, pp. 5280–5283.

Arner, P., Pollare, T., Lithell, H. and Livingston, J. N. (1987) 'Defective insulin receptor tyrosine kinase in human skeletal muscle in obesity and Type 2 (non-insulin-dependent) diabetes mellitus', *Diabetologia*, 30(6), pp. 437–440. doi: 10.1007/BF00292549.

Arruda Macedo, J. K., Fox, J. W. and Souza Castro, M. de (2015) 'Disintegrins from Snake Venoms and their Applications in Cancer Research and Therapy', *Current Protein & Peptide Science*, 16(6), pp. 532–548. doi: 10.2174/1389203716666150515125002.

Arteaga, C. L. and Engelman, J. a. (2014) 'ERBB receptors: From oncogene discovery to basic science to mechanism-based cancer therapeutics', *Cancer Cell*. Elsevier Inc., 25(3), pp. 282–303. doi: 10.1016/j.ccr.2014.02.025.

Arteaga, C. L. and Engelman, J. A. (2014) 'ERBB receptors: From oncogene discovery to basic science to mechanism-based cancer therapeutics', *Cancer Cell*. Elsevier Inc., 25(3), pp. 282–303. doi: 10.1016/j.ccr.2014.02.025.

Asiedu, M. K., Beauchamp-Perez, F. D., Ingle, J. N., Behrens, M. D., Radisky, D. C. and Knutson, K. L. (2014) 'AXL induces epithelial-to-mesenchymal transition and regulates the function of breast cancer stem cells', *Oncogene*. Nature Publishing Group, 33(10), pp. 1316–1324. doi: 10.1038/onc.2013.57.

Asmari, A., Khan, H. A. and Manthiri, R. A. (2012) 'Rapid profiling of crude scorpion venom using liquid chromatography and its relevance to species identification', *Acta Chromatographica*, 24(3), pp. 501–509. doi: 10.1556/AChrom.24.2012.3.12.

Attarde, S. S. and Pandit, S. V. (2017) 'Cytotoxic activity of NN-32 toxin from Indian spectacled cobra venom on human breast cancer cell lines', *BMC Complementary and Alternative Medicine*. BMC Complementary and Alternative Medicine, 17(503), pp. 1–9. doi: 10.1186/s12906-017-2018-3.

Avril, S., Dincer, Y., Malinowsky, K., Wolff, C., Gündisch, S., Hapfelmeier, A., Boxberg, M., Bronger, H., Becker, K. F. and Schmalfeldt, B. (2017) 'Increased PDGFR-beta and VEGFR-2 protein levels are associated with resistance to platinum-based chemotherapy and adverse outcome of ovarian cancer patients', *Oncotarget*, 8(58), pp. 97851–97861. doi: 10.18632/oncotarget.18415.

De Azevedo, R. A., Figueiredo, C. R., Ferreira, A. K., Matsuo, A. L., Massaoka, M. H., Girola, N., Auada, A. V. V., Farias, C. F., Pasqualoto, K. F. M., Rodrigues, C. P., Barbuto, J. A., Levy, D., Bydlowski, S. P., De Sá-Junior, P. L., Travassos, L. R. and Lebrun, I. (2015) 'Mastoparan induces apoptosis in B16F10-Nex2 melanoma cells via the intrinsic mitochondrial pathway and displays antitumor activity in vivo', *Peptides*. Elsevier Inc., 68, pp. 113–119. doi: 10.1016/j.peptides.2014.09.024.

Bacac, M., Fauti, T., Sam, J., Colombetti, S., Weinzierl, T., Ouaret, D., Bodmer, W., Lehmann, S., Hofer, T., Hosse, R. J., Moessner, E., Ast, O., Bruenker, P., Grau-Richards, S., Schaller, T., Seidl, A., Gerdes, C., Perro, M., Nicolini, V., *et al.* (2016) 'A novel carcinoembryonic antigen T-cell bispecific antibody (CEA TCB) for the treatment of solid tumors', *Clinical Cancer Research*,

22(13), pp. 3286–3297. doi: 10.1158/1078-0432.CCR-15-1696.

Badiola, I., Olaso, E., Crende, O., Friedman, S. L. and Vidal-Vanaclocha, F. (2012) 'Discoidin domain receptor 2 deficiency predisposes hepatic tissue to colon carcinoma metastasis', *Gut*, 61(10), pp. 1465–1472. doi: 10.1136/gutjnl-2011-300810.

Badiola, I., Villacé, P., Basaldua, I. and Olaso, E. (2011) 'Downregulation of discoidin domain receptor 2 in A375 human melanoma cells reduces its experimental liver metastasis ability', *Oncology Reports*, 26(4), pp. 971–978. doi: 10.3892/or.2011.1356.

Badr, G., Al-Sadoon, M. K., Rabah, D. M. and Sayed, D. (2013) 'Snake (Walterinnesia aegyptia) venom-loaded silica nanoparticles induce apoptosis and growth arrest in human prostate cancer cells', *Apoptosis*, 18(3), pp. 300–314. doi: 10.1007/s10495-012-0787-1.

Bae, H. J., Song, J. H., Noh, J. H., Kim, J. K., Jung, K. H., Eun, J. W., Xie, H. J., Ryu, J. C., Ahn, Y. M., Kim, S. Y., Lee, S. H., Yoo, N. J., Lee, J. Y., Park, W. S. and Nam, S. W. (2009) 'Low frequency mutation of the Ephrin receptor A3 gene in hepatocellular carcinoma', *Neoplasma*, 54(4), pp. 331–334. doi: 10.4149/neo.

Bae, J. H. and Schlessinger, J. (2010) 'Asymmetric tyrosine kinase arrangements in activation or autophosphorylation of receptor tyrosine kinases.', *Molecules and cells*, 29(5), pp. 443–448. doi: 10.1007/s10059-010-0080-5.

Bae, Song Yi, Hong, J. Y., Lee, H. J., Park, H. J. and Lee, S. K. (2015) 'Targeting the degradation of AXL receptor tyrosine kinase to overcome resistance in gefitinib-resistant non-small cell lung cancer', *Oncotarget*, 6(12), pp. 10146–10160. doi: 10.18632/oncotarget.3380.

Bae, Soo Youn, Kim, S., Lee, J. H., Lee, H. chul, Lee, S. K., Kil, W. H., Kim, S. W., Lee, J. E. and Nam, S. J. (2015) 'Poor prognosis of single hormone receptor- positive breast cancer: Similar outcome as triple-negative breast cancer', *BMC Cancer*, 15(1), pp. 1–9. doi: 10.1186/s12885-015-1121-4.

Bai, A., Meetze, K., Vo, N. Y., Kollipara, S., Mazsa, E. K., Winston, W. M., Weiler, S., Poling, L. L., Chen, T., Ismail, N. S., Jiang, J., Lerner, L., Gyuris, J. and Weng, Z. (2010) 'GP369, an FGFR2-IIIb-specific antibody, exhibits potent antitumor activity against human cancers driven by activated FGFR2 signaling', *Cancer Research*, 70(19), pp. 7630–7639. doi: 10.1158/0008-5472.CAN-10-1489.

Balakrishnan, A., Bleeker, F. E., Lamba, S., Rodolfo, M., Daniotti, M., Scarpa, A., Van Tilborg, A. A., Leenstra, S., Zanon, C. and Bardelli, A. (2007) 'Novel somatic and germline mutations in cancer candidate genes in glioblastoma, melanoma, and pancreatic carcinoma', *Cancer Research*, 67(8), pp. 3545–3550. doi: 10.1158/0008-5472.CAN-07-0065.

Balakrishnan, A., Goodpaster, T., Randolph-Habecker, J., Hoffstrom, B. G., Jalikis, F. G., Koch, L. K., Berger, C., Kosasih, P. L., Rajan, A., Sommermeyer, D., Porter, P. L. and Riddell, S. R. (2017) 'Analysis of ROR1 protein expression in human cancer and normal tissues', *Clinical Cancer Research*, 23(12), pp. 3061–3071. doi: 10.1158/1078-0432.CCR-16-2083.

Balzer, E. M., Whipple, R. A., Cho, E. H., Matrone, M. A. and Martin, S. S. (2010) 'Anti-mitotic chemotherapeutics promote adhesive responses in detached and circulating tumor cells', *Breastcancer research and treatment*, 121(1), pp. 65–78. doi: 10.1038/jid.2014.371.

Banerji, U., Dean, E. J., Alejandro Perez-Fidalgo, J., Batist, G., Bedard, P. L., You, B., Westin, S. N., Kabos, P., Garrett, M. D., Tall, M., Ambrose, H., Carl Barrett, J., Hedley Carr, T., Amy Cheung, S. Y., Corcoran, C., Cullberg, M., Davies, B. R., de Bruin, E. C., Elvin, P., *et al.* (2018) 'A phase i open-label study to identify a dosing regimen of the pan-akt inhibitor azd5363 for evaluation in solid tumors and in pik3ca-mutated breast and gynecologic cancers', *Clinical Cancer Research*, 24(9), pp. 2050–2059. doi: 10.1158/1078-0432.CCR-17-2260.

Bange, J., Prechtl, D., Cheburkin, Y., Specht, K., Harbeck, N., Schmitt, M., Knyazeva, T., Müller, S., Gärtner, S., Sures, I., Wang, H., Imyanitov, E., Häring, H. U., Knayzev, P., Iacobelli, S., Höfler, H. and Ullrich, A. (2002) 'Cancer progression and tumor cell motility are associated with the FGFR4 Arg388 allele', *Cancer Research*, 62(3), pp. 840–847.

Barton, V. N., D'Amato, N. C., Gordon, M. A., Lind, H. T., Spoelstra, N. S., Babbs, B. L., Heinz, R. E., Elias, A., Jedlicka, P., Jacobsen, B. M. and Richer, J. K. (2015) 'Multiple molecular subtypes of triple-negative breast cancer critically rely on androgen receptor and respond to enzalutamide in vivo', *Molecular Cancer Therapeutics*, 14(3), pp. 769–778. doi: 10.1158/1535-7163.MCT-14-0926.

Baselga, J. (2006) 'Targeting Tyrosine Kinases in Cancer : The Second Wave Author (s): Jose Baselga Source : Science , New Series , Vol . 312 , No . 5777 (May 26 , 2006), pp . 1175-1178', 312(5777), pp. 1175–1178.

Baselga, J., Coleman, R. E., Cortés, J. and Janni, W. (2017) 'Advances in the management of HER2-positive early breast cancer', *Critical Reviews in Oncology/Hematology*. Elsevier, 119(September), pp. 113–122. doi: 10.1016/j.critrevonc.2017.10.001.

Bayerlová, M., Menck, K., Klemm, F., Wolff, A., Pukrop, T., Binder, C., Beißbarth, T. and Bleckmann, A. (2017) 'Ror2 signaling and its relevance in breast cancer progression', *Frontiers in Oncology*, 7(JUN), pp. 1–16. doi: 10.3389/fonc.2017.00135.

Bazaa, A., Luis, J., Srairi-Abid, N., Kallech-Ziri, O., Kessentini-Zouari, R., Defilles, C., Lissitzky, J. C., El Ayeb, M. and Marrakchi, N. (2009) 'MVL-PLA2, a phospholipase A2 from Macrovipera lebetina transmediterranea venom, inhibits tumor cells adhesion and migration', *Matrix Biology*, 28(4), pp. 188–193. doi: 10.1016/j.matbio.2009.03.007.

Bazaa, A., Pasquier, E., Defilles, C., Limam, I., Kessentini-Zouari, R., Kallech-Ziri, O., Battari, A. El, Braguer, D., Ayeb, M. El, Marrakchi, N. and Luis, J. (2010) 'MVL-PLA2, a snake venom phospholipase A2, inhibits angiogenesis through an increase in microtubule dynamics and disorganization of focal adhesions', *PLoS ONE*, 5(4), pp. 1–10. doi: 10.1371/journal.pone.0010124.

Bazley, L. a. and Gullick, W. J. (2005) 'The epidermal growth factor receptor family', *Endocrine-Related Cancer*, 12, pp. 17–28. doi: 10.1677/erc.1.01032.

Béchohra, L., Laraba-Djebari, F. and Hammoudi-Triki, D. (2016a) 'Cytotoxic activity of Androctonus australis hector venom and its toxic fractions on human lung cancer cell line', *Journal of Venomous Animals and Toxins Including Tropical Diseases*. Journal of Venomous Animals and Toxins including Tropical Diseases, 22(1), pp. 1–15. doi: 10.1186/s40409-016-0085-4.

Béchohra, L., Laraba-Djebari, F. and Hammoudi-Triki, D. (2016b) 'Cytotoxic activity of Androctonus australis hector venom and its toxic fractions on human lung cancer cell line', *Journal of Venomous Animals and Toxins Including Tropical Diseases*, 22(29), pp. 1–15. doi: 10.1186/s40409-016-0085-4.

Begam, A. J., Jubie, S. and Nanjan, M. J. (2017) 'Estrogen receptor agonists/antagonists in breast cancer therapy: A critical review', *Bioorganic Chemistry*. Elsevier Inc., 71, pp. 257–274. doi: 10.1016/j.bioorg.2017.02.011.

Bei, R., Budillon, A., Masuelli, L., Cereda, V., Vitolo, D., Di Gennaro, E., Ripavecchia, V., Palumbo, C., Ionna, F., Losito, S., Modesti, A., Kraus, M. H. and Muraro, R. (2004) 'Frequent overexpression of multiple ErbB receptors by head and neck squamous cell carcinoma contrasts with rare antibody immunity in patients.', *The Journal of pathology*. England, 204(3), pp. 317–325. doi: 10.1002/path.1642.

Beiderlinden, M., Werner, P., Bahlmann, A., Kemper, J., Brezina, T., Schäfer, M., Görlinger, K.,

Seidel, H., Kienbaum, P. and Treschan, T. A. (2018) 'Monitoring of argatroban and lepirudin anticoagulation in critically ill patients by conventional laboratory parameters and rotational thromboelastometry - a prospectively controlled randomized double-blind clinical trial', *BMC Anesthesiology*. BMC Anesthesiology, 18(1), pp. 1–15. doi: 10.1186/s12871-018-0475-y.

Berardi, R., Santoni, M., Morgese, F., Ballatore, Z., Savini, A., Onofri, A., Mazzanti, P., Pistelli, M., Pierantoni, C., De Lisa, M., Caramanti, M., Pagliaretta, S., Pellei, C. and Cascinu, S. (2013) 'Novel small molecule EGFR inhibitors as candidate drugs in non-small cell lung cancer', *OncoTargets and Therapy*, 6, pp. 563–576. doi: 10.2147/OTT.S28155.

Berclaz, G., Altermatt, H. J., Rohrbach, V., Kieffer, I., Dreher, E. and Andres, A. C. (2001) 'Estrogen dependent expression of the receptor tyrosine kinase axl in normal and malignant human breast', *Annals of Oncology*. Elsevier Masson SAS, 12, pp. 819–824. doi: 10.1023/A.

Bergstrom, D., Leyton, J. V., Zereshkian, A., Chan, C., Cai, Z. and Reilly, R. M. (2016) 'Paradoxical effects of Auger electron-emitting 111In-DTPA-NLS-CSL360 radioimmunoconjugates on hCD45+ cells in the bone marrow and spleen of leukemia-engrafted NOD/SCID or NRG mice', *Nuclear Medicine and Biology*. Elsevier Inc., 43(10), pp. 635–641. doi: 10.1016/j.nucmedbio.2016.07.006.

Berlier, J. E., Rothe, A., Buller, G., Bradford, J., Gray, D. R., Filanoski, B. J., Telford, W. G., Yue, S., Liu, J., Cheung, C. Y., Chang, W., Hirsch, J. D., Beechem, J. M., Haugland, Rosaria P. and Haugland, Richard P. (2003) 'Quantitative Comparison of Long-wavelength Alexa Fluor Dyes to Cy Dyes: Fluorescence of the Dyes and Their Bioconjugates', *Journal of Histochemistry and Cytochemistry*, 51(12), pp. 1699–1712. doi: 10.1177/002215540305101214.

Bernal, M., Ruiz-Cabello, F., Concha, A., Paschen, A. and Garrido, F. (2012) 'Implication of the β2-microglobulin gene in the generation of tumor escape phenotypes', *Cancer Immunology, Immunotherapy*, 61(9), pp. 1359–1371. doi: 10.1007/s00262-012-1321-6.

Bernardes-Oliveira, E., Farias, K. J. S., Gomes, D. L., Araújo, J. M. G. De, Silva, W. D. Da, Rocha, H. A. O., Donadi, E. A., Fernandes-Pedrosa, M. D. F. and Crispim, J. C. D. O. (2019) 'Tityus serrulatus Scorpion Venom Induces Apoptosis in Cervical Cancer Cell Lines', *Evidence-based Complementary and Alternative Medicine*, 2019, pp. 1–8. doi: 10.1155/2019/5131042.

Bhagirath, T., Chingtham, B. and Mohen, Y. (2006) 'Venom of a hill centipede Scolopendra viridicornis inhibits growth of human breast tumor in mice', *Indian Journal of Pharmacology*, 38(4), pp. 291–292. doi: 10.4103/0253-7613.27031.

Bhowmik, T., Saha, P. P., Sarkar, A. and Gomes, A. (2017) 'Evaluation of cytotoxicity of a purified venom protein from Naja kaouthia (NKCT1) using gold nanoparticles for targeted delivery to cancer cell', *Chemico-Biological Interactions*. Elsevier Ltd, 261, pp. 35–49. doi: 10.1016/j.cbi.2016.11.007.

Bianchini, G., Balko, J. M., Mayer, Ingrid, A., Sanders, M. E. and Gianni, L. (2016) 'Triple-negative breast cancer: challenges and opportunities of a heterogeneous disease', *Nature Reviews Clinical Oncology*, 13(11), pp. 674–690. doi: 10.1021/acsnano.5b07425.Molecular.

Binh, D. V., Thanh, T. T. and Chi, P. V. (2010) 'Proteomic characterization of the thermostable toxins from naja naja venom', *Journal of Venomous Animals and Toxins Including Tropical Diseases*, 16(4), pp. 631–638. doi: 10.1590/S1678-91992010000400014.

Black, J., Menderes, G., Bellone, S., Schwab, C. L., Bonazzoli, E., Ferrari, F., Predolini, F., De Haydu, C., Cocco, E., Buza, N., Hui, P., Wong, S., Lopez, S., Ratner, E., Silasi, D. A., Azodi, M., Litkouhi, B., Schwartz, P. E., Goedings, P., *et al.* (2016) 'Syd985, a novel duocarmycin-based her2-targeting antibody-drug conjugate, shows antitumor activity in uterine serous carcinoma with her2/neu expression', *Molecular Cancer Therapeutics*, 15(8), pp. 1900–1909. doi: 10.1158/1535-7163.MCT-16-0163.

Blandin, A. F., Renner, G., Lehmann, M., Lelong-Rebel, I., Martin, S. and Dontenwill, M. (2015) 'ß1 Integrins As Therapeutic Targets To Disrupt Hallmarks of Cancer', *Frontiers in Pharmacology*, 6(NOV), pp. 1–10. doi: 10.3389/fphar.2015.00279.

Bonelli, S., Geeraerts, X., Bolli, E., Keirsse, J., Kiss, M., Pombo Antunes, A. R., Van Damme, H., De Vlaminck, K., Movahedi, K., Laoui, D., Raes, G. and Van Ginderachter, J. A. (2018) 'Beyond the M-CSF receptor - novel therapeutic targets in tumor-associated macrophages.', *The FEBS journal*. England, 285(4), pp. 777–787. doi: 10.1111/febs.14202.

Bonnier, F., Keating, M. E., Wróbel, T. P., Majzner, K., Baranska, M., Garcia-Munoz, A., Blanco, A. and Byrne, H. J. (2015) 'Cell viability assessment using the Alamar blue assay: A comparison of 2D and 3D cell culture models', *Toxicology in Vitro*. Elsevier Ltd, 29(1), pp. 124–131. doi: 10.1016/j.tiv.2014.09.014.

Borcherding, N., Kusner, D., Liu, G. H. and Zhang, W. (2014) 'ROR1, an embryonic protein with an emerging role in cancer biology', *Protein and Cell*, 5(7), pp. 496–502. doi: 10.1007/s13238-014-0059-7.

Borza, C. M. and Pozzi, A. (2014) 'Discoidin domain receptors in disease', *Matrix Biology*. International Society of Matrix Biology, 34, pp. 185–192. doi: 10.1016/j.matbio.2013.12.002.

Bottrall, J. L., Madaras, F., Biven, C. D., Venning, M. G. and Mirtschin, P. J. (2010) 'Proteolytic activity of Elapid and Viperid Snake venoms and its implication to digestion.', *Journal of venom research*, 1, pp. 18–28. Available at: http://www.ncbi.nlm.nih.gov/pubmed/21544178%0Ahttp://www.pubmedcentral.nih.gov/articlerender.fcgi?artid=PMC3086185.

Boucher, J., Kleinridders, A. and Kahn, C. R. (2014) 'Insulin Receptor Signaling in Normal', *Cold Spring Harb Perspect Biol 2014*, 6, p. a009191. doi: 10.1101/cshperspect.a009191.

Boulay, A., Breuleux, M., Stephan, C., Fux, C., Brisken, C., Fiche, M., Wartmann, M., Stumm, M., Lane, H. A. and Hynes, N. E. (2008) 'The ret receptor tyrosine kinase pathway functionally interacts with the ERα pathway in breast cancer', *Cancer Research*, 68(10), pp. 3743–3751. doi: 10.1158/0008-5472.CAN-07-5100.

Brabec, V. and Kasparkova, J. (2005) 'Modifications of DNA by platinum complexes: Relation to resistance of tumors to platinum antitumor drugs', *Drug Resistance Updates*, 8, pp. 131–146. doi: 10.1016/j.drup.2005.04.006.

Bradshaw, M. J., Saviola, A. J., Fesler, E. and Mackessy, S. P. (2016) 'Evaluation of cytotoxic activities of snake venoms toward breast (MCF-7) and skin cancer (A-375) cell lines', *Cytotechnology*. Springer Netherlands, 68(4), pp. 687–700. doi: 10.1007/s10616-014-9820-2.

Brand, T. M., Iida, M. and Wheeler, D. L. (2011) 'Molecular mechanisms of resistance to the EGFR monoclonal antibody cetuximab', *Cancer Biology and Therapy*, 11, pp. 777–792. doi: 10.4161/cbt.11.9.15050.

Brandes, F., Schmidt, K., Wagner, C., Redekopf, J., Schlitt, H. J., Geissler, E. K. and Lang, S. A. (2015) 'Targeting cMET with INC280 impairs tumour growth and improves efficacy of gemcitabine in a pancreatic cancer model', *BMC Cancer*, 15(1), pp. 1–14. doi: 10.1186/s12885-015-1064-9.

Brandsma, A. M., Bondza, S., Evers, M., Koutstaal, R., Nederend, M., Marco Jansen, J. H., Rösner, T., Valerius, T., Leusen, J. H. W. and Ten Broeke, T. (2019) 'Potent Fc receptor signaling by IgA leads to superior killing of cancer cells by neutrophils compared to IgG', *Frontiers in Immunology*, 10(APR). doi: 10.3389/fimmu.2019.00704.

Brantley-Sieders, D. M., Jiang, A., Sarma, K., Badu-Nkansah, A., Walter, D. L., Shyr, Y. and Chen, J. (2011) 'Eph/ephrin profiling in human breast cancer reveals significant associations

between expression level and clinical outcome', *PLoS ONE*, 6(9), pp. 1–9. doi: 10.1371/journal.pone.0024426.

Brewer, M. R., Yun, C. H., Lai, D., Lemmon, M. A., Eck, M. J. and Pao, W. (2013) 'Mechanism for activation of mutated epidermal growth factor receptors in lung cancer', *Proceedings of the National Academy of Sciences of the United States of America*, 110(38). doi: 10.1073/pnas.1220050110.

Brewster, A., Chavez-MacGregor, M. and Brown, P. (2014) 'Epidemiology, biology, and treatment of triple-negative breast cancer in women of African ancestry', *The Lancet Oncology*, 15(13), pp. e625–e634. doi: 10.1016/j.physbeh.2017.03.040.

Brideau, C., Gunter, B., Pikounis, B. and Liaw, A. (2003) 'Improved statistical methods for hit selection in high-throughput screening', *Journal of Biomolecular Screening*, 8(6), pp. 634–647. doi: 10.1177/1087057103258285.

Bringans, S., Eriksen, S., Kendrick, T., Gopalakrishnakone, P., Livk, A., Lock, R. and Lipscombe, R. (2008) 'Proteomic analysis of the venom of Heterometrus longimanus (Asian black scorpion)', *Proteomics*, 8(5), pp. 1081–1096. doi: 10.1002/pmic.200700948.

Bubien, J. K., Ji, H. L., Gillespie, G. Y., Fuller, C. M., Markert, J. M., Mapstone, T. B. and Benos, D. J. (2004) 'Cation selectivity and inhibition of malignant glioma Na+ channels by Psalmotoxin 1', *American Journal of Physiology - Cell Physiology*, 287(5 56-5), pp. 1–32. doi: 10.1152/ajpcell.00077.2004.

Bulk, E., Yu, J., Hascher, A., Koschmieder, S., Wiewrodt, R., Krug, U., Timmermann, B., Marra, A., Hillejan, L., Wiebe, K., Berdel, W. E., Schwab, A. and Müller-Tidow, C. (2012) 'Mutations of the EPHB6 Receptor Tyrosine Kinase Induce a Pro-Metastatic Phenotype in Non-Small Cell Lung Cancer', *PLoS ONE*, 7(12), pp. 1–9. doi: 10.1371/journal.pone.0044591.

Burden, S. J. (2002) 'Building the vertebrate neuromuscular synapse', *Journal of Neurobiology*, 53(4), pp. 501–511. doi: 10.1002/neu.10137.

Van Der Burg, S. H., Arens, R., Ossendorp, F., Van Hall, T. and Melief, C. J. M. (2016) 'Vaccines for established cancer: Overcoming the challenges posed by immune evasion', *Nature Reviews Cancer*. Nature Publishing Group, 16(4), pp. 219–233. doi: 10.1038/nrc.2016.16.

Burgess, A. W. (2008) 'EGFR family: structure physiology signalling and therapeutic targets.', *Growth factors (Chur, Switzerland)*, 26(October), pp. 263–274. doi: 10.1080/08977190802312844.

Burrell, K. and Zadeh, G. (2012) *Molecular Mechanisms of Tumor Angiogenesis*, *Tumour Angiogenesis*. doi: 10.1177/1947601911432334.

Bush, S. P., King, B. O., Norris, R. L. and Stockwell, S. A. (2001) 'Centipede envenomation', *Wilderness and Environmental Medicine*. Elsevier, 12, pp. 93–99. doi: 10.1580/1080-6032(2001)012.

Caballero, O. L. and Chen, Y. T. (2009) 'Cancer/testis (CT) antigens: Potential targets for immunotherapy', *Cancer Science*, 100(11), pp. 2014–2021. doi: 10.1111/j.1349-7006.2009.01303.x.

Cailleau, R., Olivé, M. and Cruciger, Q. V. J. (1978) 'Long-Term Human Breast Carcinoma Cell Lines of Metastatic Origin : Preliminary Characterization', *In vitro*, 14(11), pp. 911–915. Available at: http://www.ncbi.nlm.nih.gov/pubmed/730202.

Cairns, R. a, Harris, I. S. and Mak, T. W. (2011) 'Regulation of cancer cell metabolism.', *Nature reviews. Cancer*. Nature Publishing Group, 11(FebruAry), pp. 85–95. doi: 10.1038/nrc2981.

Calderon, L. A., Sobrinho, J. C., Zaqueo, K. D., Moura, A. A. De, Grabner, A. N., Mazzi, M. V,

Marcussi, S., Nomizo, A., Fernandes, C. F. C., Zuliani, J. P., Carvalho, B. M. A., Silva, S. L., Stábeli, R. G. and Soares, A. M. (2014) 'Antitumaral Activities of Snake Venom Proteins: New Trends in Cancer Therapy', *Biomed Research International*, 2014, pp. 1–19.

Caliskan, F., Ergene, E., Sogut, I., Hatipoglu, I., Basalp, A., Sivas, H. and Kanbak, G. (2013) 'Biological assays on the effects of Acra3 peptide from Turkish scorpion Androctonus crassicauda venom on a mouse brain tumor cell line (BC3H1) and production of specific monoclonal antibodies', *Toxicon*. Elsevier Ltd, 76, pp. 350–361. doi: 10.1016/j.toxicon.2013.09.009.

Calvez, H. Le, Mountzouris, J. and Gramatikoff, K. (2005) *Drug delivery principles and applications*, *Journal of Chemical Information and Modeling*. doi: 10.1017/CBO9781107415324.004.

Cardoso, H. J., Figueira, M. I. and Socorro, S. (2017) 'The stem cell factor (SCF)/c-KIT signalling in testis and prostate cancer', *Journal of Cell Communication and Signaling*. Journal of Cell Communication and Signaling, 11(4), pp. 297–307. doi: 10.1007/s12079-017-0399-1.

Carlomagno, F. (2012) 'Thyroid Cancer: Role of RET and Beyond', *European Thyroid Journal*, 1(1), pp. 15–23. doi: 10.1159/000336975.

Carmeliet, P. and Jain, R. K. (2011) 'Molecular mechanisms and clinical applications of angiogenesis', *Nature*, 473(7347), pp. 298–307. doi: 10.1016/S0140-6736(01)91146-8.

Carter, P. (2001) 'Improving the efficacy of antibody-based cancer therapies', *Nature Reviews Cancer*, 1(November), pp. 118–129.

De Carvalho, D. D., Schmitmeier, S., Novello, J. C. and Markland, F. S. (2001) 'Effect of BJcuL (a lectin from the venom of the snake Bothrops jararacussu) on adhesion and growth of tumor and endothelial cells', *Toxicon*, 39(10), pp. 1471–1476. doi: 10.1016/S0041-0101(01)00106-4.

Castaño, A. and Maurer, M. S. (2015) 'ALTernative Telomere Maintenance and Cancer', *Trends in Cancer*, 20(2), pp. 163–178. doi: 10.1007/s10741-014-9462-7.Natural.

Castaño, J., Davalos, V., Schwartz, S. and Arango, D. (2008) 'EPH receptors in cancer', *Histology and Histopathology*, 23(8), pp. 1011–1023. doi: 10.14670/HH-23.1011.

Cataldo, Vince D, Gibbons, D. L., Pérez-Soler, R. and Quintás-Cardama, A. (2011) 'Treatment of non-small-cell lung cancer with erlotinib or gefitinib.', *The New England journal of medicine*, 364, pp. 947–955. doi: 10.1056/NEJMct0807960.

Cataldo, Vince D., Gibbons, D. L., Pérez-Soler, R. and Quintás-Cardama, A. (2011) 'Treatment of non-small-cell lung cancer with erlotinib or gefitinib', *New England Journal of Medicine*, 364(10), pp. 947–955. doi: 10.1056/NEJMct0807960.

Catena, R., Luis-Ravelo, D., Antón, I., Zandueta, C., Salazar-Colocho, P., Larzábal, L., Calvo, A. and Lecanda, F. (2011) 'PDGFR Signaling blockade in marrow stroma impairs lung cancer bone metastasis', *Cancer Research*, 71(1), pp. 164–174. doi: 10.1158/0008-5472.CAN-10-1708.

Cavallo, F., De Giovanni, C., Nanni, P., Forni, G. and Lollini, P. L. (2011) '2011: The immune hallmarks of cancer', *Cancer Immunology, Immunotherapy*, 60, pp. 319–326. doi: 10.1007/s00262-010-0968-0.

Cazet, A., Lefebvre, J., Adriaenssens, E., Julien, S., Bobowski, M., Grigoriadis, A., Tutt, A., Tulasne, D., Le Bourhis, X. and Delannoy, P. (2010) 'GD3 synthase expression enhances proliferation and tumor growth of MDA-MB-231 breast cancer cells through c-met activation', *Molecular Cancer Research*, 8(11), pp. 1526–1535. doi: 10.1158/1541-7786.MCR-10-0302.

Cesare, A. J. and Reddel, R. R. (2010) 'Alternative lengthening of telomeres: Models, mechanisms and implications', *Nature Reviews Genetics*. Nature Publishing Group, 11(5), pp.

319–330. doi: 10.1038/nrg2763.

Le Cesne, A., Ouali, M., Leahy, M. G., Santoro, A., Hoekstra, H. J., Hohenberger, P., Van Coevorden, F., Rutkowski, P., Van Hoesel, R., Verweij, J., Bonvalot, S., Steward, W. P., Gronchi, A., Hogendoorn, P. C. W., Litiere, S., Marreaud, S., Blay, J. Y. and Van Der Graaf, W. T. A. (2014) 'Doxorubicin-based adjuvant chemotherapy in soft tissue sarcoma: Pooled analysis of two STBSG-EORTC phase III clinical trials', *Annals of Oncology*. Elsevier Masson SAS, 25(12), pp. 2425–2432. doi: 10.1093/annonc/mdu460.

Chaabane, W., User, S. D., El-Gazzah, M., Jaksik, R., Sajjadi, E., Rzeszowska-Wolny, J. and Łos, M. J. (2013) 'Autophagy, apoptosis, mitoptosis and necrosis: Interdependence between those pathways and effects on cancer', *Archivum Immunologiae et Therapiae Experimentalis*, 61(1), pp. 43–58. doi: 10.1007/s00005-012-0205-y.

Chacón, R. D. and Costanzo, M. V (2010) 'Triple-negative breast cancer', *Breast Cancer Research*, 12(Suppl 2), pp. 1–9. doi: 10.1016/j.breast.2007.11.031.

Chaim-Matyas, A., Borkow, G. and Ovadia, M. (1991) 'Isolation and characterization of a cytotoxin P4 from the venom of Naja nigricollis nigricollis preferentially active on tumor cells', *Biochemistry International*, 24(3), pp. 415–421. doi: 10.1145/2505515.2507827.

Chaisakul, J., Hodgson, W. C., Kuruppu, S. and Prasongsook, N. (2016) 'Effects of animal venoms and toxins on hallmarks of cancer', *Journal of Cancer*, 7(11), pp. 1571–1578. doi: 10.7150/jca.15309.

Chalhoub, N. and Baker, S. J. (2009) 'PTEN and the PI3-kinase pathway in cancer.', *Annual review of pathology*, 4(1), pp. 127–150. doi: 10.1146/annurev.pathol.4.110807.092311.

Challa-Malladi, M., Lieu, Y. K., Califano, O., Holmes, A. B., Bhagat, G., Murty, V. V., Dominguez-Sola, D., Pasqualucci, L. and Dalla-Favera, R. (2011) 'Combined Genetic Inactivation of β2-Microglobulin and CD58 Reveals Frequent Escape from Immune Recognition in Diffuse Large B Cell Lymphoma', *Cancer Cell*. Elsevier Inc., 20(6), pp. 728–740. doi: 10.1016/j.ccr.2011.11.006.

Chambers, M. C., Maclean, B., Burke, R., Amodei, D., Ruderman, D. L., Neumann, S., Gatto, L., Fischer, B., Pratt, B., Egertson, J., Hoff, K., Kessner, D., Tasman, N., Schlman, N., Frewen, B., Baker, T. A., Brusniak, M. Y., Paulse, C., Creasy, D., *et al.* (2012) 'A Cross-platform Toolkit for Mass Spectrometry and Proteomics', *Nature Biotechnology*, 30(10), pp. 918–920. doi: 10.1038/nbt.2377.A.

Chames, P., Van Regenmortel, M., Weiss, E. and Baty, D. (2009) 'Therapeutic antibodies: Successes, limitations and hopes for the future', *British Journal of Pharmacology*, 157(2), pp. 220–233. doi: 10.1111/j.1476-5381.2009.00190.x.

Chan, D. L. H., Segelov, E., Wong, R. S. H., Smith, A., Herbertson, R. A., Li, B. T., Tebbutt, N., Price, T. and Pavlakis, N. (2017) 'Epidermal growth factor receptor (EGFR) inhibitors for metastatic colorectal cancer', *Cochrane Database of Systematic Reviews*, 2017(6). doi: 10.1002/14651858.CD007047.pub2.

Chang, C. H., Chung, C. H., Hsu, C. C., Peng, H. C. and Huang, T. F. (2014) 'Inhibitory effects of polypeptides derived from a snake venom C-type lectin, aggretin, on tumor cell-induced platelet aggregation', *Journal of Thrombosis and Haemostasis*, 12(4), pp. 540–549. doi: 10.1111/jth.12519.

Chang, H. R., Glaspy, J., Allison, M. A., Kass, F. C., Elashoff, R., Chung, D. U. and Gornbein, J. (2010) 'Differential response of triple-negative breast cancer to a docetaxel and carboplatin-based neoadjuvant treatment', *Cancer*, 116(18), pp. 4227–4237. doi: 10.1002/cncr.25309.

Chau, W. K., Ip, C. K., Mak, A. S. C., Lai, H. C. and Wong, A. S. T. (2013) 'C-Kit mediates

chemoresistance and tumor-initiating capacity of ovarian cancer cells through activation of Wnt/β-catenin-ATP-binding cassette G2 signaling', *Oncogene*, 32(22), pp. 2767–2781. doi: 10.1038/onc.2012.290.

Chen, H. I. and Sudol, M. (1995) 'The WW domain of Yes-associated protein binds a proline-rich ligand that differs from the consensus established for Src homology 3-binding modules', *Proceedings of the National Academy of Sciences of the United States of America*, 92(17), pp. 7819–7823. doi: 10.1073/pnas.92.17.7819.

Chen, H. M., Tsai, C. H. and Hung, W. C. (2015) 'Foretinib inhibits angiogenesis, lymphangiogenesis and tumor growth of pancreatic cancer in vivo by decreasing VEGFR-2/3 and TIE-2 signaling', *Oncotarget*, 6(17), pp. 14940–14952. doi: 10.18632/oncotarget.3613.

Chen, H. X. and Sharon, E. (2013) 'IGF-1R as an anti-cancer target-trials and tribulation', *Chinese Journal of Cancer*, 32(5), pp. 242–252. doi: 10.5732/cjc.012.10263.

Chen, J., Kinoshita, T., Sukbuntherng, J., Chang, B. Y. and Elias, L. (2016) 'Ibrutinib inhibits ERBB receptor tyrosine kinases and HER2-amplified breast cancer cell growth', *Molecular Cancer Therapeutics*, 15(12), pp. 2835–2844. doi: 10.1158/1535-7163.MCT-15-0923.

Chen, K. C., Kao, P. H., Lin, S. R. and Chang, L. Sen (2009) 'Upregulation of Fas and FasL in taiwan cobra phospholipase A 2-treated human neuroblastoma SK-N-SH cells through ROS- And Ca 2+-mediated p38 MAPK activation', *Journal of Cellular Biochemistry*, 106(1), pp. 93–102. doi: 10.1002/jcb.21979.

Cheng, H., Chua, V., Liao, C., Purwin, T. J., Terai, M., Kageyama, K., Davies, M. A., Sato, T. and Aplin, A. E. (2017) 'Co-Targeting HGF/cMET Signaling with MEK Inhibitors in metastatic uveal melanoma', *Molecular Cancer Therapeutics*, 16(3), pp. 516–528. doi: 10.1158/1535-7163.MCT-16-0552.

Cherki, R. S., Kolb, E., Langut, Y., Tsveyer, L., Bajayo, N. and Meir, A. (2014) 'Two tarantula venom peptides as potent and differential NaV channels blockers', *Toxicon*. Elsevier Ltd, 77, pp. 58–67. doi: 10.1016/j.toxicon.2013.10.029.

Chiang, C. L. L., Benencia, F. and Coukos, G. (2010) 'Whole tumor antigen vaccines', *Seminars in Immunology*. Elsevier Ltd, 22(3), pp. 132–143. doi: 10.1016/j.smim.2010.02.004.

Chien, C. M., Yang, S. H., Yang, C. C., Chang, L. Sen and Lin, S. R. (2008) 'Cardiotoxin III induces c-jun N-terminal kinase-dependent apoptosis in HL-60 human leukaemia cells', *Cell biochemistry and function*, 26, pp. 111–118. doi: 10.1002/cbf.

Chien, H. P., Ueng, S. H., Chen, S. C., Chang, Y. S., Lin, Y. C., Lo, Y. F., Chang, H. K., Chuang, W. Y., Huang, Y. T., Cheung, Y. C., Shen, S. C. and Hsueh, C. (2016) 'Expression of ROR1 has prognostic significance in triple negative breast cancer', *Virchows Archiv*, 468(5), pp. 589–595. doi: 10.1007/s00428-016-1911-3.

Chiou, J. T., Shi, Y. J., Wang, L. J., Huang, C. H., Lee, Y. C. and Chang, L. Sen (2019) 'Naja atra cardiotoxin 3 elicits autophagy and apoptosis in u937 human leukemia cells through the Ca2+/PP2A/AMPK Axis', *Toxins*, 11(9). doi: 10.3390/toxins11090527.

Chiu, S. T., Chang, K. J., Ting, C. H., Shen, H. C., Li, H. and Hsieh, F. J. (2009) 'Over-expression of EphB3 enhances cell-cell contacts and suppresses tumor growth in HT-29 human colon cancer cells', *Carcinogenesis*, 30(9), pp. 1475–1486. doi: 10.1093/carcin/bgp133.

Chmielecki, J., Ross, J. S., Wang, K., Frampton, G. M., Palmer, G. A., Ali, S. M., Palma, N., Morosini, D., Miller, V. A., Yelensky, R., Lipson, D. and Stephens, P. J. (2015) 'Oncogenic Alterations in ERBB2/HER2 Represent Potential Therapeutic Targets Across Tumors From Diverse Anatomic Sites of Origin', *The Oncologist*, 20(1), pp. 7–12. doi: 10.1634/theoncologist.2014-0234.

Chockalingam, S. and Ghosh, S. S. (2014) 'Macrophage colony-stimulating factor and cancer: a review.', *Tumour biology : the journal of the International Society for Oncodevelopmental Biology and Medicine*. United States, 35(11), pp. 10635–10644. doi: 10.1007/s13277-014-2627-0.

Choi, K. E., Hwang, C. J., Gu, S. M., Park, M. H., Kim, J. H., Park, J. H., Ahn, Y. J., Kim, J. Y., Song, M. J., Song, H. S., Han, S. B. and Hong, J. T. (2014) 'Cancer cell growth inhibitory effect of bee venom via increase of death receptor 3 expression and inactivation of NF-kappa B in NSCLC cells', *Toxins*, 6(8), pp. 2210–2228. doi: 10.3390/toxins6082210.

Choudary, K. B. (2012) 'Antibody engineering and immunoconjugates for cancer therapy', *Internation journal of pharmaceutical sciences and research*, 3(10), pp. 3618–3629.

Choudhary, C. and Mann, M. (2010) 'Decoding signalling networks by mass spectrometry-based proteomics', *Nature Reviews Molecular Cell Biology*. Nature Publishing Group, 11(6), pp. 427–439. doi: 10.1038/nrm2900.

Choudhury, S. R., Gomes, Aparna, Gomes, Antony, Dattagupta, J. K. and Sen, U. (2006) 'Purification, crystallization and preliminary X-ray structural studies of a 7.2 kDa cytotoxin isolated from the venom of Daboia russelli russelli of the Viperidae family', *Acta Crystallographica Section F: Structural Biology and Crystallization Communications*, 62(3), pp. 292–294. doi: 10.1107/S1744309106005963.

Chua, H. H., Yeh, T. H., Wang, Y. P., Huang, Y. T., Sheen, T. S., Lo, Y. C., Chou, Y. C. and Tsai, C. H. (2008) 'UPREGULATION OF DISCOIDIN DOMAIN RECEPTOR 2 IN NASOPHARYNGEAL CARCINOMA', *Head and Neck*, pp. 427–436. doi: 10.1002/HED.

Chukkapalli, S., Amessou, M., Dilly, A. K., Dekhil, H., Zhao, J., Liu, Q., Bejna, A., Thomas, R. D., Bandyopadhyay, S., Bismar, T. A., Neill, D., Azoulay, L., Batist, G. and Kandouz, M. (2014) 'Role of the EphB2 receptor in autophagy, apoptosis and invasion in human breast cancer cells', *Experimental Cell Research*. Elsevier, 320(2), pp. 233–246. doi: 10.1016/j.yexcr.2013.10.022.

Chung, C. H., Chang, C. H., Hsu, C. C., Lin, K. T., Peng, H. C. and Huang, T. F. (2017) 'Aggretin Venom Polypeptide as a Novel Anti-angiogenesis Agent by Targeting Integrin alpha2beta1', *Scientific Reports*. Nature Publishing Group, 7(March), pp. 1–11. doi: 10.1038/srep43612.

Citri, A., Skaria, K. B. and Yarden, Y. (2003) 'The deaf and the dumb: The biology of ErbB-2 and ErbB-3', *Experimental Cell Research*, 284(1), pp. 54–65. doi: 10.1016/S0014-4827(02)00101-5.

Cochrane, D. R., Bernales, S., Jacobsen, B. M., Cittelly, D. M., Howe, E. N., D'Amato, N. C., Spoelstra, N. S., Edgerton, S. M., Jean, A., Guerrero, J., Gómez, F., Medicherla, S., Alfaro, I. E., McCullagh, E., Jedlicka, P., Torkko, K. C., Thor, A. D., Elias, A. D., Protter, A. A., *et al.* (2014) 'Role of the androgen receptor in breast cancer and preclinical analysis of enzalutamide', *Breast Cancer Research*, 16(1), pp. 1–19. doi: 10.1186/bcr3599.

Cohen, B. D., Baker, D. A., Soderstrom, C., Tkalcevic, G., Rossi, A. M., Miller, P. E., Tengowski, M. W., Wang, F., Gualberto, A., Beebe, J. S. and Moyer, J. D. (2005) 'Combination therapy enhances the inhibition of tumor growth with the fully human anti-type 1 insulin-like growth factor receptor monoclonal antibody CP-751,871', *Clinical Cancer Research*, 11(5), pp. 2063–2073. doi: 10.1158/1078-0432.CCR-04-1070.

Cohen, M. H., Johnson, J. R., Chen, Y., Sridhara, R. and Pazdur, R. (2005) ' FDA Drug Approval Summary: Erlotinib (Tarceva ®) Tablets ', *The Oncologist*, 10(7), pp. 461–466. doi: 10.1634/theoncologist.10-7-461.

Cohen, M. H., Williams, G. A., Sridhara, R., Chen, G. and Pazdur, R. (2003) ' FDA Drug Approval Summary: Gefitinib (ZD1839) (Iressa ®) Tablets ', *The Oncologist*, 8(4), pp. 303–306. doi: 10.1634/theoncologist.8-4-303.

Cohen, S. and Carpenter, G. (1975) 'Human Epidermal Growth Factor: Isolation and Chemical and Biological Properties', *PNAS*, 72(4), pp. 1317–1321.

Cole, C., Lau, S., Backen, A., Clamp, A., Rushton, G., Dive, C., Hodgkinson, C., McVey, R., Kitchener, H. and Jayson, G. C. (2010) 'Inhibition of FGFR2 and FGFR1 increases cisplatin sensitivity in ovarian cancer', *Cancer Biology and Therapy*, 10(5), pp. 495–504. doi: 10.4161/cbt.10.5.12585.

Conde, R., Zamudio, F. Z., Becerril, B. and Possani, L. D. (1999) 'Phospholipin, a novel heterodimeric phospholipase A2 from Pandinus imperator scorpion venom', *FEBS Letters*, 460(3), pp. 447–450. doi: 10.1016/S0014-5793(99)01392-7.

Conlon, J. M., Prajeep, M., Mechkarska, M., Arafat, K., Attoub, S., Adem, A., Pla, D. and Calvete, J. J. (2014) 'Peptides with in vitro anti-tumor activity from the venom of the Eastern green mamba, Dendroaspis angusticeps (Elapidae).', *Journal of venom research*, 5, pp. 16–21.

Cooper, O., Vlotides, G., Fukuoka, H., Greene, M. I. and Melmed, S. (2011) 'Expression and function of ErbB receptors and ligands in the pituitary', *Endocrine-Related Cancer*, 18(6), pp. 197–211. doi: 10.1530/ERC-11-0066.

Cornelissen, B. and Vallis, K. A. (2010) 'Targeting the Nucleus: An Overview of Auger-Electron Radionuclide Therapy', *Current Drug Discovery Technologies*, 7(4), pp. 263–279. doi: 10.2174/157016310793360657.

Corsa, C. A. S., Brenot, A., Grither, W. R., Van Hove, S., Loza, A. J., Zhang, K., Ponik, S. M., Liu, Y., DeNardo, D. G., Eliceiri, K. W., Keely, P. J. and Longmore, G. D. (2016) 'The Action of Discoidin Domain Receptor 2 in Basal Tumor Cells and Stromal Cancer-Associated Fibroblasts Is Critical for Breast Cancer Metastasis', *Cell Reports*. The Author(s), 15(11), pp. 2510–2523. doi: 10.1016/j.celrep.2016.05.033.

Costa, D. B. and Kobayashi, S. S. (2015) 'Whacking a mole-cule: Clinical activity and mechanisms of resistance to third generation EGFR inhibitors in EGFR mutated lung cancers with EGFR-T790M', *Translational Lung Cancer Research*, 4(6), pp. 809–815. doi: 10.3978/j.issn.2218-6751.2015.05.05.

Costa, T. R., Menaldo, D. L., Oliveira, C. Z., Santos-Filho, N. A., Teixeira, S. S., Nomizo, A., Fuly, A. L., Monteiro, M. C., de Souza, B. M., Palma, M. S., Stábeli, R. G., Sampaio, S. V. and Soares, A. M. (2008) 'Myotoxic phospholipases A2 isolated from Bothrops brazili snake venom and synthetic peptides derived from their C-terminal region: Cytotoxic effect on microorganism and tumor cells', *Peptides*, 29(10), pp. 1645–1656. doi: 10.1016/j.peptides.2008.05.021.

Costa, T. R., Menaldo, D. L., Prinholato da Silva, C., Sorrechia, R., de Albuquerque, S., Pietro, R. C. L. R., Ghisla, S., Greggi Antunes, L. M. and Sampaio, S. V. (2015) 'Evaluating the microbicidal, antiparasitic and antitumor effects of CR-LAAO from Calloselasma rhodostoma venom', *International Journal of Biological Macromolecules*. Elsevier B.V., 80, pp. 489–497. doi: 10.1016/j.ijbiomac.2015.07.004.

Couturier, O., Supiot, S., Degraef-Mougin, M., Faivre-Chauvet, A., Carlier, T., Chatal, J. F., Davodeau, F. and Cherel, M. (2005) 'Cancer radioimmunotherapy with alpha-emitting nuclides', *European Journal of Nuclear Medicine and Molecular Imaging*, 32(5), pp. 601–614. doi: 10.1007/s00259-005-1803-2.

Cox, K. J., Shomin, C. D. and Ghosh, I. (2011) 'Tinkering outside the kinase ATP box: Allosteric (type IV) and bivalent (type V) inhibitors of protein kinases', *Future Medicinal Chemistry*, 3(1), pp. 29–43. doi: 10.4155/fmc.10.272.

Cravatt, B. F., Simon, G. M. and Yates, J. R. (2007) 'The biological impact of mass-spectrometry-based proteomics', *Nature*, 450(7172), pp. 991–1000. doi: 10.1038/nature06525.

Crespo, J., Sun, H., Welling, T. H., Tian, Z. and Zou, W. (2013) 'T cell anergy, exhaustion, senescence and stemness in the tumor microenvironment', *Current Opinion in Immunology*, 25(2), pp. 214–221. doi: 10.1038/jid.2014.371.

Crusz, S. M. and Balkwill, F. R. (2015) 'Inflammation and cancer: Advances and new agents', *Nature Reviews Clinical Oncology*, 12(10), pp. 584–596. doi: 10.1038/nrclinonc.2015.105.

Cui, B., Zhang, S., Chen, L., Yu, J., Widhopf, G. F., Fecteau, J. F., Rassenti, L. Z. and Kipps, T. J. (2013) 'Targeting ROR1 inhibits epithelial-mesenchymal transition and metastasis', *Cancer Research*, 73(12), pp. 3649–3660. doi: 10.1158/0008-5472.CAN-12-3832.

Curigliano, G., Viale, G., Ghioni, M., Jungbluth, A. A., Bagnardi, V., Spagnoli, G. C., NevilleM, A. M., Nolè, F., Rotmensz, N. and Goldhirsch, A. (2011) 'Cancer-testis antigen expression in triple-negative breast cancer', *Annals of Oncology*, 22(1), pp. 98–103. doi: 10.1093/annonc/mdq325.

Van Cutsem, E., Sagaert, X., Topal, B., Haustermans, K. and Prenen, H. (2016) 'Gastric cancer', *The Lancet*. Elsevier Ltd, 388(10060), pp. 2654–2664. doi: 10.1016/S0140-6736(16)30354-3.

D'Suze, G., Rosales, A., Salazar, V. and Sevcik, C. (2010) 'Apoptogenic peptides from Tityus discrepans scorpion venom acting against the SKBR3 breast cancer cell line', *Toxicon*. Elsevier Ltd, 56(8), pp. 1497–1505. doi: 10.1016/j.toxicon.2010.09.008.

Dacic, S., Luvison, A., Evdokimova, V., Kelly, L., Siegfried, J. M., Villaruz, L. C., Socinski, M. A. and Nikiforov, Y. E. (2014) 'RET rearrangements in lung adenocarcinoma and radiation', *Journal of Thoracic Oncology*. International Association for the Study of Lung Cancer, 9(1), pp. 118–120. doi: 10.1097/JTO.0000000000000015.

Dahle, J., Abbas, N., S. Bruland, O. and H. Larsen, R. (2012) 'Toxicity and Relative Biological Effectiveness of Alpha Emitting Radioimmunoconjugates', *Current Radiopharmaceuticalse*, 4(4), pp. 321–328. doi: 10.2174/1874471011104040321.

Dai, X., Cheng, H., Bai, Z. and Li, J. (2017) 'Breast cancer cell line classification and Its relevance with breast tumor subtyping', *Journal of Cancer*, 8(16), pp. 3131–3141. doi: 10.7150/jca.18457.

Dal Corso, A., Gébleux, R., Murer, P., Soltermann, A. and Neri, D. (2017) 'A non-internalizing antibody-drug conjugate based on an anthracycline payload displays potent therapeutic activity in vivo', *Journal of Controlled Release*, 264, pp. 211–218. doi: 10.1016/j.jconrel.2017.08.040.

Damelin, M., Geles, K. G., Follettie, M. T., Yuan, P., Baxter, M., Golas, J., DiJoseph, J. F., Karnoub, M., Huang, S., Diesl, V., Behrens, C., Choe, S. E., Rios, C., Gruzas, J., Sridharan, L., Dougher, M., Kunz, A., Hamann, P. R., Evans, D., *et al.* (2011) 'Delineation of a cellular hierarchy in lung cancer reveals an oncofetal antigen expressed on tumor-initiating cells', *Cancer Research*, 71(12), pp. 4236–4246. doi: 10.1158/0008-5472.CAN-10-3919.

Damiani, R. M., Moura, D. J., Viau, C. M., Caceres, R. A., Henriques, J. A. P. and Saffi, J. (2016) 'Pathways of cardiac toxicity: comparison between chemotherapeutic drugs doxorubicin and mitoxantrone', *Archives of Toxicology*. Springer Berlin Heidelberg, 90(9), pp. 2063–2076. doi: 10.1007/s00204-016-1759-y.

Dang, C. V, Hamaker, M., Sun, P., Le, A. and Gao, P. (2011) 'Therapeutic targeting of cancer cell metabolism', *J Mol Med (Berl)*, 89(3), pp. 205–212. doi: 10.1007/s00109-011-0730-x.Therapeutic.

Das, T., Bhattacharya, S., Biswas, A., Gupta, S. Das, Gomes, Antony and Gomes, Aparna (2013) 'Inhibition of leukemic U937 cell growth by induction of apoptosis, cell cycle arrest and suppression of VEGF, MMP-2 and MMP-9 activities by cytotoxin protein NN-32 purified from Indian spectacled cobra (Naja naja) venom', *Toxicon*. Elsevier Ltd, 65, pp. 1–4. doi: 10.1016/j.toxicon.2013.01.004.

Das, T., Bhattacharya, S., Halder, B., Biswas, A., Das Gupta, S., Gomes, Antony and Gomes, Aparna (2011) 'Cytotoxic and antioxidant property of a purified fraction (NN-32) of Indian Naja naja venom on Ehrlich ascites carcinoma in BALB/c mice', *Toxicon*. Elsevier Ltd, 57(7–8), pp. 1065–1072. doi: 10.1016/j.toxicon.2011.04.012.

Dashivets, T., Stracke, J., Dengl, S., Knaupp, A., Pollmann, J., Buchner, J. and Schlothauer, T. (2016) 'Oxidation in the complementarity-determining regions differentially influences the properties of therapeutic antibodies', *mAbs*. Taylor & Francis, 8(8), pp. 1525–1535. doi: 10.1080/19420862.2016.1231277.

Davis, N. M., Sokolosky, M., Stadelman, K., Abrams, S. L., Libra, M., Candido, S., Nicoletti, F., Polesel, J., Maestro, R., D'Assoro, A., Drobot, L., Rakus, D., Gizak, A., Laidler, P., Dulinska-Litewka, J., Basecke, J., Mijatovic, S., Maksimovic-Ivanic, D., Montalto, G., *et al.* (2014) 'Deregulation of the EGFR/PI3K/PTEN/Akt/mTORC1 pathway in breast cancer: Possibilities for therapeutic intervention', *Oncotarget*, 5(13), pp. 4603–4650. doi: 10.18632/oncotarget.2209.

Day, K. C., Hiles, G. L., Kozminsky, M., Dawsey, S. J., Paul, A., Broses, L. J., Shah, R., Kunja, L. P., Hall, C., Palanisamy, N., Daignault-Newton, S., El-Sawy, L., Wilson, S. J., Chou, A., Ignatoski, K. W., Keller, E., Thomas, D., Nagrath, S., Morgan, T., *et al.* (2017) 'HER2 and EGFR overexpression support metastatic progression of prostate cancer to bone', *Cancer Research*, 77(1), pp. 74–85. doi: 10.1158/0008-5472.CAN-16-1656.

Debebe, Z. and Rathmell, W. K. (2015) 'Ror2 as a therapeutic target in cancer', *Pharmacology and Therapeutics*. Elsevier Inc., 150, pp. 143–148. doi: 10.1016/j.pharmthera.2015.01.010.

Debnath, A., Chatterjee, U., Das, M., Vedasiromoni, J. R. and Gomes, A. (2007) 'Venom of Indian monocellate cobra and Russell's viper show anticancer activity in experimental models', *Journal of Ethnopharmacology*, 111(3), pp. 681–684. doi: 10.1016/j.jep.2006.12.027.

Debnath, A., Saha, A., Gomes, Antony, Biswas, S., Chakrabarti, P., Giri, B., Biswas, A. K., Gupta, S. Das and Gomes, Aparna (2010) 'A lethal cardiotoxic-cytotoxic protein from the Indian monocellate cobra (Naja kaouthia) venom', *Toxicon*. Elsevier Ltd, 56(4), pp. 569–579. doi: 10.1016/j.toxicon.2010.05.016.

Dejmek, J., Leandersson, K., Manjer, J., Bjartell, A., Emdin, S. O., Vogel, W. F., Landberg, G. and Andersson, T. (2005) 'Expression and Signaling Activity of Wnt-5a/Discoidin Domain Receptor-1 and Syk Plays Distinct but Decisive Roles in Breast Cancer Patient Survival', *Clinical Cancer Research*, 11(2), pp. 520–528.

Demont, Y., Corbet, C., Page, A., Ataman-Önal, Y., Choquet-Kastylevsky, G., Fliniaux, I., Le Bourhis, X., Toillon, R. A., Bradshaw, R. A. and Hondermarck, H. (2012) 'Pro-nerve growth factor induces autocrine stimulation of breast cancer cell invasion through tropomyosin-related kinase A (TrkA) and sortilin protein', *Journal of Biological Chemistry*, 287(3), pp. 1923–1931. doi: 10.1074/jbc.M110.211714.

Devilard, E., Bladou, F., Ramuz, O., Karsenty, G., Dalès, P., Gravis, G., Nguyen, C., Bertucci, F., Xerri, L. and Birnbaum, D. (2006) 'FGFR1 and WT1 are markers of human prostate cancer progression', *BMC Cancer*, 6(272), pp. 1–11. doi: 10.1186/1471-2407-6-272.

DeVita, V. T. and Chu, E. (2008) 'A history of cancer chemotherapy', *Cancer Research*, 68(21), pp. 8643–8653. doi: 10.1158/0008-5472.CAN-07-6611.

Díaz-García, A., Morier-Díaz, L., Frión-Herrera, Y., Rodríguez-Sánchez, H., Caballero-Lorenzo, Y., Mendoza-Llanes, D., Riquenes-Garlobo, Y. and Fraga-Castro, J. A. (2013) 'In vitro anticancer effect of venom from Cuban scorpion Rhopalurus junceus against a panel of human cancer cell lines.', *Journal of venom research*, 4, pp. 5–12. Available at: http://www.ncbi.nlm.nih.gov/pubmed/23946884%0Ahttp://www.pubmedcentral.nih.gov/articlerender.fcgi?artid=PMC3717326.

Díaz-García, A., Ruiz-Fuentes, J. L., Rodríguez-Sánchez, H. and Fraga Castro, J. A. (2017) 'Rhopalurus junceus scorpion venom induces apoptosis in the triple negative human breast cancer cell line MDA-MB-231.', *Journal of venom research*, 8, pp. 9–13. Available at: http://www.ncbi.nlm.nih.gov/pubmed/29285349%0Ahttp://www.pubmedcentral.nih.gov/articlerender.fcgi?artid=PMC5735679.

Díaz-Zaragoza, M., Hernández-Ávila, R., Viedma-Rodríguez, R., Arenas-Aranda, D. and Ostoa-Saloma, P. (2015) 'Natural and adaptive IgM antibodies in the recognition of tumor-associated antigens of breast cancer (Review)', *Oncology Reports*, 34(3), pp. 1106–1114. doi: 10.3892/or.2015.4095.

Diepenbruck, M. and Christofori, G. (2016) 'Epithelial-mesenchymal transition (EMT) and metastasis: Yes, no, maybe?', *Current Opinion in Cell Biology*. Elsevier Ltd, 43, pp. 7–13. doi: 10.1016/j.ceb.2016.06.002.

DiLillo, D. J. and Ravetch, J. V. (2015) 'Fc-receptor interactions regulate both cytotoxic and immunomodulatory therapeutic antibody effector functions', *Cancer Immunology Research*, 3(7), pp. 704–713. doi: 10.1158/2326-6066.CIR-15-0120.

Ding, D., Guo, Y. R., Wu, R. L., Qi, W. Y. and Xu, H. M. (2016) 'Two new isoquinoline alkaloids from Scolopendra subspinipes mutilans induce cell cycle arrest and apoptosis in human glioma cancer U87 cells', *Fitoterapia*. Elsevier B.V., 110, pp. 103–109. doi: 10.1016/j.fitote.2016.03.004.

Ding, J., Chua, P. J., Bay, B. H. and Gopalakrishnakone, P. (2014) 'Scorpion venoms as a potential source of novel cancer therapeutic compounds', *Experimental Biology and Medicine*, 239(4), pp. 387–393. doi: 10.1177/1535370213513991.

Dittrich, A., Gautrey, H., Browell, D. and Tyson-Capper, A. (2014) 'The HER2 Signaling Network in Breast Cancer—Like a Spider in its Web', *Journal of Mammary Gland Biology and Neoplasia*, 19(3–4), pp. 253–270. doi: 10.1007/s10911-014-9329-5.

Diz Filho, E. B. S., Marangoni, S., Toyama, D. O., Fagundes, F. H. R., Oliveira, S. C. B., Fonseca, F. V., Calgarotto, A. K., Joazeiro, P. P. and Toyama, M. H. (2009) 'Enzymatic and structural characterization of new PLA2 isoform isolated from white venom of Crotalus durissus ruruima', *Toxicon*. Elsevier Ltd, 53(1), pp. 104–114. doi: 10.1016/j.toxicon.2008.10.021.

Donato, N. J., Martin, C. A., Perez, M., Newman, R. A., Vidal, J. C. and Etcheverry, M. (1996) 'Regulation of epidermal growth factor receptor activity by crotoxin, a snake venom phospholipase A2 toxin: A novel growth inhibitory mechanism', *Biochemical Pharmacology*, 51(11), pp. 1535–1543. doi: 10.1016/0006-2952(96)00097-4.

Dong, M. W. (2006) *Modern HPLC for Practicing Scientists*, *Modern HPLC for Practicing Scientists*. doi: 10.1002/0471973106.

Dongo, Y., Cardoso, F. C. and Lewis, R. J. (2019) 'Spider knottin pharmacology at voltage-gated sodium channels and their potential to modulate pain Pathways', *Toxins*, 11(11). doi: 10.3390/toxins11110626.

Downs-Canner, S., Magge, D., Ravindranathan, R., O'Malley, M. E., Francis, L., Liu, Z., Sheng Guo, Z., Obermajer, N. and Bartlett, D. L. (2016) 'Complement Inhibition: A Novel Form of Immunotherapy for Colon Cancer', *Annals of Surgical Oncology*, 23(2), pp. 655–662. doi: 10.1245/s10434-015-4778-7.

Drilon, A., Siena, S., Ou, S.-H. I., Patel, M., Ahn, M. J., Lee, J., Bauer, T. M., Farago, A. F., Wheler, J. J., Liu, S. V, Doebele, R., Giannetta, L., Cerea, G., Marrapese, G., Schirru, M., Amatu, A., Bencardino, K., Palmeri, L., Sartore-Bianchi, A., *et al.* (2017) 'Safety and Antitumor Activity of the Multi-Targeted Pan-TRK, ROS1, and ALK Inhibitor Entrectinib (RXDX-101): Combined Results from Two Phase 1 Trials (ALKA-372-001 and STARTRK-1)', *Cancer Discovery*, 74(4),

pp. 400–409. doi: 10.1097/CCM.0b013e31823da96d.Hydrogen.

Du, F. Le, Eckhardt, B. L., Lim, B., Litton, J. K., Moulder, S., Meric-Bernstam, F., Gonzalez-Angulo, A. M. and Ueno, N. T. (2015) 'Is the future of personalized therapy in triple-negative breast cancer based on molecular subtype?', *Oncotarget*, 6(15), pp. 12890–12908. doi: 10.18632/oncotarget.3849.

Du, Q., Hou, X., Ge, L., Li, R., Zhou, M., Wang, H., Wang, L., Wei, M., Chen, T. and Shaw, C. (2014) 'Cationicity-enhanced analogues of the antimicrobial peptides, AcrAP1 and AcrAP2, from the venom of the scorpion, Androctonus crassicauda, display potent growth modulation effects on human cancer cell lines', *International Journal of Biological Sciences*, 10(10), pp. 1097–1107. doi: 10.7150/ijbs.9859.

Du, Z. and Lovly, C. M. (2018) 'Mechanisms of receptor tyrosine kinase activation in cancer', *Molecular Cancer*. Molecular Cancer, 17(1), pp. 1–13. doi: 10.1186/s12943-018-0782-4.

Dubovskii, P. V and Utkin, Y. N. (2015) 'Antiproliferative Activity of Cobra Venom Cytotoxins', *Current Topics in Medicinal Chemistry*, 15, pp. 638–648.

Dufies, M., Jacquel, A., Belhacene, N., Robert, G., Cluzeau, T., Luciano, F., Cassuto, J. P., Raynaud, S. and Auberger, P. (2011) 'Mechanisms of AXL overexpression and function in imatinib-resistant chronic myeloid leukemia cells', *Oncotarget*, 2(11), pp. 874–885. doi: 10.18632/oncotarget.360.

Dungo, R. T. and Keating, G. M. (2013) 'Afatinib: First global approval', *Drugs*, 73(13), pp. 1503–1515. doi: 10.1007/s40265-013-0111-6.

Dutt, A., Ramos, A. H., Hammerman, P. S., Mermel, C., Cho, J., Sharifnia, T., Chande, A., Tanaka, K. E., Stransky, N., Greulich, H., Gray, N. S. and Meyerson, M. (2011) 'Inhibitor-sensitive fgfr1 amplification in human non-small cell lung cancer', *PLoS ONE*, 6(6), pp. 1–10. doi: 10.1371/journal.pone.0020351.

Dutt, A., Salvesen, H. B., Chen, T. H., Ramos, A. H., Onofrio, R. C., Hatton, C., Nicoletti, R., Winckler, W., Grewal, R., Hanna, M., Wyhs, N., Ziaugra, L., Richter, D. J., Trovik, J., Engelsen, I. B., Stefansson, I. M., Fennell, T., Cibulskis, K., Zody, M. C., *et al.* (2008) 'Drug-sensitive FGFR2 mutations in endometrial carcinoma', *Proceedings of the National Academy of Sciences of the United States of America*, 105(25), pp. 8713–8717. doi: 10.1073/pnas.0803379105.

Dyason, K., Brandt, W., Prendini, L., Verdonck, F., Tytgat, J., Du Plessis, J., Müller, G. and Van Der Walt, J. (2002) 'Determination of species-specific components in the venom of Parabuthus scorpions from southern Africa using matrix-assisted laser desorption time-of-flight mass spectrometry', *Rapid Communications in Mass Spectrometry*, 16(8), pp. 768–773. doi: 10.1002/rcm.637.

Easty, D. J., Hill, S. P., Hsu, M., Fallowfield, M. E., Florenes, V. A., Herlyn, M. and Bennett, D. C. (1999) 'Up-regulation of ephrin-a1 during melanoma progression', *International Journal of Cancer*, 84(5), pp. 494–501. doi: 10.1002/(sici)1097-0215(19991022)84:5<494::aid-ijc8>3.3.co;2-f.

Ebrahim, K., Shirazi, F. H., Mirakabadi, A. Z. and Vatanpour, H. (2015) 'Cobra venom cytotoxins; Apoptotic or necrotic agents?', *Toxicon*. Elsevier Ltd, 108, pp. 134–140. doi: 10.1016/j.toxicon.2015.09.017.

Ebrahim, K., Shirazi, F. H., Vatanpour, H., Zare, A., Kobarfard, F. and Rabiei, H. (2014) 'Anticancer activity of cobra venom polypeptide, Cytotoxin-II, against human breast adenocarcinoma cell line (MCF-7) via the induction of apoptosis', *Journal of Breast Cancer*, 17(4), pp. 314–322. doi: 10.4048/jbc.2014.17.4.314.

Ebrahim, K., Vatanpour, H., Zare, A., Shirazi, F. H. and Nakhjavani, M. (2016) 'Anticancer

activity a of caspian cobra (Naja naja oxiana) snake venom in human cancer cell lines via induction of apoptosis', *Iranian Journal of Pharmaceutical Research*, 15, pp. 101–112. doi: 10.22037/ijpr.2016.1811.

Endres, N. F., Barros, T., Cantor, A. J. and Kuriyan, J. (2014) 'Emerging concepts in the regulation of the EGF receptor and other receptor tyrosine kinases', *Trends in Biochemical Sciences*. Elsevier Ltd, 39(10), pp. 437–446. doi: 10.1016/j.tibs.2014.08.001.

Erickson, H. K. and Lambert, J. M. (2012) 'ADME of antibody-maytansinoid conjugates', *AAPS Journal*, 14(4), pp. 799–805. doi: 10.1208/s12248-012-9386-x.

Ersahin, T., Tuncbag, N. and Cetin-Atalay, R. (2015) 'PI3K/AKT/mTOR Interactive Pathway', *Molecular biosystems*, 11(7), pp. 1946–1954. doi: 10.1039/x0xx00000x.

Erzurumlu, Y., Petras, D., Goçmen, B., Hempel, B.-F., Heiss, P., Yildiz, M. Z., Süssmuth, R. D. and Nalbantsoy, A. (2017) 'Apoptotic Effects of Mount Bulgar Viper (Montivipera bulgardaghica) PLA2 and SVMPs Venom Peptide fractions on HeLa and A549 Cancer Cells', *Proceedings*, 1(10), p. 1049. doi: 10.3390/proceedings1101049.

Escoubas, P. and King, G. F. (2009) 'Venomics as a drug discovery platform', *Expert Review of Proteomics*, 3(3), pp. 1–6.

Escoubas, P. and Rash, L. (2004) 'Tarantulas: Eight-legged pharmacists and combinatorial chemists', *Toxicon*, 43(5), pp. 555–574. doi: 10.1016/j.toxicon.2004.02.007.

Fadaka, A., Ajiboye, B., Ojo, O., Adewale, O., Olayide, I. and Emuowhochere, R. (2017) 'Biology of glucose metabolization in cancer cells', *Journal of Oncological Sciences*. Elsevier Ltd, 3(2), pp. 45–51. doi: 10.1016/j.jons.2017.06.002.

Fagan, D. H., Uselman, R. R., Sachdev, D. and Yee, D. (2012) 'Acquired resistance to tamoxifen is associated with loss of the type I insulin-like growth factor receptor: Implications for breast cancer treatment', *Cancer Research*, 72(13), pp. 3372–3380. doi: 10.1158/0008-5472.CAN-12-0684.

Fakhri, A., Omranipour, R., Fakhri, S., Mirshamsi, M., Zangeneh, F., Vatanpour, H. and Pourahmad, J. (2017) 'Naja naja oxiana venom fraction selectively induces ros-mediated apoptosis in human colorectal tumor cells by directly targeting mitochondria', *Asian Pacific Journal of Cancer Prevention*, 18(8), pp. 2201–2208. doi: 10.22034/APJCP.2017.18.8.2201.

Farooqi, A. A. and Siddik, Z. H. (2015) 'Platelet-derived growth factor (PDGF) signalling in cancer: rapidly emerging signalling landscape', *Cell biochemistry and function*, 33(5), pp. 257–265. doi: 10.1002/cbf.3120.

Fenton, T. R., Garrett, M. D., Wass, M. N. and Michaelis, M. (2018) 'What really matters - response and resistance in cancer therapy', *Cancer Drug Resistance*. doi: 10.20517/cdr.2018.19.

Feofanov, A. V., Sharonov, G. V., Astapova, M. V., Rodionov, D. I., Utkin, Y. N. and Arseniev, A. S. (2005) 'Cancer cell injury by cytotoxins from cobra venom is mediated through lysosomal damage', *Biochemical Journal*, 390(1), pp. 11–18. doi: 10.1042/BJ20041892.

Ferguson, L. R., Chen, H., Collins, A. R., Connell, M., Damia, G., Dasgupta, S., Malhotra, M., Meeker, A. K., Amedei, A., Amin, A., Ashraf, S. S., Aquilano, K., Azmi, A. S., Bhakta, D., Bilsland, A., Boosani, C. S., Chen, S., Ciriolo, M. R., Fujii, H., *et al.* (2015) 'Genomic instability in human cancer: Molecular insights and opportunities for therapeutic attack and prevention through diet and nutrition', *Seminars in Cancer Biology*. Elsevier Ltd, 35, pp. S5–S24. doi: 10.1016/j.semcancer.2015.03.005.

Ferlay, J., Colombet, M., Soerjomataram, I., Mathers, C., Parkin, D. M., Piñeros, M., Znaor, A. and Bray, F. (2019) 'Estimating the global cancer incidence and mortality in 2018: GLOBOCAN sources and methods', *International Journal of Cancer*, 144(8), pp. 1941–1953. doi:

10.1002/ijc.31937.

Ferreira, S., Greene, L., Alabaster, V., Bakhle, Y. and Vane, J. (1970) 'Activity of various fractions of bradykinin potentiating factor against angiotensin I converting enzyme', *Nature*, 225(379–380), p. 1979.

Fischer, M. and Kampen, W. U. (2012) 'Radionuclide therapy of bone metastases', *Breast Care*, 7(2), pp. 100–107. doi: 10.1159/000337634.

Foley, J., Nickerson, N., Nam, S., Allen, K. T., Gilmore, J. L., Nephew, K. P. and Riese II, D. J. (2010) 'EGFR signaling in breast cancer : Bad to the bone', *Seminars in Cell and Developmental Biology*, 21(9), pp. 951–960. doi: 10.1016/j.semcdb.2010.08.009.

Ford, C. E., Lau, S. K., Zhu, C. Q., Andersson, T., Tsao, M. S. and Vogel, W. F. (2007) 'Expression and mutation analysis of the discoidin domain receptors 1 and 2 in non-small cell lung carcinoma', *British Journal of Cancer*, 96(5), pp. 808–814. doi: 10.1038/sj.bjc.6603614.

Ford, C. E., Qian Ma, S. S., Quadir, A. and Ward, R. L. (2013) 'The dual role of the novel Wnt receptor tyrosine kinase, ROR2, in human carcinogenesis', *International Journal of Cancer*, 133(4), pp. 779–787. doi: 10.1002/ijc.27984.

Fouad, Y. A. and Aanei, C. (2017) 'Revisiting the hallmarks of cancer', *American Journal of Cancer Research*, 7(5), pp. 1016–1036.

Fox, B. P. and Kandpal, R. P. (2004) 'Invasiveness of breast carcinoma cells and transcript profile: Eph receptors and ephrin ligands as molecular markers of potential diagnostic and prognostic application', *Biochemical and Biophysical Research Communications*, 318(4), pp. 882–892. doi: 10.1016/j.bbrc.2004.04.102.

Fox, B. P. and Kandpal, R. P. (2006) 'Transcriptional silencing of EphB6 receptor tyrosine kinase in invasive breast carcinoma cells and detection of methylated promoter by methylation specific PCR', *Biochemical and Biophysical Research Communications*, 340(1), pp. 268–276. doi: 10.1016/j.bbrc.2005.11.174.

Fox, B. P. and Kandpal, R. P. (2009) 'EphB6 receptor significantly alters invasiveness and other phenotypic characteristics of human breast carcinoma cells', *Oncogene*. Nature Publishing Group, 28(14), pp. 1706–1713. doi: 10.1038/onc.2009.18.

Frasca, F., Pandini, G., Scalia, P., Sciacca, L., Mineo, R., Costantino, A., Goldfine, I. D., Belfiore, A. and Vigneri, R. (1999) 'Insulin Receptor Isoform A, a Newly Recognized, High-Affinity Insulin-Like Growth Factor II Receptor in Fetal and Cancer Cells', *Molecular and Cellular Biology*, 19(5), pp. 3278–3288. doi: 10.1128/mcb.19.5.3278.

Freidenberg, G. R., Reichart, D., Olefsky, J. M. and Henry, R. R. (1988) 'Reversibility of defective adipocyte insulin receptor kinase activity in non-insulin-dependent diabetes mellitus. Effect of weight loss', *Journal of Clinical Investigation*, 82(4), pp. 1398–1406. doi: 10.1172/JCI113744.

Freier, K., Schwaenen, C., Sticht, C., Flechtenmacher, C., Mühling, J., Hofele, C., Radlwimmer, B., Lichter, P. and Joos, S. (2007) 'Recurrent FGFR1 amplification and high FGFR1 protein expression in oral squamous cell carcinoma (OSCC)', *Oral Oncology*, 43(1), pp. 60–66. doi: 10.1016/j.oraloncology.2006.01.005.

Fu, D., Calvo, J. a and Samson, L. D. (2013) 'SERIES: Genomic instability in cancer Balancing repair and tolerance of DNA damage caused by alkylating agents', *Nature Reviews Cancer*, 12(2), pp. 104–120. doi: 10.1038/nrc3185.SERIES.

Fu, D. Y., Wang, Z. M., Wang, B. L., Chen, L., Yang, W. T., Shen, Z. Z., Huang, W. and Shao, Z. M. (2010) 'Frequent epigenetic inactivation of the receptor tyrosine kinase EphA5 by promoter methylation in human breast cancer', *Human Pathology*. Elsevier Inc., 41(1), pp. 48–58. doi:

10.1016/j.humpath.2009.06.007.

Fu, H.-L., Valiathan, R. R., Arkwright, R., Sohail, A., Mihai, C., Kimarasiri, M., Mahasenan, K. V, Mobashery, S., Huang, P., Agarwal, G. and Fridman, R. (2013) 'Discoidin Domain Receptors: Unique Receptor Tyrosine Kinases in Collagen-mediated Signaling', *Journal of Biological Chemistry*, 288(11), pp. 7430–7437. doi: 10.1074/jbc.r112.444158.

Fu, P., Du, F., Yao, M., Lv, K. and Liu, Y. (2014) 'Microrna-185 inhibits proliferation by targeting c-Met in human breast cancer cells', *Experimental and Therapeutic Medicine*, 8(6), pp. 1879–1883. doi: 10.3892/etm.2014.1999.

Fuchs, J., Weiler, S. and Meier, J. (2019) 'Envenomation by a western green mamba (Dendroaspis viridis) – A report of three episodes in Switzerland', *Toxicon*. Elsevier, 168(June), pp. 76–82. doi: 10.1016/j.toxicon.2019.06.223.

Fukai, J., Yokote, H., Yamanaka, R., Arao, T., Nishio, K. and Itakura, T. (2008) 'EphA4 promotes cell proliferation and migration through a novel EphA4-FGFR1 signaling pathway in the human glioma U251 cell line', *Molecular Cancer Therapeutics*, 7(9), pp. 2768–2778. doi: 10.1158/1535-7163.MCT-07-2263.

Furman, B. L. (2012) 'The development of Byetta (exenatide) from the venom of the Gila monster as an anti-diabetic agent', *Toxicon*. Elsevier Ltd, 59(4), pp. 464–471. doi: 10.1016/j.toxicon.2010.12.016.

Fuse, N., Kuboki, Y., Kuwata, T., Nishina, T., Kadowaki, S., Shinozaki, E., Machida, N., Yuki, S., Ooki, A., Kajiura, S., Kimura, T., Yamanaka, T., Shitara, K., Nagatsuma, A. K., Yoshino, T., Ochiai, A. and Ohtsu, A. (2016) 'Prognostic impact of HER2, EGFR, and c-MET status on overall survival of advanced gastric cancer patients', *Gastric Cancer*. Springer Japan, 19(1), pp. 183–191. doi: 10.1007/s10120-015-0471-6.

Gabriel, K., Ingram, A., Austin, R., Kapoor, A., Tang, D., Majeed, F., Qureshi, T. and Al-Nedawi, K. (2013) 'Regulation of the Tumor Suppressor PTEN through Exosomes: A Diagnostic Potential for Prostate Cancer', *PLoS ONE*, 8(7). doi: 10.1371/journal.pone.0070047.

Gabriel, L. M., Sanchez, E. F., Silva, S. G. and dos Santos, R. G. (2012) 'Tumor cytotoxicity of leucurolysin-B, a P-III snake venom metalloproteinase from Bothrops leucurus', *Journal of Venomous Animals and Toxins Including Tropical Diseases*, 18(1), pp. 24–33. doi: 10.1590/s1678-91992012000100004.

Gajewski, T. F., Woo, S. R., Zha, Y., Spaapen, R., Zheng, Y., Corrales, L. and Spranger, S. (2013) 'Cancer immunotherapy strategies based on overcoming barriers within the tumor microenvironment', *Current Opinion in Immunology*. Elsevier Ltd, 25(2), pp. 268–276. doi: 10.1016/j.coi.2013.02.009.

Gajski, G. and Garaj-Vrhovac, V. (2013) 'Melittin: A lytic peptide with anticancer properties', *Environmental Toxicology and Pharmacology*. Elsevier B.V., 36(2), pp. 697–705. doi: 10.1016/j.etap.2013.06.009.

Galán, J. A., Sánchez, E. E., Rodríguez-acosta, A., Soto, J. G., Bashir, S., Mclane, M. A., Paquette-straub, C. and Pérez, J. C. (2008) 'Inhibition of Lung Tumor Colonization and Cell Migration with the Disintegrin Crotatroxin 2 Isolated from the Venom of Crotalus atrox', *Toxicon*, 51(7), pp. 1186–1196. doi: 10.1016/j.toxicon.2008.02.004.Inhibition.

Gallant, J. N., Sheehan, J. H., Shaver, T. M., Bailey, M., Lipson, D., Chandramohan, R., Brewer, M. R., York, S. J., Kris, M. G., Pietenpol, J. A., Ladanyi, M., Miller, V. A., Ali, S. M., Meiler, J. and Lovly, C. M. (2015) 'EGFR kinase domain duplication (EGFR -KDD) is a novel oncogenic driver in lung cancer that is clinically responsive to afatinib', *Cancer Discovery*, 5(11), pp. 1155–1163. doi: 10.1158/2159-8290.CD-15-0654.

Ganguly, A. and Cabral, F. (2011) 'New insights into mechanisms of resistance to microtubule inhibitors', *Biochim Biophys Acta.*, 1816(2), pp. 164–171. doi: 10.1016/j.biotechadv.2011.08.021.Secreted.

Gao, J., Chesebrough, J. W., Cartlidge, S. A., Ricketts, S. A., Incognito, L., Veldman-Jones, M., Blakey, D. C., Tabrizi, M., Jallal, B., Trail, P. A., Coats, S., Bosslet, K. and Chang, Y. S. (2011) 'Dual IGF-I/II-neutralizing antibody MEDI-573 potently inhibits IGF signaling and tumor growth', *Cancer Research*, 71(3), pp. 1029–1040. doi: 10.1158/0008-5472.CAN-10-2274.

Gao, L., Shan, B. E., Chen, J., Liu, J. H., Song, D. X. and Zhu, B. C. (2005) 'Effects of spider Macrothele raven venom on cell proliferation and cytotoxicity in HeLa cells', *Acta Pharmacologica Sinica*, 26(3), pp. 369–376. doi: 10.1111/j.1745-7254.2005.00052.x.

Garcia-Osta, A., Tsokas, P., Pollonini, G., Landau, E. M., Blitzer, R. and Alberini, C. M. (2006) 'MuSK expressed in the brain mediates cholinergic responses, synaptic plasticity, and memory formation', *Journal of Neuroscience*, 26(30), pp. 7919–7932. doi: 10.1523/JNEUROSCI.1674-06.2006.

Garg, M., Nagata, Y., Kanojia, D., Mayakonda, A., Yoshida, K., Keloth, S. H., Zang, Z. J., Okuno, Y., Shiraishi, Y., Chiba, K., Tanaka, H., Miyano, S., Ding, L. W., Alpermann, T., Sun, Q. Y., Lin, D. C., Chien, W., Madan, V., Liu, L. Z., *et al.* (2015) 'Profiling of somatic mutations in acute myeloid leukemia with FLT3-ITD at diagnosis and relapse', *Blood*, 126(22), pp. 2491–2501. doi: 10.1182/blood-2015-05-646240.

Garofalo, M., Jeon, Y. J., Nuovo, G. J., Middleton, J., Secchiero, P., Joshi, P., Alder, H., Nazaryan, N., Di Leva, G., Romano, G., Crawford, M., Nana-Sinkam, P. and Croce, C. M. (2013) 'MiR-34a/c-Dependent PDGFR-α/β Downregulation Inhibits Tumorigenesis and Enhances TRAIL-Induced Apoptosis in Lung Cancer', *PLoS ONE*, 8(6), pp. 1–12. doi: 10.1371/journal.pone.0067581.

Garrett, J. T. and Arteaga, C. L. (2011) 'Resistance to HER2-directed antibodies and tyrosine kinase inhibitors: Mechanisms and clinical implications', *Cancer Biology and Therapy*, 11, pp. 793–800. doi: 10.4161/cbt.11.9.15045.

Garrido, F., Aptsiauri, N., Doorduijn, E. M., Garcia Lora, A. M. and van Hall, T. (2016) 'The urgent need to recover MHC class I in cancers for effective immunotherapy', *Current Opinion in Immunology*. Elsevier Ltd, 39, pp. 44–51. doi: 10.1016/j.coi.2015.12.007.

Gatenby, R. a and Gillies, R. J. (2004) 'Why do cancers have high aerobic glycolysis?', *Nature reviews. Cancer*, 4(November), pp. 891–899. doi: 10.1038/nrc1478.

Gay, C. M., Balaji, K. and Byers, L. A. (2017) 'Giving AXL the axe: targeting AXL in human malignancy.', *British journal of cancer*. England, 116(4), pp. 415–423. doi: 10.1038/bjc.2016.428.

Gay, L. M., Pavlick, D., Chung, J., Ramkissoon, S., Daniel, S., Elvin, J. A., Severson, E., Bivona, T., Reckamp, K. L., Klempner, S. J., Ou, S.-H. I., Schrock, A. B., Miller, V. A., Stephens, P. J., Ross, J. S., Ganesan, S., Lovly, C., Mansfield, A. and Ali, S. M. (2017) 'Genomic profiling of 114,200 advanced cancers identifies recurrent kinase domain duplications (KDD) and oncogenic rearrangements (RE) across diverse tumor types', *Annals of Oncology*, 28(suppl_5), pp. 595–604. doi: 10.1093/annonc/mdx391.

Genander, M. and Frisén, J. (2010) 'Ephrins and Eph receptors in stem cells and cancer', *Current Opinion in Cell Biology*, 22(5), pp. 611–616. doi: 10.1016/j.ceb.2010.08.005.

Geng, M., Cao, Y. C., Chen, Y. J., Jiang, H., Bi, L. Q. and Liu, X. H. (2012) 'Loss of Wnt5a and Ror2 protein in hepatocellular carcinoma associated with poor prognosis', *World Journal of Gastroenterology*, 18(12), pp. 1328–1338. doi: 10.3748/wjg.v18.i12.1328.

Gentile, A., Lazzari, L., Benvenuti, S., Trusolino, L. and Comoglio, P. M. (2011) 'Ror1 is a pseudokinase that is crucial for met-driven tumorigenesis', *Cancer Research*, 71(8), pp. 3132–3141. doi: 10.1158/0008-5472.CAN-10-2662.

Gerson, J. N., Skariah, S., Denlinger, C. S. and Astsaturov, I. (2017) 'Perspectives of HER2-targeting in gastric and esophageal cancer', *Expert Opinion on Investigational Drugs*, 26(5), pp. 531–540. doi: 10.1080/13543784.2017.1315406.

Geuna, E., Montemurro, F., Aglietta, M. and Valabrega, G. (2012) 'Potential of afatinib in the treatment of patients with HER2-positive breast cancer', *Breast Cancer: Targets and Therapy*, 4, pp. 131–137. doi: 10.2147/BCTT.S25868.

Ghanbari, P., Mohseni, M., Tabasinezhad, M., Yousefi, B., Saei, A. A., Sharifi, S., Rashidi, M. R. and Samadi, N. (2014) 'Inhibition of survivin restores the sensitivity of breast cancer cells to docetaxel and vinblastine', *Applied Biochemistry and Biotechnology*, 174(2), pp. 667–681. doi: 10.1007/s12010-014-1125-6.

Ghazaryan, N. A., Ghulikyan, L. A., Kishmiryan, A. V., Kirakosyan, G. R., Nazaryan, O. H., Ghevondyan, T. H., Zakaryan, N. A. and Ayvazyan, N. M. (2015) 'Anti-tumor effect investigation of obtustatin and crude Macrovipera lebetina obtusa venom in S-180 sarcoma bearing mice', *European Journal of Pharmacology*, 764, pp. 340–345. doi: 10.1016/j.ejphar.2015.07.011.

Ghazaryan, N., Movsisyan, N., Macedo, J. C., Vaz, S., Ayvazyan, N., Pardo, L. and Logarinho, E. (2019) 'The antitumor efficacy of monomeric disintegrin obtustatin in S-180 sarcoma mouse model', *Investigational New Drugs*. Investigational New Drugs, 37(5), pp. 1044–1051. doi: 10.1007/s10637-019-00734-2.

Ghiso, E., Migliore, C., Ciciriello, V., Morando, E., Petrelli, A., Corso, S., De Luca, E., Gatti, G., Volante, M. and Giordano, S. (2017) 'YAP-Dependent AXL Overexpression Mediates Resistance to EGFR Inhibitors in NSCLC', *Neoplasia (United States)*. The Authors, 19(12), pp. 1012–1021. doi: 10.1016/j.neo.2017.10.003.

Gianfaldoni, S., Gianfaldoni, R., Wollina, U., Lotti, J., Tchernev, G. and Lotti, T. (2017) 'An overview on radiotherapy: From its history to its current applications in dermatology', *Open Access Macedonian Journal of Medical Sciences*, 5(4 Special Issue GlobalDermatology), pp. 521–525. doi: 10.3889/oamjms.2017.122.

Giannakakou, P., Sackett, D. and Fojo, T. (2000) 'Tubulin/microtubules: Still a promising target for new chemotherapeutic agents', *Journal of the National Cancer Institute*, 92(3), pp. 182–183. doi: 10.1093/jnci/92.3.182.

Giannelli, G., Koudelkova, P., Dituri, F. and Mikulits, W. (2016) 'Role of epithelial to mesenchymal transition in hepatocellular carcinoma', *Journal of Hepatology*. European Association for the Study of the Liver, 65(4), pp. 798–808. doi: 10.1016/j.jhep.2016.05.007.

Gianolio, D. A., Rouleau, C., Bauta, W. E., Lovett, D., Cantrell, W. R., Recio, A., Wolstenholme-Hogg, P., Busch, M., Pan, P., Stefano, J. E., Kramer, H. M., Goebel, J., Krumbholz, R. D., Roth, S., Schmid, S. M. and Teicher, B. A. (2012) 'Targeting HER2-positive cancer with dolastatin 15 derivatives conjugated to trastuzumab, novel antibody-drug conjugates', *Cancer Chemotherapy and Pharmacology*, 70(3), pp. 439–449. doi: 10.1007/s00280-012-1925-8.

Giard, D. J., Aaronson, S. A., Todaro, G. J., Arnstein, P., Kersey, J. H. and Parks, W. P. (1973) 'In vitro cultivation of human tumors: Establishment of cell lines derived from a series of solid tumors', *Journal of the National Cancer Institute*, 51(5), pp. 1417–1423. doi: 10.1093/jnci/51.5.1417.

Gimenes, S. N. C., Lopes, D. S., Alves, P. T., Azevedo, F. V. P. V., Vecchi, L., Goulart, L. R., Rodrigues, T. C. S., Santos, A. L. Q., Brites, V. L. D. C., Teixeira, T. L., Da Silva, C. V., Dias, M. H., Teixeira, S. C., Rodrigues, R. S., Yoneyama, K. A. G., Oliveira, R. A. and Rodrigues, V.

D. M. (2017) ‘Antitumoral effects of γCdcPLI, a PLA2 inhibitor from Crotalus durissus collilineatus via PI3K/Akt pathway on MDA-MB-231 breast cancer cell’, *Scientific Reports*, 7(1), pp. 15–18. doi: 10.1038/s41598-017-07082-2.

Gjerdrum, C., Tiron, C., Høiby, T., Stefansson, I., Haugen, H., Sandal, T., Collett, K., Li, S., McCormack, E., Gjertsen, B. T., Micklem, D. R., Akslen, L. A., Glackin, C. and Lorens, J. B. (2010) ‘Axl is an essential epithelial-to-mesenchymal transition-induced regulator of breast cancer metastasis and patient survival’, *Proceedings of the National Academy of Sciences of the United States of America*, 107(3), pp. 1124–1129. doi: 10.1073/pnas.0909333107.

Gjerstorff, M. F., Andersen, M. H. and Ditzel, H. J. (2015) ‘Oncogenic cancer/testis antigens: Prime candidates for immunotherapy’, *Oncotarget*, 6(18), pp. 15772–15787. doi: 10.18632/oncotarget.4694.

Goetsch, L., Caussanel, V. and Corvaia, N. (2013) ‘Biological significance and targeting of c-Met tyrosine kinase receptor in cancer Liliane’, *Frontiers in Bioscience- Landmark Edition*, 18, pp. 454–473.

Gökmen-Polar, Y., Toroni, R. A., Hocevar, B. A., Badve, S., Zhao, Q., Shen, C., Bruckheimer, E., Kinch, M. S. and Miller, K. D. (2011) ‘Dual targeting of EphA2 and ER restores Tamoxifen sensitivity in ER/EphA2-positive breast cancer’, *Breast Cancer Research and Treatment*, 127(2), pp. 375–384. doi: 10.1007/s10549-010-1004-y.

Goldenberg, J., Cipriani, V., Jackson, T. N. W., Arbuckle, K., Debono, J., Dashevsky, D., Panagides, N., Ikonomopoulou, M. P., Koludarov, I., Li, B., Santana, R. C., Nouwens, A., Jones, A., Hay, C., Dunstan, N., Allen, L., Bush, B., Miles, J. J., Ge, L., *et al.* (2018) ‘Proteomic and functional variation within black snake venoms (Elapidae: Pseudechis)’, *Comparative Biochemistry and Physiology Part - C: Toxicology and Pharmacology*. Elsevier Inc, 205, pp. 53–61. doi: 10.1016/j.cbpc.2018.01.001.

Gomes, Antony, Bhattacharjee, P., Mishra, R., Biswas, A. K., Dasgupta, S. C., Giri, B., Debnath, A., Gupta, S. Das, Das, T. and Gomes, Aparna (2010) ‘Anticancer potential of animal venoms and toxins’, *Indian Journal of Experimental Biology*, 48(2), pp. 93–103.

Gomes, Antony, Choudhury, S. R., Saha, A., Mishra, R., Giri, B., Biswas, A. K., Debnath, A. and Gomes, Aparna (2007) ‘A heat stable protein toxin (drCT-I) from the Indian Viper (Daboia russelli russelli) venom having antiproliferative, cytotoxic and apoptotic activities’, *Toxicon*, 49(1), pp. 46–56. doi: 10.1016/j.toxicon.2006.09.009.

Gómez Rave, L. J., Muñoz Bravo, A. X., Sierra Castrillo, J., Román Marín, L. M. and Corredor Pereira, C. (2019) ‘Scorpion venom: New promise in the treatment of cancer’, *Acta Biologica Colombiana*, 24(2), pp. 213–223. doi: 10.15446/abc.v24n2.71512.

Govindan, S. V and Goldenberg, D. M. (2010) ‘New antibody conjugates in cancer therapy.’, *TheScientificWorldJournal*, 10, pp. 2070–2089. doi: 10.1100/tsw.2010.191.

de Gramont, A., Van Cutsem, E., Schmoll, H. J., Tabernero, J., Clarke, S., Moore, M. J., Cunningham, D., Cartwright, T. H., Hecht, J. R., Rivera, F., Im, S. A., Bodoky, G., Salazar, R., Maindrault-Goebel, F., Shacham-Shmueli, E., Bajetta, E., Makrutzki, M., Shang, A., André, T., *et al.* (2012) ‘Bevacizumab plus oxaliplatin-based chemotherapy as adjuvant treatment for colon cancer (AVANT): A phase 3 randomised controlled trial’, *The Lancet Oncology*, 13(12), pp. 1225–1233. doi: 10.1016/S1470-2045(12)70509-0.

Grashof, D. G. B., Kerkkamp, H. M. I., Afonso, S., Archer, J., Harris, D. J., Richardson, M. K., Vonk, F. J. and Van Der Meijden, A. (2019) ‘Transcriptome annotation and characterization of novel toxins in six scorpion species’, *BMC Genomics*. BMC Genomics, 20(1), pp. 1–10. doi: 10.1186/s12864-019-6013-6.

Green, J. L., Kuntz, S. G. and Sternberg, P. W. (2008) ‘Ror receptor tyrosine kinases: orphans no

more', *Trends in Cell Biology*, 18(11), pp. 536–544. doi: 10.1016/j.tcb.2008.08.006.

Green, J., Nusse, R. and van Amerongen, R. (2014) 'The role of Ryk and Ror receptor tyrosine kinases in wnt signal transduction', *Cold Spring Harbor Perspectives in Biology*, 6(2), pp. 1–12. doi: 10.1101/cshperspect.a009175.

Gru, A. A. and Allred, D. C. (2012) 'FGFR1 amplification and the progression of non-invasive to invasive breast cancer', *Breast Cancer Research*, 14(6), pp. 14–16. doi: 10.1186/bcr3340.

Grunnet, M. and Sorensen, J. B. (2012) 'Carcinoembryonic antigen (CEA) as tumor marker in lung cancer', *Lung Cancer*. Elsevier Ireland Ltd, 76(2), pp. 138–143. doi: 10.1016/j.lungcan.2011.11.012.

Guan, M., Xu, C., Zhang, F. and Ye, C. (2009) 'Aberrant methylation of EphA7 in human prostate cancer and its relation to clinicopathologic features', *International Journal of Cancer*, 124(1), pp. 88–94. doi: 10.1002/ijc.23890.

Gucalp, A., Tolaney, S., Isakoff, S. J., Ingle, J. N., Liu, M. C., Carey, L. A., Blackwell, K., Rugo, H., Nabell, L., Forero, A., Stearns, V., Doane, A. S., Danso, M., Moynahan, M. E., Momen, L. F., Gonzalez, J. M., Akhtar, A., Giri, D. D., Patil, S., *et al.* (2013) 'Phase II trial of bicalutamide in patients with androgen receptor-positive, estrogen receptor-negative metastatic breast cancer', *Clinical Cancer Research*, 19(19), pp. 5505–5512. doi: 10.1158/1078-0432.CCR-12-3327.

Guerrab, A. El, Bamdad, M., Kwiatkowski, F., Bignon, Y. J., Penault-Llorca, F. and Aubel, C. (2016) 'Anti-EGFR monoclonal antibodies and EGFR tyrosine kinase inhibitors as combination therapy for triple-negative breast cancer', *Oncotarget*, 7(45), pp. 73618–73637. doi: 10.18632/oncotarget.12037.

Guilliams, M., Bruhns, P., Saeys, Y., Hammad, H. and Lambrecht, B. N. (2014) 'The function of Fcγ receptors in dendritic cells and macrophages', *Nature Reviews Immunology*, 14(2), pp. 94–108. doi: 10.1038/nri3582.

Gullick, W. J. (2009) 'The epidermal growth factor system of ligands and receptors in cancer', *European Journal of Cancer*. Elsevier Ltd, 45, pp. 205–210. doi: 10.1016/S0959-8049(09)70035-8.

Gullick, W. J., Marsden, J. J., Whittle, N., Ward, B., Bobrow, L. and Waterfield, M. D. (1986) 'Expression of Epidermal Growth Factor Receptors on Human Cervical, Ovarian and Vulval Carcinomas', *Cancer Research*, 46(1), pp. 285–292.

Guo, S., Colbert, L. S., Fuller, M., Zhang, Y. and Gonzalez-Perez, R. R. (2010) 'Vascular Endothelial Growth Factor Receptor -2 in Breast Cancer', *Biochimica et biophysica Acta*, 1806(1), pp. 108–121. doi: 10.1038/jid.2014.371.

Guo, Y.-T., Hou, Q.-Y. and Wang, N. (2011) 'Monoclonal antibodies in cancer therapy', *Clinical Oncology and Cancer Research*, 8, pp. 215–219. doi: 10.1007/s11805-011-0583-7.

Das Gupta, S., Debnath, A., Saha, A., Giri, B., Tripathi, G., Vedasiromoni, J. R., Gomes, Antony and Gomes, Aparna (2007) 'Indian black scorpion (Heterometrus bengalensis Koch) venom induced antiproliferative and apoptogenic activity against human leukemic cell lines U937 and K562', *Leukemia Research*, 31(6), pp. 817–825. doi: 10.1016/j.leukres.2006.06.004.

Gupta, S. Das, Gomes, Antony, Debnath, A., Saha, A. and Gomes, Aparna (2010) 'Apoptosis induction in human leukemic cells by a novel protein Bengalin, isolated from Indian black scorpion venom: Through mitochondrial pathway and inhibition of heat shock proteins', *Chemico-Biological Interactions*, 183(2), pp. 293–303. doi: 10.1016/j.cbi.2009.11.006.

Gutschner, T. and Diederichs, S. (2012) 'The Hallmarks of Cancer: A long non-coding RNA point of view', *RNA Biology*, 9(June), pp. 703–719. doi: 10.4161/rna.20481.

Gutzeit, C., Chen, K. and Cerutti, A. (2018) 'The enigmatic function of IgD: some answers at last', *European Journal of Immunology*, 48(7), pp. 1101–1113. doi: 10.1002/eji.201646547.

Ha, S. Y., Lee, J., Jang, J., Hong, J. Y., Do, I. G., Park, S. H., Park, J. O., Choi, M. G., Sohn, T. S., Bae, J. M., Kim, Sung, Kim, M., Kim, Seonwoo, Park, C. K., Kang, W. K. and Kim, K. M. (2015) 'HER2-positive gastric cancer with concomitant MET and/or EGFR overexpression: A distinct subset of patients for dual inhibition therapy', *International Journal of Cancer*, 136(7), pp. 1629–1635. doi: 10.1002/ijc.29159.

Ha, S. Y., Lee, J., Kang, S. Y., Do, I. G., Ahn, S., Park, J. O., Kang, W. K., Choi, M. G., Sohn, T. S., Bae, J. M., Kim, Sung, Kim, M., Kim, Seonwoo, Park, C. K., Ignatius Ou, S. H. and Kim, K. M. (2013) 'MET overexpression assessed by new interpretation method predicts gene amplification and poor survival in advanced gastric carcinomas', *Modern Pathology*, 26(12), pp. 1632–1641. doi: 10.1038/modpathol.2013.108.

Hafner, C., Schmitz, G., Meyer, S., Bataille, F., Hau, P., Langmann, T., Dietmaier, W., Landthaler, M. and Vogt, T. (2004) 'Differential Gene Expression of Eph Receptors and Ephrins in Benign Human Tissues and Cancers', *Clinical Chemistry*, 50(3), pp. 490–499. doi: 10.1373/clinchem.2003.026849.

Halford, M. M., Macheda, M. L., Parish, C. L., Takano, E. A., Fox, S., Layton, D., Nice, E. and Stacker, S. A. (2013) 'A Fully Human Inhibitory Monoclonal Antibody to the Wnt Receptor RYK', *PLoS ONE*, 8(9), pp. 1–14. doi: 10.1371/journal.pone.0075447.

Halford, M. M. and Stacker, S. A. (2001) 'Revelations of the RYK receptor', *BioEssays*, 23(1), pp. 34–45. doi: 10.1002/1521-1878(200101)23:1<34::AID-BIES1005>3.0.CO;2-D.

Hamanaka, R. B. and Chandel, N. S. (2012) 'Targeting glucose metabolism for cancer therapy', *Journal of Experimental Medicine*, 209, pp. 211–215. doi: 10.1084/jem.20120162.

Hamilton, G., Rath, B., Klameth, L. and Hochmair, M. (2015) 'Receptor tyrosine kinase expression of circulating tumor cells in small cell lung cancer', *Oncoscience*, 2(7), pp. 629–634. doi: 10.18632/oncoscience.179.

Hamilton, R. G., MacGlashan, D. W. and Saini, S. S. (2010) 'IgE antibody-specific activity in human allergic disease', *Immunologic Research*, 47(1–3), pp. 273–284. doi: 10.1007/s12026-009-8160-3.

Hanahan, D. and Weinberg, R. a. (2011) 'Hallmarks of cancer: The next generation', *Cell*. Elsevier Inc., 144(5), pp. 646–674. doi: 10.1016/j.cell.2011.02.013.

Hanahan, D. and Weinberg, R. a (2000) 'The Hallmarks of Cancer', *Cell*, 100, pp. 57–70.

Hanawa, M., Suzuki, S., Dobashi, Y., Yamane, T., Kono, K., Enomoto, N. and Ooi, A. (2006) 'EGFR protein overexpression and gene amplification in squamous cell carcinomas of the esophagus', *International Journal of Cancer*, 118(5), pp. 1173–1180. doi: 10.1002/ijc.21454.

Hariprasad, G., Saravanan, K., Singh, S. B., Das, U., Sharma, S., Kaur, P., Singh, T. P. and Srinivasan, A. (2009) 'Group III PLA2 from the scorpion, Mesobuthus tamulus: Cloning and recombinant expression in E. coli', *Electronic Journal of Biotechnology*, 12(3). doi: 10.2225/vol12-issue3-fulltext-7.

Hariprasad, G., Singh, B., Das, U., Ethayathulla, A. S., Kaur, P., Singh, T. P. and Srinivasan, A. (2007) 'Cloning, sequence analysis and homology modeling of a novel phospholipase A2 from Heterometrus fulvipes (Indian black scorpion)', *DNA Sequence - Journal of DNA Sequencing and Mapping*, 18(3), pp. 242–246. doi: 10.1080/10425170701243294.

Hartog, H., Wesseling, J., Boezen, H. M. and van der Graaf, W. T. A. (2007) 'The insulin-like growth factor 1 receptor in cancer: Old focus, new future', *European Journal of Cancer*, 43(13), pp. 1895–1904. doi: 10.1016/j.ejca.2007.05.021.

Harvey, A. L. (2014) 'Toxins and drug discovery', *Toxicon*. Elsevier Ltd, 92, pp. 193–200. doi: 10.1016/j.toxicon.2014.10.020.

Hatzis, C., Pusztai, L., Valero, V., Booser, D. J., Esserman, L., Lluch, A., Vidaurre, T., Holmes, F., Souchon, E., Wang, H., Martin, M., Cotrina, J., Gomez, H., Hubbard, R., Chacón, J. I., Ferrer-Lozano, J., Dyer, R., Buxton, M., Gong, Y., *et al.* (2011) 'A genomic predictor of response and survival following taxane-anthracycline chemotherapy for invasive breast cancer', *JAMA - Journal of the American Medical Association*, 305(18), pp. 1873–1881. doi: 10.1001/jama.2011.593.

Hayashi, M. A. F., Nascimento, F. D., Kerkis, A., Oliveira, V., Oliveira, E. B., Pereira, A., Rádis-Baptista, G., Nader, H. B., Yamane, T., Kerkis, I. and Tersariol, I. L. S. (2008) 'Cytotoxic effects of crotamine are mediated through lysosomal membrane permeabilization', *Toxicon*, 52(3), pp. 508–517. doi: 10.1016/j.toxicon.2008.06.029.

He, X., Lee, K. S., Kim, B. Y., Lee, K. Y., Ko, H. J., Jia, J., Yoon, H. J. and Jin, B. R. (2019) 'Centipede (Scolopendra subspinipes mutilans) venom toxin peptide exhibits cytotoxic and cell growth effects in a concentration-dependent manner', *Journal of Asia-Pacific Entomology*. Elsevier, 22(1), pp. 19–24. doi: 10.1016/j.aspen.2018.11.018.

Heaphy, C. M., Subhawong, A. P., Hong, S. M., Goggins, M. G., Montgomery, E. A., Gabrielson, E., Netto, G. J., Epstein, J. I., Lotan, T. L., Westra, W. H., Shih, I. M., Iacobuzio-Donahue, C. A., Maitra, A., Li, Q. K., Eberhart, C. G., Taube, J. M., Rakheja, D., Kurman, R. J., Wu, T. C., *et al.* (2011) 'Prevalence of the alternative lengthening of telomeres telomere maintenance mechanism in human cancer subtypes', *American Journal of Pathology*, 179(4), pp. 1608–1615. doi: 10.1016/j.ajpath.2011.06.018.

Heck, A. J. R. and Van Den Heuvel, R. H. H. (2004) 'Investigation of intact protein complexes by mass spectrometry', *Mass Spectrometry Reviews*, 23(5), pp. 368–389. doi: 10.1002/mas.10081.

Hedayati, M., Zarif Yeganeh, M., Sheikholeslami, S. and Afsari, F. (2016) 'Diversity of mutations in the RET proto-oncogene and its oncogenic mechanism in medullary thyroid cancer', *Critical Reviews in Clinical Laboratory Sciences*, 53(4), pp. 217–227. doi: 10.3109/10408363.2015.1129529.

Heinen, T. E. and Gorini da Veiga, A. B. (2011) 'Arthropod venoms and cancer', *Toxicon*. Elsevier Ltd, 57(4), pp. 497–511. doi: 10.1016/j.toxicon.2011.01.002.

Heinrich, M. C., Corless, C. L., Demetri, G. D., Blanke, C. D., Von Mehren, M., Joensuu, H., McGreevey, L. S., Chen, C. J., Van Den Abbeele, A. D., Druker, B. J., Kiese, B., Eisenberg, B., Roberts, P. J., Singer, S., Fletcher, C. D. M., Silberman, S., Dimitrijevic, S. and Fletcher, J. A. (2003) 'Kinase mutations and imatinib response in patients with metastatic gastrointestinal stromal tumor', *Journal of Clinical Oncology*, 21(23), pp. 4342–4349. doi: 10.1200/JCO.2003.04.190.

Heiskanen, M., Kononen, J., Bärlund, M., Torhorst, J., Sauter, G., Kallioniemi, A. and Kallioniemi, O. (2001) 'CGH, cDNA and tissue microarray analyses implicate FGFR2 amplification in a small subset of breast tumors', *Analytical Cellular Pathology*, 22(4), pp. 229–234. doi: 10.1155/2001/981218.

Heist, R. S., Mino-Kenudson, M., Sequist, L. V., Tammireddy, S., Morrissey, L., Christiani, D. C., Engelman, J. A. and Iafrate, A. J. (2012) 'FGFR1 amplification in squamous cell carcinoma of the lung', *Journal of Thoracic Oncology*. International Association for the Study of Lung Cancer, 7(12), pp. 1775–1780. doi: 10.1097/JTO.0b013e31826aed28.

Helleday, T., Petermann, E., Lundin, C., Hodgson, B. and Sharma, R. a (2008) 'DNA repair pathways as targets for cancer therapy.', *Nature reviews. Cancer*, 8(march), pp. 193–204. doi: 10.1038/nrc2342.

Henry, C., Llamosas, E., Knipprath-Meszaros, A., Schoetzau, A., Obermann, E., Fuenfschilling, M., Caduff, R., Fink, D., Hacker, N., Ward, R., Heinzelmann-Schwarz, V. and Ford, C. (2015) 'Targeting the ROR1 and ROR2 receptors in epithelial ovarian cancer inhibits cell migration and invasion', *Oncotarget*, 6(37), pp. 40310–40326. doi: 10.18632/oncotarget.5643.

Henry, C., Quadir, A., Hawkins, N. J., Jary, E., Llamosas, E., Kumar, D., Daniels, B., Ward, R. L. and Ford, C. E. (2014) 'Expression of the novel Wnt receptor ROR2 is increased in breast cancer and may regulate both β-catenin dependent and independent Wnt signalling', *Journal of Cancer Research and Clinical Oncology*, 141(2), pp. 243–254. doi: 10.1007/s00432-014-1824-y.

Herath, N. I., Spanevello, M. D., Sabesan, S., Newton, T., Cummings, M., Duffy, S., Lincoln, D., Boyle, G., Parsons, P. G. and Boyd, A. W. (2006) 'Over-expression of Eph and ephrin genes in advanced ovarian cancer: Ephrin gene expression correlates with shortened survival', *BMC Cancer*, 6, pp. 1–7. doi: 10.1186/1471-2407-6-144.

Heskamp, S., Boerman, O. C., Molkenboer-Kuenen, J. D. M., Wauters, C. A., Strobbe, L. J. A., Mandigers, C. M. P. W., Bult, P., Oyen, W. J. G., Van Der Graaf, W. T. A. and Van Laarhoven, H. W. M. (2015) 'Upregulation of IGF-1R expression during neoadjuvant therapy predicts poor outcome in breast cancer patients', *PLoS ONE*, 10(2), pp. 1–13. doi: 10.1371/journal.pone.0117745.

Higuchi, D. A., Almeida, M. C., Barros, C. C., Sanchez, E. F., Pesquero, P. R., Lang, E. A. S., Samaan, M., Araujo, R. C., Pesquero, J. B. and Pesquero, J. L. (2011) 'Leucurogin, a new recombinant disintegrin cloned from Bothrops leucurus (white-tailed-jararaca) with potent activity upon platelet aggregation and tumor growth', *Toxicon*. Elsevier Ltd, 58(1), pp. 123–129. doi: 10.1016/j.toxicon.2011.05.013.

Hilchie, A. L., Sharon, A. J., Haney, E. F., Hoskin, D. W., Bally, M. B., Franco, O. L., Corcoran, J. A. and Hancock, R. E. W. (2016) 'Mastoparan is a membranolytic anti-cancer peptide that works synergistically with gemcitabine in a mouse model of mammary carcinoma', *Biochimica et Biophysica Acta - Biomembranes*. Elsevier B.V., 1858(12), pp. 3195–3204. doi: 10.1016/j.bbamem.2016.09.021.

Hirsch, F. R., Scagliotti, G. V., Mulshine, J. L., Kwon, R., Curran, W. J., Wu, Y. L. and Paz-Ares, L. (2017) 'Lung cancer: current therapies and new targeted treatments', *The Lancet*, 389(10066), pp. 299–311. doi: 10.1016/S0140-6736(16)30958-8.

Ho-Yen, C. M., Green, A. R., Rakha, E. A., Brentnall, A. R., Ellis, I. O., Kermorgant, S. and Jones, J. L. (2014) 'C-Met in invasive breast cancer: Is there a relationship with the basal-like subtype?', *Cancer*, 120(2), pp. 163–171. doi: 10.1002/cncr.28386.

Ho-Yen, C. M., Jones, J. L. and Kermorgant, S. (2015) 'The clinical and functional significance of c-Met in breast cancer: A review', *Breast Cancer Research*, 17(1), pp. 1–11. doi: 10.1186/s13058-015-0547-6.

Hoch, W., Mcconville, J., Helms, S., Newsom-Davis, J., Melms, A. and Vincent, A. (2001) 'Auto-antibodies to the receptor tyrosine kinase MuSK in patients with myasthenia gravis without acetylcholine receptor antibodies', *Nature Medicine*, 7(3), pp. 365–368. doi: 10.1038/85520.

Hoesl, C., Röhrl, J. M., Schneider, M. R. and Dahlhoff, M. (2018) 'The receptor tyrosine kinase ERBB4 is expressed in skin keratinocytes and influences epidermal proliferation', *Biochimica et Biophysica Acta - General Subjects*, 1862(4), pp. 958–966. doi: 10.1016/j.bbagen.2018.01.017.

Hofmann, F. and García-Echeverría, C. (2005) 'Blocking the insulin-like growth factor-I receptor as a strategy for targeting cancer', *Drug Discovery Today*, 10(15), pp. 1041–1047. doi: 10.1016/S1359-6446(05)03512-9.

Hojjat-Farsangi, M., Moshfegh, A., Daneshmanesh, A. H., Khan, A. S., Mikaelsson, E.,

Osterborg, A. and Mellstedt, H. (2014) 'The receptor tyrosine kinase ROR1 – An oncofetal antigen for targeted cancer therapy', *Seminars in Cancer Biology*. Elsevier Ltd, 29, pp. 21–31. doi: 10.1016/j.semcancer.2014.07.005.

Hojjat-Farsangi, M., Moshfegh, A., Daneshmanesh, A. H., Khan, A. S., Mikaelsson, E., Österborg, A. and Mellstedt, H. (2014) 'The receptor tyrosine kinase ROR1 - An oncofetal antigen for targeted cancer therapy', *Seminars in Cancer Biology*. Elsevier Ltd, 29(C), pp. 21–31. doi: 10.1016/j.semcancer.2014.07.005.

Holla, V. R., Elamin, Y. Y., Bailey, A. M., Johnson, A. M., Litzenburger, B. C., Khotskaya, Y. B., Sanchez, N. S., Zeng, J., Shufean, M. A., Shaw, K. R., Mendelsohn, J., Mills, G. B., Meric-Bernstam, F. and Simon, G. R. (2017) 'ALK: a tyrosine kinase target for cancer therapy', *Molecular Case Studies*, 3(1), pp. 1–20. doi: 10.1101/mcs.a001115.

Hong, C. C., Lay, J. D., Huang, J. S., Cheng, A. L., Tang, J. L., Lin, M. T., Lai, G. M. and Chuang, S. E. (2008) 'Receptor tyrosine kinase AXL is induced by chemotherapy drugs and overexpression of AXL confers drug resistance in acute myeloid leukemia', *Cancer Letters*, 268(2), pp. 314–324. doi: 10.1016/j.canlet.2008.04.017.

Hovens, C. M., Stacker, S. A., Andres, A. C., Harpur, A. G., Ziemiecki, A. and Wilks, A. F. (1992) 'RYK, a receptor tyrosine kinase-related molecule with unusual kinase domain motifs', *Proceedings of the National Academy of Sciences of the United States of America*, 89(24), pp. 11818–11822. doi: 10.1073/pnas.89.24.11818.

Hsu, J. L. and Hung, M. C. (2016) 'The role of HER2, EGFR, and other receptor tyrosine kinases in breast cancer', *Cancer and Metastasis Reviews*, 35(4), pp. 575–588. doi: 10.1016/j.physbeh.2017.03.040.

Huang, C. W., Chen, Y. T., Tsai, H. L., Yeh, Y. S., Su, W. C., Ma, C. J., Tsai, T. N. and Wang, J. Y. (2017) 'EGFR expression in patients with stage III colorectal cancer after adjuvant chemotherapy and on cancer cell function', *Oncotarget*, 8(70), pp. 114663–114676. doi: 10.18632/oncotarget.23072.

Huang, J., Xiao, D., Li, G., Ma, J., Chen, P., Yuan, W., Hou, F., Ge, J., Zhong, M., Tang, Y., Xia, X. and Chen, Z. (2014) 'EphA2 promotes epithelial-mesenchymal transition through the Wnt/β-catenin pathway in gastric cancer cells', *Oncogene*, 33(21), pp. 2737–2747. doi: 10.1038/onc.2013.238.

Huang, L. and Fu, L. (2015) 'Mechanisms of resistance to EGFR tyrosine kinase inhibitors', *Acta Pharmaceutica Sinica B*. Elsevier, 5(5), pp. 390–401. doi: 10.1016/j.apsb.2015.07.001.

Huang, L., Wen, C., Yang, X., Lou, Q., Wang, X., Che, J., Chen, J., Yang, Z., Wu, X., Huang, M., Lan, P., Wang, L., Iwamoto, A., Wang, J. and Liu, H. (2018) 'PEAK1, acting as a tumor promoter in colorectal cancer, is regulated by the EGFR/KRas signaling axis and MIR-181d article', *Cell Death and Disease*. Springer US, 9(3). doi: 10.1038/s41419-018-0320-8.

Huang, Q., Snyder, D. S., Chu, P., Gaal, K. K., Chang, K. L. and Weiss, L. M. (2011) 'PDGFRA rearrangement leading to hyper-eosinophilia, T-lymphoblastic lymphoma, myeloproliferative neoplasm and precursor B-cell acute lymphoblastic leukemia', *Leukemia*, 25(2), pp. 371–375. doi: 10.1038/leu.2010.272.

Huang, T. F., Yeh, C. H. and Wu, W. B. (2001) 'Viper venom components affecting angiogenesis', *Haemostasis*, 31(3–6), pp. 192–206. doi: 10.1159/000048063.

Hubalek, M., Czech, T. and Müller, H. (2017) 'Biological Subtypes of Triple-Negative Breast Cancer', *Breast Care*, 12(1), pp. 8–14. doi: 10.1159/000455820.

Hubbard, S. R. and Gnanasambandan, K. (2013) 'Structure and Activation of MuSK, a Receptor Tyrosine Kinase Central to Neuromuscular Junction Formation', *Biochimica et biophysica acta*,

1834(10), pp. 2166–2169. doi: 10.1038/jid.2014.371.

Hubbard, S. R. and Miller, T. W. (2007) 'Receptor Tyrosine Kinases: Mechanisms of Activation and Signalling', *Current Opinion in Cell Biology*, 19(2), pp. 117–123. doi: 10.1016/j.ceb.2007.02.010.Receptor.

Hudis, C. A. and Gianni, L. (2011) 'Triple-Negative Breast Cancer: An Unmet Medical Need', *The Oncologist*, 16(S1), pp. 1–11. doi: 10.1634/theoncologist.2011-s1-01.

Huh, J. E., Baek, Y. H., Lee, M. H., Choi, D. Y., Park, D. S. and Lee, J. D. (2010) 'Bee venom inhibits tumor angiogenesis and metastasis by inhibiting tyrosine phosphorylation of VEGFR-2 in LLC-tumor-bearing mice', *Cancer Letters*. Elsevier Ireland Ltd, 292(1), pp. 98–110. doi: 10.1016/j.canlet.2009.11.013.

Hunter, T. (2009a) 'Tyrosine phosphorylation: thirty years and counting', *Current Opinion in Cell Biology*, 21(2), pp. 140–146. doi: 10.1016/j.ceb.2009.01.028.

Hunter, T. (2009b) 'Tyrosine phosphorylation: thirty years and counting', *Current Opinion in Cell Biology*, 21(2), pp. 140–146. doi: 10.1016/j.ceb.2009.01.028.

Hur, H., Ham, I. H., Lee, D., Jin, H., Aguilera, K. Y., Oh, H. J., Han, S. U., Kwon, J. E., Kim, Y. B., Ding, K. and Brekken, R. A. (2017) 'Discoidin domain receptor 1 activity drives an aggressive phenotype in gastric carcinoma', *BMC Cancer*. BMC Cancer, 17(1), pp. 1–11. doi: 10.1186/s12885-017-3051-9.

Huriyet, H., Cavas, T., Vatan, O. and Cinkilic, N. (2017) 'Investigation of In Vitro Cytotoxic Effects of Montivipera xanthina on Healthy and Cancer Human Lung Cell Lines', *Proceedings*, 1(10), p. 1029. doi: 10.3390/proceedings1101029.

Hynes, N. E. and MacDonald, G. (2009) 'ErbB receptors and signaling pathways in cancer', *Current Opinion in Cell Biology*, 21(2), pp. 177–184. doi: 10.1016/j.ceb.2008.12.010.

Hyuga, S., Hyuga, M., Yoshimura, M., Amakura, Y., Goda, Y. and Hanawa, T. (2013) 'Herbacetin, a constituent of ephedrae herba, suppresses the HGF-induced motility of human breast cancer MDA-MB-231 cells by inhibiting c-met and akt phosphorylation', *Planta Medica*, 79(16), pp. 1525–1530. doi: 10.1055/s-0033-1350899.

İğci, N., Nalbantsoy, A., Erkan, L. G., Akça, G. Y., Yalçın, H. T., Yalçın, M. and Göçmen, B. (2016) 'Screening of cytotoxic, anti-angiogenic, anti-tumorogenic and antimicrobial activities of anatolian vipera ammodytes (Nose-horned viper) venom', *Turkish Journal of Biochemistry*, 41(6), pp. 483–491. doi: 10.1515/tjb-2016-0195.

Iida, M., Bahrar, H., Brand, T., Pearson, H., Coan, J., Orbuch, R., Flanigan, B., Swick, A., Prabakaran, P., Lantto, J., Horak, I., Kragh, M., Salgia, R., Kimple, R. and Wheeler, D. (2016) 'Targeting the HER Family with Pan-HER Effectively Overcomes Resistance to Cetuximab', *Mol Cancer Therapy*, 15(9), pp. 2175–2186.

Iiizumi, M., Hosokawa, M., Takehara, A., Chung, S., Nakamura, T., Katagiri, T., Eguchi, H., Ohigashi, H., Ishikawa, O., Nakamura, Y. and Nakagawa, H. (2006) 'EphA4 receptor, overexpressed in pancreatic ductal adenocarcinoma, promotes cancer cell growth', *Cancer Science*, 97(11), pp. 1211–1216. doi: 10.1111/j.1349-7006.2006.00313.x.

Ikonomopoulou, M. P., Smith, J. J., Herzig, V., Pineda, S. S., Dziemborowicz, S., Er, S., Durek, T., Gilchrist, J., Alewood, P. F., Nicholson, G. M., Bosmans, F. and King, G. F. (2016) 'Isolation of two insecticidal toxins from venom of the Australian theraphosid spider Coremiocnemis tropix', *Toxicon*, 123, pp. 62–70. doi: 10.1016/j.toxicon.2016.10.013.Isolation.

Incamnoi, P., Patramanon, R., Thammasirirak, S., Chaveerach, A., Uawonggul, N., Sukprasert, S., Rungsa, P., Daduang, J. and Daduang, S. (2013) 'Heteromtoxin (HmTx), a novel heterodimeric phospholipase A 2 from Heterometrus laoticus scorpion venom', *Toxicon*, 61, pp.

62–71.

Iyer, R., Wehrmann, L., Golden, R. L., Naraparaju, K., Croucher, J. L., MacFarland, S. P., Guan, P., Kolla, V., Wei, G., Cam, N., Li, G., Hornby, Z. and Brodeur, G. M. (2016) 'Entrectinib is a Potent Inhibitor of Trk-Driven Neuroblastomas in a Xenograft Mouse Model', *Cancer Letter*, 372(2), pp. 179–186. doi: 10.1016/j.physbeh.2017.03.040.

Jackson, K. (2003) 'The evolution of venom-delivery systems in snakes', *Zoological Journal of the Linnean Society*, 137(3), pp. 337–354. doi: 10.1046/j.1096-3642.2003.00052.x.

Jackson, N. M. and Ceresa, B. P. (2016) 'Protein Kinase G facilitates EGFR-mediated cell death in MDA-MB-468 cells', *Experimental Cell Research*, 346(2), pp. 224–232. doi: 10.1016/j.yexcr.2016.07.001.

Jain, D. and Kumar, S. (2012) 'Snake Venom : A Potent Anticancer Agent', *Asian Pacific Journal of Cancer Prevention*, 13(10), pp. 4855–4860.

Jain, M. V., Paczulla, A. M., Klonisch, T., Dimgba, F. N., Rao, S. B., Roberg, K., Schweizer, F., Lengerke, C., Davoodpour, P., Palicharla, V. R., Maddika, S. and Los, M. (2013) 'Interconnections between apoptotic, autophagic and necrotic pathways: Implications for cancer therapy development', *Journal of Cellular and Molecular Medicine*, 17(1), pp. 12–29. doi: 10.1111/jcmm.12001.

Jaiswal, B. S., Kljavin, N. M., Stawiski, E. W., Chan, E., Parikh, C., Durinck, S., Chaudhuri, S., Pujara, K., Guillory, J., Edgar, K. A., Janakiraman, V., Scholz, R. P., Bowman, K. K., Lorenzo, M., Li, H., Wu, J., Yuan, W., Peters, B. A., Kan, Z., *et al.* (2013) 'Oncogenic ERBB3 Mutations in Human Cancers', *Cancer Cell*. Elsevier Inc., 23(5), pp. 603–617. doi: 10.1016/j.ccr.2013.04.012.

Jang, S. H., Choi, S. Y., Ryu, P. D. and Lee, S. Y. (2011) 'Anti-proliferative effect of Kv1.3 blockers in A549 human lung adenocarcinoma in vitro and in vivo', *European Journal of Pharmacology*. Elsevier B.V., 651, pp. 26–32. doi: 10.1016/j.ejphar.2010.10.066.

Jang, Y. J., Kim, Dong Seok, Jeon, O. H. and Kim, Doo Sik (2007) 'Saxatilin suppresses tumor-induced angiogenesis by regulating VEGF expression in NCI-H460 human lung cancer cells', *Journal of Biochemistry and Molecular Biology*, 40(3), pp. 439–443. doi: 10.5483/bmbrep.2007.40.3.439.

Jebali, J., Fakhfekh, E., Morgen, M., Srairi-Abid, N., Majdoub, H., Gargouri, A., El Ayeb, M., Luis, J., Marrakchi, N. and Sarray, S. (2014) 'Lebecin, a new C-type lectin like protein from Macrovipera lebetina venom with anti-tumor activity against the breast cancer cell line MDA-MB231', *Toxicon*. Elsevier Ltd, 86, pp. 16–27. doi: 10.1016/j.toxicon.2014.04.010.

Jechlinger, M., Sommer, A., Moriggl, R., Seither, P., Kraut, N., Capodiecci, P., Donovan, M., Cordon-Cardo, C., Beug, H. and Grünert, S. (2006) 'Autocrine PDGFR signaling promotes mammary cancer metastasis', *Journal of Clinical Investigation*, 116(6), pp. 1561–1570. doi: 10.1172/JCI24652.

Jeong, Y. J., Choi, Y., Shin, J. M., Cho, H. J., Kang, J. H., Park, K. K., Choe, J. Y., Bae, Y. S., Han, S. M., Kim, C. H., Chang, H. W. and Chang, Y. C. (2014) 'Melittin suppresses EGF-induced cell motility and invasion by inhibiting PI3K/Akt/mTOR signaling pathway in breast cancer cells', *Food and Chemical Toxicology*. Elsevier Ltd, 68, pp. 218–225. doi: 10.1016/j.fct.2014.03.022.

Ji, X. D., Li, G., Feng, Y. X., Zhao, J. S., Li, J. J., Sun, Z. J., Shi, S., Deng, Y. Z., Xu, J. F., Zhu, Y. Q., Koeffler, H. P., Tong, X. J. and Xie, D. (2011) 'EphB3 is overexpressed in non-small-cell lung cancer and promotes tumor metastasis by enhancing cell survival and migration', *Cancer Research*, 71(3), pp. 1156–1166. doi: 10.1158/0008-5472.CAN-10-0717.

Jiang, D. M., Fyles, A., Nguyen, L. T., Neel, B. G., Sacher, A., Rottapel, R., Wang, B. X., Ohashi, P. S. and Sridhar, S. S. (2019) 'Phase i study of local radiation and tremelimumab in patients with inoperable locally recurrent or metastatic breast cancer', *Oncotarget*, 10(31), pp. 2947–2958. doi: 10.18632/oncotarget.26893.

Jiang, T., Gao, G., Fan, G., Li, M. and Zhou, C. (2015) 'FGFR1 amplification in lung squamous cell carcinoma: A systematic review with meta-analysis', *Lung Cancer*, 87(1), pp. 1–7. doi: 10.1016/j.lungcan.2014.11.009.

Jo, M., Park, M. H., Kollipara, P. S., An, B. J., Song, H. S., Han, S. B., Kim, J. H., Song, M. J. and Hong, J. T. (2012) 'Anti-cancer effect of bee venom toxin and melittin in ovarian cancer cells through induction of death receptors and inhibition of JAK2/STAT3 pathway', *Toxicology and Applied Pharmacology*. Elsevier Inc., 258(1), pp. 72–81. doi: 10.1016/j.taap.2011.10.009.

Johnston, C. I., Brown, S. G. A., O'Leary, M. A., Currie, B. J., Greenberg, R., Taylor, M., Barnes, C., White, J. and Isbister, G. K. (2013) 'Mulga snake (Pseudechis australis) envenoming: A spectrum of myotoxicity, anticoagulant coagulopathy, haemolysis and the role of early antivenom therapy-Australian Snakebite Project (ASP-19)', *Clinical Toxicology*, 51(5), pp. 417–424. doi: 10.3109/15563650.2013.787535.

Jorge, R. J. B., Martins, A. M. C., Morais, I. C. O., Ximenes, R. M., Rodrigues, F. A. R., Soares, B. M., Evangelista, J. S. A. M., Toyama, M. H., Martins, A. M. A., Moraes Filho, M. O. and Monteiro, H. S. A. (2011) 'In vitro studies on Bothrops venoms cytotoxic effect on tumor cells', *Journal of Experimental Therapeutics and Oncology*, 9(3), pp. 249–253.

Jorissen, R. N., Walker, F., Pouliot, N., Garrett, T. P. J., Ward, C. W. and Burgess, A. W. (2003) 'Epidermal growth factor receptor: Mechanisms of activation and signalling', *Experimental Cell Research*, 284(1), pp. 31–53. doi: 10.1016/S0014-4827(02)00098-8.

Jover, R., Nguyen, T., Prezcarbonell, L., Zapater, P., Pay, A., Alenda, C., Rojas, E., Cubiella, J., Balaguer, F., Morillas, J. D., Clofent, J., Bujanda, L., Re, J. M., Bessa, X., Xicola, R. M., Nicolsprez, D., Castells, A., Andreu, M., Llor, X., *et al.* (2011) '5-fluorouracil adjuvant chemotherapy does not increase survival in patients with CpG island methylator phenotype colorectal cancer', *Gastroenterology*. Elsevier Inc., 140(4), pp. 1174–1181. doi: 10.1053/j.gastro.2010.12.035.

Jridi, I., Catacchio, I., Majdoub, H., Shahbazeddah, D., El Ayeb, M., Frassanito, M. A., Ribatti, D., Vacca, A. and Borchani, L. (2015) 'Hemilipin, a novel Hemiscorpius lepturus venom heterodimeric phospholipase A2, which inhibits angiogenesis in vitro and in vivo', *Toxicon*. Elsevier Ltd, 105, pp. 34–44. doi: 10.1016/j.toxicon.2015.08.022.

Kaelin, W. G. and Thompson, C. B. (2010) 'Q&A: Cancer: clues from cell metabolism.', *Nature*, 465(June), pp. 562–564. doi: 10.1038/465562a.

Kaenel, P., Mosimann, M. and Andres, A.-C. (2012) 'The multifaceted roles of Eph/ephrin signaling in breast cancer.', *Cell adhesion & migration*. United States, 6(2), pp. 138–147. doi: 10.4161/cam.20154.

Kamińska, M., Ciszewski, T., Łopacka-Szatan, K., Miotła, P. and Starosławska, E. (2015) 'Breast cancer risk factors', *Przeglad Menopauzalny*, 14(3), pp. 196–202. doi: 10.5114/pm.2015.54346.

Kampen, K. R., Scherpen, F. J. G., Garcia-Manero, G., Yang, H., Kaspers, G. J. L., Cloos, J., Zwaan, C. M., Van Den Heuvel-Eibrink, M. M., Kornblau, S. M. and De Bont, E. S. J. M. (2015) 'EphB1 suppression in acute myelogenous leukemia: Regulating the DNA damage control system', *Molecular Cancer Research*, 13(6), pp. 982–992. doi: 10.1158/1541-7786.MCR-14-0660-T.

Kang, I. C., Chung, K. H., Lee, S. J., Yun, Y., Moon, H. M. and Kim, D. S. (1998) 'Purification and molecular cloning of a platelet aggregation inhibitor from the snake (Agkistrodon halys

brevicaudus) venom', *Thrombosis Research*, 91(2), pp. 65–73. doi: 10.1016/S0049-3848(98)00053-X.

Kao, H. W., Chen, H. C., Wu, C. W. and Lin, W. C. (2003) 'Tyrosine-kinase expression profiles in human gastric cancer cell lines and their modulations with retinoic acids', *British Journal of Cancer*, 88(7), pp. 1058–1064. doi: 10.1038/sj.bjc.6600821.

Karlsson, E., Appelgren, J., Solterbeck, A., Bergenheim, M., Alvariza, V. and Bergh, J. (2014) 'Breast cancer during follow-up and progression - A population based cohort on new cancers and changed biology', *European Journal of Cancer*. Elsevier Ltd, 50(17), pp. 2916–2924. doi: 10.1016/j.ejca.2014.08.014.

Kashiwagi, S., Yashiro, M., Takashima, T., Aomatsu, N., Kawajiri, H., Ogawa, Y., Onoda, N., Ishikawa, T., Wakasa, K. and Hirakawa, K. (2013) 'C-Kit expression as a prognostic molecular marker in patients with basal-like breast cancer', *British Journal of Surgery*, 100(4), pp. 490–496. doi: 10.1002/bjs.9021.

Kato, S., Kobayashi, T., Yamada, K., Nishii, K., Sawada, H., Ishiguro, H., Itoh, M., Funahashi, H. and Nagasaka, A. (2004) 'Expression of erbB receptors mRNA in thyroid tissues.', *Biochimica et biophysica acta*. Netherlands, 1673(3), pp. 194–200. doi: 10.1016/j.bbagen.2004.04.016.

Katoh, Y. and Katoh, M. (2009) 'FGFR2-related pathogenesis and FGFR2-targeted therapeutics', *International Journal of Molecular Medicine*, 23, pp. 307–311. doi: 10.3892/ijmm.

Katso, R. M., Russell, R. B. and Ganesan, T. S. (1999) 'Functional Analysis of H-Ryk, an Atypical Member of the Receptor Tyrosine Kinase Family', *Molecular and Cellular Biology*, 19(9), pp. 6427–6440. doi: 10.1128/mcb.19.9.6427.

Katso, R. M. T., Manek, S., Ganjavi, H., Biddolph, S., Charnock, M. F. L., Bradburn, M., Wells, M. and Ganesan, T. S. (2000) 'Overexpression of H-Ryk in epithelial ovarian cancer: Prognostic significance of receptor expression', *Clinical Cancer Research*, 6(8), pp. 3271–3281.

Keating, A. K., Kim, G. K., Jones, A. E., Donson, A. M., Ware, K., Mulcahy, J. M., Salzberg, D. B., Foreman, N. K., Liang, X., Thorburn, A. and Graham, D. K. (2010) 'Inhibition of Mer and Axl receptor tyrosine kinases in astrocytoma cells leads to increased apoptosis and improved chemosensitivity', *Molecular Cancer Therapeutics*, 9(5), pp. 1298–1307. doi: 10.1158/1535-7163.MCT-09-0707.

Keegan, T. H. M., DeRouen, M. C., Press, D. J., Kurian, A. W. and Clarke, C. A. (2012) 'Occurrence of breast cancer subtypes in adolescent and young adult women', *Breast Cancer Research*, 14(2). doi: 10.1186/bcr3156.

Kelland, L. (2007) 'The resurgence of platinum-based cancer chemotherapy.', *Nature reviews. Cancer*, 7(July), pp. 573–584. doi: 10.1038/nrc2167.

Keller, J., Shroyer, K. R., Batajoo, S. K., Zhao, H. L., Dong, L. M., Hayman, M. J. and Chan, E. L. (2010) 'Combination of Phosphorylated and Truncated EGFR Correlates With Higher Tumor and Nodal Stage in Head and Neck Cancer', *Cancer Investigation*, 28(10), pp. 1054–1062. doi: 10.1161/CIRCULATIONAHA.110.956839.

Kelly, C. M. and Janjigian, Y. Y. (2016) 'The genomics and therapeutics of HER2-positive gastric cancer- from trastuzumab and beyond', *Journal of Gastrointestinal Oncology*, 7(5), pp. 750–762. doi: 10.21037/jgo.2016.06.10.

Kessenbrock, K., Plaks, V. and Werb, Z. (2010) 'Matrix Metalloproteinases: Regulators of the Tumor Microenvironment', *Cell*, 141(1), pp. 52–67. doi: 10.1016/j.cell.2010.03.015.

Kessentini-Zouari, R., Jebali, J., Taboubi, S., Srairi-Abid, N., Morjen, M., Kallech-Ziri, O., Bezzine, S., Marvaldi, J., Ayeb, M. E. L., Marrakchi, N. and Luis, J. (2010) 'CC-PLA2-1 and CC-PLA2-2, two Cerastes cerastes venom-derived phospholipases A2, inhibit angiogenesis both

in vitro and in vivo', *Laboratory Investigation*, 90(4), pp. 510–519. doi: 10.1038/labinvest.2009.137.

Khong, H. T. and Restifo, N. P. (2002) 'Natural selection of tumor variants in the generation of "tumor escape" phenotypes', *Nature Immunology*, 3(11), pp. 999–1005. Available at: https://www.ncbi.nlm.nih.gov/pmc/articles/PMC1508168/pdf/nihms10884.pdf.

Kieran, M. W., Chi, S., Goldman, S., Onar-Thomas, A., Poussaint, T. Y., Vajapeyam, S., Fahey, F., Wu, S., Turner, D. C., Stewart, C. F., Moses, M., Packer, R. J., Jakacki, R., Banerjee, A., Boyett, J. M., Fouladi, M. and Kun, L. (2015) 'A phase I trial and PK study of cediranib (AZD2171), an orally bioavailable pan-VEGFR inhibitor, in children with recurrent or refractory primary CNS tumors', *Child's Nervous System*, 31(9), pp. 1433–1445. doi: 10.1007/s00381-015-2812-5.

Kim, Dong Seok, Jang, Y. J., Jeon, O. H. and Kim, Doo Sik (2007a) 'Saxatilin, a snake venom disintegrin, suppresses TNF-a induced Ovarian Cancer Cell Invasion', *Journal of Biochemistry and Molecular Biology*, 40(2), pp. 290–294. Available at: http://www.jbmb.or.kr/jbmb/jbmb_files/[40-2]0703290828_290.pdf.

Kim, Dong Seok, Jang, Y. J., Jeon, O. H. and Kim, Doo Sik (2007b) 'Saxatilin inhibits TNF-α-induced proliferation by suppressing AP-1-dependent IL-8 expression in the ovarian cancer cell line MDAH 2774', *Molecular Immunology*, 44(6), pp. 1409–1416. doi: 10.1016/j.molimm.2006.05.001.

Kim, J. S., Kang, S. J., Jeong, H. Y., Kim, M. W., Park, S. Il, Lee, Y. K., Kim, H. S., Kim, K. S. and Park, Y. S. (2016) 'Anti-EGFR immunonanoparticles containing IL12 and salmosin genes for targeted cancer gene therapy', *International Journal of Oncology*, 49(3), pp. 1130–1138. doi: 10.3892/ijo.2016.3619.

Kim, J. W. and Dang, C. V. (2006) 'Cancer's molecular sweet tooth and the warburg effect', *Cancer Research*, 66(18), pp. 8927–8930. doi: 10.1158/0008-5472.CAN-06-1501.

Kim, M. S., Lee, W. S., Jeong, J., Kim, S. J. and Jin, W. (2015) 'Induction of metastatic potential by TrkB via activation of IL6/JAK2/STAT3 and PI3K/AKT signaling in breast cancer', *Oncotarget*, 6(37), pp. 40158–40171. doi: 10.18632/oncotarget.5522.

Kim, S. I., Kim, K. S., Kim, H. S., Kim, D. S., Jang, Y., Chung, K. H. and Park, Y. S. (2003) 'Inhibitory effect of the salmosin gene transferred by cationic liposomes on the progression of B16BL6 tumors', *Cancer Research*, 63(19), pp. 6458–6462.

Kinch, M. S., Moore, M. B. and Harpole, D. H. (2003) 'Predictive value of the EphA2 receptor tyrosine kinase in lung cancer recurrence and survival', *Clinical Cancer Research*, 9(2), pp. 613–618.

Kini, R. M. and Doley, R. (2010) 'Structure, function and evolution of three-finger toxins: Mini proteins with multiple targets', *Toxicon*. Elsevier Ltd, 56(6), pp. 855–867. doi: 10.1016/j.toxicon.2010.07.010.

Kinjo, T., Taniguchi, H., Kushima, R., Sekine, S., Oda, I., Saka, M., Gotoda, T., Kinjo, F., Fujita, J. and Shimoda, T. (2012) 'Histologic and immunohistochemical analyses of α-fetoprotein-producing cancer of the stomach', *American Journal of Surgical Pathology*, 36(1), pp. 56–65. doi: 10.1097/PAS.0b013e31823aafec.

Klein, S. and Levitzki, A. (2009) 'Targeting the EGFR and the PKB pathway in cancer', *Current Opinion in Cell Biology*, 21, pp. 185–193. doi: 10.1016/j.ceb.2008.12.006.

Kluger, H. M., Dolled-Filhart, M., Rodov, S., Kacinski, B. M., Camp, R. L. and Rimm, D. L. (2004) 'Macrophage colony-stimulating factor-1 receptor expression is associated with poor outcome in breast cancer by large cohort tissue microarray analysis.', *Clinical cancer research*.

United States, 10, pp. 173–177.

Klute, K., Nackos, E., Tasaki, S. and Tagawa, S. T. (2014) 'Microtubule inhibitor-based antibody – drug conjugates for cancer therapy', pp. 2227–2236.

Koh, C. Y. and Kini, R. M. (2012) 'From snake venom toxins to therapeutics - Cardiovascular examples', *Toxicon*. Elsevier Ltd, 59(4), pp. 497–506. doi: 10.1016/j.toxicon.2011.03.017.

Kolosov, A., Goodchild, C. S. and Cooke, I. (2010) 'CNSB004 (leconotide) causes antihyperalgesia without side effects when given intravenously: A comparison with ziconotide in a rat model of diabetic neuropathic pain', *Pain Medicine*, 11(2), pp. 262–273. doi: 10.1111/j.1526-4637.2009.00741.x.

Kondoh, H., Lleonart, M. E., Gil, J., Wang, J., Degan, P., Peters, G., Martinez, D., Carnero, A. and Beach, D. (2005) 'Glycolytic Enzymes Can Modulate Cellular Life Span Glycolytic Enzymes Can Modulate Cellular Life Span', 65(1), pp. 177–185.

Konduri, K., Gallant, J. N., Chae, Y. K., Giles, F. J., Gitlitz, B. J., Gowen, K., Ichihara, E., Owonikoko, T. K., Peddareddigari, V., Ramalingam, S. S., Reddy, S. K., Eaby-Sandy, B., Vavalà, T., Whiteley, A., Chen, H., Yan, Y., Sheehan, J. H., Meiler, J., Morosini, D., *et al.* (2016) 'EGFR fusions as novel therapeutic targets in lung cancer', *Cancer Discovery*, 6(6), pp. 601–611. doi: 10.1158/2159-8290.CD-16-0075.

Konecny, G. E., Pegram, M. D., Venkatesan, N., Finn, R., Yang, G., Rahmeh, M., Untch, M., Rusnak, D. W., Spehar, G., Mullin, R. J., Keith, B. R., Gilmer, T. M., Berger, M., Podratz, K. C. and Slamon, D. J. (2006) 'Activity of the dual kinase inhibitor lapatinib (GW572016) against HER-2-overexpressing and trastuzumab-treated breast cancer cells', *Cancer Research*, 66(3), pp. 1630–1639. doi: 10.1158/0008-5472.CAN-05-1182.

Koneczny, I., Cossins, J. and Vincent, A. (2014) 'The role of muscle-specific tyrosine kinase (MuSK) and mystery of MuSK myasthenia gravis', *Journal of Anatomy*, 224(1), pp. 29–35. doi: 10.1111/joa.12034.

Kong, Y., Hui, J., Shao, Y., Huang, S., Chen, H. and Wei, J.-F. (2013) 'Cytotoxic and anticoagulant peptide from Scolopendra subspinipes mutilans venom', *African Journal of Pharmacy and Pharmacology*, 7(31), pp. 2238–2245. doi: 10.5897/ajpp2013.3765.

Koorstra, J. B. M., Karikari, C. A., Feldmann, G., Bisht, S., Rojas, P. L., Offerhaus, G. J. A., Alvarez, H. and Maitra, A. (2009) 'The Axl receptor tyrosine kinase confers an adverse prognostic influence in pancreatic cancer and represents a new therapeutic target', *Cancer Biology and Therapy*, 8(7). doi: 10.4161/cbt.8.7.7923.

Kopparapu, P. K., Boorjian, S. A., Robinson, B. D., Downes, M., Gudas, L. J., Mongan, N. P. and Persson, J. L. (2013) 'Expression of VEGF and Its receptors VEGFR1/VEGFR2 is associated with invasiveness of bladder cancer', *Anticancer Research*, 33(6), pp. 2381–2390.

Koukourakis, M. I. (2012) 'Radiation damage and radioprotectants: New concepts in the era of molecular medicine', *British Journal of Radiology*, 85(1012), pp. 313–330. doi: 10.1259/bjr/16386034.

Koustas, E., Karamouzis, M. V., Mihailidou, C., Schizas, D. and Papavassiliou, A. G. (2017) 'Co-targeting of EGFR and autophagy signaling is an emerging treatment strategy in metastatic colorectal cancer', *Cancer Letters*. Elsevier Ltd, 396, pp. 94–102. doi: 10.1016/j.canlet.2017.03.023.

Koutras, A. K., Fountzilas, G., Kalogeras, K. T., Starakis, I., Iconomou, G. and Kalofonos, H. P. (2010) 'The upgraded role of HER3 and HER4 receptors in breast cancer', *Critical Reviews in Oncology/Hematology*. Elsevier Ireland Ltd, 74(2), pp. 73–78. doi: 10.1016/j.critrevonc.2009.04.011.

Kovacs, E., Zorn, J. A., Huang, Y., Barros, T. and Kuriyan, J. (2015) 'A Structural Perspective on the Regulation of the Epidermal Growth Factor Receptor', *Annual Review of Biochemistry*, 84(1), pp. 739–764. doi: 10.1146/annurev-biochem-060614-034402.

Kraeber-Bodéré, F., Bodet-Milin, C., Rousseau, C., Eugène, T., Pallardy, A., Frampas, E., Carlier, T., Ferrer, L., Gaschet, J., Davodeau, F., Gestin, J. F., Faivre-Chauvet, A., Barbet, J. and Chérel, M. (2014) 'Radioimmunoconjugates for the treatment of cancer', *Seminars in Oncology*, 41(5), pp. 613–622. doi: 10.1053/j.seminoncol.2014.07.004.

Kumar, P., Ferns, M. J. and Meizel, S. (2006) 'Identification of agrinSN isoform and muscle-specific receptor tyrosine kinase in sperm', *Biochemical and Biophysical Research Communications*, 342(2), pp. 522–528. doi: 10.1016/j.bbrc.2006.01.161.

Kumar, S. R., Masood, R., Spannuth, W. A., Singh, J., Scehnet, J., Kleiber, G., Jennings, N., Deavers, M., Krasnoperov, V., Dubeau, L., Weaver, F. A., Sood, A. K. and Gill, P. S. (2007) 'The receptor tyrosine kinase EphB4 is overexpressed in ovarian cancer, provides survival signals and predicts poor outcome', *British Journal of Cancer*, 96(7), pp. 1083–1091. doi: 10.1038/sj.bjc.6603642.

Kumar, S. R., Singh, J., Xia, G., Krasnoperov, V., Hassanieh, L., Ley, E. J., Scehnet, J., Kumar, N. G., Hawes, D., Press, M. F., Weaver, F. A. and Gill, P. S. (2006) 'Receptor tyrosine kinase EphB4 is a survival factor in breast cancer', *American Journal of Pathology*, 169(1), pp. 279–293. doi: 10.2353/ajpath.2006.050889.

Kumar, S., Sarkar, P. and Jain, R. (2013) 'Venoms can be a boon for cancer patients', *Forum on Immunopathological Diseases and Therapeutics*, 4(3–4), pp. 255–273. doi: 10.1615/ForumImmunDisTher.2014008152.

Lacoeuille, F., Arlicot, N. and Faivre-Chauvet, A. (2018) 'Targeted alpha and beta radiotherapy: An overview of radiopharmaceutical and clinical aspect', *Medecine Nucleaire*. Elsevier Masson SAS, 42(1), pp. 32–44. doi: 10.1016/j.mednuc.2017.12.002.

Lagadec, C., Meignan, S., Adriaenssens, E., Foveau, B., Vanhecke, E., Romon, R., Toillon, R. A., Oxombre, B., Hondermarck, H. and Le Bourhis, X. (2009) 'TrkA overexpression enhances growth and metastasis of breast cancer cells', *Oncogene*. Nature Publishing Group, 28(18), pp. 1960–1970. doi: 10.1038/onc.2009.61.

Lake, D., Corrêa, S. A. L. and Müller, J. (2016) 'Negative feedback regulation of the ERK1/2 MAPK pathway', *Cellular and Molecular Life Sciences*, 73(23), pp. 4397–4413. doi: 10.1007/s00018-016-2297-8.

Lamba, V. and Ghosh, I. (2012) 'New Directions in Targeting Protein Kinases: Focusing Upon True Allosteric and Bivalent Inhibitors', *Current Pharmaceutical Design*, 18(20), pp. 2936–2945. doi: 10.2174/138161212800672813.

Lancet, J. E., Uy, G. L., Cortes, J. E., Newell, L. F., Lin, T. L., Ritchie, E. K., Stuart, R. K., Strickland, S. A., Hogge, D., Solomon, S. R., Stone, R. M., Bixby, D. L., Kolitz, J. E., Schiller, G. J., Wieduwilt, M. J., Ryan, D. H., Hoering, A., Banerjee, K., Chiarella, M., *et al.* (2018) 'Cpx-351 (cytarabine and daunorubicin) liposome for injection versus conventional cytarabine plus daunorubicin in older patients with newly diagnosed secondary acute myeloid leukemia', *Journal of Clinical Oncology*, 36(26), pp. 2684–2692. doi: 10.1200/JCO.2017.77.6112.

Lange, A. M. and Lo, H. W. (2018) 'Inhibiting TRK proteins in clinical cancer therapy', *Cancers*, 10(4), pp. 1–15. doi: 10.3390/cancers10040105.

Larsson, O., Girnita, A. and Girnita, L. (2005) 'Role of insulin-like growth factor I receptor signalling in cancer', *British Journal of Cancer*, 92(12), pp. 2097–2101. doi: 10.1038/sj.bjc.6602627.

Latinović, Z., Leonardi, A., Petan, T., Žlajpah, M. and Križaj, I. (2017) 'Disintegrins from the venom of vipera ammodytes ammodytes efficiently inhibit migration of breast cancer cells', *Acta Chimica Slovenica*, 64(3), pp. 555–559. doi: 10.17344/acsi.2016.2924.

Lauridsen, L. P., Laustsen, A. H., Lomonte, B. and Gutiérrez, J. M. (2017) 'Exploring the venom of the forest cobra snake: Toxicovenomics and antivenom profiling of Naja melanoleuca', *Journal of Proteomics*, 150, pp. 98–108. doi: 10.1016/j.jprot.2016.08.024.

Laustsen, A. H., Lomonte, B., Lohse, B., Fernández, J. and Gutiérrez, J. M. (2015) 'Unveiling the nature of black mamba (Dendroaspis polylepis) venom through venomics and antivenom immunoprofiling: Identification of key toxin targets for antivenom development', *Journal of Proteomics*, 119, pp. 126–142. doi: 10.1016/j.jprot.2015.02.002.

Lawenda, B. D., Kelly, K. M., Ladas, E. J., Sagar, S. M., Vickers, A. and Blumberg, J. B. (2008) 'Should supplemental antioxidant administration be avoided during chemotherapy and radiation therapy?', *Journal of the National Cancer Institute*, 100(11), pp. 773–783. doi: 10.1093/jnci/djn148.

Leahy, D. J. (2004) 'Structure and function of the epidermal growth factor (EGF/ERBB) family of receptors', *Advances in Protein Chemistry*, 68, pp. 1–27. doi: 10.1016/S0065-3233(04)68001-6.

Leconet, W., Chentouf, M., Du Manoir, S., Chevalier, C., Sirvent, A., Aït-Arsa, I., Busson, M., Jarlier, M., Radosevic-Robin, N., Theillet, C., Chalbos, D., Pasquet, J. M., Pèlegrin, A., Larbouret, C. and Robert, B. (2017) 'Therapeutic activity of anti-AXL antibody against triple-negative breast cancer patient-derived xenografts and metastasis', *Clinical Cancer Research*, 23(11), pp. 2806–2816. doi: 10.1158/1078-0432.CCR-16-1316.

LeCouter, J. and Ferrara, N. (2002) 'EG-VEGF and the concept of tissue-specific angiogenic growth factors', *Seminars in Cell and Developmental Biology*, 13(1), pp. 3–8. doi: 10.1006/scdb.2001.0284.

Lee, B. Q., Kibédi, T., Stuchbery, A. E., Robertson, K. A. and Kondev, F. G. (2013) 'A model to realize the potential of auger electrons for radiotherapy', *EPJ Web of Conferences*, 63, pp. 1–5. doi: 10.1051/epjconf/20136301002.

Lee, H. J., Seo, A. N., Kim, E. J., Jang, M. H., Kim, Y. J., Kim, J. H., Kim, S. W., Ryu, H. S., Park, I. A., Im, S. A., Gong, G., Jung, K. H., Kim, H. J. and Park, S. Y. (2015) 'Prognostic and predictive values of EGFR overexpression and EGFR copy number alteration in HER2-positive breast cancer', *British Journal of Cancer*, 112(1), pp. 103–111. doi: 10.1038/bjc.2014.556.

Lee, J.-K., Choi, Y.-L., Kwon, M. and Park, P. J. (2016) 'Mechanisms and Consequences of Cancer Genome Instability: Lessons from Genome Sequencing Studies', *Annual Review of Pathology: Mechanisms of Disease*, 11(1), pp. 283–312. doi: 10.1146/annurev-pathol-012615-044446.

Lee, J. H., Kim, I. W., Kim, S. H., Kim, M. A., Yun, E. Y., Nam, S. H., Ahn, M. Y., Kang, D. and Hwang, J. S. (2015) 'Anticancer activity of the antimicrobial peptide scolopendrasin VII derived from the centipede, scolopendra subspinipes mutilans', *Journal of Microbiology and Biotechnology*, 25(8), pp. 1275–1280. doi: 10.4014/jmb.1503.03091.

Lee, M. L., Fung, S. Y., Chung, I., Pailoor, J., Cheah, S. H. and Tan, N. H. (2014) 'King cobra (Ophiophagus hannah) venom L-amino acid oxidase induces apoptosis in PC-3 cells and suppresses PC-3 solid tumor growth in a tumor xenograft mouse model', *International Journal of Medical Sciences*, 11(6), pp. 593–601. doi: 10.7150/ijms.8096.

Lee, P. C., Kakadiya, R., Su, T. L. and Lee, T. C. (2010) 'Combination of bifunctional alkylating agent and arsenic trioxide synergistically suppresses the growth of drug-resistant tumor cells', *Neoplasia*, 12(5), pp. 376–387. doi: 10.1593/neo.10110.

Lee, W. Y., Chen, H. H. W., Chow, N. H., Su, W. C., Lin, P. W. and Guo, H. R. (2005) 'Prognostic significance of co-expression of RON and MET receptors in node-negative breast cancer patients', *Clinical Cancer Research*, 11(6), pp. 2222–2228. doi: 10.1158/1078-0432.CCR-04-1761.

Lee, Y., Ma, J., Lyu, H., Huang, J., Kim, A. and Liu, B. (2014) 'Role of erbB3 receptors in cancer therapeutic resistance', *Acta Biochimica et Biophysica Sinica*, 46(January), pp. 190–198. doi: 10.1093/abbs/gmt150.

Lehenberger, S., Barkhausen, C., Cohrs, S., Fischer, E., Grünberg, J., Hohn, A., Köster, U., Schibli, R., Türler, A. and Zhernosekov, K. (2011) 'The low-energy β - and electron emitter 161Tb as an alternative to 177Lu for targeted radionuclide therapy', *Nuclear Medicine and Biology*, 38(6), pp. 917–924. doi: 10.1016/j.nucmedbio.2011.02.007.

Lehmann, B. D., Bauer, J. A., Chen, X., Sanders, M. E., Chakravarthy, A. B., Shyr, Y. and Pietenpol, J. A. (2011) 'Identification of human triple-negative breast cancer subtypes and preclinical models for selection of targeted therapies', *Journal of Clinical Investigation*, 121(7), pp. 2750–2767. doi: 10.1172/JCI45014.

Leitinger, B. (2014) *Discoidin domain receptor functions in physiological and pathological conditions*, *International Review of Cell and Molecular Biology*. doi: 10.1016/B978-0-12-800180-6.00002-5.

Lemmon, M. A. and Schlessinger, J. (2010) 'Cell signaling by receptor tyrosine kinases', *Cell*, 141(7), pp. 1117–1134. doi: 10.1016/j.cell.2010.06.011.

Leonardi, A., Gubenšek, F. and Križaj, I. (2002) 'Purification and characterisation of two hemorrhagic metalloproteinases from the venom of the long-nosed viper, Vipera ammodytes ammodytes', *Toxicon*, 40(1), pp. 55–62. doi: 10.1016/S0041-0101(01)00188-X.

Li, G., Ji, X. D., Gao, H., Zhao, J. S., Xu, J. F., Sun, Z. J., Deng, Y. Z., Shi, S., Feng, Y. X., Zhu, Y. Q., Wang, T., Li, J. J. and Xie, D. (2012) 'EphB3 suppresses non-small-cell lung cancer metastasis via a PP2A/RACK1/Akt signalling complex', *Nature Communications*. Nature Publishing Group, 3, pp. 1–10. doi: 10.1038/ncomms1675.

Li, J. J., Sun, Z. J., Yuan, Y. M., Yin, F. F., Bian, Y. G., Long, L. Y., Zhang, X. L. and Xie, D. (2017) 'EphB3 stimulates cell migration and metastasis in a kinase-dependent manner through Vav2-Rho GTPase axis in papillary thyroid cancer', *Journal of Biological Chemistry*, 292(3), pp. 1112–1121. doi: 10.1074/jbc.M116.750349.

Li, L., Huang, J. and Lin, Y. (2018) 'Snake venoms in cancer therapy: Past, present and future', *Toxins*, 10(9), pp. 1–8. doi: 10.3390/toxins10090346.

Li Lee, M., Chung, I., Yee Fung, S., Kanthimathi, M. S. and Hong Tan, N. (2014) 'Antiproliferative activity of King Cobra (Ophiophagus hannah) Venom l-Amino Acid Oxidase', *Basic and Clinical Pharmacology and Toxicology*, 114(4), pp. 336–343. doi: 10.1111/bcpt.12155.

Li, M., Wu, S., Liu, Z., Zhang, W., Xu, J., Wang, Y., Liu, J., Zhang, D., Tian, H., Li, Y. and Ye, W. (2012) 'Arenobufagin, a bufadienolide compound from toad venom, inhibits VEGF-mediated angiogenesis through suppression of VEGFR-2 signaling pathway', *Biochemical Pharmacology*. Elsevier Inc., 83(9), pp. 1251–1260. doi: 10.1016/j.bcp.2012.01.023.

Li, Q., Xiao, K. and Wang, Z. (2015) 'Cytotoxic and Apoptotic Effects of the Venom of the Scorpion Heterometrus liangi in Human KYSE-510 Cells (Esophageal cancer)', *International Conference on Mechatronics, Electronic, Industrial and Control Engineering*, pp. 750–755. doi: 10.2991/meic-15.2015.171.

Li, S., Kussie, P. and Ferguson, K. M. (2008) 'Structural Basis for EGF Receptor Inhibition by the Therapeutic Antibody IMC-11F8', *Structure*, 16(2), pp. 216–227. doi:

10.1016/j.str.2007.11.009.

Li, S., Schmitz, K. R., Jeffrey, P. D., Wiltzius, J. J. W., Kussie, P. and Ferguson, K. M. (2005) 'Structural basis for inhibition of the epidermal growth factor receptor by cetuximab', *Cancer Cell*, 7(4), pp. 301–311. doi: 10.1016/j.ccr.2005.03.003.

Li, W., Li, Y., Zhao, Y., Yuan, J. and Mao, W. (2014) 'Inhibition effects of scorpion venom extracts (Buthus matensii Karsch) on the growth of human breast cancer MCF-7 cells', *African Journal of Traditional, Complementary and Alternative Medicines*, 11(5), pp. 105–110. doi: 10.4314/ajtcam.v11i5.17.

Li, W. X. (2008) 'Canonical and non-canonical JAK-STAT signaling', *Trends in Cell Biology*, 18(October), pp. 545–551. doi: 10.1016/j.tcb.2008.08.008.

Li, X., Wang, W. and Chen, J. (2017) 'Recent progress in mass spectrometry proteomics for biomedical research', *Science China Life Sciences*, 60(10), pp. 1093–1113. doi: 10.1007/s11427-017-9175-2.

Li, X., Xu, Y., Ding, Y., Li, C., Zhao, H., Wang, J. and Meng, S. (2018) 'Posttranscriptional upregulation of HER3 by HER2 mRNA induces trastuzumab resistance in breast cancer', *Molecular Cancer*. Molecular Cancer, 17(1), pp. 1–14. doi: 10.1186/s12943-018-0862-5.

Li, Y., Jin, L., Ye, F., Ma, Q., Yang, Z., Liu, D., Yang, J., Ma, D. and Gao, Q. (2017) 'Isoform expression patterns of EPHA10 protein mediate breast cancer progression by regulating the E-Cadherin and β-catenin complex', *Oncotarget*, 8(18), pp. 30344–30356. doi: 10.18632/oncotarget.15910.

Li, Y., Ye, X., Tan, C., Hongo, J. A., Zha, J., Liu, J., Kallop, D., Ludlam, M. J. C. and Pei, L. (2009) 'Axl as a potential therapeutic target in cancer: Role of Axl in tumor growth, metastasis and angiogenesis', *Oncogene*, 28(39), pp. 3442–3455. doi: 10.1038/onc.2009.212.

Liang, G., Chen, G., Wei, X., Zhao, Y. and Li, X. (2013) 'Small molecule inhibition of fibroblast growth factor receptors in cancer', *Cytokine and Growth Factor Reviews*. Elsevier Ltd, 24(5), pp. 467–475. doi: 10.1016/j.cytogfr.2013.05.002.

Liang, Y., Xu, X., Wang, T., Li, Y., You, W., Fu, J., Liu, Y., Jin, S., Ji, Q., Zhao, W., Song, Q., Li, L., Hong, T., Huang, J., Lyu, Z. and Ye, Q. (2017) 'The EGFR/miR-338-3p/EYA2 axis controls breast tumor growth and lung metastasis', *Cell death & disease*. Nature Publishing Group, 8(7), p. e2928. doi: 10.1038/cddis.2017.325.

Liao, Z., Cao, J., Li, S., Yan, X., Hu, W., He, Q., Chen, J., Tang, J., Xie, J. and Liang, S. (2007) 'Proteomic and peptidomic analysis of the venom from Chinese tarantula Chilobrachys jingzhao', *Proteomics*, 7(11), pp. 1892–1907. doi: 10.1002/pmic.200600785.

Lim, S. H., Beers, S. A., French, R. R., Johnson, P. W. M., Glennie, M. J. and Cragg, M. S. (2010) 'Anti-CD20 monoclonal antibodies: Historical and future perspectives', *Haematologica*, 95(1), pp. 135–143. doi: 10.3324/haematol.2008.001628.

Lim, S. M., Syn, N. L., Cho, B. C. and Soo, R. A. (2018) 'Acquired resistance to EGFR targeted therapy in non-small cell lung cancer: Mechanisms and therapeutic strategies', *Cancer Treatment Reviews*. Elsevier Ltd, 65, pp. 1–10. doi: 10.1016/j.ctrv.2018.02.006.

Lin, K. L., Su, J. C., Chien, C. M., Chuang, P. W., Chang, L. Sen and Lin, S. R. (2010) 'Down-regulation of the JAK2/PI3K-mediated signaling activation is involved in Taiwan cobra cardiotoxin III-induced apoptosis of human breast MDA-MB-231 cancer cells', *Toxicon*. Elsevier Ltd, 55(7), pp. 1263–1273. doi: 10.1016/j.toxicon.2010.01.017.

Ling, Y., Sikarwar, A. and Yi, Y. (2015) 'Anti-tumor Effect of Calloselasma rhodostoma Venom on Human Breast Cancer Cell Line', *British Biotechnology Journal*, 8(2), pp. 1–9. doi: 10.9734/bbj/2015/18873.

Linger, R. M. ., Keating, A. K., Earp, H. S. and Graham, D. K. (2010) 'Taking aim at Mer and Axl receptor tyrosine kinases as novel therapeutic targets in solid tumors', *expert opinions therapeutic targets*, 14(10), pp. 1073–1090. doi: 10.1038/jid.2014.371.

Linger, R. M. A., Cohen, R. A., Cummings, C. T., Sather, S., Migdall-Wilson, J., Middleton, D. H. G., Lu, X., Barón, A. E., Franklin, W. A., Merrick, D. T., Jedlicka, P., Deryckere, D., Heasley, L. E. and Graham, D. K. (2013) 'Mer or Axl receptor tyrosine kinase inhibition promotes apoptosis, blocks growth and enhances chemosensitivity of human non-small cell lung cancer', *Oncogene*, 32(29), pp. 3420–3431. doi: 10.1038/onc.2012.355.

Linggi, B. and Carpenter, G. (2006) 'ErbB receptors: new insights on mechanisms and biology', *Trends in Cell Biology*, 16(12), pp. 649–656. doi: 10.1016/j.tcb.2006.10.008.

Lisabeth, E. M., Fernandez, C. and Pasquale, E. B. (2012) 'Cancer Somatic Mutations Disrupt Functions of the EphA3 Receptor Tyrosine Kinase Through Multiple Mechanisms', *Biochemistry*, 51(7), pp. 1464–1475. doi: 10.1161/CIRCULATIONAHA.110.956839.

Liu, C. C., Yang, H., Zhang, L. L., Zhang, Q., Chen, B. and Wang, Y. (2014) 'Biotoxins for cancer therapy', *Asian Pacific Journal of Cancer Prevention*, 15, pp. 4753–4758. doi: 10.7314/APJCP.2014.15.12.4753.

Liu, L., Greger, J., Shi, H., Liu, Y., Greshock, J., Annan, R., Halsey, W., Sathe, G. M., Martin, A. M. and Gilmer, T. M. (2009) 'Novel mechanism of lapatinib resistance in HER2-positive breast tumor cells: Activation of AXL', *Cancer Research*, 69(17), pp. 6871–6878. doi: 10.1158/0008-5472.CAN-08-4490.

Liu, Q., Yu, S., Zhao, W., Qin, S., Chu, Q. and Wu, K. (2018) 'EGFR-TKIs resistance via EGFR-independent signaling pathways', *Molecular Cancer*. Molecular Cancer, 17(1), pp. 1–9. doi: 10.1186/s12943-018-0793-1.

Liu, S., Meng, X., Chen, H., Liu, W., Miller, T., Murph, M., Lu, Y., Zhang, F., Gagea, M., Arteaga, C. L., Mills, G. B., Meric-Bernstam, F. and González-Angulo, A. M. (2014) 'Targeting tyrosine-kinases and estrogen receptor abrogates resistance to endocrine therapy in breast cancer', *Oncotarget*, 5(19), pp. 9049–9064. doi: 10.18632/oncotarget.2022.

Liu, S., Yu, M., He, Y., Xiao, L., Wang, F., Song, C., Sun, S., Ling, C. and Xu, Z. (2008) 'Melittin prevents liver cancer cell metastasis through inhibition of the Rac1-dependent pathway', *Hepatology*, 47(6), pp. 1964–1973. doi: 10.1002/hep.22240.

Liu, T. C., Jin, X., Wang, Y. and Wang, K. (2017) 'Role of epidermal growth factor receptor in lung cancer and targeted therapies', *American Journal of Cancer Research*, 7(2), pp. 187–202.

Liu, X., Wang, P., Zhang, C. and Ma, Z. (2017) 'Epidermal growth factor receptor (EGFR): A rising star in the era of precision medicine of lung cancer', *Oncotarget*, 8(30), pp. 50209–50220. doi: 10.18632/oncotarget.16854.

Liu, Y., Chen, C., Xu, Z., Scuoppo, C., Rillahan, C. D., Spitzer, B., Bosbach, B., Kastenhuber, E. R., Baslan, T., Ackermann, S., Cheng, L., Wang, Q., Niu, T., Schultz, N., Ross, L., Mills, A. A. and Lowe, S. W. (2016) 'Deletions linked to TP53 loss drive cancer through p53– independent mechanisms', *Natre*, 531(7595), pp. 471–475. doi: 10.1038/nature17157.Deletions.

Liu, Z., Zhao, Y., Li, J., Xu, S., Liu, C., Zhu, Y. and Liang, S. (2012) 'The venom of the spider Macrothele raveni induces apoptosis in the myelogenous leukemia K562 cell line', *Leukemia Research*. Elsevier Ltd, 36(8), pp. 1063–1066. doi: 10.1016/j.leukres.2012.02.025.

Logan-Collins, J., Thomas, R. M., Yu, P., Jaquish, D., Mose, E., French, R., Stuart, W., McClaine, R., Aronow, B., Hoffman, R. M., Waltz, S. E. and Lowy, A. M. (2010) 'Silencing of RON receptor signaling promotes apoptosis and gemcitabine sensitivity in pancreatic cancers', *Cancer Research*, 70(3), pp. 1130–1140. doi: 10.1158/0008-5472.CAN-09-0761.

Loibl, S. and Gianni, L. (2017a) 'HER2-positive breast cancer', *The Lancet*. Elsevier Ltd, 389(10087), pp. 2415–2429. doi: 10.1016/S0140-6736(16)32417-5.

Loibl, S. and Gianni, L. (2017b) 'HER2-positive breast cancer', *The Lancet*. Elsevier Ltd, 389(10087), pp. 2415–2429. doi: 10.1016/S0140-6736(16)32417-5.

Lopez-Gines, C., Gil-Benso, R., Ferrer-Luna, R., Benito, R., Serna, E., Gonzalez-Darder, J., Quilis, V., Monleon, D., Celda, B. and Cerdá-Nicolas, M. (2010) 'New pattern of EGFR amplification in glioblastoma and the relationship of gene copy number with gene expression profile', *Modern Pathology*, 23(6), pp. 856–865. doi: 10.1038/modpathol.2010.62.

Lovly, C. M., Gupta, A., Lipson, D., Otto, G., Brennan, T., Chung, C. T., Borinstein, S. C., Ross, J. S., Stephens, P. J., Miller, V. A. and Coffin, C. M. (2014) 'Inflammatory myofibroblastic tumors harbor multiple potentially actionable Kinase fusions', *Cancer Discovery*, 4(8), pp. 889–895. doi: 10.1158/2159-8290.CD-14-0377.

Lovly, C. M., Mcdonald, N. T., Chen, H., Ortiz-cuaran, S., Heukamp, L. C., Yan, Y., Florin, A., Ozretić, L., Lim, D., Wang, L., Chen, Z., Chen, X., Lu, P., Paik, P. K., Shen, R., Jin, H., Buettner, R., Ansén, S., Perner, S., *et al.* (2014) 'Rationale for co-targeting IGF-1R and ALK in ALK fusion positive lung cancer', *Nature Medicine*, 20(9), pp. 1027–1034. doi: 10.1038/nm.3667.Rationale.

Lovly, C. M. and Shaw, A. T. (2014) 'Molecular pathways: Resistance to kinase inhibitors and implications for therapeutic strategies', *Clinical Cancer Research*, 20(9), pp. 2249–2256. doi: 10.1158/1078-0432.CCR-13-1610.

Low, K. C. and Tergaonkar, V. (2013) 'Telomerase: Central regulator of all of the hallmarks of cancer', *Trends in Biochemical Sciences*. Elsevier Ltd, 38(9), pp. 426–434. doi: 10.1016/j.tibs.2013.07.001.

Lu, C., Wang, X., Zhu, H., Feng, J., Ni, S. and Huang, J. (2015) 'Over-expression of ROR2 and Wnt5a cooperatively correlates with unfavorable prognosis in patients with non-small cell lung cancer', *Oncotarget*, 6(28), pp. 24912–24921. doi: 10.18632/oncotarget.4701.

Lucarelli, E., Kaplan, D. and Thiele, C. J. (1997) 'Activation of trk-A but not trk-B signal transduction pathway inhibits growth of neuroblastoma cells', *European Journal of Cancer*, 33(12), pp. 2068–2070. doi: 10.1016/S0959-8049(97)00266-9.

Lucas, F. A. M. and Cristovam, S. N. (2016) 'HER2 testing in gastric cancer: An update', *World Journal of Gastroenterology*, 22(19), pp. 4619–4625. doi: 10.3748/wjg.v22.i19.4619.

Luo, H., Xu, X., Ye, M., Sheng, B. and Zhu, X. (2018) 'The prognostic value of HER2 in ovarian cancer: A meta-analysis of observational studies', *PLoS ONE*, 13(1), pp. 1–16. doi: 10.1371/journal.pone.0191972.

Luo, Y., Tsuchiya, K. D., Il Park, D., Fausel, R., Kanngurn, S., Welcsh, P., Dzieciatkowski, S., Wang, J. and Grady, W. M. (2013) 'RET is a potential tumor suppressor gene in colorectal cancer', *Oncogene*. Nature Publishing Group, 32(16), pp. 2037–2047. doi: 10.1038/onc.2012.225.

Lyu, H., Wang, S., Huang, J., Wang, B., He, Z. and Liu, B. (2018) 'Survivin-targeting miR-542-3p overcomes HER3 signaling-induced chemoresistance and enhances the antitumor activity of paclitaxel against HER2-overexpressing breast cancer', *Cancer Letters*. Elsevier Ltd, 420, pp. 97–108. doi: 10.1016/j.canlet.2018.01.065.

Ma, W., Liu, R., Qi, J. and Zhang, Y. (2014) 'Extracts of centipede Scolopendra subspinipes mutilans induce cell cycle arrest and apoptosis in A375 human melanoma cells', *Oncology Letters*, 8(1), pp. 414–420. doi: 10.3892/ol.2014.2139.

Ma, W., Zhang, D., Zheng, L., Zhan, Y. and Zhang, Y. (2015) 'Potential roles of Centipede Scolopendra extracts as a strategy against EGFR-dependent cancers', *American Journal of*

Translational Research, 7(1), pp. 39–52.

Ma, Y., Zhao, Y., Zhao, R., Zhang, W., He, Y., Wu, Y., Cao, Z., Guo, L. and Li, W. (2010) 'Molecular diversity of toxic components from the scorpion Heterometrus petersii venom revealed by proteomic and transcriptome analysis', *Proteomics*, 10(13), pp. 2471–2485. doi: 10.1002/pmic.200900763.

Maass, K. F., Kulkarni, C., Betts, A. M. and Wittrup, K. D. (2016) 'Determination of cellular processing rates for a trastuzumab-maytansinoid antibody-drug conjugate (ADC) highlights key parameters for ADC design', *AAPS Journal*. The AAPS Journal, 18(3), pp. 635–646. doi: 10.1208/s12248-016-9892-3.

Macheret, M. and Halazonetis, T. D. (2015) 'DNA Replication Stress as a Hallmark of Cancer', *Annual Review of Pathology: Mechanisms of Disease*, 10(1), pp. 425–448. doi: 10.1146/annurev-pathol-012414-040424.

Macias, M. J., Wiesner, S. and Sudol, M. (2002) 'WW and SH3 domains, two different scaffolds to recognize proline-rich ligands', *FEBS Letters*, 513(1), pp. 30–37. doi: 10.1016/S0014-5793(01)03290-2.

Maggiora, P., Marchio', S., Stella, M. C., Giai, M., Belfiore, A., De Bortoli, M., Di Renzo, M. F., Costantino, A., Sismondi, P. and Comoglio, P. M. (1998) 'Overexpression of the RON gene in human breast carcinoma', *Oncogene*, 16(22), pp. 2927–2933. doi: 10.1038/sj.onc.1201812.

Mailey, B., Artinyan, A., Khalili, J., Denitz, J., Sanchez-Luege, N., Sun, C. L., Bhatia, S., Nissen, N., Colquhoun, S. D. and Kim, J. (2011) 'Evaluation of absolute serum α-fetoprotein levels in liver transplant for hepatocellular cancer', *Archives of Surgery*, 146(1), pp. 26–33. doi: 10.1001/archsurg.2010.295.

Malih, I., Ahmad rusmili, M. R., Tee, T. Y., Saile, R., Ghalim, N. and Othman, I. (2014) 'Proteomic analysis of moroccan cobra naja haje legionis venom using tandem mass spectrometry', *Journal of Proteomics*. Elsevier B.V., 96, pp. 240–252. doi: 10.1016/j.jprot.2013.11.012.

Malo, N., Hanley, J. A., Cerquozzi, S., Pelletier, J. and Nadon, R. (2006) 'Statistical practice in high-throughput screening data analysis', *Nature Biotechnology*, 24(2), pp. 167–175. doi: 10.1038/nbt1186.

Mancheril, B. G., Aubrey Waddell, J. and Solimando, D. a (2014) 'Drug monographs: afatinib and obinutuzumab.', *Hospital pharmacy*, 49(3), pp. 237–41. doi: 10.1310/hpj4903-237.

Mar, N., Vredenburgh, J. J. and Wasser, J. S. (2015) 'Targeting HER2 in the treatment of non-small cell lung cancer', *Lung Cancer*. Elsevier Ireland Ltd, 87(3), pp. 220–225. doi: 10.1016/j.lungcan.2014.12.018.

Marchetti, A., Martella, C., Felicioni, L., Barassi, F., Salvatore, S., Chella, A., Camplese, P. P., Iarussi, T., Mucilli, F., Mezzetti, A., Cuccurullo, F., Sacco, R. and Buttitta, F. (2005) 'EGFR mutations in non-small-cell lung cancer: Analysis of a large series of cases and development of a rapid and sensitive method for diagnostic screening with potential implications on pharmacologic treatment', *Journal of Clinical Oncology*, 23(4), pp. 857–865. doi: 10.1200/JCO.2005.08.043.

Marcinkiewicz, C., Weinreb, P. H., Calvete, J. J., Kisiel, D. G., Mousa, S. A., Tuszynski, G. P. and Lobb, R. R. (2003) 'Obtustatin: A potent selective inhibitor of α1β1 integrin in Vitro and angiogenesis in Vivo', *Cancer Research*, 63(9), pp. 2020–2023.

Marcussi, S., Santos, P. R. S., Menaldo, D. L., Silveira, L. B., Santos-Filho, N. A., Mazzi, M. V., da Silva, S. L., Stábeli, R. G., Antunes, L. M. G. and Soares, A. M. (2011) 'Evaluation of the genotoxicity of Crotalus durissus terrificus snake venom and its isolated toxins on human lymphocytes', *Mutation Research - Genetic Toxicology and Environmental Mutagenesis*.

Elsevier B.V., 724(1–2), pp. 59–63. doi: 10.1016/j.mrgentox.2011.06.004.

Martinelli, E., Martini, G., Cardone, C., Troiani, T., Liguori, G., Vitagliano, D., Napolitano, S., Morgillo, F., Rinaldi, B., Melillo, R. M., Liotti, F., Nappi, A., Bianco, R., Berrino, L., Ciuffreda, L. P., Ciardiello, D., Iaffaioli, V., Botti, G., Ferraiolo, F., *et al.* (2015) 'AXL is an oncotarget in human colorectal cancer', *Oncotarget*, 6(27), pp. 23281–23296. doi: 10.18632/oncotarget.3962.

Matei, D., Emerson, R. E., Lai, Y. C., Baldridge, L. A., Rao, J., Yiannoutsos, C. and Donner, D. B. (2006) 'Autocrine activation of PDGFRα promotes the progression of ovarian cancer', *Oncogene*, 25(14), pp. 2060–2069. doi: 10.1038/sj.onc.1209232.

Matera, C., Gomila, A. M. J., Camarero, N., Libergoli, M., Soler, C. and Gorostiza, P. (2018) 'Photoswitchable Antimetabolite for Targeted Photoactivated Chemotherapy', *Journal of the American Chemical Society*, 140(46), pp. 15764–15773. doi: 10.1021/jacs.8b08249.

Matsuoka, T. (2015) 'Recent advances in the HER2 targeted therapy of gastric cancer', *World Journal of Clinical Cases*, 3(1), p. 42. doi: 10.12998/wjcc.v3.i1.42.

McArthur, H. L., Diab, A., Page, D. B., Yuan, J., Solomon, S. B., Sacchini, V., Comstock, C., Durack, J. C., Maybody, M., Sung, J., Ginsberg, A., Wong, P., Barlas, A., Dong, Z., Zhao, C., Blum, B., Patil, S., Neville, D., Comen, E. A., *et al.* (2016) 'A pilot study of preoperative single-dose ipilimumab and/or cryoablation in women with early-stage breast cancer with comprehensive immune profiling', *Clinical Cancer Research*, 22(23), pp. 5729–5737. doi: 10.1158/1078-0432.CCR-16-0190.

McClaine, R. J., Marshall, A. M., Wagh, P. K. and Waltz, S. E. (2010) 'Ron receptor tyrosine kinase activation confers resistance to tamoxifen in breast cancer cell lines', *Neoplasia*, 12(8), pp. 650–658. doi: 10.1593/neo.10476.

McGowan, J. V., Chung, R., Maulik, A., Piotrowska, I., Walker, J. M. and Yellon, D. M. (2017) 'Anthracycline Chemotherapy and Cardiotoxicity', *Cardiovascular Drugs and Therapy*. Cardiovascular Drugs and Therapy, 31(1), pp. 63–75. doi: 10.1007/s10557-016-6711-0.

Medina, P. J. and Goodin, S. (2008) 'Lapatinib: A dual inhibitor of human epidermal growth factor receptor tyrosine kinases', *Clinical Therapeutics*, 30(8), pp. 1426–1447. doi: 10.1016/j.clinthera.2008.08.008.

Medves, S. and Demoulin, J. B. (2012) 'Tyrosine kinase gene fusions in cancer: Translating mechanisms into targeted therapies', *Journal of Cellular and Molecular Medicine*, 16(2), pp. 237–248. doi: 10.1111/j.1582-4934.2011.01415.x.

Mehta, R., Katta, H., Alimirah, F., Patel, R., Murillo, G., Peng, X., Muzzio, M. and Mehta, R. G. (2013) 'Deguelin Action Involves c-Met and EGFR Signaling Pathways in Triple Negative Breast Cancer Cells', *PLoS ONE*, 8(6), pp. 1–11. doi: 10.1371/journal.pone.0065113.

Mei, H., Lian, S., Zhang, S., Wang, W., Mao, Q. and Wang, H. (2014) 'High expression of ROR2 in cancer cell correlates with unfavorable prognosis in colorectal cancer', *Biochemical and Biophysical Research Communications*. Elsevier Inc., 453(4), pp. 703–709. doi: 10.1016/j.bbrc.2014.09.141.

Menard, S., Casalini, P., Campiglio, M., Pupa, S., Agresti, R. and Tagliabue, E. (2001) 'HER2 overexpression in various tumor types, focussing on its relationship to the development of invasive breast cancer S.', *Annals of Oncology*, 12 Suppl 2(February 2001), pp. S15–S19. doi: 10.1093/annonc/12.suppl.

Menderes, G., Bonazzoli, E., Bellone, S., Black, J., Predolini, F., Pettinella, F., Masserdotti, A., Zammataro, L., Altwerger, G., Buza, N., Hui, P., Wong, S., Litkouhi, B., Ratner, E., Silasi, D. A., Azodi, M., Schwartz, P. E. and Santin, A. D. (2017) 'SYD985, a novel duocarmycin-based her2-targeting antibody–drug conjugate, shows antitumor activity in uterine and ovarian

carcinosarcoma with HER2/Neu expression', *Clinical Cancer Research*, 23(19), pp. 5836–5845. doi: 10.1158/1078-0432.CCR-16-2862.

Meric, F., Lee, W. P., Sahin, A., Zhang, H., Kung, H. J. and Hung, M. C. (2002) 'Expression profile of tyrosine kinases in breast cancer', *Clinical Cancer Research*, 8(2), pp. 361–367.

Merlino, G. T., Xu, Y. H., Clark, A. J. L., Semba, K., Toyoshima, K., Yamamoto, T. and Pastan, I. (1984) 'Amplification and Enhanced Expression of the Epidermal Growth Factor Receptor Gene in A431 Human Carcinoma Cells', *Science*, 224(4647), pp. 417–419.

Métayer, L. E., Vilalta, A., Amos Burke, G. A. and Brown, G. C. (2017) 'Anti-CD47 antibodies induce phagocytosis of live, malignant B cells by macrophages via the Fc domain, resulting in cell death by phagoptosis', *Oncotarget*, 8(37), pp. 60892–60903. doi: 10.18632/oncotarget.18492.

Mezquita, B., Mezquita, J., Pau, M. and Mezquita, C. (2010) 'A novel intracellular isoform of VEGFR-1 activates Src and promotes cell invasion in MDA-MB-231 breast cancer cells', *Journal of Cellular Biochemistry*, 110(3), pp. 732–742. doi: 10.1002/jcb.22584.

Milazzo, G., Giorgino, F., Damante, G., Sung, C., Stampfer, M. R., Vigneri, R., Goldfine, I. D. and Belfiore, A. (1992) 'Insulin Receptor Expression and Function in Human Breast Cancer Cell Lines', *Cancer Research*, 52(14), pp. 3924–3930.

Milenic, D. E., Brady, E. D. and Brechbiel, M. W. (2004) 'Antibody-targeted radiation cancer therapy', *Nature Reviews Drug Discovery*, 3(6), pp. 488–498. doi: 10.1038/nrd1413.

Miljanich, G. (2004) 'Ziconotide: Neuronal Calcium Channel Blocker for Treating Severe Chronic Pain', *Current Medicinal Chemistry*, 11(23), pp. 3029–3040. doi: 10.2174/0929867043363884.

Von Minckwitz, G., Procter, M., De Azambuja, E., Zardavas, D., Benyunes, M., Viale, G., Suter, T., Arahmani, A., Rouchet, N., Clark, E., Knott, A., Lang, I., Levy, C., Yardley, D. A., Bines, J., Gelber, R. D., Piccart, M. and Baselga, J. (2017) 'Adjuvant pertuzumab and trastuzumab in early her2-positive breast cancer', *New England Journal of Medicine*, 377(2), pp. 122–131. doi: 10.1056/NEJMoa1703643.

Mishal, R., Tahir, H. M., Zafar, K. and Arshad, M. (2013) 'Anti-Cancerous Applications of Scorpion Venom', *International Journal of Biological and Pharmaceutical Research*, 4(5), pp. 356–360.

Mishra, R., Alanazi, S., Yuan, L., Solomon, T., Thaker, T. M., Jura, N. and Garrett, J. T. (2018) 'Activating HER3 mutations in breast cancer', *Oncotarget*, 9(45), pp. 27773–27788. doi: 10.18632/oncotarget.25576.

Mishra, R., Patel, H., Alanazi, S., Yuan, L. and Garrett, J. T. (2018) 'HER3 signaling and targeted therapy in cancer', *Oncology Reviews*, 12(1), pp. 45–62. doi: 10.4081/oncol.2018.355.

Mittendorf, E. A., Philips, A. V, Meric-Bernstam, F., Qiao, N., Wu, Y., Harrington, S., Su, X., Wang, Y., Gonzalez-Angulo, A. M., Akcakanat, A., Chawla, A., Curran, M., Hwu, P., Sharma, P., Litton, J. K., Molldrem, J. J. and Alatrash, G. (2014) 'PD-L1 Expression in Triple Negative Breast Cancer Elizabeth', *Cancer immunology research*, 2(4), pp. 361–370. doi: 10.1158/2326-6066.CIR-13-0127.PD-L1.

Miyawaki, M., Yasuda, H., Tani, T., Hamamoto, J., Arai, D., Ishioka, K., Ohgino, K., Nukaga, S., Hirano, T., Kawada, I., Naoki, K., Hayashi, Y., Betsuyaku, T. and Soejima, K. (2017) 'Overcoming EGFR bypass signal-induced acquired resistance to ALK tyrosine kinase inhibitors in ALK-translocated lung cancer', *Molecular Cancer Research*, 15(1), pp. 106–114. doi: 10.1158/1541-7786.MCR-16-0211.

Miyazaki, K., Inokuchi, M., Takagi, Y., Kato, K., Kojima, K. and Sugihara, K. (2013) 'EphA4 is

a prognostic factor in gastric cancer', *BMC Clinical Pathology*, 13(1), pp. 1–9. doi: 10.1186/1472-6890-13-19.

Miyazaki, T., Kato, H., Fukuchi, M., Nakajima, M. and Kuwano, H. (2003) 'EphA2 overexpression correlates with poor prognosis in esophageal squamous cell carcinoma', *International Journal of Cancer*, 103(5), pp. 657–663. doi: 10.1002/ijc.10860.

Moga, M. A., Dimienescu, O. G., Arvătescu, C. A., Ifteni, P. and Pleş, L. (2018) 'Anticancer activity of toxins from bee and snake venom-an overview on ovarian cancer', *Molecules*, 23(692), pp. 1–21. doi: 10.3390/molecules23030692.

Mohamed, E. R., Noguchi, M., Hamed, A. R., Eldahshoury, M. Z., Hammady, A. R., Salem, E. E. and Itoh, K. (2015) 'Reduced expression of erythropoietin-producing hepatocyte B6 receptor tyrosine kinase in prostate cancer', *Oncology Letters*, 9(4), pp. 1672–1676. doi: 10.3892/ol.2015.2925.

Mohammad, R. M., Muqbil, I., Lowe, L., Yedjou, C., Hsu, H. Y., Lin, L. T., Siegelin, M. D., Fimognari, C., Kumar, N. B., Dou, Q. P., Yang, H., Samadi, A. K., Russo, G. L., Spagnuolo, C., Ray, S. K., Chakrabarti, M., Morre, J. D., Coley, H. M., Honoki, K., *et al.* (2015) 'Broad targeting of resistance to apoptosis in cancer', *Seminars in Cancer Biology*. Elsevier Ltd, 35, pp. S78–S103. doi: 10.1016/j.semcancer.2015.03.001.

Mohr, A., Chatain, N., Domoszlai, T., Rinis, N., Sommerauer, M., Vogt, M. and Müller-Newen, G. (2012) 'Dynamics and non-canonical aspects of JAK/STAT signalling', *European Journal of Cell Biology*. Elsevier GmbH., 91(6–7), pp. 524–532. doi: 10.1016/j.ejcb.2011.09.005.

Mologni, L. (2011) 'Development of RET Kinase Inhibitors for Targeted Cancer Therapy', *Current Medicinal Chemistry*, 18(2), pp. 162–175. doi: 10.2174/092986711794088308.

Monnier, J. and Samson, M. (2010) 'Prokineticins in angiogenesis and cancer', *Cancer Letters*. Elsevier Ireland Ltd, 296(2), pp. 144–149. doi: 10.1016/j.canlet.2010.06.011.

Monsuez, J. J., Charniot, J. C., Vignat, N. and Artigou, J. Y. (2010) 'Cardiac side-effects of cancer chemotherapy', *International Journal of Cardiology*. Elsevier Ireland Ltd, 144(1), pp. 3–15. doi: 10.1016/j.ijcard.2010.03.003.

Moon, D. O., Park, S. Y., Heo, M. S., Kim, K. C., Park, C., Ko, W. S., Choi, Y. H. and Kim, G. Y. (2006) 'Key regulators in bee venom-induced apoptosis are Bcl-2 and caspase-3 in human leukemic U937 cells through downregulation of ERK and Akt', *International Immunopharmacology*, 6(12), pp. 1796–1807. doi: 10.1016/j.intimp.2006.07.027.

Moore, S. W. M., Bhat, V. K., Flatt, P. R., Gault, V. A. and McClean, S. (2015) 'Isolation and characterisation of insulin-releasing compounds from Crotalus adamanteus, Crotalus vegrandis and Bitis nasicornis venom', *Toxicon*. Elsevier Ltd, 101, pp. 48–54. doi: 10.1016/j.toxicon.2015.05.002.

Moradi, M., Solgi, R., Vazirianzadeh, B., Tanzadehpanah, H. and Saidijam, M. (2018) 'Scorpion venom and its components as new pharmaceutical approach to cancer treatment, a systematic review', *International Journal of Pharmaceutical Sciences and Research*, 9(7), pp. 2604–2615. doi: 10.13040/IJPSR.0975-8232.9(7).2604-15.

Morandi, A., Plaza-Menacho, I. and Isacke, C. M. (2011) 'RET in breast cancer: Functional and therapeutic implications', *Trends in Molecular Medicine*, 17(3), pp. 149–157. doi: 10.1016/j.molmed.2010.12.007.

Moreno, M. and Giralt, E. (2015) 'Three valuable peptides from bee and wasp venoms for therapeutic and biotechnological use: Melittin, apamin and mastoparan', *Toxins*, 7(4), pp. 1126–1150. doi: 10.3390/toxins7041126.

Morgenstern, D. and King, G. F. (2013) 'The venom optimization hypothesis revisited', *Toxicon*.

Elsevier Ltd, 63(1), pp. 120–128. doi: 10.1016/j.toxicon.2012.11.022.

Morgillo, F., Della Corte, C. M., Fasano, M. and Ciardiello, F. (2016) 'Mechanisms of resistance to EGFR-targeted drugs: Lung cancer', *ESMO Open*, 1(3), pp. 1–9. doi: 10.1136/esmoopen-2016-000060.

Morioka, K., Tanikawa, C., Ochi, K., Daigo, Y., Katagiri, T., Kawano, H., Kawaguchi, H., Myoui, A., Yoshikawa, H., Naka, N., Araki, N., Kudawara, I., Ieguchi, M., Nakamura, K., Nakamura, Y. and Matsuda, K. (2009) 'Orphan receptor tyrosine kinase ROR2 as a potential therapeutic target for osteosarcoma', *Cancer Science*, 100(7), pp. 1227–1233. doi: 10.1111/j.1349-7006.2009.01165.x.

Mosch, B., Reissenweber, B., Neuber, C. and Pietzsch, J. (2010) 'Eph Receptors and Ephrin Ligands: Important Players in Angiogenesis and Tumor Angiogenesis', *Journal of Oncology*, pp. 1–12. doi: 10.1155/2010/135285.

Moschetta, M., Basile, A., Ferrucci, A., Frassanito, M. A., Rao, L., Ria, R., Solimando, A. G., Giuliani, N., Boccarelli, A., Fumarola, F., Coluccia, M., Rossini, B., Ruggieri, S., Nico, B., Maiorano, E., Ribatti, D., Roccaro, A. M. and Vacca, A. (2013) 'Novel targeting of phospho-cMET overcomes drug resistance and induces antitumor activity in multiple myeloma', *Clinical Cancer Research*, 19(16), pp. 4371–4382. doi: 10.1158/1078-0432.CCR-13-0039.

Moudi, M., Go, R., Yien, C. Y. S. and Nazre, M. (2013) 'Vinca alkaloids', *international journal of preventative medicine*, 4(11), pp. 1231–1235. doi: 10.1007/BF00569574.

Mueller, S. B. and Kontos, C. D. (2016) 'Tie1: An orphan receptor provides context for angiopoietin-2/Tie2 signaling', *Journal of Clinical Investigation*, 126(9), pp. 3188–3191. doi: 10.1172/JCI89963.

Mukherjee, A. K., Saviola, A. J., Burns, P. D. and Mackessy, S. P. (2015) 'Apoptosis induction in human breast cancer (MCF-7) cells by a novel venom l-amino acid oxidase (Rusvinoxidase) is independent of its enzymatic activity and is accompanied by caspase-7 activation and reactive oxygen species production', *Apoptosis*. Springer US, 20(10), pp. 1358–1372. doi: 10.1007/s10495-015-1157-6.

Mukohara, T. (2011) 'Mechanisms of resistance to anti-human epidermal growth factor receptor 2 agents in breast cancer', *Cancer Science*, 102(1), pp. 1–8. doi: 10.1111/j.1349-7006.2010.01711.x.

Müller, C., Van Der Meulen, N. P., Benešová, M. and Schibli, R. (2017) 'Therapeutic radiometals beyond 177Lu and 90Y: Production and application of promising α-particle, β--particle, and auger electron emitters', *Journal of Nuclear Medicine*, 58, pp. 91S-96S. doi: 10.2967/jnumed.116.186825.

Muller, S. P., Silva, V. A. O., Silvestrini, A. V. P., de Macedo, L. H., Caetano, G. F., Reis, R. M. and Mazzi, M. V. (2018) 'Crotoxin from Crotalus durissus terrificus venom: In vitro cytotoxic activity of a heterodimeric phospholipase A2 on human cancer-derived cell lines', *Toxicon*. Elsevier Ltd, 156, pp. 13–22. doi: 10.1016/j.toxicon.2018.10.306.

Mulvihill, M. J., Cooke, A., Rosenfeld-Franklin, M., Buck, E., Foreman, K., Landfair, D., Oconnor, M., Pirritt, C., Sun, Y., Yao, Y., Arnold, L. D., Gibson, N. W. and Ji, Q. S. (2009) 'Discovery of OSI-906: A selective and orally efficacious dual inhibitor of the IGF-1 receptor and insulin receptor', *Future Medicinal Chemistry*, 1(6), pp. 1153–1171. doi: 10.4155/fmc.09.89.

Munn, D. H. and Bronte, V. (2016) 'Immune mechanisms in the tumor microenvironment', *Current Opinion in Chemical Biology*, 39, pp. 1–6. doi: 10.1016/j.physbeh.2017.03.040.

Munshi, N., Jeay, S., Li, Y., Chen, C. R., France, D. S., Ashwell, M. A., Hill, J., Moussa, M. M., Leggett, D. S. and Li, C. J. (2010) 'ARQ 197, a novel and selective inhibitor of the human c-Met

receptor tyrosine kinase with antitumor activity', *Molecular Cancer Therapeutics*, 9(6), pp. 1544–1553. doi: 10.1158/1535-7163.MCT-09-1173.

Muraoka-Cook, R. S. (2008) 'ErbB4/HER4: Role in Mammary Gland Development, Differentiation and Growth Inhibition', *J Mammary Gland Biol Neoplasia*, 13(2), pp. 235–246. doi: 10.1016/j.biotechadv.2011.08.021.Secreted.

Nafie, M. S., Abdel Daim, M. M., Ali, I. A. I., Nabil, Z. I., Tantawy, M. A. and Abdel-Rahman, M. A. (2020) 'Antitumor efficacy of the Egyptian Scorpion Venom Androctonus Australis: in vitro and in vivo study', *The Journal of Basic and Applied Zoology*. The Journal of Basic and Applied Zoology, 81(1), pp. 1–10. doi: 10.1186/s41936-020-00147-1.

Nagano, K., Maeda, Y., Kanasaki, S. I., Watanabe, T., Yamashita, T., Inoue, M., Higashisaka, K., Yoshioka, Y., Abe, Y., Mukai, Y., Kamada, H., Tsutsumi, Y. and Tsunoda, S. I. (2014) 'Ephrin receptor A10 is a promising drug target potentially useful for breast cancers including triple negative breast cancers', *Journal of Controlled Release*. Elsevier B.V., 189, pp. 72–79. doi: 10.1016/j.jconrel.2014.06.010.

Nagano, K., Yamashita, T., Inoue, M., Higashisaka, K., Yoshioka, Y., Abe, Y., Mukai, Y., Kamada, H., Tsutsumi, Y. and Tsunoda, S. I. (2014) 'Eph receptor A10 has a potential as a target for a prostate cancer therapy', *Biochemical and Biophysical Research Communications*. Elsevier Inc., 450(1), pp. 545–549. doi: 10.1016/j.bbrc.2014.06.007.

Nagatsuma, A. K., Aizawa, M., Kuwata, T., Doi, T., Ohtsu, A., Fujii, H. and Ochiai, A. (2015) 'Expression profiles of HER2, EGFR, MET and FGFR2 in a large cohort of patients with gastric adenocarcinoma', *Gastric Cancer*, 18(2), pp. 227–238. doi: 10.1007/s10120-014-0360-4.

Nakai, K., Hung, M. C. and Yamaguchi, H. (2016) 'A perspective on anti-EGFR therapies targeting triple-negative breast cancer', *American Journal of Cancer Research*, 6(8), pp. 1609–1623.

Nakamura, R., Kataoka, H., Sato, N., Kanamori, M., Ihara, M., Igarashi, H., Ravshanov, S., Wang, Y. J., Li, Z. Y., Shimamura, T., Kobayashi, T., Konno, H., Shinmura, K., Tanaka, M. and Sugimura, H. (2005) 'EPHA2/EFNA1 expression in human gastric cancer', *Cancer Science*, 96(1), pp. 42–47. doi: 10.1111/j.1349-7006.2005.00007.x.

Nalbantsoy, A., Hempel, B. F., Petras, D., Heiss, P., Göçmen, B., Iğci, N., Yildiz, M. Z. and Süssmuth, R. D. (2017) 'Combined venom profiling and cytotoxicity screening of the Radde's mountain viper (Montivipera raddei) and Mount Bulgar Viper (Montivipera bulgardaghica) with potent cytotoxicity against human A549 lung carcinoma cells', *Toxicon*, 135, pp. 71–83. doi: 10.1016/j.toxicon.2017.06.008.

Naumann, G. B., Silva, L. F., Silva, L., Faria, G., Richardson, M., Evangelista, K., Kohlhoff, M., Gontijo, C. M. F., Navdaev, A., De Rezende, F. F., Eble, J. A. and Sanchez, E. F. (2011) 'Cytotoxicity and inhibition of platelet aggregation caused by an l-amino acid oxidase from Bothrops leucurus venom', *Biochimica et Biophysica Acta - General Subjects*. Elsevier B.V., 1810(7), pp. 683–694. doi: 10.1016/j.bbagen.2011.04.003.

Navalkissoor, S. and Grossman, A. (2019) 'Targeted Alpha Particle Therapy for Neuroendocrine Tumours: The Next Generation of Peptide Receptor Radionuclide Therapy', *Neuroendocrinology*, 108(3), pp. 256–264. doi: 10.1159/000494760.

Newton, A. C. (2010) 'Protein kinase C: poised to signal.', *American journal of physiology. Endocrinology and metabolism*, 298(35), pp. E395–E402. doi: 10.1152/ajpendo.00477.2009.

Nguyen, M., Miyakawa, S., Kato, J., Mori, T., Arai, T., Armanini, M., Gelmon, K., Yerushalmi, R., Leung, S., Gao, D., Landes, G., Haak-Frendscho, M., Elias, K. and Simmons, A. D. (2015) 'Preclinical Efficacy and Safety Assessment of an Antibody-Drug Conjugate Targeting the c-RET Proto-Oncogene for Breast Carcinoma', *Clinical Cancer Research*, 21(24), pp. 5552–5562.

doi: 10.1158/1078-0432.CCR-15-0468.

Niederst, M. J., Sequist, L. V., Poirier, J. T., Mermel, C. H., Lockerman, E. L., Garcia, A. R., Katayama, R., Costa, C., Ross, K. N., Moran, T., Howe, E., Fulton, L. E., Mulvey, H. E., Bernardo, L. A., Mohamoud, F., Miyoshi, N., VanderLaan, P. A., Costa, D. B., Jänne, P. A., *et al.* (2015) 'RB loss in resistant EGFR mutant lung adenocarcinomas that transform to small-cell lung cancer', *Nature Communications*, 6, pp. 199–203. doi: 10.1038/ncomms7377.

Nikoletopoulou, V., Markaki, M., Palikaras, K. and Tavernarakis, N. (2013) 'Crosstalk between apoptosis, necrosis and autophagy', *Biochimica et Biophysica Acta - Molecular Cell Research*. Elsevier B.V., 1833(12), pp. 3448–3459. doi: 10.1016/j.bbamcr.2013.06.001.

Ning, Q., Liu, C., Hou, L., Meng, M., Zhang, X., Luo, M., Shao, S., Zuo, X. and Zhao, X. (2013) 'Vascular Endothelial Growth Factor Receptor-1 Activation Promotes Migration and Invasion of Breast Cancer Cells through Epithelial-Mesenchymal Transition', *PLoS ONE*, 8(6), pp. 1–11. doi: 10.1371/journal.pone.0065217.

Nishikawa, H. and Sakaguchi, S. (2014) 'Regulatory T cells in cancer immunotherapy', *Current Opinion in Immunology*. Elsevier Ltd, 27(1), pp. 1–7. doi: 10.1016/j.coi.2013.12.005.

Nolte, S., de Castro Damasio, D., Baréa, A. C., Gomes, J., Magalhães, A., Mello Zischler, L. F. C., Stuelp-Campelo, P. M., Elífio-Esposito, S. L., Roque-Barreira, M. C., Reis, C. A. and Moreno-Amaral, A. N. (2012) 'BJcuL, a lectin purified from Bothrops jararacussu venom, induces apoptosis in human gastric carcinoma cells accompanied by inhibition of cell adhesion and actin cytoskeleton disassembly', *Toxicon*, 59(1), pp. 81–85. doi: 10.1016/j.toxicon.2011.10.012.

Nome, R., Hernes, E., Bogsrud, T. V., Bjøro, T. and Fosså, S. D. (2015) 'Changes in prostate-specific antigen, markers of bone metabolism and bone scans after treatment with radium-223', *Scandinavian Journal of Urology*, 49(3), pp. 211–217. doi: 10.3109/21681805.2014.982169.

Noren, N. K., Foos, G., Hauser, C. A. and Pasquale, E. B. (2006) 'The EphB4 receptor suppresses breast cancer cell tumorigenicity through an Abl-Crk pathway', *Nature Cell Biology*, 8(8), pp. 815–825. doi: 10.1038/ncb1438.

Noren, N. K., Lu, M., Freeman, A. L., Koolpe, M. and Pasquale, E. B. (2004) 'Interplay between EphB4 on tumor cells and vascular ephrin-B2 regulates tumor growth', *Proceedings of the National Academy of Sciences of the United States of America*, 101(15), pp. 5583–5588. doi: 10.1073/pnas.0401381101.

Noren, N. K. and Pasquale, E. B. (2007) 'Paradoxes of the EphB4 receptor in cancer', *Cancer Research*, 67(9), pp. 3994–3997. doi: 10.1158/0008-5472.CAN-07-0525.

Nukaga, S., Yasuda, H., Tsuchihara, K., Hamamoto, J., Masuzawa, K., Kawada, I., Naoki, K., Matsumoto, S., Mimaki, S., Ikemura, S., Goto, K., Betsuyaku, T. and Soejima, K. (2017) 'Amplification of EGFR wild-type alleles in non-small cell lung cancer cells confers acquired resistance to mutation-selective EGFR tyrosine kinase inhibitors', *Cancer Research*, 77(8), pp. 2078–2089. doi: 10.1158/0008-5472.CAN-16-2359.

Nunes, E. S., Souza, M. A. A., Vaz, A. F. M., Silva, T. G., Aguiar, J. S., Batista, A. M., Guerra, M. M. P., Guarnieri, M. C., Coelho, L. C. B. B. and Correia, M. T. S. (2012) 'Cytotoxic effect and apoptosis induction by Bothrops leucurus venom lectin on tumor cell lines', *Toxicon*. Elsevier Ltd, 59(7–8), pp. 667–671. doi: 10.1016/j.toxicon.2012.03.002.

Núñez, V., Otero, R., Barona, J., Saldarriaga, M., Osorio, R. G., Fonnegra, R., Jiménez, S. L., Díaz, A. and Quintana, J. C. (2004) 'Neutralization of the edema-forming, defibrinating and coagulant effects of Bothrops asper venom by extracts of plants used by healers in Columbia', *Brazilian Journal of Medical and Biological Research*, 37(7), pp. 969–977. doi: 10.1590/S0100-879X2004000700005.

O'Brien, J., Wilson, I., Orton, T. and Pognan, F. (2000) 'Investigation of the Alamar Blue (resazurin) fluorescent dye for the assessment of mammalian cell cytotoxicity', *European Journal of Biochemistry*, 267(17), pp. 5421–5426. doi: 10.1046/j.1432-1327.2000.01606.x.

Ochiai, H., Archer, G. E., Herndon II, J. E., Kuan, C. T., Mitchell, D. A., Bigner, D. D., Pastan, I. H. and Sampson, J. H. (2008) 'EGFRvIII-targeted immunotoxin induces antitumor immunity that is inhibited in the absence of CD4+ and CD8+ T cells', *Cancer Immunology, Immunotherapy*, 57(1), pp. 115–121. doi: 10.1161/CIRCULATIONAHA.110.956839.

Oconnell, M. P., Fiori, J. L., Xu, M., Carter, A. D., Frank, B. P., Camilli, T. C., French, A. D., Dissanayake, S. K., Indig, F. E., Bernier, M., Taub, D. D., Hewitt, S. M. and Weeraratna, A. T. (2010) 'The orphan tyrosine kinase receptor, ROR2, mediates Wnt5A signaling in metastatic melanoma', *Oncogene*, 29(1), pp. 34–44. doi: 10.1038/onc.2009.305.

Olayioye, M. a, Neve, R. M., Lane, H. a and Hynes, N. E. (2000) 'The ErbB signaling network: receptor heterodimerization in development and cancer.', *The EMBO journal*, 19(13), pp. 3159–3167. doi: 10.1093/emboj/19.13.3159.

Oliveira, I. S. de, Manzini, R. V., Ferreira, I. G., Cardoso, I. A., Bordon, K. de C. F., Machado, A. R. T., Antunes, L. M. G., Rosa, J. C. and Arantes, E. C. (2018) 'Cell migration inhibition activity of a non-RGD disintegrin from Crotalus durissus collilineatus venom', *Journal of Venomous Animals and Toxins including Tropical Diseases*. Journal of Venomous Animals and Toxins including Tropical Diseases, 24(28), pp. 1–10. doi: 10.1186/s40409-018-0167-6.

Olsen, J. V., Ong, S. E. and Mann, M. (2004) 'Trypsin cleaves exclusively C-terminal to arginine and lysine residues', *Molecular and Cellular Proteomics*, 3(6), pp. 608–614. doi: 10.1074/mcp.T400003-MCP200.

Olvera, F., Rosales, A., Olvera, A., Diaz, P., Sevcik, C., Salazar, V., Alagón, A., Hernández, H. and D'Suze, G. (2016) 'An efficient approach to clone and express active Neopladine 2, an anticancer peptide from Tityus discrepans scorpion venom', *Process Biochemistry*. Elsevier Ltd, 51(5), pp. 624–631. doi: 10.1016/j.procbio.2016.02.013.

Ong, S. E. and Mann, M. (2005) 'Mass Spectrometry–Based Proteomics Turns Quantitative', *Nature Chemical Biology*, 1(5), pp. 252–262. doi: 10.1038/nchembio736.

Ono, M. and Kuwano, M. (2006) 'Molecular mechanisms of epidermal growth factor receptor (EGFR) activation and response to gefitinib and other EGFR-targeting drugs.', *Clinical cancer research : an official journal of the American Association for Cancer Research*. United States, 12(24), pp. 7242–7251. doi: 10.1158/1078-0432.CCR-06-0646.

Oršolić, N. (2009) 'Potentiation of bleomycin lethality in hela and V79 cells by bee venom', *Arhiv za Higijenu Rada i Toksikologiju*, 60(3), pp. 317–326. doi: 10.2478/10004-1254-60-2009-1936.

Ortiz, E., Gurrola, G. B., Schwartz, E. F. and Possani, L. D. (2015) 'Scorpion venom components as potential candidates for drug development', *Toxicon*, 93, pp. 125–135. doi: 10.1016/j.toxicon.2014.11.233.

Oshima, T., Akaike, M., Yoshihara, K., Shiozawa, M., Yamamoto, N., Sato, T., Akihito, N., Nagano, Y., Fujii, S., Kunisaki, C., Wada, N., Rino, Y., Tanaka, K., Masuda, M. and Imada, T. (2008) 'Overexpression of EphA4 gene and reduced expression of EphB2 gene correlates with liver metastasis in colorectal cancer', *International Journal of Oncology*, 33, pp. 573–577. doi: 10.3892/ijo.

Ott, I. and Gust, R. (2007) 'Non platinum metal complexes as anti-cancer drugs', *Archiv der Pharmazie*, 340, pp. 117–126. doi: 10.1002/ardp.200600151.

Ou, S. H. I., Schrock, A. B., Bocharov, E. V., Klempner, S. J., Haddad, C. K., Steinecker, G., Johnson, M., Gitlitz, B. J., Chung, J., Campregher, P. V., Ross, J. S., Stephens, P. J., Miller, V.

A., Suh, J. H., Ali, S. M. and Velcheti, V. (2017) ‘HER2 Transmembrane Domain (TMD) Mutations (V659/G660) That Stabilize Homo- and Heterodimerization Are Rare Oncogenic Drivers in Lung Adenocarcinoma That Respond to Afatinib’, *Journal of Thoracic Oncology*. Elsevier Inc, 12(3), pp. 446–457. doi: 10.1016/j.jtho.2016.11.2224.

Oun, R., Moussa, Y. E. and Wheate, N. J. (2018) ‘The side effects of platinum-based chemotherapy drugs: A review for chemists’, *Dalton Transactions*. Royal Society of Chemistry, 47(19), pp. 6645–6653. doi: 10.1039/c8dt00838h.

Paatero, I. and Elenius, K. (2008) ‘ErbB4 and its isoforms: Patentable drug targets?’, *Recent Patents on DNA and Gene Sequences*, 2(1), pp. 27–33. doi: 10.2174/187221508783406602.

Paccez, J. D., Vasques, G. J., Correa, R. G., Vasconcellos, J. F., Duncan, K., Gu, X., Bhasin, M., Libermann, T. A. and Zerbini, L. F. (2013) ‘The tyrosine receptor kinase of Axl is an essential regulator of prostate cancer proliferation and tumour growth and represents a new therapeutic target’, *oncogene*, 32(6), pp. 689–698. doi: 10.1038/onc.2012.89.The.

Pagliaro, L. C., Williams, D. L., Daliani, D., Williams, M. B., Osai, W., Kincaid, M., Wen, S., Thall, P. F. and Pettaway, C. A. (2010) ‘Neoadjuvant paclitaxel, ifosfamide, and cisplatin chemotherapy for metastatic penile cancer: A phase II study’, *Journal of Clinical Oncology*, 28(24), pp. 3851–3857. doi: 10.1200/JCO.2010.29.5477.

Pal, S. K., Gomes, Aparna, Dasgupta, S. C. and Gomes, Antony (2002) ‘Snake venom as therapeutic agents: From toxin to drug development’, *Indian Journal of Experimental Biology*, pp. 1353–1358.

Palmer, T. D., Ashby, W. J., Lewis, J. D. and Zijlstra, A. (2011) ‘Targeting tumor cell motility to prevent metastasis’, *Advanced Drug Delivery Reviews*, 63(8), pp. 568–581. doi: 10.1038/jid.2014.371.

Panda, Subhamay, Kumari, L. and Panda, Santamay (2016) ‘Structural Understanding of Cytotoxin 1 of Naja Sputatrix: a Potential Anticancer Agent’, *Journal of Drug Delivery and Therapeutics*, 6(3), pp. 59–63. doi: 10.22270/jddt.v6i3.1212.

Park, H. S., Jang, M. H., Kim, E. J., Kim, H. J., Lee, H. J., Kim, Y. J., Kim, J. H., Kang, E., Kim, S. W., Kim, I. A. and Park, S. Y. (2014) ‘High EGFR gene copy number predicts poor outcome in triple-negative breast cancer’, *Modern Pathology*. Nature Publishing Group, 27(9), pp. 1212–1222. doi: 10.1038/modpathol.2013.251.

Park, I. K., Mundy-Bosse, B., Whitman, S. P., Zhang, X., Warner, S. L., Bearss, D. J., Blum, W., Marcucci, G. and Caligiuri, M. A. (2015) ‘Receptor tyrosine kinase Axl is required for resistance of leukemic cells to FLT3-targeted therapy in acute myeloid leukemia’, *Leukemia*. Nature Publishing Group, 29(12), pp. 2382–2389. doi: 10.1038/leu.2015.147.

Park, M. H., Choi, M. S., Kwak, D. H., Oh, K. W., Yoon, D. Y., Han, S. B., Song, H. S., Song, M. J. and Hong, J. T. (2011) ‘Anti-cancer effect of bee venom in prostate cancer cells through activation of caspase pathway via inactivation of NF-κB’, *The Prostate*, 71(8), pp. 801–812. doi: 10.1002/pros.21296.

Pasquale, E. B. (2010) ‘Eph receptors and ephrins in cancer: bidirectional signalling and beyond.’, *Nature reviews. Cancer*. England, 10(3), pp. 165–180. doi: 10.1038/nrc2806.

Pastan, I., Hassan, R., FitzGerald, D. J. and Kreitman, R. J. (2007) ‘ Immunotoxin Treatment of Cancer * ’, *Annual Review of Medicine*, 58(1), pp. 221–237. doi: 10.1146/annurev.med.58.070605.115320.

Paulson, K. G., Tegeder, A., Willmes, C., Iyer, J. G., Afanasiev, O. K., Schrama, D., Koba, S., Thibodeau, R., Nagase, K., Simonson, W. T., Seo, A., Koelle, D. M., Madeleine, M., Bhatia, S., Nakajima, H., Sano, S., Hardwick, J. S., Disis, M. L., Cleary, M. A., *et al.* (2014) ‘Downregulation

of MHC-I expression is prevalent but reversible in Merkel cell carcinoma Kelly', *Cancer immunology research*, 2(11), pp. 1071–1079. doi: 10.1038/jid.2014.371.

Payne, G. (2003) 'Progress in immunoconjugate cancer therapeutics', *Cancer Cell*, 3(March), pp. 207–212. doi: 10.1016/S1535-6108(03)00057-6.

Peace, B. E., Toney-Earley, K., Collins, M. H. and Waltz, S. E. (2005) 'Ron receptor signaling augments mammary tumor formation and metastasis in a murine model of breast cancer', *Cancer Research*, 65(4), pp. 1285–1293. doi: 10.1158/0008-5472.CAN-03-3580.

Peichoto, M. E., Tavares, F. L., Santoro, M. L. and MacKessy, S. P. (2012) 'Venom proteomes of South and North American opisthoglyphous (Colubridae and Dipsadidae) snake species: A preliminary approach to understanding their biological roles', *Comparative Biochemistry and Physiology - Part D: Genomics and Proteomics*. Elsevier Inc., 7(4), pp. 361–369. doi: 10.1016/j.cbd.2012.08.001.

Peng, W., Chen, J. Q., Liu, C., Malu, S., Creasy, C., Tetzlaff, M. T., Xu, C., McKenzie, J. A., Zhang, C., Liang, X., Williams, L. J., Deng, W., Chen, G., Mbofung, R., Lazar, A. J., Torres-Cabala, C. A., Cooper, Z. A., Chen, P. L., Tieu, T. N., *et al.* (2016) 'Loss of PTEN promotes resistance to T cell–mediated immunotherapy', *Cancer Discovery*, 6(2), pp. 202–216. doi: 10.1158/2159-8290.CD-15-0283.

Pennington, M. W., Czerwinski, A. and Norton, R. S. (2018) 'Peptide therapeutics from venom: Current status and potential', *Bioorganic and Medicinal Chemistry*. The Authors, 26(10), pp. 2738–2758. doi: 10.1016/j.bmc.2017.09.029.

Pereañez, J. A., Núñez, V., Huancahuire-Vega, S., Marangoni, S. and Ponce-Soto, L. A. (2009) 'Biochemical and biological characterization of a PLA2 from crotoxin complex of Crotalus durissus cumanensis', *Toxicon*, 53(5), pp. 534–542. doi: 10.1016/j.toxicon.2009.01.021.

Peters, G. J., Van Der Wilt, C. L., Van Moorsel, C. J. A., Kroep, J. R., Bergman, A. M. and Ackland, S. P. (2000) 'Basis for effective combination cancer chemotherapy with antimetabolites', *Pharmacology and Therapeutics*, 87(2–3), pp. 227–253. doi: 10.1016/S0163-7258(00)00086-3.

Petty, A., Myshkin, E., Qin, H., Guo, H., Miao, H., Tochtrop, G. P., Hsieh, J. T., Page, P., Liu, L., Lindner, D. J., Acharya, C., MacKerell, A. D., Ficker, E., Song, J. and Wang, B. (2012) 'A small molecule agonist of EphA2 receptor tyrosine kinase inhibits tumor cell migration in vitro and prostate cancer metastasis in vivo', *PLoS ONE*, 7(8), pp. 1–14. doi: 10.1371/journal.pone.0042120.

Phan, L. M., Fuentes-Mattei, E., Wu, W., Velazquez-Torres, G., Sircar, K., Wood, C. G., Hai, T., Jimenez, C., Cote, G. J., Ozsari, L., Hofmann, M. C., Zheng, S., Verhaak, R., Pagliaro, L., Cortez, M. A., Lee, M. H., Yeung, S. C. J. and Habra, M. A. (2015) 'Hepatocyte Growth Factor/cMET Pathway Activation Enhances Cancer Hallmarks in Adrenocortical Carcinoma', *Cancer Research*, 75(19), pp. 4131–4142. doi: 10.1158/0008-5472.CAN-14-3707.

Phaopongthai, J., Noiphrom, J., Phaopongthai, S., Pakmanee, N. and Sichaem, J. (2015) 'Biological activities of Peristrophe bivalvis extracts : promising potential', *Natural Product Research*, 30(6), pp. 697–699. doi: 10.1080/14786419.2015.1038810.

Phay, J. E. and Shah, M. H. (2010) 'Targeting RET receptor tyrosine kinase activation in cancer', *Clinical Cancer Research*, 16(24), pp. 5936–5941. doi: 10.1158/1078-0432.CCR-09-0786.

Pietrantonio, F., Vernieri, C., Siravegna, G., Mennitto, A., Berenato, R., Perrone, F., Gloghini, A., Tamborini, E., Lonardi, S., Morano, F., Picciani, B., Busico, A., Volpi, C. C., Martinetti, A., Battaglin, F., Bossi, I., Pellegrinelli, A., Milione, M., Cremolini, C., *et al.* (2017) 'Heterogeneity of acquired resistance to anti-EGFR monoclonal antibodies in patients with metastatic colorectal cancer', *Clinical Cancer Research*, 23(10), pp. 2414–2422. doi: 10.1158/1078-0432.CCR-16-

1863.

Pillai, R. N., Behera, M., Berry, L. D., Rossi, M. R., Kris, M. G., Johnson, B. E., Bunn, P. A., Ramalingam, S. S. and Khuri, F. R. (2017) 'HER2 mutations in lung adenocarcinomas: A report from the Lung Cancer Mutation Consortium', *Cancer*, 123(21), pp. 4099–4105. doi: 10.1002/cncr.30869.

Pillai, S. K. K., Tay, A., Nair, S. and Leong, C. O. (2012) 'Triple-negative breast cancer is associated with EGFR, CK5/6 and c-KIT expression in Malaysian women', *BMC Clinical Pathology*, 12, pp. 11–13. doi: 10.1186/1472-6890-12-18.

Pirpour Tazehkand, A., Akbarzadeh, M., Velaie, K., Sadeghi, M. R. and Samadi, N. (2018) 'The role of Her2-Nrf2 axis in induction of oxaliplatin resistance in colon cancer cells', *Biomedicine and Pharmacotherapy*. Elsevier, 103(February), pp. 755–766. doi: 10.1016/j.biopha.2018.04.105.

Pizzitola, I., Anjos-Afonso, F., Rouault-Pierre, K., Lassailly, F., Tettamanti, S., Spinelli, O., Biondi, A., Biagi, E. and Bonnet, D. (2014) 'Chimeric antigen receptors against CD33/CD123 antigens efficiently target primary acute myeloid leukemia cells in vivo', *Leukemia*. Nature Publishing Group, 28(8), pp. 1596–1605. doi: 10.1038/leu.2014.62.

Pohlmann, P. R., Mayer, I. a. and Mernaugh, R. (2009) 'Resistance to trastuzumab in breast cancer', *Clinical Cancer Research*, 15, pp. 7479–7491. doi: 10.1158/1078-0432.CCR-09-0636.

Pollak, M. (2008) 'Insulin and insulin-like growth factor signalling in neoplasia', *Nature Reviews Cancer*, 8(12), pp. 915–928. doi: 10.1038/nrc2536.

Polonelli, L., Pontón, J., Elguezabal, N., Moragues, M. D., Casoli, C., Pilotti, E., Ronzi, P., Dobroff, A. S., Rodrigues, E. G., Juliano, M. A., Maffei, D. L., Magliani, W., Conti, S. and Travassos, L. R. (2008) 'Antibody complementarity-determining regions (CDRs) can display differential antimicrobial, antiviral and antitumor activities', *PLoS ONE*, 3(6). doi: 10.1371/journal.pone.0002371.

Pondé, N., Brandão, M., El-Hachem, G., Werbrouck, E. and Piccart, M. (2018) 'Treatment of advanced HER2-positive breast cancer: 2018 and beyond', *Cancer Treatment Reviews*. Elsevier, 67(February), pp. 10–20. doi: 10.1016/j.ctrv.2018.04.016.

Powles, T., Eder, J. P., Fine, G. D., Braiteh, F. S., Loriot, Y., Cruz, C., Bellmunt, J., Burris, H. A., Petrylak, D. P., Teng, S. L., Shen, X., Boyd, Z., Hedge, P. S., Chen, D. S. and Vogelzang, N. J. (2014) 'MPDL3280A (Anti-PD-L1) treatment leads to clinical activity in metastatic bladder cancer', *Nature*. American Urological Association Education and Research, Inc., 515(558–562), p. 956. doi: 10.1016/j.juro.2015.07.017.

Premratanachai, P. and Chanchao, C. (2014) 'Review of the anticancer activities of bee products', *Asian Pac J Trop Biomed*, 4(5), pp. 337–344. doi: 10.12980/APJTB.4.2014C1262.

Presta, M., Chiodelli, P., Giacomini, A., Rusnati, M. and Ronca, R. (2017) 'Fibroblast growth factors (FGFs) in cancer: FGF traps as a new therapeutic approach', *Pharmacology and Therapeutics*. Elsevier Inc., 179, pp. 171–187. doi: 10.1016/j.pharmthera.2017.05.013.

Previdi, S., Abbadessa, G., Dalò, F., France, D. S. and Broggini, M. (2012) 'Breast cancer-derived bone metastasis can be effectively reduced through specific c-MET inhibitor tivantinib (ARQ 197) and shRNA c-MET knockdown', *Molecular Cancer Therapeutics*, 11(1), pp. 214–223. doi: 10.1158/1535-7163.MCT-11-0277.

Qiu, L., Zhou, C., Sun, Y., Di, W., Scheffler, E., Healey, S., Kouttab, N., Chu, W. and Wan, Y. (2006) 'Crosstalk between EGFR and TrkB enhances ovarian cancer cell migration and proliferation', *International Journal of Oncology*, 29(4), pp. 1003–1011. doi: 10.3892/ijo.29.4.1003.

Quan, J., Yahata, T., Adachi, S., Yoshihara, K. and Tanaka, K. (2011) 'Identification of receptor tyrosine kinase, discoidin domain receptor 1 (DDR1), as a potential biomarker for serous ovarian cancer', *International Journal of Molecular Sciences*, 12(2), pp. 971–982. doi: 10.3390/ijms12020971.

Quast, I., Keller, C. W., Maurer, M. A., Giddens, J. P., Tackenberg, B., Wang, L. X., Münz, C., Nimmerjahn, F., Dalakas, M. C. and Lünemann, J. D. (2015) 'Sialylation of IgG Fc domain impairs complement-dependent cytotoxicity', *Journal of Clinical Investigation*, 125(11), pp. 4160–4170. doi: 10.1172/JCI82695.

Quesnelle, K. M., Boehm, A. L. and Grandis, J. R. (2007) 'STAT-mediated EGFR signaling in cancer', *Journal of Cellular Biochemistry*, 102(June), pp. 311–319. doi: 10.1002/jcb.21475.

Rady, I., Siddiqui, I. A., Rady, M. and Mukhtar, H. (2017) 'Melittin, a major peptide component of bee venom, and its conjugates in cancer therapy', *Cancer Letters*, 402, pp. 16–31. doi: 10.1016/j.physbeh.2017.03.040.

Raghav, K. P., Wang, W., Liu, S., Chavez-MacGregor, M., Meng, X., Hortobagyi, G. N., Mills, G. B., Meric-Bernstam, F., Blumenschein, G. R. and Gonzalez-Angulo, A. M. (2012) 'cMET and phospho-cMET protein levels in breast cancers and survival outcomes', *Clinical Cancer Research*, 18(8), pp. 2269–2277. doi: 10.1158/1078-0432.CCR-11-2830.

Rammal, H., Saby, C., Magnien, K., Van-Gulick, L., Garnotel, R., Buache, E., Btaouri, H. El, Jeannesson, P. and Morjani, H. (2016) 'Discoidin Domain Receptors: Potential Actors and Targets in Cancer', *Frontiers in Pharmacology*, 7(March), pp. 1–13. doi: 10.3389/fphar.2016.00346.

Rampersad, S. N. (2012) 'Multiple applications of alamar blue as an indicator of metabolic function and cellular health in cell viability bioassays', *Sensors (Switzerland)*, 12(9), pp. 12347–12360. doi: 10.3390/s120912347.

Ranchoux, B., Günther, S., Quarck, R., Chaumais, M. C., Dorfmüller, P., Antigny, F., Dumas, S. J., Raymond, N., Lau, E., Savale, L., Jaïs, X., Sitbon, O., Simonneau, G., Stenmark, K., Cohen-Kaminsky, S., Humbert, M., Montani, D. and Perros, F. (2015) 'Chemotherapy-induced pulmonary hypertension: Role of alkylating agents', *American Journal of Pathology*. American Society for Investigative Pathology, 185(2), pp. 356–371. doi: 10.1016/j.ajpath.2014.10.021.

Rankin, E. B., Fuh, K. C., Taylor, T. E., Krieg, A. J., Musser, M., Yuan, J., Wei, K., Kuo, C. J., Longacre, T. A. and Giaccia, A. J. (2010) 'AXL is an essential factor and therapeutic target for metastatic ovarian cancer', *Cancer Research*, 70(19), pp. 7570–7579. doi: 10.1158/0008-5472.CAN-10-1267.

Rapisarda, A. and Melillo, G. (2012) *Role of the VEGF/VEGFR Axis in Cancer Biology and Therapy*. 1st edn, *Advances in Cancer Research*. 1st edn. Elsevier Inc. doi: 10.1016/B978-0-12-386503-8.00006-5.

Rasmussen, N. R., Wright, T. M., Brooks, S. A., Hacker, K. E., Debebe, Z., Sendor, A. B., Walker, M. P., Major, M. Ben, Green, J., Wahl, G. M. and Rathmell, W. K. (2013) 'Receptor tyrosine kinase-like orphan receptor 2 (Ror2) expression creates a poised state of wnt signaling in renal cancer', *Journal of Biological Chemistry*, 288(36), pp. 26301–26310. doi: 10.1074/jbc.M113.466086.

Regan, J. L., Kendrick, H., Magnay, F. A., Vafaizadeh, V., Groner, B. and Smalley, M. J. (2012) 'C-Kit is required for growth and survival of the cells of origin of Brca1-mutation-associated breast cancer', *Oncogene*. Nature Publishing Group, 31(7), pp. 869–883. doi: 10.1038/onc.2011.289.

van Rhijn, B. W. G., van Tilborg, A. A. G., Lurkin, I., Bonaventure, J., de Vries, A., Thiery, J. P., van der Kwast, T. H. and Zwarthoff, E. C. (2002) 'Novel fibroblast growth factor receptor 3

(FGFR3) mutations in bladder cancer previously identified in non-lethal skeletal disorders', *European Journal of Human Genetics*, 10(12), pp. 819–824. doi: 10.1038/sj.ejhg.5200883.

Ricart, A. D. (2011) 'Antibody-drug conjugates of calicheamicin derivative: Gemtuzumab ozogamicin and inotuzumab ozogamicin', *Clinical Cancer Research*, 17(20), pp. 6417–6427. doi: 10.1158/1078-0432.CCR-11-0486.

Rita de, R. de C., Hyslop, S., Dorce, V. A. C., Antunes, E. and Rowan, E. G. (2019) 'Scorpion venom increases acetylcholine release by prolonging the duration of somatic nerve action potentials', *Neuropharmacology*, 153, pp. 41–52. doi: 10.1016/j.neuropharm.2019.04.013.

Van Rite, B. D., Lazrak, Y. A., Pagnon, M. L., Palwai, N. R., Neves, L. F. F., McFetridge, P. S. and Harrison, R. G. (2011) 'Enzyme prodrug therapy designed to target l-methioninase to the tumor vasculature', *Cancer Letters*, 301(2), pp. 177–184. doi: 10.1016/j.canlet.2010.11.013.

Robertson, S. C., Meyer, A. N., Hart, K. C., Galvin, B. D., Webster, M. K. and Donoghue, D. J. (1998) 'Activating mutations in the extracellular domain of the fibroblast growth factor receptor 2 function by disruption of the disulfide bond in the third immunoglobulin-like domain', *Proceedings of the National Academy of Sciences of the United States of America*, 95(8), pp. 4567–4572. doi: 10.1073/pnas.95.8.4567.

Robinson, D., He, F., Pretlow, T. and Kung, H. J. (1996) 'A tyrosine kinase profile of prostate carcinoma', *Proceedings of the National Academy of Sciences of the United States of America*, 93(12), pp. 5958–5962. doi: 10.1073/pnas.93.12.5958.

Rodrigues, E. G., Dobroff, A. S. S., Cavarsan, C. F., Paschoalin, T., Nimrichter, L., Mortara, R. A., Santos, E. L., Fázio, M. A., Miranda, A., Daffre, S. and Travassos, L. R. (2008) 'Effective topical treatment of subcutaneous murine B16F10-Nex2 melanoma by the antimicrobial peptide gomesin', *Neoplasia*, 10(1), pp. 61–68. doi: 10.1593/neo.07885.

Rodríguez-Antona, C., Pallares, J., Montero-Conde, C., Inglada-Pérez, L., Castelblanco, E., Landa, I., Leskelä, S., Leandro-García, L. J., López-Jiménez, E., Letón, R., Cascón, A., Lerma, E., Martin, M. C., Carralero, M. C., Mauricio, D., Cigudosa, J. C., Matias-Guiu, X. and Robledo, M. (2010) 'Overexpression and activation of EGFR and VEGFR2 in medullary thyroid carcinomas is related to metastasis', *Endocrine-Related Cancer*, 17(1), pp. 7–16. doi: 10.1677/ERC-08-0304.

Roidl, A., Berger, H. J., Kumar, S., Bange, J., Knyazev, P. and Ullrich, A. (2009) 'Resistance to chemotherapy is associated with fibroblast growth factor receptor 4 up-regulation', *Clinical Cancer Research*, 15(6), pp. 2058–2066. doi: 10.1158/1078-0432.CCR-08-0890.

Roskoski, R. (2014a) 'ErbB/HER protein-tyrosine kinases: Structures and small molecule inhibitors', *Pharmacological Research*. Elsevier Ltd, 87, pp. 42–59. doi: 10.1016/j.phrs.2014.06.001.

Roskoski, R. (2014b) 'The ErbB/HER family of protein-tyrosine kinases and cancer', *Pharmacological Research*. Elsevier Ltd, 79, pp. 34–74. doi: 10.1016/j.phrs.2013.11.002.

Rothman, J. (2017) 'The Rediscovery of Bisantrene: A Review of the Literature', *International Journal of Cancer Research & Therapy*, 2(2). doi: 10.33140/ijcrt/02/02/00006.

Roy, V. and Perez, E. a (2009) 'Beyond trastuzumab: small molecule tyrosine kinase inhibitors in HER-2-positive breast cancer.', *The oncologist*, 14, pp. 1061–1069. doi: 10.1634/theoncologist.2009-0142.

Rudrammaji, L. M. S. and Gowda, T. V. (1998) 'Purification and characterization of three acidic, cytotoxic phospholipases A2 from Indian cobra (Naja naja naja) venom', *Toxicon*, 36(6), pp. 921–932. doi: 10.1016/S0041-0101(97)00097-4.

Rugo, H. S., Olopade, O. I., DeMichele, A., Yau, C., Van't Veer, L. J., Buxton, M. B., Hogarth,

M., Hylton, N. M., Paoloni, M., Perlmutter, J., Symmans, W. F., Yee, D., Chien, A. J., Wallace, A. M., Kaplan, H. G., Boughey, J. C., Haddad, T. C., Albain, K. S., Liu, M. C., *et al.* (2016) 'Adaptive randomization of veliparib-carboplatin treatment in breast cancer', *New England Journal of Medicine*, 375(1), pp. 23–34. doi: 10.1056/NEJMoa1513749.

Ruiz-Ferrer, M., Torroglosa, A., Luzón-Toro, B., Fernández, R. M., Antiñolo, G., Mulligan, L. M. and Borrego, S. (2011) 'Novel mutations at RET ligand genes preventing receptor activation are associated to Hirschsprung's disease', *Journal of Molecular Medicine*, 89(5), pp. 471–480. doi: 10.1007/s00109-010-0714-2.

Russo, A., Franchina, T., Ricciardi, G. R. R., Picone, A., Ferraro, G., Mariangela Zanghì, Toscano, G., Giordano, A. and Adamo, V. (2015) 'A decade of EGFR inhibition in EGFR-mutated non small cell lung cancer (NSCLC): Old successes and future perspectives', *Oncotarget*, 6(29), pp. 26814–26825. doi: 10.18632/oncotarget.4254.

Russo, A., Franchina, T., Ricciardi, G. R. R., Smiroldo, V., Picciotto, M., Zanghì, M., Rolfo, C. and Adamo, V. (2017) 'Third generation EGFR TKIs in EGFR-mutated NSCLC: Where are we now and where are we going', *Critical Reviews in Oncology/Hematology*. Elsevier Ireland Ltd, 117, pp. 38–47. doi: 10.1016/j.critrevonc.2017.07.003.

Russo, M., Misale, S., Wei, G., Siravegna, G., Crisafulli, G., Lazzari, L., Corti, G., Rospo, G., Novara, L., Mussolin, B., Bartolini, A., Cam, N., Patel, R., Yan, S., Shoemaker, R., Wild, R., di Nicolantonio, F., Sartore-Bianchi, A., Li, G., *et al.* (2016) 'Acquired resistance to the TRK inhibitor entrectinib in colorectal cancer', *Cancer Discovery*, 6(1), pp. 36–44. doi: 10.1158/2159-8290.CD-15-0940.

Saigusa, S., Tanaka, K., Ohi, M., Toiyama, Y., Yasuda, H., Kitajima, T., Okugawa, Y., Inoue, Y., Mohri, Y. and Kusunoki, M. (2015) 'Clinical implications of Fas/Fas ligand expression in patients with esophageal squamous cell carcinoma following neoadjuvant chemoradiotherapy', *Molecular and Clinical Oncology*, 3(1), pp. 151–156. doi: 10.3892/mco.2014.431.

Salem, M. L., Shoukry, N. M., Teleb, W. K., Abdel-Daim, M. M. and Abdel-Rahman, M. A. (2016) 'In vitro and in vivo antitumor effects of the Egyptian scorpion Androctonus amoreuxi venom in an Ehrlich ascites tumor model', *SpringerPlus*. Springer International Publishing, 5(1), pp. 1–12. doi: 10.1186/s40064-016-2269-3.

Sallinen, H., Anttila, M., Gröhn, O., Koponen, J., Hämäläinen, K., Kholova, I., Kosma, V. M., Heinonen, S., Alitalo, K. and Ylä-Herttuala, S. (2011) 'Cotargeting of VEGFR-1 and -3 and angiopoietin receptor Tie2 reduces the growth of solid human ovarian cancer in mice', *Cancer Gene Therapy*, 18(2), pp. 100–109. doi: 10.1038/cgt.2010.56.

Samel, M., Vija, H., Rönnholm, G., Siigur, J., Kalkkinen, N. and Siigur, E. (2006) 'Isolation and characterization of an apoptotic and platelet aggregation inhibiting l-amino acid oxidase from Vipera berus berus (common viper) venom', *Biochimica et Biophysica Acta - Proteins and Proteomics*, 1764(4), pp. 707–714. doi: 10.1016/j.bbapap.2006.01.021.

Sánchez, E. E., Rodríguez-Acosta, A., Palomar, R., Lucena, S. E., Bashir, S., Soto, J. G. and Pérez, J. C. (2009) 'Colombistatin: A disintegrin isolated from the venom of the South American snake (bothrops colombiensis) that effectively inhibits platelet aggregation and SK-Mel-28 cell adhesion', *Archives of Toxicology*, 83(3), pp. 271–279. doi: 10.1007/s00204-008-0358-y.

Sánchez, N. S. and Königsberg, M. (2006) 'Using yeast to easily determine mitochondrial functionality with 1-(4,5-dimethylthiazol-2-yl)-3,5-diphenyltetrazolium bromide (MTT) assay', *Biochemistry and Molecular Biology Education*, 34(3), pp. 209–212. doi: 10.1002/bmb.2006.49403403209.

Sarduy, R., Brito, V., Castillo, A., Soto, Y., Griñán, T., Marleau, S. and Vázquez, A. M. (2017) 'Dose-dependent induction of an idiotypic cascade by anti-glycosaminoglycan monoclonal antibody in apoE-/- mice: Association with atheroprotection', *Frontiers in Immunology*, 8(MAR),

pp. 1–8. doi: 10.3389/fimmu.2017.00232.

Sarfo-Poku, C., Eshun, O. and Lee, K. H. (2016) 'Medical application of scorpion venom to breast cancer: A mini-review', *Toxicon*. Elsevier Ltd, 122, pp. 109–112. doi: 10.1016/j.toxicon.2016.09.005.

Satitmanwiwat, S., Changsangfa, C., Khanuengthong, A., Promthep, K., Roytrakul, S., Arpornsuwan, T., Saikhun, K. and Sritanaudomchai, H. (2016) 'The scorpion venom peptide BmKn2 induces apoptosis in cancerous but not in normal human oral cells', *Biomedicine and Pharmacotherapy*. Elsevier Masson SAS, 84, pp. 1042–1050. doi: 10.1016/j.biopha.2016.10.041.

Satose, V., Menon, S., Pardhi, V., Pendse, S. and Choursiya, V. (2018) 'Evaluation of Anticancer Properties From Venom Fraction Of Trimeresurus malabaricus (Malabar Pit Viper) Snake', 03(06).

Savage, H. P. and Baumgarth, N. (2015) 'Characteristics of natural antibody–secreting cells Hannah', *Annals of the new york academy of science*, 1362(1), pp. 132–142. doi: 10.1016/j.physbeh.2017.03.040.

Savant, S., La Porta, S., Budnik, A., Busch, K., Hu, J., Tisch, N., Korn, C., Valls, A. F., Benest, A. V., Terhardt, D., Qu, X., Adams, R. H., Baldwin, H. S., Ruiz de Almodóvar, C., Rodewald, H. R. and Augustin, H. G. (2015) 'The Orphan Receptor Tie1 Controls Angiogenesis and Vascular Remodeling by Differentially Regulating Tie2 in Tip and Stalk Cells', *Cell Reports*, 12(11), pp. 1761–1773. doi: 10.1016/j.celrep.2015.08.024.

Sawan, S., Yaacoub, T., Hraoui-Bloquet, S., Sadek, R., Hleihel, W., Fajloun, Z. and Karam, M. (2017) 'Montivipera bornmuelleri venom selectively exhibits high cytotoxic effects on keratinocytes cancer cell lines', *Experimental and Toxicologic Pathology*. Elsevier GmbH., 69(4), pp. 173–178. doi: 10.1016/j.etp.2017.01.001.

Scarborough, R. M., Naughton, M. A., Teng, W., Rose, J. W., Phillips, D. R., Nannizzi, L., Arfsten, A., Campbell, A. M. and Charo, I. F. (1993) 'Design of potent and specific integrin antagonists. Peptide antagonists with high specificity for glycoprotein IIb-IIIa', *Journal of Biological Chemistry*, 268(2), pp. 1066–1073.

Schardt, J. S., Oubaid, J. M., William, S. C., Howard, J. L., Aloimonos, C. M., Bookstaver, M. L., Lamichhane, T. N., Sokic, S., Liyasova, M. S., O'Neill, M., Andersson, T., Hussain, A., Lipkowitz, S. and Jay, S. M. (2017) 'Engineered Multivalency Enhances Affibody-Based HER3 Inhibition and Downregulation in Cancer Cells', *molecular Pharmaceutics*, 14(4), pp. 1047–1056. doi: 10.1016/j.physbeh.2017.03.040.

Schmandt, R. E., Broaddus, R., Lu, K. H., Shvartsman, H., Thornton, A., Malpica, A., Sun, C., Bodurka, D. C. and Gershenson, D. M. (2003) 'Expression of c-ABL, c-KIT, and platelet-derived growth factor receptor-β in ovarian serous carcinoma and normal ovarian surface epithelium', *Cancer*, 98(4), pp. 758–764. doi: 10.1002/cncr.11561.

Schmid, P., Cortes, J., Pusztai, L., McArthur, H., Kümmel, S., Bergh, J., Denkert, C., Park, Y. H., Hui, R., Harbeck, N., Takahashi, M., Foukakis, T., Fasching, P. A., Cardoso, F., Untch, M., Jia, L., Karantza, V., Zhao, J., Aktan, G., *et al.* (2020) 'Pembrolizumab for Early Triple-Negative Breast Cancer', *New England Journal of Medicine*, 382(9), pp. 810–821. doi: 10.1056/nejmoa1910549.

Schulze, W. X., Deng, L. and Mann, M. (2005) 'Phosphotyrosine interactome of the ErbB-receptor kinase family', *Molecular Systems Biology*, 1(1). doi: 10.1038/msb4100012.

Sciacca, L., Costantino, A., Pandini, G., Mineo, R., Frasca, F., Scalia, P., Sbraccia, P., Goldfine, I. D., Vigneri, R. and Belfiore, A. (1999) 'Insulin receptor activation by IGF-II in breast cancers: Evidence for a new autocrine/paracrine mechanism', *Oncogene*, 18(15), pp. 2471–2479. doi: 10.1038/sj.onc.1202600.

Sclabas, G. M., Fujioka, S., Schmidt, C., Li, Z., Frederick, W. A. I., Yang, W., Yokoi, K., Evans, D. B., Abbruzzese, J. L., Hess, K. R., Zhang, W., Fidler, I. J. and Chiao, P. J. (2005) 'Overexpression of tropomysin-related kinase B in metastatic human pancreatic cancer cells', *Clinical Cancer Research*, 11(2 I), pp. 440–449.

Scott, A. M., Wolchok, J. D. and Old, L. J. (2012) 'Antibody therapy of cancer', *Nature Reviews Cancer*. Nature Publishing Group, 12(April), pp. 278–287. doi: 10.1038/nrc3236.

Seidel, U. J. E., Schlegel, P. and Lang, P. (2013) 'Natural killer cell mediated antibody-dependent cellular cytotoxicity in tumor immunotherapy with therapeutic antibodies', *Frontiers in Immunology*, 4(MAR), pp. 1–8. doi: 10.3389/fimmu.2013.00076.

Seliger, B. (2005) 'Strategies of tumor immune evasion', *BioDrugs*, 19(6), pp. 347–354. doi: 10.2165/00063030-200519060-00002.

Selvaggi, G., Novello, S., Torri, V., Leonardo, E., De Giuli, P., Borasio, P., Mossetti, C., Ardissone, F., Lausi, P. and Scagliotti, G. V. (2004) 'Epidermal growth factor receptor overexpression correlates with a poor prognosis in completely resected non-small-cell lung cancer', *Annals of Oncology*, 15(1), pp. 28–32. doi: 10.1093/annonc/mdh011.

Sequist, L. V., Soria, J. C., Goldman, J. W., Wakelee, H. A., Gadgeel, S. M., Varga, A., Papadimitrakopoulou, V., Solomon, B. J., Oxnard, G. R., Dziadziuszko, R., Aisner, D. L., Doebele, R. C., Galasso, C., Garon, E. B., Heist, R. S., Logan, J., Neal, J. W., Mendenhall, M. A., Nichols, S., *et al.* (2015) 'Rociletinib in EGFR-mutated non-small-cell lung cancer', *New England Journal of Medicine*, 372(18), pp. 1700–1709. doi: 10.1056/NEJMoa1413654.

Sequist, L. V., Yang, J. C. H., Yamamoto, N., O'Byrne, K., Hirsh, V., Mok, T., Geater, S. L., Orlov, S., Tsai, C. M., Boyer, M., Su, W. C., Bennouna, J., Kato, T., Gorbunova, V., Lee, K. H., Shah, R., Massey, D., Zazulina, V., Shahidi, M., *et al.* (2013) 'Phase III study of afatinib or cisplatin plus pemetrexed in patients with metastatic lung adenocarcinoma with EGFR mutations', *Journal of Clinical Oncology*, 31(27), pp. 3327–3334. doi: 10.1200/JCO.2012.44.2806.

Sergina, N. V and Moasser, M. M. (2007) 'The HER family and cancer: emerging molecular mechanisms and therapeutic targets', *Trends Mol Med.*, 13(12), pp. 527–534. doi: 10.1016/j.biotechadv.2011.08.021.Secreted.

Sezgintürk, M. K. (2011) 'A new impedimetric biosensor utilizing VEGF receptor-1 (Flt-1): Early diagnosis of vascular endothelial growth factor in breast cancer', *Biosensors and Bioelectronics*, 26(10), pp. 4032–4039. doi: 10.1016/j.bios.2011.03.025.

Sforza, V., Martinelli, E., Ciardiello, F., Gambardella, V., Napolitano, S., Martini, G., Corte, C. Della, Cardone, C., Ferrara, M. L., Reginelli, A., Liguori, G., Belli, G. and Troiani, T. (2016) 'Mechanisms of resistance to anti-epidermal growth factor receptor inhibitors in metastatic colorectal cancer', *World Journal of Gastroenterology*, 22(28), pp. 6345–6361. doi: 10.3748/wjg.v22.i28.6345.

Shahbazi, B., Najafabadi, Z. S., Goudarzi, H., Sajadi, M., Tahoori, F. and Bagheri, M. (2019) 'Cytotoxic effects of Pseudocerastes persicus venom and its HPLC fractions on lung cancer cells', *Journal of Venomous Animals and Toxins including Tropical Diseases*, (February 2019), pp. 1–11.

Shanbhag, V. K. L. (2015) 'Applications of snake venoms in treatment of cancer', *Asian Pacific Journal of Tropical Biomedicine*. Hainan Medical University, 5(4), pp. 275–276. doi: 10.1016/S2221-1691(15)30344-0.

Sharma, S. K. and Bagshawe, K. D. (2017a) 'Antibody Directed Enzyme Prodrug Therapy (ADEPT): Trials and tribulations', *Advanced Drug Delivery Reviews*. Elsevier B.V., 118, pp. 2–7. doi: 10.1016/j.addr.2017.09.009.

Sharma, S. K. and Bagshawe, K. D. (2017b) 'Translating antibody directed enzyme prodrug therapy (ADEPT) and prospects for combination', *Expert Opinion on Biological Therapy*. Taylor & Francis, 17(1), pp. 1–13. doi: 10.1080/14712598.2017.1247802.

Sharma, S. V., Bell, D. W., Settleman, J. and Haber, D. A. (2007) 'Epidermal growth factor receptor mutations in lung cancer', *Nature Reviews Cancer*, 7(3), pp. 169–181. doi: 10.1038/nrc2088.

Shear, W. A. (2015) 'The chemical defenses of millipedes (diplopoda): Biochemistry, physiology and ecology', *Biochemical Systematics and Ecology*. Elsevier Ltd, 61, pp. 78–117. doi: 10.1016/j.bse.2015.04.033.

Sheff, M. A. and Thorn, K. S. (2004) 'Optimized cassettes for fluorescent protein tagging in Saccharomyces cerevisiae', *Yeast*, 21(8), pp. 661–670. doi: 10.1002/yea.1130.

Shen, Y., Chen, X., He, J., Liao, D. and Zu, X. (2018) 'Axl inhibitors as novel cancer therapeutic agents.', *Life sciences*. Netherlands, 198, pp. 99–111. doi: 10.1016/j.lfs.2018.02.033.

Sheng, Z., Wang, J., Dong, Y., Ma, H., Zhou, H., Sugimura, H., Lu, G. and Zhou, X. (2008) 'EphB1 is underexpressed in poorly differentiated colorectal cancers', *Pathobiology*, 75(5), pp. 274–280. doi: 10.1159/000151707.

Shi, F., Telesco, S. E., Liu, Y., Radhakrishnan, R. and Lemmona, M. A. (2010) 'ErbB3/HER3 intracellular domain is competent to bind ATP and catalyze autophosphorylation', *Proceedings of the National Academy of Sciences of the United States of America*, 107(17), pp. 7692–7697. doi: 10.1073/pnas.1002753107.

Shibuya, M. (2014) 'Vegf-vegfr signals in health and disease', *Biomolecules and Therapeutics*, 22(1), pp. 1–9. doi: 10.4062/biomolther.2013.113.

Shieh, Y. S., Lai, C. Y., Kao, Y. R., Shiah, S. G., Chu, Y. W., Lee, H. S. and Wu, C. W. (2005) 'Expression of Axl in lung adenocarcinoma and correlation with tumor progression', *Neoplasia*, 7(12), pp. 1058–1064. doi: 10.1593/neo.05640.

Shin, S.-Y., Rath, O., Choo, S.-M., Fee, F., McFerran, B., Kolch, W. and Cho, K.-H. (2009) 'Positive- and negative-feedback regulations coordinate the dynamic behavior of the Ras-Raf-MEK-ERK signal transduction pathway.', *Journal of cell science*, 122, pp. 425–435. doi: 10.1242/jcs.036319.

Siddle, H. V., Kreiss, A., Tovar, C., Yuen, C. K., Cheng, Y., Belov, K., Swift, K., Pearse, A. M., Hamede, R., Jones, M. E., Skjødt, K., Woods, G. M. and Kaufman, J. (2013) 'Reversible epigenetic down-regulation of MHC molecules by devil facial tumour disease illustrates immune escape by a contagious cancer', *Proceedings of the National Academy of Sciences of the United States of America*, 110(13), pp. 5103–5108. doi: 10.1073/pnas.1219920110.

Siena, S., Sartore-Bianchi, A., Marsoni, S., Hurwitz, H. I., McCall, S. J., Penault-Llorca, F., Srock, S., Bardelli, A. and Trusolino, L. (2018) 'Targeting the human epidermal growth factor receptor 2 (HER2) oncogene in colorectal cancer', *Annals of Oncology*, 29(5), pp. 1108–1119. doi: 10.1093/annonc/mdy100.

Da Silva, S. L., Rowan, E. G., Albericio, F., Stábeli, R. G., Calderon, L. A. and Soares, A. M. (2014) 'Animal toxins and their advantages in biotechnology and pharmacology', *BioMed Research International*, 2014, pp. 2–4. doi: 10.1155/2014/951561.

Simon, N., Antignani, A., Sarnovsky, R., Hewitt, S. M. and FitzGerald, D. (2016) 'Targeting a cancer-specific epitope of the epidermal growth factor receptor in triple-negative breast cancer', *Journal of the National Cancer Institute*, 108(8), pp. 1–8. doi: 10.1093/jnci/djw028.

Singh, H., Hansen, T. M., Patel, N. and Brindle, N. P. J. (2012) 'The molecular balance between receptor tyrosine kinases Tie1 and Tie2 is dynamically controlled by VEGF and TNFα and

regulates angiopoietin signalling', *PLoS ONE*, 7(1), pp. 1–9. doi: 10.1371/journal.pone.0029319.

Singh, H., Werner, L., DeAngelo, D., Ballen, K., Amrein, P., Wadleigh, M., Neuberg, D., Fox, E., Stone, R. and Attar, E. (2010) 'Clinical outcome of patients with acute promyelocytic leukemia and FLT3 mutations', *American Journal of Hematology*, 85(12), pp. 956–957. doi: 10.1002/ajh.21867.Clinical.

Singh, M. and Jadhav, H. R. (2018) 'Targeting non-small cell lung cancer with small-molecule EGFR tyrosine kinase inhibitors', *Drug Discovery Today*. Elsevier Ltd, 23(3), pp. 745–753. doi: 10.1016/j.drudis.2017.10.004.

Sivakumar, G. (2013) 'Colchicine Semisynthetics: Chemotherapeutics for Cancer?', *Current Medicinal Chemistry*, 20(7), pp. 892–898. doi: 10.2174/0929867311320070005.

Skirnisdottir, I., Seidal, T. and Akerud, H. (2016) 'The relationship of the angiogenesis regulators VEGF-A, VEGF-R1 and VEGF-R2 to p53 status and prognostic factors in epithelial ovarian carcinoma in FIGO-stages I-II', *International Journal of Oncology*, 48(3), pp. 998–1006. doi: 10.3892/ijo.2016.3333.

Sledge, G. W. and Miller, K. D. (2003) 'Exploiting the hallmarks of cancer: The future conquest of breast cancer', *European Journal of Cancer*, 39, pp. 1668–1675. doi: 10.1016/S0959-8049(03)00273-9.

Smith, H. M., Smith, R. B. and Sawin, H. L. (1977) 'A summary of snake classification (Reptilia, Serpentes)', *Journal of Herpetology*, 11(2), pp. 115–121.

Sohn, J., Liu, S., Parinyanitikul, N., Lee, J., Hort obagyi, G. N., Mills, G. B., Ueno, N. T. and Gonzalez-Angulo, A. M. (2014) 'cMET activation and EGFR-directed therapy resistance in triple-negative breast cancer', *Journal of Cancer*, 5(9), pp. 745–753. doi: 10.7150/jca.9696.

Solca, F., Dahl, G., Zoephel, A., Bader, G., Sanderson, M., Klein, C., Kraemer, O., Himmelsbach, F., Haaksma, E. and Adolf, G. R. (2012) 'Target binding properties and cellular activity of afatinib (BIBW 2992), an irreversible ErbB family blocker.', *The Journal of pharmacology and experimental therapeutics*, 343, pp. 342–50. doi: 10.1124/jpet.112.197756.

Soletti, R. C., del Barrio, L., Daffre, S., Miranda, A., Borges, H. L., Moura-Neto, V., Lopez, M. G. and Gabilan, N. H. (2010) 'Peptide gomesin triggers cell death through L-type channel calcium influx, MAPK/ERK, PKC and PI3K signaling and generation of reactive oxygen species', *Chemico-Biological Interactions*. Elsevier Ireland Ltd, 186(2), pp. 135–143. doi: 10.1016/j.cbi.2010.04.012.

Solt, L. A. and Burris, T. P. (2012) 'Action of RORs and Their Ligands in (Patho)physiology', *Trends in Endocrinology & Metabolism*, 23(12), pp. 619–627. doi: 10.1161/CIRCULATIONAHA.110.956839.

Somay Doğan, T., İğci, N., Biber, A., Gerekçi, S., Hüsnügil, H. H., İzbirak, A. and Özen, C. (2018) 'Peptidomic characterization and bioactivity of protoiurus kraepelini (Scorpiones: Iuridae) venom', *Turkish Journal of Biology*, 42(6), pp. 490–497. doi: 10.3906/biy-1804-35.

Sommer, A., Kopitz, C., Schatz, C. A., Nising, C. F., Mahlert, C., Lerchen, H. G., Stelte-Ludwig, B., Hammer, S., Greven, S., Schuhmacher, J., Braun, M., Zierz, R., Wittemer-Rump, S., Harrenga, A., Dittmer, F., Reetz, F., Apeler, H., Jautelat, R., Huynh, H., *et al.* (2016) 'Preclinical efficacy of the auristatin-based antibody-drug conjugate BAY 1187982 for the treatment of FGFR2-positive solid tumors', *Cancer Research*, 76(21), pp. 6331–6339. doi: 10.1158/0008-5472.CAN-16-0180.

Song, X., Weng, H., Logsdon, C. D., Rashid, A., Fleming, J. B., Abbruzzese, J. L., Gomez, H. F., Evans, D. B. and Wang, H. (2011) 'Overexpression of receptor tyrosine kinase Axl promotes tumor cell invasion and survival in pancreatic ductal adenocarcinoma', *Cancer*, 117(4), pp. 734–

743. doi: 10.1002/cncr.25483.

Sonnenschein, C. and Soto, A. M. (2013) 'The aging of the 2000 and 2011 Hallmarks of Cancer reviews: A critique', *Journal of Biosciences*, 38(September), pp. 651–663. doi: 10.1007/s12038-013-9335-6.

Stadler, C., Rexhepaj, E., Singan, V. R., Murphy, R. F., Pepperkok, R., Uhlén, M., Simpson, J. C. and Lundberg, E. (2013) 'Immunofluorescence and fluorescent-protein tagging show high correlation for protein localization in mammalian cells', *Nature Methods*, 10(4), pp. 315–323. doi: 10.1038/nmeth.2377.

Stanley, A., Ashrafi, G. H., Seddon, A. M. and Modjtahedi, H. (2017) 'Synergistic effects of various Her inhibitors in combination with IGF-1R, C-MET and Src targeting agents in breast cancer cell lines', *Scientific Reports*, 7(1), pp. 1–15. doi: 10.1038/s41598-017-04301-8.

Steeghs, N., Nortier, J. W. R. and Gelderblom, H. (2007) 'Small molecule tyrosine kinase inhibitors in the treatment of solid tumors: An update of recent developments', *Annals of Surgical Oncology*, 14(2), pp. 942–953. doi: 10.1245/s10434-006-9227-1.

Steinberg, S. F. (2008) 'Structural basis of protein kinase C isoform function.', *Physiological reviews*, 88, pp. 1341–1378. doi: 10.1152/physrev.00034.2007.

Steiner, M. and Neri, D. (2011) 'Antibody-radionuclide conjugates for cancer therapy: Historical considerations and new trends', *Clinical Cancer Research*, 17, pp. 6406–6416. doi: 10.1158/1078-0432.CCR-11-0483.

Stephenson, S., Slomka, S., Douglas, E. L., Hewett, P. J. and Hardingham, J. E. (2001) 'Receptor protein tyrosine kinase EphB4 is up-regulated in colon cancer', *BMC Molecular Biology*, 2(15), pp. 1–9.

Stewart, E. L., Tan, S. Z., Liu, G. and Tsao, M. S. (2015) 'Known and putative mechanisms of resistance to EGFR targeted therapies in NSCLC patients with EGFR mutations-a review', *Translational Lung Cancer Research*, 4(1), pp. 67–81. doi: 10.3978/j.issn.2218-6751.2014.11.06.

Stockert, J. C., Horobin, R. W., L, C. L. and Blazquez-Castro, A. (2018) 'Tetrazolium salts and formazan products in cell biology: viability assessment, fluorescence imaging, and labeling perspectives', *Acta Histochemica*, 120(3), pp. 159–167.

Stockmann, H., Adamczyk, B., Hayes, J. and Rudd, P. M. (2013) 'Automated, High-Throughput IgG-Antibody Glycoprofiling Platform', *Analytical chemistry*, 85, pp. 8841–8849.

Stransky, N., Cerami, E., Schalm, S., Kim, J. L. and Lengauer, C. (2014) 'The landscape of kinase fusions in cancer', *Nature Communications*. Nature Publishing Group, 5. doi: 10.1038/ncomms5846.

Su, J. C., Lin, K. L., Chien, C. M., Chuang, P. W., Chang, L. Sen and Lin, S. R. (2010) 'Concomitant inactivation of the epidermal growth factor receptor, phosphatidylinositol 3-kinase/Akt and Janus tyrosine kinase 2/signal transducer and activator of transcription 3 signalling pathways in cardiotoxin III-treated A549 cells', *Clinical and Experimental Pharmacology and Physiology*, 37, pp. 833–840. doi: 10.1111/j.1440-1681.2010.05397.x.

Sudol, M., Chen, H. I., Bougeret, C., Einbond, A. and Bork, P. (1995) 'Characterization of a novel protein-binding module - the W W domain', *FEBS Letters*, 369, pp. 67–71.

Sugimoto, T., Kuroda, H., Horii, Y., Moritake, H., Tanaka, T. and Hattori, S. (2001) 'Signal transduction pathways through TRK-A and TRK-B receptors in human neuroblastoma cells', *Japanese Journal of Cancer Research*, 92(2), pp. 152–160. doi: 10.1111/j.1349-7006.2001.tb01077.x.

Suhf, S. M. and Kim, D. S. (1996) 'Identification of the Snake Venom Substance That Induces

Apoptosis', *Biochemical and Biophysical Research Communications*, 224, pp. 134–139. doi: 10.1111/j.1742-7843.2008.00229.x.

Sukari, A., Nagasaka, M., Al-Hadidi, A. and Lum, L. G. (2016) 'Cancer immunology and immunotherapy', *Anticancer Research*, 36(11), pp. 5593–5606. doi: 10.21873/anticanres.11144.

Sun, L. K., Yoshii, Y., Hyodo, A., Tsurushima, H., Saito, A., Harakuni, T., Li, Y. P., Kariya, K., Nozaki, M. and Morine, N. (2003) 'Apoptotic effect in the glioma cells induced by specific protein extracted from Okinawa Habu (Trimeresurus flavoviridis) venom in relation to oxidative stress', *Toxicology in Vitro*, 17(2), pp. 169–177. doi: 10.1016/S0887-2333(03)00010-9.

Sun, M. N., Zhao, X. J., Zhao, H. D., Zhang, W. G., Li, F. L., Chen, M. Z., Li, H. and Li, G. (2013) 'Recombinant Escherichia coli Trx-JZTX-III represses the proliferation of mouse hepatocellular carcinoma cells through induction of cell cycle arrest', *Molecular Medicine Reports*, 7(6), pp. 1800–1804. doi: 10.3892/mmr.2013.1432.

Sun, W. L., Chen, J., Wang, Y. P. and Zheng, H. (2011) 'Autophagy protects breast cancer cells from epirubicin-induced apoptosis and facilitates epirubicin-resistance development', *Autophagy*, 7(9), pp. 1035–1044. doi: 10.4161/auto.7.9.16521.

Surawska, H., Ma, P. C. and Salgia, R. (2004) 'The role of ephrins and Eph receptors in cancer', *Cytokine and Growth Factor Reviews*, 15(6), pp. 419–433. doi: 10.1016/j.cytogfr.2004.09.002.

Suthe, S. R., Yao, H. P., Weng, T. H., Hu, C. Y., Feng, L., Wu, Z. G. and Wang, M. H. (2018) 'RON receptor tyrosine kinase as a therapeutic target for eradication of triple-negative breast cancer: Efficacy of anti-RON ADC ZT/G4-MMAE', *Molecular Cancer Therapeutics*, 17(12), pp. 2654–2664. doi: 10.1158/1535-7163.MCT-18-0252.

Swenson, S., Costa, F., Minea, R., Sherwin, R. P., Ernst, W., Fujii, G., Yang, D. and Markland, F. S. (2004) 'Intravenous liposomal delivery of the snake venom disintegrin contortrostatin limits breast cancer progression', *Molecular Cancer Therapeutics*, 3(4), pp. 499–511.

Tabchy, A., Valero, V., Vidaurre, T., Lluch, A., Gomez, H., Martin, M., Qi, Y., Barajas-Figueroa, L. J., Souchon, E., Coutant, C., Doimi, F. D., Ibrahim, N. K., Gong, Y., Hortobagyi, G. N., Hess, K. R., Symmans, W. F. and Pusztai, L. (2010) 'Evaluation of a 30-gene paclitaxel, fluorouracil, doxorubicin, and cyclophosphamide chemotherapy response predictor in a multicenter randomized trial in breast cancer', *Clinical Cancer Research*, 16(21), pp. 5351–5361. doi: 10.1158/1078-0432.CCR-10-1265.

Takai, K., Drain, A. P., Lawson, D. A., Littlepage, L. E., Karpuj, M., Kessenbrock, K., Le, A., Inoue, K., Weaver, V. M. and Werb, Z. (2018) 'Discoidin domain receptor 1 (DDR1) ablation promotes tissue fibrosis and hypoxia to induce aggressive basal-like breast cancers', *Genes and Development*, 32(3–4), pp. 244–257. doi: 10.1101/gad.301366.117.

Takegawa, N. and Yonesaka, K. (2017) 'HER2 as an Emerging Oncotarget for Colorectal Cancer Treatment After Failure of Anti-Epidermal Growth Factor Receptor Therapy', *Clinical Colorectal Cancer*. Elsevier Inc., 16(4), pp. 247–251. doi: 10.1016/j.clcc.2017.03.001.

Takeuchi, K., Soda, M., Togashi, Y., Suzuki, R., Sakata, S., Hatano, S., Asaka, R., Hamanaka, W., Ninomiya, H., Uehara, H., Lim Choi, Y., Satoh, Y., Okumura, S., Nakagawa, K., Mano, H. and Ishikawa, Y. (2012) 'RET, ROS1 and ALK fusions in lung cancer', *Nature Medicine*, 18(3), pp. 378–381. doi: 10.1038/nm.2658.

Tan, K. K., Ler, S. G., Gunaratne, J., Bay, B. H. and Ponnampalam, G. (2017) 'In vitro cytotoxicity of L-amino acid oxidase from the venom of Crotalus mitchellii pyrrhus', *Toxicon*. Elsevier Ltd, 139, pp. 20–30. doi: 10.1016/j.toxicon.2017.09.012.

Tanaka, K., Okugawa, Y., Toiyama, Y., Inoue, Y., Saigusa, S., Kawamura, M., Araki, T., Uchida, K., Mohri, Y. and Kusunoki, M. (2014) 'Brain-Derived Neurotrophic Factor (BDNF)-induced

Tropomyosin-related kinase B (Trk B) signaling is a potential therapeutic target for peritoneal carcinomatosis arising from colorectal cancer', *PLoS ONE*, 9(5), pp. 1–12. doi: 10.1371/journal.pone.0096410.

Tang, K. D., Holzapfel, B. M., Liu, J., Lee, T. K. W., Ma, S., Jovanovic, L., An, J., Russell, P. J., Clements, J. A., Hutmacher, D. W. and Ling, M. T. (2016) 'Tie-2 regulates the stemness and metastatic properties of prostate cancer cells', *Oncotarget*, 7(3), pp. 2572–2584. doi: 10.18632/oncotarget.3950.

Tang, X. X., Robinson, M. E., Riceberg, J. S., Kim, D. Y., Kung, B., Titus, T. B., Hayashi, S., Flake, A. W., Carpentieri, D. and Ikegaki, N. (2004) 'Favorable neuroblastoma genes and molecular therapeutics of neuroblastoma', *Clinical Cancer Research*, 10(17), pp. 5837–5844. doi: 10.1158/1078-0432.CCR-04-0395.

Tang, X. X., Zhao, H., Robinson, M. E., Cohen, B., Cnaan, A., London, W., Cohn, S. L., Cheung, N. V, Brodeur, G. M., Evans, A. E. and Ikegaki, N. (2000) 'Implications of EPHB6, EFNB2, and EFNB3 expressions in human neuroblastoma', *PNAS*, 97(20), pp. 10936–10941.

Tarafdar, A., Hopcroft, L. E. M., Gallipoli, P., Pellicano, F., Cassels, J., Hair, A., Korfi, K., Jørgensen, H. G., Vetrie, D., Holyoake, T. L. and Michie, A. M. (2017) 'CML cells actively evade host immune surveillance through cytokine-mediated downregulation of MHC-II expression', *Blood*, 129(2), pp. 199–208. doi: 10.1182/blood-2016-09-742049.

Tavares, C., Maciel, T., Burin, S., Ambrósio, L., Ghisla, S., Sampaio, S. and Castro, F. (2016) 'L-Amino acid oxidase isolated from Calloselasma rhodostoma snake venom induces cytotoxicity and apoptosis in JAK2V617F-positive cell lines', *Revista Brasileira de Hematologia e Hemoterapia*. Associação Brasileira de Hematologia, Hemoterapia e Terapia Celular, 38(2), pp. 128–134. doi: 10.1016/j.bjhh.2016.03.004.

Tavazoie, S. F., Alarcon, C., Oskarsson, T., Padua, D., Wang, Q., Bos, P. D., Gerald, W. L. and Massague, J. (2008) 'Endogenous human microRNAs that suppress breast cancer metastasis', *Nature*, 451(7175), pp. 147–152. doi: 10.1038/nature06487.Endogenous.

Teicher, B. a. and Chari, R. V. J. (2011) 'Antibody conjugate therapeutics: Challenges and potential', *Clinical Cancer Research*, 17, pp. 6389–6397. doi: 10.1158/1078-0432.CCR-11-1417.

Teixeira, T. L., Oliveira Silva, V. A., da Cunha, D. B., Polettini, F. L., Thomaz, C. D., Pianca, A. A., Zambom, F. L., da Silva Leitão Mazzi, D. P., Reis, R. M. and Mazzi, M. V. (2016) 'Isolation, characterization and screening of the in vitro cytotoxic activity of a novel L-amino acid oxidase (LAAOcdt) from Crotalus durissus terrificus venom on human cancer cell lines', *Toxicon*, 119, pp. 203–217. doi: 10.1016/j.toxicon.2016.06.009.

Templeton, A. J., Diez-Gonzalez, L., Ace, O., Vera-Badillo, F., Šeruga, B., Jordán, J., Amir, E., Pandiella, A. and Ocaña, A. (2014) 'Prognostic relevance of receptor tyrosine kinase expression in breast cancer: A meta-analysis', *Cancer Treatment Reviews*. Elsevier Ltd, 40(9), pp. 1048–1055. doi: 10.1016/j.ctrv.2014.08.003.

Terai, T. and Nagano, T. (2013) 'Small-molecule fluorophores and fluorescent probes for bioimaging', *Pflugers Archiv European Journal of Physiology*, 465(3), pp. 347–359. doi: 10.1007/s00424-013-1234-z.

Tesniere, A., Schlemmer, F., Boige, V., Kepp, O., Martins, I., Ghiringhelli, F., Aymeric, L., Michaud, M., Apetoh, L., Barault, L., Mendiboure, J., Pignon, J. P., Jooste, V., Van Endert, P., Ducreux, M., Zitvogel, L., Piard, F. and Kroemer, G. (2010) 'Immunogenic death of colon cancer cells treated with oxaliplatin', *Oncogene*. Nature Publishing Group, 29(4), pp. 482–491. doi: 10.1038/onc.2009.356.

Tettamanti, S., Marin, V., Pizzitola, I., Magnani, C. F., Giordano Attianese, G. M. P., Cribioli, E., Maltese, F., Galimberti, S., Lopez, A. F., Biondi, A., Bonnet, D. and Biagi, E. (2013) 'Targeting

of acute myeloid leukaemia by cytokine-induced killer cells redirected with a novel CD123-specific chimeric antigen receptor', *British Journal of Haematology*, 161(3), pp. 389–401. doi: 10.1111/bjh.12282.

Thangam, R., Gunasekaran, P., Kaveri, K., Sridevi, G., Sundarraj, S., Paulpandi, M. and Kannan, S. (2012) 'A novel disintegrin protein from Naja naja venom induces cytotoxicity and apoptosis in human cancer cell lines in vitro', *Process Biochemistry*. Elsevier Ltd, 47(8), pp. 1243–1249. doi: 10.1016/j.procbio.2012.04.020.

Thiele, C. J., Li, Z. and McKee, A. E. (2009) 'On Trk - the TrkB signal transduction pathway is an increasingly important target in cancer biology', *Clinical Cancer Research*, 15(19), pp. 5962–5967. doi: 10.1158/1078-0432.CCR-08-0651.

Thielemann, A., Baszczuk, A., Kopczyński, Z., Kopczyński, P. and Grodecka-Gazdecka, S. (2013) 'Clinical usefulness of assessing VEGF and soluble receptors sVEGFR-1 and sVEGFR-2 in women with breast cancer', *Annals of Agricultural and Environmental Medicine*, 20(2), pp. 293–297.

Thobe, M. N., Gurusamy, D., Pathrose, P. and Waltz, S. E. (2010) 'The Ron receptor tyrosine kinase positively regulates angiogenic chemokine production in prostate cancer cells', *Oncogene*. Nature Publishing Group, 29(2), pp. 214–226. doi: 10.1038/onc.2009.331.

Thomas, R. M., Toney, K., Fenoglio-Preiser, C., Revelo-Penafiel, M. P., Hingorani, S. R., Tuveson, D. A., Waltz, S. E. and Lowy, A. M. (2007) 'The RON receptor tyrosine kinase mediates oncogenic phenotypes in pancreatic cancer cells and is increasingly expressed during pancreatic cancer progression', *Cancer Research*, 67(13), pp. 6075–6082. doi: 10.1158/0008-5472.CAN-06-4128.

Thomas, S. A., Grami, Z., Mehta, S., Patel, K., North, W. and Hospital, F. (2016) 'Adverse Effects of 5-fluorouracil: Focus on Rare Side Effects', *Cancer Cell & Microenvironment*, pp. 3–6. doi: 10.14800/ccm.1266.

Thomasson, M., Hedman, H., Junttila, T. T., Elenius, K., Ljungberg, B. and Henriksson, R. (2004) 'ErbB4 is downregulated in renal cell carcinoma--a quantitative RT-PCR and immunohistochemical analysis of the epidermal growth factor receptor family.', *Acta oncologica (Stockholm, Sweden)*. England, 43(5), pp. 453–459.

Tian, Y., Wang, H., Li, B., Ke, M., Wang, J., Dou, J. and Zhou, C. (2013) 'The cathelicidin-BF Lys16 mutant Cbf-K16 selectively inhibits non-small cell lung cancer proliferation in vitro', *Oncology Reports*, 30(5), pp. 2502–2510. doi: 10.3892/or.2013.2693.

Tolaney, S. M., Barry, W. T., Dang, C. T., Yardley, D. A., Moy, B., Marcom, P. K., Albain, K. S., Rugo, H. S., Ellis, M., Shapira, I., Wolff, A. C., Carey, L. A., Overmoyer, B. A., Partridge, A. H., Guo, H., Hudis, C. A., Krop, I. E., Burstein, H. J. and Winer, E. P. (2015) 'Adjuvant paclitaxel and trastuzumab for node-negative, HER2-positive breast cancer', *New England Journal of Medicine*, 372(2), pp. 134–141. doi: 10.1056/NEJMoa1406281.

Tomlinson, D. C., Baldo, O., Hamden, P. and Knowles, M. A. (2007) 'FGFR3 protein expression and its relationship to mutation status and prognostic variables in bladder cancer', *Journal of Pathology*, 213(1), pp. 91–98. doi: 10.1002/path.2207.

Tong-ngam, P., Roytrakul, S. and Sritanaudomchai, H. (2015) 'BmKn-2 scorpion venom peptide for killing oral cancer cells by apoptosis', *Asian Pacific Journal of Cancer Prevention*, 16(7), pp. 2807–2811. doi: 10.7314/APJCP.2015.16.7.2807.

Toosi, B. M., El Zawily, A., Truitt, L., Shannon, M., Allonby, O., Babu, M., DeCoteau, J., Mousseau, D., Ali, M., Freywald, T., Gall, A., Vizeacoumar, F. S., Kirzinger, M. W., Geyer, C. R., Anderson, D. H., Kim, T. H., Welm, A. L., Siegel, P., Vizeacoumar, F. J., *et al.* (2018) 'EPHB6 augments both development and drug sensitivity of triple-negative breast cancer tumours',

Oncogene. Springer US, 37(30), pp. 4073–4093. doi: 10.1038/s41388-018-0228-x.

Torres-Larios, A., Gurrola, G. B., Zamudio, F. Z. and Possani, L. D. (2000) 'Hadrurin, A new antimicrobial peptide from the venom of the scorpion Hadrurus aztecus', *European Journal of Biochemistry*, 267(16), pp. 5023–5031. doi: 10.1046/j.1432-1327.2000.01556.x.

Toy, K. A., Valiathan, Rajeshwari R, Nunez, F., Kidwell, K. M., Gonzalez, M. E., Fridman, R. and Kleer, C. G. (2015) 'Tyrosine Kinase Discoidin Domain Receptors DDR1 and DDR2 are Coordinately Deregulated in Triple Negative Breast Cancer Kathy', *Breast Cancer Research*, 150(1), pp. 9–18. doi: 10.1007/s10549-015-3285-7.Tyrosine.

Toy, K. A., Valiathan, Rajeshwari R., Núñez, F., Kidwell, K. M., Gonzalez, M. E., Fridman, R. and Kleer, C. G. (2015) 'Tyrosine Kinase Discoidin Domain Receptors DDR1 and DDR2 are Coordinately Deregulated in Triple Negative Breast Cancer', 150(1), pp. 9–18. doi: 10.1055/s-0035-1563737.Venous.

Toyama, D. O., Marangoni, S., Diz-Filho, E. B. S., Oliveira, S. C. B. and Toyama, M. H. (2009) 'Effect of umbelliferone (7-hydroxycoumarin, 7-HOC) on the enzymatic, edematogenic and necrotic activities of secretory phospholipase A2 (sPLA2) isolated from Crotalus durissus collilineatus venom', *Toxicon*. Elsevier Ltd, 53(4), pp. 417–426. doi: 10.1016/j.toxicon.2008.12.018.

Trentini, M. M., das Neves, R. C., Santos, B. de P. O., DaSilva, R. A., de Souza, A. C. B., Mortari, M. R., Schwartz, E. F., Kipnis, A. and Junqueira-Kipnis, A. P. (2017) 'Non-disulfide-bridge peptide 5.5 from the scorpion Hadrurus gertschi inhibits the growth of Mycobacterium abscessus subsp. massiliense', *Frontiers in Microbiology*, 8(FEB), pp. 1–11. doi: 10.3389/fmicb.2017.00273.

Trim, S. A. and Trim, C. M. (2013) 'Venom: the sharp end of pain therapeutics', *British Journal of Pain*, 7(4), pp. 179–188. doi: 10.1177/2049463713502005.

Truitt, L., Freywald, T., DeCoteau, J., Sharfe, N. and Freywald, A. (2010) 'The EphB6 receptor cooperates with c-Cbl to regulate the behavior of breast cancer cells', *Cancer Research*, 70(3), pp. 1141–1153. doi: 10.1158/0008-5472.CAN-09-1710.

Tsai, P. C., Chu, C. L., Chiu, C. C., Chang, L. Sen and Lin, S. R. (2014) 'Cardiotoxin III suppresses hepatocyte growth factor-stimulated migration and invasion of MDA-MB-231 cells', *Cell Biochemistry and Function*, 32(6), pp. 485–495. doi: 10.1002/cbf.3041.

Tsai, P. C., Fu, Y. S., Chang, L. Sen and Lin, S. R. (2016) 'Taiwan cobra cardiotoxin III suppresses EGF/EGFR-mediated epithelial-to-mesenchymal transition and invasion of human breast cancer MDA-MB-231 cells', *Toxicon*. Elsevier Ltd, 111, pp. 108–120. doi: 10.1016/j.toxicon.2016.01.051.

Tsai, P. C., Hsieh, C. Y., Chiu, C. C., Wang, C. K., Chang, L. Sen and Lin, S. R. (2012) 'Cardiotoxin III suppresses MDA-MB-231 cell metastasis through the inhibition of EGF/EGFR-mediated signaling pathway', *Toxicon*. Elsevier Ltd, 60(5), pp. 734–743. doi: 10.1016/j.toxicon.2012.05.019.

Tsao, A. S. (2012) 'Carboplatin- or Cisplatin-Based Chemotherapy in First-Line Treatment of Small-Cell Lung Cancer: The COCIS Meta-Analysis of Individual Patient Data', *Yearbook of Medicine*. Mosby, Inc., 2012, pp. 151–152. doi: 10.1016/s0084-3873(12)00211-8.

Tsouko, E., Wang, J., Frigo, D. E., Aydogdu, E. and Williams, C. (2015) 'miR-200a inhibits migration of triple-negative breast cancer cells through direct repression of the EPHA2 oncogene', *Carcinogenesis*, 36(9), pp. 1051–1060. doi: 10.1093/carcin/bgv087.

Tsujioka, H., Yotsumoto, F., Shirota, K., Horiuchi, S., Yoshizato, T., Kuroki, M. and Miyamoto, S. (2010) 'Emerging strategies for ErbB ligand-based targeted therapy for cancer', *Anticancer*

Research, 30, pp. 3107–3112.

Tu, W. C., Wu, C. C., Hsieh, H. L., Chen, C. Y. and Hsu, S. L. (2008) 'Honeybee venom induces calcium-dependent but caspase-independent apoptotic cell death in human melanoma A2058 cells', *Toxicon*, 52(2), pp. 318–329. doi: 10.1016/j.toxicon.2008.06.007.

Turner, N., Pearson, A., Sharpe, R., Lambros, M., Geyer, F., Lopez-Garcia, M. A., Natrajan, R., Marchio, C., Iorns, E., Mackay, A., Gillett, C., Grigoriadis, A., Tutt, A., Reis-Filho, J. S. and Ashworth, A. (2010) 'FGFR1 amplification drives endocrine therapy resistance and is a therapeutic target in breast cancer.', *Cancer research*. United States, 70(5), pp. 2085–2094. doi: 10.1158/0008-5472.CAN-09-3746.

Ueno, N. T. and Zhang, D. (2011) 'Targeting EGFR in triple negative breast cancer', *Journal of Cancer*, 2(1), pp. 324–328. doi: 10.7150/jca.2.324.

Ullrich, A. and Schlessinger, J. (1990) 'Signal transduction by receptors with tyrosine kinase activity', *Cell*, 61(2), pp. 203–212. doi: 10.1016/0092-8674(90)90801-K.

Undheim, E. A. B., Jenner, R. A. and King, G. F. (2016) 'Centipede venoms as a source of drug leads', *Expert Opinion on Drug Discovery*, 11(12), pp. 1139–1149. doi: 10.1080/17460441.2016.1235155.

Untch, M. and Lück, H. J. (2010) 'Lapatinib - Member of a new generation of ErbB-Targeting drugs', *Breast Care*, 5(suppl 1), pp. 8–12. doi: 10.1159/000285750.

Ustach, C. V., Huang, W., Conley-LaComb, M. K., Lin, C. Y., Che, M., Abrams, J. and Kim, H. R. C. (2010) 'A novel signaling axis of matriptase/PDGF-D/β-PDGFR in human prostate cancer', *Cancer Research*, 70(23), pp. 9631–9640. doi: 10.1158/0008-5472.CAN-10-0511.

Vaidyanathan, G. and R. Zalutsky, M. (2012) 'Applications of 211At and 223Ra in Targeted Alpha-Particle Radiotherapy', *Current Radiopharmaceuticalse*, 4(4), pp. 283–294. doi: 10.2174/1874471011104040283.

Valdez-Cruz, N. A., Batista, C. V. F. and Possani, L. D. (2004) 'Phaiodactylipin, a glycosylated heterodimeric phospholipase A2 from the venom of the scorpion Anuroctonus phaiodactylus', *European Journal of Biochemistry*, 271(8), pp. 1453–1464. doi: 10.1111/j.1432-1033.2004.04047.x.

Valdez-Velazquéz, L. L., Romero-Gutierrez, M. T., Delgado-Enciso, I., Dobrovinskaya, O., Melnikov, V., Quintero-Hernández, V., Ceballos-Magaña, S. G., Gaitan-Hinojosa, M. A., Coronas, F. I., Puebla-Perez, A. M., Zamudio, F., De La Cruz-García, I., Vázquez-Vuelvas, O. F., Soriano-Hernandez, A. D. and Possani, L. D. (2016) 'Comprehensive analysis of venom from the scorpion Centruroides tecomanus reveals compounds with antimicrobial, cytotoxic, and insecticidal activities', *Toxicon*, 118, pp. 95–103. doi: 10.1016/j.toxicon.2016.04.046.

Valencia, K., Ormazábal, C., Zandueta, C., Luis-Ravelo, D., Antón, I., Pajares, M. J., Agorreta, J., Montuenga, L. M., Martínez-Canarias, S., Leitinger, B. and Lecanda, F. (2012) 'Inhibition of collagen receptor discoidin domain receptor-1 (DDR1) reduces cell survival, homing, and colonization in lung cancer bone metastasis', *Clinical Cancer Research*, 18(4), pp. 969–980. doi: 10.1158/1078-0432.CCR-11-1686.

Valenzuela, M. M. A., Neidigh, J. W. and Wall, N. R. (2014) 'Antimetabolite Treatment for Pancreatic Cancer', *Chemotherapy*, 3(3), pp. 1–16. doi: 10.4172/2167-7700.1000137.

Valiathan, R. R., Marco, M., Leitinger, B., Kleer, C. G. and Fridman, R. (2012) 'Discoidin Domain Receptor Tyrosine Kinases: New Players in Cancer Progression', 31(1–2), pp. 295–321. doi: 10.1007/s10555-012-9346-z.DISCOIDIN.

Valtola, R., Salven, P., Taipale, J., Joensuu, H., Rehn, M., Pihlajaniemi, T., Weich, H. and Alitalo, K. (1999) 'VEGFR-3 and Its Ligand VEGF-C Are Associated with Angiogenesis in Breast

Cancer', *American Journal of Pathology*, 154(5), pp. 1–10. Available at: papers2://publication/uuid/591EA31B-2332-43A6-BF67-292DF41DFB56.

Vanuopadath, M., Shaji, S. K., Raveendran, D., Nair, B. G. and Nair, S. S. (2020) 'Delineating the venom toxin arsenal of Malabar pit viper (Trimeresurus malabaricus) from the Western Ghats of India and evaluating its immunological cross-reactivity and in vitro cytotoxicity', *International Journal of Biological Macromolecules*. Elsevier B.V., 148, pp. 1029–1045. doi: 10.1016/j.ijbiomac.2020.01.226.

Veikkolainen, V., Vaparanta, K., Halkilahti, K., Iljin, K., Sundvall, M. and Elenius, K. (2011) 'Function of ERBB4 is determined by alternative splicing', *Cell Cycle*, 10(16), pp. 2647–2657. doi: 10.4161/cc.10.16.17194.

Velcheti, V., Schalper, K. A., Carvajal, D. E., Anagnostou, V. K., Syrigos, K. N., Sznol, M., Herbst, R. S., Gettinger, S. N., Chen, L. and Rimm, D. L. (2014) 'Programmed death ligand-1 expression in non-small cell lung cancer', *Laboratory Investigation*. Nature Publishing Group, 94(1), pp. 107–116. doi: 10.1038/labinvest.2013.130.

Vella, V., Malaguarnera, R., Nicolosi, M. L., Palladino, C., Spoleti, C., Massimino, M., Vigneri, P., Purrello, M., Ragusa, M., Morrione, A. and Belfiore, A. (2017) 'Discoidin domain receptor 1 modulates insulin receptor signaling and biological responses in breast cancer cells', *Oncotarget*, 8(26), pp. 43248–43270. doi: 10.18632/oncotarget.18020.

Verma, A., Warner, S. L., Vankayalapati, H., Bearss, D. J. and Sharma, S. (2011) 'Targeting Axl and Mer kinases in cancer', *Molecular Cancer Therapeutics*, 10(10), pp. 1763–1773. doi: 10.1158/1535-7163.MCT-11-0116.

Verma, V. A., Pillow, T. H., Depalatis, L., Li, G., Phillips, G. L., Polson, A. G., Raab, H. E., Spencer, S. and Zheng, B. (2015) 'The cryptophycins as potent payloads for antibody drug conjugates', *Bioorganic and Medicinal Chemistry Letters*. Elsevier Ltd, 25(4), pp. 864–868. doi: 10.1016/j.bmcl.2014.12.070.

Vidal, M., Paré, L. and Prat, A. (2016) 'Molecular classification of breast cancer', *Management of Breast Diseases: Second Edition*, 27(1), pp. 203–219. doi: 10.1007/978-3-319-46356-8_12.

Vinay, D. S., Ryan, E. P., Pawelec, G., Talib, W. H., Stagg, J., Elkord, E., Lichtor, T., Decker, W. K., Whelan, R. L., Kumara, H. M. C. S., Signori, E., Honoki, K., Georgakilas, A. G., Amin, A., Helferich, W. G., Boosani, C. S., Guha, G., Ciriolo, M. R., Chen, S., *et al.* (2015) 'Immune evasion in cancer: Mechanistic basis and therapeutic strategies', *Seminars in Cancer Biology*. Elsevier Ltd, 35, pp. S185–S198. doi: 10.1016/j.semcancer.2015.03.004.

Vinnedge, L. M. P., Benight, N. M., Wagh, P. K., Pease, N. A., Nashu, M. A., Serrano-lopez, J., Adams, A. K., Cancelas, J. A., Waltz, S. E. and Wells, S. I. (2015) 'The DEK oncogene promotes cellular proliferation through paracrine Wnt signaling in Ron receptor positive breast cancers', *Oncogene*, 34(18), pp. 2325–2336. doi: 10.1038/onc.2014.173.The.

Vu, T. and Claret, F. X. (2012) 'Trastuzumab: Updated Mechanisms of Action and Resistance in Breast Cancer', *Frontiers in Oncology*, 2(June), pp. 1–6. doi: 10.3389/fonc.2012.00062.

Vyas, V. K., Brahmbhatt, K., Bhatt, H. and Parmar, U. (2013) 'Therapeutic potential of snake venom in cancer therapy: Current perspectives', *Asian Pacific Journal of Tropical Biomedicine*, 3(2), pp. 156–162. doi: 10.1016/S2221-1691(13)60042-8.

Wadood, A., Ali, S. A., Sattar, R., Lodhi, M. A. and Ul-Haq, Z. (2012) 'A Novel Pharmacophore Model to Identify Leads for Simultaneous Inhibition of Anti-coagulation and Anti-inflammatory Activities of Snake Venom Phospholipase A 2', *Chemical Biology and Drug Design*, 79(4), pp. 431–441. doi: 10.1111/j.1747-0285.2011.01281.x.

Wagenfeld, A., Saunders, P. T. K., Whitaker, L. and Critchley, H. O. D. (2016) 'Selective

progesterone receptor modulators (SPRMs): progesterone receptor action, mode of action on the endometrium and treatment options in gynecological therapies', *Expert Opinion on Therapeutic Targets*. Taylor & Francis, 20(9), pp. 1045–1054. doi: 10.1080/14728222.2016.1180368.

Wagstaff, S. C., Favreau, P., Cheneval, O., Laing, G. D., Wilkinson, M. C., Miller, R. L., Stöcklin, R. and Harrison, R. A. (2008) 'Molecular characterisation of endogenous snake venom metalloproteinase inhibitors', *Biochemical and Biophysical Research Communications*, 365(4), pp. 650–656. doi: 10.1016/j.bbrc.2007.11.027.

Wahba, H. A. and El-Hadaad, H. A. (2015) 'Current approaches in treatment of triple-negative breast cancer', *Cancer Biology and Medicine*, 12(2), pp. 106–116. doi: 10.7497/j.issn.2095-3941.2015.0030.

Walker, S. R., Chaudhury, M., Nelson, E. A. and Frank, D. A. (2010) 'Microtubule-targeted chemotherapeutic agents inhibit Signal Transducer and Activator of Transcription 3 (STAT3) signaling', *Molecular Pharmacology*, 78(5), pp. 903–908. doi: 10.1124/mol.110.066316.

Wang, D., Qian, G., Zhang, H., Magliocca, K. R., Nannapaneni, S., Amin, A. R. M. R., Rossi, M., Patel, M., El-Deiry, M., Wadsworth, J. T., Chen, Z., Khuri, F. R., Shin, D. M., Saba, N. F. and Chen, Z. G. (2017) 'HER3 targeting sensitizes HNSCC to cetuximab by reducing HER3 activity and HER2/HER3 dimerization: Evidence from cell line and patient-derived xenograft models', *Clinical Cancer Research*, 23(3), pp. 677–686. doi: 10.1158/1078-0432.CCR-16-0558.

Wang, H., Ke, M., Tian, Y., Wang, J., Li, B., Wang, Y., Dou, J. and Zhou, C. (2013) 'BF-30 selectively inhibits melanoma cell proliferation via cytoplasmic membrane permeabilization and DNA-binding in vitro and in B16F10-bearing mice', *European Journal of Pharmacology*. Elsevier, 707(1–3), pp. 1–10. doi: 10.1016/j.ejphar.2013.03.028.

Wang, Haiyan, Wen, J., Wang, Hai, Guo, Q., Shi, S., Shi, Q., Zhou, X., Liu, Q., Lu, G. and Wang, J. (2014) 'Loss of expression of EphB1 protein in serous carcinoma of ovary associated with metastasis and poor survival', *International Journal of Clinical and Experimental Pathology*, 7(1), pp. 313–321.

Wang, J. H., Xie, Y., Wu, J. C., Han, R., Reid, P. F., Qin, Z. H. and He, J. K. (2012) 'Crotoxin enhances the antitumor activity of gefinitib (Iressa) in SK-MES-1 human lung squamous carcinoma cells', *Oncology Reports*, 27, pp. 1341–1347. doi: 10.3892/or.2012.1677.

Wang, J., Kataoka, H., Suzuki, M., Sato, N., Nakamura, R., Tao, H., Maruyama, K., Isogaki, J., Kanaoka, S., Ihara, M., Tanaka, M., Kanamori, M., Nakamura, T., Shinmura, K. and Sugimura, H. (2005) 'Downregulation of EphA7 by hypermethylation in colorectal cancer', *Oncogene*, 24(36), pp. 5637–5647. doi: 10.1038/sj.onc.1208720.

Wang, Jun, Wang, B., Chu, H. and Yao, Y. (2016) 'Intrinsic resistance to EGFR tyrosine kinase inhibitors in advanced non-small-cell lung cancer with activating EGFR mutations', *OncoTargets and Therapy*, 9, pp. 3711–3726. doi: 10.2147/OTT.S106399.

Wang, Junxiong, Yang, S., Cai, X., Dong, J., Chen, Z., Wang, R., Zhang, S., Cao, H., Lu, D., Jin, T., Nie, Y., Hao, J. and Fan, D. (2016) 'Berberine inhibits EGFR signaling and enhances the antitumor effects of EGFR inhibitors in gastric cancer', *Oncotarget*, 7(46), pp. 76076–76086. doi: 10.18632/oncotarget.12589.

Wang, L. F., Fokas, E., Juricko, J., You, A., Rose, F., Pagenstecher, A., Engenhart-Cabillic, R. and An, H. X. (2008) 'Increased expression of EphA7 correlates with adverse outcome in primary and recurrent glioblastoma multiforme patients', *BMC Cancer*, 8, pp. 1–9. doi: 10.1186/1471-2407-8-79.

Wang, M. H., Lee, W., Weis, M. T. and Tao, H. P. (2007) 'Altered expression of the RON receptor tyrosine kinase in various epithelial cancers and its contribution to tumourigenic phenotypes in thyroid cancer cells', *Journal of Pathology*, 213(October), pp. 402–411. doi: 10.1002/path.

Wang, Q., Quan, H., Zhao, J., Xie, C., Wang, L. and Lou, L. (2013a) 'RON confers lapatinib resistance in HER2-positive breast cancer cells', *Cancer Letters*. Elsevier Ireland Ltd, 340(1), pp. 43–50. doi: 10.1016/j.canlet.2013.06.022.

Wang, Q., Quan, H., Zhao, J., Xie, C., Wang, L. and Lou, L. (2013b) 'RON confers lapatinib resistance in HER2-positive breast cancer cells', *Cancer Letters*. Elsevier Ireland Ltd, 340(1), pp. 43–50. doi: 10.1016/j.canlet.2013.06.022.

Wang, R., Li, L., Zhang, S., Li, Y., Wang, X., Miao, Q. and Zhen, Y. (2018) 'A novel enediyne-integrated antibody–drug conjugate shows promising antitumor efficacy against CD30+ lymphomas', *Molecular Oncology*, 12(3), pp. 339–355. doi: 10.1002/1878-0261.12166.

Wang, S.-C. and Hung, M.-C. (2009) 'Nuclear translocation of the epidermal growth factor receptor family membrane tyrosine kinase receptors.', *Clinical cancer research : an official journal of the American Association for Cancer Research*, 15, pp. 6484–6489. doi: 10.1158/1078-0432.CCR-08-2813.

Wang, X. C., Katso, R., Butler, R., Hanby, A. M., Poulsom, R., Jones, T., Sheer, D. and Ganesan, T. S. (1996) 'H-RYK, an unusual receptor kinase: Isolation and analysis of expression in ovarian cancer', *Molecular Medicine*, 2(2), pp. 189–203. doi: 10.1007/bf03401616.

Wang, Y.-N., Yamaguchi, H., Hsu, J.-M. and Hung, M.-C. (2010) 'Nuclear trafficking of the epidermal growth factor receptor family membrane proteins.', *Oncogene*. Nature Publishing Group, 29(28), pp. 3997–4006. doi: 10.1038/onc.2010.157.

Wang, Y. M., Parmelee, J., Guo, Y. W. and Tsai, I. H. (2010) 'Absence of phospholipase A2 in most Crotalus horridus venom due to translation blockage: Comparison with Crotalus horridus atricaudatus venom', *Toxicon*. Elsevier Ltd, 56(1), pp. 93–100. doi: 10.1016/j.toxicon.2010.03.015.

Warkentin, T. E. (2004) 'Bivalent direct thrombin inhibitors: Hirudin and bivalirudin', *Best Practice and Research: Clinical Haematology*, 17(1), pp. 105–125. doi: 10.1016/j.beha.2004.02.002.

Warrell, D. A. (2010) 'Snake bite', *The Lancet*. Elsevier Ltd, 375(9708), pp. 77–88. doi: 10.1016/S0140-6736(09)61754-2.

Webb, T. R., Slavish, J., George, R. E., Look, A. T., Xue, L., Jiang, Q., Cui, X., Rentrop, W. B. and Morris, S. W. (2009) 'Anaplastic lymphoma kinase: Role in cancer pathogenesis and small-molecule inhibitor development for therapy', *Expert Review of Anticancer Therapy*, 9(3), pp. 331–356. doi: 10.1586/14737140.9.3.331.

Weigel, M. T., Meinhold-Heerlein, I., Bauerschlag, D. O., Schem, C., Bauer, M., Jonat, W., Maass, N. and Mundhenke, C. (2009) 'Combination of imatinib and vinorelbine enhances cell growth inhibition in breast cancer cells via PDGFR β signalling', *Cancer Letters*. Elsevier Ireland Ltd, 273(1), pp. 70–79. doi: 10.1016/j.canlet.2008.07.040.

Weiner, L. M., Dhodapkar, M. V and Ferrone, S. (2009) 'Monoclonal Antibodies for Cancer Immunotherapy', *Lancet*, 373(9668), pp. 1033–1040. doi: 10.1038/jid.2014.371.

Weiner, L. M., Murray, J. C. and Shuptrine, C. W. (2012) 'Antibody-based immunotherapy of cancer', *Cell*. Elsevier Inc., 148(6), pp. 1081–1084. doi: 10.1016/j.cell.2012.02.034.

Weiner, L. M., Surana, R. and Wang, S. (2010) 'Monoclonal antibodies: versatile platforms for cancer immunotherapy.', *Nature reviews. Immunology*, 10, pp. 317–327. doi: 10.1038/nri2744.

Weitsman, G., Barber, P. R., Nguyen, L. K., Lawler, K., Patel, G., Woodman, N., Kelleher, M. T., Pinder, S. E., Rowley, M., Ellis, P. A., Purushotham, A. D., Coolen, A. C., Kholodenko, B. N., Vojnovic, B., Gillett, C. and Ng, T. (2016) 'HER2-HER3 dimer quantification by FLIM-FRET predicts breast cancer metastatic relapse independently of HER2 IHC status', *Oncotarget*,

7(32), pp. 51012–51026. doi: 10.18632/oncotarget.9963.

Whittaker, S. R., Barlow, C., Martin, M. P., Mancusi, C., Wagner, S., Self, A., Barrie, E., Te Poele, R., Sharp, S., Brown, N., Wilson, S., Jackson, W., Fischer, P. M., Clarke, P. A., Walton, M. I., McDonald, E., Blagg, J., Noble, M., Garrett, M. D., *et al.* (2018) 'Molecular profiling and combinatorial activity of CCT068127: a potent CDK2 and CDK9 inhibitor', *Molecular Oncology*, 12(3), pp. 287–304. doi: 10.1002/1878-0261.12148.

Wiesner, T., He, J., Yelensky, R., Esteve-Puig, R., Botton, T., Yeh, I., Lipson, D., Otto, G., Brennan, K., Murali, R., Garrido, M., Miller, V. A., Ross, J. S., Berger, M. F., Sparatta, A., Palmedo, G., Cerroni, L., Busam, K. J., Kutzner, H., *et al.* (2014) 'Kinase fusions are frequent in Spitz tumours and spitzoid melanomas', *Nature Communications*. Nature Publishing Group, 5. doi: 10.1038/ncomms4116.

Wild, D., Frischknecht, M., Zhang, H., Morgenstern, A., Bruchertseifer, F., Boisclair, J., Provencher-Bolliger, A., Reubi, J. C. and Maecke, H. R. (2011) 'Alpha- versus beta-particle radiopeptide therapy in a human prostate cancer model (213Bi-DOTA-PESIN and 213Bi-AMBA versus 177Lu-DOTA-PESIN)', *Cancer Research*, 71(3), pp. 1009–1018. doi: 10.1158/0008-5472.CAN-10-1186.

Wilden, P. A., Kahn, C. R., Siddle, K. and White, M. F. (1992) 'Insulin receptor kinase domain autophosphorylation regulates receptor enzymatic function', *Journal of Biological Chemistry*, 267(23), pp. 16660–16668.

Wilson, D., Boyle, G. M., McIntyre, L., Nolan, M. J., Parsons, P. G., Smith, J. J., Tribolet, L., Loukas, A., Liddell, M. J., Rash, L. D. and Daly, N. L. (2017) 'The aromatic head group of spider toxin polyamines influences toxicity to cancer cells', *Toxins*, 9(11), pp. 1–13. doi: 10.3390/toxins9110346.

Wingerd, J. S., Mozar, C. A., Ussing, C. A., Murali, S. S., Chin, Y. K. Y., Cristofori-Armstrong, B., Durek, T., Gilchrist, J., Vaughan, C. W., Bosmans, F., Adams, D. J., Lewis, R. J., Alewood, P. F., Mobli, M., Christie, M. J. and Rash, L. D. (2017) 'The tarantula toxin β/δ-TRTX-Pre1a highlights the importance of the S1-S2 voltage-sensor region for sodium channel subtype selectivity', *Scientific Reports*, 7(1), pp. 1–15. doi: 10.1038/s41598-017-01129-0.

Wojtukiewicz, M. Z., Hempel, D., Sierko, E., Tucker, S. C. and Honn, K. V. (2017) 'Antiplatelet agents for cancer treatment: a real perspective or just an echo from the past?', *Cancer and Metastasis Reviews*. Cancer and Metastasis Reviews, 36(2), pp. 305–329. doi: 10.1007/s10555-017-9683-z.

Wong, A. L. a and Lee, S.-C. (2012) 'Mechanisms of Resistance to Trastuzumab and Novel Therapeutic Strategies in HER2-Positive Breast Cancer.', *International journal of breast cancer*, 2012, p. 415170. doi: 10.1155/2012/415170.

Wong, K.-K., Engelman, J. A. and Cantley, L. C. (2010) 'Targeting the PI3K signaling pathway in cancer therapy.', *Curr Opin Genet Dev.*, 20(1), pp. 1–7. doi: 10.1080/07853890600551037.

Woo, S. R., Turnis, M. E., Goldberg, M. V., Bankoti, J., Selby, M., Nirschl, C. J., Bettini, M. L., Gravano, D. M., Vogel, P., Liu, C. L., Tangsombatvisit, S., Grosso, J. F., Netto, G., Smeltzer, M. P., Chaux, A., Utz, P. J., Workman, C. J., Pardoll, D. M., Korman, A. J., *et al.* (2012) 'Immune inhibitory molecules LAG-3 and PD-1 synergistically regulate T-cell function to promote tumoral immune escape', *Cancer Research*, 72(4), pp. 917–927. doi: 10.1158/0008-5472.CAN-11-1620.

Woof, J. M. and Russell, M. W. (2011) 'Structure and function relationships in IgA', *Mucosal Immunology*. Nature Publishing Group, 4(6), pp. 590–597. doi: 10.1038/mi.2011.39.

Wu, F.-L., Zhang, J., Li, W., Bian, B.-X., Hong, Y.-D., Song, Z.-Y., Wang, H.-Y., Cui, F.-B., Li, R.-T., Liu, Q., Jiang, X.-D., Li, X.-M. and Zheng, J.-N. (2017) 'Enhanced antiproliferative activity of antibody-functionalized polymeric nanoparticles for targeted delivery of anti-miR-21

to HER2 positive gastric cancer', *Oncotarget*, 8(40), pp. 67189–67202. doi: 10.18632/oncotarget.18066.

Wu, P., Nielsen, T. E. and Clausen, M. H. (2015) 'FDA-approved small-molecule kinase inhibitors', *Trends in Pharmacological Sciences*, 36(7), pp. 422–439. doi: 10.1016/j.tips.2015.04.005.

Wu, Q., Suo, Z., Kristensen, G. B., Baekelandt, M. and Nesland, J. M. (2006) 'The prognostic impact of EphB2/B4 expression on patients with advanced ovarian carcinoma', *Gynecologic Oncology*, 102(1), pp. 15–21. doi: 10.1016/j.ygyno.2005.11.034.

Wu, R., Connolly, D., Ngelangel, C., Bosch, F. X., Muñoz, N. and Cho, K. R. (2000) 'Somatic mutations of fibroblast growth factor receptor 3 (FGFR3) are uncommon in carcinomas of the uterine cervix', *Oncogene*, 19(48), pp. 5543–5546. doi: 10.1038/sj.onc.1203934.

Wu, S., Nie, Y., Zeng, X. C., Cao, H., Zhang, L., Zhou, L., Yang, Y., Luo, X. and Liu, Y. (2014) 'Genomic and functional characterization of three new venom peptides from the scorpion Heterometrus spinifer', *Peptides*. Elsevier Inc., 53, pp. 30–41. doi: 10.1016/j.peptides.2013.12.012.

Wu, X., Liu, X., Koul, S., Lee, C. Y., Zhang, Z. and Halmos, B. (2014) 'AXL kinase as a novel target for cancer therapy', *Oncotarget*, 5(20), pp. 9546–9563. Available at: www.impactjournals.com/oncotarget%5Cnwww.impactjournals.com/oncotarget/.

Xi, G. M., Sun, B., Jiang, H. H., Kong, F., Yuan, H. Q. and Lou, H. X. (2010) 'Bisbibenzyl derivatives sensitize vincristine-resistant KB/VCR cells to chemotherapeutic agents by retarding P-gp activity', *Bioorganic and Medicinal Chemistry*. Elsevier Ltd, 18(18), pp. 6725–6733. doi: 10.1016/j.bmc.2010.07.055.

Xia, G., Kumar, S. R., Stein, J. P., Singh, J., Krasnoperov, V., Zhu, S., Hassanieh, L., Smith, D. L., Buscarini, M., Broek, D., Quinn, D. I., Weaver, F. A. and Gill, P. S. (2006) 'EphB4 receptor tyrosine kinase is expressed in bladder cancer and provides signals for cell survival', *Oncogene*, 25(5), pp. 769–780. doi: 10.1038/sj.onc.1209108.

Xiao, K. F., Zhou, J., Wang, Z., Fu, W. H. and Lu, X. Y. (2012) 'Effect of the venom of the scorpion Heterometrus liangi on the expression of P21 and caspase-3 gene in human KYSE-510 cell', *Advanced Materials Research*, 345, pp. 399–404. doi: 10.4028/www.scientific.net/AMR.345.399.

Xiao, Z., Carrasco, R., Kinneer, K., Sabol, D., Jallal, B., Coats, S. and Tice, D. A. (2012) 'EphB4 promotes or suppresses Ras/MEK/ERK pathway in a context-dependent manner', *Cancer Biology & Therapy*, 13(8), pp. 630–637. doi: 10.4161/cbt.20080.

Xie, S., Li, Y., Li, X., Wang, L., Yang, N., Wang, Y. and Wei, H. (2015) 'Mer receptor tyrosine kinase is frequently overexpressed in human non-small cell lung cancer, confirming resistance to erlotinib', *Oncotarget*, 6(11), pp. 9206–9219. doi: 10.18632/oncotarget.3280.

Xie, X., Rui, W., He, W., Shao, Y., Sun, F., Zhou, W., Wu, Y. and Zhu, Y. (2017) 'Discoidin domain receptor 1 activity drives an aggressive phenotype in bladder cancer', *American Journal of Translational Research*, 9(5), pp. 2500–2507.

Xu, D., Yuan, L., Liu, X., Li, M., Zhang, F., Gu, X. Y., Zhang, D., Yang, Y., Cui, B., Tong, J., Zhou, J. and Yu, Z. (2016) 'EphB6 overexpression and Apc mutation together promote colorectal cancer', *Oncotarget*, 7(21), pp. 31111–31121. doi: 10.18632/oncotarget.9080.

Xu, F., Zhong, W., Li, J., Shanshen, Z., Cui, J., Nesland, J. M. and Suo, Z. (2005) 'Predictive value of EphA2 and EphrinA-1 expression in oesophageal squamous cell carcinoma', *Anticancer Research*, 25(4), pp. 2943–2950.

Xu, X., Duan, Z., Di, Z., He, Y., Li, J., Li, Z., Xie, C., Zeng, X., Cao, Z., Wu, Y., Liang, S. and

Li, W. (2014) ‘Proteomic analysis of the venom from the scorpion Mesobuthus martensii’, *Journal of Proteomics*. Elsevier B.V., 106, pp. 162–180. doi: 10.1016/j.jprot.2014.04.032.

Yam, C., Mani, S. A. and Moulder, S. L. (2017) ‘Targeting the Molecular Subtypes of Triple Negative Breast Cancer: Understanding the Diversity to Progress the Field’, *The Oncologist*, 22(9), pp. 1086–1093. doi: 10.1634/theoncologist.2017-0095.

Yamaguchi, N., Lucena-Araujo, A. R., Nakayama, S., de Figueiredo-Pontes, L. L., Gonzalez, D. A., Yasuda, H., Kobayashi, S. and Costa, D. B. (2014) ‘Dual ALK and EGFR inhibition targets a mechanism of acquired resistance to the tyrosine kinase inhibitor crizotinib in ALK rearranged lung cancer’, *Lung Cancer*. Elsevier Ireland Ltd, 83(1), pp. 37–43. doi: 10.1016/j.lungcan.2013.09.019.

Yamashiro, D. J., Liu, X. G., Lee, C. P., Nakagawara, A., Ikegaki, N., McGregor, L. M., Baylin, S. B. and Brodeur, G. M. (1997) ‘Expression and function of trk-C in favourable human neuroblastomas’, *European Journal of Cancer*, 33(12), pp. 2054–2057. doi: 10.1016/S0959-8049(97)00309-2.

Yan, J. D., Liu, Y., Zhang, Z. Y., Liu, G. Y., Xu, J. H., Liu, L. Y. and Hu, Y. M. (2015) ‘Expression and prognostic significance of VEGFR-2 in breast cancer’, *Pathology Research and Practice*. Elsevier GmbH., 211(7), pp. 539–543. doi: 10.1016/j.prp.2015.04.003.

Yan, S., Jiao, X., Zou, H. and Li, K. (2015) ‘Prognostic significance of c-Met in breast cancer: A meta-analysis of 6010 cases’, *Diagnostic Pathology*. Diagnostic Pathology, 10(1), pp. 1–10. doi: 10.1186/s13000-015-0296-y.

Yang, L., Li, Y., Shen, E., Cao, F., Li, L., Li, X., Wang, X., Kariminia, S., Chang, B., Li, H. and Li, Q. (2017) ‘NRG1-dependent activation of HER3 induces primary resistance to trastuzumab in HER2-overexpressing breast cancer cells’, *International Journal of Oncology*, 51(5), pp. 1553–1562. doi: 10.3892/ijo.2017.4130.

Yang, S. H., Baek, H. A., Lee, H. J., Park, H. S., Jang, K. Y., Kang, M. J., Lee, D. G., Lee, Y. C., Moon, W. S. and Chung, M. J. (2010) ‘Discoidin domain receptor 1 is associated with poor prognosis of non-small cell lung carcinomas’, *Oncology Reports*, 24, pp. 311–319. doi: 10.3892/or.

Yang, S. H., Chien, C. M., Lu, M. C., Lin, Y. H., Hu, X. W. and Lin, S. R. (2006) ‘Up-regulation of Bax and endonuclease G, and down-modulation of Bcl-X L involved in cardiotoxin III-induced apoptosis in K562 cells’, *Experimental and Molecular Medicine*, 38(4), pp. 435–444. doi: 10.1038/emm.2006.51.

Yang, S. H., Chien, C. M., Lu, M. C., Lu, Y. J., Wu, Z. Z. and Lin, S. R. (2005) ‘Cardiotoxin III induces apoptosis in K562 cells through a mitochondrial-mediated pathway’, *Clinical and Experimental Pharmacology and Physiology*, 32(7), pp. 515–520. doi: 10.1111/j.1440-1681.2005.04223.x.

Yang, S. H., Lu, M. C., Chien, C. M., Tsai, C. H., Lu, Y. J., Hour, T. C. and Lin, S. R. (2005) ‘Induction of apoptosis in human leukemia K562 cells by cardiotoxin III’, *Life Sciences*, 76(21), pp. 2513–2522. doi: 10.1016/j.lfs.2005.01.001.

Yang, Z., Yang, N., Ou, Q., Xiang, Y., Jiang, T., Wu, X., Bao, H., Tong, X., Wang, X., Shao, Y. W., Liu, Y., Wang, Y. and Zhou, C. (2018) ‘Investigating novel resistance mechanisms to third-generation EGFR tyrosine kinase inhibitor osimertinib in non–small cell lung cancer patients’, *Clinical Cancer Research*, 24(13), pp. 3097–3107. doi: 10.1158/1078-0432.CCR-17-2310.

Yaswen, P., MacKenzie, K. L., Keith, W. N., Hentosh, P., Rodier, F., Zhu, J., Firestone, G. L., Matheu, A., Carnero, A., Bilsland, A., Sundin, T., Honoki, K., Fujii, H., Georgakilas, A. G., Amedei, A., Amin, A., Helferich, B., Boosani, C. S., Guha, G., *et al.* (2015) ‘Therapeutic targeting of replicative immortality’, *Seminars in Cancer Biology*. Elsevier Ltd, 35, pp. S104–S128. doi:

10.1016/j.semcancer.2015.03.007.

Ye, B., Xie, Y., Qin, Z. H., Wu, J. C., Han, R. and He, J. K. (2011) 'Anti-tumor activity of CrTX in human lung adenocarcinoma cell line A549', *Acta Pharmacologica Sinica*. Nature Publishing Group, 32(11), pp. 1397–1401. doi: 10.1038/aps.2011.116.

Yen, C. Y., Liang, S. S., Han, L. Y., Chou, H. L., Chou, C. K., Lin, S. R. and Chiu, C. C. (2013) 'Cardiotoxin III inhibits proliferation and migration of oral cancer cells through MAPK and MMP signaling', *The Scientific World Journal*, 2013, pp. 1–5. doi: 10.1155/2013/650946.

Yilmaz, E., Celik, O., Simsek, Y., Turkcuoglu, I., Celik, E., Gül, M., Hascalik, S. and Aydin, E. (2012) 'C-Kit proto-oncogene expression in endometrial hyperplasia and endometrial cancer', *Archives of Gynecology and Obstetrics*, 286(1), pp. 197–200. doi: 10.1007/s00404-012-2276-8.

Yu, H. A., Suzawa, K., Jordan, E., Zehir, A., Ni, A., Kim, R., Kris, M. G., Hellmann, M. D., Li, B. T., Somwar, R., Solit, D. B., Berger, M. F., Arcila, M., Riely, G. J. and Ladanyi, M. (2018) 'Concurrent alterations in EGFR-mutant lung cancers associated with resistance to EGFR kinase inhibitors and characterization of MTOR as a mediator of resistance', *Clinical Cancer Research*, 24(13), pp. 3108–3118. doi: 10.1158/1078-0432.CCR-17-2961.

Yu, J., Bulk, E., Ji, P., Hascher, A., Tang, M., Metzger, R., Marra, A., Serve, H., Berdel, W. E., Wiewroth, R., Koschmieder, S. and Müller-Tidow, C. (2010) 'The EPHB6 receptor tyrosine kinase is a metastasis suppressor that is frequently silenced by promoter DNA hypermethylation in non-small cell lung cancer', *Clinical Cancer Research*, 16(8), pp. 2275–2283. doi: 10.1158/1078-0432.CCR-09-2000.

Yu, S. F., Zheng, B., Go, M., Lau, J., Spencer, S., Raab, H., Soriano, R., Jhunjhunwala, S., Cohen, R., Caruso, M., Polakis, P., Flygare, J. and Polson, A. G. (2015) 'A novel anti-CD22 anthracycline-based antibody-drug conjugate (ADC) that overcomes resistance to auristatin-based ADCs', *Clinical Cancer Research*, 21(14), pp. 3298–3306. doi: 10.1158/1078-0432.CCR-14-2035.

Yu, X., Ghamande, S., Liu, H, Xue, L., Zhao, S., Tan, W., Zhao, L., Tang, S., Wu, D., Korkaya, H., Maihle, N. and Liu, HY (2018) 'Targeting EGFR/HER2/HER3 with a Three-in-One Aptamer-siRNA Chimera Confers Superior Activity against HER2+ Breast Cancer', *Mol Ther Nucleic Acids*, 10, pp. 317–330. doi: 10.1016/j.omtn.2017.12.015.

Yuan, T. L. and Cantley, L. C. (2008) 'PI3K pathway alterations in cancer: variations on a theme.', *Oncogene*, 27, pp. 5497–5510. doi: 10.1038/onc.2008.245.

Yuan, W. J., Ge, J., Chen, Z. K., Wu, S. Bin, Shen, H., Yang, P., Hu, B., Zhang, G. W. and Chen, Z. H. (2009) 'Over-expression of EphA2 and ephrinA-1 in human gastric adenocarcinoma and its prognostic value for postoperative patients', *Digestive Diseases and Sciences*, 54(11), pp. 2410–2417. doi: 10.1007/s10620-008-0649-4.

Zah, E., Lin, M. Y., Silva-Benedict, A., Jensen, M. C. and Chen, Y. Y. (2016) 'T cells expressing CD19/CD20 bi-specific chimeric antigen receptors prevent antigen escape by malignant B cells', *Cancer immunology research*, 4(6), pp. 498–508. doi: 10.1016/j.physbeh.2017.03.040.

Zainal Abidin, S. A., Rajadurai, P., Chowdhury, M. E. H., Ahmad Rusmili, M. R., Othman, I. and Naidu, R. (2018) 'Cytotoxic, Antiproliferative and Apoptosis-inducing Activity of L-Amino Acid Oxidase from Malaysian Calloselasma rhodostoma on Human Colon Cancer Cells', *Basic and Clinical Pharmacology and Toxicology*, 123(5), pp. 577–588. doi: 10.1111/bcpt.13060.

Zamunér, S. R., Da Cruz-Höfling, M. A., Corrado, A. P., Hyslop, S. and Rodrigues-Simioni, L. (2004) 'Comparison of the neurotoxic and myotoxic effects of Brazilian Bothrops venoms and their neutralization by commercial antivenom', *Toxicon*, 44(3), pp. 259–271. doi: 10.1016/j.toxicon.2004.05.029.

Zargan, J., Sajad, M., Umar, S., Naime, Mohammad, Ali, S. and Khan, H. A. (2011) 'Scorpion (Androctonus crassicauda) venom limits growth of transformed cells (SH-SY5Y and MCF-7) by cytotoxicity and cell cycle arrest', *Experimental and Molecular Pathology*, 91(1), pp. 447–454. doi: 10.1016/j.yexmp.2011.04.008.

Zargan, J., Sajad, M., Umar, S., Naime, M., Ali, S. and Khan, H. A. (2011) 'Scorpion (Odontobuthus doriae) venom induces apoptosis and inhibits DNA synthesis in human neuroblastoma cells', *Molecular and Cellular Biochemistry*, 348(1–2), pp. 173–181. doi: 10.1007/s11010-010-0652-x.

Zargan, J., Umar, S., Sajad, M., Naime, M., Ali, S. and Khan, H. A. (2011) 'Scorpion venom (Odontobuthus doriae) induces apoptosis by depolarization of mitochondria and reduces S-phase population in human breast cancer cells (MCF-7)', *Toxicology in Vitro*. Elsevier Ltd, 25(8), pp. 1748–1756. doi: 10.1016/j.tiv.2011.09.002.

Závada, J., Valenta, J., Kopecký, O., Stach, Z. and Leden, P. (2011) 'Black mamba dendroaspis polylepis bite: a case report.', *Prague medical report*, 112(4), pp. 298–304.

Zelinski, D. P., Zantek, N. D., Stewart, J. C., Irizarry, A. R. and Kinch, M. S. (2001) 'EphA2 overexpression causes tumorigenesis of mammary epithelial cells', *Cancer Research*, 61(5), pp. 2301–2306.

Zereshkian, A., Leyton, J. V., Cai, Z., Bergstrom, D., Weinfeld, M. and Reilly, R. M. (2014) 'The human polynucleotide kinase/phosphatase (hPNKP) inhibitor A12B4C3 radiosensitizes human myeloid leukemia cells to Auger electron-emitting anti-CD123 111In-NLS-7G3 radioimmunoconjugates', *Nuclear Medicine and Biology*. Elsevier Inc., 41(5), pp. 377–383. doi: 10.1016/j.nucmedbio.2014.02.003.

Zhang, Hongtao, Berezov, A., Wang, Q., Zhang, G., Drebin, J., Murali, R. and Greene, M. I. (2007) 'ErbB receptors: from oncogenes to targeted cancer therapies', 117(8), pp. 2051–2058. doi: 10.1172/JCI32278.The.

Zhang, Hua, Pelzer, A. M., Kiang, D. T. and Yee, D. (2007) 'Down-regulation of type I insulin-like growth factor receptor increases sensitivity of breast cancer cells to insulin', *Cancer Research*, 67(1), pp. 391–397. doi: 10.1158/0008-5472.CAN-06-1712.

Zhang, H., Teng, M., Niu, L., Wang, Yubao, Wang, Yuzhen, Liu, Q., Huang, Q., Hao, Q., Dong, Y. and Liu, P. (2004) 'Purification, partial characterization, crystallization and structural determination of AHP-LAAO, a novel L-amino-acid oxidase with cell apoptosis-inducing activity from Agkistrodon halys pallas venom', *Acta Crystallographica Section D: Biological Crystallography*, 60(5), pp. 974–977. doi: 10.1107/S0907444904000046.

Zhang, J. H., Wang, L. H., Li, X. J., Wang, A. P., Reng, L. Q., Xia, F. G., Yang, Z. P., Jiang, J., Wang, X. D. and Wen, C. Y. (2014) 'Expression of Ang-2 / Tie-2 and PI3K / AKT in Colorectal Cancer', *Asian Pacific Journal of Cancer Prevention*, 15(20), pp. 8651–8656.

Zhang, J., Wang, L. S., Ye, S. L., Luo, P. and Wang, B. L. (2015) 'Blockage of tropomyosin receptor kinase a (TrkA) enhances chemo-sensitivity in breast cancer cells and inhibits metastasis in vivo', *International Journal of Clinical and Experimental Medicine*, 8(1), pp. 634–641.

Zhang, L. and Cui, L. (2007) 'A cytotoxin isolated from Agkistrodon acutus snake venom induces apoptosis via Fas pathway in A549 cells', *Toxicology in Vitro*, 21(6), pp. 1095–1103. doi: 10.1016/j.tiv.2007.04.008.

Zhang, L. and Wei, L. J. (2007) 'ACTX-8, a cytotoxic l-amino acid oxidase isolated from Agkistrodon acutus snake venom, induces apoptosis in Hela cervical cancer cells', *Life Sciences*, 80(13), pp. 1189–1197. doi: 10.1016/j.lfs.2006.12.024.

Zhang, L. and Wu, W. T. (2008) 'Isolation and characterization of ACTX-6: A cytotoxic L-amino

acid oxidase from Agkistrodon acutus snake venom', *Natural Product Research*, 22(6), pp. 554–563. doi: 10.1080/14786410701592679.

Zhang, S., Chen, L., Cui, B., Chuang, H. Y., Yu, J., Wang-Rodriguez, J., Tang, L., Chen, G., Basak, G. W. and Kipps, T. J. (2012) 'ROR1 is expressed in human breast cancer and associated with enhanced tumor-cell growth', *PLoS ONE*, 7(3), pp. 1–12. doi: 10.1371/journal.pone.0031127.

Zhang, S., Chen, L., Wang-Rodriguez, J., Zhang, L., Cui, B., Frankel, W., Wu, R. and Kipps, T. J. (2012) 'The onco-embryonic antigen ROR1 is expressed by a variety of human cancers', *American Journal of Pathology*, 181(6), pp. 1903–1910. doi: 10.1016/j.ajpath.2012.08.024.

Zhang, S., Cui, B., Lai, H., Liu, G., Ghia, E. M., Widhopf, G. F., Zhang, Z., Wu, C. C. N., Chen, L., Wu, R., Schwab, R., Carson, D. A. and Kipps, T. J. (2014) 'Ovarian cancer stem cells express ROR1, which can be targeted for anti -cancer-stem-cell therapy', *Proceedings of the National Academy of Sciences of the United States of America*, 111(48), pp. 17266–17271. doi: 10.1073/pnas.1419599111.

Zhang, X. Y. and Zhang, P. Y. (2016) 'Scorpion venoms in gastric cancer (Review)', *Oncology Letters*, 12(5), pp. 3683–3686. doi: 10.3892/ol.2016.5134.

Zhang, Y. and Weinberg, R. A. (2018) 'Epithelial-to-mesenchymal transition in cancer: complexity and opportunities EMT: a naturally occurring transdifferentia-tion program', *Frontiers of medicine*, 12(4), pp. 1–13. doi: 10.1007/s11684-018-0656-6.

Zhang, Y. X., Knyazev, P. G., Cheburkin, Y. V., Sharma, K., Knyazev, Y. P., Orfi, L., Szabadkai, I., Daub, H., Kéri, G. and Ullrich, A. (2008) 'AXL is a potential target for therapeutic intervention in breast cancer progression', *Cancer Research*, 68(6), pp. 1905–1915. doi: 10.1158/0008-5472.CAN-07-2661.

Zhang, Y., Xia, M., Jin, K., Wang, S., Wei, H., Fan, C., Wu, Y., Li, Xiaoling, Li, Xiayu, Li, G., Zeng, Z. and Xiong, W. (2018) 'Function of the c-Met receptor tyrosine kinase in carcinogenesis and associated therapeutic opportunities', *Molecular Cancer*. Molecular Cancer, 17(1), pp. 1–14. doi: 10.1186/s12943-018-0796-y.

Zhang, Y. Y., Wu, L. C., Wang, Z. P., Wang, Z. X., Jia, Q., Jiang, G. S. and Zhang, W. D. (2009) 'Anti-proliferation Effect of Polypeptide Extracted from Scorpion Venom on Human Prostate Cancer Cells in vitro', *Journal of Clinical Medicine Research*, 1(1), pp. 24–31. doi: 10.4021/jocmr2009.01.1220.

Zhang, Y., Yuan, Jia, Zhang, H. Y., Simayi, D., Li, P. D., Wang, Y. H., Li, F. and Zhang, W. J. (2012) 'Natural resistance to apoptosis correlates with resistance to chemotherapy in colorectal cancer cells', *Clinical and Experimental Medicine*, 12(2), pp. 97–103. doi: 10.1007/s10238-011-0146-5.

Zhang, Z., Lee, Jae Cheol, Lin, L., Olivas, V., Au, V., LaFramboise, T., Abdel-Rahman, M., Wang, X., Levine, A. D., Rho, J. K., Choi, Y. J., Choi, C. M., Kim, S. W., Jang, S. J., Park, Y. S., Kim, W. S., Lee, D. H., Lee, J. S., Miller, V. A., *et al.* (2012) 'Activation of the AXL kinase causes resistance to EGFR-targeted therapy in lung cancer', *Nature Genetics*, 44(8), pp. 852–860. doi: 10.1038/ng.2330.

Zhao, B., Wang, L., Qiu, H., Zhang, M., Sun, L., Peng, P., Yu, Q. and Yuan, X. (2017) 'Mechanisms of resistance to anti-EGFR therapy in colorectal cancer', *Oncotarget*, 8(3), pp. 3980–4000. doi: 10.18632/oncotarget.14012.

Zhao, S., Du, X. Y., Chen, J. S., Zhou, Y. C. and Song, J. G. (2002) 'Secretory phospholipase A2 inhibits epidermal growth factor-induced receptor activation', *Experimental Cell Research*, 279(2), pp. 354–364. doi: 10.1006/excr.2002.5622.

Zhao, Y. J. and Li, G. C. (2013) 'Tumor markers for hepatocellular carcinoma', *Molecular and Clinical Oncology*, 1, pp. 593–598. doi: 10.3892/mco.2013.119.

Zheng, L., He, H., Shen, X. and Sun, Y. (2017) 'Centipede Scolopendra suppresses cell growth in human epidermoid carcinoma cell A431', *Bangladesh Journal of Pharmacology*, 12(3), pp. 299–307. doi: 10.3329/bjp.v12i3.32525.

Zhi, Y., Li, B., Yao, C., Li, H., Chen, P., Bao, J., Qin, T., Wang, Y., Lu, T. and Lu, S. (2018) 'Discovery of the selective and efficacious inhibitors of FLT3 mutations', *European Journal of Medicinal Chemistry*. Elsevier Masson SAS, 155, pp. 303–315. doi: 10.1016/j.ejmech.2018.06.010.

Zhong, Y., Song, B., Mo, G., Yuan, Mingwei, Li, H., Wang, P., Yuan, Minglong and Lu, Q. (2014) 'A novel neurotoxin from venom of the Spider, Brachypelma albopilosum', *PLoS ONE*, 9(10), pp. 2–7. doi: 10.1371/journal.pone.0110221.

Zhou, D., Ren, K., Wang, J., Ren, H., Yang, W., Wang, W., Li, Q., Liu, X. and Tang, F. (2018) 'Erythropoietin-producing hepatocellular A6 overexpression is a novel biomarker of poor prognosis in patients with breast cancer', *Oncology Letters*, 15(4), pp. 5257–5263. doi: 10.3892/ol.2018.7919.

Zhou, J. and Giannakakou, P. (2005) 'Targeting microtubules for cancer chemotherapy.', *Current medicinal chemistry. Anti-cancer agents*, 5, pp. 65–71. doi: 10.2174/1568011053352569.

Zhou, J., Qi, Y., Diao, Q., Wu, L., Du, X., Li, Y. and Sun, L. (2013) 'Cytotoxicity of melittin and apamin in human hepatic L02 and HepG2 cells in vitro', *Toxin Reviews*, 32(4), pp. 60–67. doi: 10.3109/15569543.2013.852108.

Zhou, Q., Nakada, M. T., Arnold, C., Shieh, K. Y. and Markland, F. S. (1999) 'Contortrostatin, a dimeric disintegrin from Agkistrodon contortrix contortrix, inhibits angiogenesis', *Angiogenesis*, 3(3), pp. 259–269. doi: 10.1023/A:1009059210733.

Zhou, Q., Sherwin, R. P., Parrish, C., Richters, V., Groshen, S. G., Tsao-Wei, D. and Markland, F. S. (2000) 'Contortrostatin, a dimeric disintegrin from Agkistrodon contortrix contortrix, inhibits breast cancer progression', *Breast Cancer Research and Treatment*, 61(3), pp. 249–260. doi: 10.1023/A:1006457903545.

Zhou, S., Wang, L., Li, G., Zhang, Z. and Wang, J. (2014) 'Decreased expression of receptor tyrosine kinase of EphB1 protein in renal cell carcinomas', *International Journal of Clinical and Experimental Pathology*, 7(7), pp. 4254–4260. doi: 10.21037/tau.2016.s137.

Zhu, C., Sempkowski, M., Holleran, T., Linz, T., Bertalan, T., Josefsson, A., Bruchertseifer, F., Morgenstern, A. and Sofou, S. (2017) 'Alpha-particle radiotherapy: For large solid tumors diffusion trumps targeting', *Biomaterials*. Elsevier Ltd, 130, pp. 67–75. doi: 10.1016/j.biomaterials.2017.03.035.

Zhu, X. and Zhou, W. (2015) 'The emerging regulation of VEGFR-2 in triple-negative breast cancer', *Frontiers in Endocrinology*, 6(OCT), pp. 1–7. doi: 10.3389/fendo.2015.00159.

Zhu, Y., Wang, Y., Guan, B., Rao, Q., Wang, J., Ma, H., Zhang, Z. and Zhou, X. (2014) 'C-kit and PDGFRA gene mutations in triple negative breast cancer', *International Journal of Clinical and Experimental Pathology*, 7(7), pp. 4280–4285.

Zucali, P. A., Ruiz, M. G., Giovannetti, E., Destro, A., Varella-Garcia, M., Floor, K., Ceresoli, G. L., Rodriguez, J. A., Garassino, I., Comoglio, P., Roncalli, M., Santoro, A. and Giaccone, G. (2008) 'Role of cMET expression in non-small-cell lung cancer patients treated with EGFR tyrosine kinase inhibitors', *Annals of Oncology*, 19(9), pp. 1605–1612. doi: 10.1093/annonc/mdn240.

Zwick, E., Bange, J. and Ullrich, A. (2002) 'Receptor tyrosine kinases as targets for anticancer

drugs', *Trends in Molecular Medicine*, 8(1), pp. 17–23. doi: 10.1016/S1471-4914(01)02217-1.

Appendix

Appendix I: Chapter 2: Cell Line Authentication STR report

OJG, UK
(O) 1980 611315 E: culturecollections@phe.gov.uk W: wwwphe•culturecoflections.org.uk
@ECACC @NCTC 3000 @NCPF

Statement

We have now completed DNA analysis of the sample presented for cell line authentication. Analysis has been conducted using the Promega Powerplex 16 HS kit which analyses the differences at 16 distinct hypervariable genetic loci. (Please note that some cell lines may exhibit genetic instability as they proliferate leading to discrepancies within the DNA profiles examined).

Summary

A short tandem repeat (STR) DNA Profile has been generated from the sample provided by Carol Trim of Canterbury Christ Church University. The sample name is MDA-MB-468. The profile is shown in the table below together with the STR profile for cell line MDA-MB468 from the Cellosaurus website (ref. CVCL_0419). The profiles match 100%. This indicates these cell lines were generated from the same source material. Please refer to the detailed results on the second page for further information and interpretation and the notes below on interpreting cell line STR profiles.

Notes on interpretation of cell line STR profiles:

The outcome percentage is calculated using a formula which compares the number of alleles present against the number of alleles shared between the two DNA profiles. The outcome is designated one of the following statements based upon the outcome percentage (more data on the interpretation Of cell line STR profiles can be found on the International Cell Line Authentication committee (ICLAC) website using the following link www.iclac.org/resources/match-criteria-worksheet

(1) For two cell lines with STR profiles matching greater than 80% they are considered to have been generated from the same source.
(2) For two cell lines with STR profiles matching between 56-79% they are unlikely to have been generated from the same source but further investigation should be carried out.
(3) For two cell lines with STR profiles matching less than 56% are considered to be unrelated, that is, to have been generated from independent sources.
(4) On occasion, the cell line STR profile may match one of the cell lines on the intemational list of misidentified cell lines curated by ICLAC. If this is the case this will be indicated in the summary statement. This list can be found at www.iclac.ora/wp-content/uploads!Cross-Contaminations• v8o.pdf

Summary statement prepared by:
Edward Bumett

@ECACC @NCTC_3000 @NCPV @NCPF

Collections, Public Health Salisbury, SP4 (O) 1980 611315 E:
W:

Case Number

Date Sample Tested 15/3/2018
Date Sample
Reported 21/3/2018

Sample Name	SempWComparison Profile Source	Sample Reference
MDA.MB.468	Cellosaurus MOA-MB-468 CVCL_0419	RS 03 D1015666 9514 LW6000087-18

Table of Allelic Data	Genotypes	
STR Locus	Test Sample - MOA-MB-468 Canterbury Christ Church University	Database Sample — Cellosaurus MDA-MB-468 CVCL_0419
AMEL		
CSFIPO	12, 12	12, 12
D13S317	12, 12	12, 12
DI 6S539		
	17 17	17, 17
D21S11	27, 28	27, 28
D3S1358	15. 15	15, 15
D5S818	12, 12	12, 12
D7S820	8t8	
D8S1179	13, 13	13, 13
FGA	23, 23	23, 23
PENTA D	8, 10	8, 10
PENTA E		
THOI		
TPOX		
vWA	18, 18	18, 18

Public Health England, Porton Down, Salisbury, SP4 OJG, UK
+44 (O) 1980 611315 E: culturecollections@phe.gov.uk W: mwg.phe•cuiturecoltections.org.uk
@ECACC @NCTC_3000@NCPF

ECACC European Collection of Authenticated Cell Cultures
Operated by Public Health England

We have now completed DNA analysis of the sample presented for cell line authentication. Analysis has been conducted using the Promega Powerplex 16 HS kit which analyses the differences at 16 distinct hypervariable genetic loci. (Please note that some cell lines may exhibit genetic instability as they proliferate leading to discrepancies within the DNA profiles examined).

Summary

A short tandem repeat (STR) DNA Profile has been generated from the sample provided by Carol Trim of Canterbury Christ Church University. The sample name is A431. The profile is shown in the table below together with the STR profile for cell line A431 from the Cellosaurus website (ref. CVCL_0037). The profiles match 93% (28/30 alleles).This indicates these cell lines were generated from the same source material. Please refer to the detailed results on the second page for further information and interpretation and the notes below on interpreting cell line STR profiles.

Notes on interpretation of cell line STR profiles:

The outcome percentage is calculated using a formula which compares the number of alleles present against the number of alleles shared between the two DNA profiles. The outcome is designated one of the following statements based upon the outcome percentage (more data on the interpretation of cell line STR profiles can be found on the Intemational Celt Line Authentication committee (ICLAC) website using the following link www.iclac.org/resources/match-criteria-worksheet

(1) For two cell lines with STR profiles matching greater than 80% they are considered to have been generated from the same source.
(2) For two cell lines with STR profiles matching between 56-79% they are unlikely to have been generated from the same source but further investigation should be carried out.
(3) For two cell lines with STR profiles matching less than 56% are considered to be unrelated, that is, to have been generated from independent sources.
(4) On occasion, the cell line STR profile may match one of the cell tines on the intemational list of misidentified cell lines curated by ICLAC. If this is the case this will be indicated in the summary statement. This list can be found at www.iclac.org/wp-contenVup!oads/Cross-Contaminations.vs O.pdf

Laboratory Report

Cell Line

Test Requested Authentication

Date Sample Tested 15/3/2018

Date Sample Reported 21/3/2018

Sample Name	Sampte/Comparison Profile Source	Sample Reference
A431	Cellosaurus A431 CVCL_0037	RS 02 D1015665 9514 LW6000087-18

Table of Allelic Data	Genotypes	
STR Locus	Test Sample — A431 Canterbury Christ Church University	Database Sample Cellosaurus A431 CVCL_0037
AMEL		
CSFIPO	11, 12	11, 12
D13S317	13, 13	9, 13
DI 6S539	12, 14	12, 14
DI 8S51	n/d	13, 17
D21S11	28, 30	28, 30
D3S1358	14, 14	14, 14
D5S818	12, 13	12, 13
D7S820	10, 10	10, 10
D8S1179	13, 13	13, 13
FGA	20, 20	20, 20
PENTA D	9, 11	9, 11
PENTA E	13, 13	12, 13
THOI		
TPOX	11, 11	11, 11
vWA	15, 17	15, 17

Appendix II: Chapter 2: Bradford Assay Methodology

Bradford Protocol for Samples with Low Protein Concentration

Preparation of known protein concentrations: -

2mg of bovine serum albumin (BSA) (Fisher, U.K.) were dissolved in 1ml PBS to produce a 2 mg/ml stock solution, which was aliquoted and stored at -20 for future use. 100µl of the 2 mg/ml BSA stock were diluted in 1.9ml of PBS to produce a new 100 µg/ml starting stock concentration. Using the 100 µg/ml BSA stock a serial dilution of BSA was produced.

Final BSA concentration (µg/ml)	Volume of 100 µg/ml BSA stock (µl)	Volume of PBS (µl)
0	0	500
10	50	450
20	100	400
30	150	350
40	200	300
50	250	250
60	300	200

BSA Standard Curve dilution table for samples containing low protein concentrations

Preparation of Cell lysate dilutions: -

30µl of each protein lysate, were diluted to produce 3 different protein concentrations for comparison again Bovine Serum Albumin (BSA) standards (Fisher, UK). Dilutions of cell lysates were produced.

Final lysate dilution	Volume of undiluted cell lysate (µl)	Volume of PBS (µl)
1/50	10	490
1/100	5	495
1/200	5	995

Cell lysate sample dilutions for Bradford Assay analysis

Once the BSA standards and protein lysate dilutions were prepared 100µl of each were loaded into 96 well plates in triplicate (Figure 2.1).

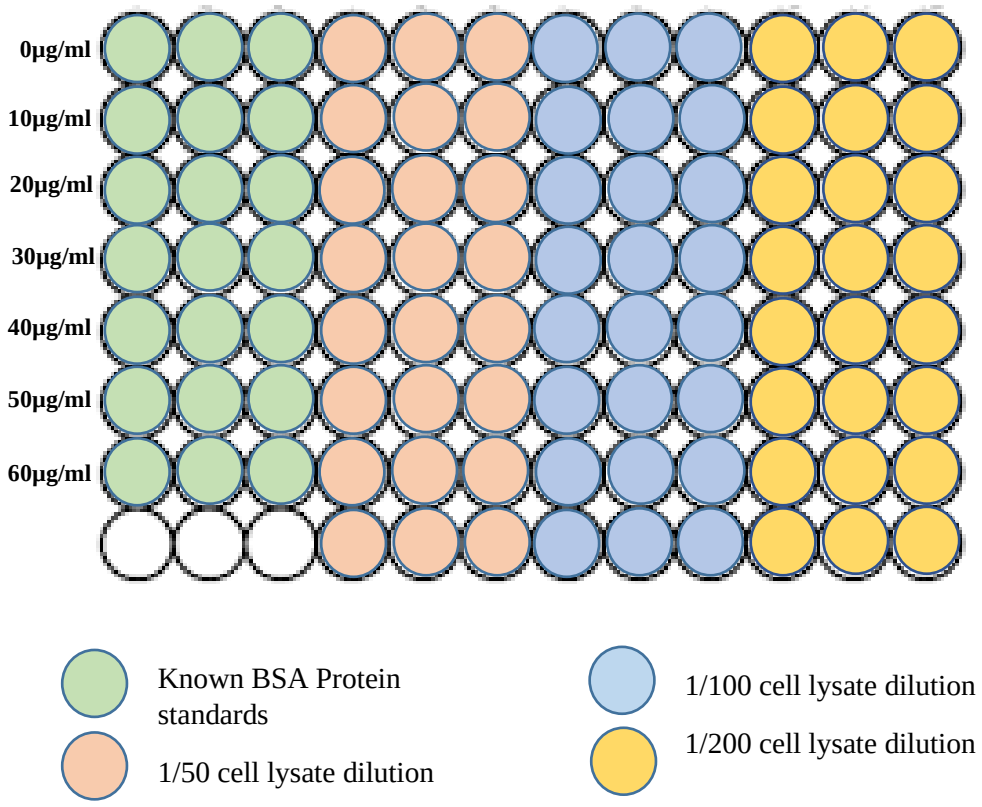

General plate layout for Bradford Assay

Plate layout includes BSA standard curve and 1/50, 1/100 and1/200 dilutions of lysate samples

Bradford Protocol for Samples with High Protein Concentration

Preparation of known protein concentrations: -

2mg of BSA (Fisher, U.K.) were dissolved in 1 ml PBS to produce a 2 mg/ml stock solution, which was aliquoted and stored at -20. This stock was used to produce a serial dilution of BSA.

	Final BSA concentration (µg/ml)	Volume of 2 mg/ml BSA stock (µl)	Volume of PBS (µl)
A	2000	300	0
B	1500	125	375
C	1000	325	325
D	750	175 of **B**	175
E	500	325 of **C**	325
F	250	325 of **E**	325
	0		400

BSA Standard Curve dilution table for samples containing high protein concentrations

Dilutions of cell lysate samples were produced and the 96 well plate layout loaded up (as in section **2.3.1.1.** 5µl of each sample and BSA standard were loaded into the 96 well plate in triplicate and 200µl of 1x Bradford reagent (Bio-Rad, UK) added to each well. Once mixed the plate was incubated for 10 min to enable the blue colour to develop. The absorbency of each well in the plate was read at 595nm using the Fluostar plate reader (BMG Labtech, UK). Protein concentrations were then calculated using the absorbencies and concentrations of the known BSA standards.

Appendix III: Chapter 3: Plate Layout for Resazurin Cell Number Assay

	1	**2**	**3**	**4**	**5**	**6**
A	$2x10^5$	$2x10^5$	$2x10^5$	$2x10^5$	$2x10^5$	$2x10^5$
B	$2x10^5$	$2x10^5$	$2x10^5$	$2x10^5$	$2x10^5$	$2x10^5$
C	$1x10^5$	$1x10^5$	$1x10^5$	$1x10^5$	$1x10^5$	$1x10^5$
D	$1x10^5$	$1x10^5$	$1x10^5$	$1x10^5$	$1x10^5$	$1x10^5$
E	$5x10^4$	$5x10^4$	$5x10^4$	$5x10^4$	$5x10^4$	$5x10^4$
F	$5x10^4$	$5x10^4$	$5x10^4$	$5x10^4$	$5x10^4$	$5x10^4$
G	$2.5x10^4$	$2.5x10^4$	$2.5x10^4$	$2.5x10^4$	$2.5x10^4$	$2.5x10^4$
H	$2.5x10^4$	$2.5x10^4$	$2.5x10^4$	$2.5x10^4$	$2.5x10^4$	$2.5x10^4$

Appendix III: Determining the Ideal Cell Number for Resazurin Cell Viability Assay.

MDA-MB-468 and A431 cells were plated out in sextuplicate at the 4 cell concentrations and left to adhere overnight. Cells were either treated for 2h with a cytotoxic dose of whole *N. nigricollis* venom (100µg/ml) **(Blue),** or with DMEM media containing no venom **(Pink)**. After 2h all treatment was removed and 50µl of 160 µM Resazurin (diluted from a 1.6 mM Resazurin stock in supplemented DMEM) was added to all wells. The change in fluorescence was monitored for 5h using a BMG Fluostar plate reader (ex.544 nm, em.590 nm)

Appendix IV: Chapter 3: Plate Layout for Resazurin Z' Assay

	1	2	3	4	5	6	7	8	9	10	11	12
A	+	+	+	+	+	+	-	-	-	-	-	-
B	+	+	+	+	+	+	-	-	-	-	-	-
C	+	+	+	+	+	+	-	-	-	-	-	-
D	+	+	+	+	+	+	-	-	-	-	-	-
E	-	-	-	-	-	-	+	+	+	+	+	+
F	-	-	-	-	-	-	+	+	+	+	+	+
G	-	-	-	-	-	-	+	+	+	+	+	+
H	-	-	-	-	-	-	+	+	+	+	+	+

Appendix IV: Plate Layout for 96-well Resazurin assay Z' Assay.

MDA-MB-468 and A431 cells were plated out across a whole 96 well plate at a concentration of $2x10^5$ and $1x10^5$ cells/well respectively and left to adhere overnight. Cells were treated with either a cytotoxic dose of *N. nigricollis* venom (100µg/ml) **(+VE Control)** or with DMEM media containing no venom **(-VE Control)** for 2h. After 2h 50µl of 160 µM Resazurin (diluted from 1.6 mM Resazurin stock in DMEM) was added to all wells and the change in fluorescence monitored for 5h using a BMG Fluostar plate reader (ex.544 nm, em.590 nm)

Appendix V: Chapter 3: Resazurin Snake Panel Plate Layout

	1	2	3	4	5	6	7	8	9	10	11	12
A	+VE	+VE	+VE	P.wei	P.wei	P.wei	N.sia	N.sia	N.sia	-VE	-VE	-VE
B	N.nig	N.nig	N.nig	N.atr	N.atr	N.atr	N.naj	N.naj	N.naj	O.han	O.han	O.han
C	D.pol	D.pol	D.pol	D.vir	D.vir	D.vir	C.rho	C.rho	C.rho	C.atr	C.atr	C.atr
D	C.rru	C.rru	C.rru	C.dve	C.dve	C.dve	C.ins	C.ins	C.ins	S.mil	S.mil	S.mil
E	M.xan	M.xan	M.xan	A.cco	A.cco	A.cco	V.aam	V.aam	V.aam	B.asp	B.asp	B.asp
F	-VE	-VE	-VE							+VE	+VE	+VE
G												
H												

Appendix V: Resazurin Cell Viability Assay, Snake Panel Plate Layout

A431 and MDA-MB-468 Cells were plated at a concentration of $1x10^5$ and $2x10^5$ cells/well respectively. Cells were treated in triplicate with each venom shown above. For each Resazurin assay, snake venoms were used at a concentration of 2 mg/ml, 200 µg/ml or 20 µg/ml for 2h. +ve control wells were treated with 100µg/ml whole *N. nigricollis* venom. -ve control wells were untreated and remained in fresh supplemented DMEM for the duration incubation period

Appendix VI: Chapter 3: Resazurin Invertebrate Panel Plate Layout

	1	2	3	4	5	6	7	8	9	10	11	12
A	A.aus			H.ari			H.swa			P.kra		
B	P.lio			A.cor			A.gen			A.met		
C	B.boe			H.lbo			H.mac			P.cam		
D	P.for			P.lug			T.cup			T.pru		
E	T.str			S.har			S.sud			C.gig		
F	E.foe			P.map			A.sex					
G	+ve						-ve					
H												

Appendix VI: Resazurin Cell Viability Assay, Snake Panel Plate Layout

A431 and MDA-MB-468 Cells were plated at a concentration of $1x10^5$ and $2x10^5$ cells/well respectively. Cells were treated in triplicate with each venom shown above. For each Resazurin assay, snake venoms were used at a concentration of 200 µg/ml or 20 µg/ml for 2h. +ve control wells were treated with 100µg/ml Whole *N. nigricollis* venom. -ve control wells were untreated and remained in fresh supplemented DMEM for the duration of the incubation period

Appendix VII: Chapter 3: Resazurin Assay Screens of Snake Panel

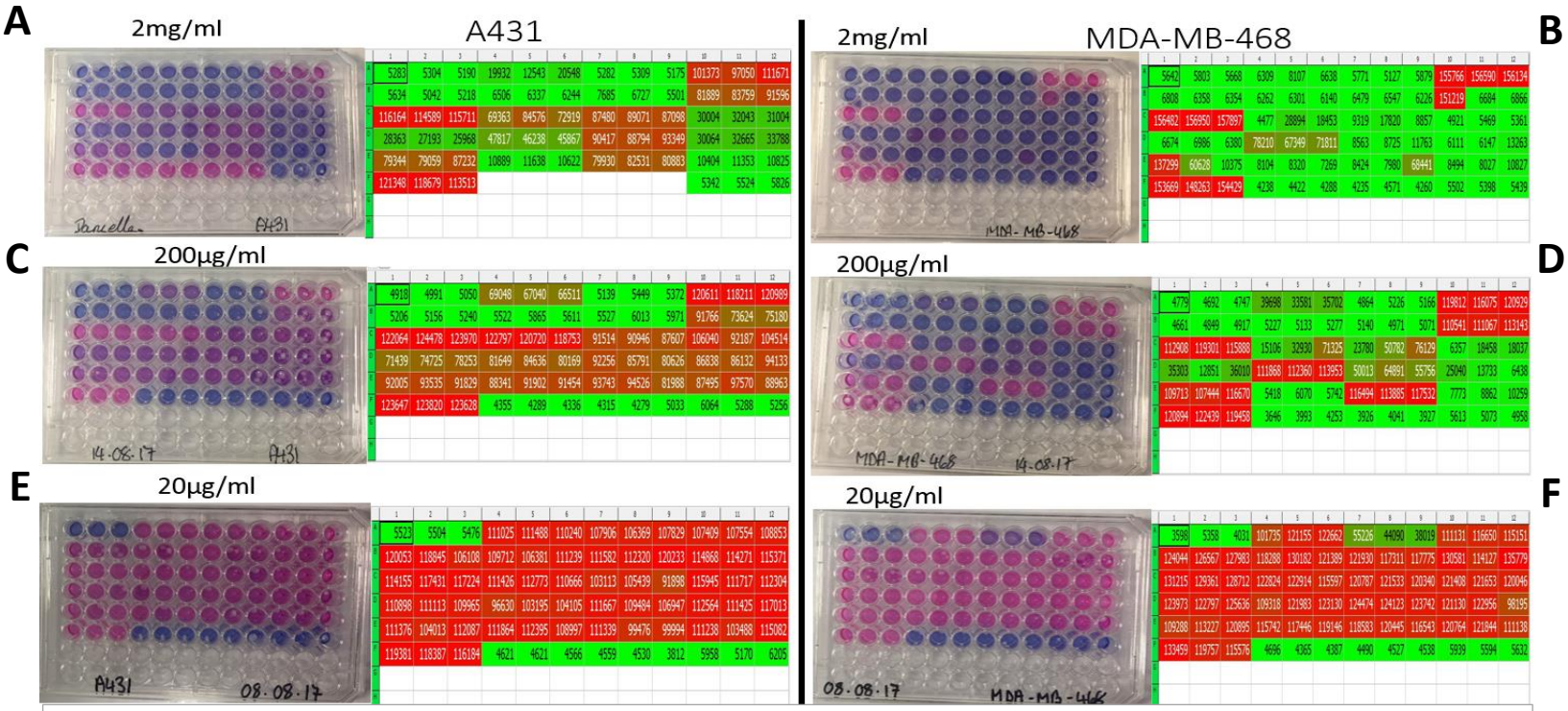

Appendix VII: Resazurin Assays Screens of Snake Panel

Figure. A and B. show the plate and plate reader images for A431 and MDA-MB-468 treated with a panel of snake venoms at a final conc. of 2 mg/ml. Figs. C and D. show the plate and plate reader images for A431 and MDA-MB-468 treated with a panel of snake venoms at a final conc. of 200 µg/ml. Figures. E and F. show the plate and plate reader images for A431 and MDA-MB-468 treated with a panel of snake venoms at a final conc. of 20 µg/ml. All venoms doses were run in triplicate and in accordance with the plate layout previously determined in Figure.4.3. **+VE control:** Cells treated for 2h with a cytotoxic dose of *N. nigricollis* venom (100 µg/ml), **-VE control:** DMEM media containing no venom . Green colour-coded wells indicate low levels of resazurin fluorescence (no/low resazurin metabolism-cellular toxicity), whilst red colour-coded wells indicate high levels of resazurin fluorescence indicative of continued cellular viability.

Appendix VIII: Chapter 4: Table of Concentrations of Crude venoms used for Kinome Arrays

Whole Venom	DS11 Readings for Whole Venoms (mg/ml)				Av. (mg/ml)	SD. (mg/ml)
A. geniculata	257.38	258.49	259.19	260.24	**258.8**	**±1.04**
C. durissus vegrandis	62.67	60.57	60.13	65.88	**62**	**±2.27**
D. viridis	288.21	277.01	277.18	278.86	**280.32**	**±4.62**
H. swammerdami	97.5	100.33	101.99	104.47	**101.07**	**±2.53**
P. liosoma	215.13	216.42	217.95	215.49	**216.28**	**±1.09**
N. naja	226.93	241.16	262.53	279.6	**252.55**	**±20.11**

Appendix VIII: Table of Concentrations of Whole Venoms Ascertained by DeNovix DS11 Spectrophotometry

Protein concentration of multiple microlitres were read and an average protein (Av.) concentration and standard deviation (SD.) in mg/ml calculated.

Appendix IX: Chapter 4: Kinome Array Receptor Phospho-RTK Array layout Template

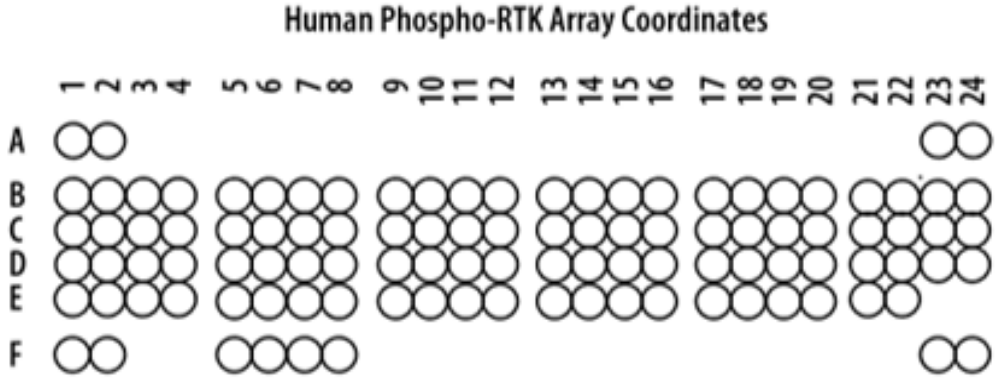

Coordinate	Receptor Family	RTK/Control		Coordinate	Receptor Family	RTK/Control
A1, A2	References	----------		D1, D2	Tie	Tie-2
A23, A24	References	----------		D3, D4	NGF R	Trk A
B1, B2	EGF R	EGF R		D5, D6	NGF R	Trk B
B3, B4	EGF R	ErbB2		D7, D8	NGF R	Trk C
B5, B6	EGF R	ErbB3		D9, D10	VEGF R	VEGF R1
B7, B8	EGF R	ErbB4		D11, D12	VEGF R	VEGF R2
B9, B10	FGF R	FGF R1		D13, D14	VEGF R	VEGF R3
B11, B12	FGF R	FGF R2a		D15, D16	MuSK	MuSK
B13, B14	FGF R	FGF R3		D17, D18	Eph R	Eph A1
B15, B16	FGF R	FGF R4		D19, D20	Eph R	Eph A2
B17, B18	Insulin R	Insulin R		D21, D22	Eph R	Eph A3
B19, B20	Insulin R	IGF-IR		D23, D24	Eph R	Eph A4
B21, B22	Axl	Axl		E1, E2	Eph R	Eph A6
B23, B24	Axl	Dtk		E3, E4	Eph R	Eph A7
C1, C2	Axl	Mer		E5, E6	Eph R	Eph B1
C3, C4	HGF R	HGF R		E7, E8	Eph R	Eph B2
C5, C6	HGF R	MSP R		E9, E10	Eph R	Eph B4
C7, C8	PDGF R	PDGF Rα		E11, E12	Eph R	Eph B6
C9, C10	PDGF R	PDGF Rβ		E13, E14	Insulin R	ALK
C11, C12	PDGF R	SCF R		E15, E16	----------	DDR1
C13, C14	PDGF R	Flt-3		E17, E18	----------	DDR2
C15, C16	PDGF R	M-CSF R		E19, E20	Eph R	Eph A5
C17, C18	Ret	c-RET		E21, E22	Eph R	Eph A10
C19, C20	ROR	ROR1		F1, F2	References	----------
C21, C22	ROR	ROR2		F5, F6	Eph R	EphB3
C23, C24	Tie	Tie-1		F7, F8	----------	RYK
				F23, F24	Control (-)	PBS

Appendix IX: Human p-RTK Kinome Blot Coordinates

The table displays a list of each RTK probed for on the kinome array membranes, the sub-family of RTKs they belong to, and their relevant coordinate location on each blot.

Appendix X: Chapter 4: Kinome Array Analysis Report Raw Data

Image Report: 2016-05-26 45s

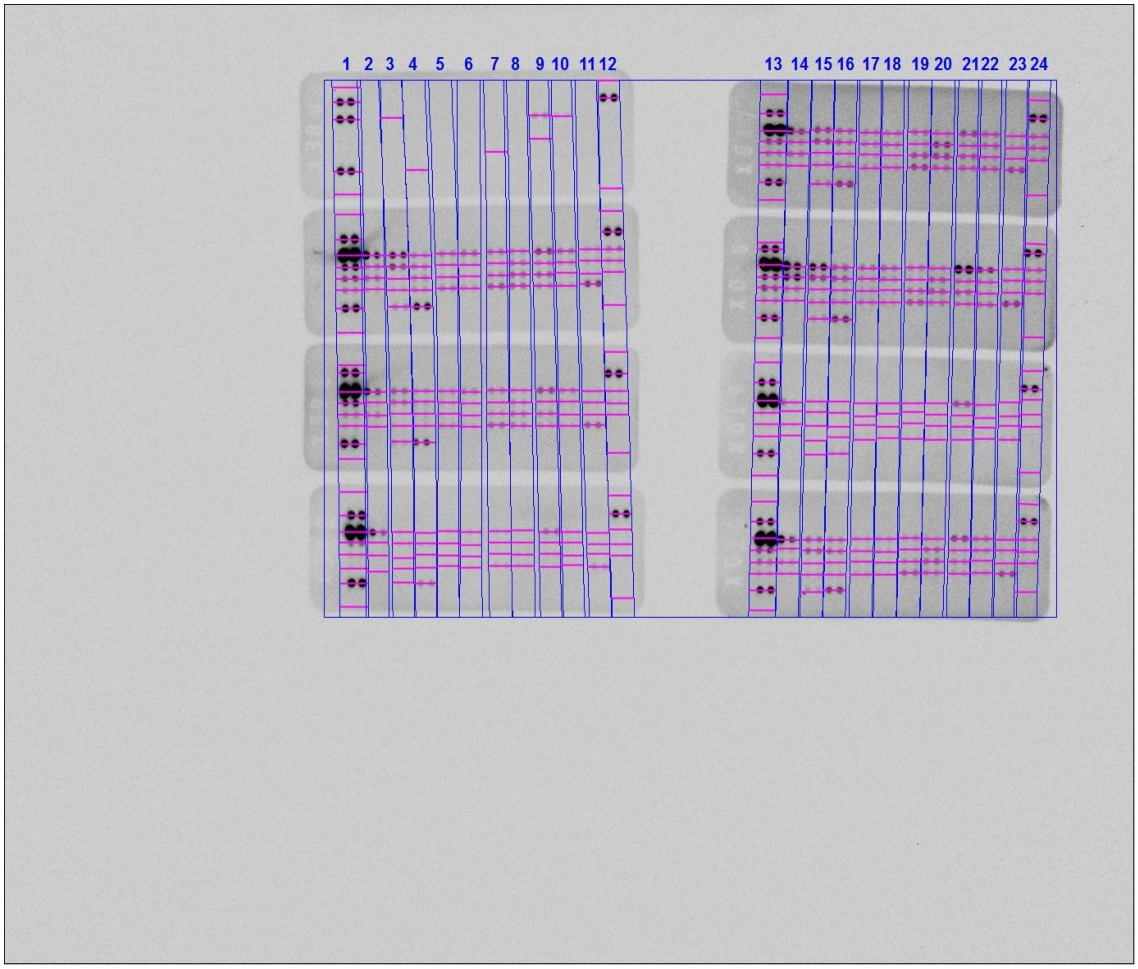

F:\Kinome blot work\kinome blot images\doc images\2016-05-26 45s.scn

Acquisition Information

Imager	ChemiDoc™ Touch
Exposure Time (sec)	45.000 (Manual)
Serial Number	732BR1296
Software Version	1.1.0.04
Application	Chemiluminescence
Excitation Source	No Illumination
Emission Filter	No Filter
Binning	2x2

Image Information

Acquisition Date	27/05/2016 01:40:33
User Name	
Image Area (mm)	X: 210.0 Y: 168.1
Pixel Size (um)	X: 152.3 Y: 152.3

Data Range (Int)	500 - 65535

Analysis Settings

	Automatically detected lanes with manual adjustments Band detection: Bands detected with different sensitivity per lane Manually adjusted bands Lane Background Subtraction: Lane background subtracted with disk size: 10 Lane width: Variable

Lane And Band Analysis:

Lane 1

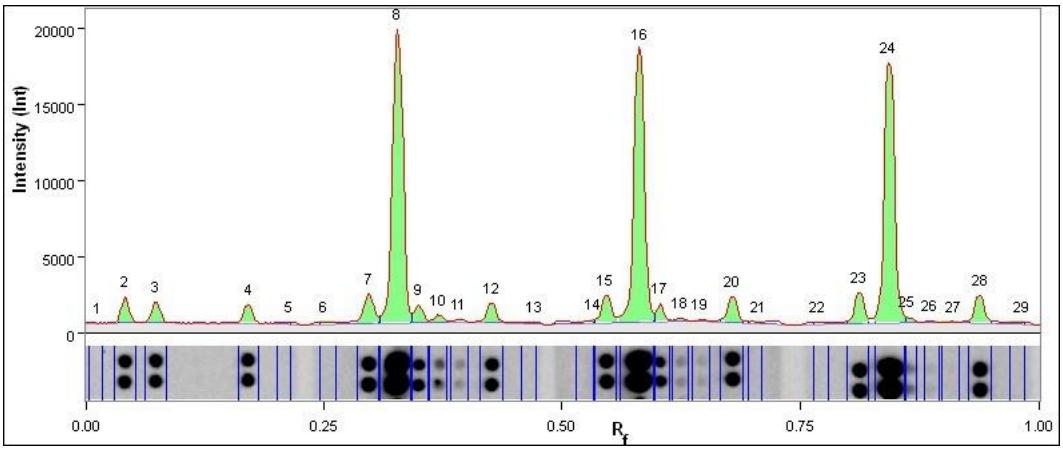

Band No.	Band Label	Mol. Wt. (KDa)	Relative Front	Volume (Int)	Abs. Quant.	Rel. Quant.	Band %	Lane %
1		N/A	0.015	6,580	N/A	N/A	0.0	0.0
2		N/A	0.042	428,820	N/A	N/A	1.8	1.7
3		N/A	0.075	373,380	N/A	N/A	1.5	1.5
4		N/A	0.172	354,795	N/A	N/A	1.5	1.4
5		N/A	0.214	40,005	N/A	N/A	0.2	0.2
6		N/A	0.251	70,805	N/A	N/A	0.3	0.3
7		N/A	0.298	654,290	N/A	N/A	2.7	2.6
8		N/A	0.327	6,480,425	N/A	N/A	26.6	25.8
9		N/A	0.350	333,795	N/A	N/A	1.4	1.3
10		N/A	0.371	142,240	N/A	N/A	0.6	0.6
11		N/A	0.392	54,180	N/A	N/A	0.2	0.2
12		N/A	0.426	387,345	N/A	N/A	1.6	1.5
13		N/A	0.472	47,950	N/A	N/A	0.2	0.2
14		N/A	0.533	72,415	N/A	N/A	0.3	0.3
15		N/A	0.546	624,400	N/A	N/A	2.6	2.5
16		N/A	0.582	6,143,445	N/A	N/A	25.2	24.5

17		N/A	0.603	279,825	N/A	N/A	1.1	1.1
18		N/A	0.624	58,695	N/A	N/A	0.2	0.2
19		N/A	0.645	35,280	N/A	N/A	0.1	0.1
20		N/A	0.679	542,395	N/A	N/A	2.2	2.2
21		N/A	0.707	48,930	N/A	N/A	0.2	0.2
22		N/A	0.768	53,970	N/A	N/A	0.2	0.2
23		N/A	0.812	659,120	N/A	N/A	2.7	2.6
24		N/A	0.843	5,728,135	N/A	N/A	23.5	22.8
25		N/A	0.862	71,540	N/A	N/A	0.3	0.3
26		N/A	0.885	22,715	N/A	N/A	0.1	0.1
27		N/A	0.911	24,360	N/A	N/A	0.1	0.1
28		N/A	0.938	587,300	N/A	N/A	2.4	2.3
29		N/A	0.982	64,785	N/A	N/A	0.3	0.3

Band Detection	Automatically detected bands with sensitivity: Low
Lane Background	Lane background subtracted with disk size: 10
Lane Width	5.33 mm

Lane 2

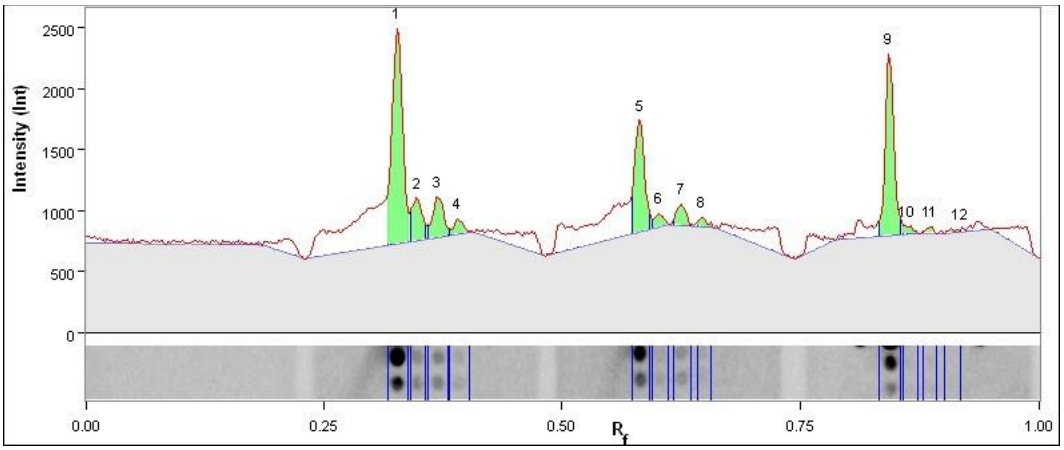

Band No.	Band Label	Mol. Wt. (KDa)	Relative Front	Volume (Int)	Abs. Quant.	Rel. Quant.	Band %	Lane %
1		N/A	0.327	399,756	N/A	N/A	34.3	16.4
2		N/A	0.348	75,208	N/A	N/A	6.5	3.1
3		N/A	0.370	80,556	N/A	N/A	6.9	3.3
4		N/A	0.391	26,572	N/A	N/A	2.3	1.1
5		N/A	0.582	201,824	N/A	N/A	17.3	8.3
6		N/A	0.601	21,280	N/A	N/A	1.8	0.9
7		N/A	0.626	35,000	N/A	N/A	3.0	1.4
8		N/A	0.647	13,804	N/A	N/A	1.2	0.6
9		N/A	0.843	280,700	N/A	N/A	24.1	11.5
10		N/A	0.862	12,908	N/A	N/A	1.1	0.5
11		N/A	0.887	9,100	N/A	N/A	0.8	0.4

12		N/A	0.919	7,812	N/A	N/A	0.7	0.3

Band Detection	Automatically detected bands with advanced settings
Lane Background	Lane background subtracted with disk size: 10
Lane Width	4.26 mm

Lane 3

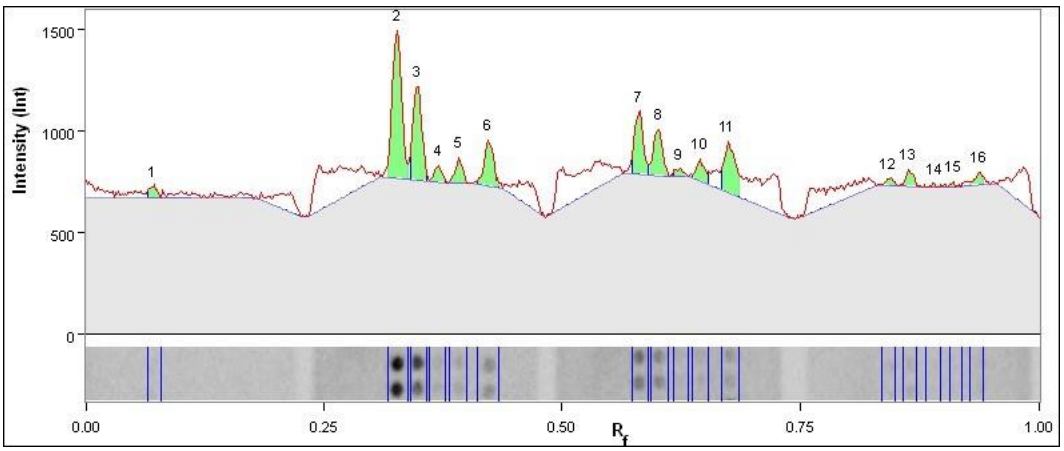

Band No.	Band Label	Mol. Wt. (KDa)	Relative Front	Volume (Int)	Abs. Quant.	Rel. Quant.	Band %	Lane %
1		N/A	0.071	11,396	N/A	N/A	1.8	0.8
2		N/A	0.327	166,936	N/A	N/A	26.9	11.5
3		N/A	0.348	98,896	N/A	N/A	15.9	6.8
4		N/A	0.371	15,652	N/A	N/A	2.5	1.1
5		N/A	0.392	21,364	N/A	N/A	3.4	1.5
6		N/A	0.423	52,108	N/A	N/A	8.4	3.6
7		N/A	0.580	66,668	N/A	N/A	10.7	4.6
8		N/A	0.601	47,460	N/A	N/A	7.6	3.3
9		N/A	0.622	7,308	N/A	N/A	1.2	0.5
10		N/A	0.645	24,556	N/A	N/A	4.0	1.7
11		N/A	0.674	67,508	N/A	N/A	10.9	4.6
12		N/A	0.843	6,832	N/A	N/A	1.1	0.5
13		N/A	0.864	14,504	N/A	N/A	2.3	1.0
14		N/A	0.891	3,528	N/A	N/A	0.6	0.2
15		N/A	0.911	3,752	N/A	N/A	0.6	0.3
16		N/A	0.937	11,956	N/A	N/A	1.9	0.8

Band Detection	Automatically detected bands with advanced settings
Lane Background	Lane background subtracted with disk size: 10
Lane Width	4.26 mm

Lane 4

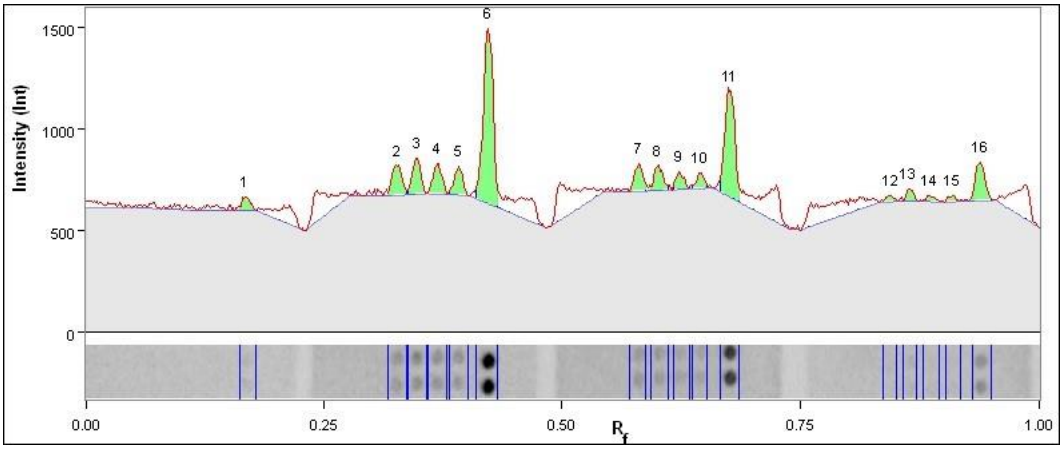

Band No.	Band Label	Mol. Wt. (KDa)	Relative Front	Volume (Int)	Abs. Quant.	Rel. Quant.	Band %	Lane %
1		N/A	0.169	15,960	N/A	N/A	2.2	1.2
2		N/A	0.327	41,580	N/A	N/A	5.9	3.0
3		N/A	0.348	40,964	N/A	N/A	5.8	3.0
4		N/A	0.370	35,728	N/A	N/A	5.0	2.6
5		N/A	0.392	30,940	N/A	N/A	4.4	2.2
6		N/A	0.423	225,064	N/A	N/A	31.7	16.2
7		N/A	0.580	32,676	N/A	N/A	4.6	2.4
8		N/A	0.600	29,400	N/A	N/A	4.1	2.1
9		N/A	0.622	18,760	N/A	N/A	2.6	1.4
10		N/A	0.645	16,520	N/A	N/A	2.3	1.2
11		N/A	0.676	142,576	N/A	N/A	20.1	10.3
12		N/A	0.844	6,496	N/A	N/A	0.9	0.5
13		N/A	0.864	12,096	N/A	N/A	1.7	0.9
14		N/A	0.885	7,028	N/A	N/A	1.0	0.5
15		N/A	0.909	6,636	N/A	N/A	0.9	0.5
16		N/A	0.938	47,656	N/A	N/A	6.7	3.4

Band Detection	Automatically detected bands with advanced settings
Lane Background	Lane background subtracted with disk size: 10
Lane Width	4.26 mm

Lane 5

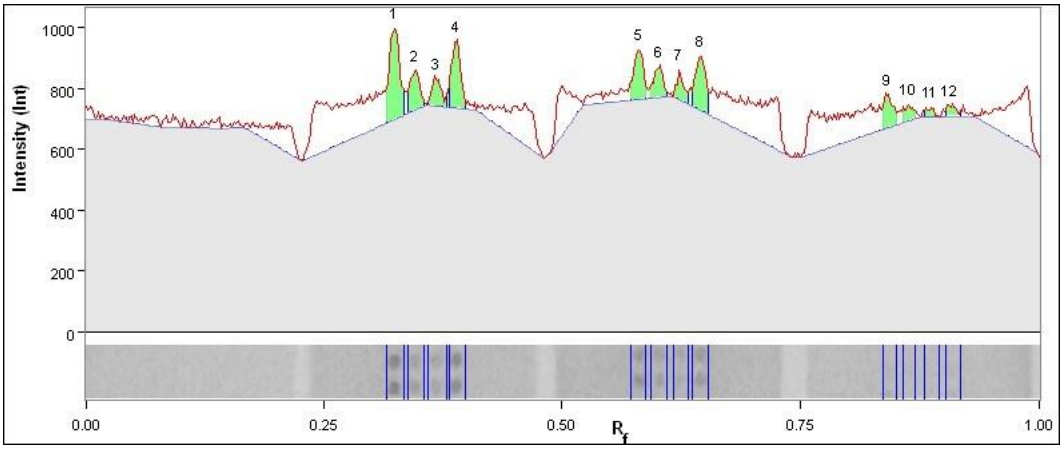

Band No.	Band Label	Mol. Wt. (KDa)	Relative Front	Volume (Int)	Abs. Quant.	Rel. Quant.	Band %	Lane %
1		N/A	0.324	74,956	N/A	N/A	21.6	5.8
2		N/A	0.345	29,428	N/A	N/A	8.5	2.3
3		N/A	0.368	24,024	N/A	N/A	6.9	1.8
4		N/A	0.389	45,920	N/A	N/A	13.2	3.5
5		N/A	0.580	37,828	N/A	N/A	10.9	2.9
6		N/A	0.601	22,568	N/A	N/A	6.5	1.7
7		N/A	0.622	18,116	N/A	N/A	5.2	1.4
8		N/A	0.645	45,136	N/A	N/A	13.0	3.5
9		N/A	0.841	24,640	N/A	N/A	7.1	1.9
10		N/A	0.864	10,500	N/A	N/A	3.0	0.8
11		N/A	0.887	5,544	N/A	N/A	1.6	0.4
12		N/A	0.906	8,652	N/A	N/A	2.5	0.7

Band Detection	Automatically detected bands with advanced settings
Lane Background	Lane background subtracted with disk size: 10
Lane Width	4.26 mm

Lane 6

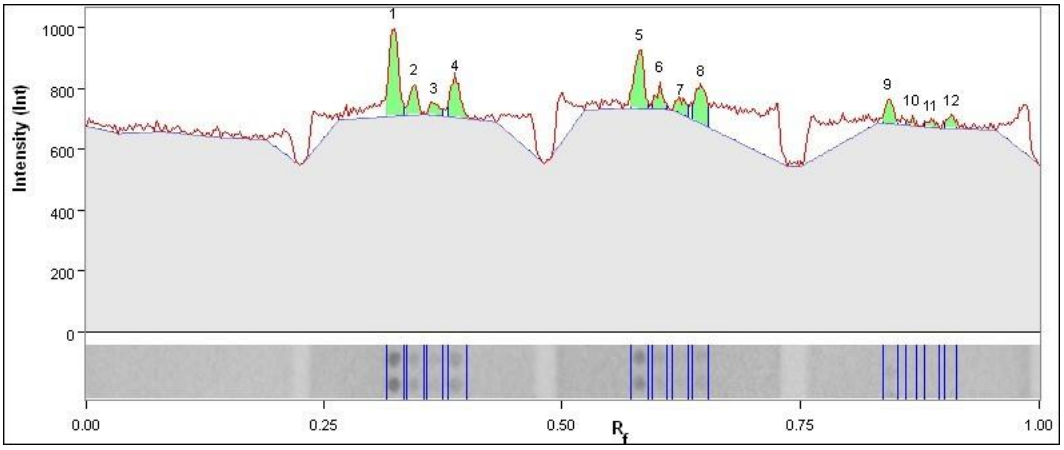

Band No.	Band Label	Mol. Wt. (KDa)	Relative Front	Volume (Int)	Abs. Quant.	Rel. Quant.	Band %	Lane %
1		N/A	0.324	67,620	N/A	N/A	24.4	7.0
2		N/A	0.345	19,908	N/A	N/A	7.2	2.0
3		N/A	0.366	11,200	N/A	N/A	4.0	1.2
4		N/A	0.389	31,500	N/A	N/A	11.4	3.2
5		N/A	0.582	45,696	N/A	N/A	16.5	4.7
6		N/A	0.603	14,560	N/A	N/A	5.2	1.5
7		N/A	0.626	14,896	N/A	N/A	5.4	1.5
8		N/A	0.647	36,260	N/A	N/A	13.1	3.7
9		N/A	0.843	16,940	N/A	N/A	6.1	1.7
10		N/A	0.867	4,088	N/A	N/A	1.5	0.4
11		N/A	0.888	5,264	N/A	N/A	1.9	0.5
12		N/A	0.909	9,492	N/A	N/A	3.4	1.0

Band Detection	Automatically detected bands with advanced settings
Lane Background	Lane background subtracted with disk size: 10
Lane Width	4.26 mm

Lane 7

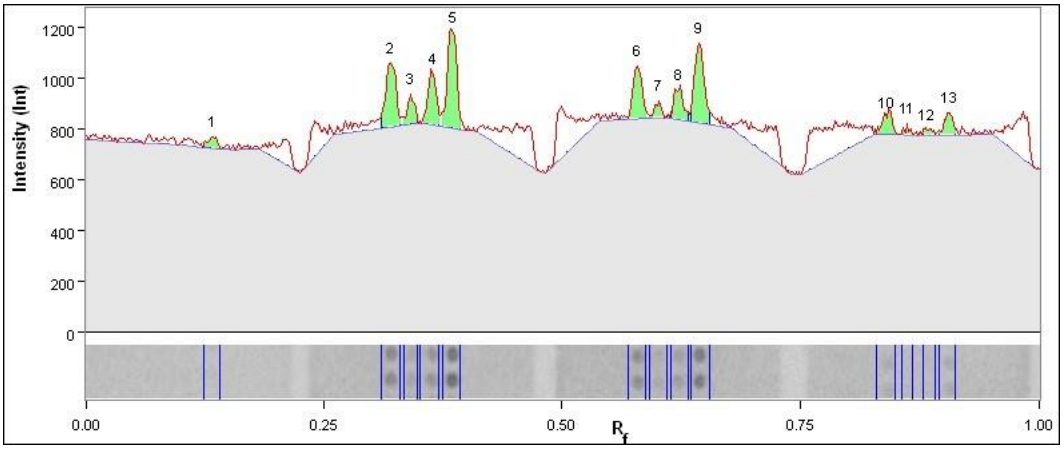

Band No.	Band Label	Mol. Wt. (KDa)	Relative Front	Volume (Int)	Abs. Quant.	Rel. Quant.	Band %	Lane %
1		N/A	0.135	9,856	N/A	N/A	2.5	1.0
2		N/A	0.321	57,260	N/A	N/A	14.4	5.6
3		N/A	0.342	17,836	N/A	N/A	4.5	1.8
4		N/A	0.365	39,396	N/A	N/A	9.9	3.9
5		N/A	0.386	80,444	N/A	N/A	20.3	7.9
6		N/A	0.579	42,000	N/A	N/A	10.6	4.1
7		N/A	0.601	10,164	N/A	N/A	2.6	1.0
8		N/A	0.622	26,404	N/A	N/A	6.6	2.6
9		N/A	0.643	66,500	N/A	N/A	16.7	6.5
10		N/A	0.841	19,880	N/A	N/A	5.0	2.0

11		N/A	0.862	4,284	N/A	N/A	1.1	0.4
12		N/A	0.883	5,488	N/A	N/A	1.4	0.5
13		N/A	0.906	17,612	N/A	N/A	4.4	1.7
Band Detection		Automatically detected bands with advanced settings						
Lane Background		Lane background subtracted with disk size: 10						
Lane Width		4.26 mm						

Lane 8

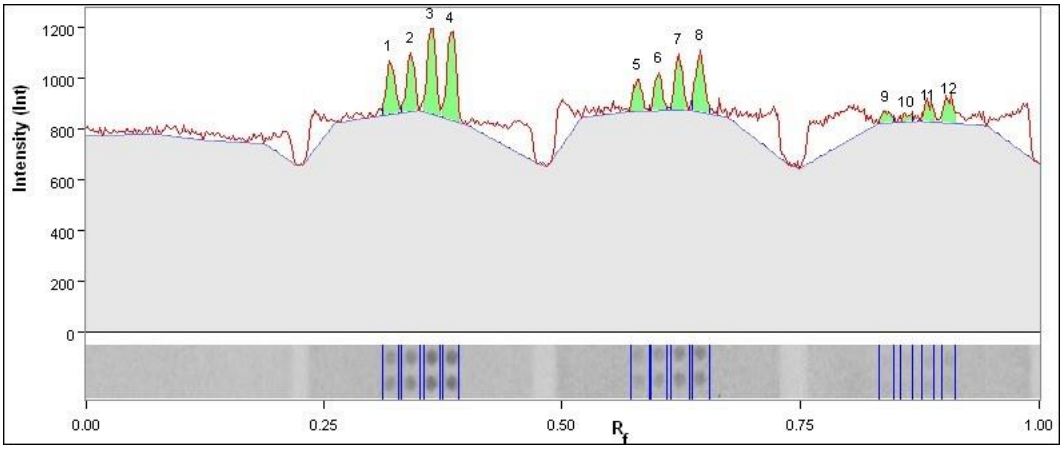

Band No.	Band Label	Mol. Wt. (KDa)	Relative Front	Volume (Int)	Abs. Quant.	Rel. Quant.	Band %	Lane %
1		N/A	0.319	37,968	N/A	N/A	9.9	3.6
2		N/A	0.342	39,648	N/A	N/A	10.3	3.7
3		N/A	0.363	61,544	N/A	N/A	16.0	5.8
4		N/A	0.384	67,004	N/A	N/A	17.4	6.3
5		N/A	0.579	22,456	N/A	N/A	5.8	2.1
6		N/A	0.601	24,528	N/A	N/A	6.4	2.3
7		N/A	0.622	36,540	N/A	N/A	9.5	3.4
8		N/A	0.645	43,092	N/A	N/A	11.2	4.1
9		N/A	0.840	9,856	N/A	N/A	2.6	0.9
10		N/A	0.862	6,384	N/A	N/A	1.7	0.6
11		N/A	0.885	14,644	N/A	N/A	3.8	1.4
12		N/A	0.906	21,140	N/A	N/A	5.5	2.0
Band Detection		Automatically detected bands with advanced settings						
Lane Background		Lane background subtracted with disk size: 10						
Lane Width		4.26 mm						

Lane 9

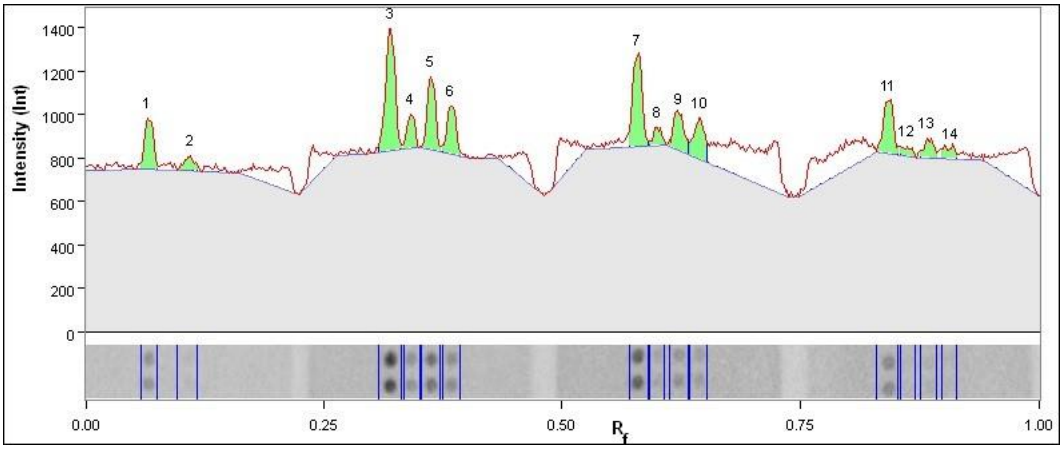

Band No.	Band Label	Mol. Wt. (KDa)	Relative Front	Volume (Int)	Abs. Quant.	Rel. Quant.	Band %	Lane %
1		N/A	0.066	45,640	N/A	N/A	7.5	3.4
2		N/A	0.110	15,792	N/A	N/A	2.6	1.2
3		N/A	0.321	115,892	N/A	N/A	19.1	8.6
4		N/A	0.342	27,048	N/A	N/A	4.5	2.0
5		N/A	0.363	61,124	N/A	N/A	10.1	4.6
6		N/A	0.384	44,716	N/A	N/A	7.4	3.3
7		N/A	0.579	90,608	N/A	N/A	14.9	6.8
8		N/A	0.600	15,512	N/A	N/A	2.6	1.2
9		N/A	0.622	42,672	N/A	N/A	7.0	3.2
10		N/A	0.645	44,940	N/A	N/A	7.4	3.4
11		N/A	0.843	57,372	N/A	N/A	9.5	4.3
12		N/A	0.862	9,688	N/A	N/A	1.6	0.7
13		N/A	0.883	20,076	N/A	N/A	3.3	1.5
14		N/A	0.908	15,064	N/A	N/A	2.5	1.1

Band Detection	Automatically detected bands with advanced settings
Lane Background	Lane background subtracted with disk size: 10
Lane Width	4.26 mm

Lane 10

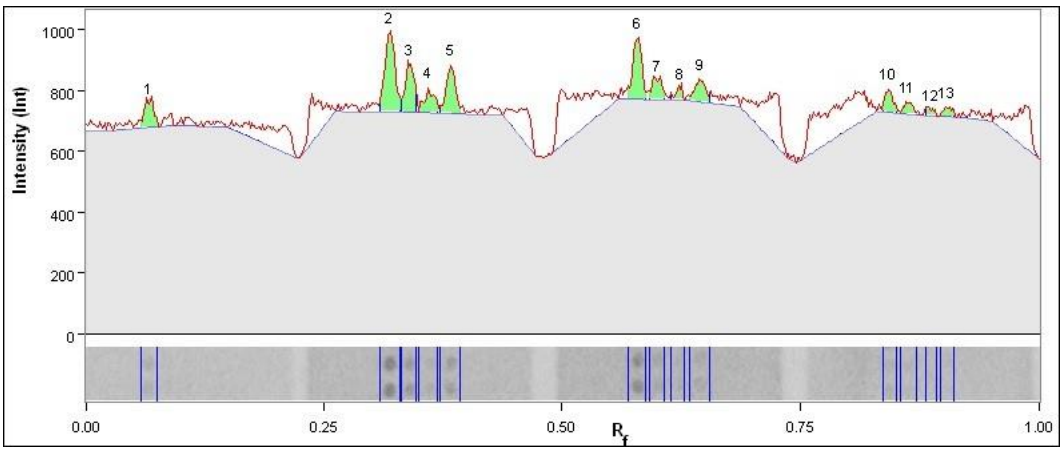

Band No.	Band Label	Mol. Wt. (KDa)	Relative Front	Volume (Int)	Abs. Quant.	Rel. Quant.	Band %	Lane %
1		N/A	0.068	21,840	N/A	N/A	7.2	2.2
2		N/A	0.319	65,044	N/A	N/A	21.3	6.6
3		N/A	0.340	35,560	N/A	N/A	11.7	3.6
4		N/A	0.360	20,076	N/A	N/A	6.6	2.0
5		N/A	0.384	35,812	N/A	N/A	11.7	3.7
6		N/A	0.579	44,520	N/A	N/A	14.6	4.5
7		N/A	0.600	17,752	N/A	N/A	5.8	1.8
8		N/A	0.624	7,504	N/A	N/A	2.5	0.8
9		N/A	0.645	20,832	N/A	N/A	6.8	2.1
10		N/A	0.843	14,504	N/A	N/A	4.8	1.5
11		N/A	0.862	9,940	N/A	N/A	3.3	1.0
12		N/A	0.887	4,368	N/A	N/A	1.4	0.4
13		N/A	0.904	7,252	N/A	N/A	2.4	0.7

Band Detection	Automatically detected bands with advanced settings
Lane Background	Lane background subtracted with disk size: 10
Lane Width	4.26 mm

Lane 11

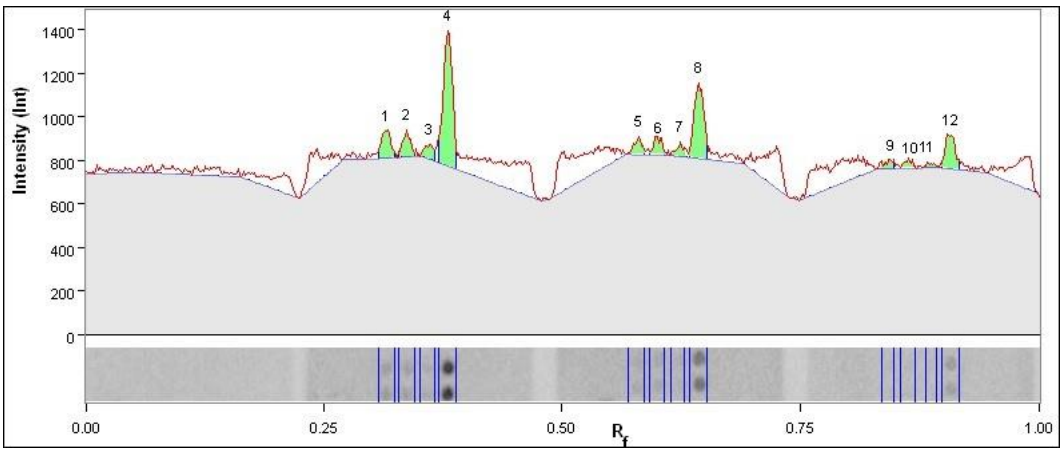

Band No.	Band Label	Mol. Wt. (KDa)	Relative Front	Volume (Int)	Abs. Quant.	Rel. Quant.	Band %	Lane %
1		N/A	0.316	26,684	N/A	N/A	7.4	2.3
2		N/A	0.337	21,952	N/A	N/A	6.0	1.9
3		N/A	0.361	15,512	N/A	N/A	4.3	1.4
4		N/A	0.381	129,696	N/A	N/A	35.7	11.3
5		N/A	0.580	15,092	N/A	N/A	4.2	1.3
6		N/A	0.601	15,680	N/A	N/A	4.3	1.4
7		N/A	0.624	11,060	N/A	N/A	3.0	1.0
8		N/A	0.643	72,828	N/A	N/A	20.1	6.4
9		N/A	0.844	7,476	N/A	N/A	2.1	0.7
10		N/A	0.865	7,588	N/A	N/A	2.1	0.7
11		N/A	0.883	3,528	N/A	N/A	1.0	0.3
12		N/A	0.908	35,812	N/A	N/A	9.9	3.1

Band Detection	Automatically detected bands with advanced settings
Lane Background	Lane background subtracted with disk size: 10
Lane Width	4.26 mm

Lane 12

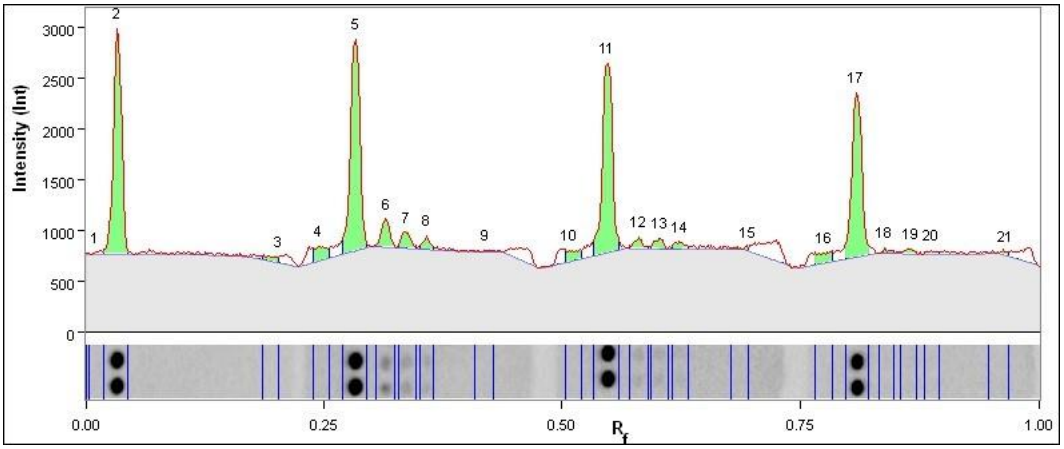

Band No.	Band Label	Mol. Wt. (KDa)	Relative Front	Volume (Int)	Abs. Quant.	Rel. Quant.	Band %	Lane %
1		N/A	0.002	644	N/A	N/A	0.0	0.0
2		N/A	0.034	395,528	N/A	N/A	20.9	16.9
3		N/A	0.204	15,652	N/A	N/A	0.8	0.7
4		N/A	0.245	36,904	N/A	N/A	1.9	1.6
5		N/A	0.284	426,636	N/A	N/A	22.5	18.2
6		N/A	0.316	50,316	N/A	N/A	2.7	2.1
7		N/A	0.337	33,376	N/A	N/A	1.8	1.4
8		N/A	0.358	18,760	N/A	N/A	1.0	0.8
9		N/A	0.420	4,564	N/A	N/A	0.2	0.2
10		N/A	0.507	29,568	N/A	N/A	1.6	1.3

11		N/A	0.548	403,200	N/A	N/A	21.3	17.2
12		N/A	0.580	21,308	N/A	N/A	1.1	0.9
13		N/A	0.603	21,252	N/A	N/A	1.1	0.9
14		N/A	0.624	15,708	N/A	N/A	0.8	0.7
15		N/A	0.695	8,204	N/A	N/A	0.4	0.3
16		N/A	0.775	33,824	N/A	N/A	1.8	1.4
17		N/A	0.809	344,316	N/A	N/A	18.2	14.7
18		N/A	0.838	7,392	N/A	N/A	0.4	0.3
19		N/A	0.865	11,144	N/A	N/A	0.6	0.5
20		N/A	0.887	7,560	N/A	N/A	0.4	0.3
21		N/A	0.966	9,940	N/A	N/A	0.5	0.4

Band Detection	Automatically detected bands with advanced settings
Lane Background	Lane background subtracted with disk size: 10
Lane Width	4.26 mm

Lane 13

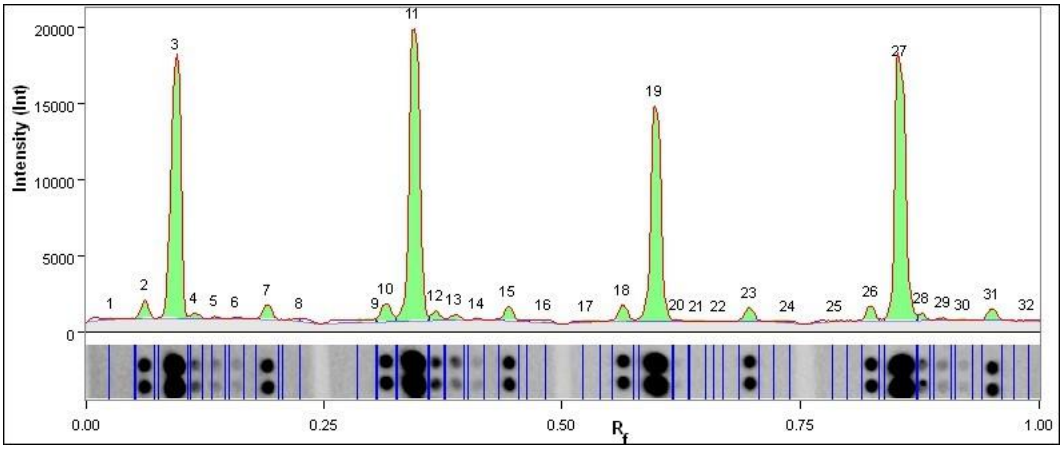

Band No.	Band Label	Mol. Wt. (KDa)	Relative Front	Volume (Int)	Abs. Quant.	Rel. Quant.	Band %	Lane %
1		N/A	0.028	14,751	N/A	N/A	0.1	0.1
2		N/A	0.063	296,340	N/A	N/A	1.2	1.2
3		N/A	0.096	5,089,161	N/A	N/A	20.7	20.2
4		N/A	0.115	91,179	N/A	N/A	0.4	0.4
5		N/A	0.136	34,287	N/A	N/A	0.1	0.1
6		N/A	0.159	30,558	N/A	N/A	0.1	0.1
7		N/A	0.191	279,147	N/A	N/A	1.1	1.1
8		N/A	0.225	45,540	N/A	N/A	0.2	0.2
9		N/A	0.305	91,014	N/A	N/A	0.4	0.4
10		N/A	0.316	406,593	N/A	N/A	1.7	1.6
11		N/A	0.345	6,142,191	N/A	N/A	25.0	24.4
12		N/A	0.368	166,089	N/A	N/A	0.7	0.7

13		N/A	0.387	98,340	N/A	N/A	0.4	0.4
14		N/A	0.412	20,130	N/A	N/A	0.1	0.1
15		N/A	0.444	266,739	N/A	N/A	1.1	1.1
16		N/A	0.481	72,204	N/A	N/A	0.3	0.3
17		N/A	0.527	22,374	N/A	N/A	0.1	0.1
18		N/A	0.564	314,391	N/A	N/A	1.3	1.2
19		N/A	0.598	4,405,038	N/A	N/A	17.9	17.5
20		N/A	0.621	24,750	N/A	N/A	0.1	0.1
21		N/A	0.642	15,741	N/A	N/A	0.1	0.1
22		N/A	0.665	3,564	N/A	N/A	0.0	0.0
23		N/A	0.697	262,383	N/A	N/A	1.1	1.0
24		N/A	0.737	45,804	N/A	N/A	0.2	0.2
25		N/A	0.786	14,883	N/A	N/A	0.1	0.1
26		N/A	0.823	270,732	N/A	N/A	1.1	1.1
27		N/A	0.854	5,695,008	N/A	N/A	23.1	22.6
28		N/A	0.877	105,864	N/A	N/A	0.4	0.4
29		N/A	0.900	48,048	N/A	N/A	0.2	0.2
30		N/A	0.921	16,797	N/A	N/A	0.1	0.1
31		N/A	0.951	220,209	N/A	N/A	0.9	0.9
32		N/A	0.989	5,775	N/A	N/A	0.0	0.0

Band Detection	Automatically detected bands with advanced settings
Lane Background	Lane background subtracted with disk size: 10
Lane Width	5.03 mm

Lane 14

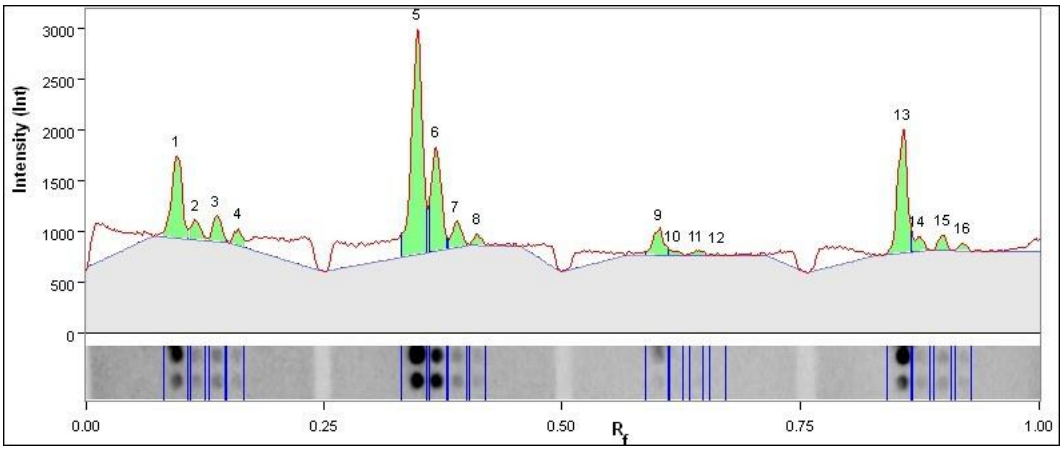

Band No.	Band Label	Mol. Wt. (KDa)	Relative Front	Volume (Int)	Abs. Quant.	Rel. Quant.	Band %	Lane %
1		N/A	0.097	202,776	N/A	N/A	12.5	6.9
2		N/A	0.117	40,460	N/A	N/A	2.5	1.4
3		N/A	0.138	54,852	N/A	N/A	3.4	1.9
4		N/A	0.160	33,432	N/A	N/A	2.1	1.1

5		N/A	0.348	543,144	N/A	N/A	33.4	18.5
6		N/A	0.368	231,840	N/A	N/A	14.2	7.9
7		N/A	0.389	57,176	N/A	N/A	3.5	1.9
8		N/A	0.412	21,448	N/A	N/A	1.3	0.7
9		N/A	0.601	67,004	N/A	N/A	4.1	2.3
10		N/A	0.618	10,164	N/A	N/A	0.6	0.3
11		N/A	0.642	11,900	N/A	N/A	0.7	0.4
12		N/A	0.663	3,920	N/A	N/A	0.2	0.1
13		N/A	0.857	275,632	N/A	N/A	16.9	9.4
14		N/A	0.874	30,912	N/A	N/A	1.9	1.1
15		N/A	0.900	29,176	N/A	N/A	1.8	1.0
16		N/A	0.921	13,412	N/A	N/A	0.8	0.5

Band Detection	Automatically detected bands with advanced settings
Lane Background	Lane background subtracted with disk size: 10
Lane Width	4.26 mm

Lane 15

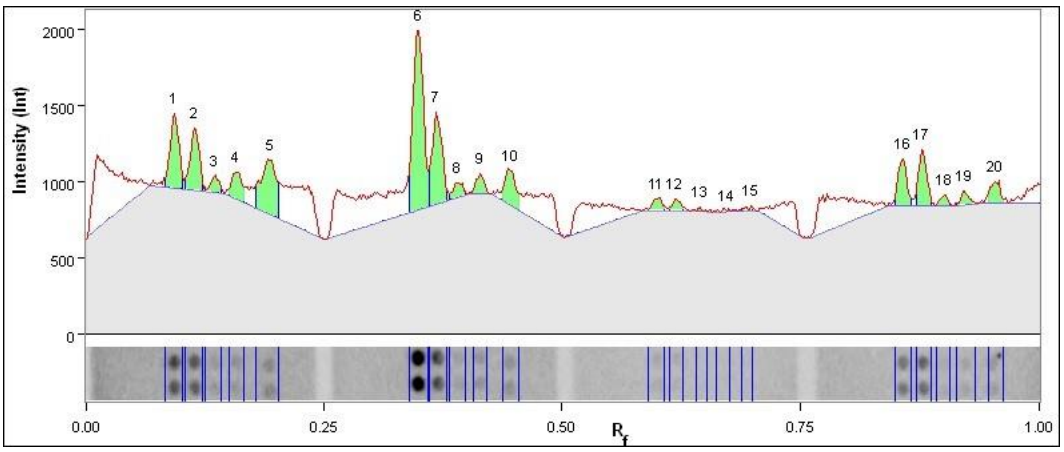

Band No.	Band Label	Mol. Wt. (KDa)	Relative Front	Volume (Int)	Abs. Quant.	Rel. Quant.	Band %	Lane %
1		N/A	0.094	94,864	N/A	N/A	8.7	3.9
2		N/A	0.115	79,128	N/A	N/A	7.3	3.2
3		N/A	0.136	21,084	N/A	N/A	1.9	0.9
4		N/A	0.159	43,764	N/A	N/A	4.0	1.8
5		N/A	0.194	118,552	N/A	N/A	10.9	4.8
6		N/A	0.350	277,536	N/A	N/A	25.5	11.3
7		N/A	0.368	123,396	N/A	N/A	11.3	5.0
8		N/A	0.391	20,636	N/A	N/A	1.9	0.8
9		N/A	0.415	23,632	N/A	N/A	2.2	1.0
10		N/A	0.446	58,716	N/A	N/A	5.4	2.4
11		N/A	0.600	18,956	N/A	N/A	1.7	0.8
12		N/A	0.619	13,468	N/A	N/A	1.2	0.6

13		N/A	0.645	3,052	N/A	N/A	0.3	0.1
14		N/A	0.673	3,052	N/A	N/A	0.3	0.1
15		N/A	0.699	4,424	N/A	N/A	0.4	0.2
16		N/A	0.857	60,564	N/A	N/A	5.6	2.5
17		N/A	0.877	65,268	N/A	N/A	6.0	2.7
18		N/A	0.901	12,208	N/A	N/A	1.1	0.5
19		N/A	0.922	16,632	N/A	N/A	1.5	0.7
20		N/A	0.955	31,192	N/A	N/A	2.9	1.3
Band Detection		Automatically detected bands with advanced settings						
Lane Background		Lane background subtracted with disk size: 10						
Lane Width		4.26 mm						

Lane 16

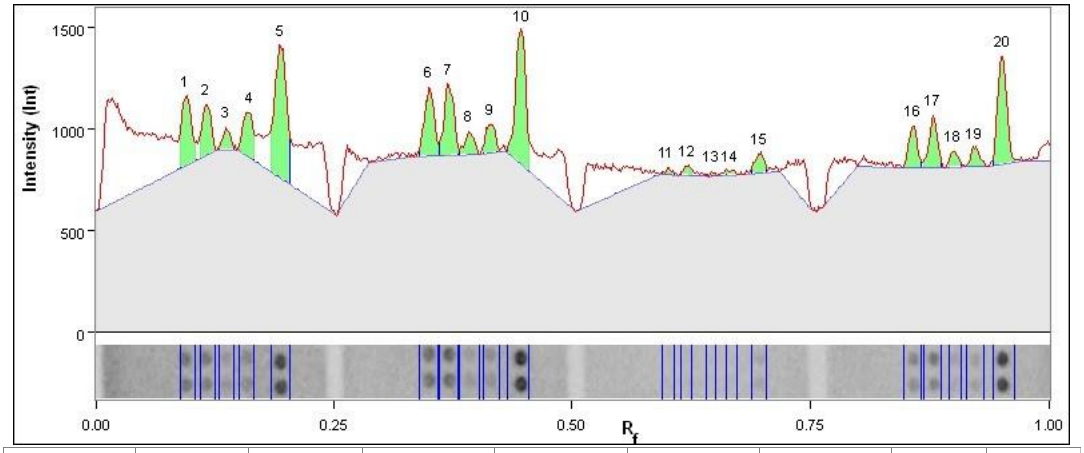

Band No.	Band Label	Mol. Wt. (KDa)	Relative Front	Volume (Int)	Abs. Quant.	Rel. Quant.	Band %	Lane %
1		N/A	0.096	82,880	N/A	N/A	8.1	3.6
2		N/A	0.117	49,448	N/A	N/A	4.8	2.1
3		N/A	0.138	19,572	N/A	N/A	1.9	0.8
4		N/A	0.162	54,964	N/A	N/A	5.3	2.4
5		N/A	0.194	171,136	N/A	N/A	16.7	7.4
6		N/A	0.350	75,740	N/A	N/A	7.4	3.3
7		N/A	0.371	79,240	N/A	N/A	7.7	3.4
8		N/A	0.392	25,368	N/A	N/A	2.5	1.1
9		N/A	0.415	32,312	N/A	N/A	3.1	1.4
10		N/A	0.447	159,404	N/A	N/A	15.5	6.9
11		N/A	0.600	4,928	N/A	N/A	0.5	0.2
12		N/A	0.621	8,428	N/A	N/A	0.8	0.4
13		N/A	0.647	2,380	N/A	N/A	0.2	0.1
14		N/A	0.666	3,920	N/A	N/A	0.4	0.2
15		N/A	0.697	19,964	N/A	N/A	1.9	0.9
16		N/A	0.857	42,252	N/A	N/A	4.1	1.8
17		N/A	0.878	48,580	N/A	N/A	4.7	2.1
18		N/A	0.900	14,952	N/A	N/A	1.5	0.6

19		N/A	0.922	20,076	N/A	N/A	2.0	0.9
20		N/A	0.951	111,944	N/A	N/A	10.9	4.9
Band Detection	Automatically detected bands with advanced settings							
Lane Background	Lane background subtracted with disk size: 10							
Lane Width	4.26 mm							

Lane 17

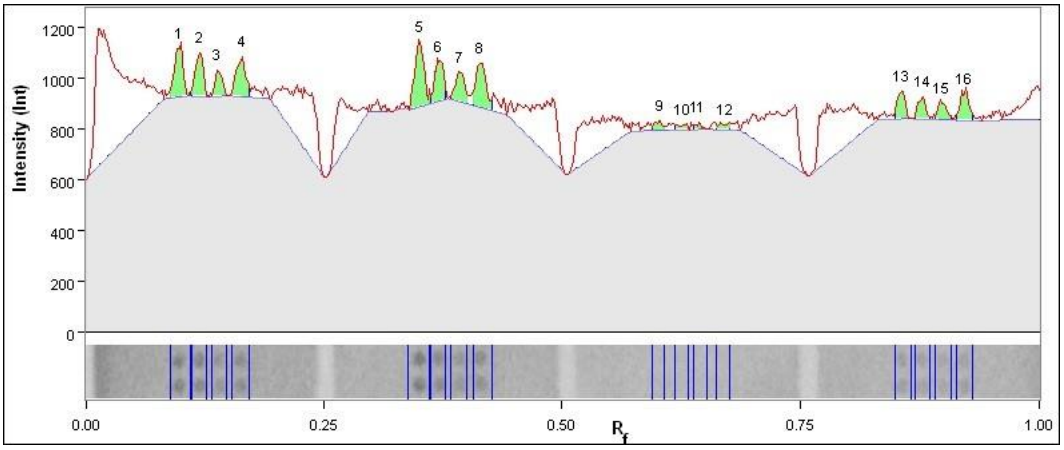

Band No.	Band Label	Mol. Wt. (KDa)	Relative Front	Volume (Int)	Abs. Quant.	Rel. Quant.	Band %	Lane %
1		N/A	0.099	39,480	N/A	N/A	10.8	2.4
2		N/A	0.120	31,248	N/A	N/A	8.5	1.9
3		N/A	0.139	16,128	N/A	N/A	4.4	1.0
4		N/A	0.165	33,432	N/A	N/A	9.1	2.1
5		N/A	0.352	53,620	N/A	N/A	14.7	3.3
6		N/A	0.371	32,732	N/A	N/A	8.9	2.0
7		N/A	0.394	24,920	N/A	N/A	6.8	1.5
8		N/A	0.415	42,336	N/A	N/A	11.6	2.6
9		N/A	0.603	6,972	N/A	N/A	1.9	0.4
10		N/A	0.627	4,004	N/A	N/A	1.1	0.2
11		N/A	0.643	3,024	N/A	N/A	0.8	0.2
12		N/A	0.671	6,720	N/A	N/A	1.8	0.4
13		N/A	0.856	19,152	N/A	N/A	5.2	1.2
14		N/A	0.878	15,260	N/A	N/A	4.2	0.9
15		N/A	0.898	14,056	N/A	N/A	3.8	0.9
16		N/A	0.922	22,904	N/A	N/A	6.3	1.4
Band Detection	Automatically detected bands with advanced settings							
Lane Background	Lane background subtracted with disk size: 10							
Lane Width	4.26 mm							

Lane 18

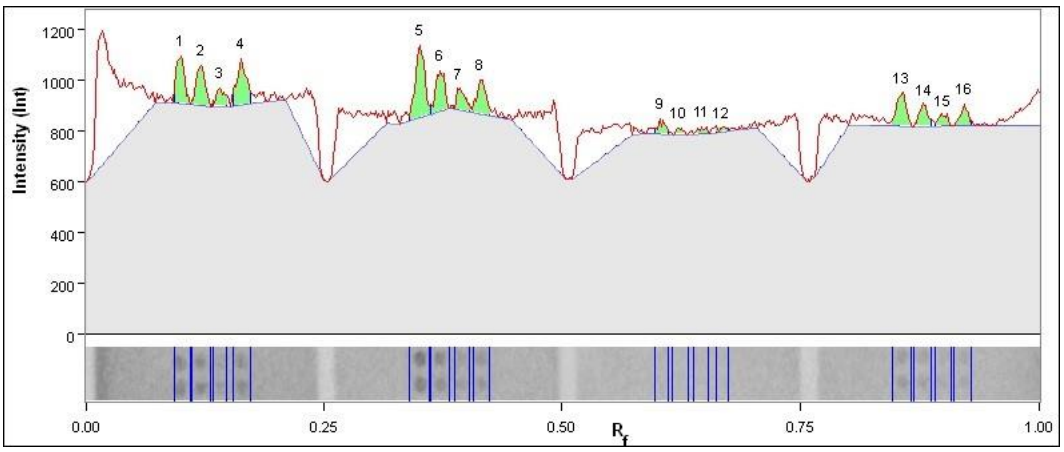

Band No.	Band Label	Mol. Wt. (KDa)	Relative Front	Volume (Int)	Abs. Quant.	Rel. Quant.	Band %	Lane %
1		N/A	0.100	36,736	N/A	N/A	10.3	2.6
2		N/A	0.122	31,528	N/A	N/A	8.9	2.2
3		N/A	0.141	14,728	N/A	N/A	4.1	1.0
4		N/A	0.164	38,360	N/A	N/A	10.8	2.7
5		N/A	0.352	60,592	N/A	N/A	17.0	4.2
6		N/A	0.373	32,900	N/A	N/A	9.3	2.3
7		N/A	0.392	17,948	N/A	N/A	5.0	1.3
8		N/A	0.415	27,692	N/A	N/A	7.8	1.9
9		N/A	0.603	9,212	N/A	N/A	2.6	0.6
10		N/A	0.622	4,452	N/A	N/A	1.3	0.3
11		N/A	0.647	4,956	N/A	N/A	1.4	0.3
12		N/A	0.668	3,556	N/A	N/A	1.0	0.2
13		N/A	0.856	29,456	N/A	N/A	8.3	2.1
14		N/A	0.880	18,424	N/A	N/A	5.2	1.3
15		N/A	0.900	9,716	N/A	N/A	2.7	0.7
16		N/A	0.922	15,316	N/A	N/A	4.3	1.1

Band Detection	Automatically detected bands with advanced settings
Lane Background	Lane background subtracted with disk size: 10
Lane Width	4.26 mm

Lane 19

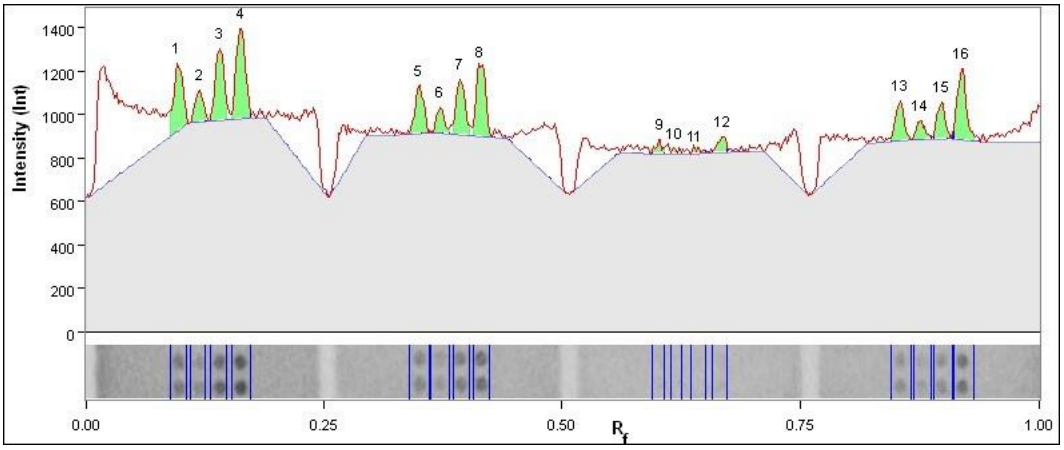

Band No.	Band Label	Mol. Wt. (KDa)	Relative Front	Volume (Int)	Abs. Quant.	Rel. Quant.	Band %	Lane %
1		N/A	0.097	60,760	N/A	N/A	10.1	3.3
2		N/A	0.120	26,796	N/A	N/A	4.5	1.5
3		N/A	0.141	64,932	N/A	N/A	10.8	3.5
4		N/A	0.164	83,720	N/A	N/A	14.0	4.6
5		N/A	0.350	42,448	N/A	N/A	7.1	2.3
6		N/A	0.373	22,372	N/A	N/A	3.7	1.2
7		N/A	0.394	50,456	N/A	N/A	8.4	2.7
8		N/A	0.415	70,000	N/A	N/A	11.7	3.8
9		N/A	0.603	9,716	N/A	N/A	1.6	0.5
10		N/A	0.619	4,900	N/A	N/A	0.8	0.3
11		N/A	0.640	5,320	N/A	N/A	0.9	0.3
12		N/A	0.669	12,488	N/A	N/A	2.1	0.7
13		N/A	0.854	33,684	N/A	N/A	5.6	1.8
14		N/A	0.875	15,904	N/A	N/A	2.7	0.9
15		N/A	0.898	31,024	N/A	N/A	5.2	1.7
16		N/A	0.919	64,736	N/A	N/A	10.8	3.5

Band Detection	Automatically detected bands with advanced settings
Lane Background	Lane background subtracted with disk size: 10
Lane Width	4.26 mm

Lane 20

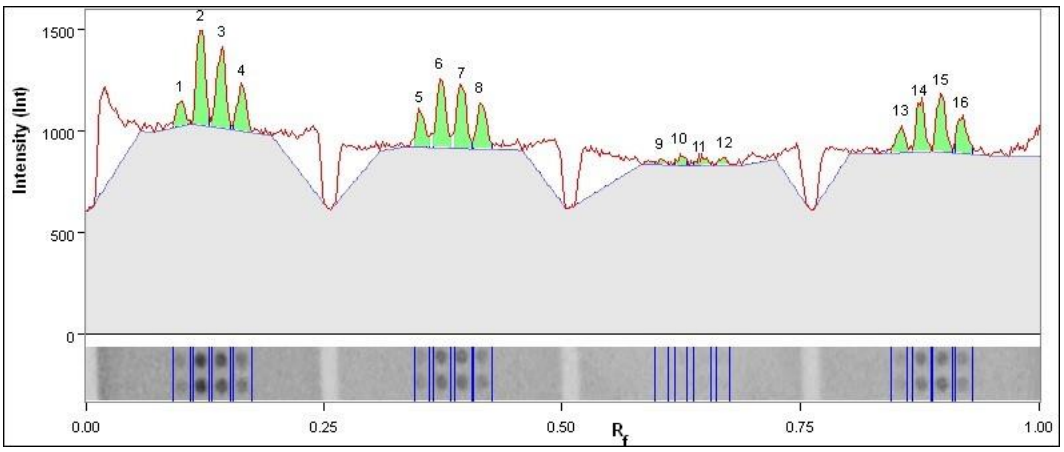

Band No.	Band Label	Mol. Wt. (KDa)	Relative Front	Volume (Int)	Abs. Quant.	Rel. Quant.	Band %	Lane %
1		N/A	0.100	25,844	N/A	N/A	3.8	1.5
2		N/A	0.122	93,128	N/A	N/A	13.8	5.3
3		N/A	0.144	80,444	N/A	N/A	11.9	4.6
4		N/A	0.165	46,564	N/A	N/A	6.9	2.7
5		N/A	0.352	37,660	N/A	N/A	5.6	2.1
6		N/A	0.373	70,476	N/A	N/A	10.4	4.0
7		N/A	0.395	66,416	N/A	N/A	9.8	3.8
8		N/A	0.415	49,560	N/A	N/A	7.3	2.8
9		N/A	0.603	4,928	N/A	N/A	0.7	0.3
10		N/A	0.624	8,484	N/A	N/A	1.3	0.5
11		N/A	0.645	10,164	N/A	N/A	1.5	0.6
12		N/A	0.671	6,692	N/A	N/A	1.0	0.4
13		N/A	0.856	25,900	N/A	N/A	3.8	1.5
14		N/A	0.875	48,412	N/A	N/A	7.2	2.8
15		N/A	0.898	61,572	N/A	N/A	9.1	3.5
16		N/A	0.919	40,124	N/A	N/A	5.9	2.3

Band Detection	Automatically detected bands with advanced settings
Lane Background	Lane background subtracted with disk size: 10
Lane Width	4.26 mm

Lane 21

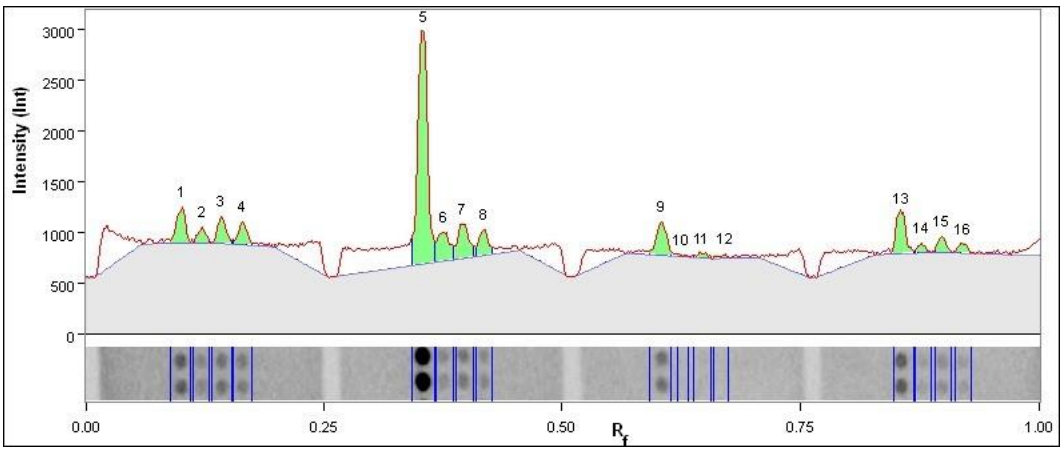

Band No.	Band Label	Mol. Wt. (KDa)	Relative Front	Volume (Int)	Abs. Quant.	Rel. Quant.	Band %	Lane %
1		N/A	0.102	82,040	N/A	N/A	6.3	3.0
2		N/A	0.123	30,604	N/A	N/A	2.3	1.1
3		N/A	0.143	55,580	N/A	N/A	4.3	2.0
4		N/A	0.165	51,184	N/A	N/A	3.9	1.9
5		N/A	0.355	558,488	N/A	N/A	42.9	20.6
6		N/A	0.376	93,100	N/A	N/A	7.1	3.4
7		N/A	0.395	89,628	N/A	N/A	6.9	3.3
8		N/A	0.418	58,688	N/A	N/A	4.5	2.2
9		N/A	0.605	83,748	N/A	N/A	6.4	3.1
10		N/A	0.626	4,144	N/A	N/A	0.3	0.2
11		N/A	0.647	13,104	N/A	N/A	1.0	0.5
12		N/A	0.671	7,644	N/A	N/A	0.6	0.3
13		N/A	0.856	101,332	N/A	N/A	7.8	3.7
14		N/A	0.877	18,256	N/A	N/A	1.4	0.7
15		N/A	0.898	33,992	N/A	N/A	2.6	1.3
16		N/A	0.921	21,028	N/A	N/A	1.6	0.8

Band Detection	Automatically detected bands with advanced settings
Lane Background	Lane background subtracted with disk size: 10
Lane Width	4.26 mm

Lane 22

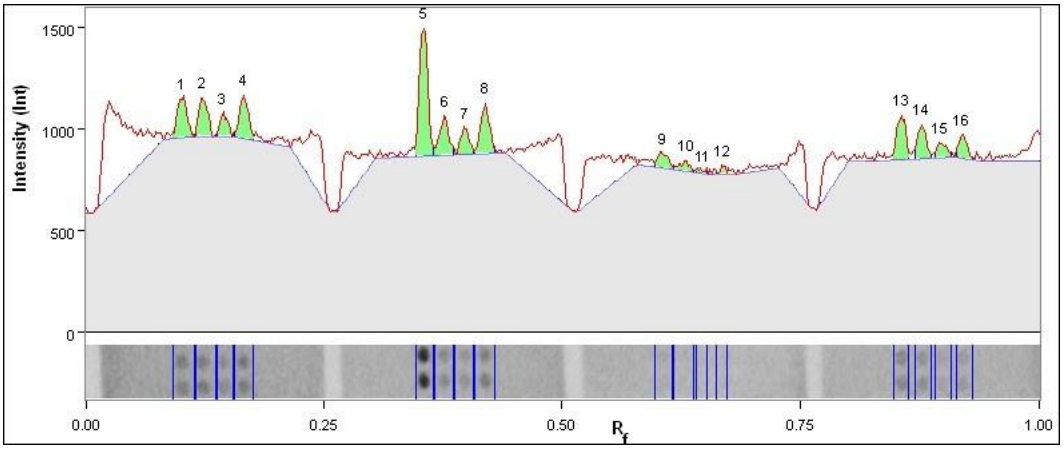

Band No.	Band Label	Mol. Wt. (KDa)	Relative Front	Volume (Int)	Abs. Quant.	Rel. Quant.	Band %	Lane %
1		N/A	0.102	45,304	N/A	N/A	8.1	2.7
2		N/A	0.123	40,208	N/A	N/A	7.2	2.4
3		N/A	0.144	22,456	N/A	N/A	4.0	1.3
4		N/A	0.167	44,632	N/A	N/A	8.0	2.6
5		N/A	0.355	126,868	N/A	N/A	22.8	7.5
6		N/A	0.378	41,160	N/A	N/A	7.4	2.4
7		N/A	0.399	26,936	N/A	N/A	4.8	1.6
8		N/A	0.420	49,924	N/A	N/A	9.0	3.0
9		N/A	0.606	19,264	N/A	N/A	3.5	1.1
10		N/A	0.630	11,536	N/A	N/A	2.1	0.7
11		N/A	0.648	4,340	N/A	N/A	0.8	0.3
12		N/A	0.669	5,908	N/A	N/A	1.1	0.4
13		N/A	0.856	46,200	N/A	N/A	8.3	2.7
14		N/A	0.877	32,760	N/A	N/A	5.9	1.9
15		N/A	0.896	17,472	N/A	N/A	3.1	1.0
16		N/A	0.919	21,840	N/A	N/A	3.9	1.3
Band Detection		Automatically detected bands with advanced settings						
Lane Background		Lane background subtracted with disk size: 10						
Lane Width		4.26 mm						

Lane 23

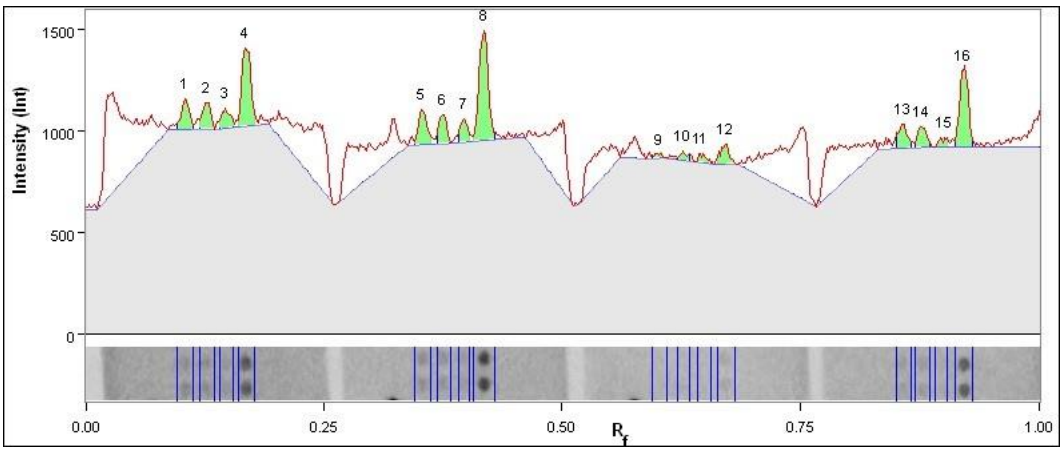

Band No.	Band Label	Mol. Wt. (KDa)	Relative Front	Volume (Int)	Abs. Quant.	Rel. Quant.	Band %	Lane %
1		N/A	0.105	27,160	N/A	N/A	5.5	1.4
2		N/A	0.128	25,004	N/A	N/A	5.0	1.3
3		N/A	0.147	18,312	N/A	N/A	3.7	1.0
4		N/A	0.169	79,240	N/A	N/A	16.0	4.2
5		N/A	0.353	32,732	N/A	N/A	6.6	1.7
6		N/A	0.374	23,632	N/A	N/A	4.8	1.2
7		N/A	0.397	18,340	N/A	N/A	3.7	1.0
8		N/A	0.418	108,304	N/A	N/A	21.8	5.7
9		N/A	0.601	4,396	N/A	N/A	0.9	0.2
10		N/A	0.627	8,036	N/A	N/A	1.6	0.4
11		N/A	0.645	7,504	N/A	N/A	1.5	0.4
12		N/A	0.671	18,312	N/A	N/A	3.7	1.0
13		N/A	0.857	22,848	N/A	N/A	4.6	1.2
14		N/A	0.877	19,572	N/A	N/A	3.9	1.0
15		N/A	0.901	8,764	N/A	N/A	1.8	0.5
16		N/A	0.921	74,172	N/A	N/A	14.9	3.9

Band Detection	Automatically detected bands with advanced settings
Lane Background	Lane background subtracted with disk size: 10
Lane Width	4.26 mm

Lane 24

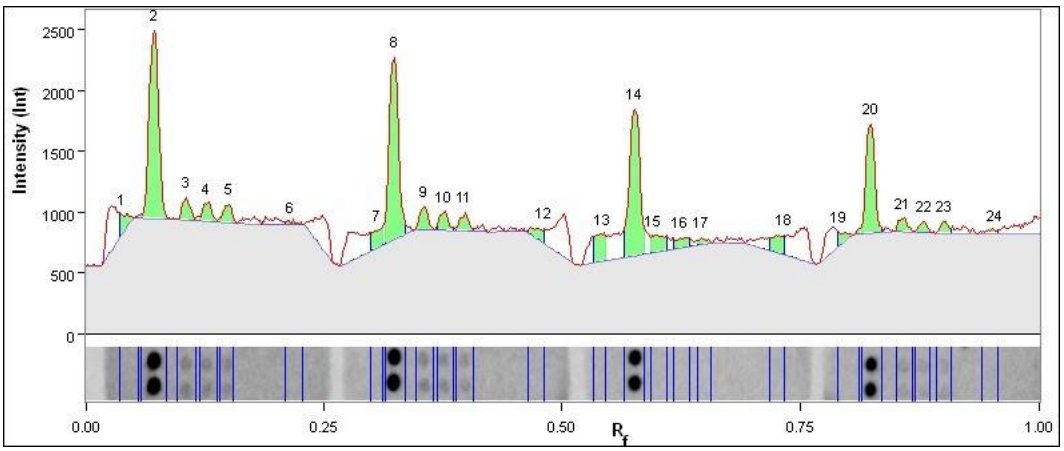

Band No.	Band Label	Mol. Wt. (KDa)	Relative Front	Volume (Int)	Abs. Quant.	Rel. Quant.	Band %	Lane %
1		N/A	0.039	24,976	N/A	N/A	1.4	0.9
2		N/A	0.073	355,908	N/A	N/A	19.7	12.8
3		N/A	0.107	39,536	N/A	N/A	2.2	1.4
4		N/A	0.128	35,784	N/A	N/A	2.0	1.3
5		N/A	0.151	31,808	N/A	N/A	1.8	1.1
6		N/A	0.216	6,748	N/A	N/A	0.4	0.2
7		N/A	0.306	37,436	N/A	N/A	2.1	1.4
8		N/A	0.324	345,520	N/A	N/A	19.2	12.5
9		N/A	0.355	38,724	N/A	N/A	2.1	1.4
10		N/A	0.376	33,180	N/A	N/A	1.8	1.2
11		N/A	0.399	30,744	N/A	N/A	1.7	1.1
12		N/A	0.483	30,324	N/A	N/A	1.7	1.1
13		N/A	0.543	63,924	N/A	N/A	3.5	2.3
14		N/A	0.577	314,524	N/A	N/A	17.5	11.4
15		N/A	0.596	45,388	N/A	N/A	2.5	1.6
16		N/A	0.624	25,732	N/A	N/A	1.4	0.9
17		N/A	0.647	9,744	N/A	N/A	0.5	0.4
18		N/A	0.733	44,716	N/A	N/A	2.5	1.6
19		N/A	0.791	19,404	N/A	N/A	1.1	0.7
20		N/A	0.823	193,816	N/A	N/A	10.8	7.0
21		N/A	0.857	24,780	N/A	N/A	1.4	0.9
22		N/A	0.880	17,752	N/A	N/A	1.0	0.6
23		N/A	0.901	22,008	N/A	N/A	1.2	0.8
24		N/A	0.955	9,828	N/A	N/A	0.5	0.4

Band Detection	Automatically detected bands with advanced settings
Lane Background	Lane background subtracted with disk size: 10

Appendix XI: Chapter 4: Table of Increases and Decreases to Combined RTK Phosphotyrosine/Expression Levels

	A. gen	*C.dve*	*D.vir*	*H.swa*	*N.naj*
EGFR	X	X	X	X	X
HER2	X	√	X	√	√
HER3	√	√	X	X	√
HER4	X	√	X	√	X
FGF R1	√	√	X	X	√
FGF R2 alpha	√	√	X	X	X
FGF R3	X	√	X	X	X
FGF R4	X	√	X	X	X
Insulin R	X	X	√	X	X
IGF-I R	X	√	X	X	X
Axl	X	√	X	X	X
Dtk	√	X	X	X	√
Mer	√	√	√	√	X
HGF R	√	√	√	X	√
MSP R	X	√	X	X	√
PDGF R alpha	X	√	X	X	X
PDGF R beta	X	√	X	X	X
SCF R	X	√	X	X	X
Flt-3	X	√	X	X	X
M-CSF R	X	√	X	√	X
c-RET	X	√	√	X	X
ROR1	X	√	X	X	√
ROR2	X	√	X	X	X
Tie-1	X	X	X	X	X
Tie-2	√	√	X	√	√
Trk A	√	√	X	X	√
Trk B	X	√	X	X	√
Trk C	√	√	X	X	X
VEGF R1	X	√	X	X	X
VEGF R2	X	√	X	X	X
VEGF R3	X	√	X	X	X
MuSK	X	√	X	X	X
Eph A1	X	√	X	X	X
Eph A2	X	√	X	X	√
Eph A3	X	√	X	X	X
Eph A4	X	√	X	X	X
Eph A5	X	√	X	X	X
Eph A6	√	√	√	X	X
Eph A7	√	√	X	X	X
Eph A10	X	√	X	X	X
Eph B1	X	√	X	√	X
Eph B3	X	√	X	√	X
Eph B2	X	√	X	X	X
Eph B4	√	√	X	X	X
Eph B6	√	√	X	X	X
ALK	X	√	X	X	X
DDR1	X	√	X	X	X
DDR2	√	√	X	X	X
RYK	√	√	X	X	X

Appendix XI: Changes in RTK Expression/Phosphorylation State in Response to Treatment with Whole Venoms

The table displays 2-fold or greater reductions or increases in the combined phosphorylation/expression profile of each of 49 receptor tyrosine kinases in response to 5 whole venom treatments. **Greater than 2-fold upregulations in green, greater than 2-fold downregulation in red.**

Appendix XII: Chapter 5: PY20 ELISA Cell Number Optimisation Plate Layout

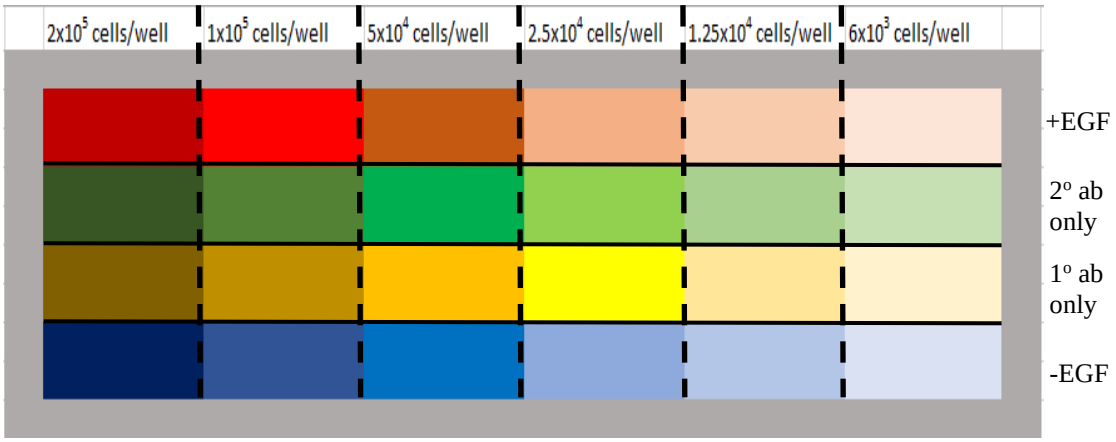

Appendix XII: Plate Layout to Determine the Optimal Cell Number for PY20 ELISAs

MDA-MB-468 and A431 cells were plated out in quadruplicate at varying cell concentrations of $2x10^5$, $1x10^5$, $5x10^4$, $2.5x10^4$, $1.25x10^4$ and $6x10^3$ cells/well. All cell concentrations were treated with differing combinations EGF, 1º and 2º antibody to enable the max phosphorylation, min phosphorylation and non-specific antibody binding to be assessed in both cell lines at all cell concentrations.

Rows 1+2: Treatment: EGF, 1^0ab, 2^0ab **(Max Phosphorylation)**
Rows 3+4: Treatment: EGF, 2^0ab only **(2º background control)**
Rows 5+6: Treatment: EGF, 1^0ab only **(1º background control)**
Rows 7+8: Treatment: No EGF, 1^0ab, 2^0ab **(background phosphorylation control (min))**

Appendix XIII: Chapter 5: PY20 ELISA Optimisation, Cell Number and Secondary Antibody Combination Plate Layout

A

	1	2	3	4	5	6	7	8	9	10	11	12
A	+ EGF and 1 ab		+ EGF, 1 ab and 1/10,000 2ab	+ EGF, 1 ab and 1/10,000 2ab	+ EGF and 1 ab		+ EGF and 1 ab		+ EGF, 1 ab and 1/10,000 2ab	+ EGF, 1 ab and 1/10,000 2ab	+ EGF and 1 ab	
B	+ EGF and 1/10,000 2ab		+ EGF, 1 ab and 1/10,000 2ab	+ EGF, 1 ab and 1/10,000 2ab	+ EGF and 1/10,000 2ab		+ EGF and 1/10,000 2ab		+ EGF, 1 ab and 1/10,000 2ab	+ EGF, 1 ab and 1/10,000 2ab	+ EGF and 1/10,000 2ab	
C	+ EGF and 1/20,000 2ab		+ EGF, 1 ab and 1/20,000 2ab	+ EGF, 1 ab and 1/20,000 2ab	+ EGF and 1/20,000 2ab		+ EGF and 1/20,000 2ab		+ EGF, 1 ab and 1/20,000 2ab	+ EGF, 1 ab and 1/20,000 2ab	+ EGF and 1/20,000 2ab	
D	+ EGF and 1/40,000 2ab		+ EGF, 1 ab and 1/20,000 2ab	+ EGF, 1 ab and 1/20,000 2ab	+ EGF and 1/40,000 2ab		+ EGF and 1/40,000 2ab		+ EGF, 1 ab and 1/20,000 2ab	+ EGF, 1 ab and 1/20,000 2ab	+ EGF and 1/40,000 2ab	
E	+EGF and NO abs		+ EGF, 1 ab and 1/40,000 2ab	+ EGF, 1 ab and 1/40,000 2ab	+EGF and NO abs		+EGF and NO abs		+ EGF, 1 ab and 1/40,000 2ab	+ EGF, 1 ab and 1/40,000 2ab	+EGF and NO abs	
F	- EGF, 1 ab and 1/10,000 2ab		+ EGF, 1 ab and 1/40,000 2ab	+ EGF, 1 ab and 1/40,000 2ab	- EGF, 1 ab and 1/10,000 2ab		- EGF, 1 ab and 1/10,000 2ab		+ EGF, 1 ab and 1/40,000 2ab	+ EGF, 1 ab and 1/40,000 2ab	- EGF, 1 ab and 1/10,000 2ab	
G	- EGF, 1 ab and 1/20,000 2ab		-EGF and NO abs	-EGF and NO abs	- EGF, 1 ab and 1/20,000 2ab		- EGF, 1 ab and 1/20,000 2ab		-EGF and NO abs	-EGF and NO abs	- EGF, 1 ab and 1/20,000 2ab	
H	- EGF, 1 ab and 1/40,000 2ab		-EGF and NO abs	-EGF and NO abs	- EGF, 1 ab and 1/40,000 2ab		- EGF, 1 ab and 1/40,000 2ab		-EGF and NO abs	-EGF and NO abs	- EGF, 1 ab and 1/40,000 2ab	
	$5X10^4$ Cells			$2X10^5$ Cells			$1X10^5$ Cells			$2X10^5$ Cells		
	MDA-MB-468						A431					

B

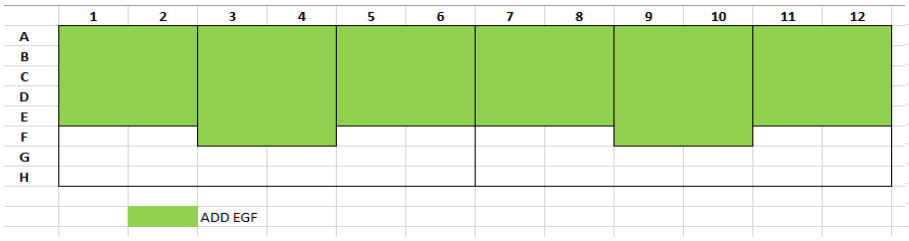

C

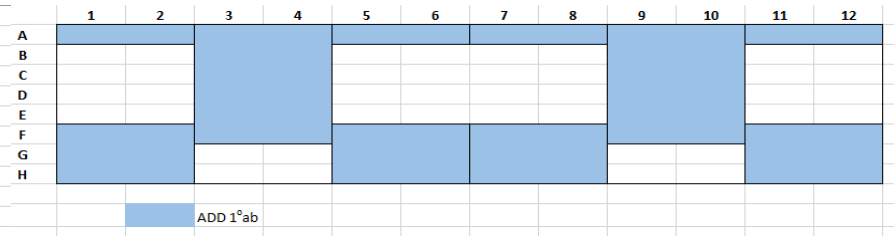

D

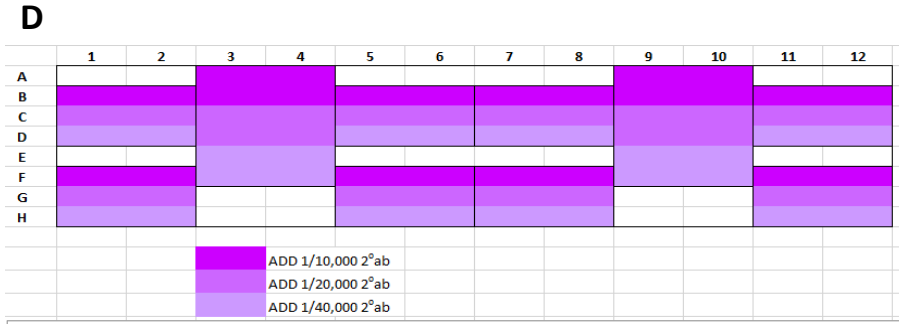

E

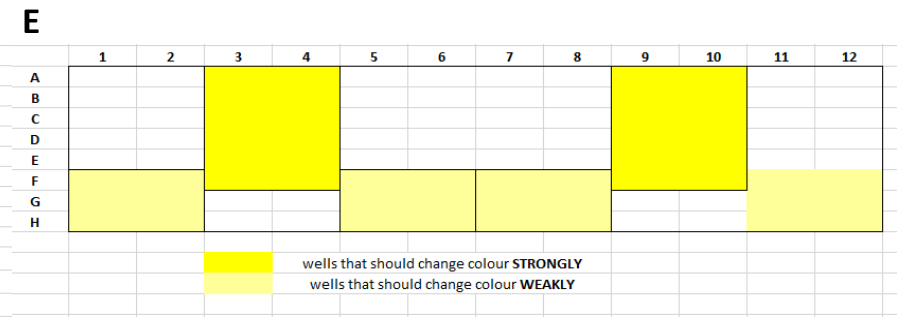

Appendix XIII: Cell and 2º ab Plate Layouts

Displays the final overall treatment and cell number of each well of a 96 well plates (A), the wells which specifically received the addition of $1x10^{-7}$M EGF (B), the wells which specifically received the addition of 1/1000 PY20 1º ab (C), the wells which received 1/10,000, 1/20,000 or 1/40,000 2º ab (D) and the predicted final expected TMB colour changed wells (E)

Appendix XIV: Chapter 5: PY20 ELISA Z' Assay Plate Layout

	1	2	3	4	5	6	7	8	9	10	11	12
A	+	+	+	+	+	+	-	-	-	-	-	-
B	+	+	+	+	+	+	-	-	-	-	-	-
C	+	+	+	+	+	+	-	-	-	-	-	-
D	+	+	+	+	+	+	-	-	-	-	-	-
E	-	-	-	-	-	-	+	+	+	+	+	+
F	-	-	-	-	-	-	+	+	+	+	+	+
G	-	-	-	-	-	-	+	+	+	+	+	+
H	-	-	-	-	-	-	+	+	+	+	+	+

Appendix XIV: Plate Layout for 96-well PY20 ELISA Z' Assay

MDA-MB-468 and A431 cells were plated out across a whole 96 well plate at a concentration of $5x10^4$ and $1x10^5$ cells/well respectively and left to adhere overnight. Cells were treated with either $1x10^{-7}$M EGF **(+VE Control)** or with supplemented DMEM media **(-VE Control)** for 5mins. After 5mins, cells were fixed using paraformaldehyde and the optimised PY20 ELISA protocol carried out as via **2.4.2**

Appendix XV: Chapter 5: PY20 ELISA Snake Panel Plate Layout

	1	2	3	4	5	6	7	8	9	10	11	12
A	+EGF	+EGF	+EGF	1°ab only	1°ab only	1°ab only	2°ab only	2°ab only	2°ab only	-EGF	-EGF	-EGF
B	P.wei	P.wei	N.sia	N.sia	N.nig	N.nig	N.atr	N.atr	N.naj	N.naj	O.han	O.han
C	P.wei	P.wei	N.sia	N.sia	N.nig	N.nig	N.atr	N.atr	N.naj	N.naj	O.han	O.han
D	D.pol	D.pol	D.vir	D.vir	C.rho	C.rho	C.atr	C.atr	C.rru	C.rru	C.dve	C.dve
E	D.pol	D.pol	D.vir	D.vir	C.rho	C.rho	C.atr	C.atr	C.rru	C.rru	C.dve	C.dve
F	C.ins	C.ins	S.mil	S.mil	M.xan	M.xan	A.cco	A.cco	V.aam	V.aam	B.asp	B.asp
G	C.ins	C.ins	S.mil	S.mil	M.xan	M.xan	A.cco	A.cco	V.aam	V.aam	B.asp	B.asp
H	-EGF	-EGF	-EGF	2°ab only	2°ab only	2°ab only	1°ab only	1°ab only	1°ab only	+EGF	+EGF	+EGF

Appendix XV: Plate layout for Snake Panel ELISA Screening

A panel of whole snake venoms were screened in quadruplicate at a concentration of 20µg/ml. Wells of cells were dosed as via the example plate layout above. Plate included +ve EGF controls (Max abs), -ve EGF controls (background cell phosphorylation levels) and 1° and 2° ab only controls (non-specific antibody binding controls).

Appendix XVI: Chapter 5: PY20 ELISA Invertebrate Panel Plate Layout

	1	2	3	4	5	6	7	8	9	10	11	12
A	+EGF	+EGF	+EGF	1° ab only	1° ab only	1° ab only	2° ab only	2° ab only	2° ab only	-EGF	-EGF	-EGF
B	A.aus	A.aus	A.aus	H.ari	H.ari	H.ari	H.swa	H.swa	H.swa	P.kra	P.kra	P.kra
C	P.lio	P.lio	P.lio	A.cor	A.cor	A.cor	A.gen	A.gen	A.gen	A.met	A.met	A.met
D	B.boe	B.boe	B.boe	H.lbo	H.lbo	H.lbo	H.mac	H.mac	H.mac	P.cam	P.cam	P.cam
E	P.for	P.for	P.for	P.lug	P.lug	P.lug	T.cup	T.cup	T.cup	T.pru	T.pru	T.pru
F	T.str	T.str	T.str	S.har	S.har	S.har	S.sud	S.sud	S.sud	C.gig	C.gig	C.gig
G	E.foe	E.foe	E.foe	A.sex	A.sex	A.sex	P.mar	P.mar	P.mar			
H	-EGF	-EGF	-EGF	2° ab only	2° ab only	2° ab only	1° ab only	1° ab only	1° ab only	+EGF	+EGF	+EGF

Appendix XVI: Plate layout for Invertebrate Panel ELISA Screening

A panel of whole invertebrate venoms were screened in triplicate at a concentration of 100µg/ml. Wells of cells were dosed as via the example plate layout above. Plate included +ve EGF controls (Max abs), -ve EGF controls (background cell phosphorylation levels) and 1° and 2° ab only controls (non-specific antibody binding controls).

Appendix XVII: Chapter 5: Table of Minitab Normality Test, Equal Variance and Residual P-Values for Whole Snake and Invertebrate Venom PY20 ELISA Data Sets

Normality Test P-Values			
MDA-MB-468 Cells		A431 Cells	
P.wei	0.484	P.wei	0.125
N.sia	0.190	N.sia	0.211
N.nig	0.315	N.nig	0.281
N.atr	0.146	N.atr	0.277
N.naj	0.513	N.naj	0.128
O.han	0.210	O.han	0.207
D.pol	0.342	D.pol	0.628
D.vir	0.146	D.vir	0.503
C.rho	0.838	C.rho	0.870
C.atr	0.230	C.atr	0.160
C.rru	0.164	C.rru	0.608
C.dve	0.176	C.dve	0.116
C.ins	0.722	C.ins	0.254
S.mil	0.578	S.mil	0.511
M.xan	0.406	M.xan	0.186
V.aam	0.360	V.aam	0.314
A.cco	0.143	A.cco	0.358
B.asp	0.128	B.asp	0.401
+EGF	0.065	+EGF	0.095
A.aus	0.348	A.aus	0.227

H.ari	0.292	H.ari	0.457
H.swa	0.506	H.swa	0.627
P.kra	0.078	P.kra	0.329
P.lio	0.227	P.lio	0.239
A.cor	0.227	A.cor	0.630
A.gen	0.595	A.gen	0.227
A.met	0.227	A.met	0616
B.boe	0.391	B.boe	0.617
H.lbo	0.156	H.lbo	0.227
H.mac	0.581	H.mac	0.181
P.cam	0.027	P.cam	0.227
P.for	0.142	P.for	0.627
P.lug	0.120	P.lug	0.283
T.cup	0.554	T.cup	0.242
T.pru	0.227	T.pru	0.612
T.str	0.227	T.str	0.621
S.har	0.227	S.har	0.623
S.sud	0.077	S.sud	0.122
C.gig	0.227	C.gig	0.249
E.foe	0.073	E.foe	0.524
P.map	0.576	P.map	0.298
A.sex	0.227	A.sex	0.071
+EGF	0.469	+EGF	0.839
Equal Variance Test P-Values			
Snake Panel	0.359	Snake Panel	0.491
Invertebrate Panel	0.603	Invertebrate Panel	0.653
ANOVA Residuals P-Value			
Snake Panel	0.256	Snake Panel	0.062
Invertebrate Panel	0.931	Invertebrate Panel	0.218

Appendix XVIII: Chapter 5: ImageLab Analysis Reports of Whole Snake Panel PY20 and Actin Western Blot

Image Report: 2018-08-29 MDA-MB-468 snake panel PY20 240s

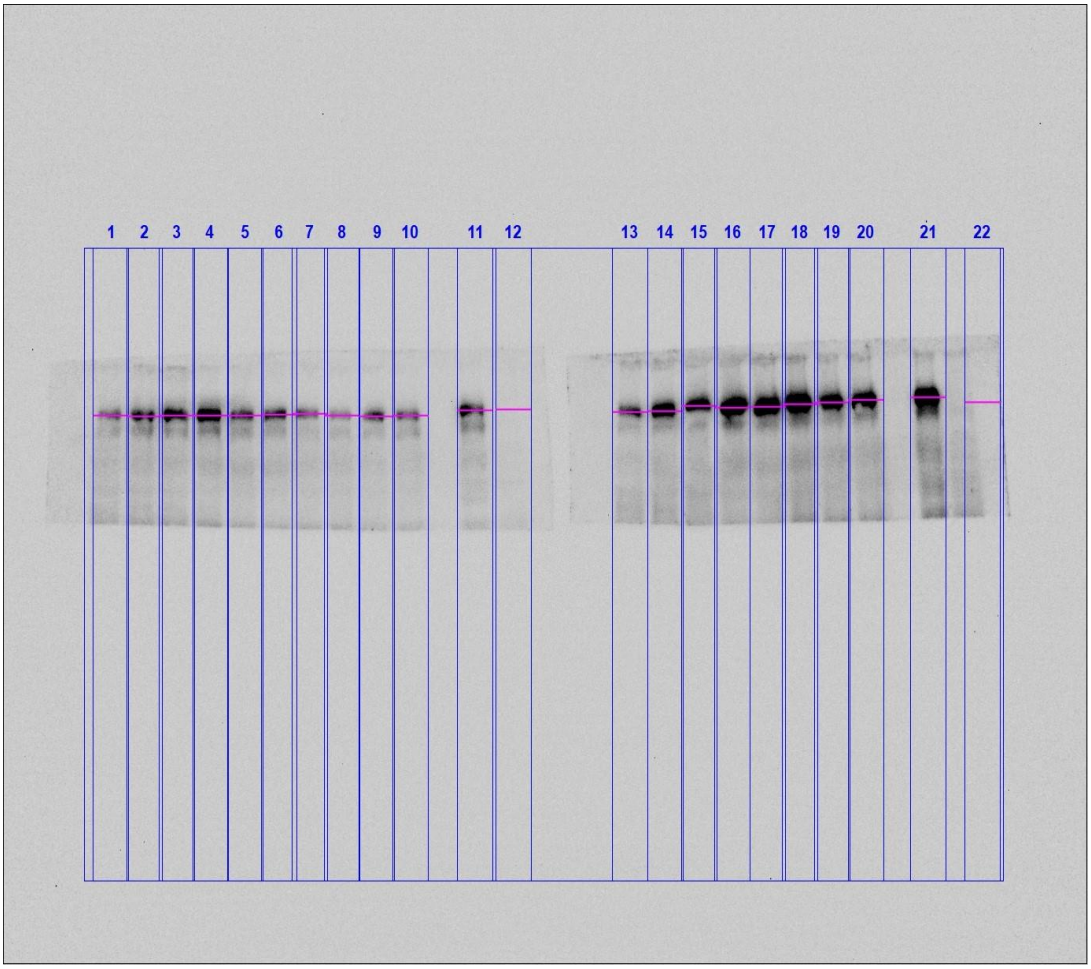

G:\Chemidoc Touch Images 2018-08-29_16.56.54\mda snake panel\2018-08-29 mda snake panel py20 240s.scn

Acquisition Information

Imager	ChemiDoc™ Touch
Exposure Time (sec)	240.000 (Manual)
Serial Number	732BR1296
Software Version	1.1.0.04
Application	Chemiluminescence
Excitation Source	No Illumination
Emission Filter	No Filter
Binning	2x2

Image Information

Acquisition Date	29/08/2018 22:59:28
User Name	
Image Area (mm)	X: 173.6 Y: 138.9
Pixel Size (um)	X: 125.9 Y: 125.9
Data Range (Int)	500 - 10536

Analysis Settings

Detection	Lane detection: Manually created lanes Band detection: Manually adjusted bands Lane Background Subtraction: Lane background subtracted with disk size: 10 Lane width: 5.66 mm

Lane And Band Analysis

Lane 1

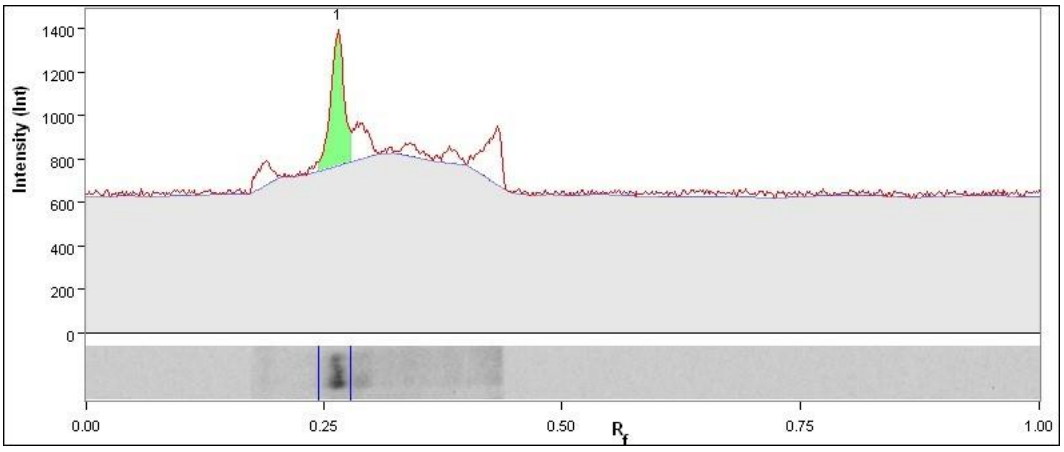

Band No.	Band Label	Mol. Wt. (KDa)	Relative Front	Volume (Int)	Abs. Quant.	Rel. Quant.	Band %	Lane %
1		N/A	0.265	356,040	N/A	N/A	100.0	31.1

Lane Background	Lane background subtracted with disk size: 10
Lane Width	5.66 mm

Lane 2

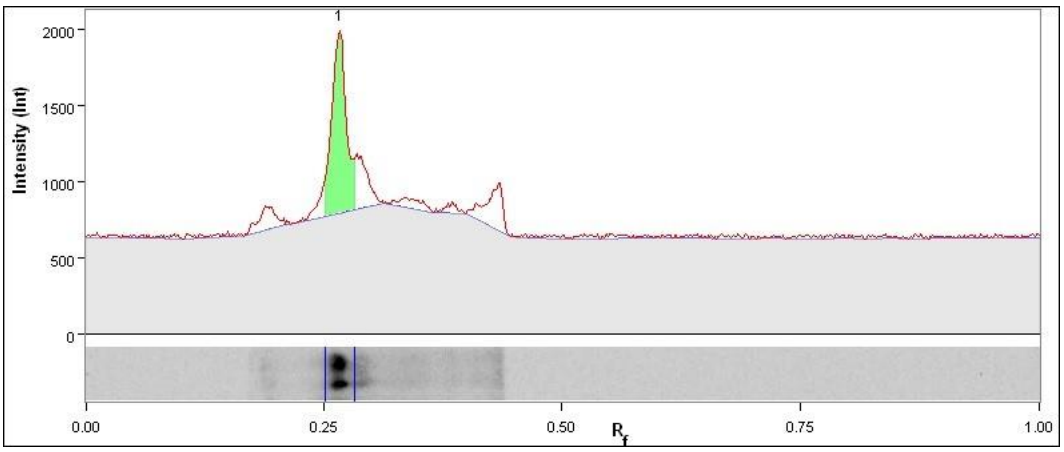

Band No.	Band Label	Mol. Wt. (KDa)	Relative Front	Volume (Int)	Abs. Quant.	Rel. Quant.	Band %	Lane %
1		N/A	0.266	763,470	N/A	N/A	100.0	44.6

Lane Background	Lane background subtracted with disk size: 10
Lane Width	5.66 mm

Lane 3

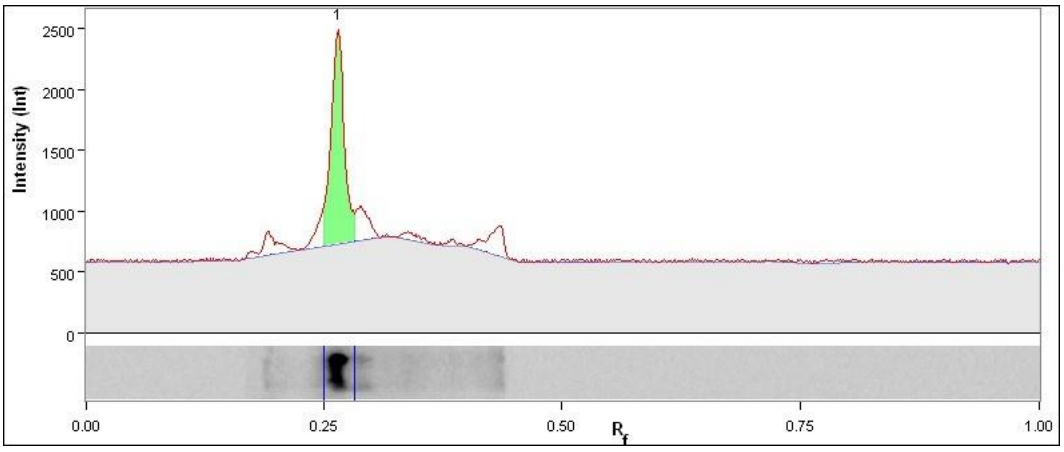

Band No.	Band Label	Mol. Wt. (KDa)	Relative Front	Volume (Int)	Abs. Quant.	Rel. Quant.	Band %	Lane %
1		N/A	0.265	1,077,750	N/A	N/A	100.0	54.3

Lane Background	Lane background subtracted with disk size: 10
Lane Width	5.66 mm

Lane 4

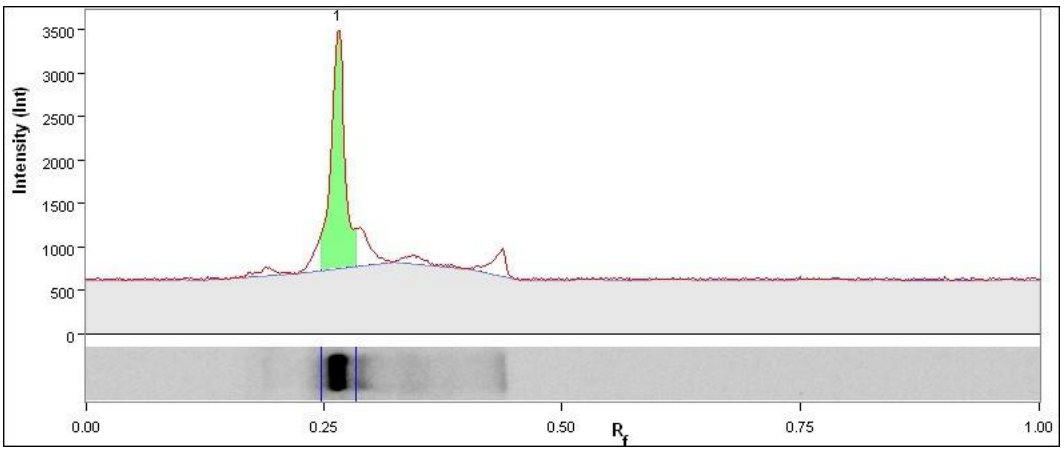

Band No.	Band Label	Mol. Wt. (KDa)	Relative Front	Volume (Int)	Abs. Quant.	Rel. Quant.	Band %	Lane %
1		N/A	0.265	1,647,990	N/A	N/A	100.0	62.1

Lane Background	Lane background subtracted with disk size: 10
Lane Width	5.66 mm

Lane 5

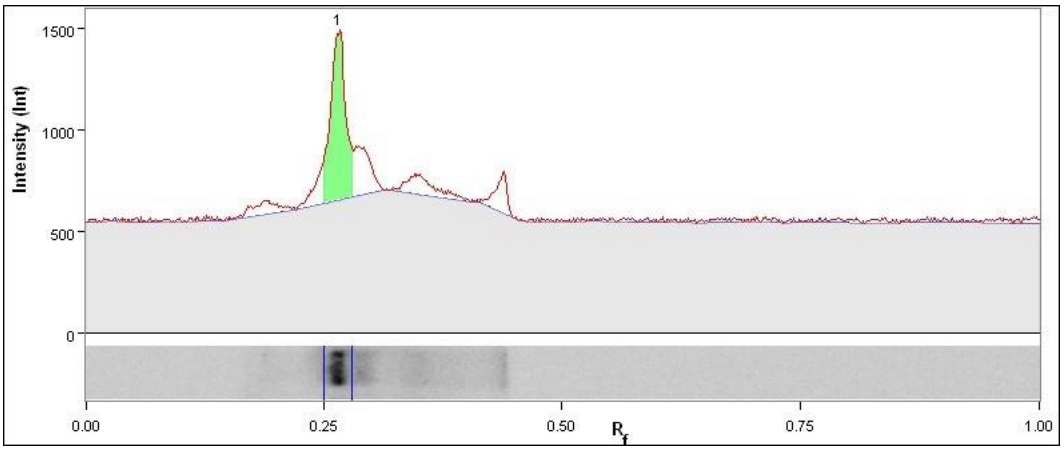

Band No.	Band Label	Mol. Wt. (KDa)	Relative Front	Volume (Int)	Abs. Quant.	Rel. Quant.	Band %	Lane %
1		N/A	0.265	615,150	N/A	N/A	100.0	40.6

Lane Background	Lane background subtracted with disk size: 10
Lane Width	5.66 mm

Lane 6

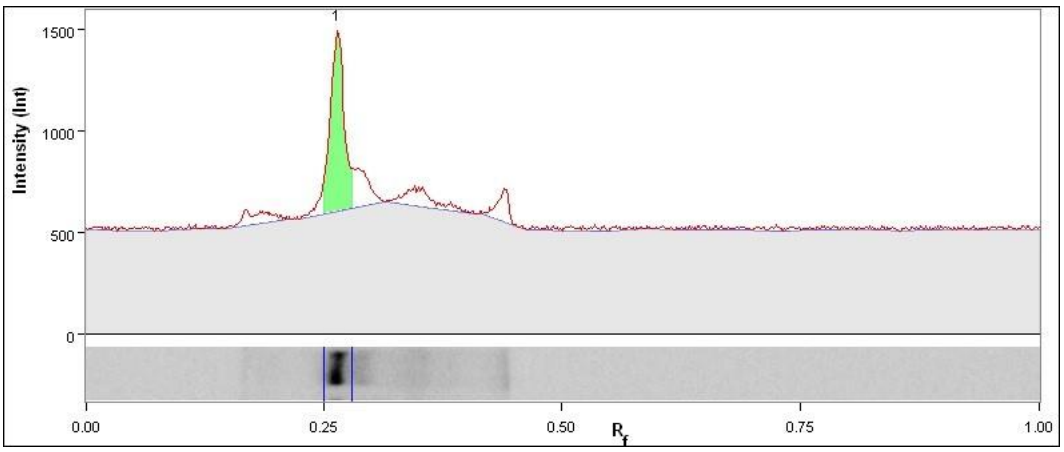

Band No.	Band Label	Mol. Wt. (KDa)	Relative Front	Volume (Int)	Abs. Quant.	Rel. Quant.	Band %	Lane %
1		N/A	0.264	646,110	N/A	N/A	100.0	44.5

Lane Background	Lane background subtracted with disk size: 10
Lane Width	5.66 mm

Lane 7

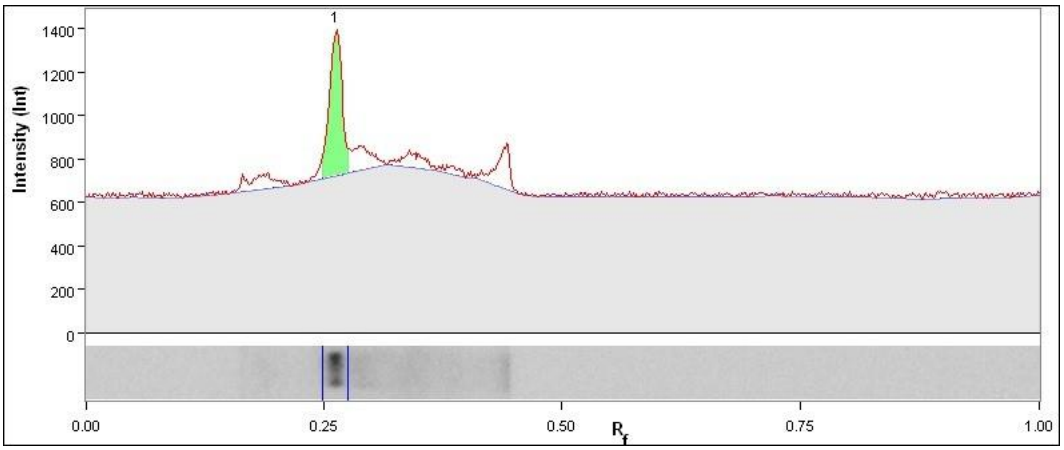

Band No.	Band Label	Mol. Wt. (KDa)	Relative Front	Volume (Int)	Abs. Quant.	Rel. Quant.	Band %	Lane %
1		N/A	0.262	358,560	N/A	N/A	100.0	34.8

Lane Background	Lane background subtracted with disk size: 10
Lane Width	5.66 mm

Lane 8

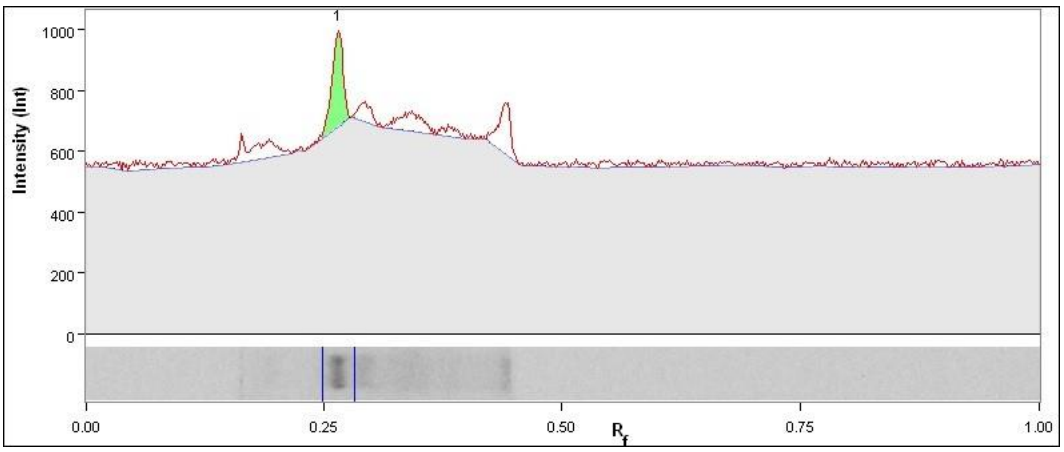

Band No.	Band Label	Mol. Wt. (KDa)	Relative Front	Volume (Int)	Abs. Quant.	Rel. Quant.	Band %	Lane %
1		N/A	0.265	172,485	N/A	N/A	100.0	21.8

Lane Background	Lane background subtracted with disk size: 10
Lane Width	5.66 mm

Lane 9

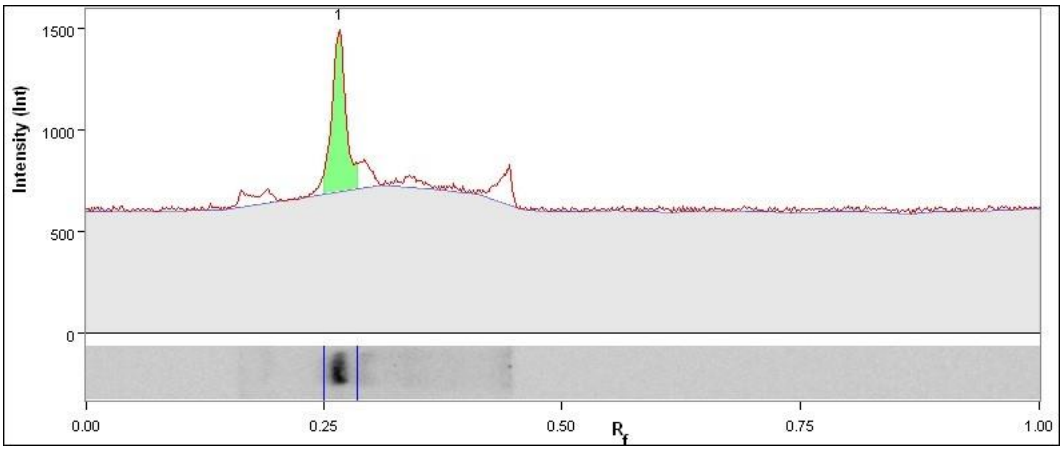

Band No.	Band Label	Mol. Wt. (KDa)	Relative Front	Volume (Int)	Abs. Quant.	Rel. Quant.	Band %	Lane %
1		N/A	0.266	498,240	N/A	N/A	100.0	44.1

Lane Background	Lane background subtracted with disk size: 10
Lane Width	5.66 mm

Lane 10

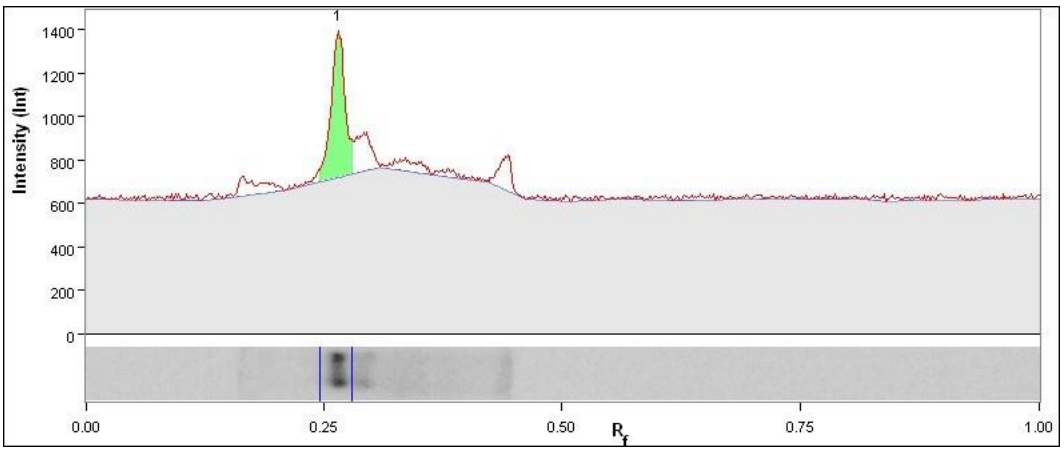

Band No.	Band Label	Mol. Wt. (KDa)	Relative Front	Volume (Int)	Abs. Quant.	Rel. Quant.	Band %	Lane %
1		N/A	0.265	410,445	N/A	N/A	100.0	39.3

Lane Background	Lane background subtracted with disk size: 10
Lane Width	5.66 mm

Lane 11

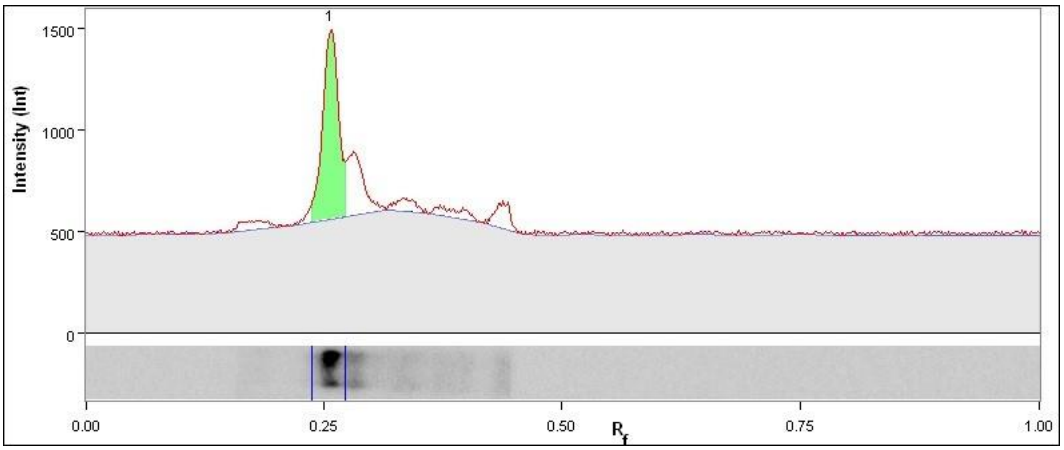

Band No.	Band Label	Mol. Wt. (KDa)	Relative Front	Volume (Int)	Abs. Quant.	Rel. Quant.	Band %	Lane %
1		N/A	0.257	806,085	N/A	N/A	100.0	47.7

Lane Background	Lane background subtracted with disk size: 10
Lane Width	5.66 mm

Lane 12

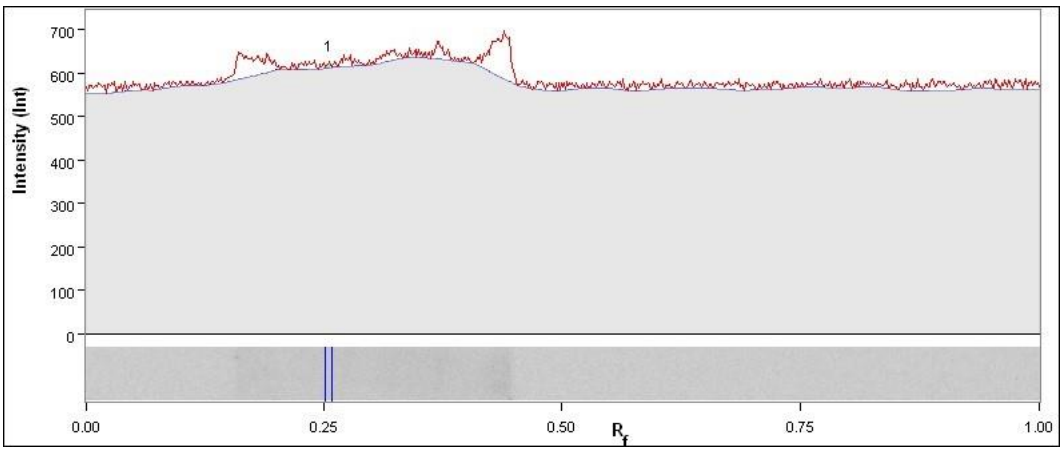

Band No.	Band Label	Mol. Wt. (KDa)	Relative Front	Volume (Int)	Abs. Quant.	Rel. Quant.	Band %	Lane %
1		N/A	0.255	2,385	N/A	N/A	100.0	0.5

Lane Background	Lane background subtracted with disk size: 10
Lane Width	5.66 mm

Lane 13

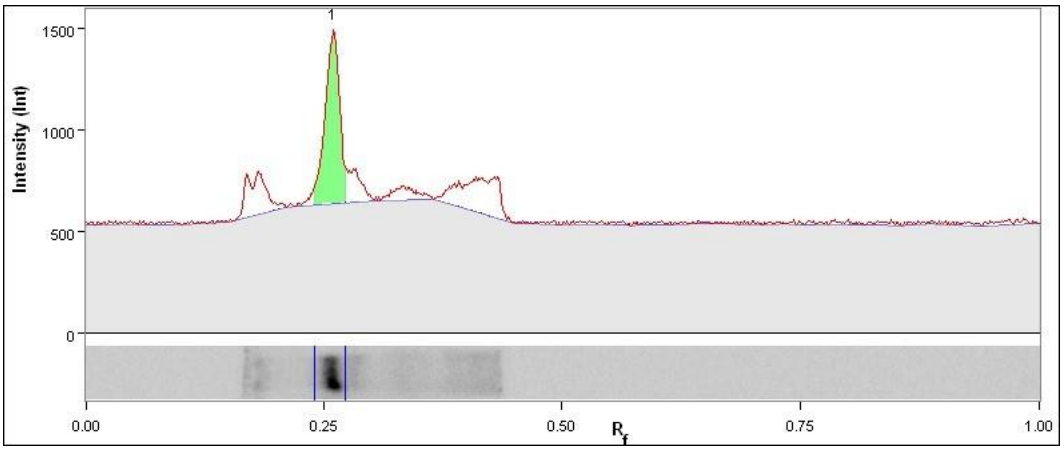

Band No.	Band Label	Mol. Wt. (KDa)	Relative Front	Volume (Int)	Abs. Quant.	Rel. Quant.	Band %	Lane %
1		N/A	0.260	596,700	N/A	N/A	100.0	36.3

Lane Background	Lane background subtracted with disk size: 10
Lane Width	5.66 mm

Lane 14

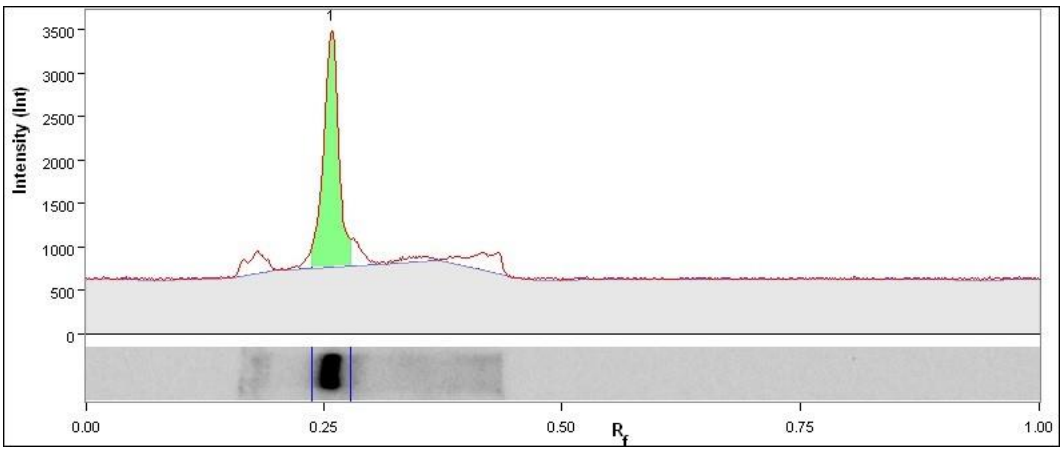

Band No.	Band Label	Mol. Wt. (KDa)	Relative Front	Volume (Int)	Abs. Quant.	Rel. Quant.	Band %	Lane %
1		N/A	0.258	1,704,420	N/A	N/A	100.0	61.9

Lane Background	Lane background subtracted with disk size: 10
Lane Width	5.66 mm

Lane 15

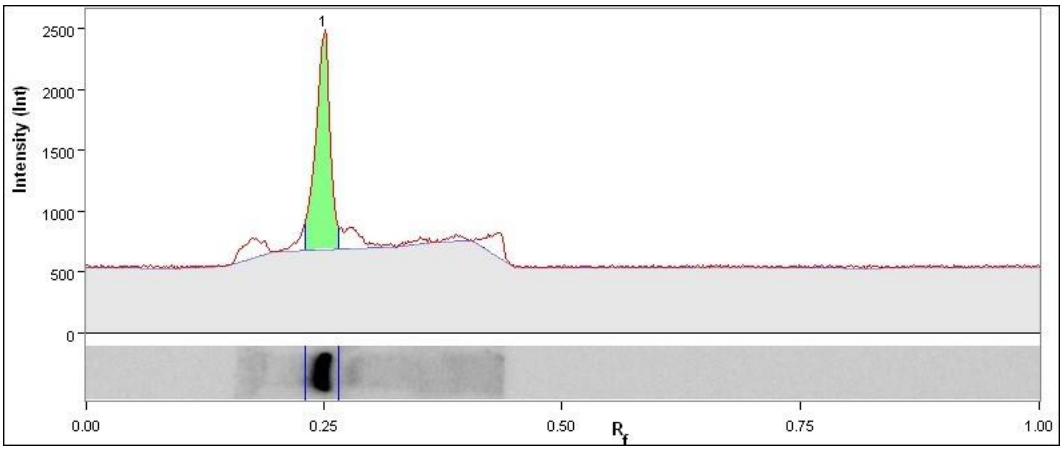

Band No.	Band Label	Mol. Wt. (KDa)	Relative Front	Volume (Int)	Abs. Quant.	Rel. Quant.	Band %	Lane %
1		N/A	0.250	1,219,770	N/A	N/A	100.0	57.6

Lane Background	Lane background subtracted with disk size: 10
Lane Width	5.66 mm

Lane 16

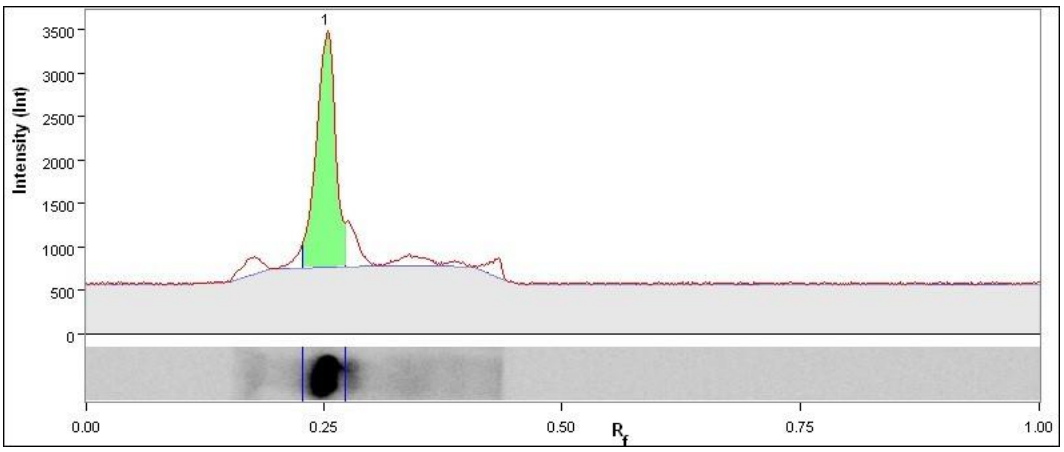

Band No.	Band Label	Mol. Wt. (KDa)	Relative Front	Volume (Int)	Abs. Quant.	Rel. Quant.	Band %	Lane %
1		N/A	0.253	2,345,445	N/A	N/A	100.0	67.1

Lane Background	Lane background subtracted with disk size: 10
Lane Width	5.66 mm

Lane 17

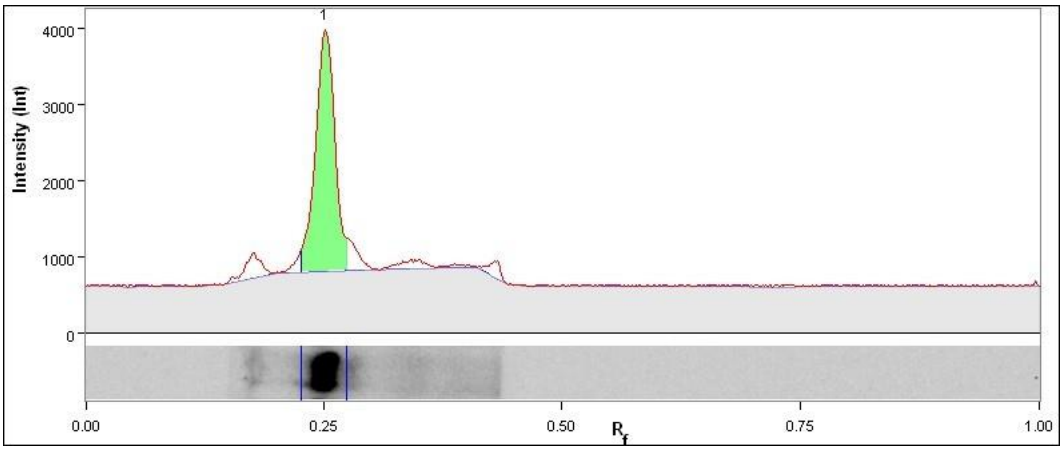

Band No.	Band Label	Mol. Wt. (KDa)	Relative Front	Volume (Int)	Abs. Quant.	Rel. Quant.	Band %	Lane %
1		N/A	0.251	2,567,295	N/A	N/A	100.0	71.0

Lane Background	Lane background subtracted with disk size: 10
Lane Width	5.66 mm

Lane 18

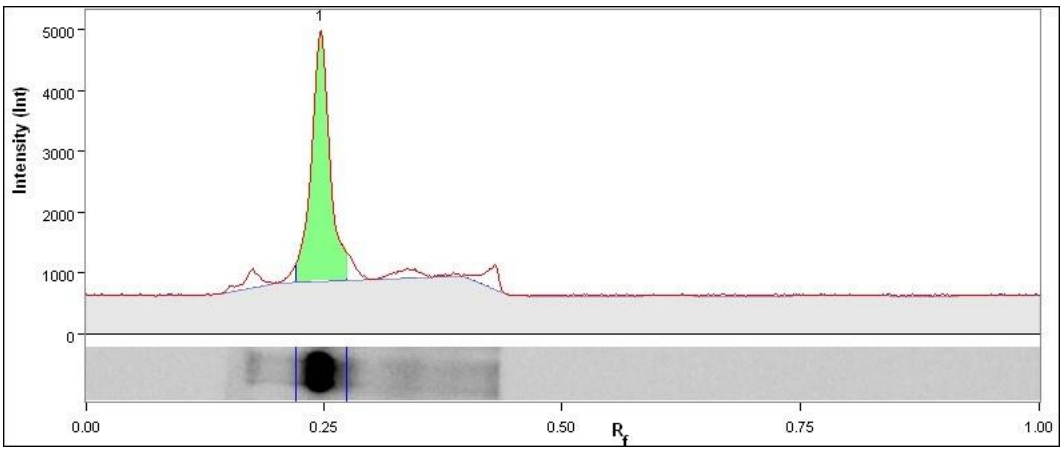

Band No.	Band Label	Mol. Wt. (KDa)	Relative Front	Volume (Int)	Abs. Quant.	Rel. Quant.	Band %	Lane %
1		N/A	0.247	3,079,215	N/A	N/A	100.0	73.1

Lane Background	Lane background subtracted with disk size: 10
Lane Width	5.66 mm

Lane 19

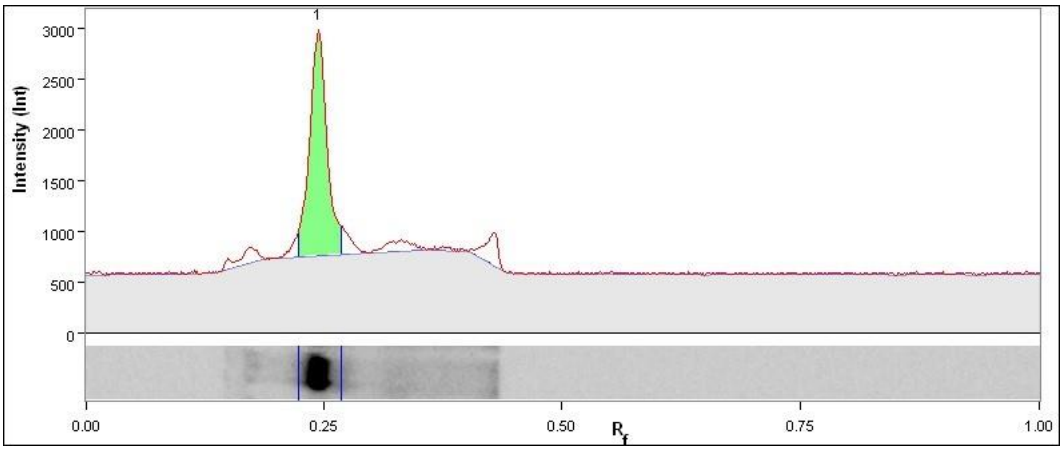

Band No.	Band Label	Mol. Wt. (KDa)	Relative Front	Volume (Int)	Abs. Quant.	Rel. Quant.	Band %	Lane %
1		N/A	0.245	1,693,125	N/A	N/A	100.0	64.1

Lane Background	Lane background subtracted with disk size: 10
Lane Width	5.66 mm

Lane 20

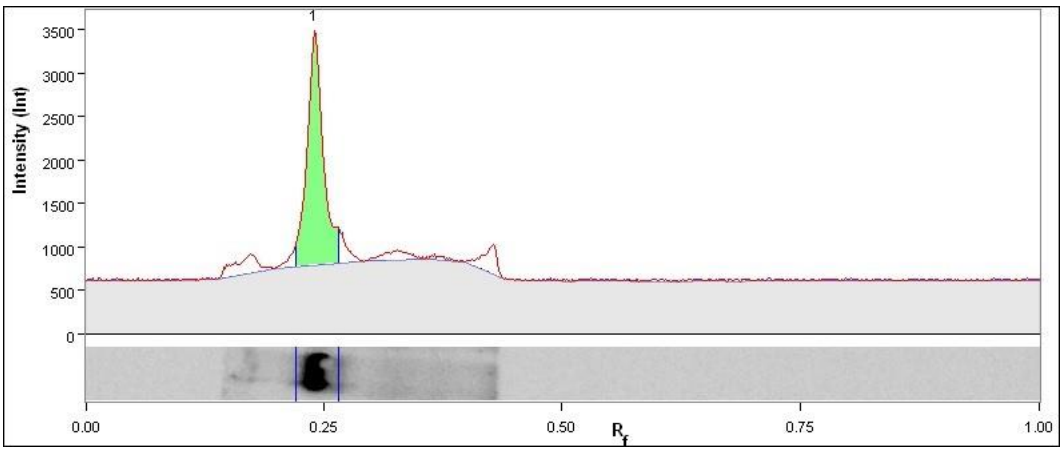

Band No.	Band Label	Mol. Wt. (KDa)	Relative Front	Volume (Int)	Abs. Quant.	Rel. Quant.	Band %	Lane %
1		N/A	0.240	1,791,135	N/A	N/A	100.0	62.0

Lane Background	Lane background subtracted with disk size: 10
Lane Width	5.66 mm

Lane 21

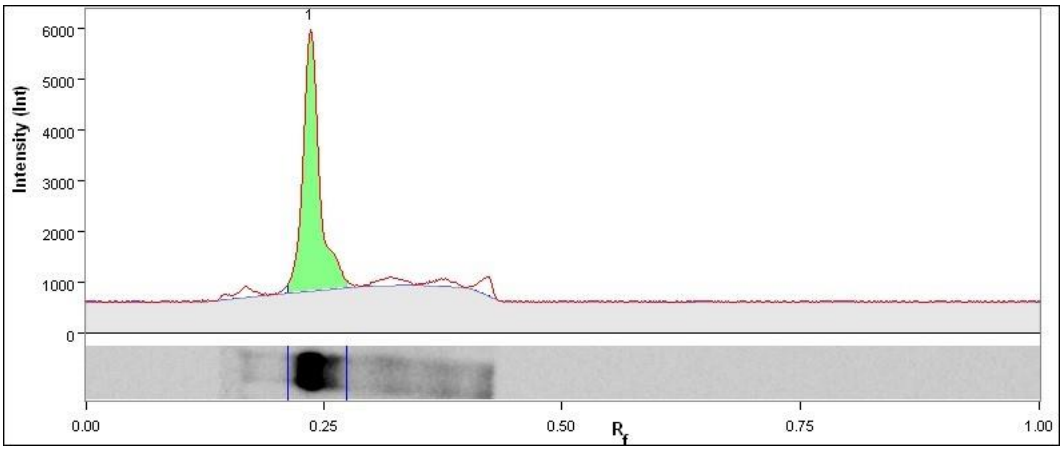

Band No.	Band Label	Mol. Wt. (KDa)	Relative Front	Volume (Int)	Abs. Quant.	Rel. Quant.	Band %	Lane %
1		N/A	0.236	3,559,320	N/A	N/A	100.0	76.9

Lane Background	Lane background subtracted with disk size: 10
Lane Width	5.66 mm

Lane 22

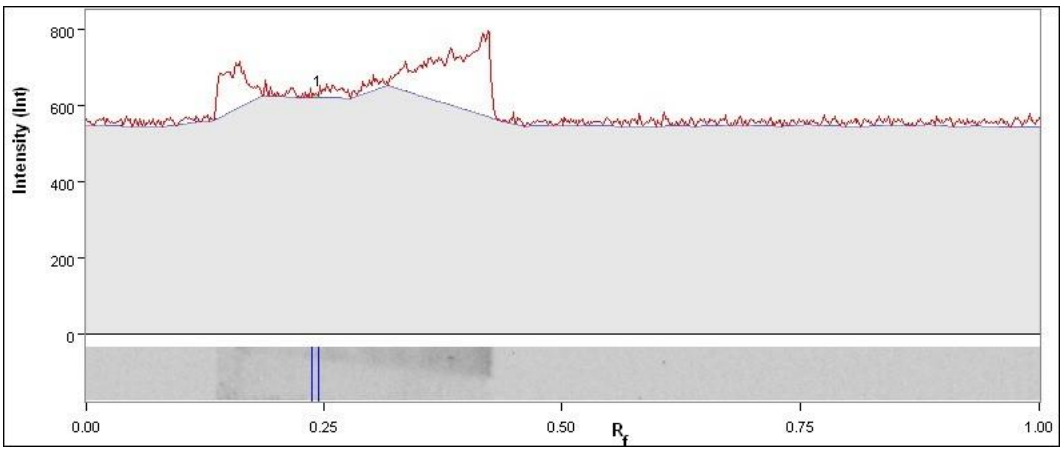

Band No.	Band Label	Mol. Wt. (KDa)	Relative Front	Volume (Int)	Abs. Quant.	Rel. Quant.	Band %	Lane %
1		N/A	0.246	3,825	N/A	N/A	100.0	0.4

Lane Background	Lane background subtracted with disk size: 10
Lane Width	5.66 mm

Image Report: 2018-08-29 MDA-MB-468 snake actin 60s

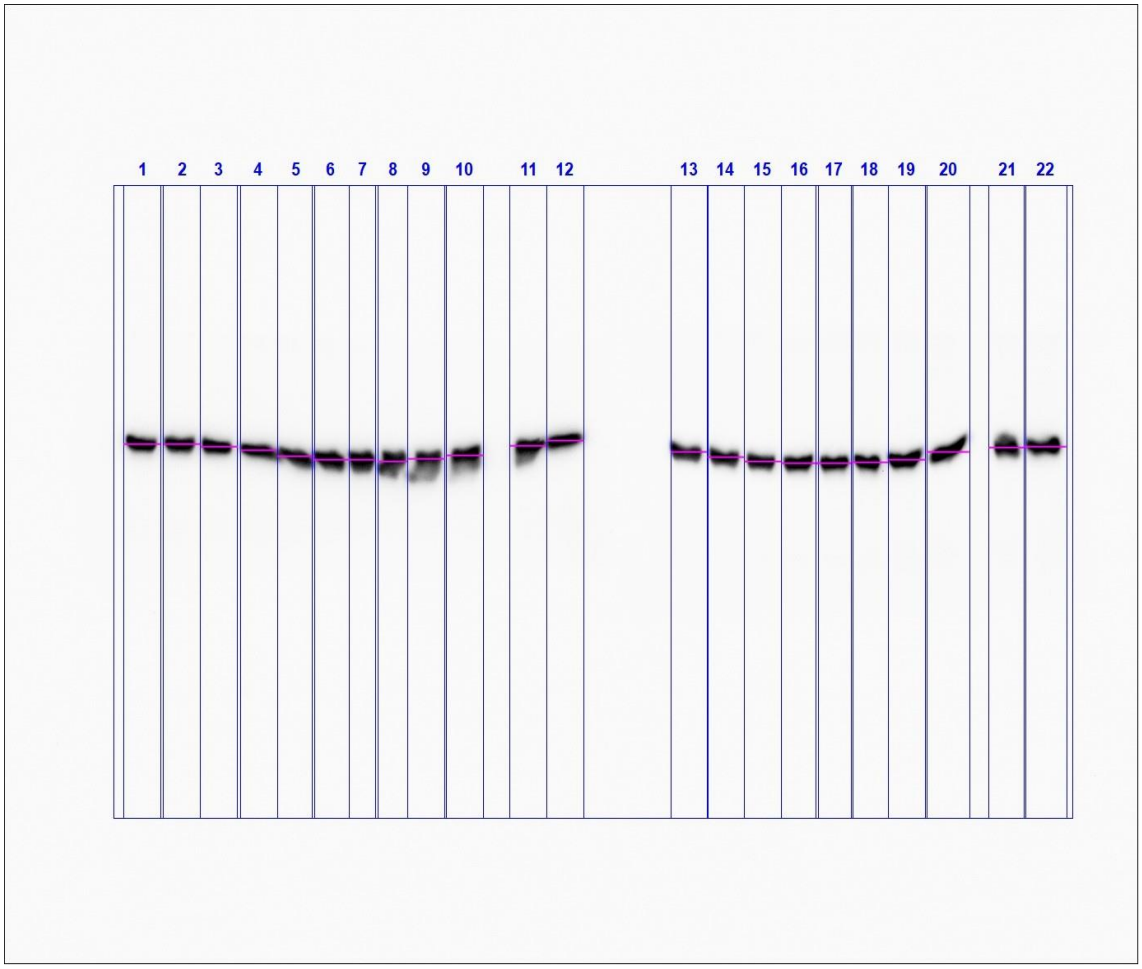

G:\Chemidoc Touch Images 2018-08-29_16.56.54\mda snake panel\2018-08-29 mda snake actin 60s.scn

Acquisition Information

Imager	ChemiDoc™ Touch
Exposure Time (sec)	60.000 (Manual)
Serial Number	732BR1296
Software Version	1.1.0.04
Application	Chemiluminescence
Excitation Source	No Illumination
Emission Filter	No Filter
Binning	2x2

Image Information

Acquisition Date	29/08/2018 22:47:45
User Name	
Image Area (mm)	X: 173.6 Y: 138.9
Pixel Size (um)	X: 125.9 Y: 125.9
Data Range (Int)	502 - 28362

Analysis Settings

	Manually created lanes Band detection: Manually adjusted bands Lane Background Subtraction: Lane background subtracted with disk size: 10 Lane width: Variable

Lane And Band Analysis

Lane 1

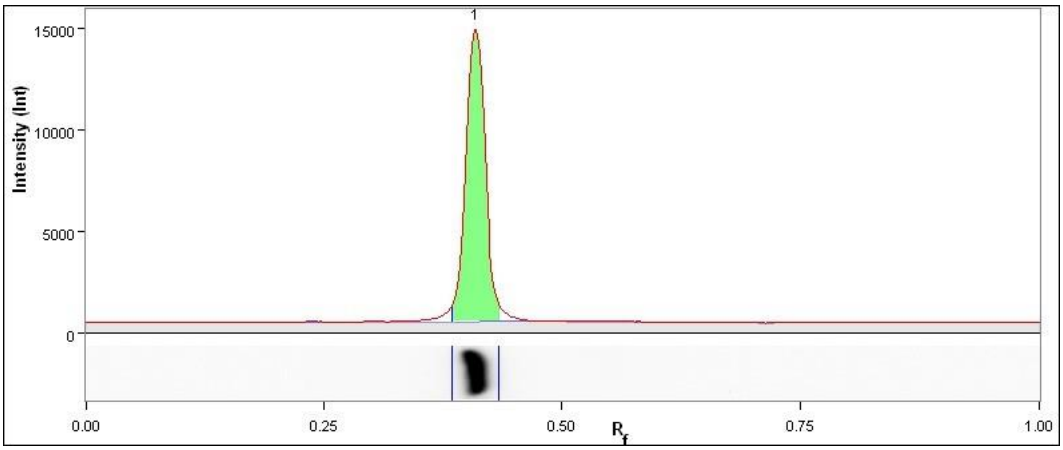

Band No.	Band Label	Mol. Wt. (KDa)	Relative Front	Volume (Int)	Abs. Quant.	Rel. Quant.	Band %	Lane %
1		N/A	0.409	14,123,025	N/A	N/A	100.0	91.6

Lane Background	Lane background subtracted with disk size: 10
Lane Width	5.66 mm

Lane 2

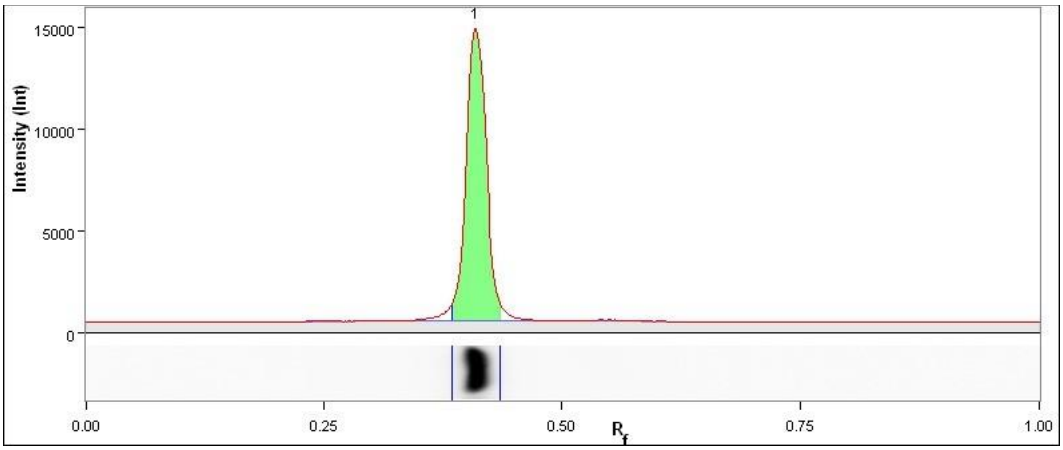

Band No.	Band Label	Mol. Wt. (KDa)	Relative Front	Volume (Int)	Abs. Quant.	Rel. Quant.	Band %	Lane %
1		N/A	0.409	14,056,875	N/A	N/A	100.0	92.0
Lane Background		Lane background subtracted with disk size: 10						
Lane Width		5.66 mm						

Lane 3

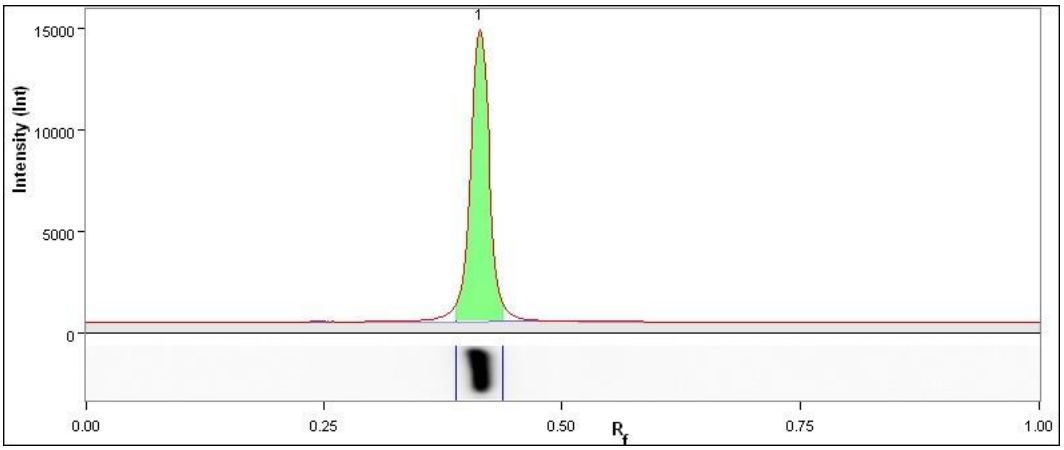

Band No.	Band Label	Mol. Wt. (KDa)	Relative Front	Volume (Int)	Abs. Quant.	Rel. Quant.	Band %	Lane %
1		N/A	0.413	13,736,565	N/A	N/A	100.0	90.7
Lane Background		Lane background subtracted with disk size: 10						
Lane Width		5.66 mm						

Lane 4

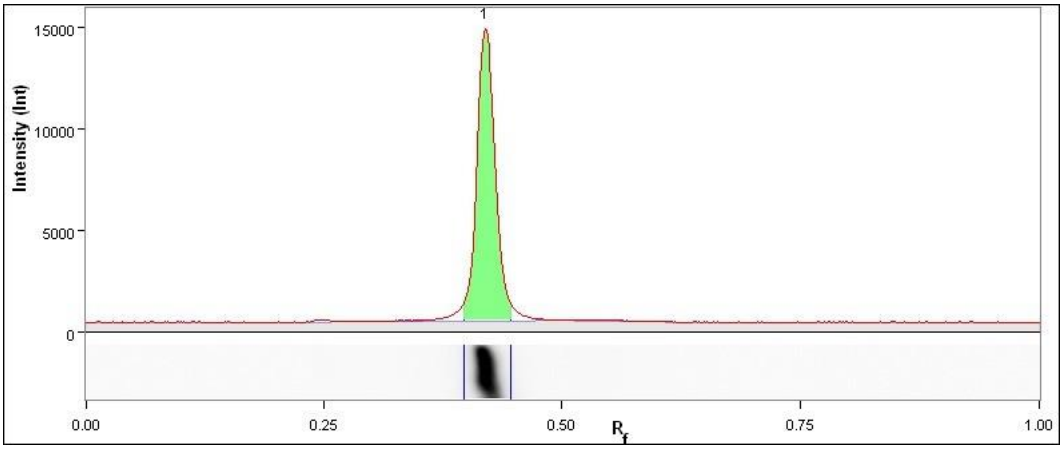

Band No.	Band Label	Mol. Wt. (KDa)	Relative Front	Volume (Int)	Abs. Quant.	Rel. Quant.	Band %	Lane %
1		N/A	0.419	14,506,110	N/A	N/A	100.0	91.2
Lane Background		Lane background subtracted with disk size: 10						
Lane Width		5.66 mm						

Lane 5

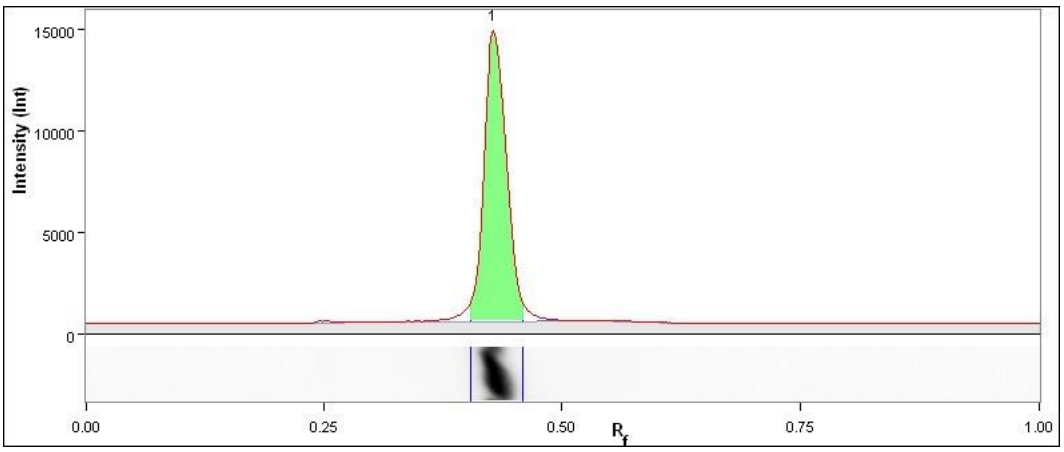

Band No.	Band Label	Mol. Wt. (KDa)	Relative Front	Volume (Int)	Abs. Quant.	Rel. Quant.	Band %	Lane %
1		N/A	0.429	15,603,030	N/A	N/A	100.0	92.3

Lane Background	Lane background subtracted with disk size: 10
Lane Width	5.66 mm

Lane 6

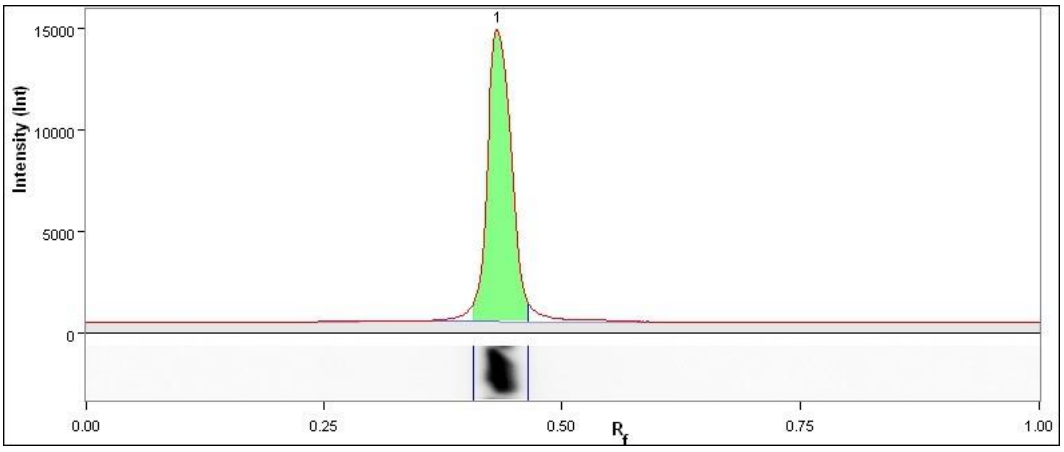

Band No.	Band Label	Mol. Wt. (KDa)	Relative Front	Volume (Int)	Abs. Quant.	Rel. Quant.	Band %	Lane %
1		N/A	0.434	17,082,855	N/A	N/A	100.0	91.3

Lane Background	Lane background subtracted with disk size: 10
Lane Width	5.66 mm

Lane 7

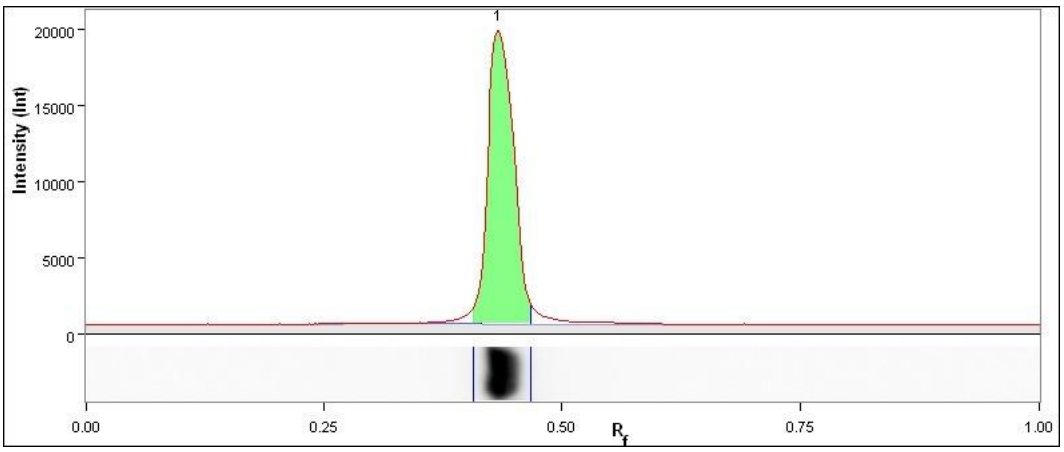

Band No.	Band Label	Mol. Wt. (KDa)	Relative Front	Volume (Int)	Abs. Quant.	Rel. Quant.	Band %	Lane %
1		N/A	0.434	14,384,992	N/A	N/A	100.0	91.4

Lane Background	Lane background subtracted with disk size: 10
Lane Width	4.03 mm

Lane 8

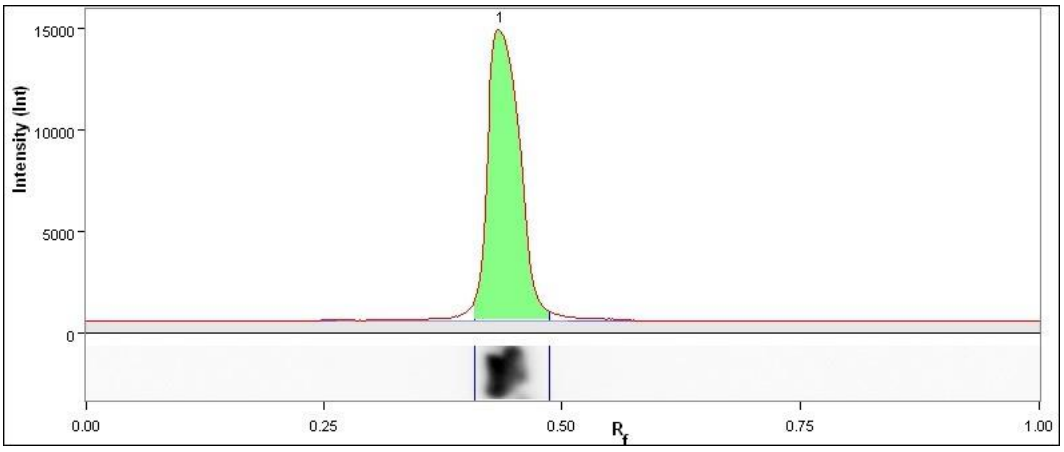

Band No.	Band Label	Mol. Wt. (KDa)	Relative Front	Volume (Int)	Abs. Quant.	Rel. Quant.	Band %	Lane %
1		N/A	0.437	16,280,820	N/A	N/A	100.0	93.4

Lane Background	Lane background subtracted with disk size: 10
Lane Width	4.53 mm

Lane 9

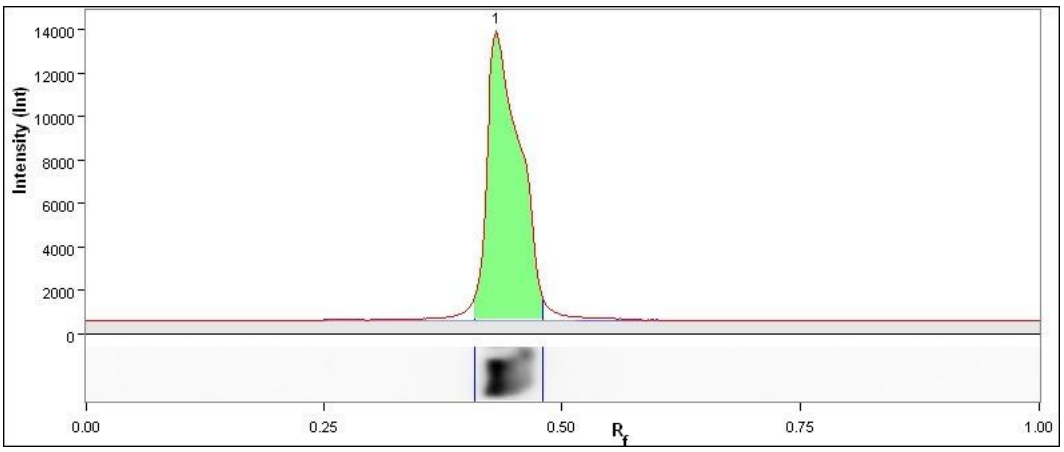

Band No.	Band Label	Mol. Wt. (KDa)	Relative Front	Volume (Int)	Abs. Quant.	Rel. Quant.	Band %	Lane %
1		N/A	0.433	18,478,035	N/A	N/A	100.0	92.1

Lane Background	Lane background subtracted with disk size: 10
Lane Width	5.66 mm

Lane 10

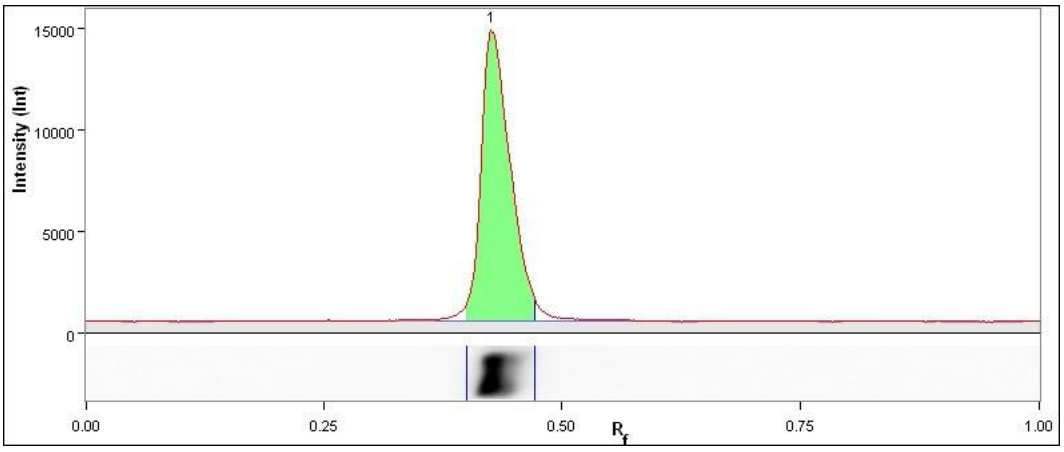

Band No.	Band Label	Mol. Wt. (KDa)	Relative Front	Volume (Int)	Abs. Quant.	Rel. Quant.	Band %	Lane %
1		N/A	0.427	19,074,690	N/A	N/A	100.0	93.1

Lane Background	Lane background subtracted with disk size: 10
Lane Width	5.66 mm

Lane 11

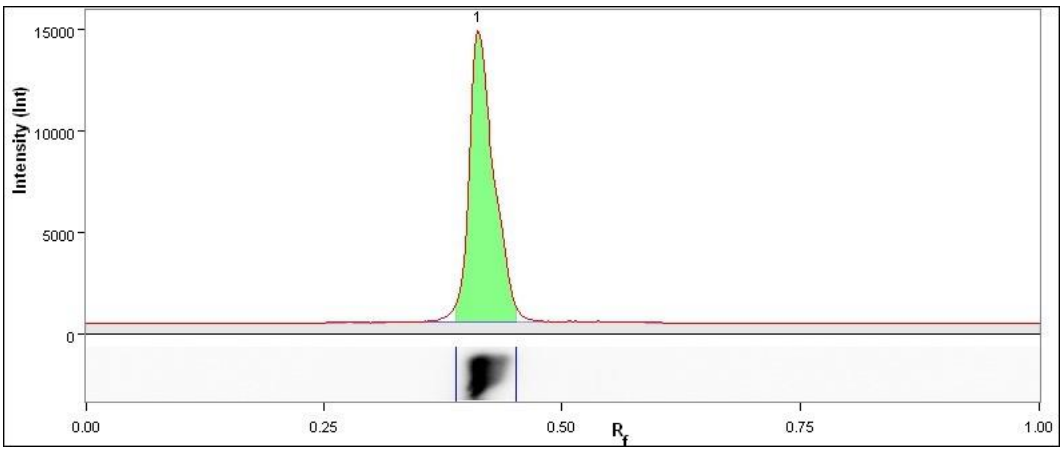

Band No.	Band Label	Mol. Wt. (KDa)	Relative Front	Volume (Int)	Abs. Quant.	Rel. Quant.	Band %	Lane %
1		N/A	0.412	17,044,335	N/A	N/A	100.0	94.8

Lane Background	Lane background subtracted with disk size: 10
Lane Width	5.66 mm

Lane 12

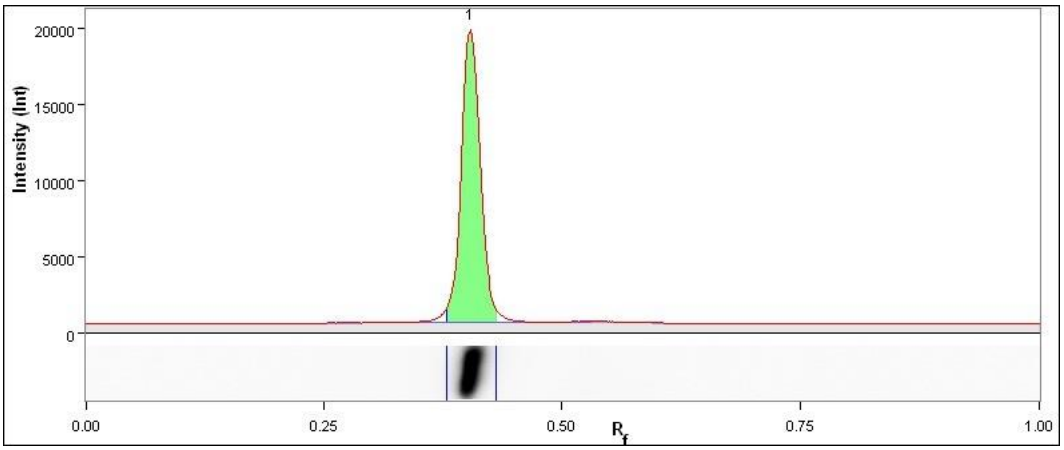

Band No.	Band Label	Mol. Wt. (KDa)	Relative Front	Volume (Int)	Abs. Quant.	Rel. Quant.	Band %	Lane %
1		N/A	0.404	15,078,195	N/A	N/A	100.0	93.7

Lane Background	Lane background subtracted with disk size: 10
Lane Width	5.66 mm

Lane 13

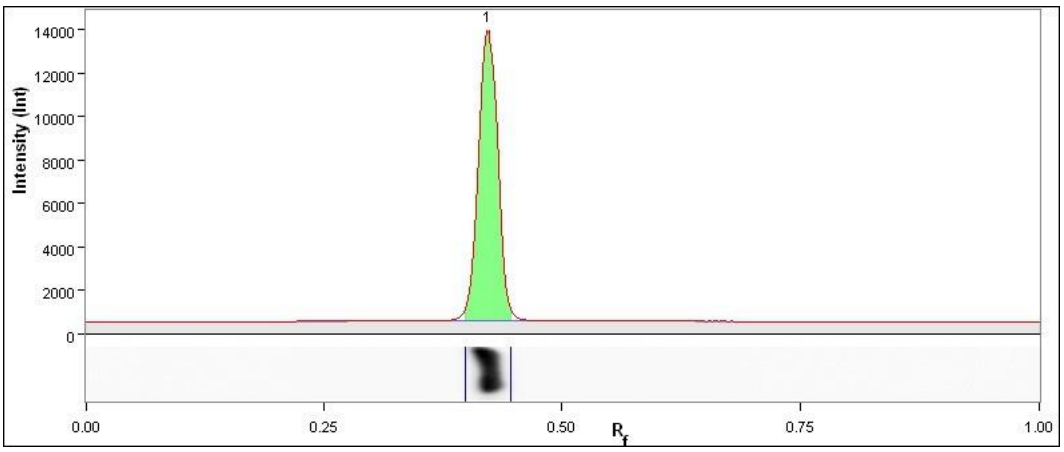

Band No.	Band Label	Mol. Wt. (KDa)	Relative Front	Volume (Int)	Abs. Quant.	Rel. Quant.	Band %	Lane %
1		N/A	0.422	12,264,165	N/A	N/A	100.0	95.0

Lane Background	Lane background subtracted with disk size: 10
Lane Width	5.66 mm

Lane 14

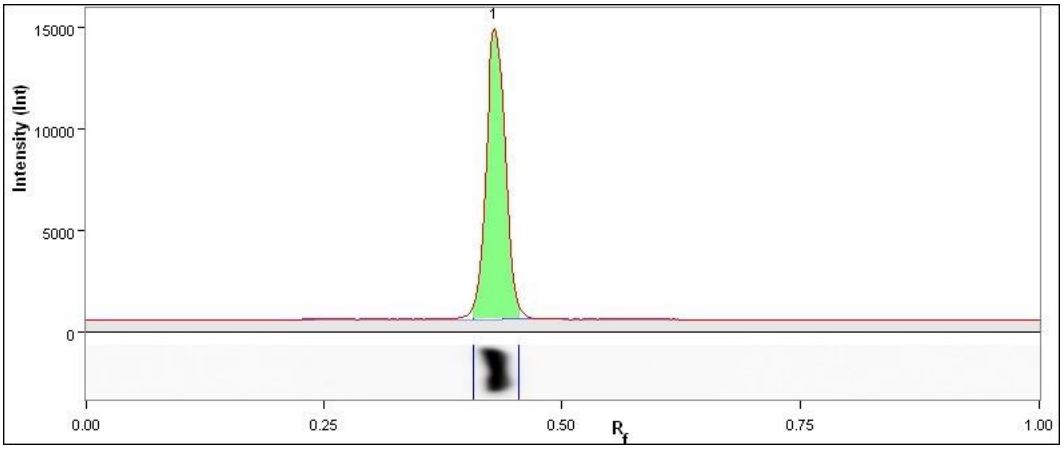

Band No.	Band Label	Mol. Wt. (KDa)	Relative Front	Volume (Int)	Abs. Quant.	Rel. Quant.	Band %	Lane %
1		N/A	0.430	12,385,125	N/A	N/A	100.0	94.5

Lane Background	Lane background subtracted with disk size: 10
Lane Width	5.66 mm

Lane 15

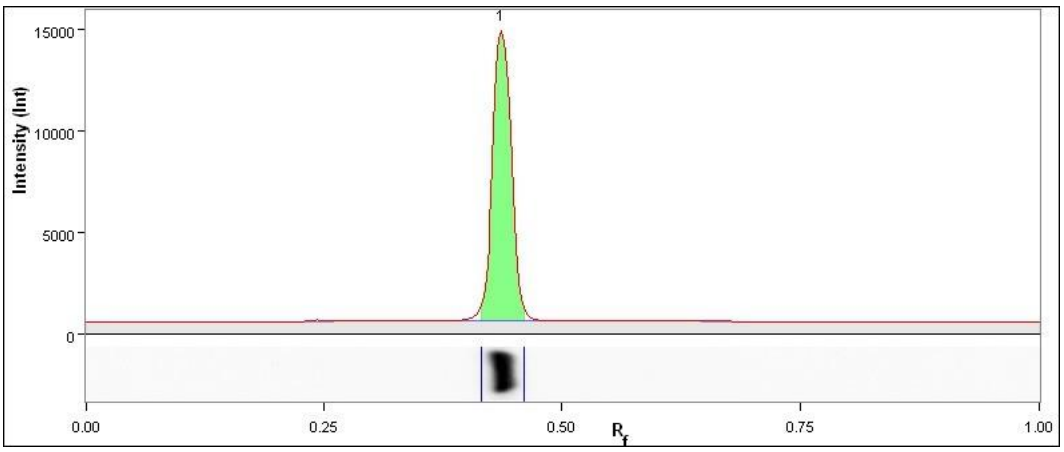

Band No.	Band Label	Mol. Wt. (KDa)	Relative Front	Volume (Int)	Abs. Quant.	Rel. Quant.	Band %	Lane %
1		N/A	0.437	11,555,550	N/A	N/A	100.0	93.8

Lane Background	Lane background subtracted with disk size: 10
Lane Width	5.66 mm

Lane 16

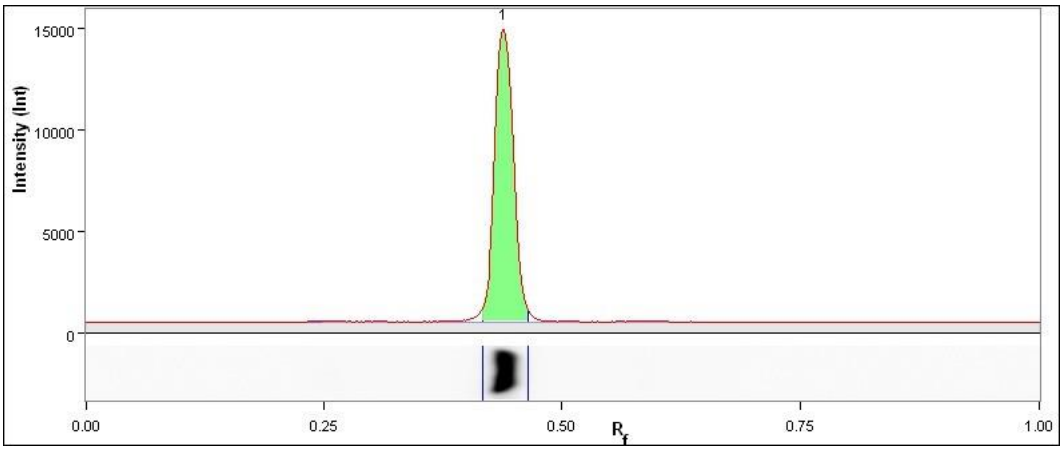

Band No.	Band Label	Mol. Wt. (KDa)	Relative Front	Volume (Int)	Abs. Quant.	Rel. Quant.	Band %	Lane %
1		N/A	0.440	13,674,690	N/A	N/A	100.0	94.0

Lane Background	Lane background subtracted with disk size: 10
Lane Width	5.66 mm

Lane 17

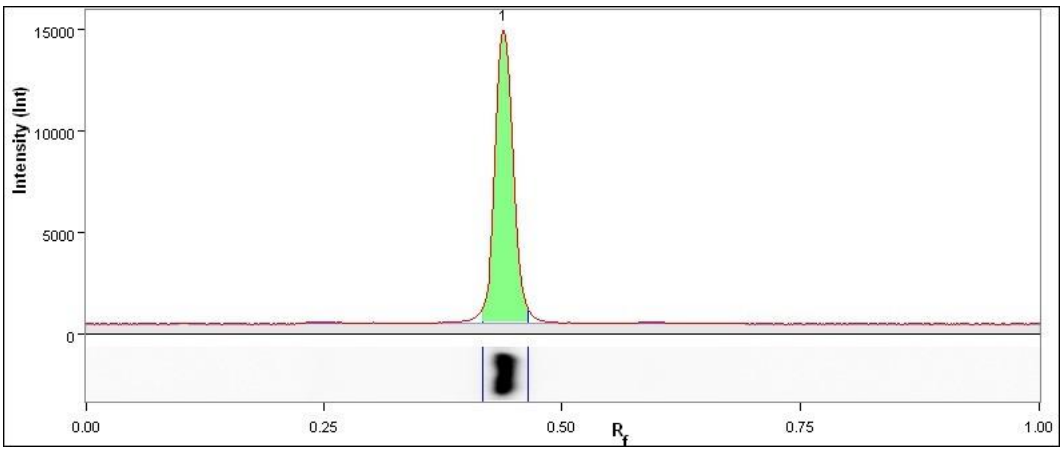

Band No.	Band Label	Mol. Wt. (KDa)	Relative Front	Volume (Int)	Abs. Quant.	Rel. Quant.	Band %	Lane %
1		N/A	0.440	13,615,470	N/A	N/A	100.0	92.6

Lane Background	Lane background subtracted with disk size: 10
Lane Width	5.66 mm

Lane 18

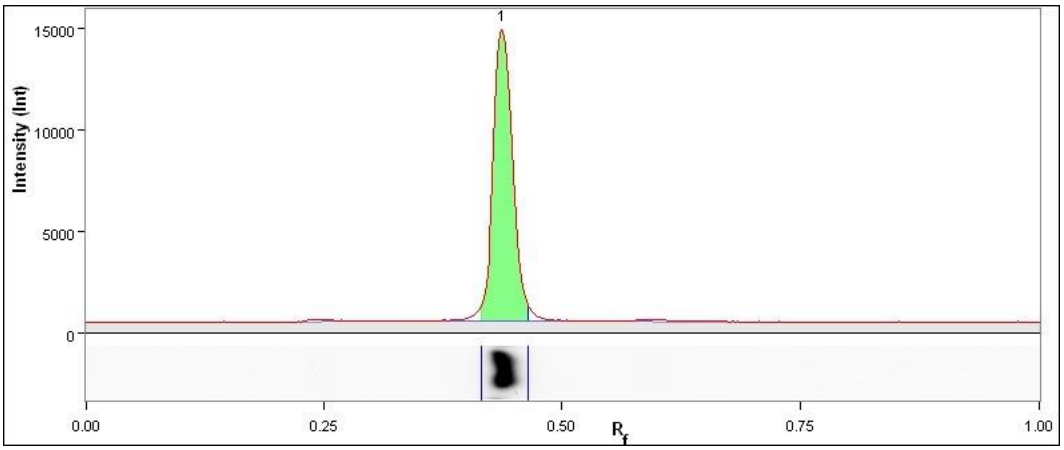

Band No.	Band Label	Mol. Wt. (KDa)	Relative Front	Volume (Int)	Abs. Quant.	Rel. Quant.	Band %	Lane %
1		N/A	0.438	13,153,545	N/A	N/A	100.0	91.4

Lane Background	Lane background subtracted with disk size: 10
Lane Width	5.66 mm

Lane 19

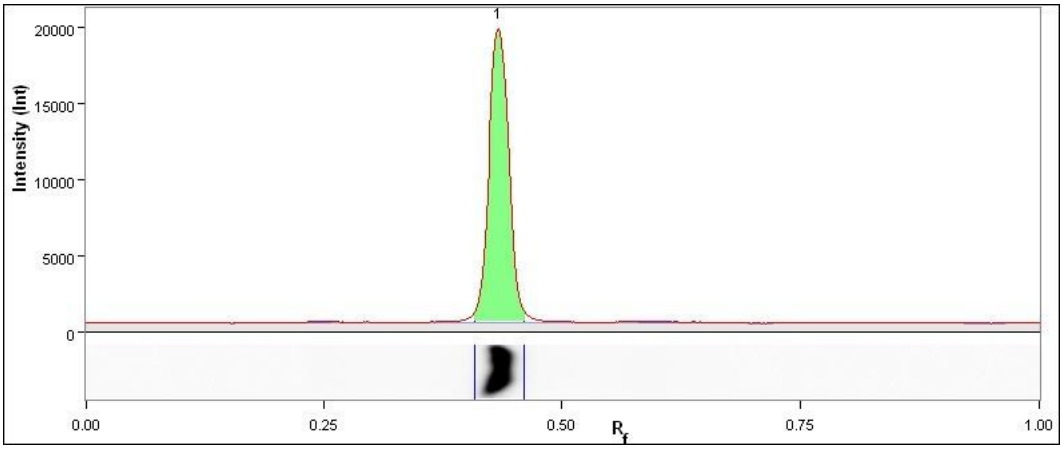

Band No.	Band Label	Mol. Wt. (KDa)	Relative Front	Volume (Int)	Abs. Quant.	Rel. Quant.	Band %	Lane %
1		N/A	0.434	17,175,150	N/A	N/A	100.0	93.8

Lane Background	Lane background subtracted with disk size: 10
Lane Width	5.66 mm

Lane 20

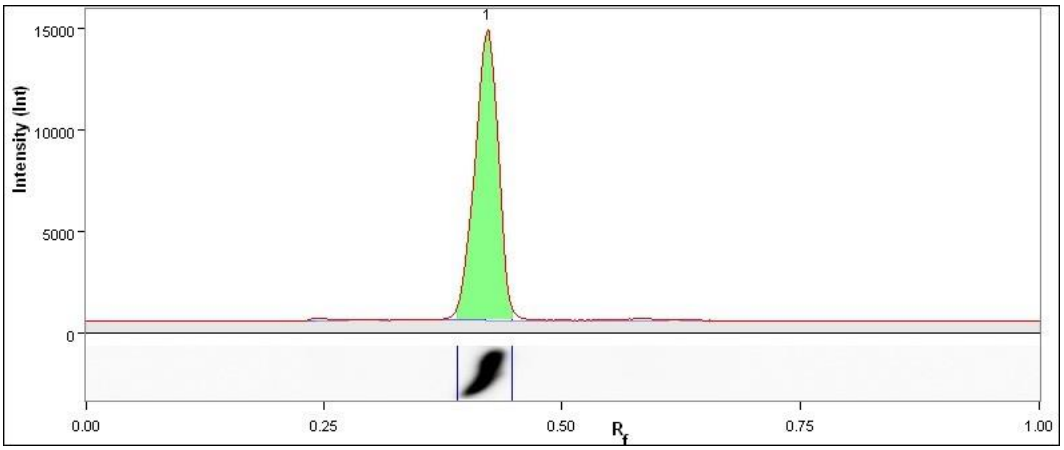

Band No.	Band Label	Mol. Wt. (KDa)	Relative Front	Volume (Int)	Abs. Quant.	Rel. Quant.	Band %	Lane %
1		N/A	0.422	17,738,344	N/A	N/A	100.0	94.9

Lane Background	Lane background subtracted with disk size: 10
Lane Width	6.54 mm

Lane 21

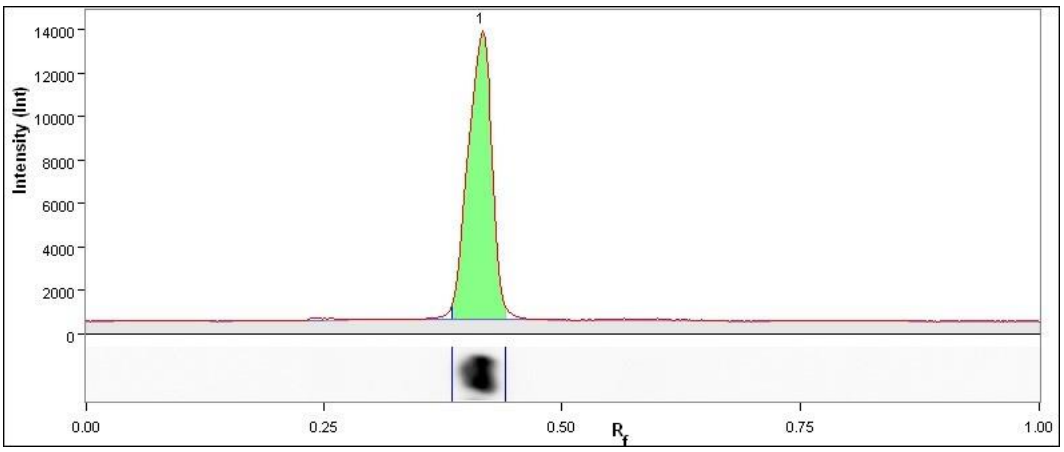

Band No.	Band Label	Mol. Wt. (KDa)	Relative Front	Volume (Int)	Abs. Quant.	Rel. Quant.	Band %	Lane %
1		N/A	0.415	13,878,945	N/A	N/A	100.0	93.6

Lane Background	Lane background subtracted with disk size: 10
Lane Width	5.66 mm

Lane 22

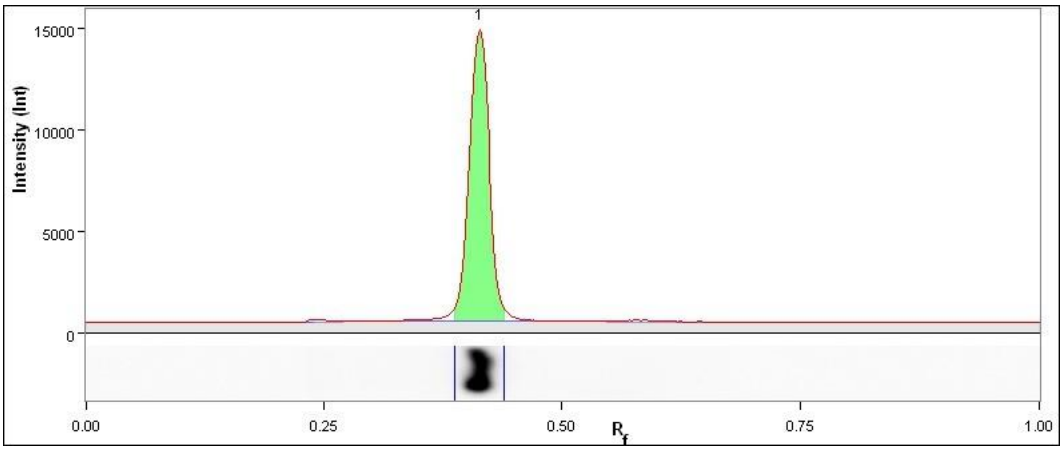

Band No.	Band Label	Mol. Wt. (KDa)	Relative Front	Volume (Int)	Abs. Quant.	Rel. Quant.	Band %	Lane %
1		N/A	0.413	16,896,152	N/A	N/A	100.0	91.4

Lane Background	Lane background subtracted with disk size: 10
Lane Width	6.54 mm

Appendix XIX: Chapter 5: ImageLab Analysis Reports of Whole Snake and Invertebrate Venom Dose Response Western Blots

MDA-MB-468, C.dve PY20 Analysis:

Image Report: 2020-02-07 MDA-MB-468 C.dve PY20

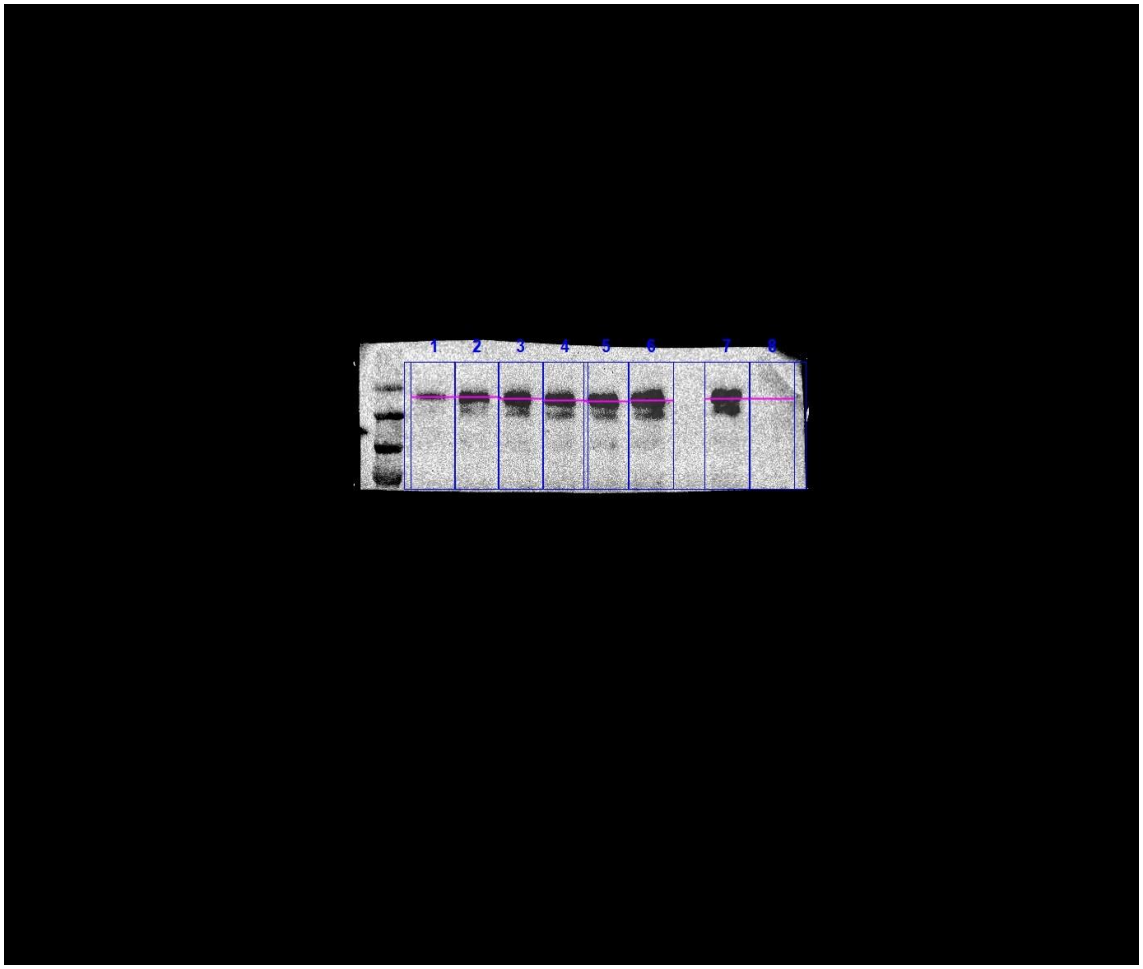

Acquisition Information

Imager	Merged Image

Image Information

Acquisition Date	13/02/2020 11:51:49
User Name	Danielle McCullough
Image Area (mm)	X: 210.0 Y: 168.1
Pixel Size (um)	X: 152.3 Y: 152.3
Data Range (Int)	17477 - 65534

Analysis Settings

	Manually created lanes Band detection: Manually adjusted bands Lane Background Subtraction: Lane background subtracted with disk size: 10 Lane width: 8.22 mm

Lane And Band Analysis

Lane 1

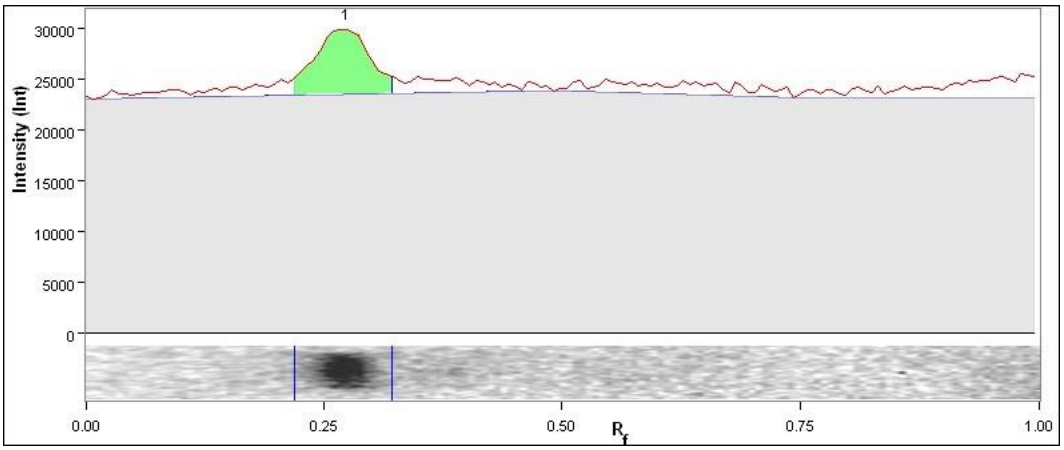

Band No.	Band Label	Mol. Wt. (KDa)	Relative Front	Volume (Int)	Abs. Quant.	Rel. Quant.	Band %	Lane %
1		N/A	0.279	3,466,044	N/A	N/A	100.0	35.1
Lane Background		Lane background subtracted with disk size: 10						
Lane Width		8.22 mm						

Lane 2

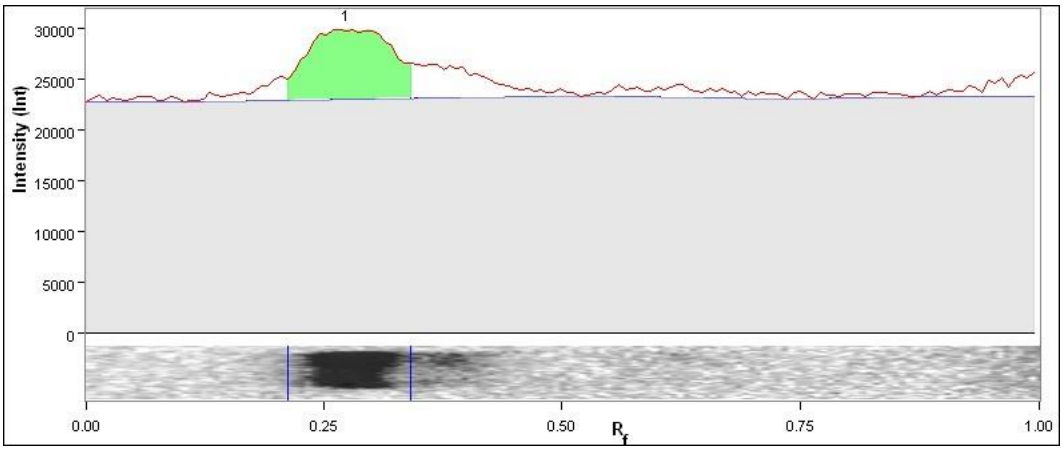

Band No.	Band Label	Mol. Wt. (KDa)	Relative Front	Volume (Int)	Abs. Quant.	Rel. Quant.	Band %	Lane %
1		N/A	0.279	5,996,646	N/A	N/A	100.0	48.4
Lane Background		Lane background subtracted with disk size: 10						
Lane Width		8.22 mm						

Lane 3

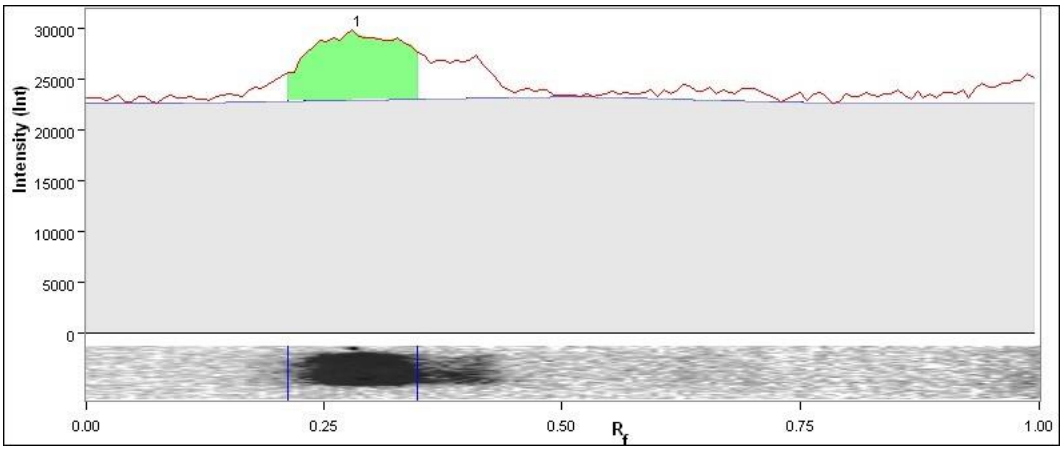

Band No.	Band Label	Mol. Wt. (KDa)	Relative Front	Volume (Int)	Abs. Quant.	Rel. Quant.	Band %	Lane %
1		N/A	0.293	6,691,518	N/A	N/A	100.0	46.2
Lane Background		Lane background subtracted with disk size: 10						
Lane Width		8.22 mm						

Lane 4

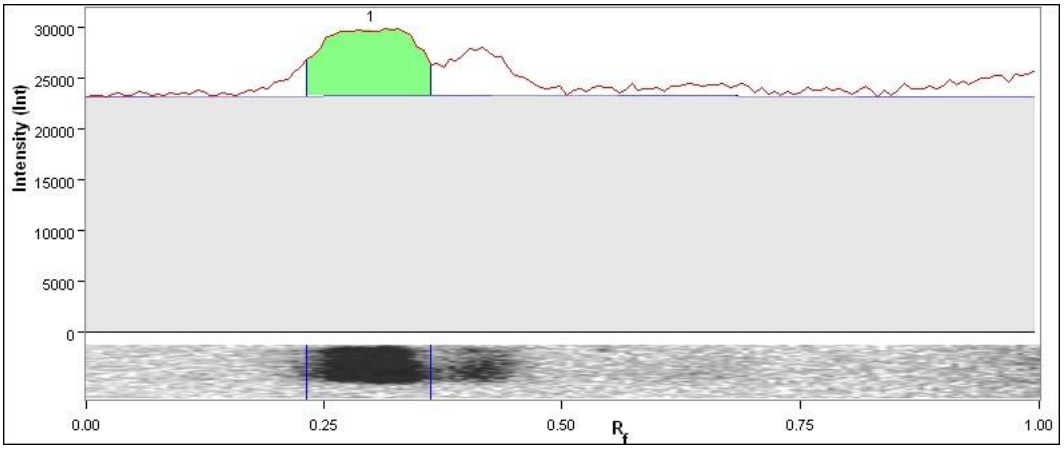

Band No.	Band Label	Mol. Wt. (KDa)	Relative Front	Volume (Int)	Abs. Quant.	Rel. Quant.	Band %	Lane %
1		N/A	0.306	6,207,246	N/A	N/A	100.0	43.0
Lane Background		Lane background subtracted with disk size: 10						
Lane Width		8.22 mm						

Lane 5

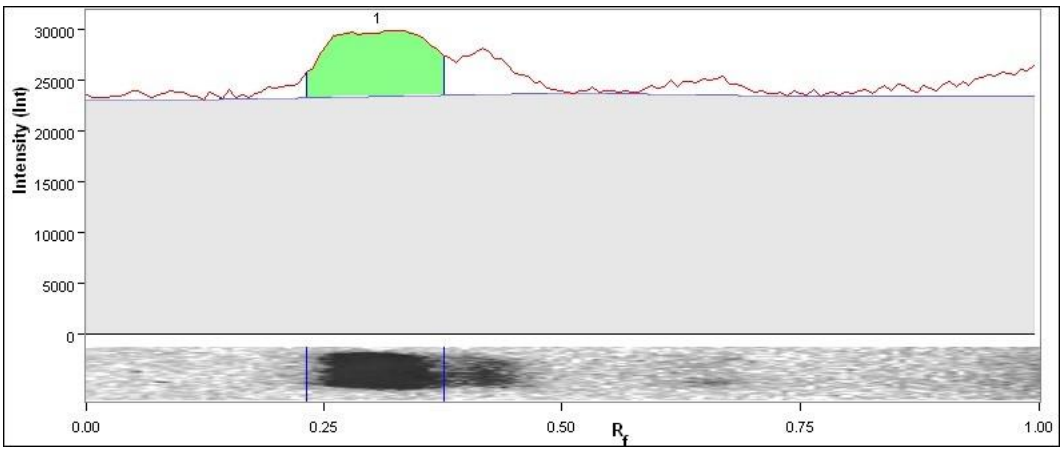

Band No.	Band Label	Mol. Wt. (KDa)	Relative Front	Volume (Int)	Abs. Quant.	Rel. Quant.	Band %	Lane %
1		N/A	0.313	6,698,052	N/A	N/A	100.0	47.0

Lane Background	Lane background subtracted with disk size: 10
Lane Width	8.22 mm

Lane 6

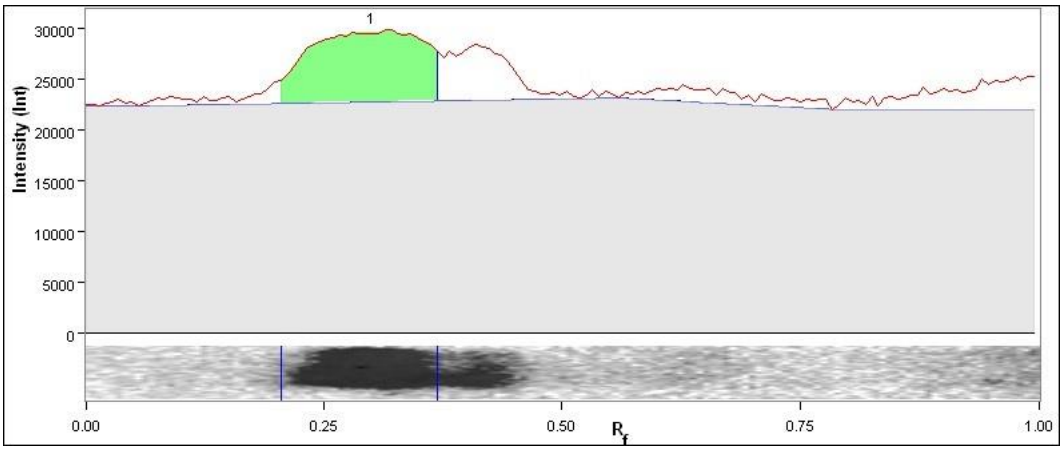

Band No.	Band Label	Mol. Wt. (KDa)	Relative Front	Volume (Int)	Abs. Quant.	Rel. Quant.	Band %	Lane %
1		N/A	0.306	8,424,054	N/A	N/A	100.0	46.0

Lane Background	Lane background subtracted with disk size: 10
Lane Width	8.22 mm

Lane 7

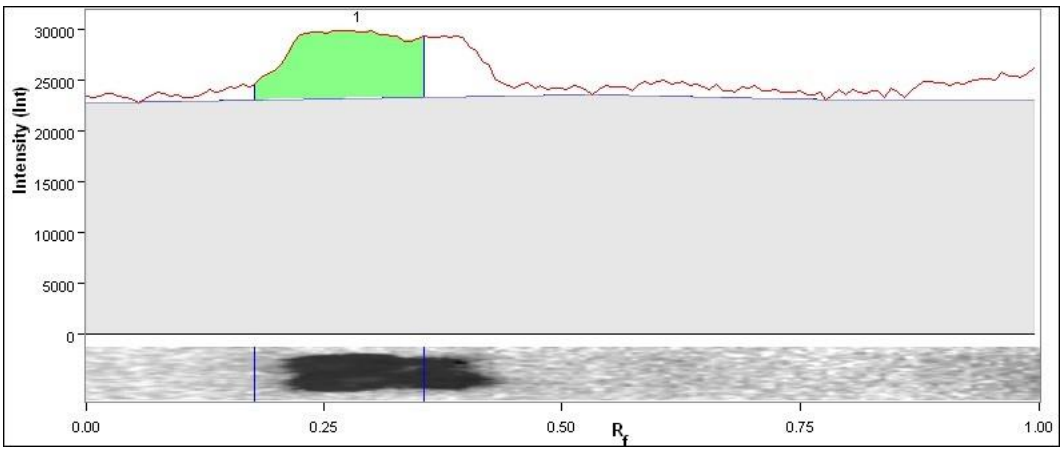

Band No.	Band Label	Mol. Wt. (KDa)	Relative Front	Volume (Int)	Abs. Quant.	Rel. Quant.	Band %	Lane %
1		N/A	0.293	8,713,008	N/A	N/A	100.0	49.4

Lane Background	Lane background subtracted with disk size: 10
Lane Width	8.22 mm

Lane 8

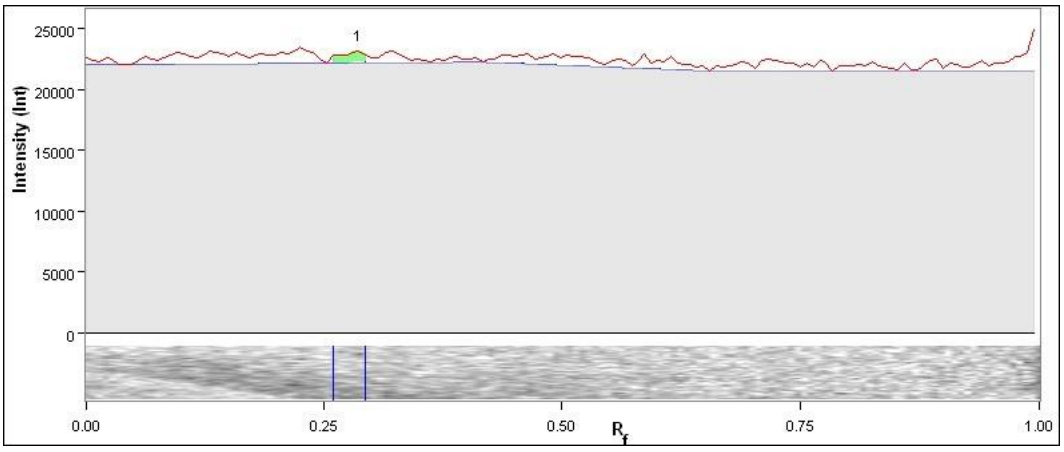

Band No.	Band Label	Mol. Wt. (KDa)	Relative Front	Volume (Int)	Abs. Quant.	Rel. Quant.	Band %	Lane %
1		N/A	0.293	276,534	N/A	N/A	100.0	5.3

Lane Background	Lane background subtracted with disk size: 10
Lane Width	8.22 mm

MDA-MB-468, C.dve Actin Analysis:

Image Report: 2020-02-07 MDA-MB-468 C.dve Actin

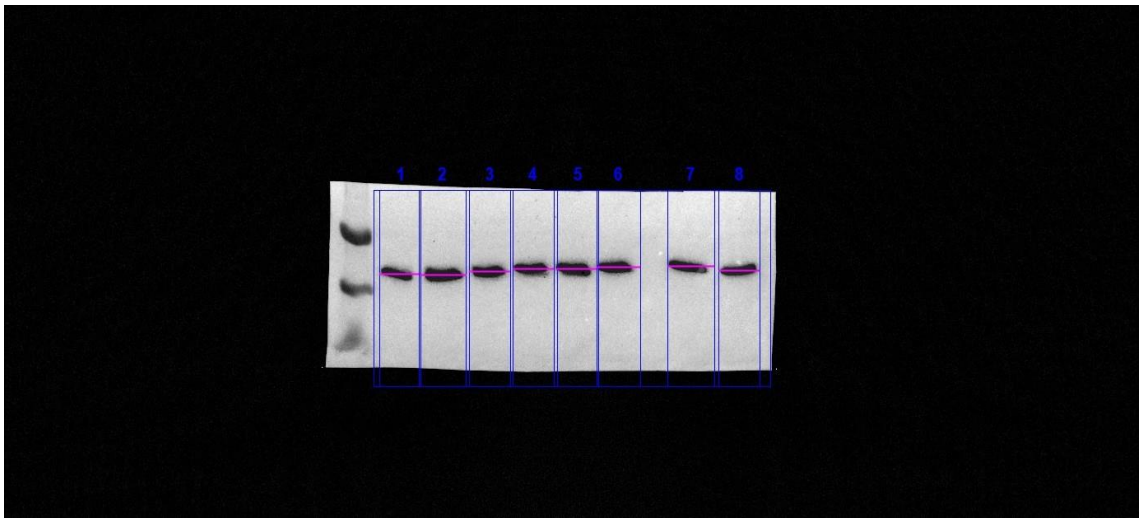

Acquisition Information

Imager	Merged Image

Image Information

Acquisition Date	13/02/2020 11:57:17
User Name	Danielle McCullough
Image Area (mm)	X: 210.0 Y: 168.1
Pixel Size (um)	X: 152.3 Y: 152.3
Data Range (Int)	7806 - 65534

Notes

Merged images:
Image 1: 2020-02-07 mda actin c.dve, invert panel 2 invert panel 1 60s
Image 2: 2020-02-07 mda actin, c.dve, invert panel2 invert panel 1

Analysis Settings

Detection	Lane detection: Manually created lanes Band detection: Manually adjusted bands Lane Background Subtraction: Lane background subtracted with disk size: 10 Lane width: Variable

Lane And Band Analysis

Lane 1

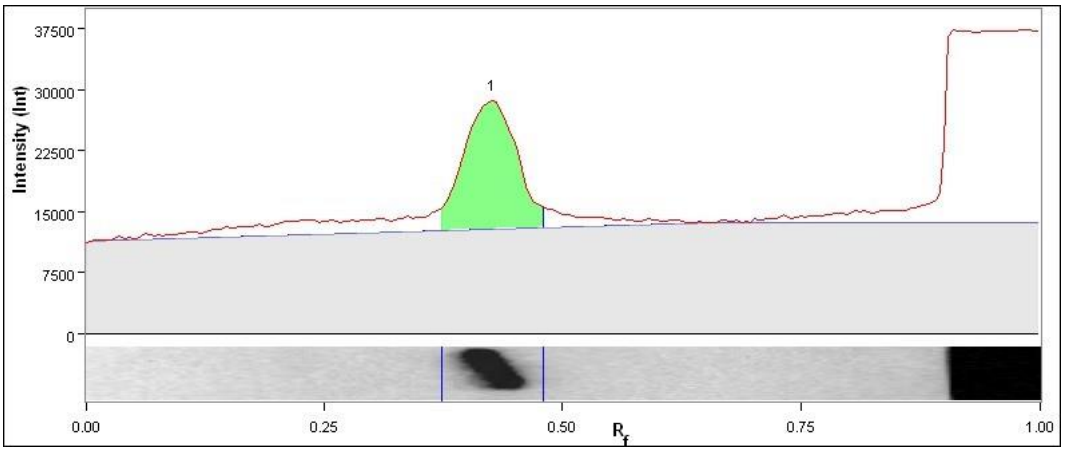

Band No.	Band Label	Mol. Wt. (KDa)	Relative Front	Volume (Int)	Abs. Quant.	Rel. Quant.	Band %	Lane %
1		N/A	0.429	13,106,100	N/A	N/A	100.0	24.2
Lane Background		Lane background subtracted with disk size: 10						
Lane Width		7.61 mm						

Lane 2

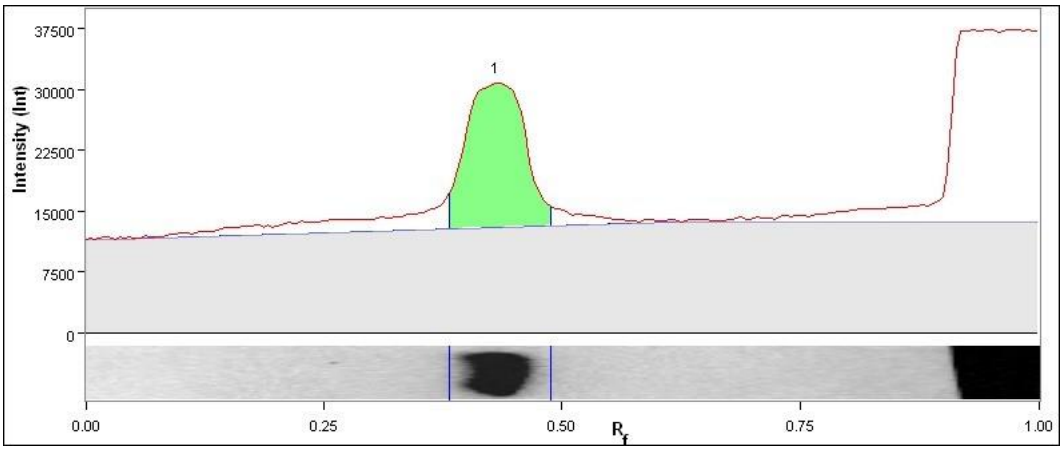

Band No.	Band Label	Mol. Wt. (KDa)	Relative Front	Volume (Int)	Abs. Quant.	Rel. Quant.	Band %	Lane %
1		N/A	0.434	18,847,791	N/A	N/A	100.0	29.8
Lane Background		Lane background subtracted with disk size: 10						
Lane Width		8.68 mm						

Lane 3

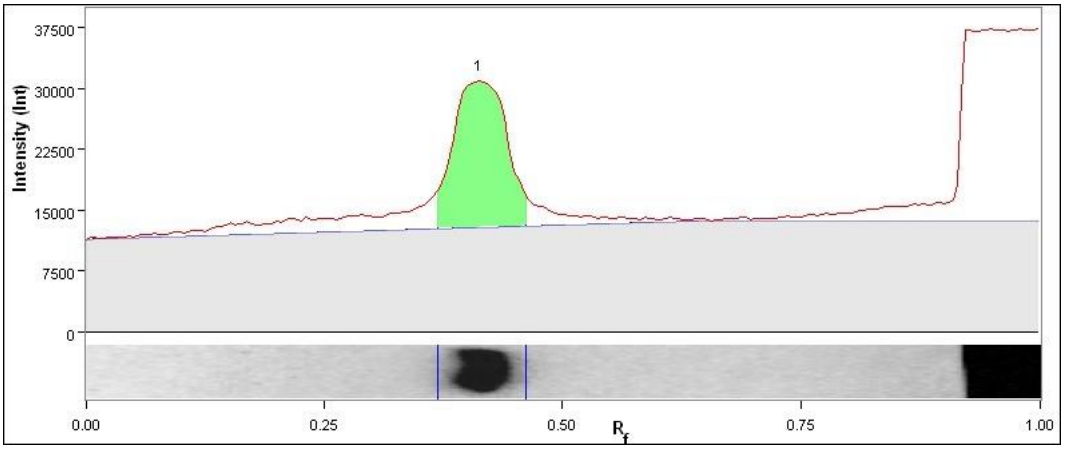

Band No.	Band Label	Mol. Wt. (KDa)	Relative Front	Volume (Int)	Abs. Quant.	Rel. Quant.	Band %	Lane %
1		N/A	0.416	15,338,450	N/A	N/A	100.0	29.3

Lane Background	Lane background subtracted with disk size: 10
Lane Width	7.61 mm

Lane 4

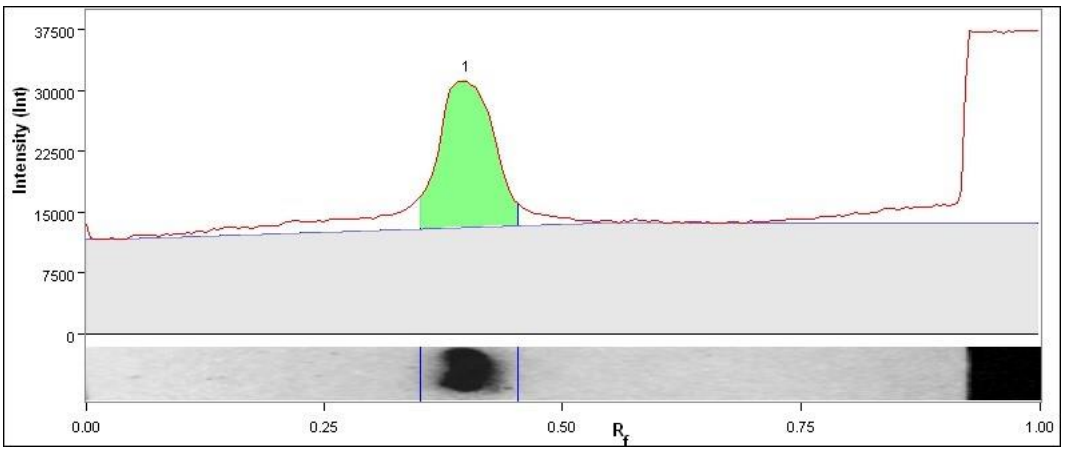

Band No.	Band Label	Mol. Wt. (KDa)	Relative Front	Volume (Int)	Abs. Quant.	Rel. Quant.	Band %	Lane %
1		N/A	0.403	15,571,850	N/A	N/A	100.0	31.4

Lane Background	Lane background subtracted with disk size: 10
Lane Width	7.61 mm

Lane 5

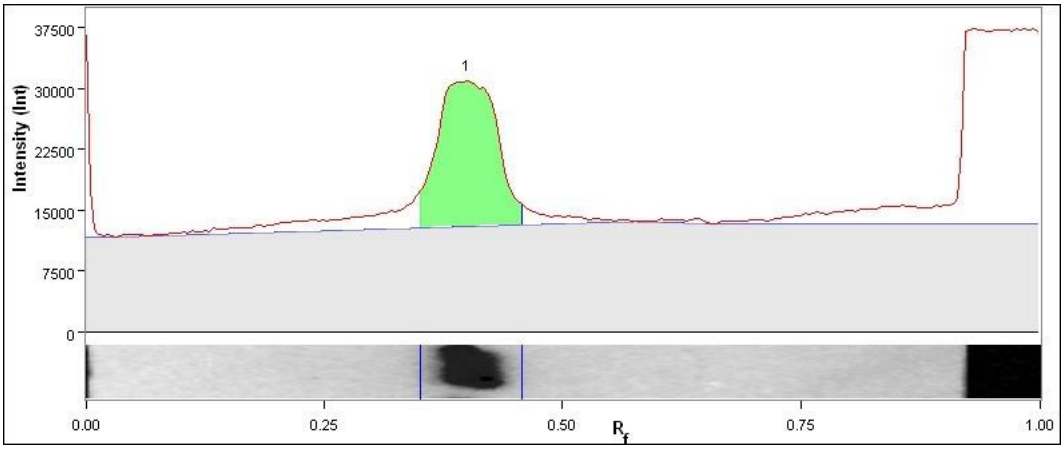

Band No.	Band Label	Mol. Wt. (KDa)	Relative Front	Volume (Int)	Abs. Quant.	Rel. Quant.	Band %	Lane %
1		N/A	0.403	16,952,650	N/A	N/A	100.0	31.1

Lane Background	Lane background subtracted with disk size: 10
Lane Width	7.61 mm

Lane 6

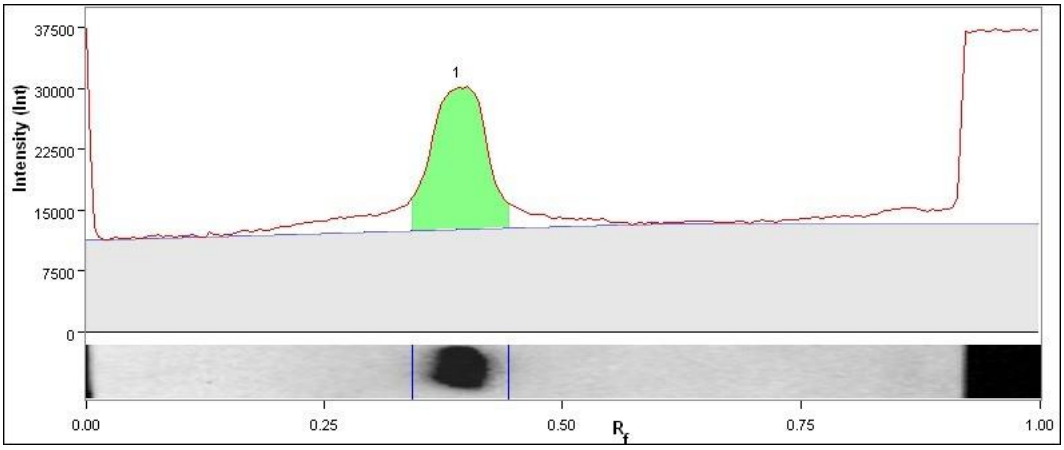

Band No.	Band Label	Mol. Wt. (KDa)	Relative Front	Volume (Int)	Abs. Quant.	Rel. Quant.	Band %	Lane %
1		N/A	0.394	16,327,445	N/A	N/A	100.0	29.3

Lane Background	Lane background subtracted with disk size: 10
Lane Width	8.07 mm

Lane 7

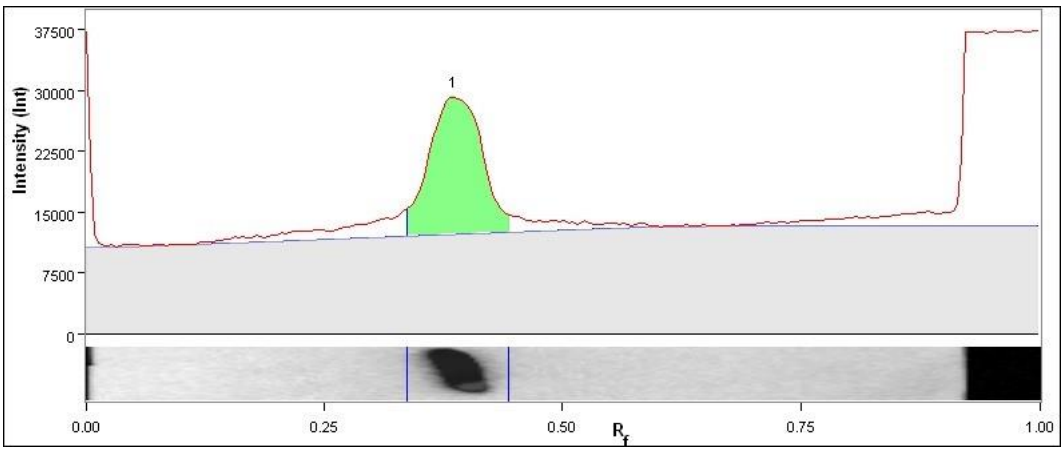

Band No.	Band Label	Mol. Wt. (KDa)	Relative Front	Volume (Int)	Abs. Quant.	Rel. Quant.	Band %	Lane %
1		N/A	0.389	16,024,638	N/A	N/A	100.0	28.1

Lane Background	Lane background subtracted with disk size: 10
Lane Width	8.68 mm

Lane 8

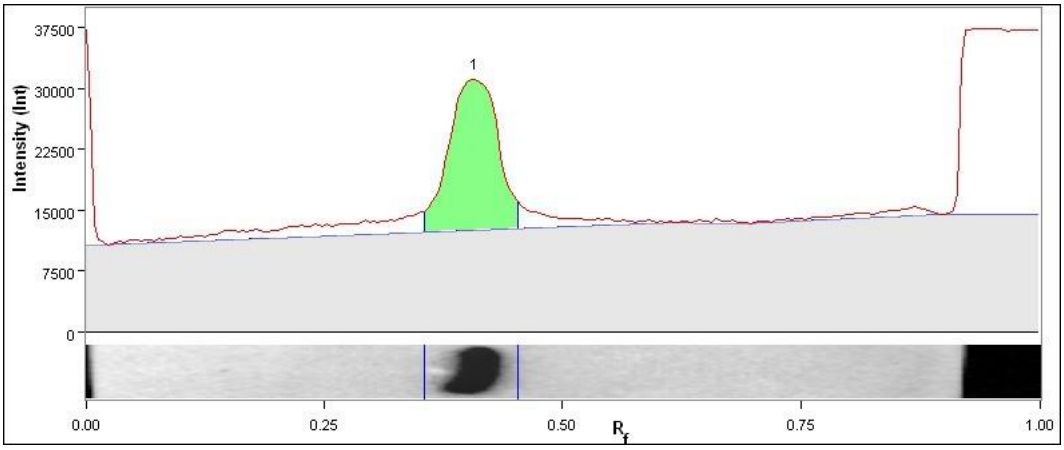

Band No.	Band Label	Mol. Wt. (KDa)	Relative Front	Volume (Int)	Abs. Quant.	Rel. Quant.	Band %	Lane %
1		N/A	0.412	14,555,700	N/A	N/A	100.0	29.2

Lane Background	Lane background subtracted with disk size: 10
Lane Width	7.61 mm

MDA-MB-468, S,sub PY20 Analysis:

Image Report: 2017-04-20 MDA-MB-468, S.sud PY20 60s

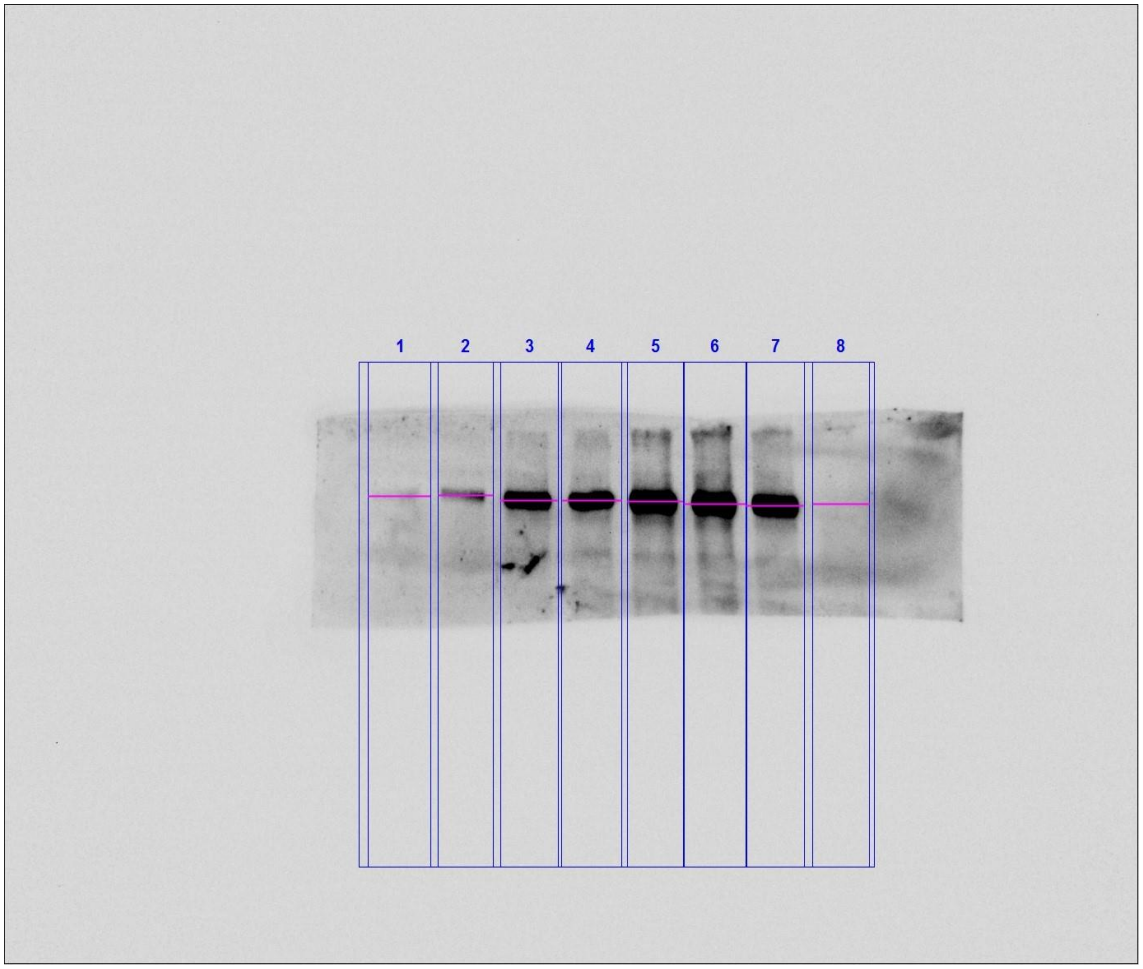

Acquisition Information

Imager	ChemiDoc™ Touch
Exposure Time (sec)	60.000 (Manual)
Serial Number	732BR1296
Software Version	1.1.0.04
Application	Chemiluminescence
Excitation Source	No Illumination
Emission Filter	No Filter
Binning	2x2

Image Information

Acquisition Date	20/04/2017 20:16:42
User Name	
Image Area (mm)	X: 143.4 Y: 114.8
Pixel Size (um)	X: 104.0 Y: 104.0
Data Range (Int)	531 - 39565

Analysis Settings

Detection	Lane detection: Manually created lanes Band detection: Automatically detected bands with custom sensitivity: 50 Manually adjusted bands Lane Background Subtraction: Lane background subtracted with disk size: 10 Lane width: Variable

Lane And Band Analysis

Lane 1

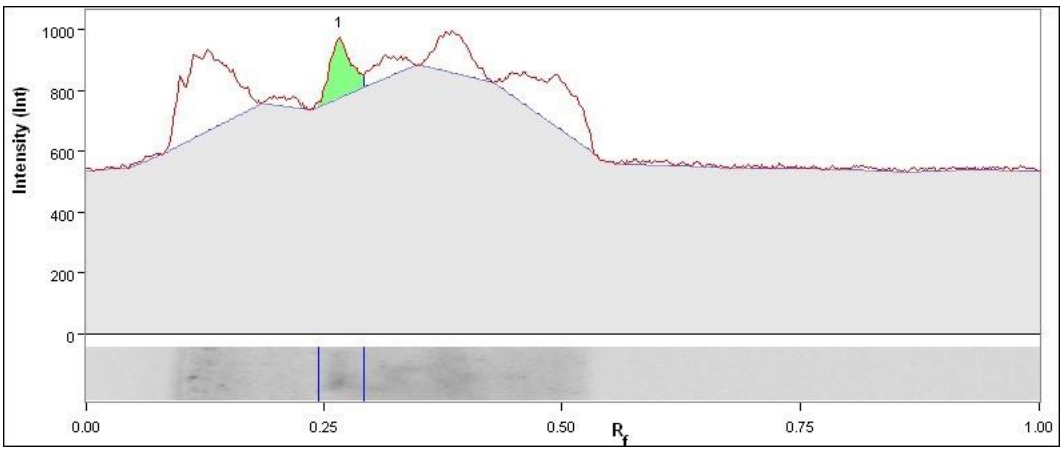

Band No.	Band Label	Mol. Wt. (KDa)	Relative Front	Volume (Int)	Abs. Quant.	Rel. Quant.	Band %	Lane %
1		N/A	0.267	269,420	N/A	N/A	100.0	11.6

Band Detection	Automatically detected bands with custom sensitivity: 50
Lane Background	Lane background subtracted with disk size: 10
Lane Width	7.90 mm

Lane 2

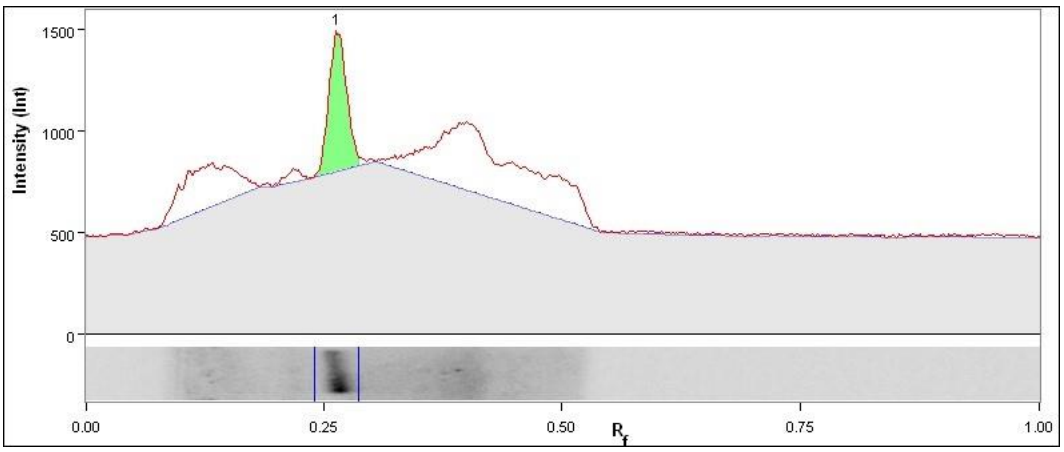

Band No.	Band Label	Mol. Wt. (KDa)	Relative Front	Volume (Int)	Abs. Quant.	Rel. Quant.	Band %	Lane %
1		N/A	0.265	778,272	N/A	N/A	100.0	20.0
Band Detection		Automatically detected bands with custom sensitivity: 50						
Lane Background		Lane background subtracted with disk size: 10						

Lane 3

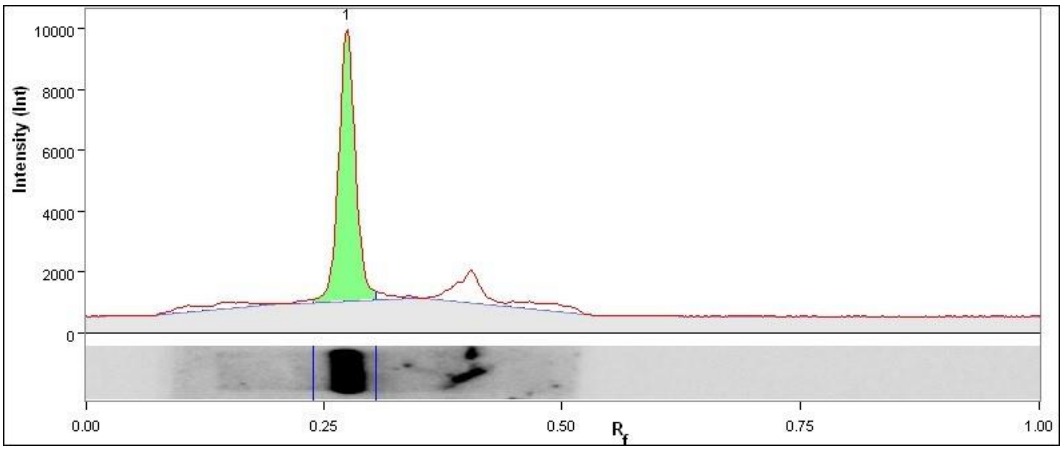

Band No.	Band Label	Mol. Wt. (KDa)	Relative Front	Volume (Int)	Abs. Quant.	Rel. Quant.	Band %	Lane %
1		N/A	0.275	8,837,080	N/A	N/A	100.0	70.3
Band Detection		Automatically detected bands with custom sensitivity: 50						
Lane Background		Lane background subtracted with disk size: 10						
Lane Width		7.28 mm						

Lane 4

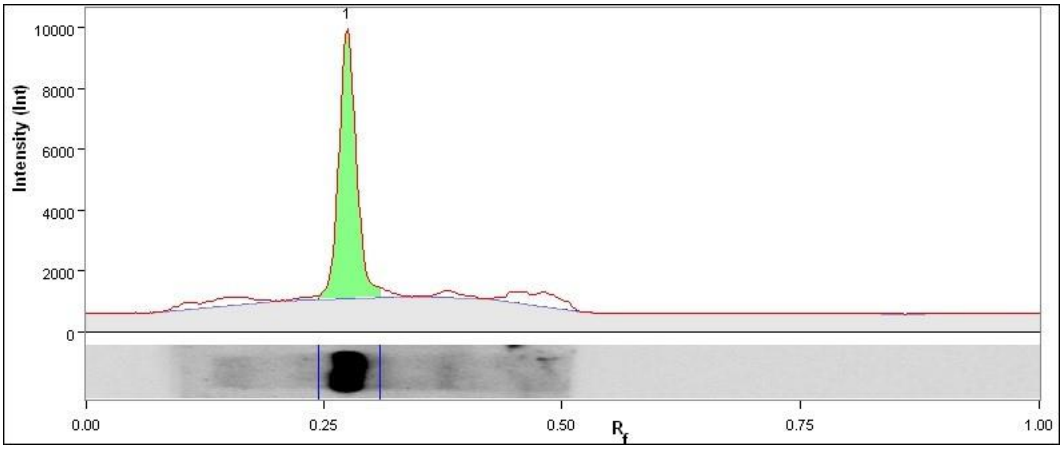

Band No.	Band Label	Mol. Wt. (KDa)	Relative Front	Volume (Int)	Abs. Quant.	Rel. Quant.	Band %	Lane %
1		N/A	0.275	8,689,628	N/A	N/A	100.0	74.4
Band Detection		Automatically detected bands with custom sensitivity: 50						
Lane Background		Lane background subtracted with disk size: 10						

Lane Width	7.59 mm

Lane 5

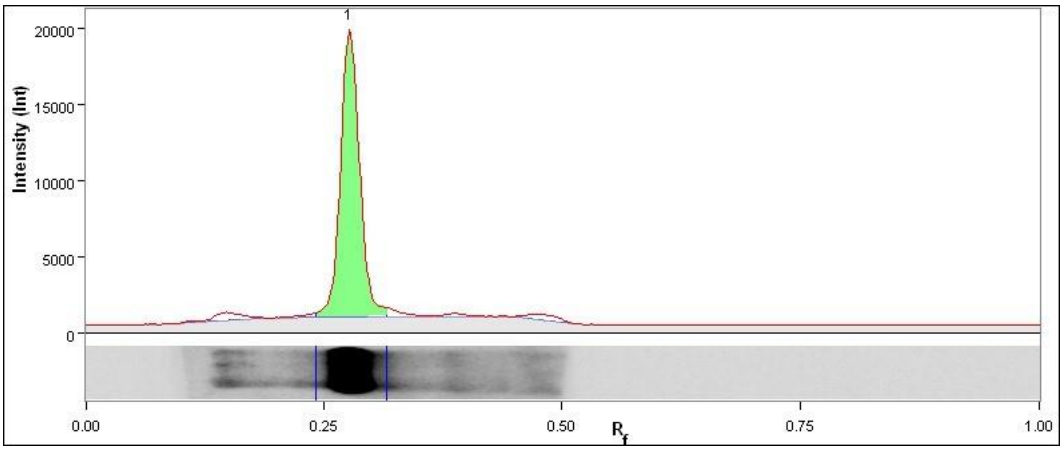

Band No.	Band Label	Mol. Wt. (KDa)	Relative Front	Volume (Int)	Abs. Quant.	Rel. Quant.	Band %	Lane %
1		N/A	0.277	20,785,560	N/A	N/A	100.0	88.5

Band Detection	Automatically detected bands with custom sensitivity: 50
Lane Background	Lane background subtracted with disk size: 10
Lane Width	7.07 mm

Lane 6

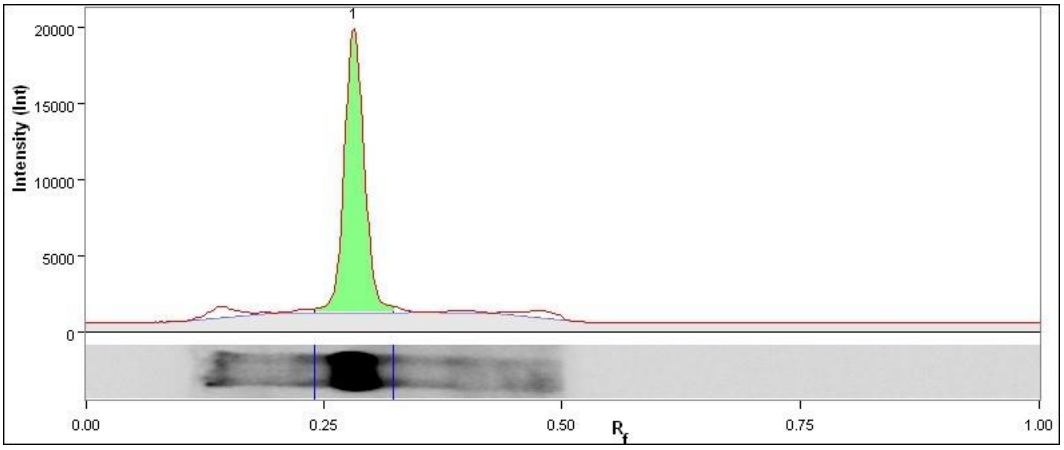

Band No.	Band Label	Mol. Wt. (KDa)	Relative Front	Volume (Int)	Abs. Quant.	Rel. Quant.	Band %	Lane %
1		N/A	0.282	20,676,675	N/A	N/A	100.0	86.5

Band Detection	Automatically detected bands with custom sensitivity: 50
Lane Background	Lane background subtracted with disk size: 10
Lane Width	7.80 mm

Lane 7

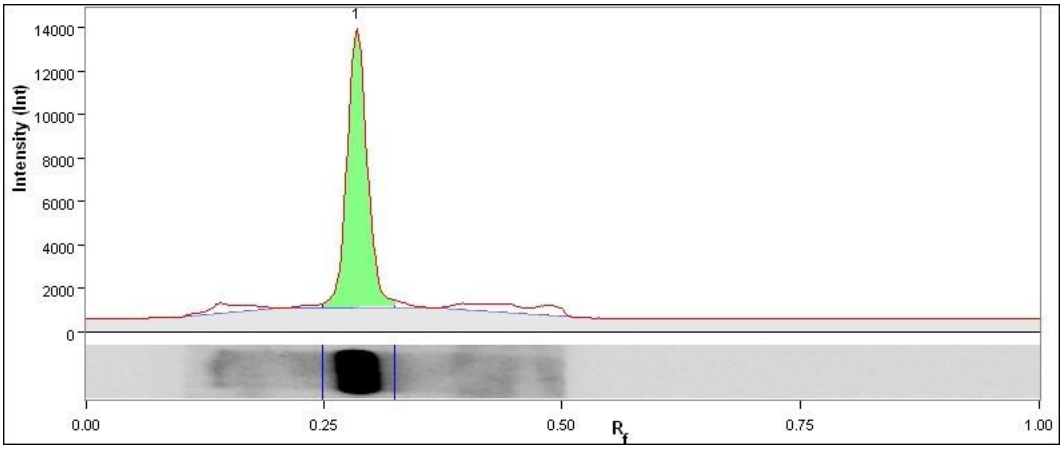

Band No.	Band Label	Mol. Wt. (KDa)	Relative Front	Volume (Int)	Abs. Quant.	Rel. Quant.	Band %	Lane %
1		N/A	0.286	13,666,590	N/A	N/A	100.0	80.9

Band Detection	Automatically detected bands with custom sensitivity: 50
Lane Background	Lane background subtracted with disk size: 10
Lane Width	7.28 mm

Lane 8

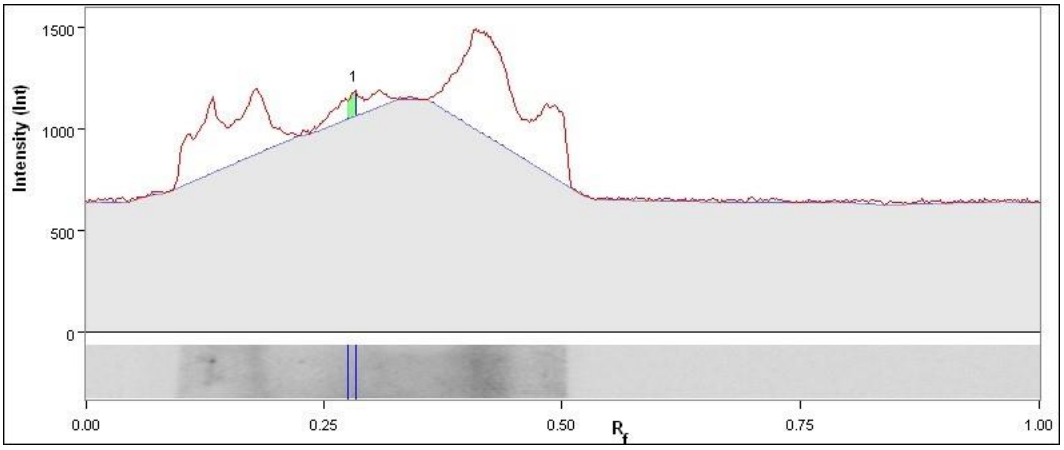

Band No.	Band Label	Mol. Wt. (KDa)	Relative Front	Volume (Int)	Abs. Quant.	Rel. Quant.	Band %	Lane %
1		N/A	0.282	45,747	N/A	N/A	100.0	1.4

Band Detection	Automatically detected bands with custom sensitivity: 50
Lane Background	Lane background subtracted with disk size: 10
Lane Width	7.18 mm

MDA-MB-468, S.sub Actin Analysis:

Image Report: 2017-04-20 MDA-MB-468, S.sud Actin 15s

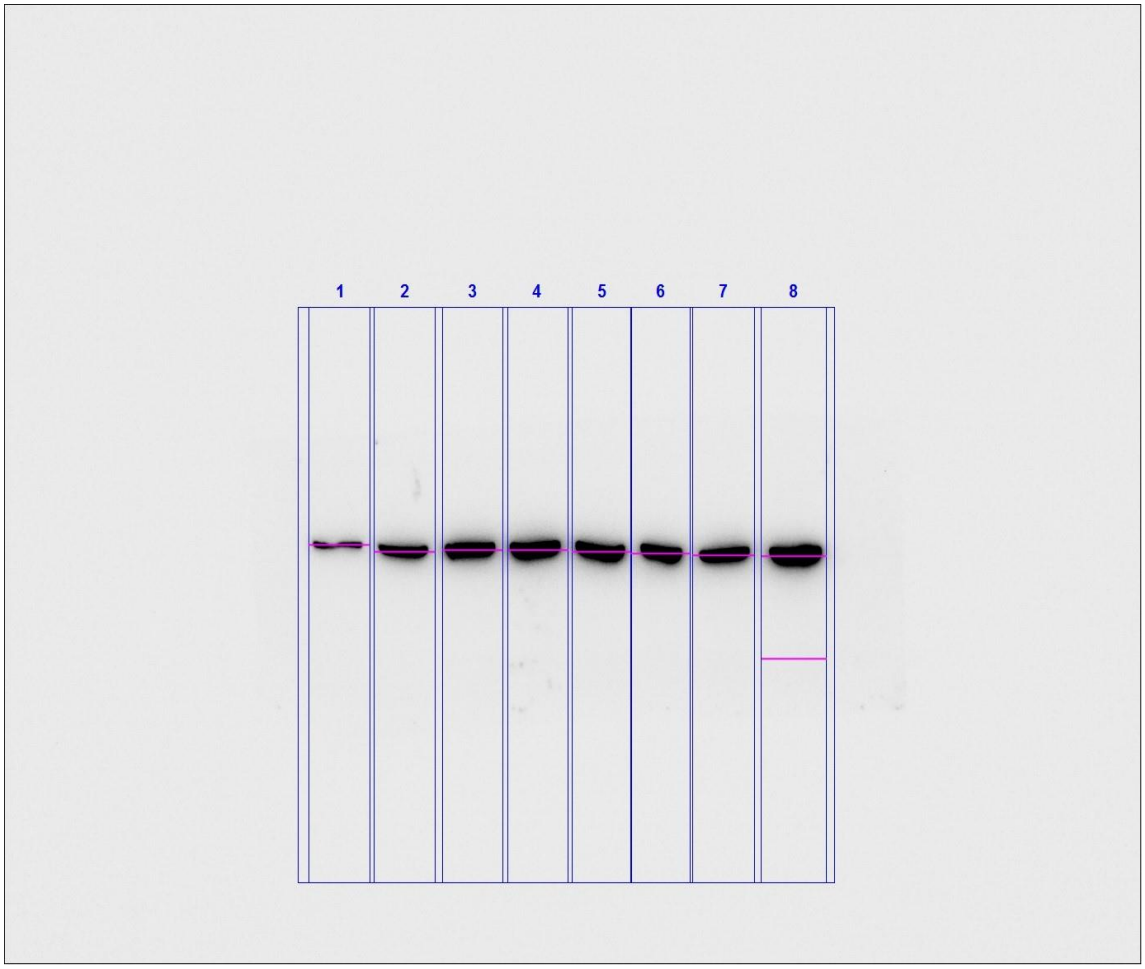

Acquisition Information

Imager	ChemiDoc™ Touch
Exposure Time (sec)	15.000 (Manual)
Serial Number	732BR1296
Software Version	1.1.0.04
Application	Chemiluminescence
Excitation Source	No Illumination
Emission Filter	No Filter
Binning	2x2

Image Information

Acquisition Date	20/04/2017 19:53:59
User Name	
Image Area (mm)	X: 143.4 Y: 114.8
Pixel Size (um)	X: 104.0 Y: 104.0
Data Range (Int)	528 - 35812

Analysis Settings

Detection	Lane detection: Manually created lanes Band detection: Automatically detected bands with custom sensitivity: 50 Manually adjusted bands Lane Background Subtraction: Lane background subtracted with disk size: 10 Lane width: Variable

Lane And Band Analysis

Lane 1

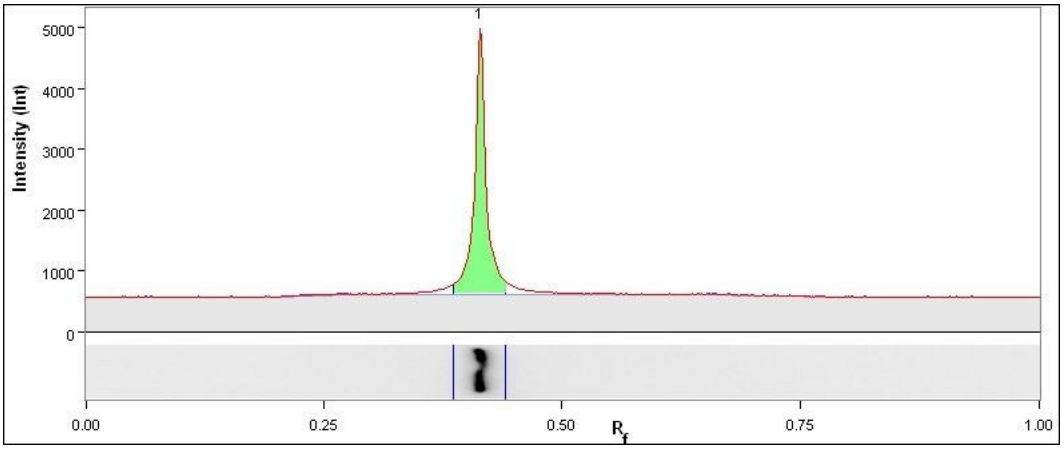

Band No.	Band Label	Mol. Wt. (KDa)	Relative Front	Volume (Int)	Abs. Quant.	Rel. Quant.	Band %	Lane %
1		N/A	0.414	3,559,548	N/A	N/A	100.0	82.4

Band Detection	Automatically detected bands with custom sensitivity: 50
Lane Background	Lane background subtracted with disk size: 10
Lane Width	7.70 mm

Lane 2

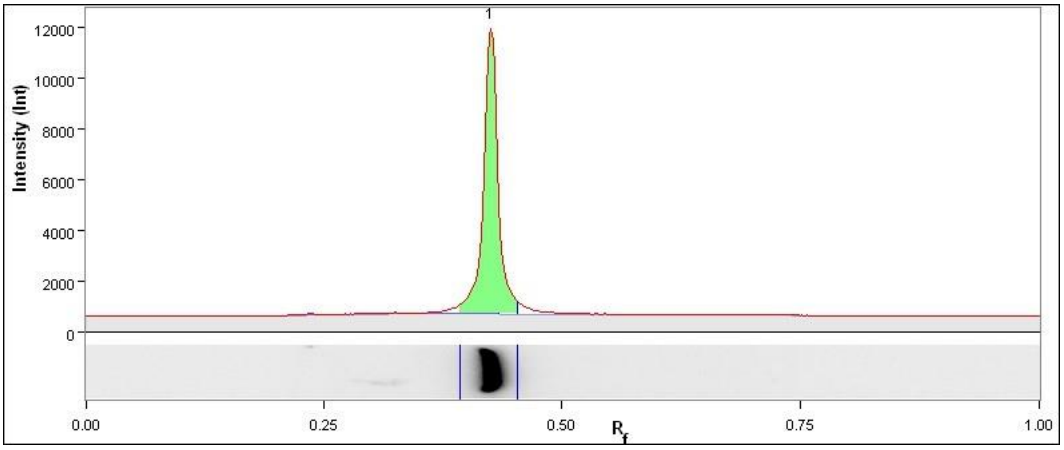

Band No.	Band Label	Mol. Wt. (KDa)	Relative Front	Volume (Int)	Abs. Quant.	Rel. Quant.	Band %	Lane %
1		N/A	0.426	9,820,096	N/A	N/A	100.0	89.6

Band Detection	Automatically detected bands with custom sensitivity: 50
Lane Background	Lane background subtracted with disk size: 10

Lane 3

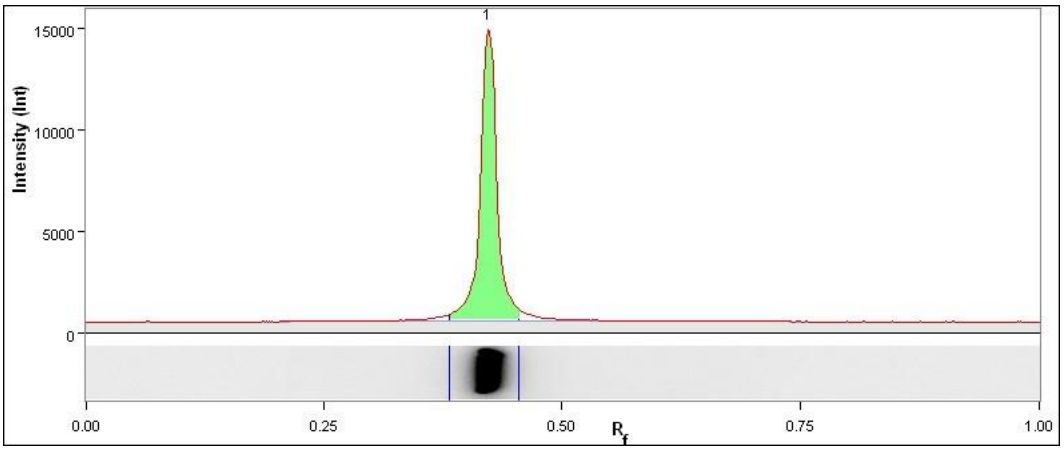

Band No.	Band Label	Mol. Wt. (KDa)	Relative Front	Volume (Int)	Abs. Quant.	Rel. Quant.	Band %	Lane %
1		N/A	0.423	16,705,977	N/A	N/A	100.0	92.7

Band Detection	Automatically detected bands with custom sensitivity: 50
Lane Background	Lane background subtracted with disk size: 10
Lane Width	7.59 mm

Lane 4

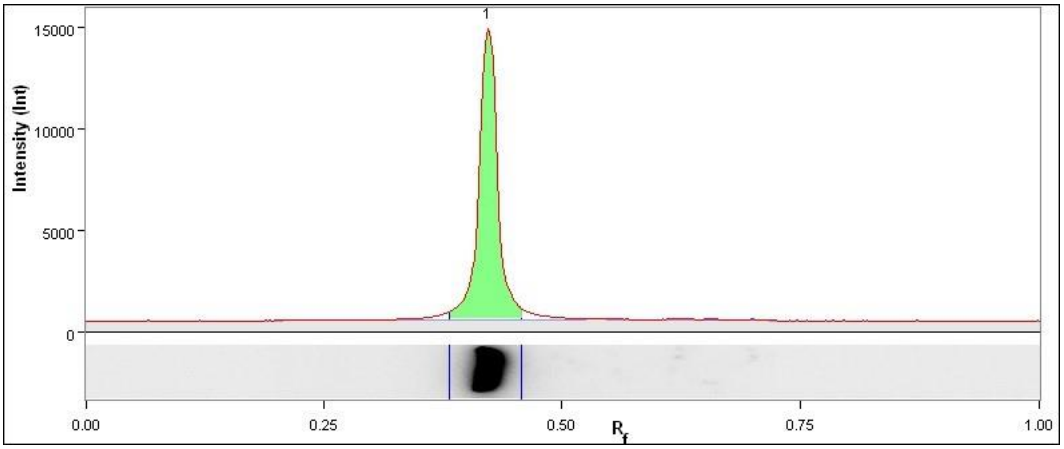

Band No.	Band Label	Mol. Wt. (KDa)	Relative Front	Volume (Int)	Abs. Quant.	Rel. Quant.	Band %	Lane %
1		N/A	0.423	18,847,797	N/A	N/A	100.0	92.3

Band Detection	Automatically detected bands with custom sensitivity: 50
Lane Background	Lane background subtracted with disk size: 10

Lane Width	7.59 mm

Lane 5

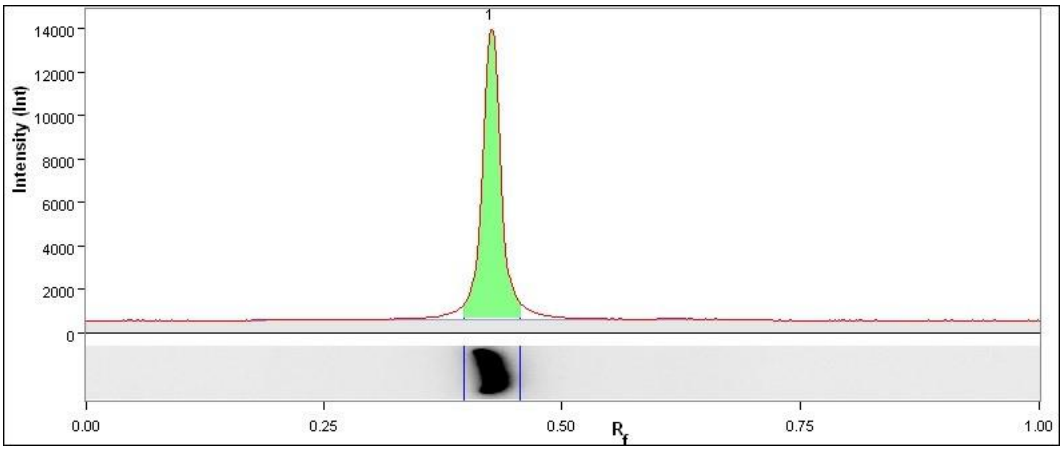

Band No.	Band Label	Mol. Wt. (KDa)	Relative Front	Volume (Int)	Abs. Quant.	Rel. Quant.	Band %	Lane %
1		N/A	0.426	16,337,808	N/A	N/A	100.0	90.6

Band Detection	Automatically detected bands with custom sensitivity: 50
Lane Background	Lane background subtracted with disk size: 10
Lane Width	7.49 mm

Lane 6

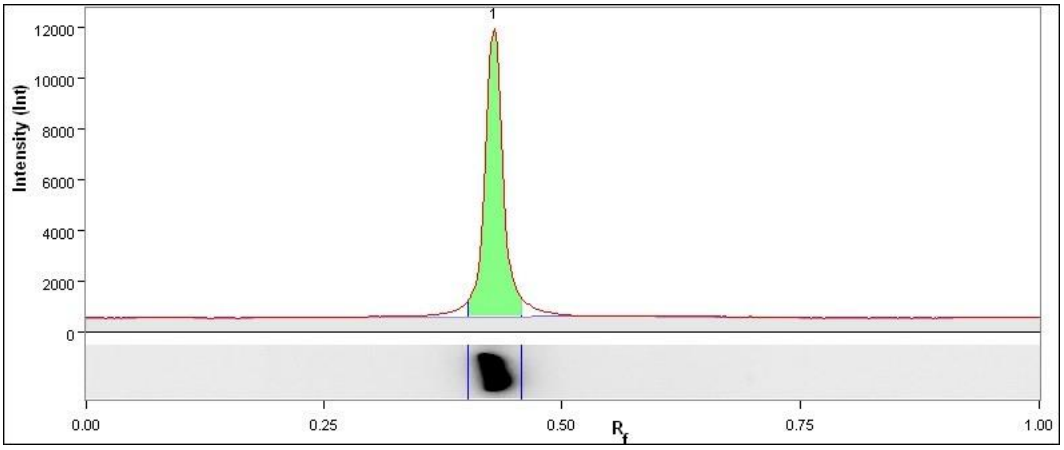

Band No.	Band Label	Mol. Wt. (KDa)	Relative Front	Volume (Int)	Abs. Quant.	Rel. Quant.	Band %	Lane %
1		N/A	0.429	13,892,328	N/A	N/A	100.0	88.4

Band Detection	Automatically detected bands with custom sensitivity: 50
Lane Background	Lane background subtracted with disk size: 10
Lane Width	7.49 mm

Lane 7

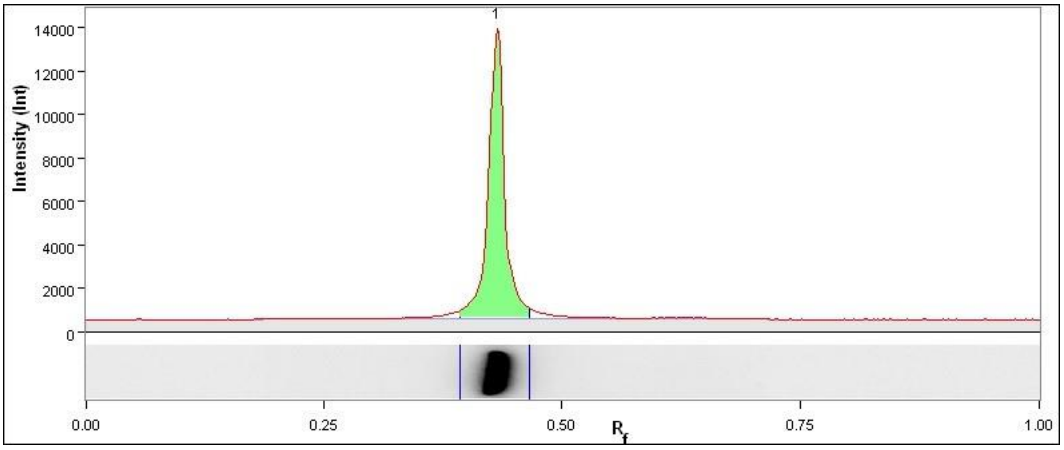

Band No.	Band Label	Mol. Wt. (KDa)	Relative Front	Volume (Int)	Abs. Quant.	Rel. Quant.	Band %	Lane %
1		N/A	0.432	14,939,475	N/A	N/A	100.0	91.9

Band Detection	Automatically detected bands with custom sensitivity: 50
Lane Background	Lane background subtracted with disk size: 10
Lane Width	7.80 mm

Lane 8

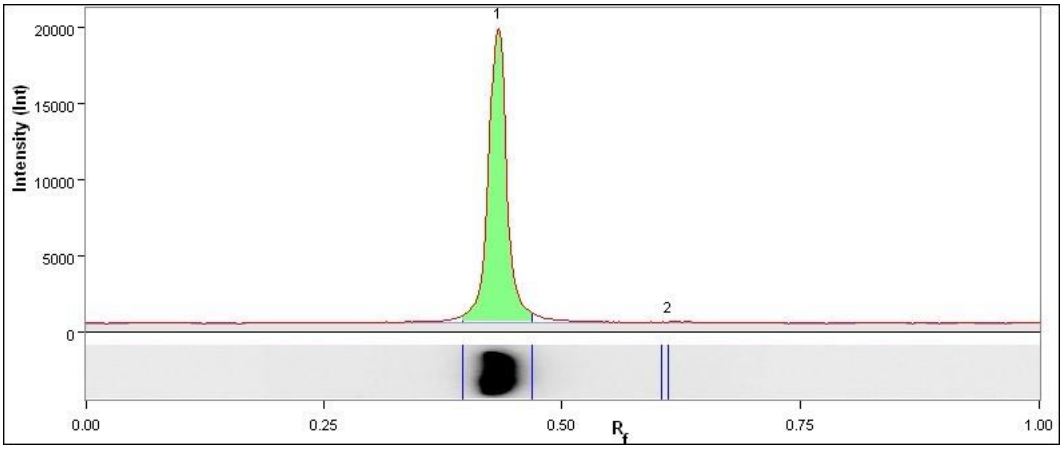

Band No.	Band Label	Mol. Wt. (KDa)	Relative Front	Volume (Int)	Abs. Quant.	Rel. Quant.	Band %	Lane %
1		N/A	0.434	25,916,345	N/A	N/A	99.9	94.2
2		N/A	0.613	15,326	N/A	N/A	0.1	0.1

Band Detection	Automatically detected bands with custom sensitivity: 50
Lane Background	Lane background subtracted with disk size: 10
Lane Width	8.22 mm

MDA-MB-468, S.har PY20 Analysis:

Image Report: 2017-04-20 MDA-MB-468, S.har py20 120s

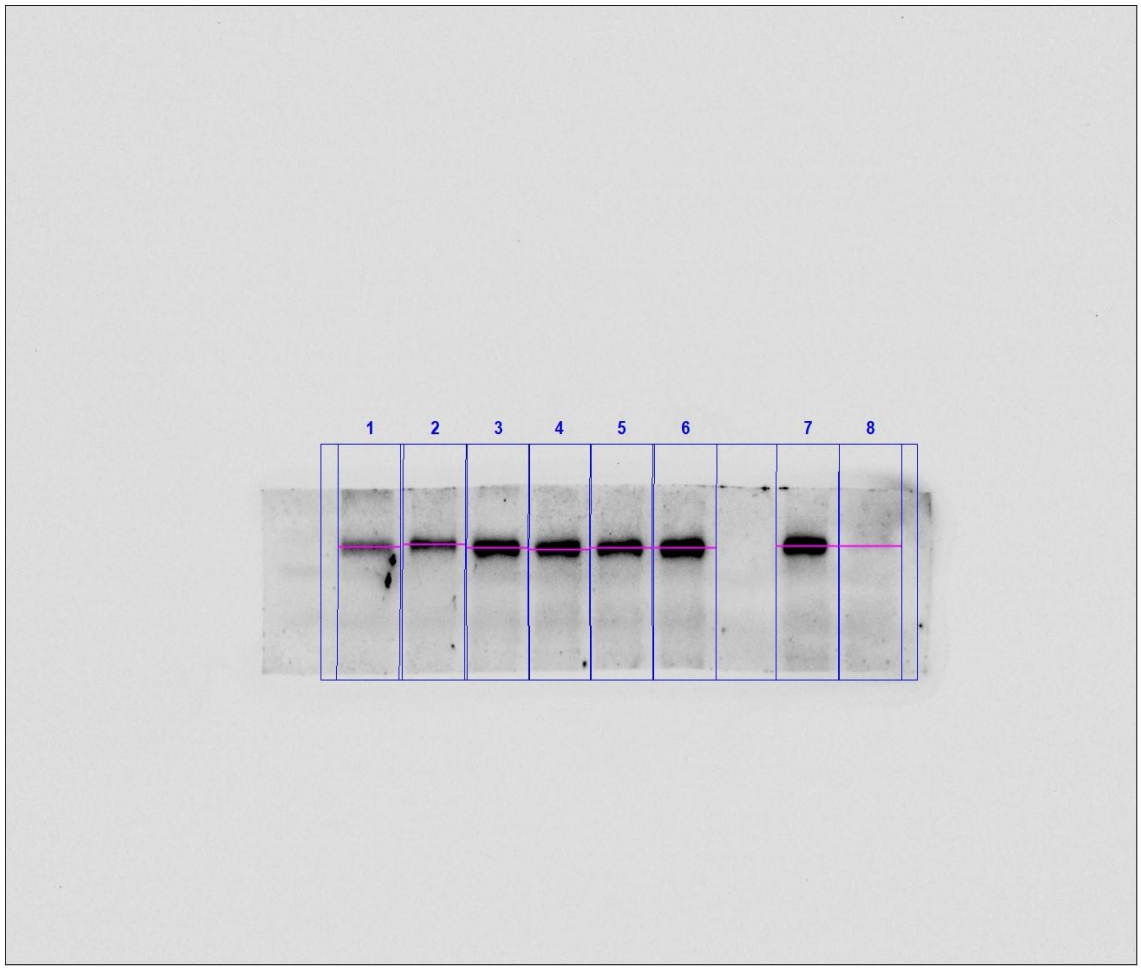

Acquisition Information

Imager	ChemiDoc™ Touch
Exposure Time (sec)	120.000 (Manual)
Serial Number	732BR1296
Software Version	1.1.0.04
Application	Chemiluminescence
Excitation Source	No Illumination
Emission Filter	No Filter
Binning	2x2

Image Information

Acquisition Date	20/04/2017 23:06:08
User Name	

Image Area (mm)	X: 143.4 Y: 114.8
Pixel Size (um)	X: 104.0 Y: 104.0
Data Range (Int)	530 - 21101

Analysis Settings

Detection	Lane detection: Automatically detected lanes with manual adjustments Band detection: Manually adjusted bands Lane Background Subtraction: Lane background subtracted with disk size: 10 Lane width: 7.90 mm

Lane And Band Analysis

Lane 1

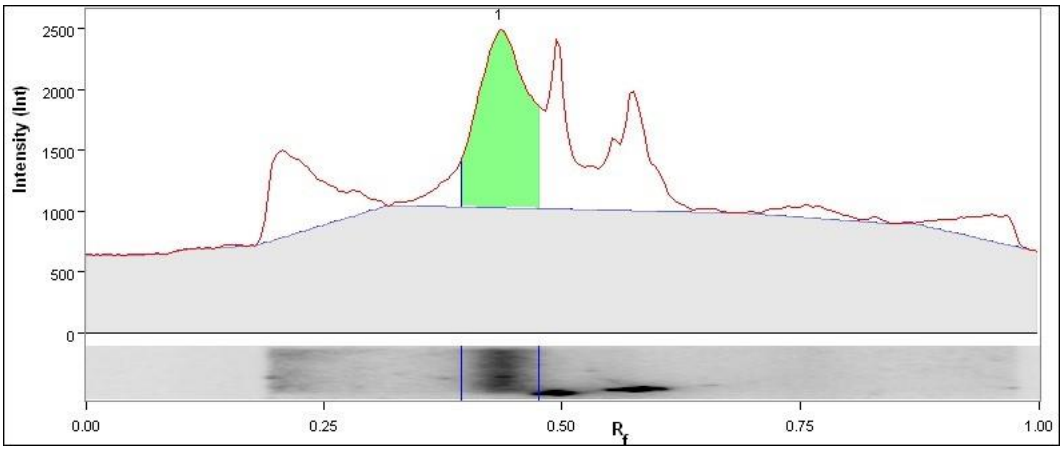

Band No.	Band Label	Mol. Wt. (KDa)	Relative Front	Volume (Int)	Abs. Quant.	Rel. Quant.	Band %	Lane %
1		N/A	0.438	1,875,832	N/A	N/A	100.0	35.5

Lane Background	Lane background subtracted with disk size: 10
Lane Width	7.90 mm

Lane 2

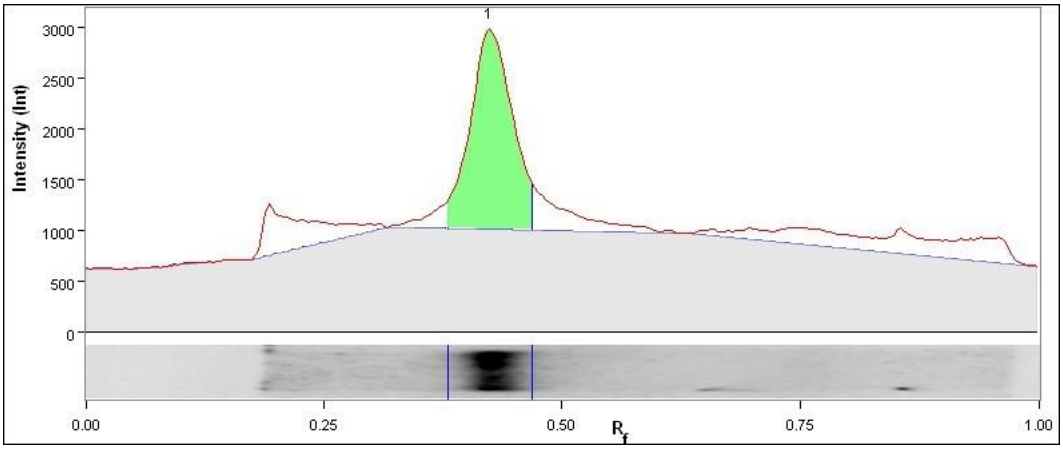

Band No.	Band Label	Mol. Wt. (KDa)	Relative Front	Volume (Int)	Abs. Quant.	Rel. Quant.	Band %	Lane %
1		N/A	0.426	2,198,756	N/A	N/A	100.0	49.8
Lane Background		Lane background subtracted with disk size: 10						
Lane Width		7.90 mm						

Lane 3

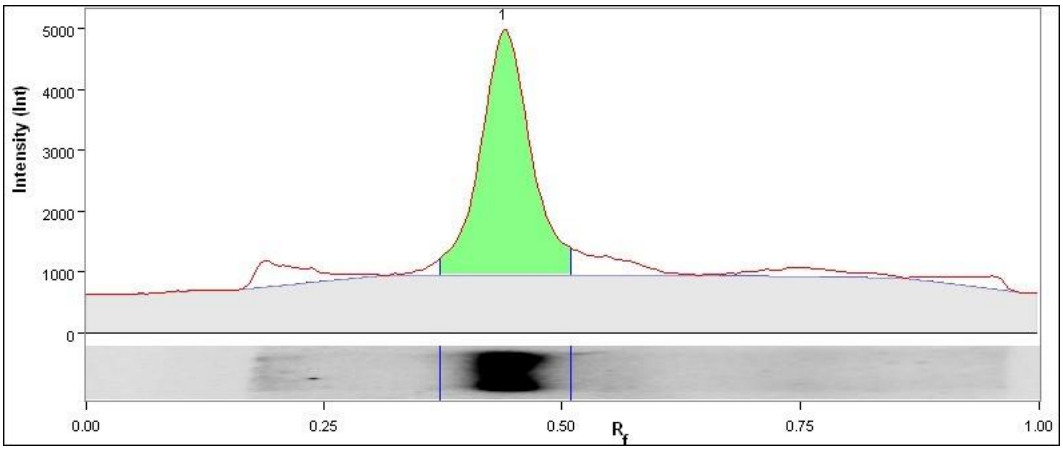

Band No.	Band Label	Mol. Wt. (KDa)	Relative Front	Volume (Int)	Abs. Quant.	Rel. Quant.	Band %	Lane %
1		N/A	0.441	5,352,756	N/A	N/A	100.0	74.7
Lane Background		Lane background subtracted with disk size: 10						
Lane Width		7.90 mm						

Lane 4

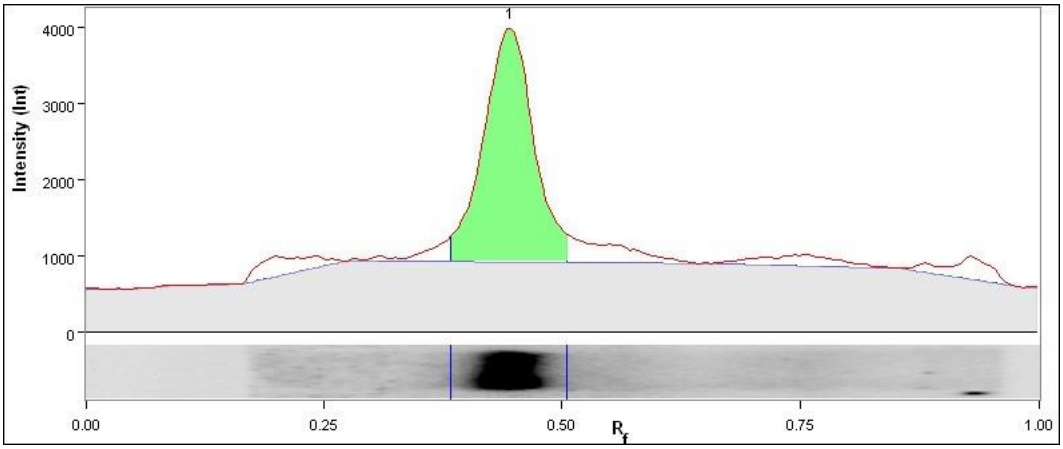

Band No.	Band Label	Mol. Wt. (KDa)	Relative Front	Volume (Int)	Abs. Quant.	Rel. Quant.	Band %	Lane %
1		N/A	0.449	4,559,088	N/A	N/A	100.0	70.8
Lane Background		Lane background subtracted with disk size: 10						
Lane Width		7.90 mm						

Lane 5

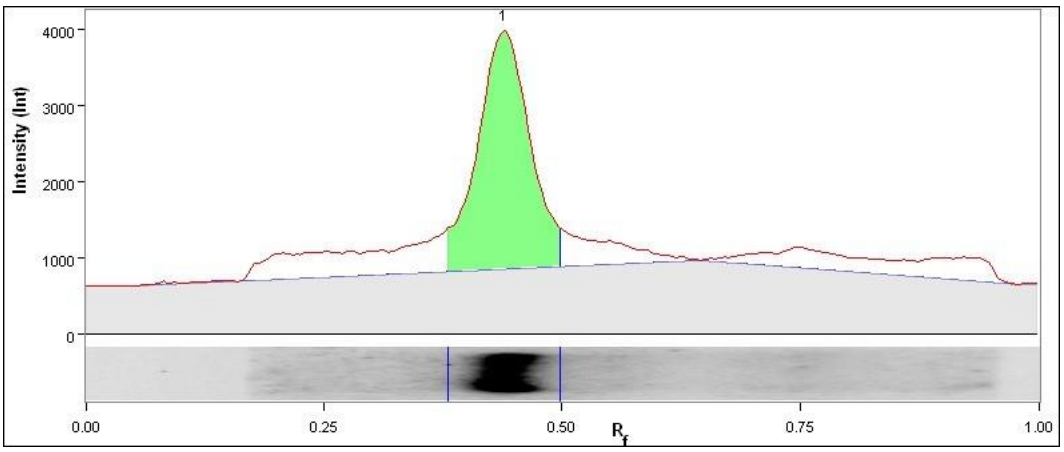

Band No.	Band Label	Mol. Wt. (KDa)	Relative Front	Volume (Int)	Abs. Quant.	Rel. Quant.	Band %	Lane %
1		N/A	0.441	4,359,968	N/A	N/A	100.0	55.1

Lane Background	Lane background subtracted with disk size: 10
Lane Width	7.90 mm

Lane 6

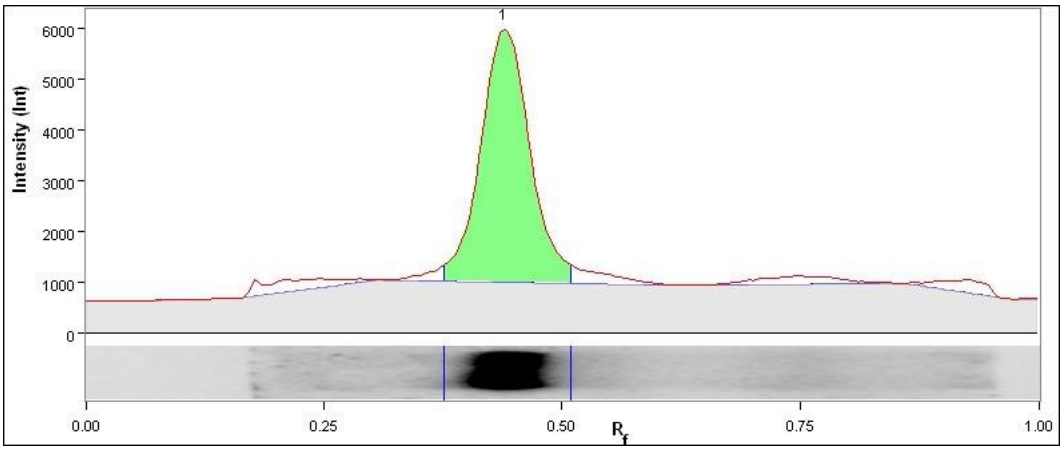

Band No.	Band Label	Mol. Wt. (KDa)	Relative Front	Volume (Int)	Abs. Quant.	Rel. Quant.	Band %	Lane %
1		N/A	0.441	6,665,276	N/A	N/A	100.0	80.3

Lane Background	Lane background subtracted with disk size: 10
Lane Width	7.90 mm

Lane 7

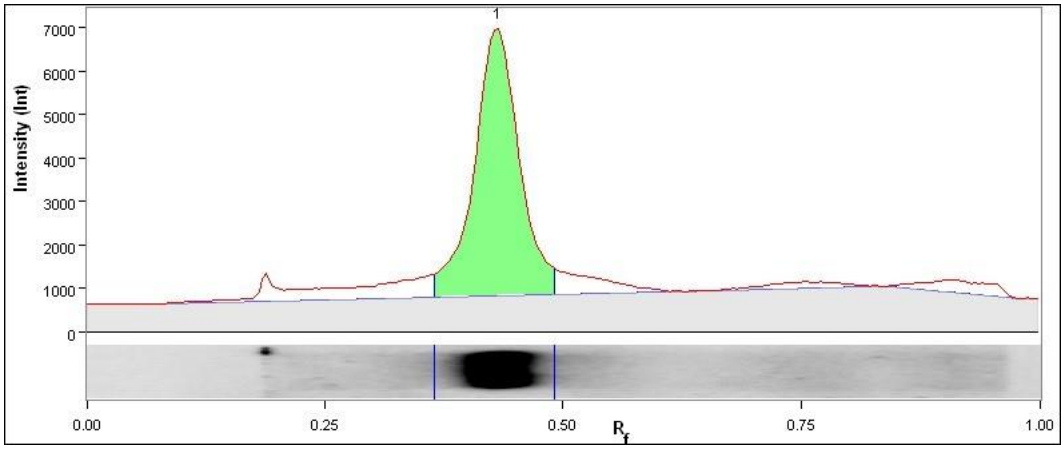

Band No.	Band Label	Mol. Wt. (KDa)	Relative Front	Volume (Int)	Abs. Quant.	Rel. Quant.	Band %	Lane %
1		N/A	0.434	7,188,688	N/A	N/A	100.0	70.5

Lane Background	Lane background subtracted with disk size: 10
Lane Width	7.90 mm

Lane 8

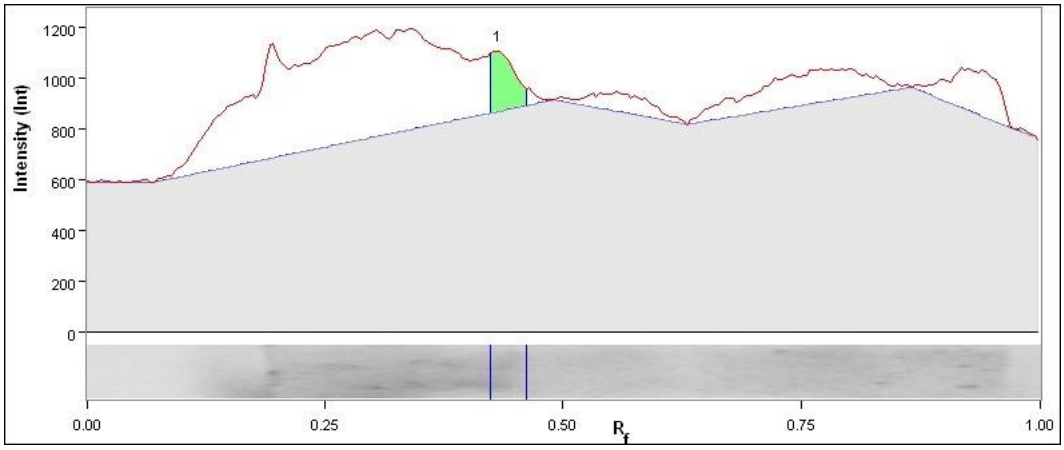

Band No.	Band Label	Mol. Wt. (KDa)	Relative Front	Volume (Int)	Abs. Quant.	Rel. Quant.	Band %	Lane %
1		N/A	0.434	139,384	N/A	N/A	100.0	4.3

Lane Background	Lane background subtracted with disk size: 10
Lane Width	7.90 mm

MDA-MB-468, S.har Actin Analysis:

Image Report: 2017-04-20 MDA-MB-468, S.har Actin 15s

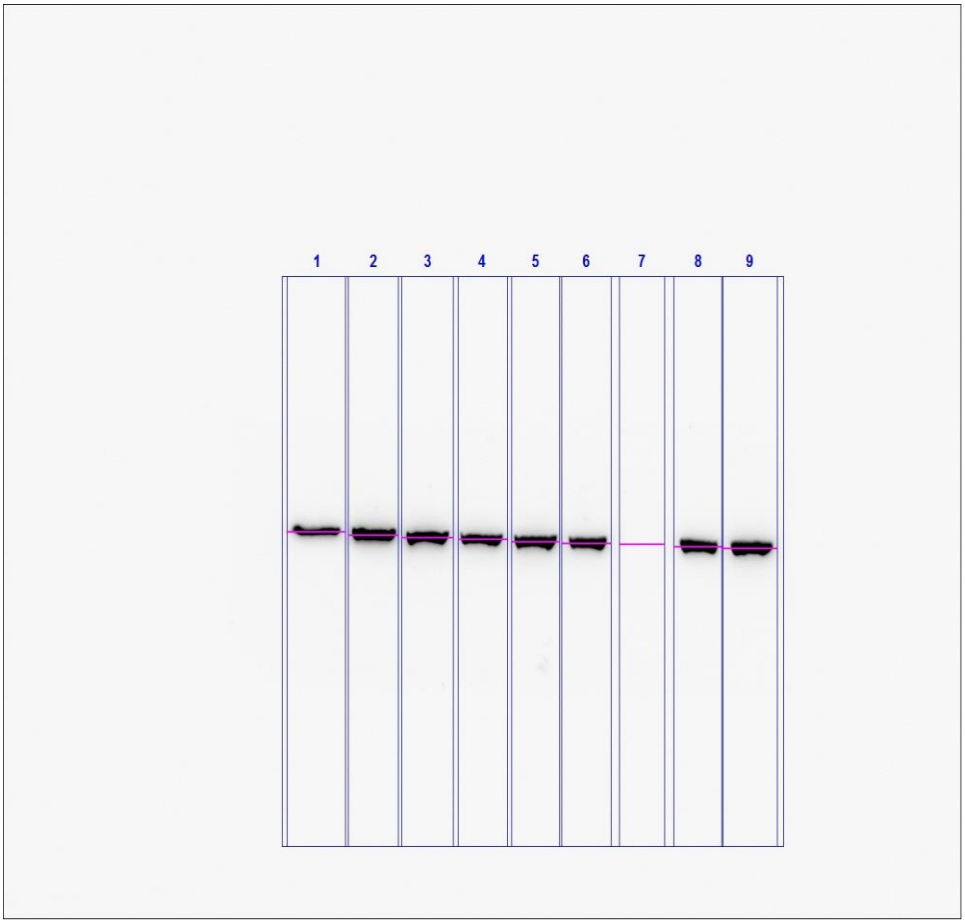

Acquisition Information

Imager	ChemiDoc™ Touch
Exposure Time (sec)	15.000 (Manual)
Serial Number	732BR1296
Software Version	1.1.0.04
Application	Chemiluminescence
Excitation Source	No Illumination
Emission Filter	No Filter
Binning	2x2

Image Information

Acquisition Date	20/04/2017 22:46:15
User Name	
Image Area (mm)	X: 143.4 Y: 114.8
Pixel Size (um)	X: 104.0 Y: 104.0
Data Range (Int)	529 - 33871

Analysis Settings

Detection	Lane detection: Manually created lanes Band detection: Automatically detected bands with custom sensitivity: 95 Manually adjusted bands Lane Background Subtraction: Lane background subtracted with disk size: 10 Lane width: Variable

Lane And Band Analysis

Lane 1

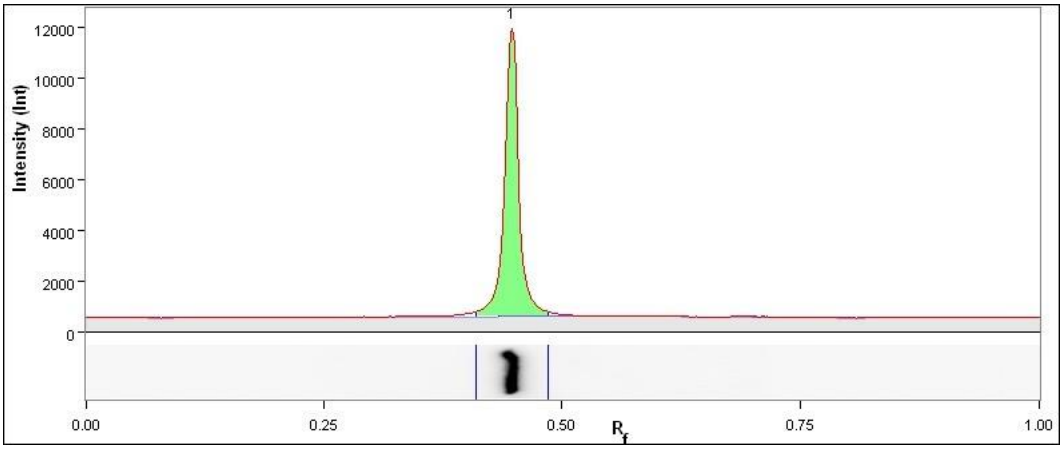

Band No.	Band Label	Mol. Wt. (KDa)	Relative Front	Volume (Int)	Abs. Quant.	Rel. Quant.	Band %	Lane %
1		N/A	0.448	12,897,696	N/A	N/A	100.0	93.2

Band Detection	Automatically detected bands with custom sensitivity: 95
Lane Background	Lane background subtracted with disk size: 10
Lane Width	8.74 mm

Lane 2

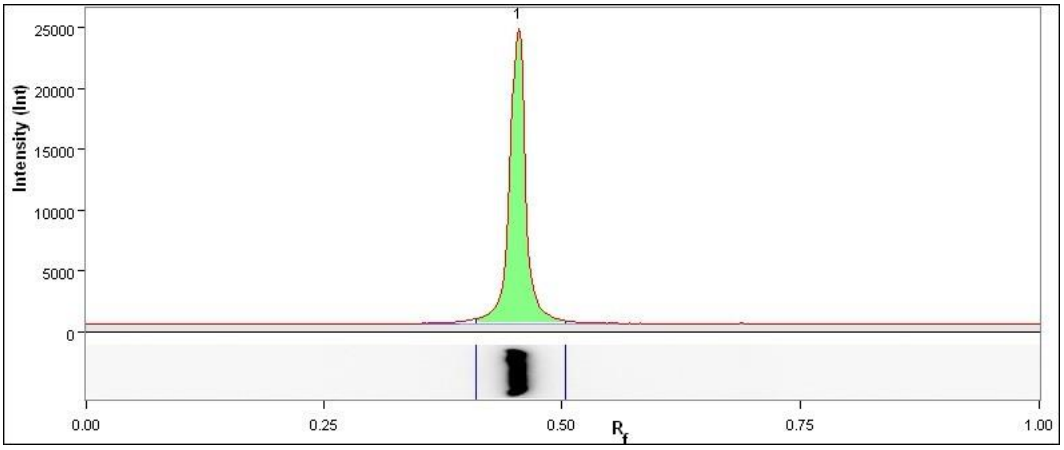

Band No.	Band Label	Mol. Wt. (KDa)	Relative Front	Volume (Int)	Abs. Quant.	Rel. Quant.	Band %	Lane %
1		N/A	0.454	24,635,160	N/A	N/A	100.0	95.3

Band Detection	Automatically detected bands with custom sensitivity: 95
Lane Background	Lane background subtracted with disk size: 10
Lane Width	7.49 mm

Lane 3

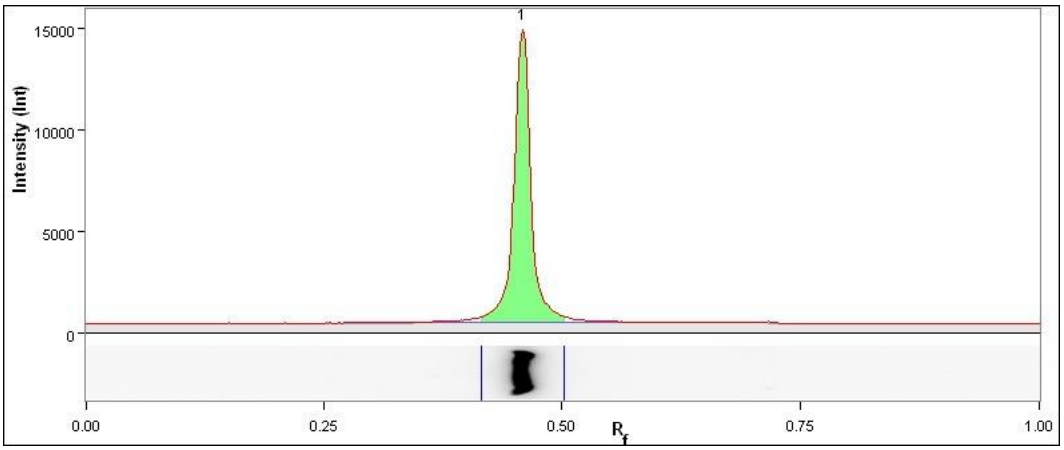

Band No.	Band Label	Mol. Wt. (KDa)	Relative Front	Volume (Int)	Abs. Quant.	Rel. Quant.	Band %	Lane %
1		N/A	0.459	20,904,926	N/A	N/A	100.0	93.4

Band Detection	Automatically detected bands with custom sensitivity: 95
Lane Background	Lane background subtracted with disk size: 10
Lane Width	7.70 mm

Lane 4

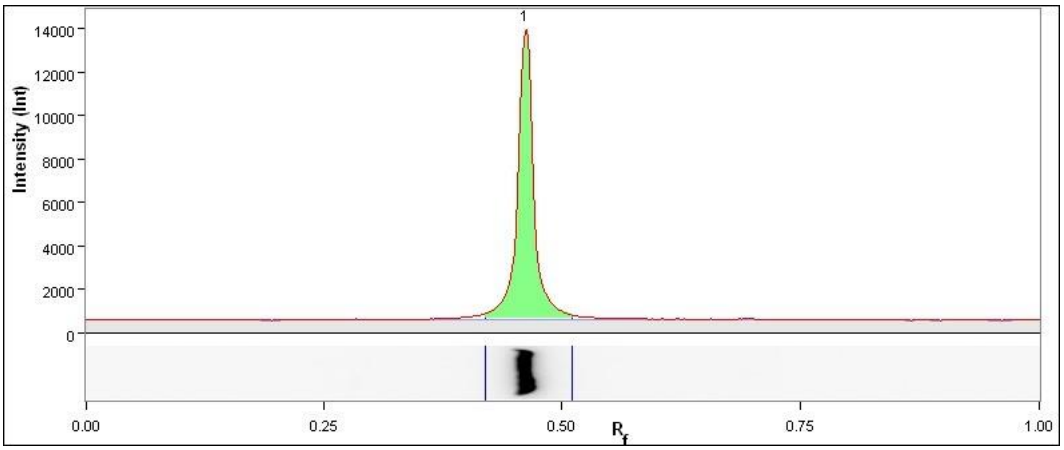

Band No.	Band Label	Mol. Wt. (KDa)	Relative Front	Volume (Int)	Abs. Quant.	Rel. Quant.	Band %	Lane %
1		N/A	0.461	14,716,809	N/A	N/A	100.0	94.3

Band Detection	Automatically detected bands with custom sensitivity: 95
Lane Background	Lane background subtracted with disk size: 10
Lane Width	7.38 mm

Lane 5

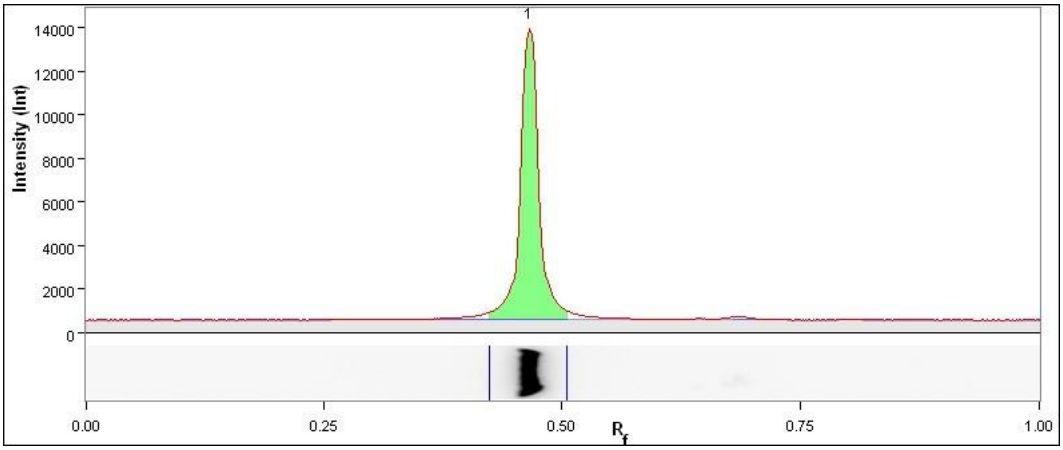

Band No.	Band Label	Mol. Wt. (KDa)	Relative Front	Volume (Int)	Abs. Quant.	Rel. Quant.	Band %	Lane %
1		N/A	0.466	16,295,523	N/A	N/A	100.0	92.0

Band Detection	Automatically detected bands with custom sensitivity: 95
Lane Background	Lane background subtracted with disk size: 10
Lane Width	7.18 mm

Lane 6

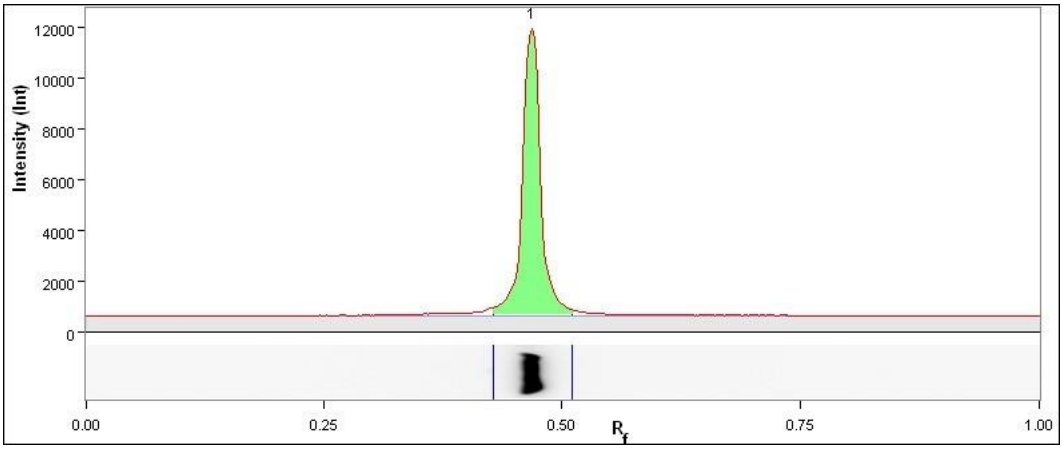

Band No.	Band Label	Mol. Wt. (KDa)	Relative Front	Volume (Int)	Abs. Quant.	Rel. Quant.	Band %	Lane %
1		N/A	0.469	12,965,452	N/A	N/A	100.0	92.7

Band Detection	Automatically detected bands with custom sensitivity: 95
Lane Background	Lane background subtracted with disk size: 10
Lane Width	7.38 mm

Lane 7

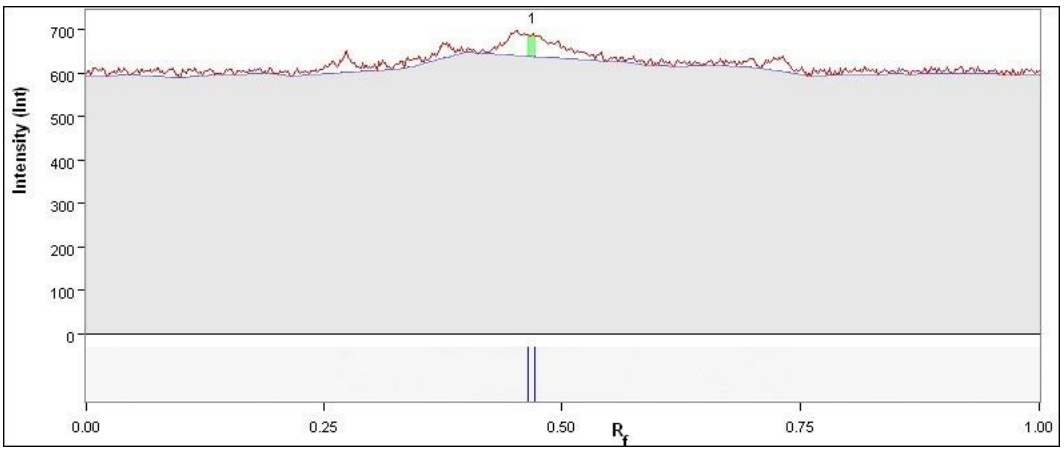

Band No.	Band Label	Mol. Wt. (KDa)	Relative Front	Volume (Int)	Abs. Quant.	Rel. Quant.	Band %	Lane %
1		N/A	0.470	20,410	N/A	N/A	100.0	3.5

Band Detection	Automatically detected bands with custom sensitivity: 95
Lane Background	Lane background subtracted with disk size: 10
Lane Width	6.76 mm

Lane 8

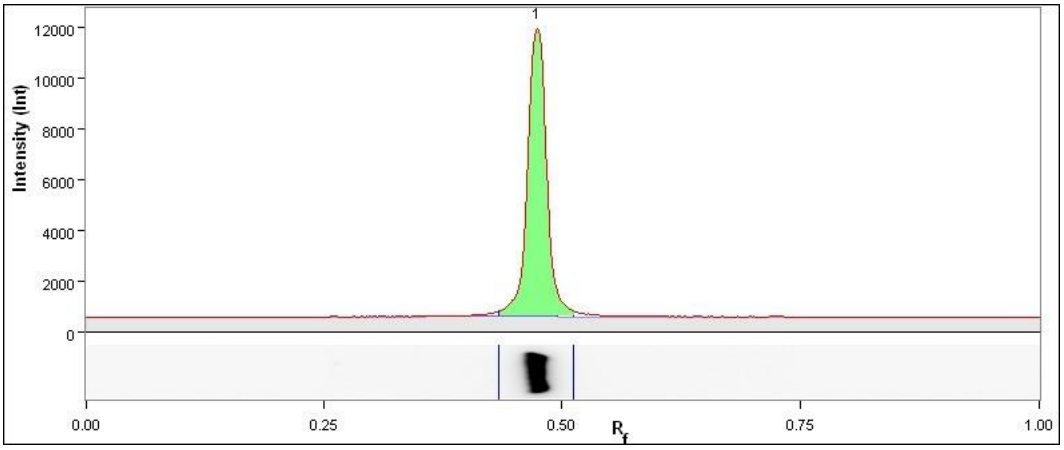

Band No.	Band Label	Mol. Wt. (KDa)	Relative Front	Volume (Int)	Abs. Quant.	Rel. Quant.	Band %	Lane %
1		N/A	0.475	14,555,781	N/A	N/A	100.0	94.5

Band Detection	Automatically detected bands with custom sensitivity: 95
Lane Background	Lane background subtracted with disk size: 10
Lane Width	7.38 mm

Lane 9

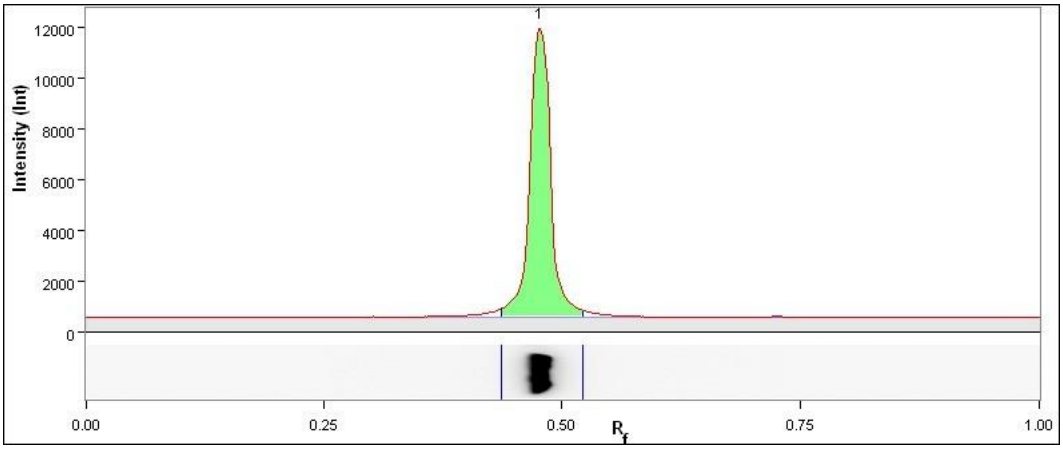

Band No.	Band Label	Mol. Wt. (KDa)	Relative Front	Volume (Int)	Abs. Quant.	Rel. Quant.	Band %	Lane %
1		N/A	0.477	17,969,360	N/A	N/A	100.0	93.5

Band Detection	Automatically detected bands with custom sensitivity: 95
Lane Background	Lane background subtracted with disk size: 10
Lane Width	8.32 mm

MDA-MB-468, H.swa and N.naj PY20 Analysis:

Image Report: 2016-08-19 MDA-MB-468 H.swa, (top) N.naj (bottom) py20 60s

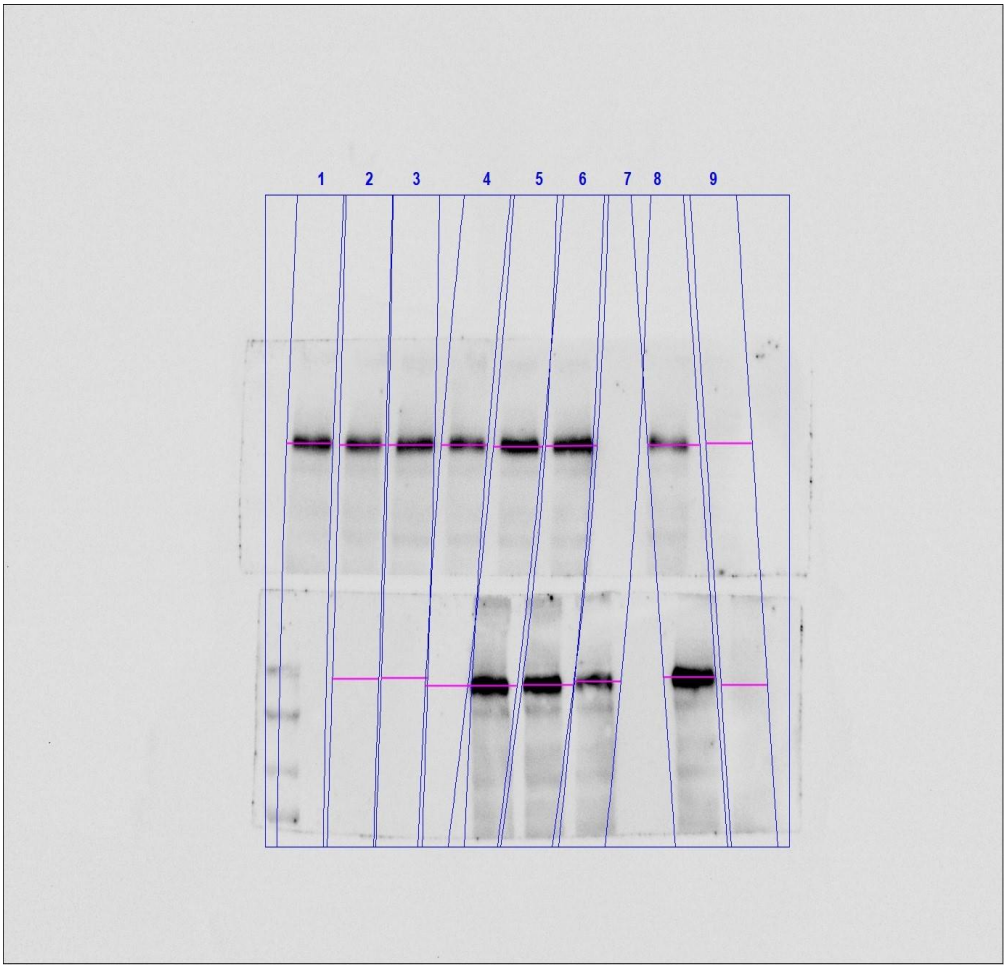

Acquisition Information

Imager	ChemiDoc™ Touch
Exposure Time (sec)	60.000 (Manual)
Serial Number	732BR1296
Software Version	1.1.0.04
Application	Chemiluminescence
Excitation Source	No Illumination
Emission Filter	No Filter
Binning	2x2

Image Information

Acquisition Date	19/08/2016 21:23:37
User Name	
Image Area (mm)	X: 155.0 Y: 124.1
Pixel Size (um)	X: 112.4 Y: 112.4

Data Range (Int)	501 - 11396

Analysis Settings

Detection	Lane detection: Automatically detected lanes with manual adjustments Band detection: Bands detected with different sensitivity per lane Manually adjusted bands Lane Background Subtraction: Lane background subtracted with disk size: 10 Lane width: Variable

Lane And Band Analysis

Lane 1

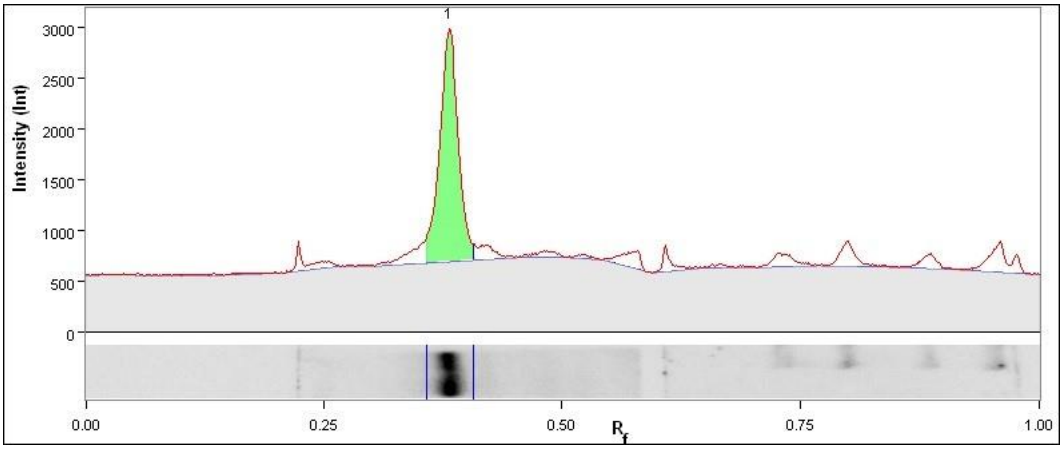

Band No.	Band Label	Mol. Wt. (KDa)	Relative Front	Volume (Int)	Abs. Quant.	Rel. Quant.	Band %	Lane %
1		N/A	0.381	2,861,760	N/A	N/A	100.0	55.1

Band Detection	Automatically detected bands with sensitivity: Low
Lane Background	Lane background subtracted with disk size: 10
Lane Width	7.19 mm

Lane 2

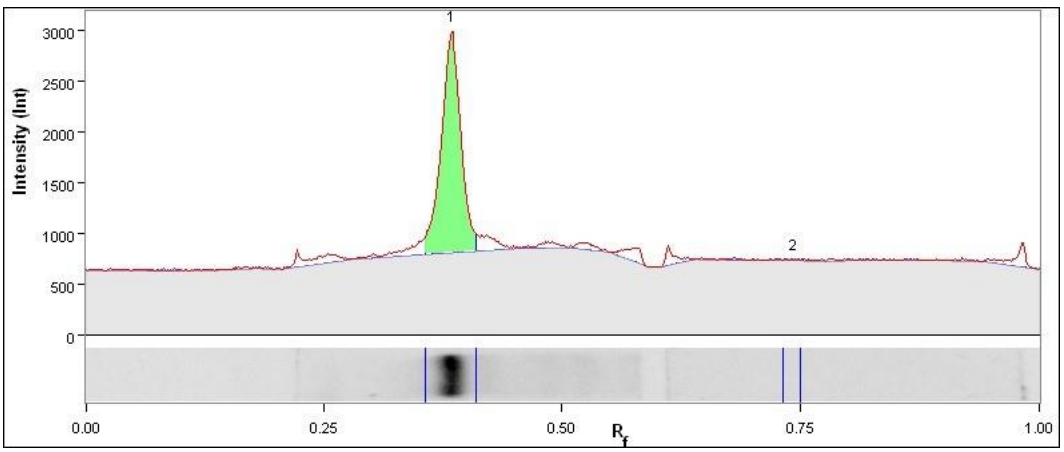

Band No.	Band Label	Mol. Wt. (KDa)	Relative Front	Volume (Int)	Abs. Quant.	Rel. Quant.	Band %	Lane %
1		N/A	0.384	2,525,312	N/A	N/A	99.5	66.1
2		N/A	0.743	11,648	N/A	N/A	0.5	0.3

Band Detection	Automatically detected bands with sensitivity: Low
Lane Background	Lane background subtracted with disk size: 10
Lane Width	7.19 mm

Lane 3

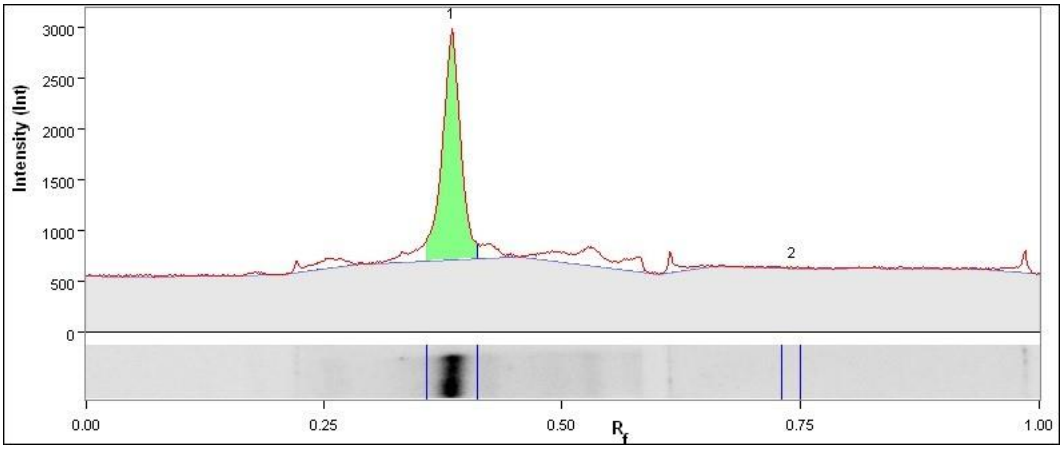

Band No.	Band Label	Mol. Wt. (KDa)	Relative Front	Volume (Int)	Abs. Quant.	Rel. Quant.	Band %	Lane %
1		N/A	0.384	2,847,360	N/A	N/A	99.6	60.0
2		N/A	0.741	11,968	N/A	N/A	0.4	0.3

Band Detection	Automatically detected bands with sensitivity: Low
Lane Background	Lane background subtracted with disk size: 10
Lane Width	7.19 mm

Lane 4

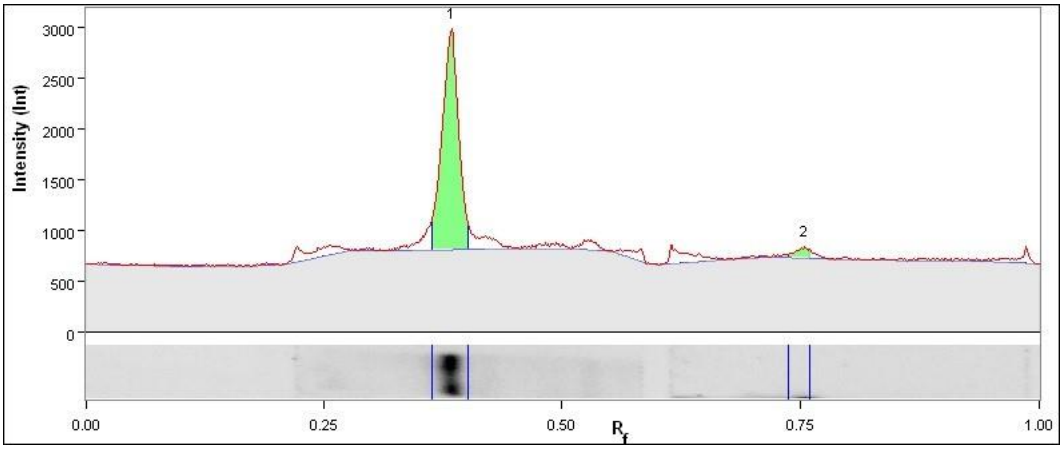

Band No.	Band Label	Mol. Wt. (KDa)	Relative Front	Volume (Int)	Abs. Quant.	Rel. Quant.	Band %	Lane %
1		N/A	0.384	2,146,560	N/A	N/A	95.9	57.7
2		N/A	0.753	90,944	N/A	N/A	4.1	2.4
Lane Background		Lane background subtracted with disk size: 10						
Lane Width		7.19 mm						

Lane 5

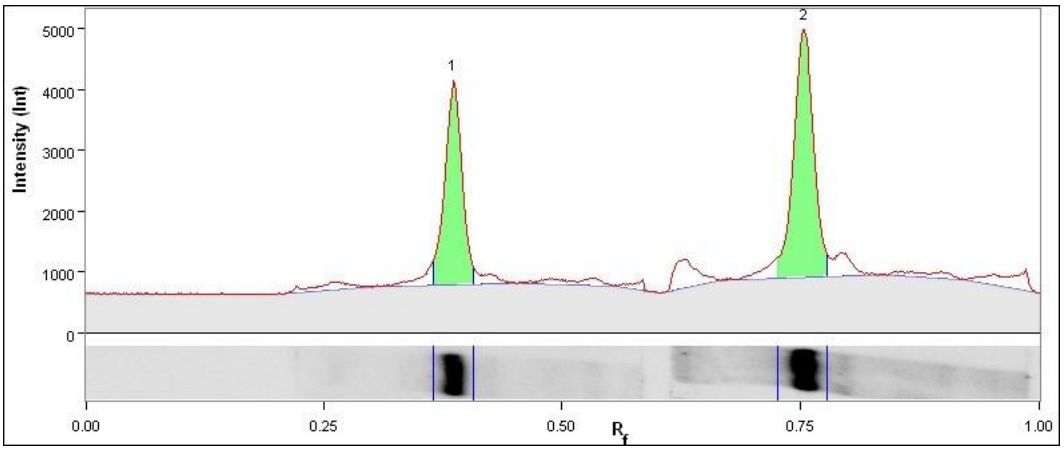

Band No.	Band Label	Mol. Wt. (KDa)	Relative Front	Volume (Int)	Abs. Quant.	Rel. Quant.	Band %	Lane %
1		N/A	0.387	3,678,460	N/A	N/A	41.8	29.3
2		N/A	0.753	5,124,140	N/A	N/A	58.2	40.8
Lane Background		Lane background subtracted with disk size: 10						
Lane Width		7.64 mm						

Lane 6

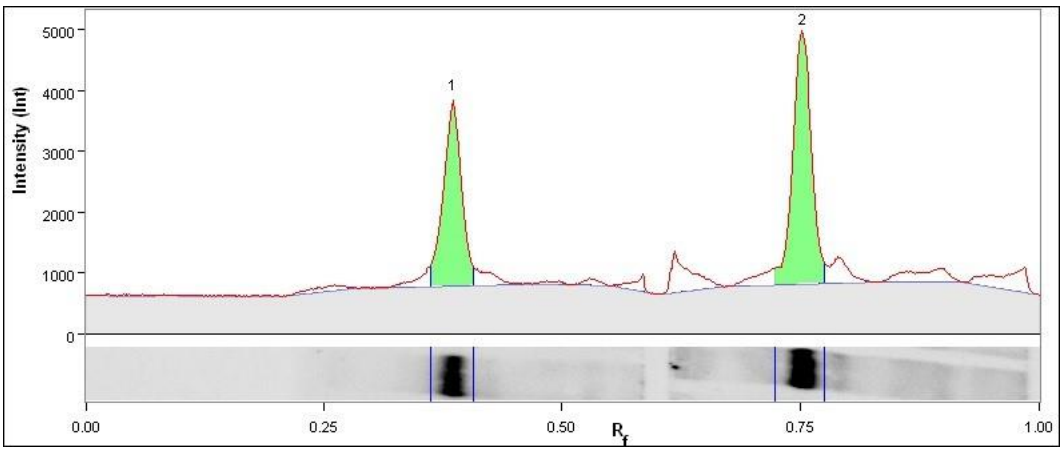

Band No.	Band Label	Mol. Wt. (KDa)	Relative Front	Volume (Int)	Abs. Quant.	Rel. Quant.	Band %	Lane %
1		N/A	0.385	3,743,404	N/A	N/A	42.0	27.6
2		N/A	0.752	5,179,450	N/A	N/A	58.0	38.2
Band Detection		Automatically detected bands with sensitivity: Low						

Lane Background	Lane background subtracted with disk size: 10
Lane Width	7.98 mm

Lane 7

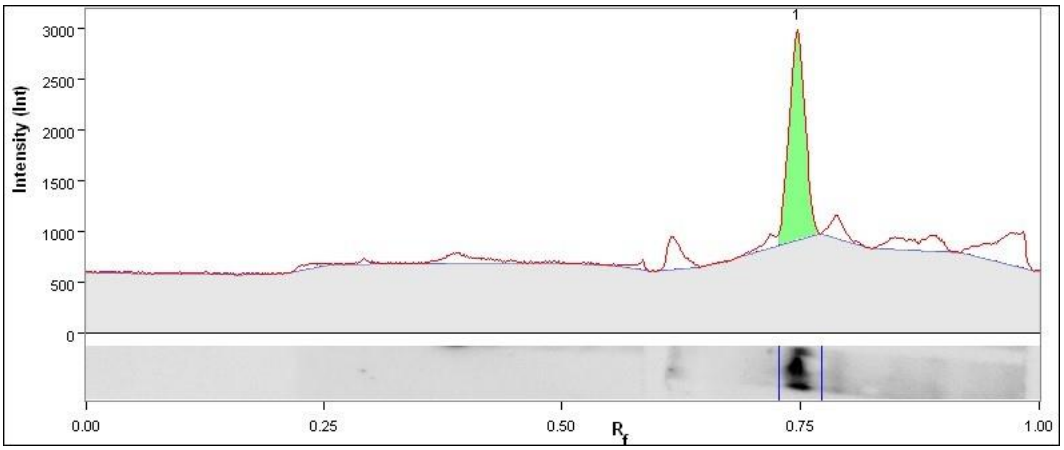

Band No.	Band Label	Mol. Wt. (KDa)	Relative Front	Volume (Int)	Abs. Quant.	Rel. Quant.	Band %	Lane %
1		N/A	0.747	2,109,952	N/A	N/A	100.0	46.7

Band Detection	Automatically detected bands with sensitivity: Low
Lane Background	Lane background subtracted with disk size: 10
Lane Width	7.19 mm

Lane 8

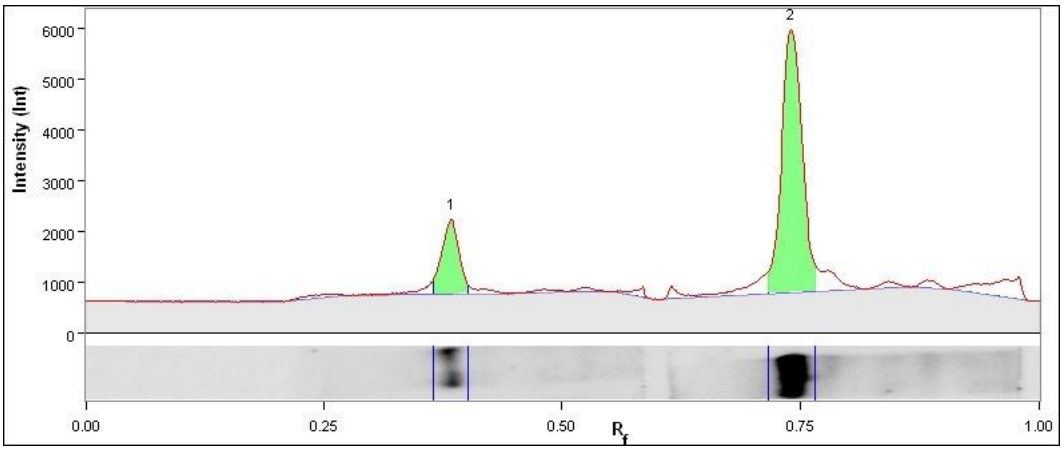

Band No.	Band Label	Mol. Wt. (KDa)	Relative Front	Volume (Int)	Abs. Quant.	Rel. Quant.	Band %	Lane %
1		N/A	0.384	1,749,744	N/A	N/A	19.6	13.9
2		N/A	0.740	7,190,280	N/A	N/A	80.4	57.2

Band Detection	Automatically detected bands with sensitivity: Low
Lane Background	Lane background subtracted with disk size: 10
Lane Width	8.09 mm

Lane 9

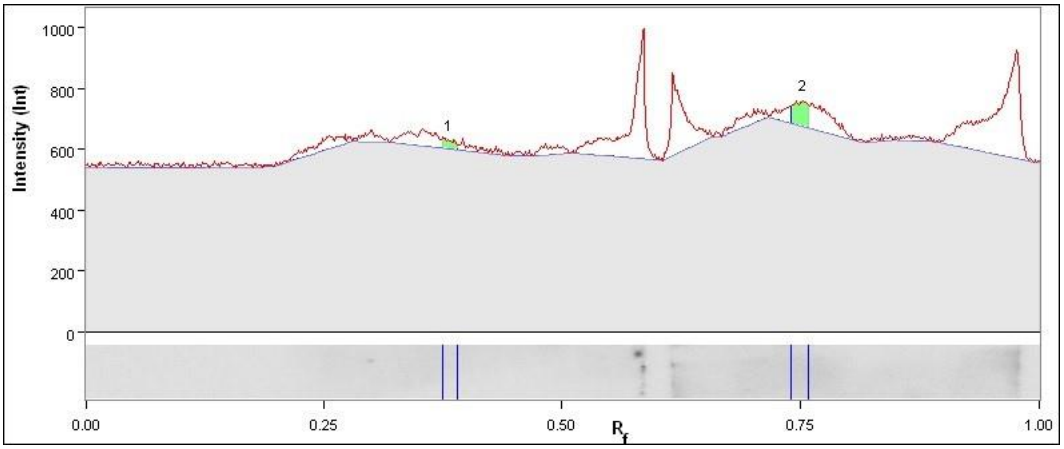

Band No.	Band Label	Mol. Wt. (KDa)	Relative Front	Volume (Int)	Abs. Quant.	Rel. Quant.	Band %	Lane %
1		N/A	0.381	25,600	N/A	N/A	23.4	1.2
2		N/A	0.752	83,776	N/A	N/A	76.6	3.9

Band Detection	Automatically detected bands with sensitivity: Low
Lane Background	Lane background subtracted with disk size: 10
Lane Width	7.19 mm

MDA-MB-468, H.swa and N.naj Actin Analysis:

Image Report: 2016-08-19 H.swa (top), N.naj (bottom) actin 60s

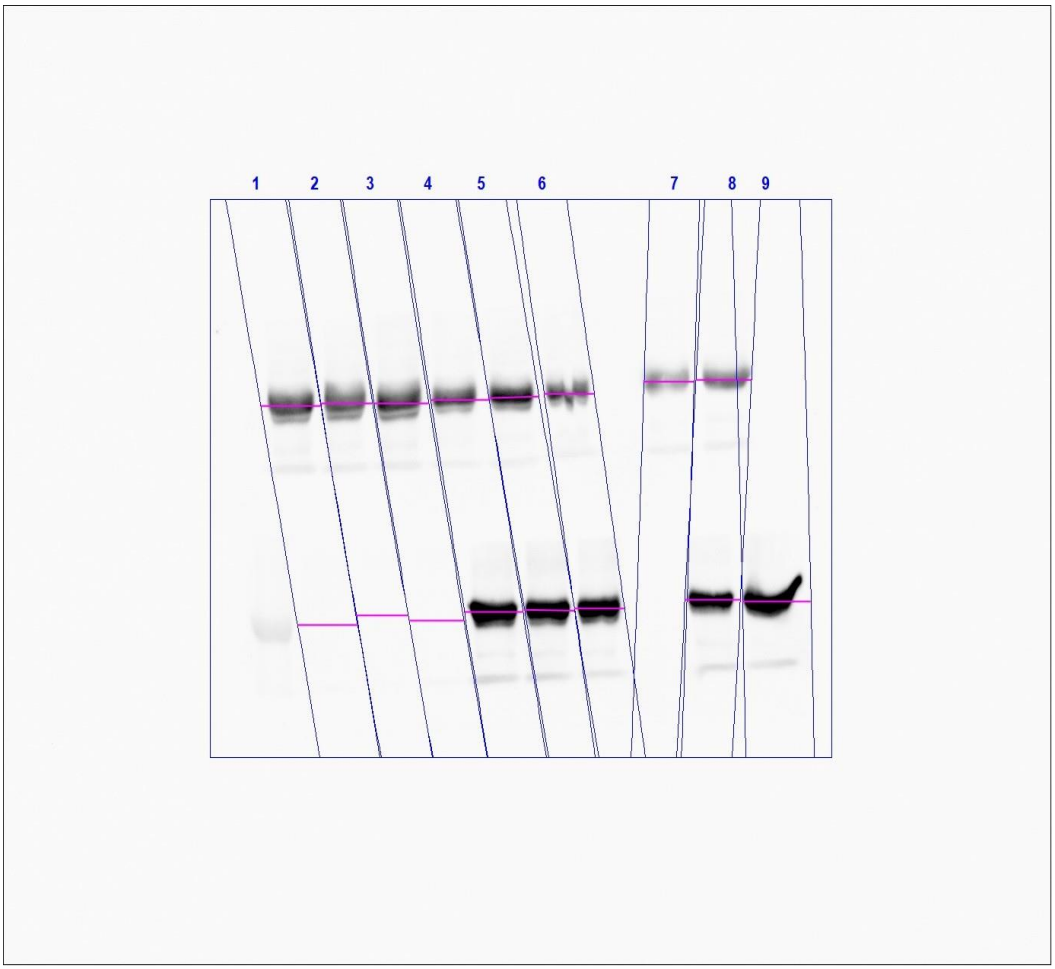

Acquisition Information

Imager	ChemiDoc™ Touch
Exposure Time (sec)	60.000 (Manual)
Serial Number	732BR1296
Software Version	1.1.0.04
Application	Chemiluminescence
Excitation Source	No Illumination
Emission Filter	No Filter
Binning	2x2

Image Information

Acquisition Date	19/08/2016 21:03:14
User Name	
Image Area (mm)	X: 155.0 Y: 124.1
Pixel Size (um)	X: 112.4 Y: 112.4

Data Range (Int)	503 - 43677

Analysis Settings

Detection	Lane detection: Automatically detected lanes with manual adjustments Band detection: Automatically detected bands with sensitivity: Low Manually adjusted bands Lane Background Subtraction: Lane background subtracted with disk size: 10 Lane width: Variable

Lane And Band Analysis

Lane 1

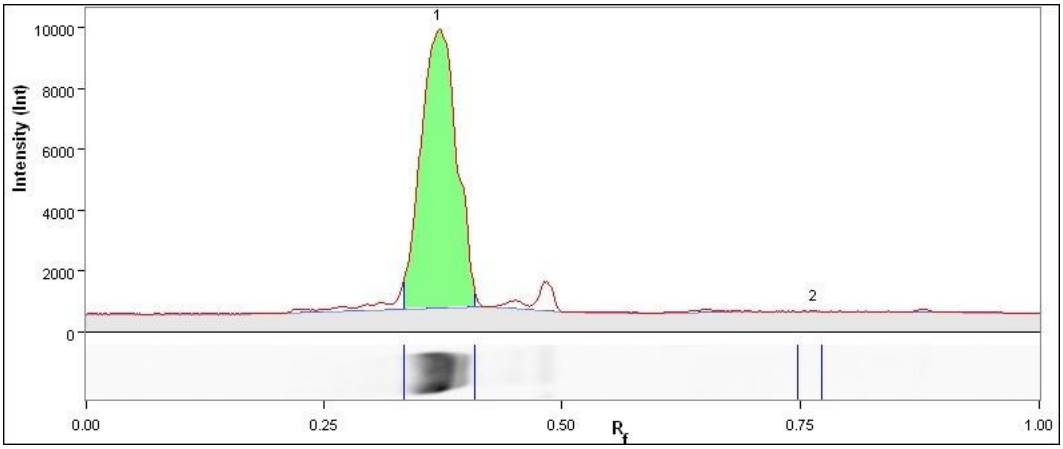

Band No.	Band Label	Mol. Wt. (KDa)	Relative Front	Volume (Int)	Abs. Quant.	Rel. Quant.	Band %	Lane %
1		N/A	0.371	21,981,829	N/A	N/A	99.9	87.9
2		N/A	0.763	18,565	N/A	N/A	0.1	0.1

Band Detection	Automatically detected bands with sensitivity: Low
Lane Background	Lane background subtracted with disk size: 10
Lane Width	8.88 mm

Lane 2

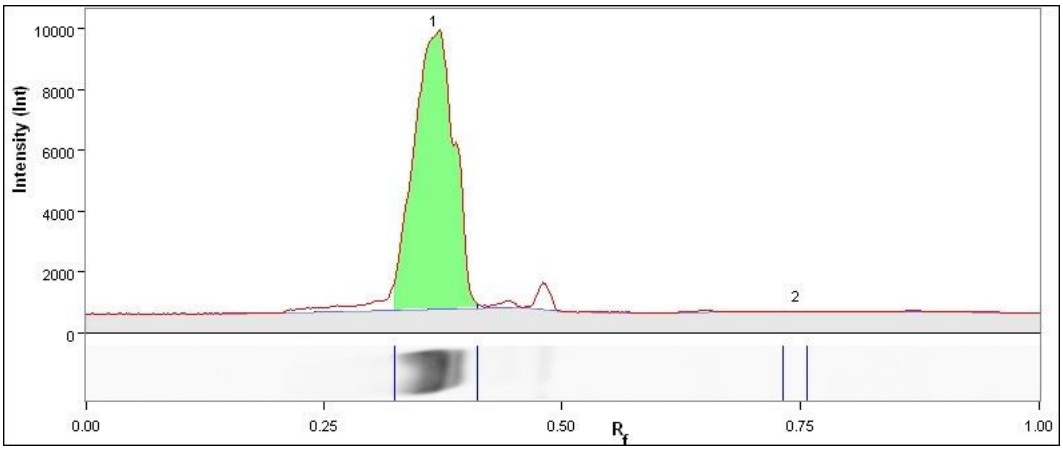

Band No.	Band Label	Mol. Wt. (KDa)	Relative Front	Volume (Int)	Abs. Quant.	Rel. Quant.	Band %	Lane %
1		N/A	0.366	20,161,320	N/A	N/A	100.0	89.5
2		N/A	0.746	7,616	N/A	N/A	0.0	0.0

Band Detection	Automatically detected bands with sensitivity: Low
Lane Background	Lane background subtracted with disk size: 10
Lane Width	7.64 mm

Lane 3

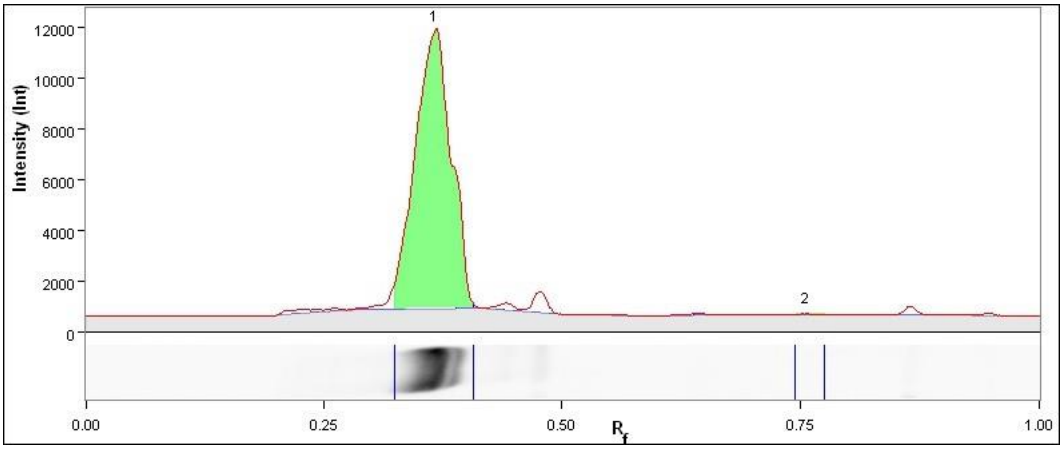

Band No.	Band Label	Mol. Wt. (KDa)	Relative Front	Volume (Int)	Abs. Quant.	Rel. Quant.	Band %	Lane %
1		N/A	0.366	23,447,736	N/A	N/A	99.9	90.5
2		N/A	0.755	28,584	N/A	N/A	0.1	0.1

Band Detection	Automatically detected bands with sensitivity: Low
Lane Background	Lane background subtracted with disk size: 10
Lane Width	8.09 mm

Lane 4

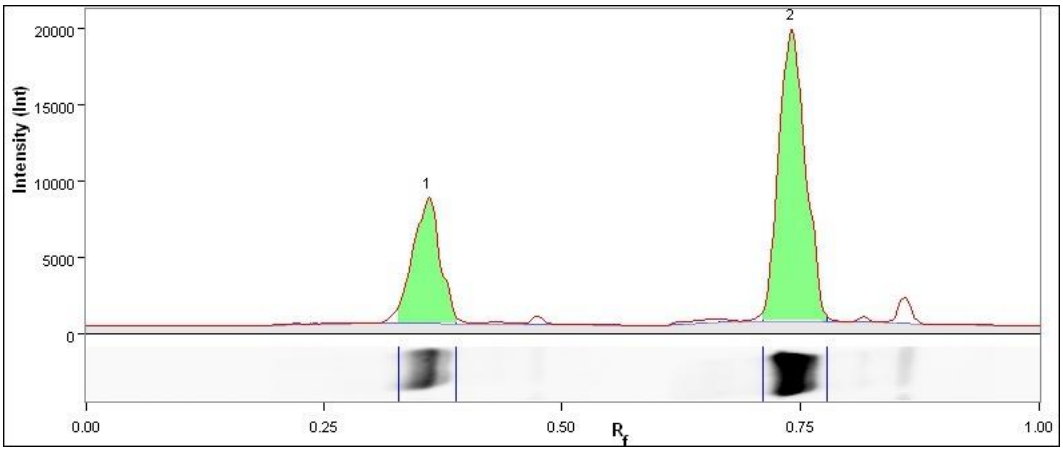

Band No.	Band Label	Mol. Wt. (KDa)	Relative Front	Volume (Int)	Abs. Quant.	Rel. Quant.	Band %	Lane %
1		N/A	0.360	16,768,136	N/A	N/A	30.4	27.8

2		N/A	0.740	38,456,264	N/A	N/A	69.6	63.7
Band Detection		Automatically detected bands with sensitivity: Low						
Lane Background		Lane background subtracted with disk size: 10						
Lane Width		8.65 mm						

Lane 5

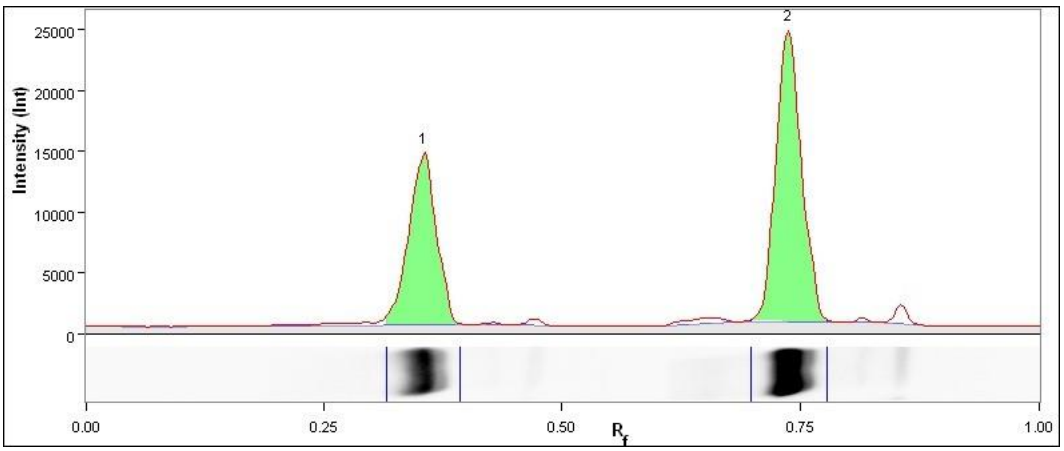

Band No.	Band Label	Mol. Wt. (KDa)	Relative Front	Volume (Int)	Abs. Quant.	Rel. Quant.	Band %	Lane %
1		N/A	0.355	21,868,704	N/A	N/A	38.8	36.0
2		N/A	0.737	34,559,184	N/A	N/A	61.2	56.9
Band Detection		Automatically detected bands with sensitivity: Low						
Lane Background		Lane background subtracted with disk size: 10						
Lane Width		7.42 mm						

Lane 6

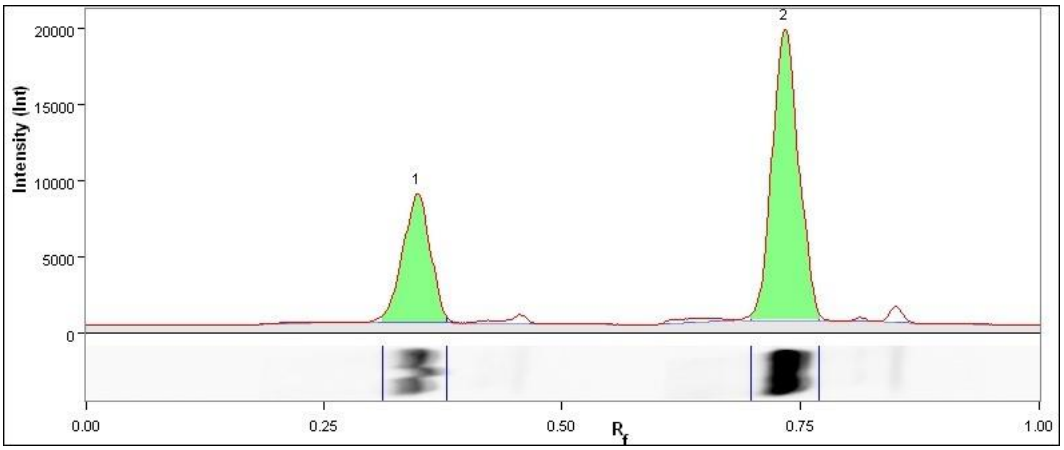

Band No.	Band Label	Mol. Wt. (KDa)	Relative Front	Volume (Int)	Abs. Quant.	Rel. Quant.	Band %	Lane %
1		N/A	0.349	14,556,498	N/A	N/A	31.4	29.2
2		N/A	0.734	31,832,790	N/A	N/A	68.6	63.8
Band Detection		Automatically detected bands with sensitivity: Low						

Lane Background	Lane background subtracted with disk size: 10
Lane Width	7.42 mm

Lane 7

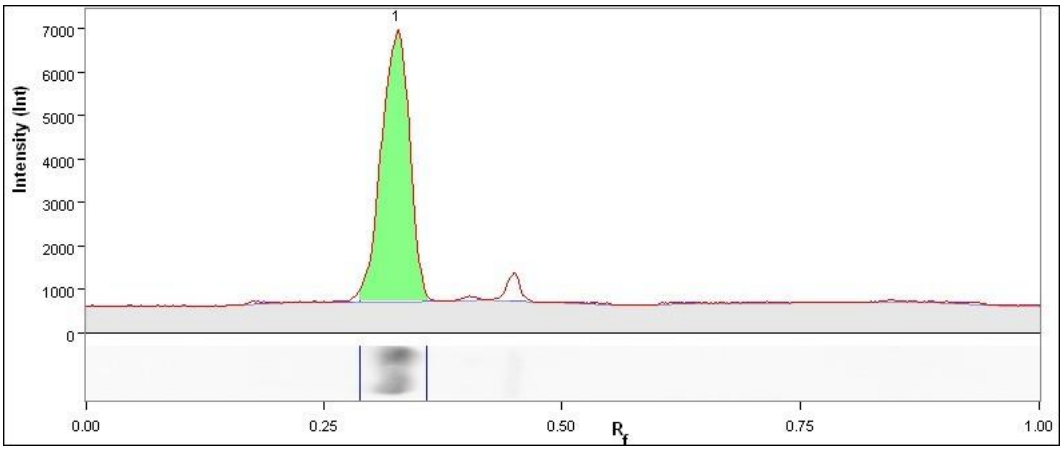

Band No.	Band Label	Mol. Wt. (KDa)	Relative Front	Volume (Int)	Abs. Quant.	Rel. Quant.	Band %	Lane %
1		N/A	0.327	9,371,340	N/A	N/A	100.0	88.4

Band Detection	Automatically detected bands with sensitivity: Low
Lane Background	Lane background subtracted with disk size: 10
Lane Width	7.42 mm

Lane 8

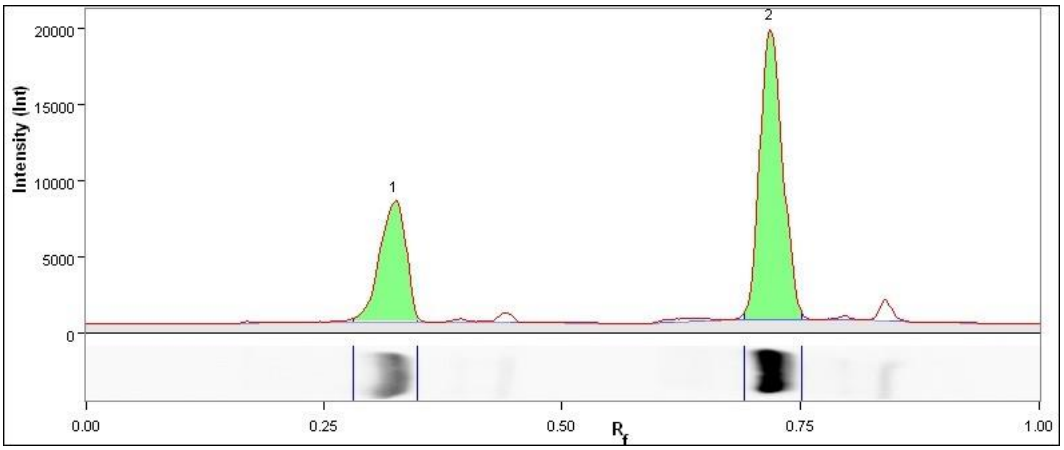

Band No.	Band Label	Mol. Wt. (KDa)	Relative Front	Volume (Int)	Abs. Quant.	Rel. Quant.	Band %	Lane %
1		N/A	0.324	12,721,126	N/A	N/A	32.5	29.9
2		N/A	0.718	26,450,674	N/A	N/A	67.5	62.2

Band Detection	Automatically detected bands with sensitivity: Low
Lane Background	Lane background subtracted with disk size: 10
Lane Width	8.21 mm

Lane 9

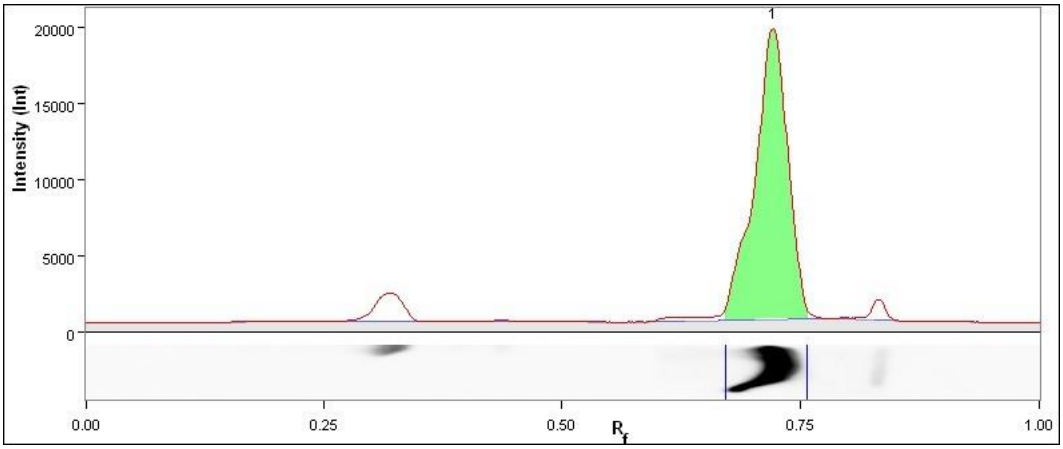

Band No.	Band Label	Mol. Wt. (KDa)	Relative Front	Volume (Int)	Abs. Quant.	Rel. Quant.	Band %	Lane %
1		N/A	0.721	45,849,870	N/A	N/A	100.0	86.3

Band Detection	Automatically detected bands with sensitivity: Low
Lane Background	Lane background subtracted with disk size: 10
Lane Width	10.12 mm

MDA-MB-468, A.gen PY20 Analysis:

Image Report: 2016-08-19 MDA-MB-468 A.gen py20 60s

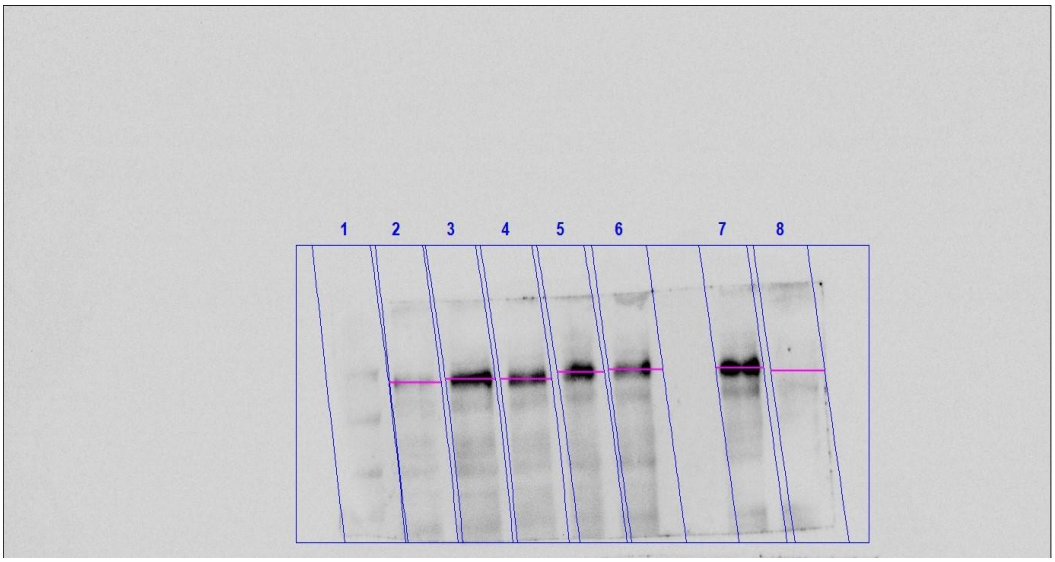

Acquisition Information

Imager	ChemiDoc™ Touch
Exposure Time (sec)	60.000 (Manual)
Serial Number	732BR1296

Software Version	1.1.0.04
Application	Chemiluminescence
Excitation Source	No Illumination
Emission Filter	No Filter
Binning	2x2

Image Information

Acquisition Date	19/08/2016 21:12:54
User Name	
Image Area (mm)	X: 155.0 Y: 124.1
Pixel Size (um)	X: 112.4 Y: 112.4
Data Range (Int)	501 - 9060

Analysis Settings

Detection	Lane detection: Automatically detected lanes with manual adjustments Band detection: Manually adjusted bands Lane Background Subtraction: Lane background subtracted with disk size: 10 Lane width: Variable

Lane And Band Analysis

Lane 1

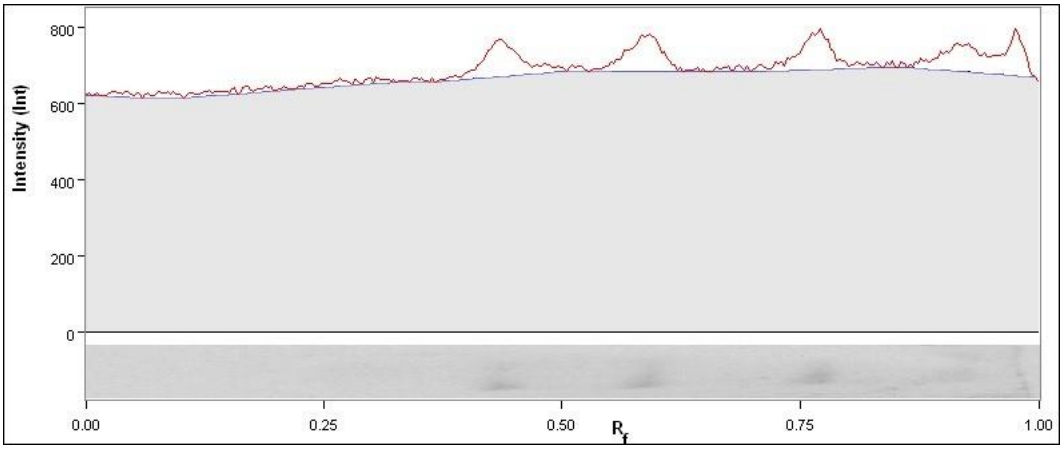

Band No.	Band Label	Mol. Wt. (KDa)	Relative Front	Volume (Int)	Abs. Quant.	Rel. Quant.	Band %	Lane %

Lane Background	Lane background subtracted with disk size: 10
Lane Width	9.33 mm

Lane 2

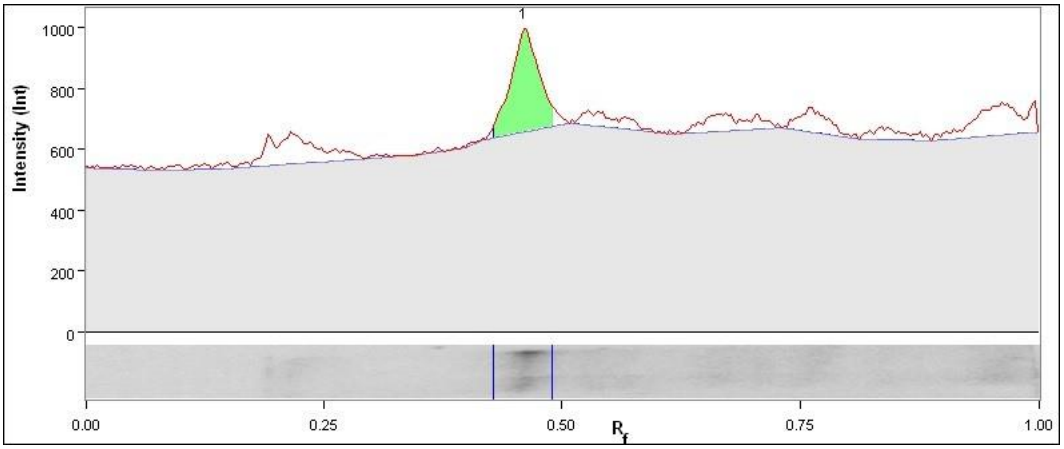

Band No.	Band Label	Mol. Wt. (KDa)	Relative Front	Volume (Int)	Abs. Quant.	Rel. Quant.	Band %	Lane %
1		N/A	0.462	325,611	N/A	N/A	100.0	31.0

Lane Background	Lane background subtracted with disk size: 10
Lane Width	7.76 mm

Lane 3

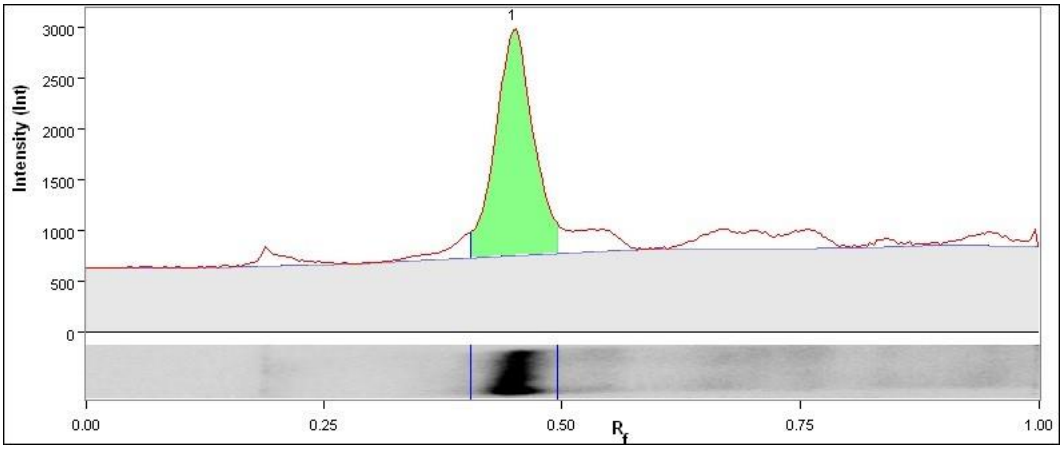

Band No.	Band Label	Mol. Wt. (KDa)	Relative Front	Volume (Int)	Abs. Quant.	Rel. Quant.	Band %	Lane %
1		N/A	0.450	2,365,770	N/A	N/A	100.0	61.3

Lane Background	Lane background subtracted with disk size: 10
Lane Width	7.42 mm

Lane 4

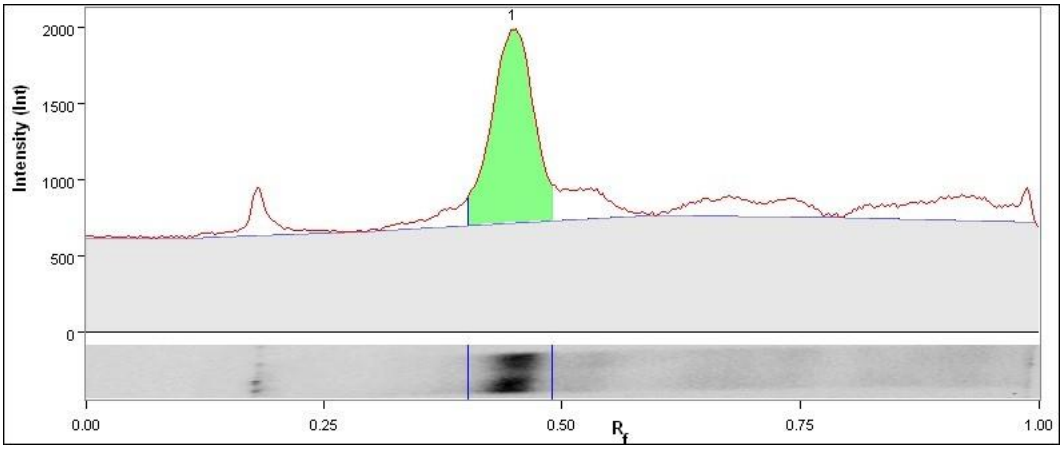

Band No.	Band Label	Mol. Wt. (KDa)	Relative Front	Volume (Int)	Abs. Quant.	Rel. Quant.	Band %	Lane %
1		N/A	0.450	1,581,408	N/A	N/A	100.0	49.1

Lane Background	Lane background subtracted with disk size: 10
Lane Width	7.64 mm

Lane 5

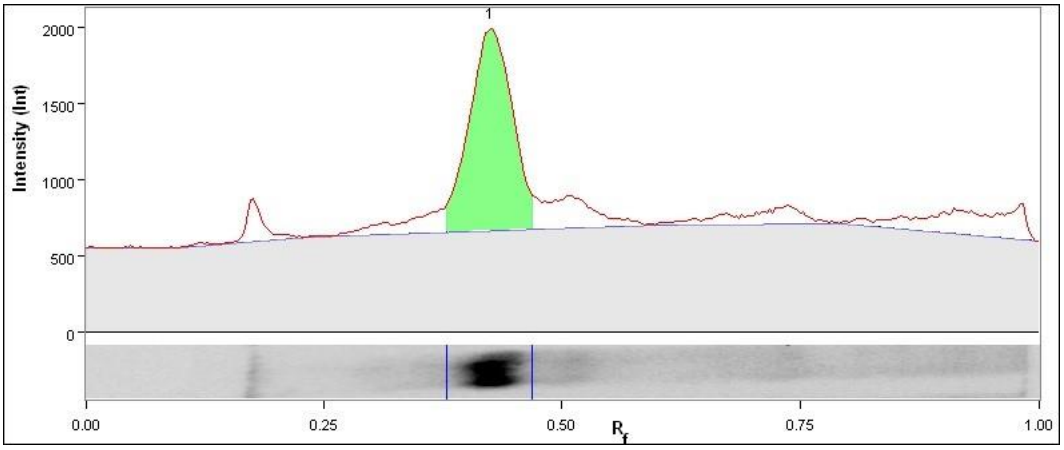

Band No.	Band Label	Mol. Wt. (KDa)	Relative Front	Volume (Int)	Abs. Quant.	Rel. Quant.	Band %	Lane %
1		N/A	0.427	1,736,310	N/A	N/A	100.0	53.6

Lane Background	Lane background subtracted with disk size: 10
Lane Width	6.97 mm

Lane 6

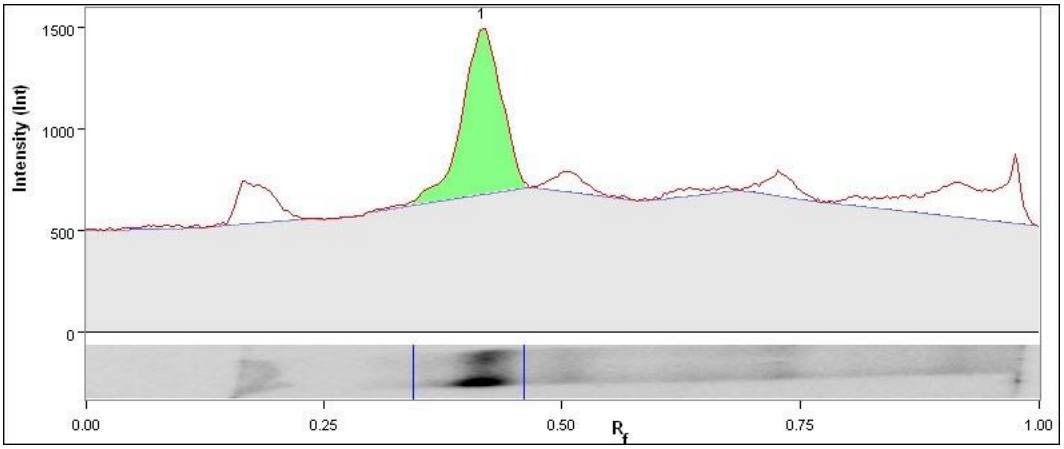

Band No.	Band Label	Mol. Wt. (KDa)	Relative Front	Volume (Int)	Abs. Quant.	Rel. Quant.	Band %	Lane %
1		N/A	0.418	1,252,296	N/A	N/A	100.0	46.9

Lane Background	Lane background subtracted with disk size: 10
Lane Width	8.09 mm

Lane 7

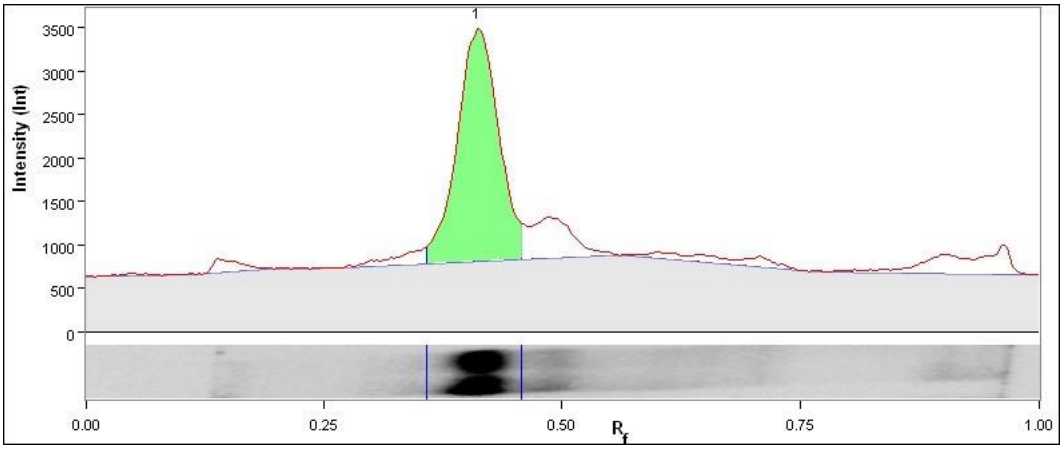

Band No.	Band Label	Mol. Wt. (KDa)	Relative Front	Volume (Int)	Abs. Quant.	Rel. Quant.	Band %	Lane %
1		N/A	0.412	2,950,731	N/A	N/A	100.0	64.3

Lane Background	Lane background subtracted with disk size: 10
Lane Width	7.08 mm

Lane 8

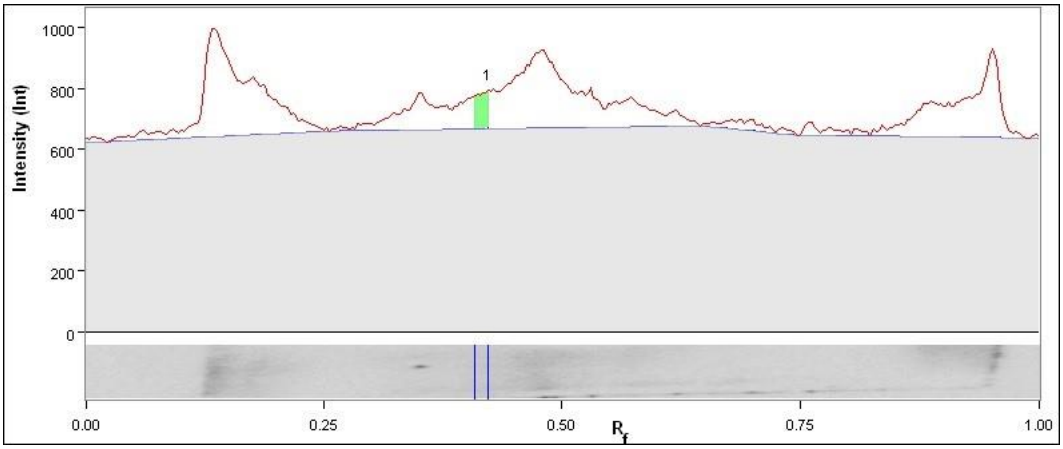

Band No.	Band Label	Mol. Wt. (KDa)	Relative Front	Volume (Int)	Abs. Quant.	Rel. Quant.	Band %	Lane %
1		N/A	0.424	51,049	N/A	N/A	100.0	2.8

Lane Background	Lane background subtracted with disk size: 10
Lane Width	7.98 mm

MDA-MB-468, A.gen Actin Analysis:

Image Report: 2016-08-19 MDA-MB-468 A.gen Actin 60s

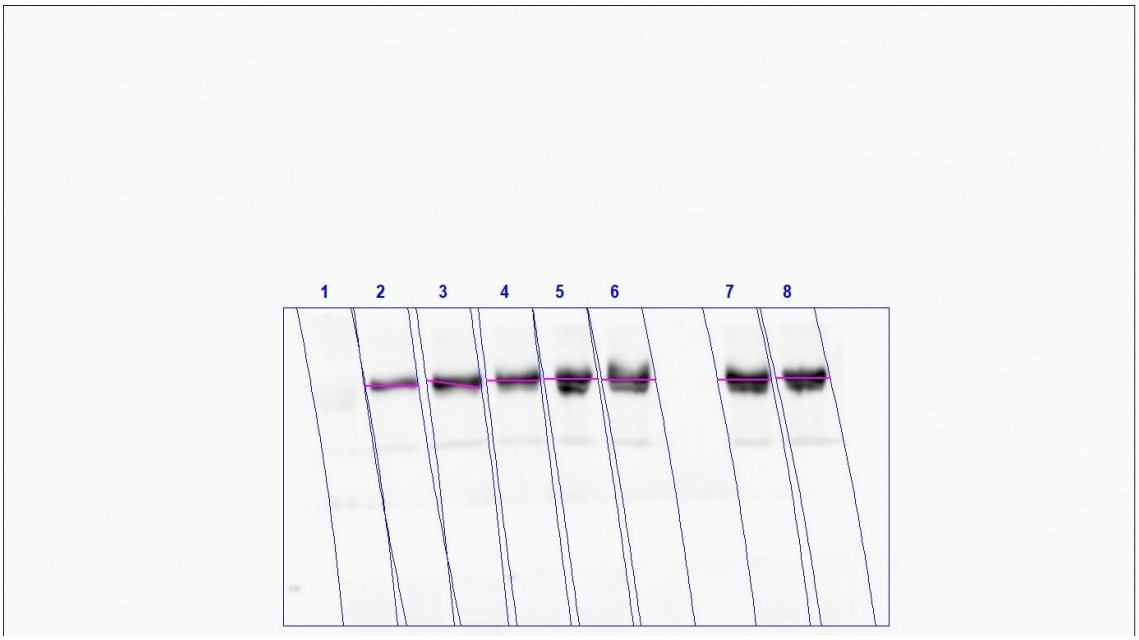

Acquisition Information

Imager	ChemiDoc™ Touch
Exposure Time (sec)	60.000 (Manual)
Serial Number	732BR1296
Software Version	1.1.0.04
Application	Chemiluminescence
Excitation Source	No Illumination
Emission Filter	No Filter
Binning	2x2

Image Information

Acquisition Date	19/08/2016 21:06:19
User Name	
Image Area (mm)	X: 155.0 Y: 124.1
Pixel Size (um)	X: 112.4 Y: 112.4
Data Range (Int)	503 - 44187

Analysis Settings

Detection	Lane detection: Automatically detected lanes with manual adjustments Band detection: Manually adjusted bands Lane Background Subtraction: Lane background subtracted with disk size: 10 Lane width: 7.42 mm

Lane And Band Analysis

Lane 1

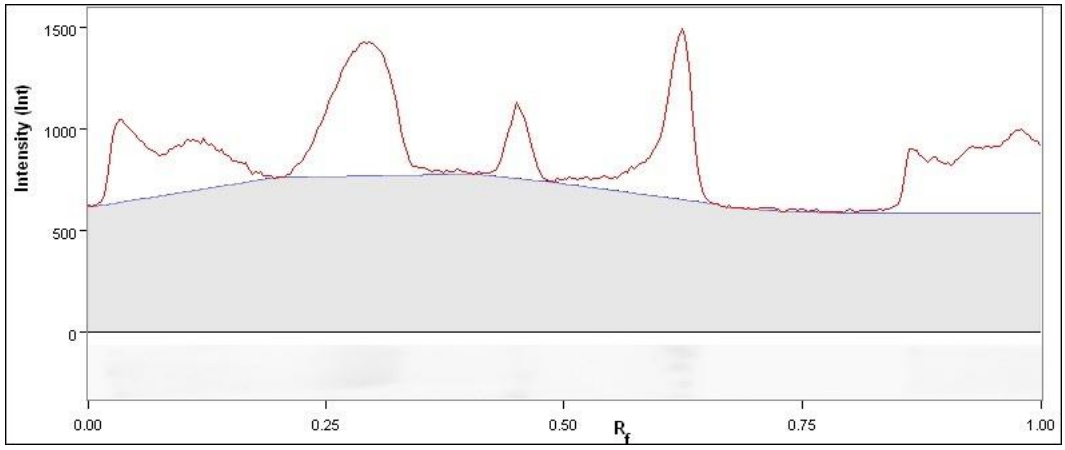

Band No.	Band Label	Mol. Wt. (KDa)	Relative Front	Volume (Int)	Abs. Quant.	Rel. Quant.	Band %	Lane %

Lane Background	Lane background subtracted with disk size: 10
Lane Width	7.42 mm

Lane 2

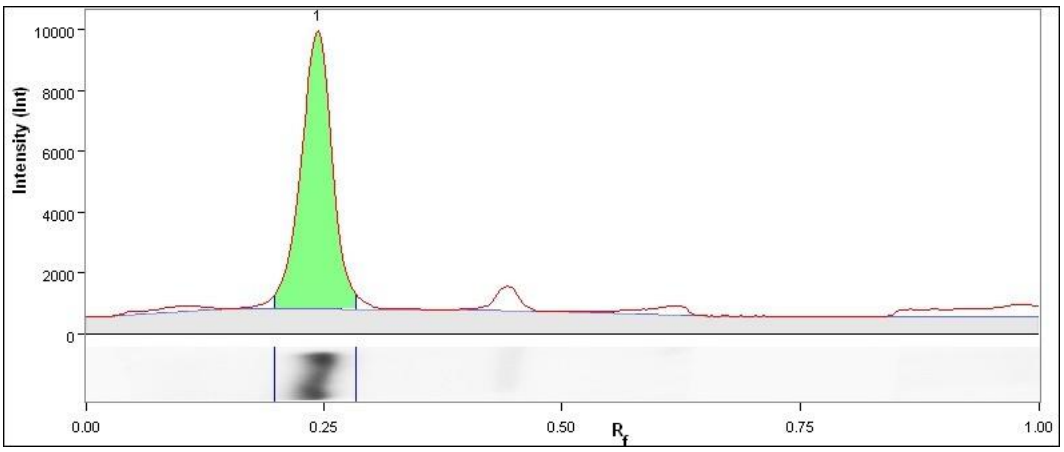

Band No.	Band Label	Mol. Wt. (KDa)	Relative Front	Volume (Int)	Abs. Quant.	Rel. Quant.	Band %	Lane %
1		N/A	0.247	9,943,626	N/A	N/A	100.0	75.9

Lane Background	Lane background subtracted with disk size: 10
Lane Width	7.42 mm

Lane 3

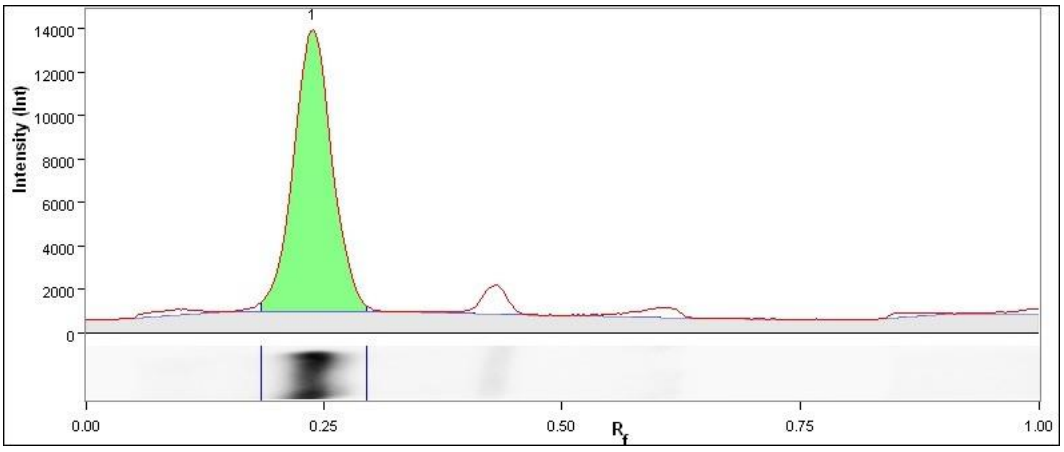

Band No.	Band Label	Mol. Wt. (KDa)	Relative Front	Volume (Int)	Abs. Quant.	Rel. Quant.	Band %	Lane %
1		N/A	0.241	15,998,334	N/A	N/A	100.0	84.7

Lane Background	Lane background subtracted with disk size: 10
Lane Width	7.42 mm

Lane 4

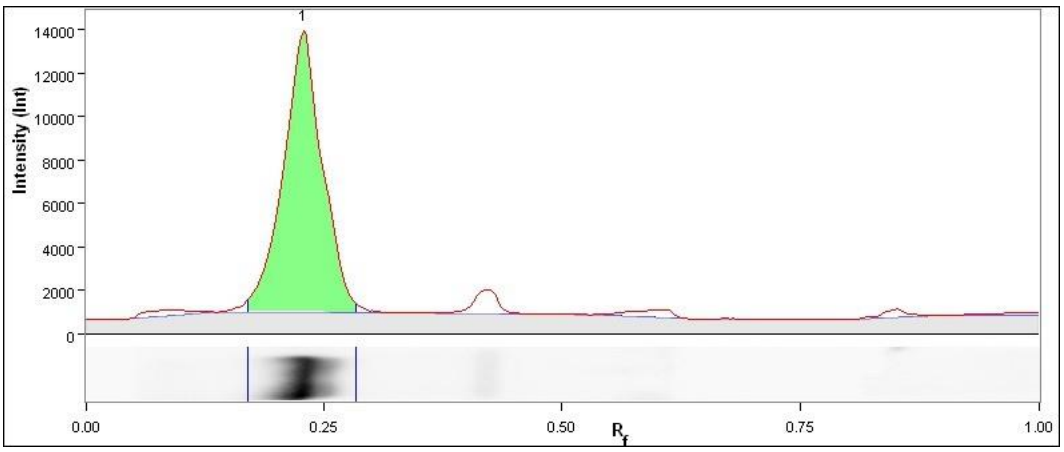

Band No.	Band Label	Mol. Wt. (KDa)	Relative Front	Volume (Int)	Abs. Quant.	Rel. Quant.	Band %	Lane %
1		N/A	0.230	15,361,698	N/A	N/A	100.0	86.0

Lane Background	Lane background subtracted with disk size: 10
Lane Width	7.42 mm

Lane 5

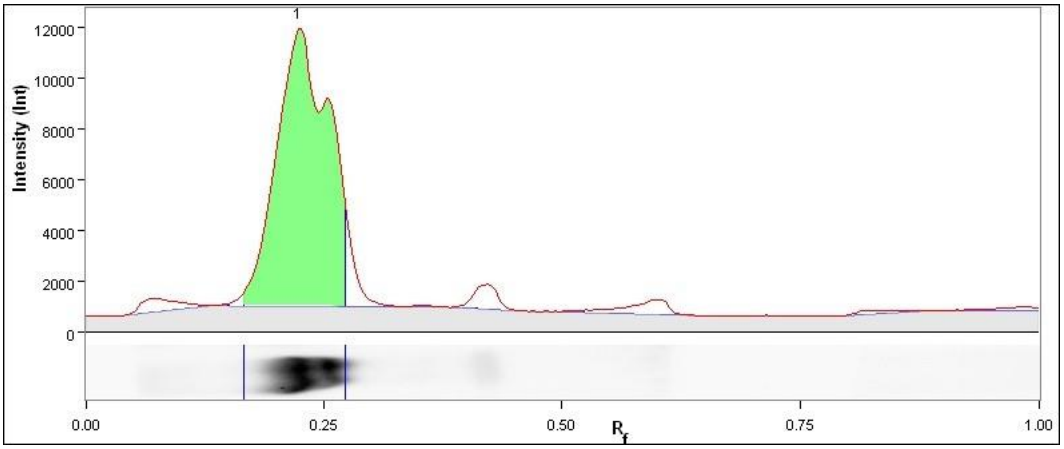

Band No.	Band Label	Mol. Wt. (KDa)	Relative Front	Volume (Int)	Abs. Quant.	Rel. Quant.	Band %	Lane %
1		N/A	0.225	18,427,398	N/A	N/A	100.0	84.1

Lane Background	Lane background subtracted with disk size: 10
Lane Width	7.42 mm

Lane 6

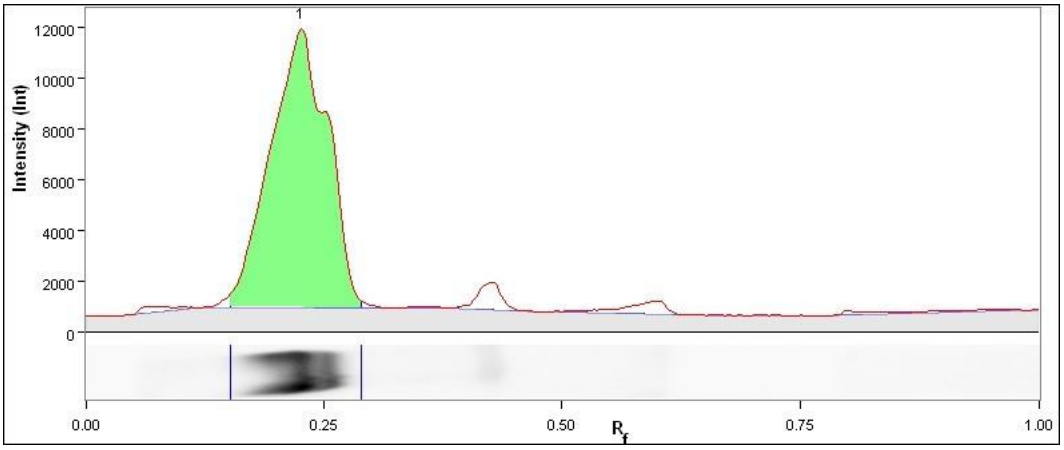

Band No.	Band Label	Mol. Wt. (KDa)	Relative Front	Volume (Int)	Abs. Quant.	Rel. Quant.	Band %	Lane %
1		N/A	0.227	20,039,514	N/A	N/A	100.0	89.2

Lane Background	Lane background subtracted with disk size: 10
Lane Width	7.42 mm

Lane 7

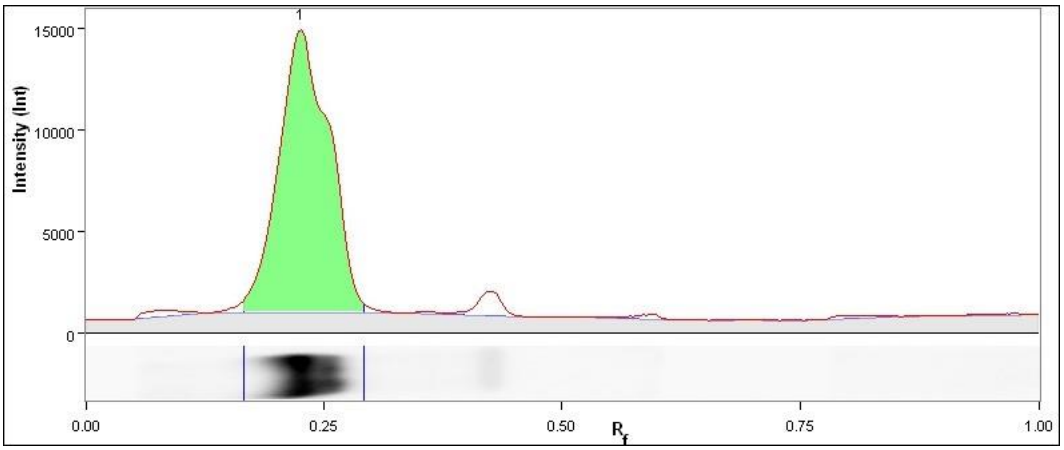

Band No.	Band Label	Mol. Wt. (KDa)	Relative Front	Volume (Int)	Abs. Quant.	Rel. Quant.	Band %	Lane %
1		N/A	0.227	22,617,210	N/A	N/A	100.0	90.5

Lane Background	Lane background subtracted with disk size: 10
Lane Width	7.42 mm

Lane 8

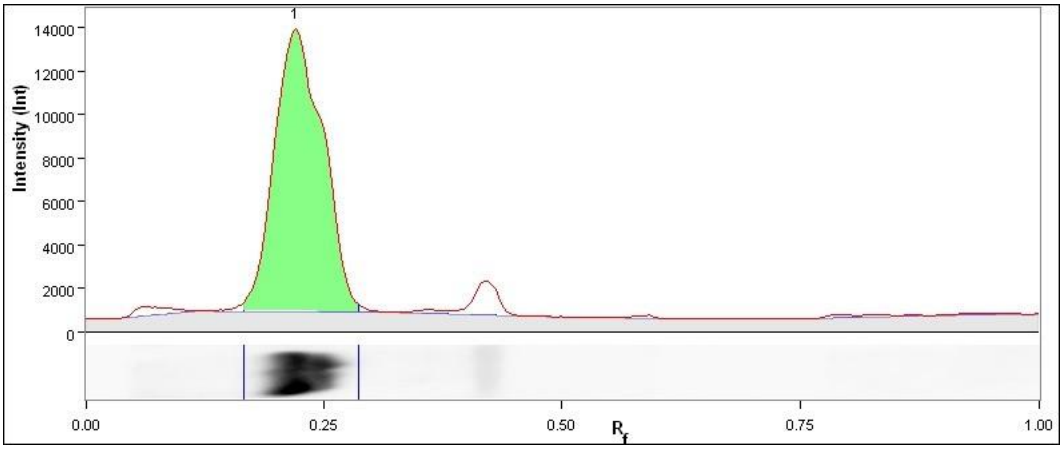

Band No.	Band Label	Mol. Wt. (KDa)	Relative Front	Volume (Int)	Abs. Quant.	Rel. Quant.	Band %	Lane %
1		N/A	0.222	20,904,180	N/A	N/A	100.0	88.6

Lane Background	Lane background subtracted with disk size: 10
Lane Width	7.42 mm

MDA-MB-468, B.boe PY20 Analysis:

Image Report: 2016-08-31 MDA-MB-468 B.boe PY20 15s

Acquisition Information

Imager	ChemiDoc™ Touch
Exposure Time (sec)	15.000 (Manual)
Serial Number	732BR1296
Software Version	1.1.0.04
Application	Chemiluminescence
Excitation Source	No Illumination
Emission Filter	No Filter
Binning	3x3

Image Information

Acquisition Date	31/08/2016 21:01:03
User Name	
Image Area (mm)	X: 158.1 Y: 126.7
Pixel Size (um)	X: 172.1 Y: 172.1
Data Range (Int)	501 - 32029

Analysis Settings

Detection	Lane detection: Manually created lanes Band detection: Manually adjusted bands Lane Background Subtraction: Lane background subtracted with disk size: 10 Lane width: 7.57 mm

Lane And Band Analysis

Lane 1

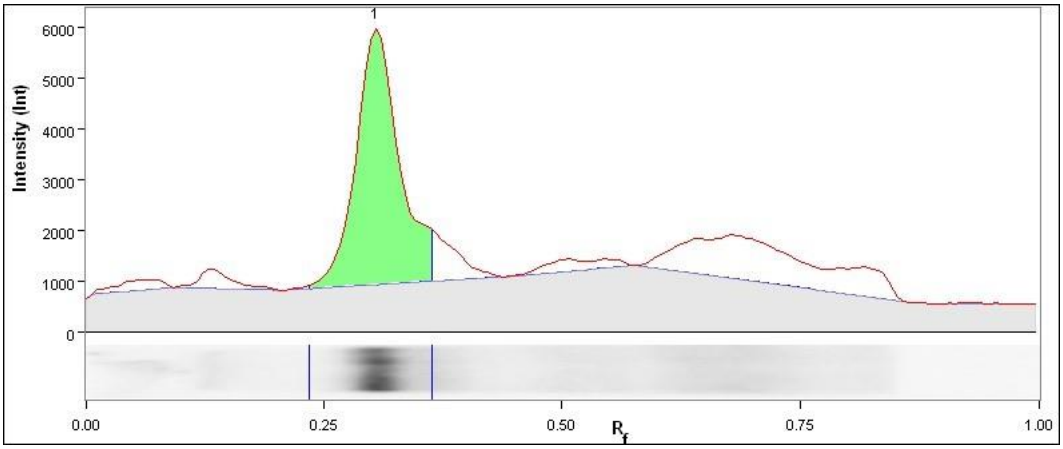

Band No.	Band Label	Mol. Wt. (KDa)	Relative Front	Volume (Int)	Abs. Quant.	Rel. Quant.	Band %	Lane %
1		N/A	0.309	2,609,728	N/A	N/A	100.0	55.5

Lane Background	Lane background subtracted with disk size: 10
Lane Width	7.57 mm

Lane 2

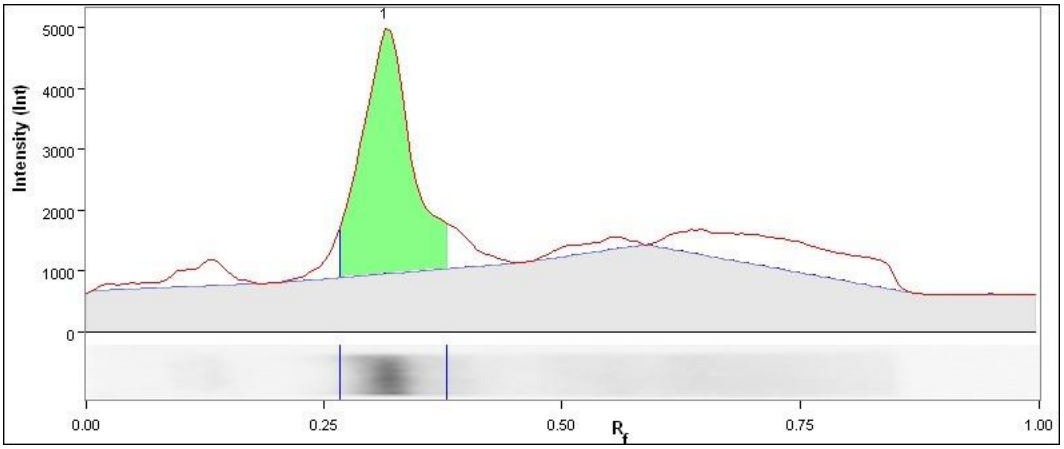

Band No.	Band Label	Mol. Wt. (KDa)	Relative Front	Volume (Int)	Abs. Quant.	Rel. Quant.	Band %	Lane %
1		N/A	0.319	2,157,056	N/A	N/A	100.0	57.1

Lane Background	Lane background subtracted with disk size: 10
Lane Width	7.57 mm

Lane 3

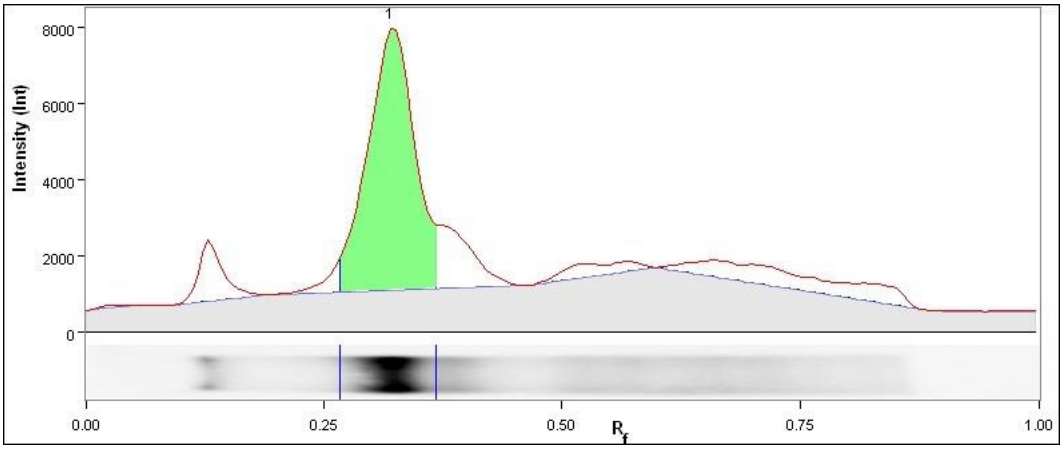

Band No.	Band Label	Mol. Wt. (KDa)	Relative Front	Volume (Int)	Abs. Quant.	Rel. Quant.	Band %	Lane %
1		N/A	0.324	3,894,396	N/A	N/A	100.0	60.1

Lane Background	Lane background subtracted with disk size: 10
Lane Width	7.57 mm

Lane 4

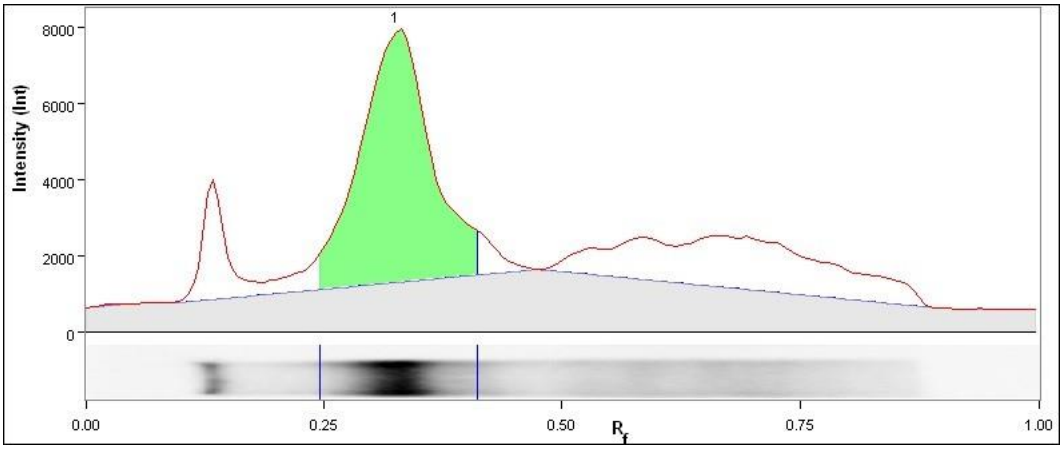

Band No.	Band Label	Mol. Wt. (KDa)	Relative Front	Volume (Int)	Abs. Quant.	Rel. Quant.	Band %	Lane %
1		N/A	0.330	5,178,228	N/A	N/A	100.0	53.6

Lane Background	Lane background subtracted with disk size: 10
Lane Width	7.57 mm

Lane 5

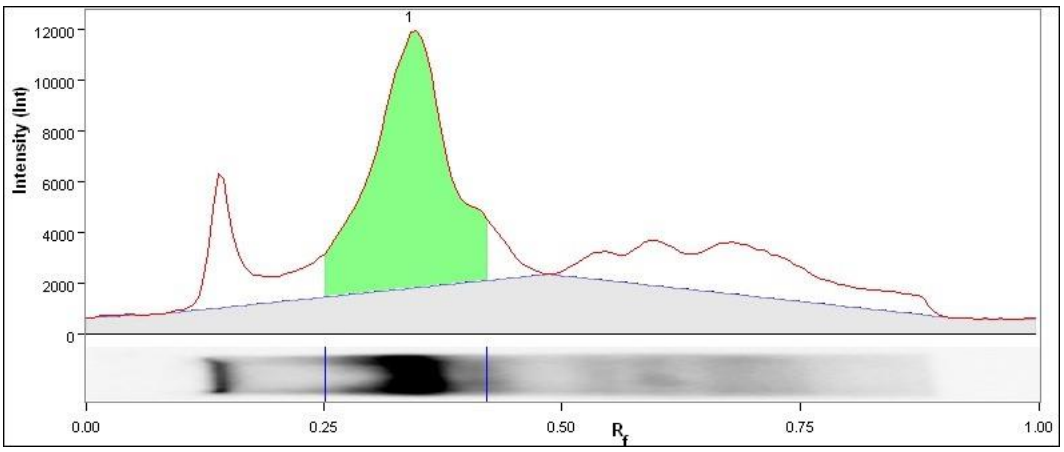

Band No.	Band Label	Mol. Wt. (KDa)	Relative Front	Volume (Int)	Abs. Quant.	Rel. Quant.	Band %	Lane %
1		N/A	0.346	8,386,576	N/A	N/A	100.0	54.5

Lane Background	Lane background subtracted with disk size: 10
Lane Width	7.57 mm

Lane 6

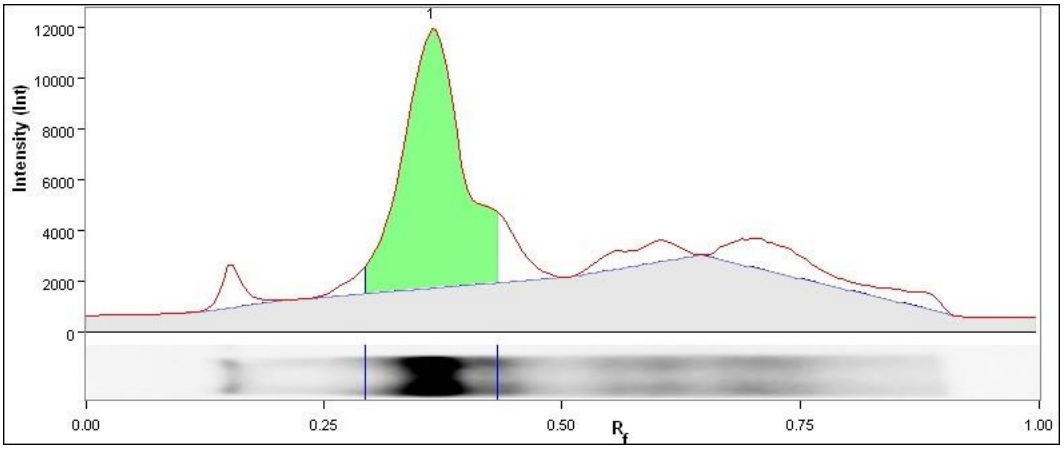

Band No.	Band Label	Mol. Wt. (KDa)	Relative Front	Volume (Int)	Abs. Quant.	Rel. Quant.	Band %	Lane %
1		N/A	0.367	7,157,568	N/A	N/A	100.0	68.2

Lane Background	Lane background subtracted with disk size: 10
Lane Width	7.57 mm

Lane 7

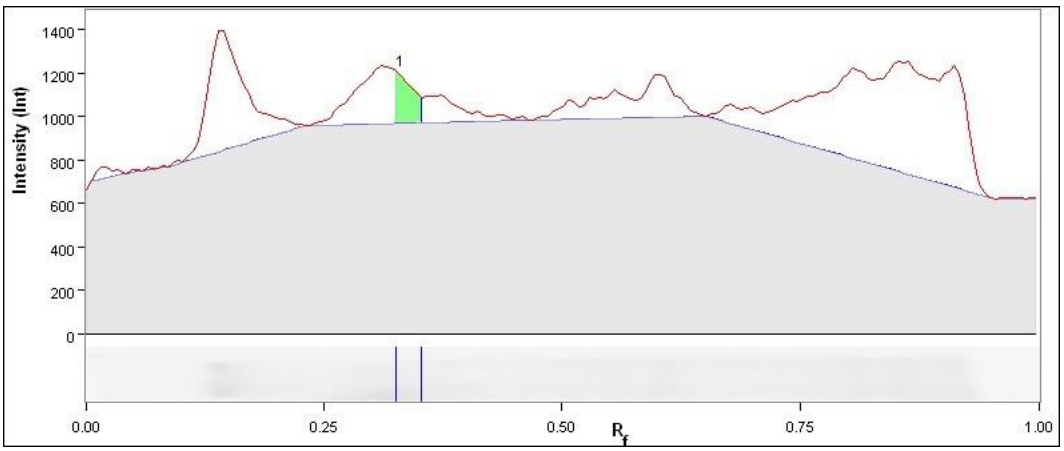

Band No.	Band Label	Mol. Wt. (KDa)	Relative Front	Volume (Int)	Abs. Quant.	Rel. Quant.	Band %	Lane %
1		N/A	0.335	44,044	N/A	N/A	100.0	3.4

Lane Background	Lane background subtracted with disk size: 10
Lane Width	7.57 mm

Lane 8

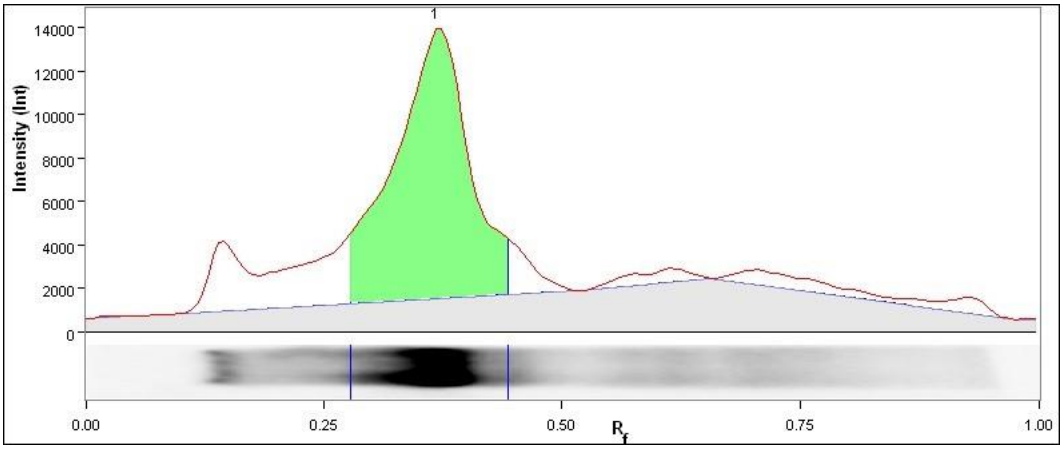

Band No.	Band Label	Mol. Wt. (KDa)	Relative Front	Volume (Int)	Abs. Quant.	Rel. Quant.	Band %	Lane %
1		N/A	0.372	10,432,224	N/A	N/A	100.0	66.2

Lane Background	Lane background subtracted with disk size: 10
Lane Width	7.57 mm

MDA-MB-468, B.boe Actin Analysis:

Image Report: 2016-08-31 MDA-MB-468 B.boe actin 30s

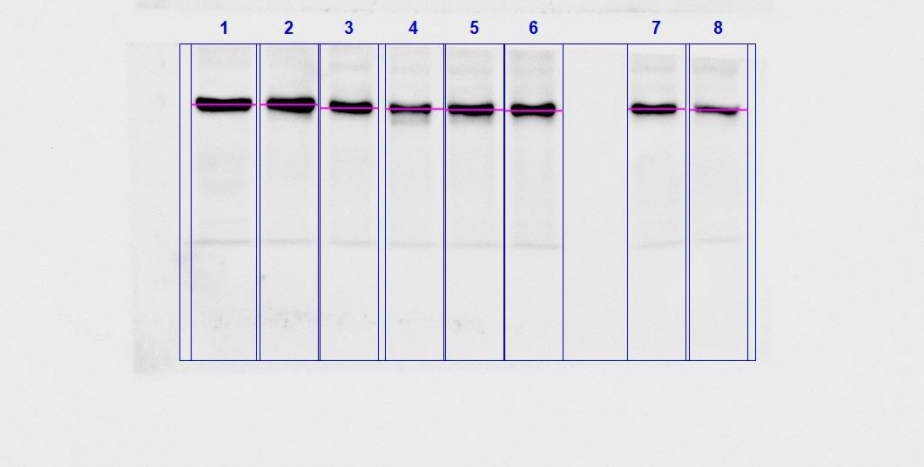

Acquisition Information

Imager	ChemiDoc™ Touch
Exposure Time (sec)	30.000 (Manual)
Serial Number	732BR1296
Software Version	1.1.0.04
Application	Chemiluminescence

Excitation Source	No Illumination
Emission Filter	No Filter
Binning	2x2

Image Information

Acquisition Date	31/08/2016 20:51:43
User Name	
Image Area (mm)	X: 158.1 Y: 126.6
Pixel Size (um)	X: 114.7 Y: 114.7
Data Range (Int)	500 - 40323

Analysis Settings

Detection	Lane detection: Manually created lanes Band detection: Manually adjusted bands Lane Background Subtraction: Lane background subtracted with disk size: 10 Lane width: Variable

Lane And Band Analysis

Lane 1

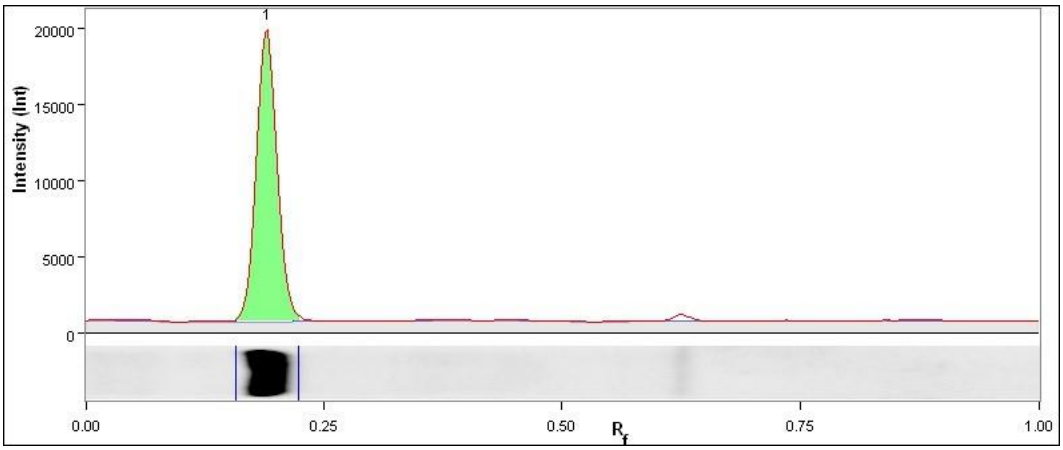

Band No.	Band Label	Mol. Wt. (KDa)	Relative Front	Volume (Int)	Abs. Quant.	Rel. Quant.	Band %	Lane %
1		N/A	0.192	14,550,075	N/A	N/A	100.0	92.7

Lane Background	Lane background subtracted with disk size: 10
Lane Width	8.60 mm

Lane 2

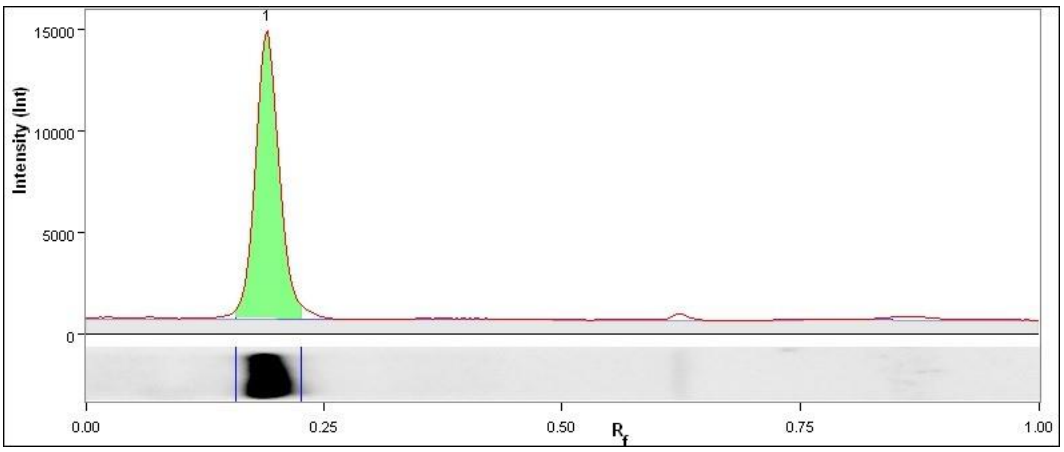

Band No.	Band Label	Mol. Wt. (KDa)	Relative Front	Volume (Int)	Abs. Quant.	Rel. Quant.	Band %	Lane %
1		N/A	0.192	11,735,854	N/A	N/A	100.0	89.3

Lane Background	Lane background subtracted with disk size: 10
Lane Width	7.68 mm

Lane 3

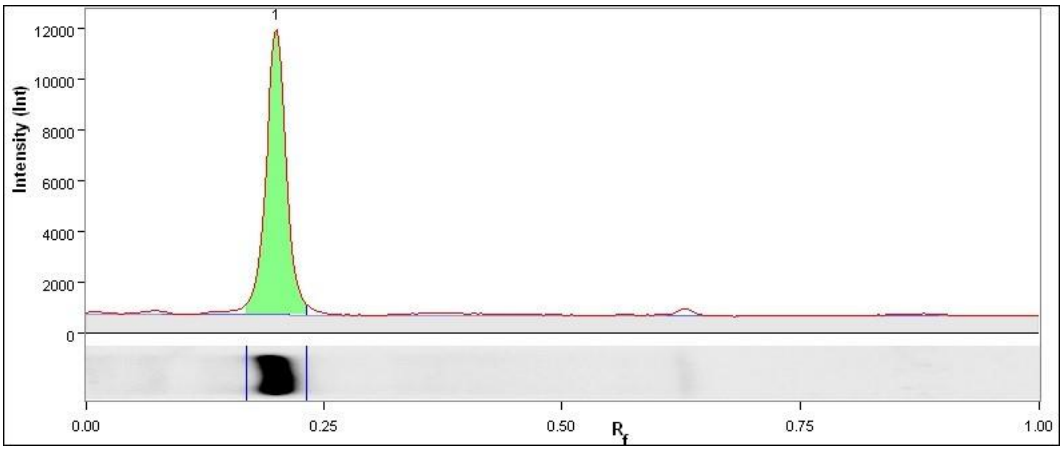

Band No.	Band Label	Mol. Wt. (KDa)	Relative Front	Volume (Int)	Abs. Quant.	Rel. Quant.	Band %	Lane %
1		N/A	0.203	7,853,405	N/A	N/A	100.0	87.1

Lane Background	Lane background subtracted with disk size: 10
Lane Width	7.68 mm

Lane 4

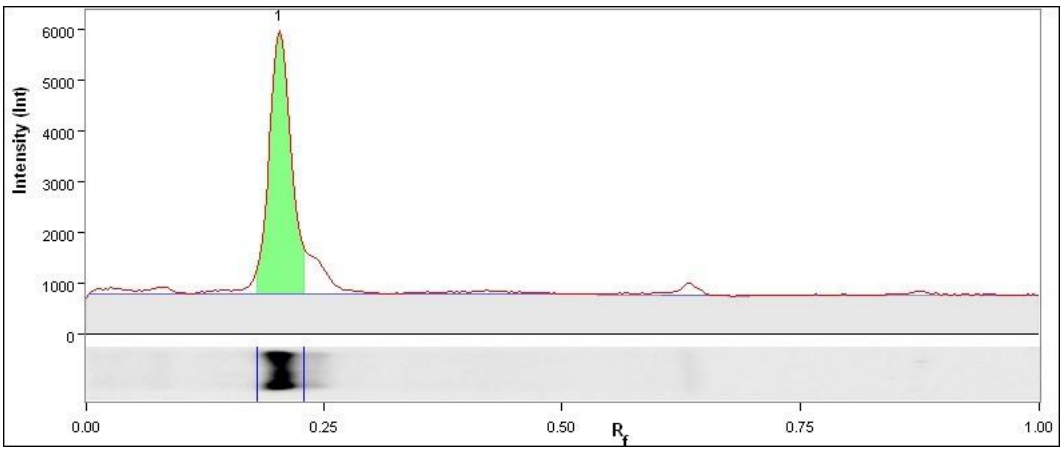

Band No.	Band Label	Mol. Wt. (KDa)	Relative Front	Volume (Int)	Abs. Quant.	Rel. Quant.	Band %	Lane %
1		N/A	0.206	3,437,971	N/A	N/A	100.0	71.7

Lane Background	Lane background subtracted with disk size: 10
Lane Width	7.68 mm

Lane 5

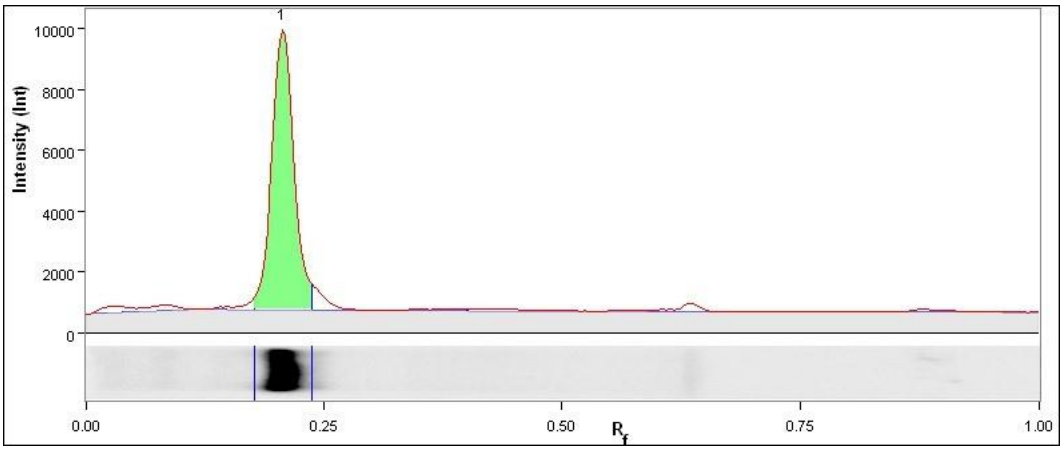

Band No.	Band Label	Mol. Wt. (KDa)	Relative Front	Volume (Int)	Abs. Quant.	Rel. Quant.	Band %	Lane %
1		N/A	0.209	6,771,087	N/A	N/A	100.0	81.6

Lane Background	Lane background subtracted with disk size: 10
Lane Width	7.68 mm

Lane 6

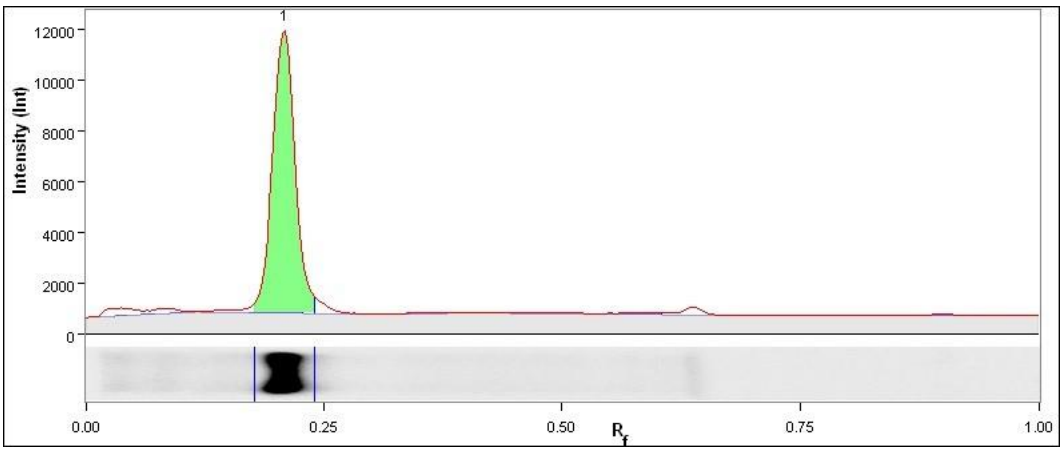

Band No.	Band Label	Mol. Wt. (KDa)	Relative Front	Volume (Int)	Abs. Quant.	Rel. Quant.	Band %	Lane %
1		N/A	0.212	7,724,631	N/A	N/A	100.0	85.4

Lane Background	Lane background subtracted with disk size: 10
Lane Width	7.68 mm

Lane 7

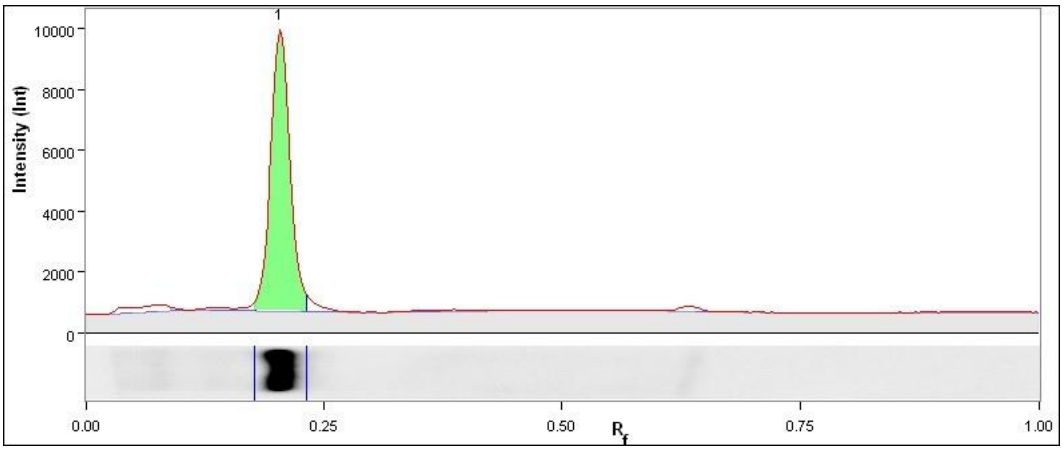

Band No.	Band Label	Mol. Wt. (KDa)	Relative Front	Volume (Int)	Abs. Quant.	Rel. Quant.	Band %	Lane %
1		N/A	0.206	5,918,177	N/A	N/A	100.0	84.9

Lane Background	Lane background subtracted with disk size: 10
Lane Width	7.68 mm

Lane 8

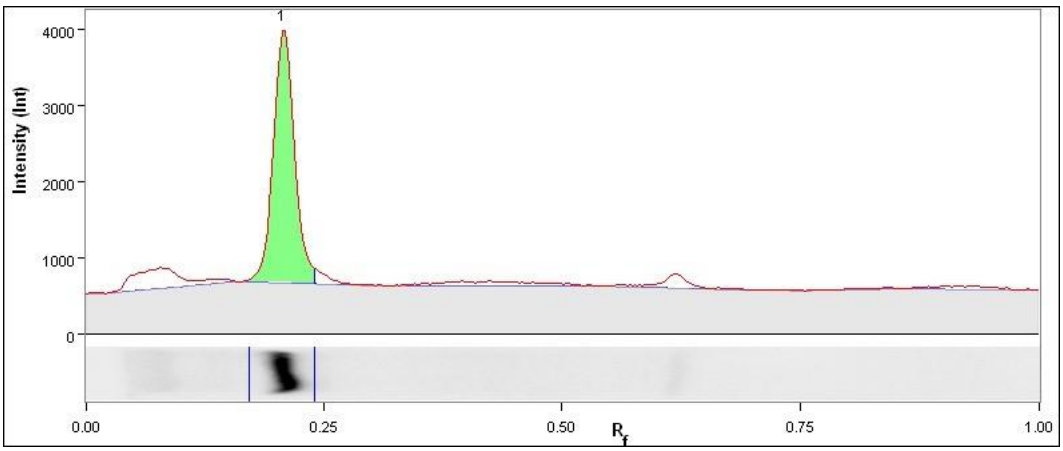

Band No.	Band Label	Mol. Wt. (KDa)	Relative Front	Volume (Int)	Abs. Quant.	Rel. Quant.	Band %	Lane %
1		N/A	0.209	2,550,757	N/A	N/A	100.0	68.3

Lane Background	Lane background subtracted with disk size: 10
Lane Width	7.68 mm

MDA-MB-468, D.vir PY20 Analysis:

Image Report: 2016-05-13 MDA-MB-468 D.vir PY20

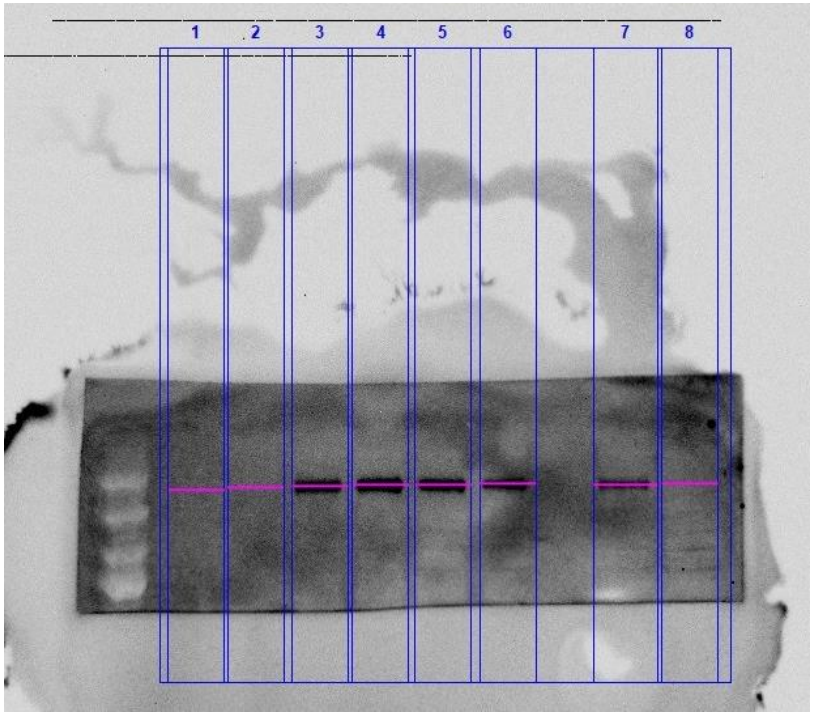

Acquisition Information

Imager	ChemiDoc™ Touch

Exposure Time (sec)	300.000 (Manual)
Serial Number	732BR1296
Software Version	1.1.0.04
Application	Chemiluminescence
Excitation Source	No Illumination
Emission Filter	No Filter
Binning	3x3

Image Information

Acquisition Date	13/05/2016 21:39:07
User Name	
Image Area (mm)	X: 155.0 Y: 124.1
Pixel Size (um)	X: 168.7 Y: 168.7
Data Range (Int)	6 - 65525

Analysis Settings

	Manually created lanes Band detection: Manually adjusted bands Lane Background Subtraction: Lane background subtracted with disk size: 10 Lane width: Variable

Lane and Band Analysis

Lane 1

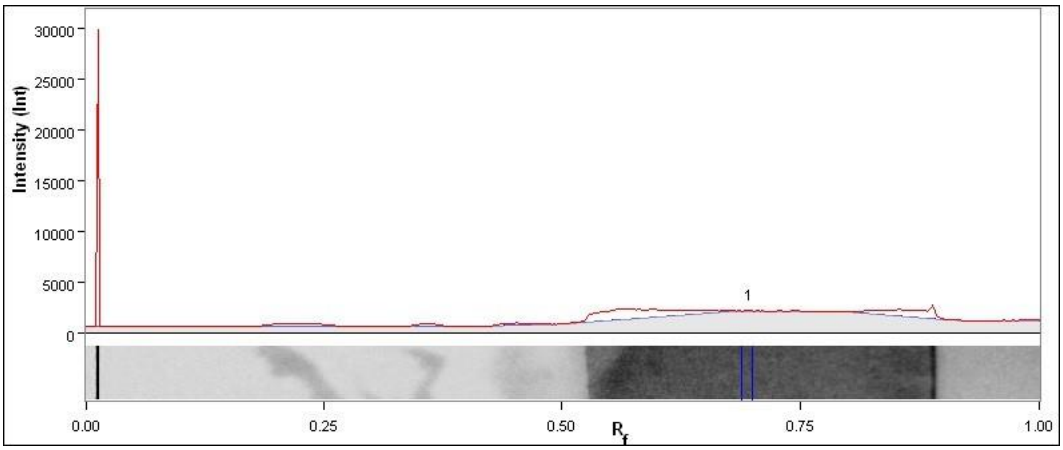

Band No.	Band Label	Mol. Wt. (KDa)	Relative Front	Volume (Int)	Abs. Quant.	Rel. Quant.	Band %	Lane %
1		N/A	0.698	12,685	N/A	N/A	100.0	0.2

Lane Background	Lane background subtracted with disk size: 10
Lane Width	7.25 mm

Lane 2

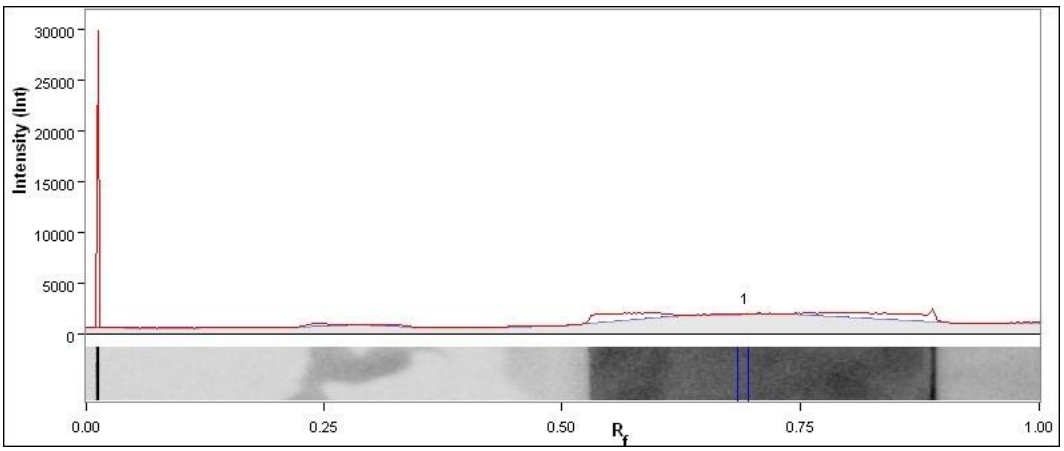

Band No.	Band Label	Mol. Wt. (KDa)	Relative Front	Volume (Int)	Abs. Quant.	Rel. Quant.	Band %	Lane %
1		N/A	0.693	14,878	N/A	N/A	100.0	0.3

Lane Background	Lane background subtracted with disk size: 10
Lane Width	7.25 mm

Lane 3

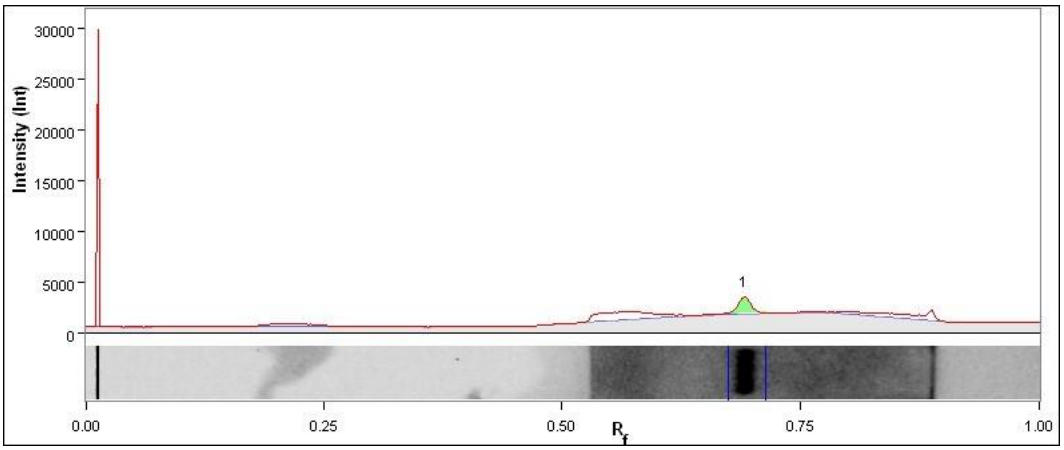

Band No.	Band Label	Mol. Wt. (KDa)	Relative Front	Volume (Int)	Abs. Quant.	Rel. Quant.	Band %	Lane %
1		N/A	0.691	622,468	N/A	N/A	100.0	12.6

Lane Background	Lane background subtracted with disk size: 10
Lane Width	7.25 mm

Lane 4

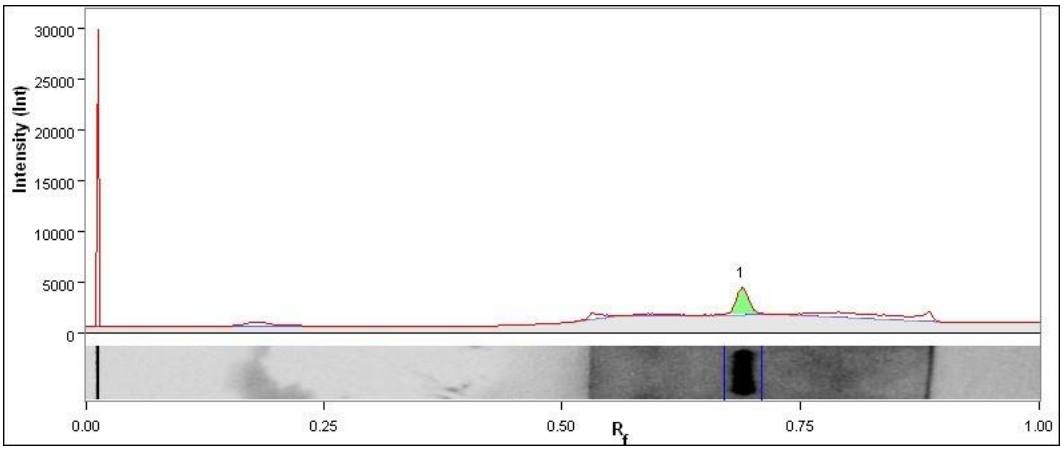

Band No.	Band Label	Mol. Wt. (KDa)	Relative Front	Volume (Int)	Abs. Quant.	Rel. Quant.	Band %	Lane %
1		N/A	0.689	967,844	N/A	N/A	100.0	20.2
Lane Background		Lane background subtracted with disk size: 10						
Lane Width		7.25 mm						

Lane 5

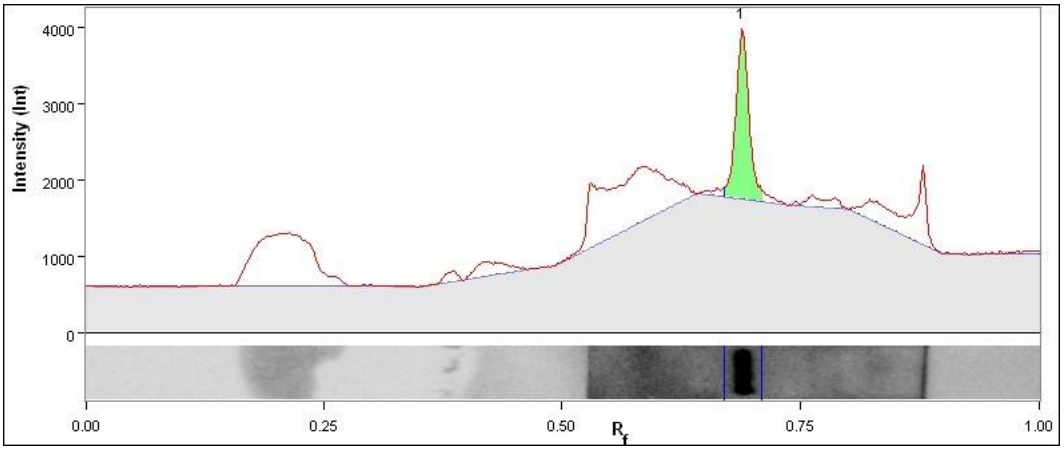

Band No.	Band Label	Mol. Wt. (KDa)	Relative Front	Volume (Int)	Abs. Quant.	Rel. Quant.	Band %	Lane %
1		N/A	0.689	782,299	N/A	N/A	100.0	18.2
Lane Background		Lane background subtracted with disk size: 10						
Lane Width		7.25 mm						

Lane 6

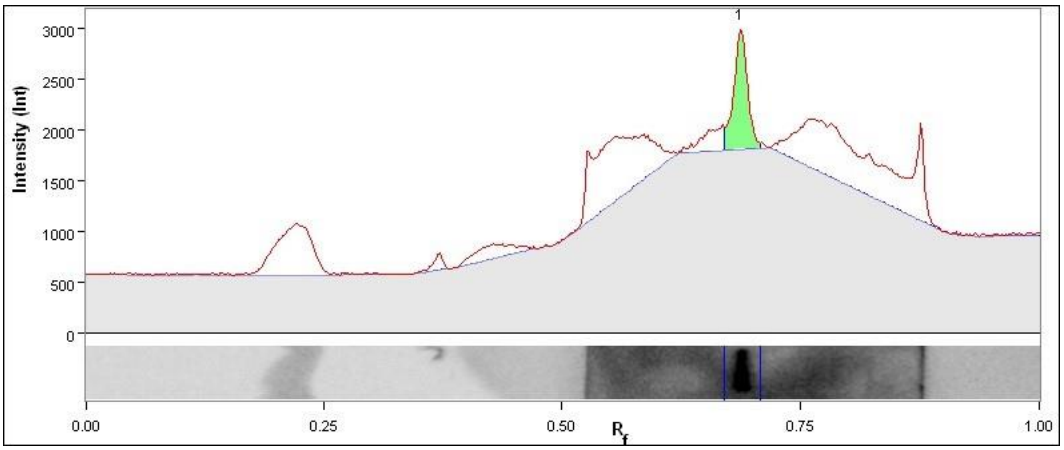

Band No.	Band Label	Mol. Wt. (KDa)	Relative Front	Volume (Int)	Abs. Quant.	Rel. Quant.	Band %	Lane %
1		N/A	0.687	460,616	N/A	N/A	100.0	11.9

Lane Background	Lane background subtracted with disk size: 10
Lane Width	7.25 mm

Lane 7

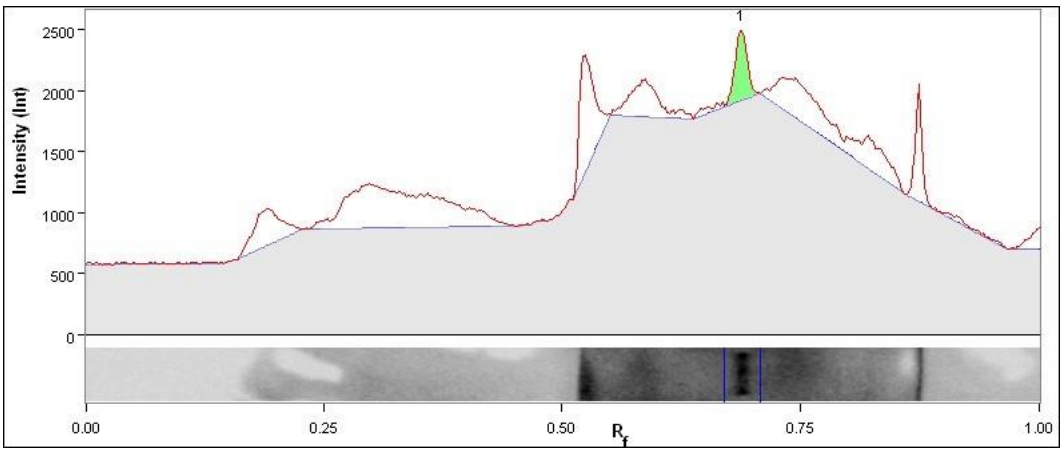

Band No.	Band Label	Mol. Wt. (KDa)	Relative Front	Volume (Int)	Abs. Quant.	Rel. Quant.	Band %	Lane %
1		N/A	0.689	228,046	N/A	N/A	100.0	6.6

Lane Background	Lane background subtracted with disk size: 10
Lane Width	8.26 mm

Lane 8

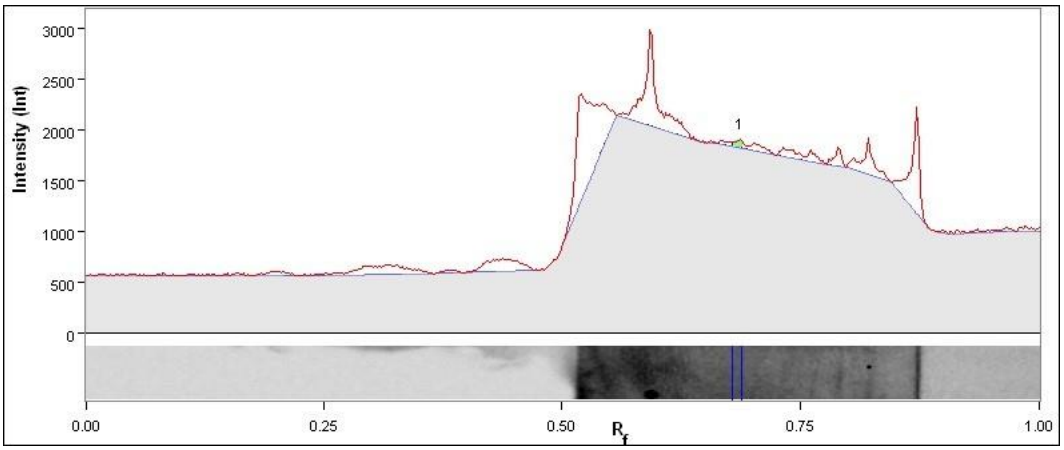

Band No.	Band Label	Mol. Wt. (KDa)	Relative Front	Volume (Int)	Abs. Quant.	Rel. Quant.	Band %	Lane %
1		N/A	0.687	18,748	N/A	N/A	100.0	1.0
Lane Background		Lane background subtracted with disk size: 10						
Lane Width		7.25 mm						

MDA-MB-468, D.vir Actin Analysis:

Image Report: 2016-05-13 MDA-MB-468 D.vir actin

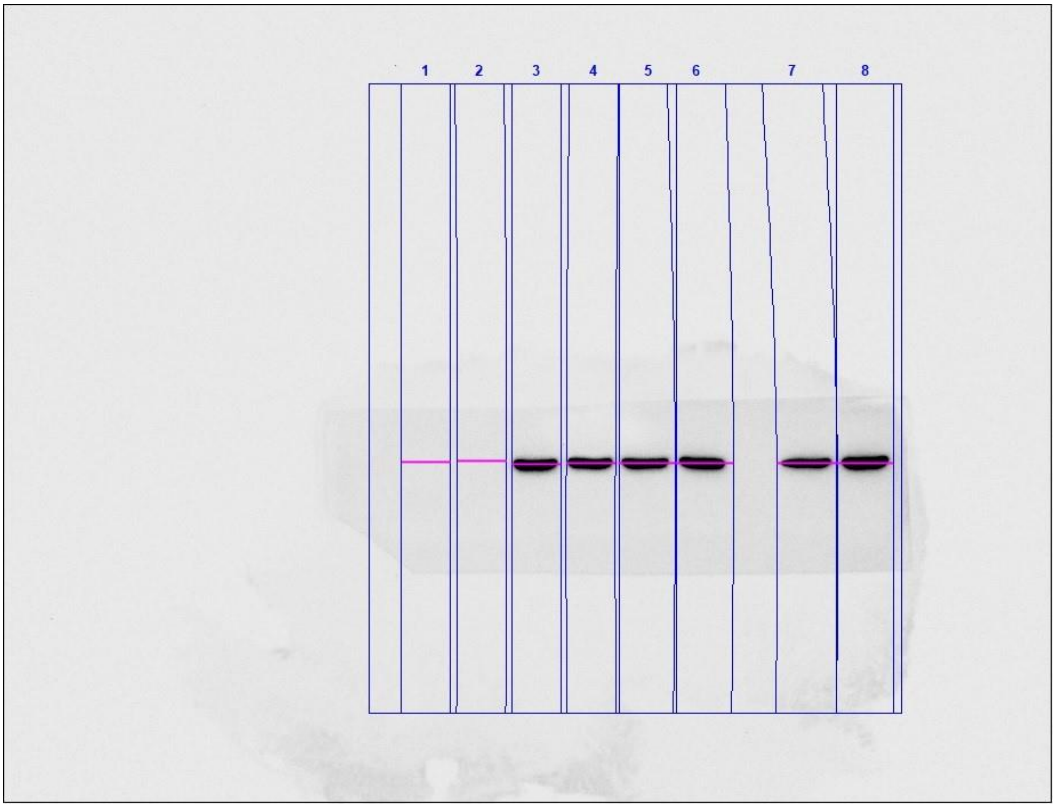

Acquisition Information

Imager	ChemiDoc™ Touch
Exposure Time (sec)	30.000 (Manual)
Serial Number	732BR1296
Software Version	1.1.0.04
Application	Chemiluminescence
Excitation Source	No Illumination
Emission Filter	No Filter
Binning	3x3

Image Information

Acquisition Date	13/05/2016 21:23:42
User Name	
Image Area (mm)	X: 155.0 Y: 124.1
Pixel Size (um)	X: 168.7 Y: 168.7
Data Range (Int)	501 - 46543

Analysis Settings

	Automatically detected lanes with manual adjustments Band detection: Manually adjusted bands Lane Background Subtraction: Lane background subtracted with disk size: 10 Lane width: Variable

Lane And Band Analysis

Lane 1

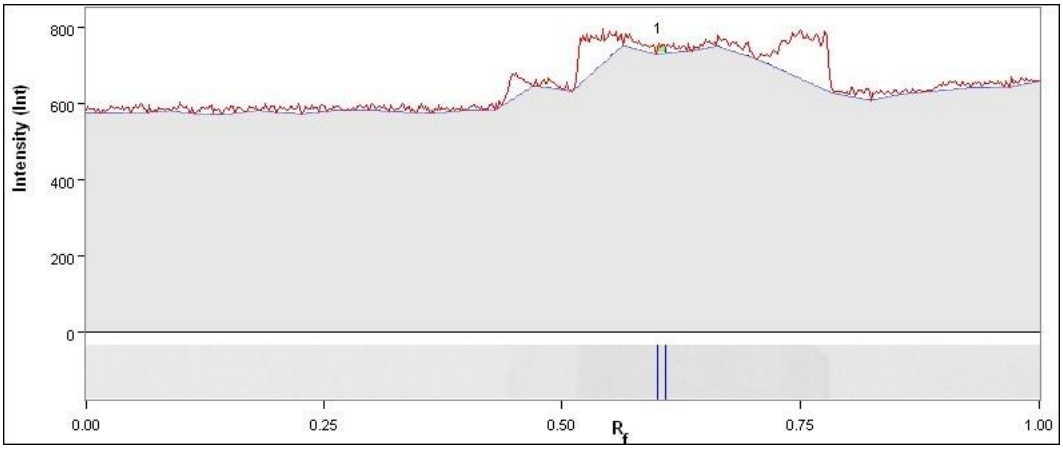

Band No.	Band Label	Mol. Wt. (KDa)	Relative Front	Volume (Int)	Abs. Quant.	Rel. Quant.	Band %	Lane %
1		N/A	0.602	5,977	N/A	N/A	100.0	1.1

Lane Background	Lane background subtracted with disk size: 10
Lane Width	7.25 mm

Lane 2

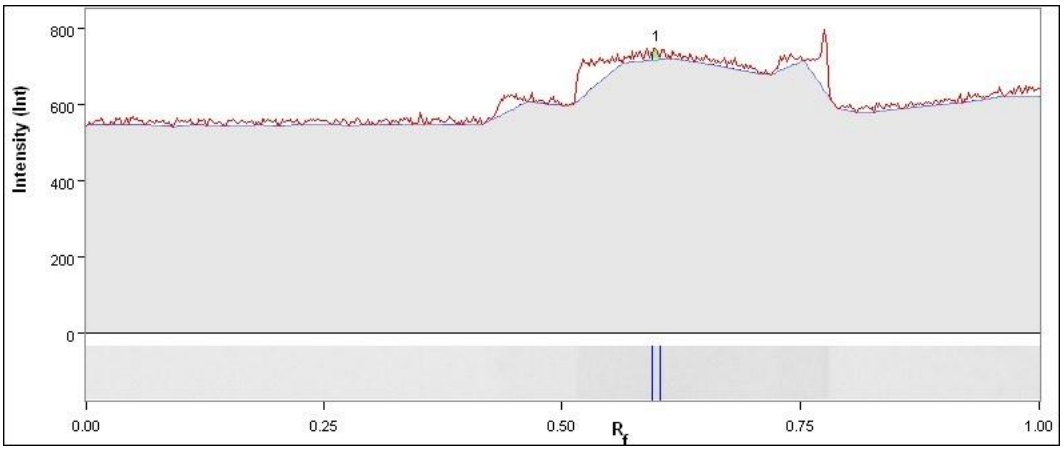

Band No.	Band Label	Mol. Wt. (KDa)	Relative Front	Volume (Int)	Abs. Quant.	Rel. Quant.	Band %	Lane %
1		N/A	0.600	5,977	N/A	N/A	100.0	1.4

Lane Background	Lane background subtracted with disk size: 10
Lane Width	7.25 mm

Lane 3

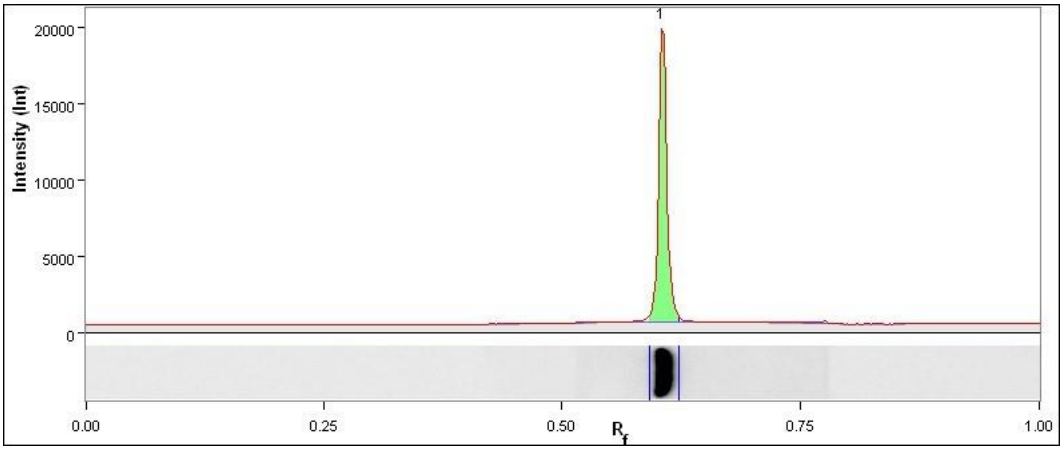

Band No.	Band Label	Mol. Wt. (KDa)	Relative Front	Volume (Int)	Abs. Quant.	Rel. Quant.	Band %	Lane %
1		N/A	0.605	5,964,659	N/A	N/A	100.0	90.7

Lane Background	Lane background subtracted with disk size: 10
Lane Width	7.25 mm

Lane 4

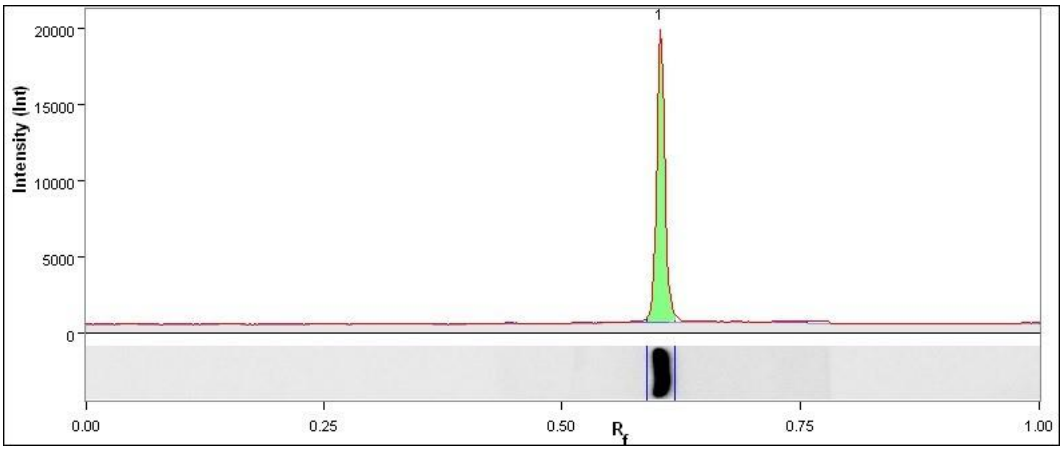

Band No.	Band Label	Mol. Wt. (KDa)	Relative Front	Volume (Int)	Abs. Quant.	Rel. Quant.	Band %	Lane %
1		N/A	0.603	5,521,157	N/A	N/A	100.0	89.5

Lane Background	Lane background subtracted with disk size: 10
Lane Width	7.25 mm

Lane 5

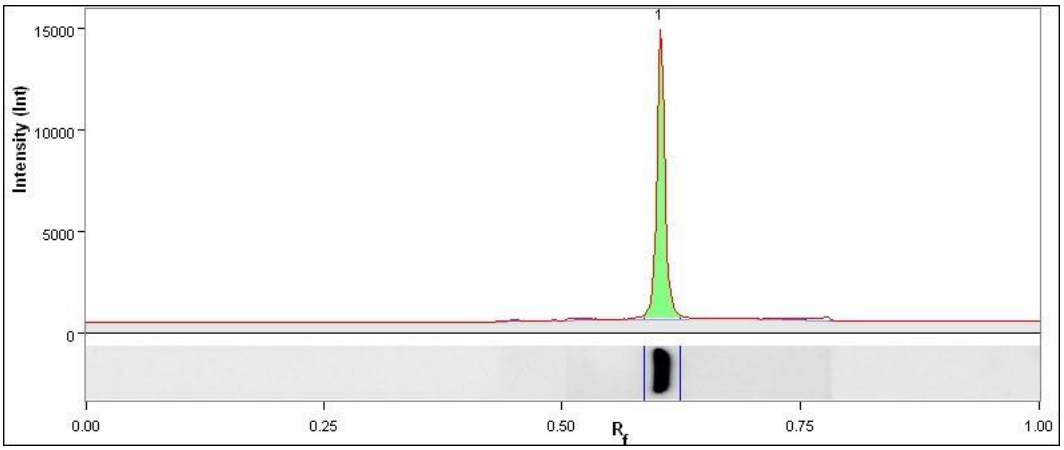

Band No.	Band Label	Mol. Wt. (KDa)	Relative Front	Volume (Int)	Abs. Quant.	Rel. Quant.	Band %	Lane %
1		N/A	0.603	5,171,150	N/A	N/A	100.0	86.0

Lane Background	Lane background subtracted with disk size: 10
Lane Width	8.43 mm

Lane 6

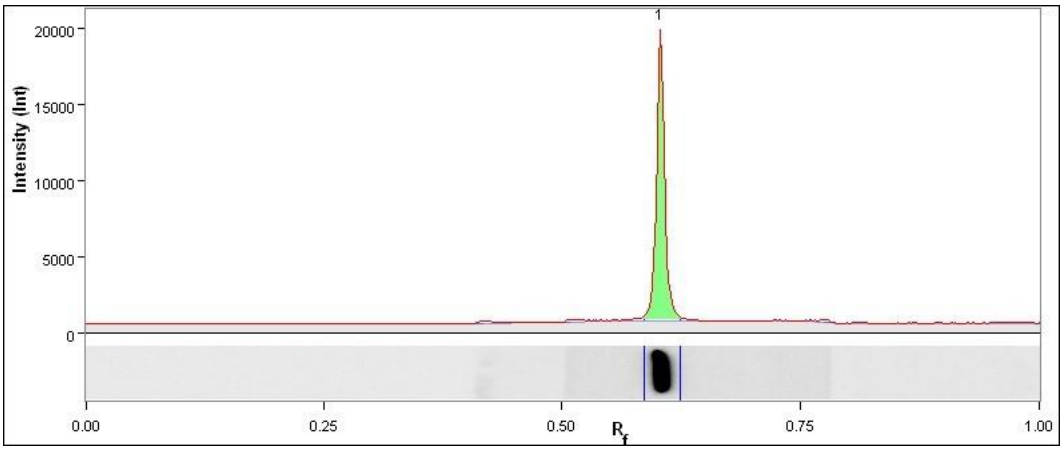

Band No.	Band Label	Mol. Wt. (KDa)	Relative Front	Volume (Int)	Abs. Quant.	Rel. Quant.	Band %	Lane %
1		N/A	0.603	6,277,998	N/A	N/A	100.0	88.3

Lane Background	Lane background subtracted with disk size: 10
Lane Width	8.60 mm

Lane 7

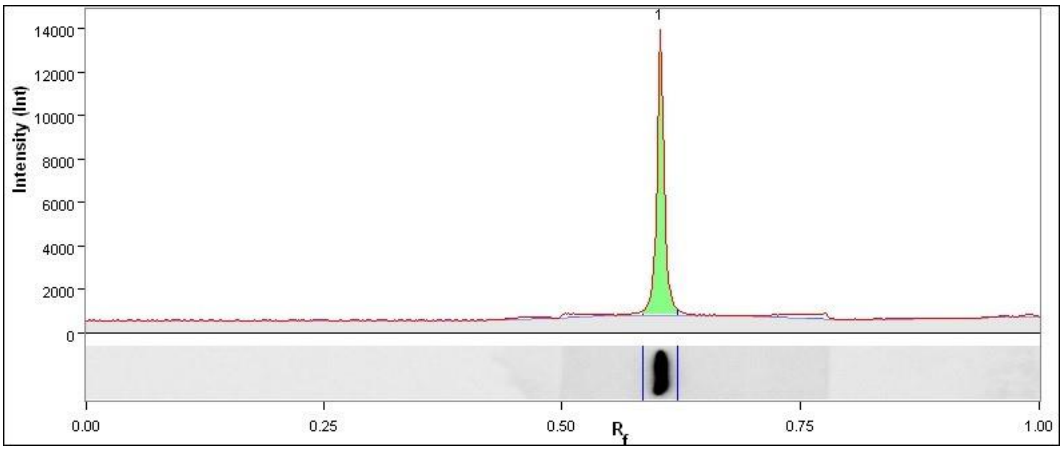

Band No.	Band Label	Mol. Wt. (KDa)	Relative Front	Volume (Int)	Abs. Quant.	Rel. Quant.	Band %	Lane %
1		N/A	0.603	4,200,091	N/A	N/A	100.0	78.6

Lane Background	Lane background subtracted with disk size: 10
Lane Width	8.94 mm

Lane 8

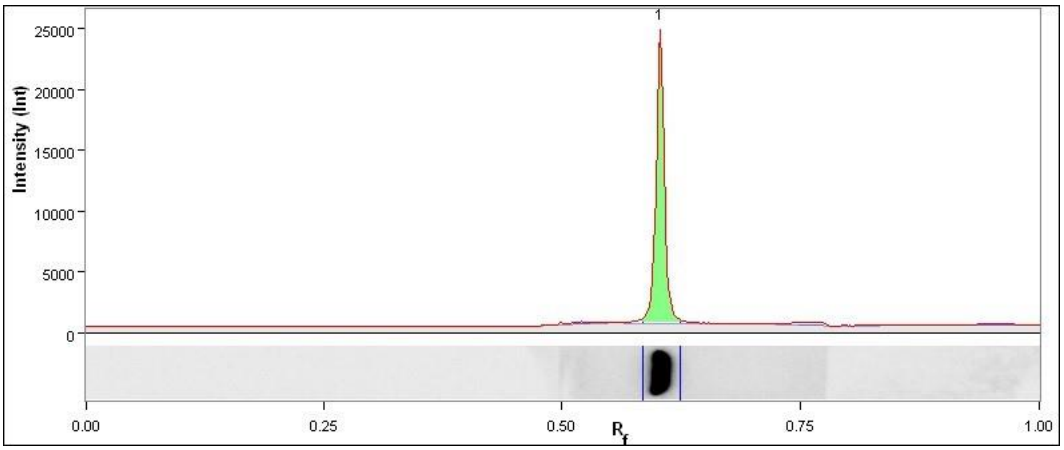

Band No.	Band Label	Mol. Wt. (KDa)	Relative Front	Volume (Int)	Abs. Quant.	Rel. Quant.	Band %	Lane %
1		N/A	0.603	8,731,250	N/A	N/A	100.0	88.0

Lane Background	Lane background subtracted with disk size: 10
Lane Width	8.43 mm

Appendix XX: Chapter 6: Plate Layout to Determine the Optimal Plate and Cell Number Combination for EGF Alexa Fluor-488 Competition Assays

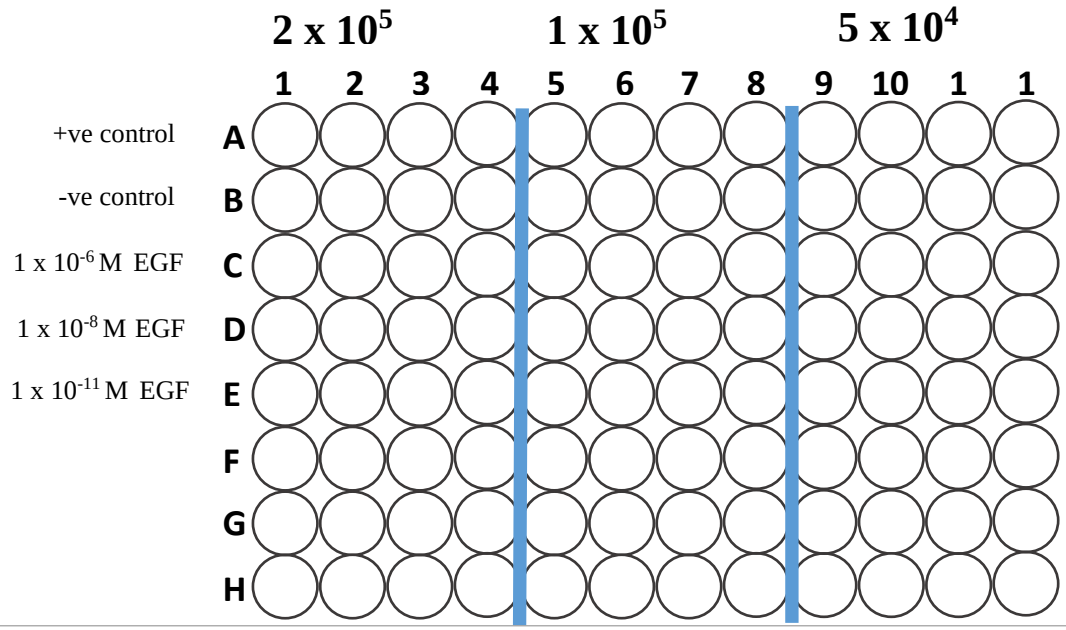

Appendix XX: Plate layout used to determine the best cell and plate combination to take forward for EGF Alexa Fluor-488 competitive binding assay

Cells were plated out at 3 different concentrations/well and treated in quadruplicate with varying concentrations of non-fluorescent EGF to simulate competitive binding by an EGF-antagonist. **+VE control:** EGF Alexa Fluor-488 only (max fluorescence), **-VE control**: PBS only (min fluorescence)

Appendix XXI: Chapter 6: Plate Layout of EGF Alexa Fluor-488 Snake Venom Competition Assay

	1	2	3	4	5	6	7	8	9	10	11	12
A	+VE	+VE	+VE	P.wei	P.wei	P.wei	N.sia	N.sia	N.sia	-VE	-VE	-VE
B	N.nig	N.nig	N.nig	N.atr	N.atr	N.atr	N.naj	N.naj	N.naj	O.han	O.han	O.han
C	D.pol	D.pol	D.pol	D.vir	D.vir	D.vir	C.rho	C.rho	C.rho	C.atr	C.atr	C.atr
D	C.rru	C.rru	C.rru	C.dve	C.dve	C.dve	C.ins	C.ins	C.ins	S.mil	S.mil	S.mil
E	M.xan	M.xan	M.xan	A.cco	A.cco	A.cco	V.aam	V.aam	V.aam	B.asp	B.asp	B.asp
F	-VE	-VE	-VE							+VE	+VE	+VE
G												
H												

Appendix XXI: EGF Competitive Binding Assay, Snake panel plate layout

Cells were plated at a concentration of $2x10^5$ cells/well and treated in triplicate with each venom shown above. All snake venoms were used at a concentration of 2 mg/ml (100µg of protein/well). All wells apart from –ve control wells were treated with $1x10^{-7}$M EGF Alexa Flour-488 for 5mins before fluorescence was read using BMG Labtech Fluostar plate reader (ex.485nm, em.520nm).

+VE control: EGF Alexa Fluor-488 only (max fluorescence), **-VE control**: PBS only (min fluorescence)

Appendix XXII: Chapter 6: Plate Layout of EGF Alexa Fluor-488 Invertebrate Venom Competition Assay

	1	2	3	4	5	6	7	8	9	10	11	12
A	-VE	-VE	-VE	-VE	-VE	-VE	+VE	+VE	+VE	+VE	+VE	+VE
B	A.aus	A.aus	A.aus	H.ari	H.ari	H.ari	H.swa	H.swa	H.swa	L.qui	L.qui	L.qui
C	P.kra	P.kra	P.kra	P.lio	P.lio	P.lio	A.cor	A.cor	A.cor	A.gen	A.gen	A.gen
D	A.met	A.met	A.met	B.boe	B.boe	B.boe	H.lbo	H.lbo	H.lbo	H.mac	H.mac	H.mac
E	P.cam	P.cam	P.cam	P.for	P.for	P.for	P.lug	P.lug	P.lug	T.cup	T.cup	T.cup
F	T.pru	T.pru	T.pru	T.str	T.str	T.str	S.har	S.har	S.har	S.sub	S.sub	S.sub
G	C.gig	C.gig	C.gig	E.foe	E.foe	E.foe	P.map	P.map	P.map	Venom Only Controls		
H	+VE	+VE	+VE	+VE	+VE	+VE	-VE	-VE	-VE	-VE	-VE	-VE

Appendix XXII: EGF Competitive Binding Assay, Invertebrate panel plate layout

Cells were plated at a concentration of $2x10^5$ cells/well and treated in triplicate with each venom shown above. All Invertebrate venoms were used at a concentration of 2 mg/ml (100µg of protein/well). All wells apart from –ve control wells were treated with $1x10^{-7}$M EGF Alexa Flour-488 for 5mins before the fluorescence was read using BMG Fluostar plate reader (ex.485nm, em.520nm).

+VE control: EGF Alexa Fluor-488 only (max fluorescence), **-VE control**: PBS only (min fluorescence)

Appendix XXIII: Chapter 7: Reverse Phase HPLC Parameters

Detection wavelengths	215 and 280nm
Collection wavelength	215nm or 280nm
Collection Mode	Threshold/Slope
Up Slope Threshold	0.1U/s
Down Slope Threshold	0.5U/s
Lower Collection Threshold	5U
Upper Collection Threshold	3000U
Column Flow Rate	1ml/min
Max Peak Duration	4min

Appendix XXIII: Detection and Collection Parameters of the RP HPLC Protocol

Protocol set up and used for the collection of fractions from whole venoms from snakes and invertebrate.

Appendix XXIV: Chapter 7: Table of Minitab Normality Test, Equal Variance and Residual P-Values for Snake and Invertebrate Fraction PY20 ELISA Data Sets

Normality Test P-Values			
Elapid Venoms			
MDA-MB-468 Cells		A431 Cells	
P.wei_R6	0.550	P.wei_R6	0.431
P.wei_R7	0.217	P.wei_R7	0.785
P.wei_R8	0.253		-
P.wei_R9	0.157	P.wei_R9	0.081
P.wei_R10	0.775	P.wei_R10	0.862
+EGF	0.227	+EGF	0.510
N.naj_R1	-	N.naj_R1	0.845
N.naj_R2	-	N.naj_R2	0.159
N.naj_R3	-	N.naj_R3	0.658
N.naj_R4	-	N.naj_R4	0.791
N.naj_R6	-	N.naj_R6	0.128
N.naj_R7	0.785	N.naj_R7	0.113
N.naj_R8	0.559	N.naj_R8	0.141
N.naj_R9	0.788	N.naj_R9	0.053
N.naj_R10	0.426	N.naj_R10	0.443
N.naj_R11	0.433	N.naj_R11	0.705
N.naj_R12	0.325	N.naj_R12	0.387
N.naj_R13	0.848	N.naj_R13	0.294
N.naj_R14	-	N.naj_R14	0.852
N.naj_R15	-	N.naj_R15	0.100
N.naj_R16	-	N.naj_R16	0.210
+EGF	0.258	+EGF	0.124

O.han_R6	0.130	O.han_R6	-
O.han_R11	-	O.han_R11	0.545
O.han_R12	0.759	O.han_R12	0.581
O.han_R19	0.227	O.han_R19	-
+EGF	0.596	+EGF	0.680
Crotalid Venoms			
C.dve_R1	0.799	C.dve_R1	0.227
C.dve_R2	0.762	C.dve_R2	-
C.dve_R3	0.610	C.dve_R3	0.227
C.dve_R4	0.543	C.dve_R4	-
C.dve_R6	0.073	C.dve_R6	0.227
C.dve_R7	0.210	C.dve_R7	0.335
C.dve_R8	0.230	C.dve_R8	0.103
C.dve_R9	0.563	C.dve_R9	0.726
C.dve_R10	0.798	C.dve_R10	0.150
C.dve_R12	0.430	C.dve_R12	0.307
C.dve_R13	0.132	C.dve_R13	0.515
C.dve_R14	0.160	C.dve_R14	0.349
C.dve_R15	0.512	C.dve_R15	-
C.dve_R16	0.386	C.dve_R16	-
+EGF	0.821	+EGF	0.588
C.rho_R1	-	C.rho_R1	0.227
C.rho_R2	-	C.rho_R2	0.450
C.rho_R3	-	C.rho_R3	0.154
C.rho_R7	0.163	C.rho_R7	0.118
C.rho_R8	-	C.rho_R8	0.447
C.rho_R9	-	C.rho_R9	0.625
C.rho_R14	-	C.rho_R14	0.377
C.rho_R15	-	C.rho_R15	0.575
+EGF	0.296	+EGF	0.721
S.mil_R1	-	S.mil_R1	0.363
S.mil_R2	-	S.mil_R2	0.309
S.mil_R3	0.284	S.mil_R3	-
S.mil_R5	0.267	S.mil_R5	0.103
S.mil_R6	0.228	S.mil_R6	0.232
S.mil_R7	0.543	S.mil_R7	0.370
S.mil_R8	0.405	S.mil_R8	0.227
S.mil_R9	0.299	S.mil_R9	0.076
S.mil_R13	0.502	S.mil_R13	0.604
S.mil_R15	0.848	S.mil_R15	-
+EGF	0.147	+EGF	0.514
Invertebrate Venoms			
A.gen_R2	0.089	A.gen_R2	-
A.gen_R22	-	A.gen_R22	0.486
A.gen_R25	-	A.gen_R25	0.672
A.gen_R26	-	A.gen_R26	0.256

A.gen_R27	-	A.gen_R27	0.266
A.gen_R28	0.250	A.gen_R28	0.297
A.gen_R29	-	A.gen_R29	0.516
A.gen_R30	-	A.gen_R30	0.396
A.gen_R31	-	A.gen_R31	0.547
A.gen_R32	-	A.gen_R32	0.055
A.gen_R37	-	A.gen_R37	0.100
+EGF plate 1	0.672	+EGF plate 1	-
+EGF Plate 2	0.290	+EGF Plate 2	0.454
B.boe_R5	0.073	B.boe_R5	-
B.boe_R6	0.511	B.boe_R6	-
B.boe_R7	0.227	B.boe_R7	-
B.boe_R10	0.227	B.boe_R10	-
B.boe_R11	0.598	B.boe_R11	-
B.boe_R13	0.602	B.boe_R13	-
B.boe_R14	0.227	B.boe_R14	-
B.boe_R15	-	B.boe_R15	0.630
B.boe_R16	-	B.boe_R16	0.209
B.boe_R17	-	B.boe_R17	0.227
B.boe_R18	0.227	B.boe_R18	0.472
B.boe_R19	0.227	B.boe_R19	0.436
B.boe_R20	0.231	B.boe_R20	0.124
B.boe_R21	0.176	B.boe_R21	0.159
B.boe_R22	0.227	B.boe_R22	0.597
B.boe_R23	0.227	B.boe_R23	0.554
B.boe_R24	-	B.boe_R24	0.566
B.boe_R25	-	B.boe_R25	0.163
B.boe_R26	-	B.boe_R26	0.524
+EGF	0.060	+EGF	0.413
H.swa_R2	0.295	H.swa_R2	-
H.swa_R7	0.840	H.swa_R7	0.059
H.swa_R8	0.564	H.swa_R8	0.407
H.swa_R9	0.372	H.swa_R9	-
H.swa_R13	0.593	H.swa_R13	0.227
+EGF	0.309	+EGF	0.580
H.swa_R19	-	H.swa_R19	0.227
H.swa_R23	0.157	H.swa_R23	0.566
H.swa_R27	0.058	H.swa_R27	-
H.swa_R28	0.340	H.swa_R28	-
H.swa_R29	0.586	H.swa_R29	0.542
H.swa_R30	0.532	H.swa_R30	0.494
H.swa_R36	0.319	H.swa_R36	-
H.swa_R37	0.492	H.swa_R37	0.630
H.swa_R40	-	H.swa_R40	0.352
+EGF	0.895	+EGF	0.095

Appendix XXV: Chapter 7: Table of Equal Variance and Residual P-Values for Snake and Invertebrate Fraction PY20 ELISA Data Sets

Equal Variance Test P-Values			
Elapid Venoms			
MDA-MB-468 Cells		A431 Cells	
P.wei	0.214	P.wei	0.536
N.naj	0.378	N.naj	0.002
O.han	0.102	O.han	0.194
Crotalid Venoms			
C.dve	0.350	C.dve	0.084
C.rho	0.000	C.rho	0.636
S.mil	0.337	S.mil	0.688
Invertebrate Venoms			
A.gen Plate 1	0.593	A.gen Plate 1	-
A.gen Plate 2	0.899	A.gen Plate 2	0.317
B.boe	0.727	B.boe	0.355
H.swa Plate 1	0.557	H.swa Plate 1	0.401
H.swa Plate 2	0.478	H.swa Plate 2	0.418
ANOVA Residual Test P-Values			
Elapid Venoms			
MDA-MB-468 Cells		A431 Cells	
P.wei	0.720	P.wei	0.298
N.naj	0.751	N.naj	N/A
O.han	0.407	O.han	0.675
Crotalid Venoms			
C.dve	0.477	C.dve	0.548
C.rho	N/A	C.rho	0.325
S.mil	0.135	S.mil	0.301
Invertebrate Venoms			
A.gen Plate 1	N/A	A.gen Plate 1	-
A.gen Plate 2	N/A	A.gen Plate 2	0.603
B.boe	0.588	B.boe	0.076
H.swa Plate 1	0.875	H.swa Plate 1	0.858
H.swa Plate 2	0.998	H.swa Plate 2	0.143

Appendix XXVI: Chapter 7: ANOVA Data Analyses of Venom Fractions

A

Analysis of Variance of MDA, C.dve Fractions

Source	DF	Adj SS	Adj MS	F-Value	P-Value
Subscripts	10	1.5432	0.15432	6.05	0.000
Error	25	0.6378	0.02551		
Total	35	2.1810			

Model Summary

S	R-sq	R-sq(adj)	R-sq(pred)
0.0970647	89.19%	85.75%	80.77%

Grouping Information Using the Tukey Method and 95% Confidence

Subscripts	N	Mean	Grouping		
+EGF	4	1.5555	A		
C.dve_R6	4	1.2247	B		
C.dve_R16	4	1.1943	B		
C.dve_R10	4	1.1109	B	C	
C.dve_R2	4	1.0961	B	C	
C.dve_R12	4	1.0911	B	C	
C.dve_R3	4	1.0648	B	C	
C.dve_R4	3	1.0570	B	C	
C.dve_R9	4	1.0198	B	C	
C.dve_R15	4	0.9388		C	D
C.dve_R1	4	0.9285		C	D
C.dve_R13	4	0.7709			D E
C.dve_R14	4	0.7597			D E
C.dve_R8	4	0.6365			E
C.dve_R7	4	0.5873			E

Means that do not share a letter are significantly different.

B

Analysis of Variance of A431, C.dve Fractions

Source	DF	Adj SS	Adj MS	F-Value	P-Value
Subscripts	10	1.5432	0.15432	6.05	0.000
Error	25	0.6378	0.02551		
Total	35	2.1810			

Model Summary

S	R-sq	R-sq(adj)	R-sq(pred)
0.159723	70.76%	59.06%	40.49%

Grouping Information Using the Tukey Method and 95% Confidence

Subscripts	N	Mean	Grouping	
+EGF	4	1.0454	A	
C.dve_R14	4	0.8348	A	B
C.dve_R3	2	0.8300	A	B
C.dve_R10	4	0.8287	A	B
C.dve_R9	4	0.819	A	B
C.dve_R1	2	0.797	A	B
C.dve_R6	2	0.7531	A	B
C.dve_R13	4	0.4887		B
C.dve_R12	3	0.4882		B
C.dve_R7	4	0.4365		B
C.dve_R8	3	0.4285		B

Means that do not share a letter are significantly different.

Statistical Analysis of MDA-MB-468 and A431 cells treated with *C. durissus vegrandis* Fractions

Fractions identified through analysis of EGFR ELISA data to cause 20% or greater reduction in EGFR phosphorylation were selected for further statistical analysis. (A) Statistical analysis of *C. durissus vegrandis* fractions identified to cause reductions ≥20% in EGFR phosphorylation in MDA-MB-468. (B) Statistical analysis of *C. durissus vegrandis* fractions identified to cause reductions ≥20% in EGFR phosphorylation in A431. ANOVA statistical analysis was undertaken, generating a P value and R-sq value for level of significance. Post Hoc Tukey's Test analysis identified fractions causing significant reductions from +EGF-only treated cells. Results of significant differences are highlighted in yellow boxes.

A

Analysis of Variance

Source	DF	Adj SS	Adj MS	F-Value	P-Value
Subscripts	8	2.2268	0.27835	12.97	0.000
Error	27	0.5797	0.02147		
Total	35	2.8065			

Model Summary

S	R-sq	R-sq(adj)	R-sq(pred)
0.146523	79.35%	73.23%	63.28%

Grouping Information Using the Tukey Method and 95% Confidence

Subscripts	N	Mean	Grouping		
+EGF	4	1.633	A		
S.mil_R5	4	1.3116	A	B	
S.mil_R15	4	1.2661		B	
S.mil_R3	4	1.2642		B	
S.mil_R9	4	1.2057		B	
S.mil_R13	4	1.1334		B	
S.mil_R6	4	1.0529		B	
S.mil_R7	4	1.0460		B	
S.mil_R8	4	0.6476			C

Means that do not share a letter are significantly different.

B

Analysis of Variance

Source	DF	Adj SS	Adj MS	F-Value	P-Value
Subscripts	8	0.3586	0.044826	6.81	0.000
Error	21	0.1382	0.006579		
Total	29	0.4968			

Model Summary

S	R-sq	R-sq(adj)	R-sq(pred)
0.0811138	72.19%	61.59%	43.70%

Grouping Information Using the Tukey Method and 95% Confidence

Subscripts	N	Mean	Grouping		
+EGF	4	0.7671	A		
S.mil_R2	3	0.6103	A	B	
S.mil_R1	4	0.6059	A	B	
S.mil_R9	3	0.5532		B	C
S.mil_R6	4	0.5372		B	C
S.mil_R5	3	0.5334		B	C
S.mil_R13	4	0.5246		B	C
S.mil_R8	2	0.4711		B	C
S.mil_R7	3	0.3395			C

Means that do not share a letter are significantly different.

Statistical Analysis of MDA-MB-468 and A431 cells treated with *S. miliarius* Fractions

Fractions identified through analysis of EGFR ELISA data to cause 20% or greater reduction in EGFR phosphorylation were selected for further statistical analysis. (A) Statistical analysis of *S. miliarius* fractions identified to cause reductions ≥20% in EGFR phosphorylation in MDA-MB-468. (B) Statistical analysis of *S. miliarius* fractions identified to cause reductions ≥20% in EGFR phosphorylation in A431. ANOVA statistical analysis was undertaken, generating a P value and R-sq value for level of significance. Post Hoc Tukey's Test analysis identified fractions causing significant reductions from +EGF-only treated cells. Results of significant differences are highlighted in yellow boxes.

A

Descriptive Statistics

Sample	N	Median
C.rho_R7	4	0.94181
+EGF	4	1.21046

Estimation for Difference

Difference	CI for Difference	Achieved Confidence
-0.266878	(-0.440278, -0.0635005)	96.96%

Test

Null hypothesis $H_0: \eta_1 - \eta_2 = 0$

Alternative hypothesis $H_1: \eta_1 - \eta_2 \neq 0$

W-Value	P-Value
10.00	0.030

B

Analysis of Variance

Source	DF	Adj SS	Adj MS	F-Value	P-Value
Subscripts	8	0.7149	0.08936	2.26	0.061
Error	23	0.9107	0.03960		
Total	31	1.6256			

Model Summary

S	R-sq	R-sq(adj)	R-sq(pred)
0.198989	43.98%	24.49%	0.00%

Grouping Information Using the Tukey Method and 95% Confidence

Subscripts	N	Mean	Grouping		
+EGF	4	1.0623	A		
C.rho_R3	4	0.854	A	B	
C.rho_R9	3	0.8401	A	B	
C.rho_R15	4	0.8359	A	B	
C.rho_R14	4	0.8314	A	B	
C.rho_R8	4	0.817	A	B	
C.rho_R2	4	0.732	A	B	
C.rho_R1	2	0.6648	A	B	
C.rho_R7	3	0.4541		B	

Means that do not share a letter are significantly different.

Two-sample T-Test

Descriptive Statistics

Sample	N	Mean	StDev	SE Mean
C.rho_R7	3	0.4541	0.0999	0.058
+EGF	4	1.062	0.169	0.084

Test

Null hypothesis $H_0: \mu_1 - \mu_2 = 0$

Alternative hypothesis $H_1: \mu_1 - \mu_2 \neq 0$

T-Value	DF	P-Value
-5.48	5	0.003

Statistical Analysis of MDA-MB-468 and A431 cells treated with *C. rhodostoma* Fractions

Fractions identified through analysis of EGFR ELISA data to cause 20% or greater reduction in EGFR phosphorylation were selected for further statistical analysis. (A) Statistical analysis of *C. rhodostoma* fractions identified to cause reductions ≥20% in EGFR phosphorylation in MDA-MB-468. (B) Statistical analysis of *C. rhodostoma* fractions identified to cause reductions ≥20% in EGFR phosphorylation in A431. ANOVA statistical analysis was undertaken, generating a P value and R-sq value for level of significance. Post Hoc Tukey's Test analysis identified fractions causing significant reductions from +EGF-only treated cells. Additional T-test analysis of A431 sample C.rho_R7 generated a P value. Results of significant differences are highlighted in yellow boxes

A

Analysis of Variance

Source	DF	Adj SS	Adj MS	F-Value	P-Value
Subscripts	2	0.6477	0.32387	24.65	0.000
Error	9	0.1182	0.01314		
Total	11	0.7660			

Model Summary

S	R-sq	R-sq(adj)	R-sq(pred)
0.114619	84.56%	81.13%	72.56%

Grouping Information Using the Tukey Method and 95% Confidence

Subscripts	N	Mean	Grouping	
+EGF	4	1.5860	A	
N.naj_R13	4	1.1145		B
N.naj_R7	4	1.0743		B

Means that do not share a letter are significantly different.

B

Analysis of Variance

Source	DF	Adj SS	Adj MS	F-Value	P-Value
Subscripts	11	2.483	0.2257	2.17	0.044
Error	32	3.333	0.1042		
Total	43	5.816			

Model Summary

S	R-sq	R-sq(adj)	R-sq(pred)
0.322726	42.69%	22.99%	0.00%

Grouping Information Using the Tukey Method and 95% Confidence

Subscripts	N	Mean	Grouping		
+EGF	3	1.390	A		
N.naj_R16	3	1.2552	A	B	
N.naj_R4	4	1.0290	A	B	
N.naj_R6	3	1.012	A	B	
N.naj_R2	4	0.955	A	B	
N.naj_R13	4	0.876	A	B	
N.naj_R1	4	0.874	A	B	
N.naj_R15	4	0.810	A	B	
N.naj_R3	4	0.786	A	B	
N.naj_R14	4	0.7278	A	B	
N.naj_R8	3	0.5299	A	B	
N.naj_R7	4	0.4928		B	

Means that do not share a letter are significantly different.

Statistical Analysis of MDA-MB-468 and A431 cells treated with *N. naja* Fractions

Fractions identified through analysis of EGFR ELISA data to cause 20% or greater reduction in EGFR phosphorylation were selected for further statistical analysis. (A) Statistical analysis of *N. naja* fractions identified to cause reductions ≥20% in EGFR phosphorylation in MDA-MB-468. (B) Statistical analysis of *N. naja* fractions identified to cause reductions ≥20% in EGFR phosphorylation in A431. ANOVA statistical analysis was undertaken, generating a P value and R-sq value for level of significance. Post Hoc Tukey's Test analysis identified fractions causing significant reductions from +EGF-only treated cells. Results of significant differences are highlighted in yellow boxes.

A

Analysis of Variance

Source	DF	Adj SS	Adj MS	F-Value	P-Value
Subscripts	5	0.50674	0.101348	25.09	0.000
Error	15	0.06060	0.004040		
Total	20	0.56734			

Model Summary

S	R-sq	R-sq(adj)	R-sq(pred)
0.0635609	89.32%	85.76%	74.14%

Grouping Information Using the Tukey Method and 95% Confidence

Subscripts	N	Mean	Grouping		
+ EGF	2	0.9728	A		
P.wei_R9	4	0.6445		B	
P.wei_R8	3	0.6098		B	
P.wei_R6	4	0.6024		B	
P.wei_R7	4	0.4353			C
P.wei_R10	4	0.4274			C

Means that do not share a letter are significantly different.

B

Analysis of Variance

Source	DF	Adj SS	Adj MS	F-Value	P-Value
Subscripts	4	0.4172	0.10430	6.89	0.003
Error	13	0.1967	0.01513		
Total	17	0.6139			

Model Summary

S	R-sq	R-sq(adj)	R-sq(pred)
0.123013	67.96%	58.10%	38.18%

Grouping Information Using the Tukey Method and 95% Confidence

Subscripts	N	Mean	Grouping		
+ EGF	3	0.7013	A		
P.wei_R6	4	0.5581	A	B	
P.wei_R9	3	0.4807	A	B	C
P.wei_R10	4	0.3721		B	C
P.wei_R7	4	0.2528			C

Means that do not share a letter are significantly different.

Statistical Analysis of MDA-MB-468 and A431 cells treated with *Pseudechis rossignoli* Fractions

Fractions identified through analysis of EGFR ELISA data to cause 20% or greater reduction in EGFR phosphorylation were selected for further statistical analysis. (A) Statistical analysis of *P. rossignoli* fractions identified to cause reductions ≥20% in EGFR phosphorylation in MDA-MB-468. (B) Statistical analysis of *P. rossignoli* fractions identified to cause reductions ≥20% in EGFR phosphorylation in A431. ANOVA statistical analysis was undertaken, generating a P value and R-sq value for level of significance. Post Hoc Tukey's Test analysis identified fractions causing significant reductions from +EGF-only treated cells. Results of significant differences are highlighted in yellow boxes.

A

Analysis of Variance

Source	DF	Adj SS	Adj MS	F-Value	P-Value
Subscripts	3	0.4123	0.13743	5.98	0.008
Error	14	0.3217	0.02298		
Total	17	0.7339			

Model Summary

S	R-sq	R-sq(adj)	R-sq(pred)
0.151579	56.17%	46.78%	35.97%

Grouping Information Using the Tukey Method and 95% Confidence

Subscripts	N	Mean	Grouping
+EGF	8	1.3887	A
O.han_R12	4	1.1033	B
O.han_R6	4	1.1033	B
O.han_R19	2	1.0256	B

Means that do not share a letter are significantly different.

B

Analysis of Variance

Source	DF	Adj SS	Adj MS	F-Value	P-Value
Subscripts	2	0.3295	0.16477	4.39	0.040
Error	11	0.4127	0.03752		
Total	13	0.7422			

Model Summary

S	R-sq	R-sq(adj)	R-sq(pred)
0.193694	44.40%	34.29%	15.89%

Grouping Information Using the Tukey Method and 95% Confidence

Subscripts	N	Mean	Grouping	
+EGF	6	1.281	A	
O.han_R11	4	1.0288	A	B
O.han_R12	4	0.9308		B

Means that do not share a letter are significantly different.

Statistical Analysis of MDA-MB-468 and A431 cells treated with *Ophiophagus hannah* Fractions

Fractions identified through analysis of EGFR ELISA data to cause 20% or greater reduction in EGFR phosphorylation were selected for further statistical analysis. (A) Statistical analysis of *O. hannah* fractions identified to cause reductions ≥20% in EGFR phosphorylation in MDA-MB-468. (B) Statistical analysis of *O. hannah* fractions identified to cause reductions ≥20% in EGFR phosphorylation in A431. ANOVA statistical analysis was undertaken, generating a P value and R-sq value for level of significance. Post Hoc Tukey's Test analysis identified fractions causing significant reductions from +EGF-only treated cells. Results of significant differences are highlighted in yellow boxes.

A

Analysis of Variance

Source	DF	Adj SS	Adj MS	F-Value	P-Value
Subscripts	13	9.3511	0.71932	19.28	0.000
Error	21	0.7835	0.03731		
Total	34	10.1346			

Model Summary

S	R-sq	R-sq(adj)	R-sq(pred)
0.193155	92.27%	87.48%	76.44%

Grouping Information Using the Tukey Method and 95% Confidence

Subscripts	N	Mean	Grouping
+ve	3	2.317	A
B.boe_R21	3	1.7142	B
B.boe_R19	2	1.7121	A B
B.boe_R22	2	1.710	A B
B.boe_R11	3	1.626	B
B.boe_R13	3	1.5746	B C
B.boe_R18	2	1.514	B C D
B.boe_R14	2	1.276	B C D E
B.boe_R5	3	1.1268	B C D E
B.boe_R23	2	0.944	C D E F
B.boe_R7	2	0.879	D E F
B.boe_R10	2	0.7110	E F
B.boe_R20	3	0.708	E F
B.boe_R6	3	0.4857	F

Means that do not share a letter are significantly different.

B

Analysis of Variance

Source	DF	Adj SS	Adj MS	F-Value	P-Value
Subscripts	12	0.6002	0.05002	3.91	0.002
Error	26	0.3322	0.01278		
Total	38	0.9324			

Model Summary

S	R-sq	R-sq(adj)	R-sq(pred)
0.113031	64.37%	47.93%	28.87%

Grouping Information Using the Tukey Method and 95% Confidence

Subscripts	N	Mean	Grouping	
+EGF	4	1.649	A	
B.boe_R17	2	1.40447	A	B
B.boe_R16	3	1.3918	A	B
B.boe_R25	3	1.3911	A	B
B.boe_R15	3	1.3821	A	B
B.boe_R18	3	1.36462	A	B
B.boe_R26	3	1.3273		B
B.boe_R22	3	1.3151		B
B.boe_R24	3	1.3036		B
B.boe_R23	3	1.2500		B
B.boe_R21	3	1.2244		B
B.boe_R20	3	1.2029		B
B.boe_R19	3	1.1970		B

Means that do not share a letter are significantly different.

Statistical Analysis of MDA-MB-468 and A431 cells treated with *Brachypelma boehmei* Fractions

Fractions identified through analysis of EGFR ELISA data to cause 20% or greater reduction in EGFR phosphorylation were selected for further statistical analysis. (A) Statistical analysis of *B. boehmei* fractions identified to cause reductions ≥20% in EGFR phosphorylation in MDA-MB-468. (B) Statistical analysis of *B. boehmei* fractions identified to cause reductions ≥20% in EGFR phosphorylation in A431. ANOVA statistical analysis was undertaken, generating a P value and R-sq value for level of significance. Post Hoc Tukey's Test analysis identified fractions causing significant reductions from +EGF-only treated cells. Results of significant differences are highlighted in yellow boxes.

A

Descriptive Statistics

Sample	N	Mean	StDev	SE Mean
A.gen_R2	4	0.3570	0.0419	0.021
+EGF	4	0.6347	0.0529	0.026

Test

Null hypothesis	$H_0: \mu_1 - \mu_2 = 0$
Alternative hypothesis	$H_1: \mu_1 - \mu_2 \neq 0$

T-Value	DF	P-Value
-8.23	6	0.000

Descriptive Statistics

Sample	N	Mean	StDev	SE Mean
A.gen_R28	4	0.4329	0.0527	0.026
+EGF_1	4	0.5738	0.0507	0.025

Test

Null hypothesis	$H_0: \mu_1 - \mu_2 = 0$
Alternative hypothesis	$H_1: \mu_1 - \mu_2 \neq 0$

T-Value	DF	P-Value
-3.85	6	0.008

B

Analysis of Variance

Source	DF	Adj SS	Adj MS	F-Value	P-Value
Subscripts	11	0.3784	0.03440	1.40	0.215
Error	35	0.8587	0.02453		
Total	46	1.2371			

Model Summary

S	R-sq	R-sq(adj)	R-sq(pred)
0.156635	30.59%	8.77%	0.00%

Grouping Information Using the Tukey Method and 95% Confidence

Subscripts	N	Mean	Grouping
+EGF	4	0.8054	A
A.gen_R37	4	0.6442	A
A.gen_R25	4	0.5809	A
A.gen_R31	4	0.5744	A
A.gen_R29	4	0.5684	A
A.gen_R32	4	0.5590	A
A.gen_R28	4	0.546	A
A.gen_R30	4	0.5383	A
A.gen_R22	4	0.5145	A
A.gen_R27	4	0.490	A
A.gen_R26	4	0.4728	A
A.gen_R21	3	0.437	A

Means that do not share a letter are significantly different.

Statistical Analysis of MDA-MB-468 and A431 cells treated with *Acanthoscurria geniculata* Fractions

Fractions identified through analysis of EGFR ELISA data to cause 20% or greater reduction in EGFR phosphorylation were selected for further statistical analysis. (A) Statistical analysis of *A. geniculata* fractions identified to cause reductions ≥20% in EGFR phosphorylation in MDA-MB-468. (B) Statistical analysis of *A. geniculata* fractions identified to cause reductions ≥20% in EGFR phosphorylation in A431. ANOVA statistical analysis was undertaken, generating a P value and R-sq value for level of significance. Post Hoc Tukey's Test analysis identified fractions causing significant reductions from +EGF-only treated cells. Results of significant differences are highlighted in yellow boxes.

A

Analysis of Variance

Source	DF	Adj SS	Adj MS	F-Value	P-Value
Subscripts	5	1.0015	0.20029	7.40	0.001
Error	19	0.5145	0.02708		
Total	24	1.5159			

Model Summary

S	R-sq	R-sq(adj)	R-sq(pred)
0.164554	66.06%	57.13%	40.09%

Grouping Information Using the Tukey Method and 95% Confidence

Subscripts	N	Mean	Grouping		
+ve EGF	7	0.8968	A		
H.swa_R2	3	0.6622	A	B	
H.swa_R13	3	0.540	A	B	
H.swa_R7	4	0.527		B	
H.swa_R9	4	0.4786		B	
H.swa_R8	4	0.3333		B	

Means that do not share a letter are significantly different.

B

Analysis of Variance

Source	DF	Adj SS	Adj MS	F-Value	P-Value
Subscripts	7	3.1110	0.44443	16.04	0.000
Error	25	0.6927	0.02771		
Total	32	3.8037			

Model Summary

S	R-sq	R-sq(adj)	R-sq(pred)
0.166453	81.79%	76.69%	69.23%

Grouping Information Using the Tukey Method and 95% Confidence

Subscripts	N	Mean	Grouping			
+ve EGF	7	1.5599	A			
H.swa_R27	3	1.2302	A	B	C	
H.swa_R28	4	1.2243	A	B		
H.swa_R23	3	0.9123		B	C	D
H.swa_R36	4	0.8974		B	C	D
H.swa_R37	4	0.867		B	C	D
H.swa_R29	4	0.8319			C	D
H.swa_R30	4	0.6593				D

Means that do not share a letter are significantly different.

Statistical Analysis of MDA-MB-468 cells treated with *Heterometrus swammerdami* Fractions

Fractions identified through analysis of EGFR ELISA data to cause 20% or greater reduction in EGFR phosphorylation were selected for further statistical analysis. (A & B) Statistical analysis of *H. swammerdami* fractions identified to cause reductions ≥20% in EGFR phosphorylation in MDA-MB-468 cells. ANOVA statistical analysis was undertaken, generating a P value and R-sq value for level of significance. Post Hoc Tukey's Test analysis identified fractions causing significant reductions from +EGF-only treated cells. Results of significant differences are highlighted in yellow boxes.

A

Analysis of Variance

Source	DF	Adj SS	Adj MS	F-Value	P-Value
Subscripts	3	0.3885	0.12950	7.53	0.004
Error	12	0.2064	0.01720		
Total	15	0.5949			

Model Summary

S	R-sq	R-sq(adj)	R-sq(pred)
0.131155	65.30%	56.63%	44.19%

Grouping Information Using the Tukey Method and 95% Confidence

Subscripts	N	Mean	Grouping		
+EGF	7	0.5711	A		
H.swa_R13	2	0.3417	A	B	
H.swa_R7	3	0.3037	A	B	
H.swa_R8	4	0.2070		B	

Means that do not share a letter are significantly different.

B

Analysis of Variance

Source	DF	Adj SS	Adj MS	F-Value	P-Value
Subscripts	6	0.4459	0.07432	3.60	0.019
Error	16	0.3304	0.02065		
Total	22	0.7764			

Model Summary

S	R-sq	R-sq(adj)	R-sq(pred)
0.143710	57.44%	41.48%	20.15%

Grouping Information Using the Tukey Method and 95% Confidence

Subscripts	N	Mean	Grouping		
+EGF	6	0.6476	A		
H.swa_R19	2	0.5087	A	B	
H.swa_R37	3	0.4878	A	B	
H.swa_R23	3	0.456	A	B	
H.swa_R29	3	0.4240	A	B	
H.swa_R40	3	0.3559	A	B	
H.swa_R30	3	0.20710		B	

Means that do not share a letter are significantly different.

Statistical Analysis of A431 cells treated with *Heterometrus swammerdami* Fractions

Fractions identified through analysis of EGFR ELISA data to cause 20% or greater reduction in EGFR phosphorylation were selected for further statistical analysis. (A & B) Statistical analysis of *H. swammerdami* fractions identified to cause reductions ≥20% in EGFR phosphorylation in A431 cells. ANOVA statistical analysis was undertaken, generating a P value and R-sq value for level of significance. Post Hoc Tukey's Test analysis identified fractions causing significant reductions from +EGF-only treated cells. Results of significant differences are highlighted in yellow boxes.

Appendix XXVII: Chapter 7: Mass Spectrometry Data Reports from Peak Proteins for Fractions B.boe_R6, C.dve_R7 and H.swa_R30

PEAK PROTEINS
Peak Proteins
Based at the BioHub, Alderley Park, Cheshire, SK10 4TG
Company Registration 9265797

04.10.2019

Venomtech samples:

3 duplicate samples provided:

C.dve_R7

H.swa_R30

B.boe_R6

Peptide Mapping Preparation:

- 50ul of 100mM Ammonium bicarbonate was added to reconstitute the sample.
- 5ul of 100mM DTT in 100mM ammonium bicarbonate was added, incubated at 65°C for 30 minutes.
- 5ul of 500mM iodoacetamide in 100mM ammonium bicarbonate was added, incubated at RT in the dark for 30 minutes.
- 10ul of25ng/ul trypsin in 50mM ammonium bicarbonate was added. The samples were incubated overnight at 37 °C.
- 10ul of digest was taken and 10ul 0f 0.1% trifluoroacetic acid was added.

10ul of sample was loaded onto the Sciex Exion LC and a 10 minute reverse phase gradient was used. Buffer A was 0.1% formic acid and Buffer B was 0.1% formic acid 100% acetonitrile. The flow was set to 300ul starting at 5% B leading to 45% B over 15 minutes before a 95% B wash and equilibration at 5%B. A Phenomenex Lunar 1.6um, PS C18, 100A 150x2.1mm column was used. The flow from the column was passed into the Sciex X500B mass spectrometer collecting data in positive ion mode. To enable ionisation of the eluate the source was set to 400°C, 5500V with gas at 30psi. A TOF mass window of 300 to 1800Da was collected scanning at 1.2seconds. MSMS data was collected using an Information Dependent Acquisition method where up to 10 MSMS were collected per scan. The X500B was calibrated with positive calibration mix, the error for this experiment was estimated at 1ppm. The data was searched against Swissprot using Mascot. See data below.

PEAK PROTEINS
Peak Proteins
Based at the BioHub, Alderley Park, Cheshire, SK10 4TG
Company Registration 9265797

Intact Mass Analysis:

The samples were reconstituted with 40ul of 0.1% formic acid/5% acetonitrile. 10ul of sample was loaded onto the Sciex Exion LC and a 5 minute reverse phase gradient was used. Buffer A was 0.1% formic acid and Buffer B was 0.1% formic acid 100% acetonitrile. The flow was set to 500ul starting at 5% B leading

to 45% B over 3 minutes before a 95% B wash and equilibration at 5%B. A Phenomenex Jupiter 5um, C4, 300A 50x2.1mm column was used. The flow from the column was passed into the Sciex X500B mass spectrometer collecting data in positive ion mode. To enable ionisation of the eluate the source was set to 400^{o}C, 5500V with gas at 50psi. A TOF mass window of 500 to 3000Da was collected scanning at 0.5 seconds. The X500B was calibrated with positive calibration mix, the error for this experiment was estimated at 0.5Da. The resultant TIC was deconvoluted using BioToolKit software. See spectrum below.

Results Summary:

Sample	Intact Mass	Peptide Mapping	Comments
C.dve_R7	14184Da	Basic phospholipase PA2BA_CRODR Venom nerve growth factor NGFV_CRODU	PA2BA – 14199Da mass(- 14Da for disulphides) 1Da out ?
H.swa_R30	8896Da plus others	Phospholipase A2 PA2_HETFU Cytotoxin 3SA1-….	No H.swa matches (only 9 seqs in uniprot)
B.boe_R6	No significant data	No significant data	

PEAK PROTEINS
Peak Proteins
Based at the BioHub, Alderley Park, Cheshire, SK10 4TG
Company Registration 9265797

C.dve_R7

Peptide Mapping:

1. PA2BA_CRODR **Mass:** 14988 **Score:** 368 **Matches:** 15(10) **Sequences:** 8(6) **emPAI:** 5.65
Basic phospholipase A2 A OS=Crotalus durissus ruruima OX=221570 PE=1 SV=1
☐ Check to include this hit in error tolerant search or archive report

Query	Observed	Mr(expt)	Mr(calc)	ppm	Miss	Score	Expect	Rank	Unique	Peptide
☑ 29	409.7123	817.4101	817.4116	-1.80	0	44	0.0089	1		R.VAAECLR.R
☑ 30	409.7141	817.4136	817.4116	2.48	0	(33)	0.19	1		R.VAAECLR.R
☑ 76	443.2105	884.4065	884.4062	0.36	0	(51)	0.0021	1		K.SGYITCGK.G
☑ 77	443.2108	884.4070	884.4062	0.95	0	51	0.0019	1		K.SGYITCGK.G
☑ 85	450.2574	898.5002	898.5025	-2.50	0	(36)	0.046	1		-.HLLQFNK.M
☑ 86	450.2593	898.5040	898.5025	1.67	0	37	0.037	1		-.HLLQFNK.M
☑ 100	462.7521	923.4895	923.4899	-0.33	1	20	4.3	1		K.MIKFETR.K
110	**470.7520**	**939.4894**	**939.4848**	**4.96**	**1**	**(5)**	**1.1e+002**	**2**		**K.MIKFETR.K + Oxidation (M)**
☑ 177	592.8049	1183.5953	1183.5913	3.38	0	40	0.038	1	U	K.WDIYPYSLK.S
☑ 196	649.7810	1297.5474	1297.5437	2.79	0	64	0.00016	1		K.YGYMFYPDSR.C
☑ 199	657.7771	1313.5397	1313.5387	0.79	0	(63)	0.00019	1		K.YGYMFYPDSR.C + Oxidation (M)
☑ 227	502.5188	1504.5344	1504.5356	-0.80	0	(28)	0.37	1		R.CCFVHDCCYGK.L
☑ 228	502.5197	1504.5374	1504.5356	1.16	0	29	0.28	1		R.CCFVHDCCYGK.L
☑ 249	871.8327	1741.6509	1741.6494	0.81	0	82	2.1e-006	1		K.GTWCEEQICECDR.V
☑ 250	871.8332	1741.6519	1741.6494	1.38	0	(82)	2.1e-006	1		K.GTWCEEQICECDR.V

---

2. NGFV_CRODU **Mass:** 27558 **Score:** 280 **Matches:** 8(5) **Sequences:** 6(4) **emPAI:** 1.12
Venom nerve growth factor OS=Crotalus durissus terrificus OX=8732 PE=2 SV=1
☐ Check to include this hit in error tolerant search or archive report

Query	Observed	Mr(expt)	Mr(calc)	ppm	Miss	Score	Expect	Rank	Unique	Peptide
☑ 23	389.2089	776.4033	776.4028	0.55	0	46	0.0065	1	U	K.TTATDIR.G
☑ 126	481.7352	961.4558	961.4545	1.32	0	44	0.018	1	U	K.QYFFETK.C
☑ 165	556.2680	1110.5214	1110.5240	-2.36	0	30	0.52	1	U	R.NPNPVPTGCR.G
☑ 166	556.2688	1110.5231	1110.5240	-0.85	0	(28)	0.84	1	U	R.NPNPVPTGCR.G
☑ 195	640.3110	1278.6075	1278.6060	1.11	0	71	3.7e-005	1	U	R.IDSACVCVISR.K
☑ 211	682.3235	1362.6325	1362.6350	-1.87	0	70	4.3e-005	1	U	K.ALTMEGNQASWR.F
☑ 215	690.3271	1378.6396	1378.6299	7.04	0	(57)	0.001	1	U	K.ALTMEGNQASWR.F + Oxidation (M)
☑ 220	476.5595	1426.6568	1426.6558	0.70	1	19	6.3	1	U	K.CRNPNPVPTGCR.G

Intact Mass: Main peak at 14184.28Da

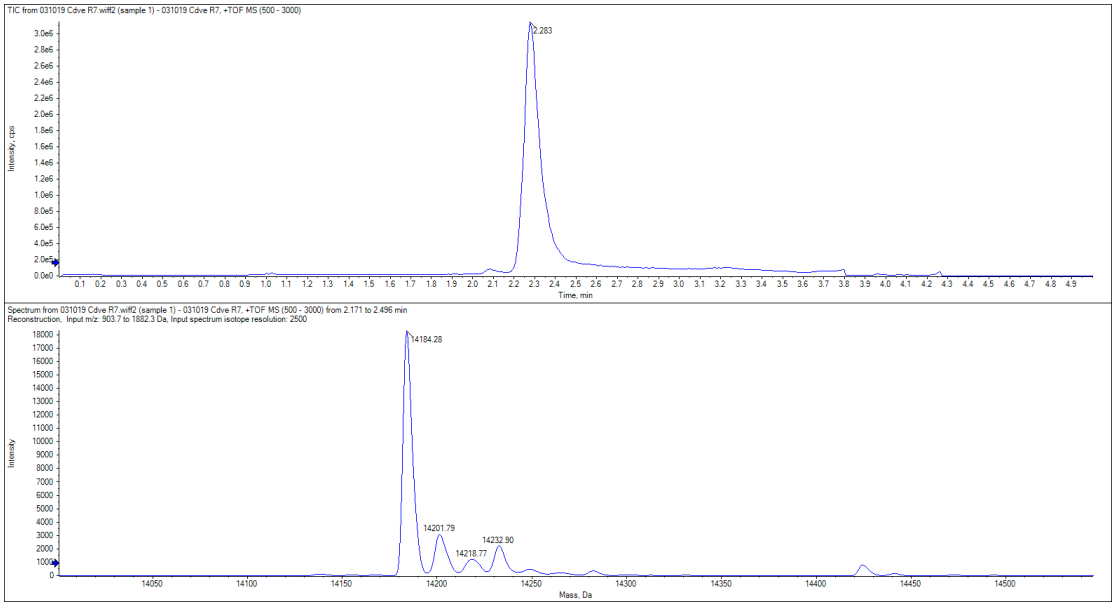

Peak Proteins
Based at the BioHub, Alderley Park, Cheshire, SK10 4TG
Company Registration 9265797

H.swa_R30

Peptide Mapping:

		Score	Mass	Matches	Sequences	emPAI	
2.1	PA2_HETFU	80	11992	5 (5)	3 (3)	1.81	Phospholipase A2 large subunit (Fragment) OS=Heterometrus fulvipes OX=141248 PE=2 SV=1

5 peptide matches (3 non-duplicate, 2 duplicate)

Auto-fit to window

Query	Dupes	Observed	Mr(expt)	Mr(calc)	ppm	M	Score	Expect	Rank	U	Peptide
149	1	441.2229	880.4312	880.4290	2.50	0	49	0.0064	1	U	K.YGLTNEGK.Y
215		474.1965	946.3785	946.3711	7.89	0	19	0.017	1	U	K.YTMMNCK.C
683	1	523.5636	1567.6690	1567.6685	0.31	0	43	0.002	1	U	R.THDHCDNIAAGETK.Y

1 subset or intersection (2 subset proteins in total)

	Score	Mass	Subset of	
IPTXI_PANIM	50	19279	2.1	Phospholipase A2 imperatoxin-1 OS=Pandinus imperator OX=55084 PE=1 SV=1
1 sameset of IPTXI_PANIM				
PA2_HOTTA	50	19188		Phospholipase A2 OS=Hottentotta tamulus OX=34647 PE=1 SV=1

		Score	Mass	Matches	Sequences	emPAI	
3	3SA1_NAJNA	46					Cytotoxin 1 OS=Naja naja OX=35670 PE=1 SV=1
3.1	3SA1_NAJNA	46	7243	3 (2)	2 (2)	2.06	Cytotoxin 1 OS=Naja naja OX=35670 PE=1 SV=1
	4 samesets of 3SA1_NAJNA						
	3SA3_NAJNA	46	7197	3 (2)	2 (2)		Cytotoxin 3 OS=Naja naja OX=35670 PE=1 SV=1
	3SA7A_NAJKA	46	7197	3 (2)	2 (2)		Cytotoxin 2 OS=Naja kaouthia OX=8649 PE=1 SV=1
	3SA7_NAJNA	46	7244	3 (2)	2 (2)		Cytotoxin 7 OS=Naja naja OX=35670 PE=1 SV=1
	3SA8_NAJNA	46	7245	3 (2)	2 (2)		Cytotoxin 8 OS=Naja naja OX=35670 PE=1 SV=2

3 peptide matches (2 non-duplicate, 1 duplicate)

Auto-fit to window

Query	Dupes	Observed	Mr(expt)	Mr(calc)	ppm	M	Score	Expect	Rank	U	Peptide
70	1	409.2635	816.5124	816.5109	1.79	0	38	0.007	1	U	K.LIPLAYK.T
218		474.7191	947.4236	947.4205	3.27	0	35	0.0056	1	U	R.GCIDVCPK.N

Intact Mass: Mixture of peaks, 4-5 main peaks ranging from 7900-9000Da

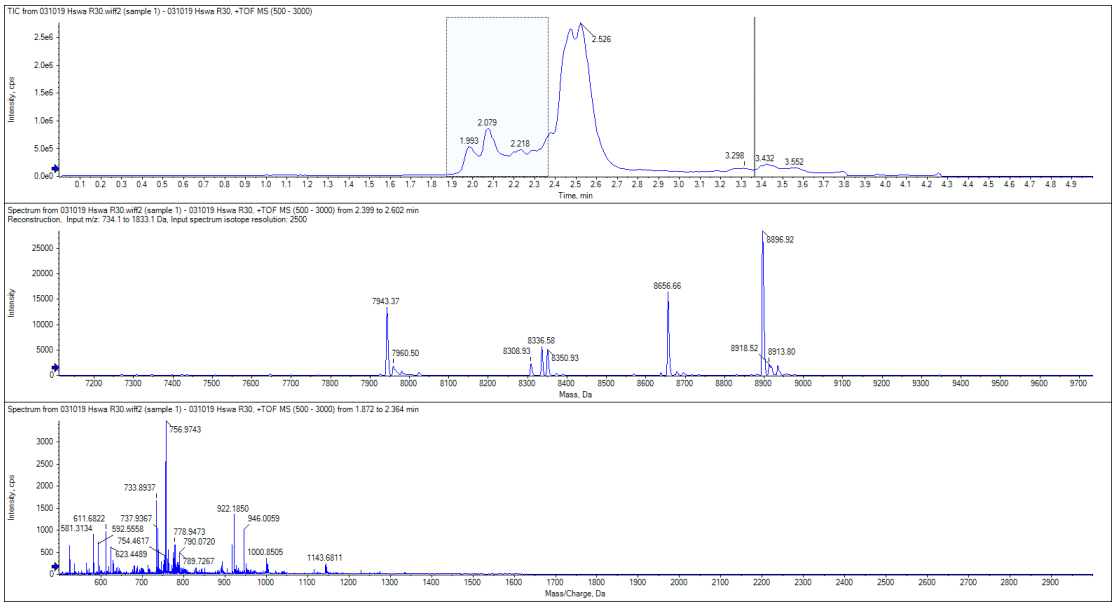

PEAK PROTEINS
Peak Proteins
Based at the BioHub, Alderley Park, Cheshire, SK10 4TG
Company Registration 9265797

B.boe_R6

Peptide Mapping: No significant results.

Intact Mass: No significant results.

C.dve_R7

Protein View: PA2BA_CRODR

Basic phospholipase A2 A OS=Crotalus durissus ruruima OX=221570 PE=1 SV=1

Database:	SwissProt
Score:	368
Nominal mass (M_r):	14988
Calculated pI:	8.74
Taxonomy:	Crotalus durissus ruruima

Sequence similarity is available as an NCBI BLAST search of PA2BA_CRODR against nr.

Search parameters

MS data file:	C:\Rachel\031019 Cdve R7 pm.mgf
Enzyme:	Trypsin: cuts C-term side of KR unless next residue is P.
Fixed modifications:	Carbamidomethyl (C)
Variable modifications:	Oxidation (M), Phospho (ST), Phospho (Y)

Protein sequence coverage: 59%

Matched peptides shown in ***bold red***.

```
  1 HLLQFNKMIK FETRKNAIPF YAFYGCYCGW GGRGRPKDAT DRCCFVHDCC
 51 YGKLAKCNTK WDIYPYSLKS GYITCGKGTW CEEQICECDR VAAECLRRSL
101 STYKYGYMFY PDSRCRGPSE TC
```

Unformatted sequence string: 122 residues (for pasting into other applications).

Sort peptides by ◉ Residue Number ○ Increasing Mass ○ Decreasing Mass

Show predicted peptides also

Query	Start – End	Observed	Mr(expt)	Mr(calc)	ppm	M	Score	Expect	Rank	U	Peptide
85	1 – 7	450.2574	898.5002	898.5025	-2.50	0	36	0.046	1		-.HLLQFNK.M
86	1 – 7	450.2593	898.5040	898.5025	1.67	0	37	0.037	1		-.HLLQFNK.M
100	8 – 14	462.7521	923.4895	923.4899	-0.33	1	20	4.3	1		K.MIKFETR.K
110	8 – 14	470.7520	939.4894	939.4848	4.96	1	5	1.1e+002	2		K.MIKFETR.K + Oxidation (M)
227	43 – 53	502.5188	1504.5344	1504.5356	-0.80	0	28	0.37	1		R.CCFVHDCCYGK.L
228	43 – 53	502.5197	1504.5374	1504.5356	1.16	0	29	0.28	1		R.CCFVHDCCYGK.L
177	61 – 69	592.8049	1183.5953	1183.5913	3.38	0	40	0.038	1	U	K.WDIYPYSLK.S
76	70 – 77	443.2105	884.4065	884.4062	0.36	0	51	0.0021	1		K.SGYITCGK.G
77	70 – 77	443.2108	884.4070	884.4062	0.95	0	51	0.0019	1		K.SGYITCGK.G
249	78 – 90	871.8327	1741.6509	1741.6494	0.81	0	82	2.1e-006	1		K.GTWCEEQICECDR.V
250	78 – 90	871.8332	1741.6519	1741.6494	1.38	0	82	2.1e-006	1		K.GTWCEEQICECDR.V
29	91 – 97	409.7123	817.4101	817.4116	-1.80	0	44	0.0089	1		R.VAAECLR.R
30	91 – 97	409.7141	817.4136	817.4116	2.48	0	33	0.19	1		R.VAAECLR.R
196	105 – 114	649.7810	1297.5474	1297.5437	2.79	0	64	0.00016	1		K.YGYMFYPDSR.C
199	105 – 114	657.7771	1313.5397	1313.5387	0.79	0	63	0.00019	1		K.YGYMFYPDSR.C + Oxidation (M)

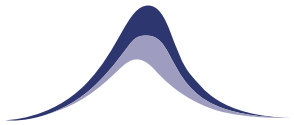

PEAK PROTEINS

Peak Proteins
Based at the BioHub, Alderley Park, Cheshire, SK10 4TG
Company Registration 9265797

Protein View: NGFV_CRODU

Venom nerve growth factor OS=Crotalus durissus terrificus OX=8732 PE=2 SV=1

Database: SwissProt
Score: 280
Nominal mass (M$_r$): 27558
Calculated pI: 8.90
Taxonomy: Crotalus durissus terrificus

Sequence similarity is available as an NCBI BLAST search of NGFV_CRODU against nr.

Search parameters

MS data file: C:\Rachel\031019 Cdve R7 pm.mgf
Enzyme: Trypsin: cuts C-term side of KR unless next residue is P.
Fixed modifications: Carbamidomethyl (C)
Variable modifications: Oxidation (M), Phospho (ST), Phospho (Y)

Protein sequence coverage: 20%

Matched peptides shown in ***bold red***.

```
  1 MSMLCYTLII AFLIGIWAAP KSEDNVPLGS PATSDLSDTS CAKTHEALKT
 51 SRNIDQHYPA PKGAEDQEFG SAANIIVDPK LFQKRRFQSP RVLFSTQPPP
101 LSRDEQSVDN ANSLNRNIRA KREDHPVHKR GEYSVCDSVN VWVANKTTAT
151 DIRGNLVTVM VDVNINNNVY KQYFFETKCR NPNPVPTGCR GIDARHWNSY
201 CTTTNTFVKA LTMEGNQASW RFIRIDSACV CVISRKNENF G
```

Unformatted sequence string: 241 residues (for pasting into other applications).

Sort peptides by ◉ Residue Number ○ Increasing Mass ○ Decreasing Mass

Show predicted peptides also

Query	Start – End	Observed	Mr(expt)	Mr(calc)	ppm	M	Score	Expect	Rank	U	Peptide
23	147 – 153	389.2089	776.4033	776.4028	0.55	0	46	0.0065	1	U	K.TTATDIR.G
126	172 – 178	481.7352	961.4558	961.4545	1.32	0	44	0.018	1	U	K.QYFFETK.C
220	179 – 190	476.5595	1426.6568	1426.6558	0.70	1	19	6.3	1	U	K.CRNPNPVPTGCR.G
165	181 – 190	556.2680	1110.5214	1110.5240	-2.36	0	30	0.52	1	U	R.NPNPVPTGCR.G
166	181 – 190	556.2688	1110.5231	1110.5240	-0.85	0	28	0.84	1	U	R.NPNPVPTGCR.G
211	210 – 221	682.3235	1362.6325	1362.6350	-1.87	0	70	4.3e-005	1	U	K.ALTMEGNQASWR.F
215	210 – 221	690.3271	1378.6396	1378.6299	7.04	0	57	0.001	1	U	K.ALTMEGNQASWR.F + Oxidation (M)
195	225 – 235	640.3110	1278.6075	1278.6060	1.11	0	71	3.7e-005	1	U	R.IDSACVCVISR.K

H.swa_R30

Protein View: PA2_HETFU

Phospholipase A2 large subunit (Fragment) OS=Heterometrus fulvipes OX=141248 PE=2 SV=1

Database: SwissProt
Score: 80
Nominal mass (M$_r$): 11992
Calculated pI: 7.46
Taxonomy: Heterometrus fulvipes

Sequence similarity is available as an NCBI BLAST search of PA2_HETFU against nr.

Search parameters

MS data file: C:\Rachel\031019 Hswa R30 pm.mgf
Enzyme: Trypsin: cuts C-term side of KR unless next residue is P.
Fixed modifications: Carbamidomethyl (C)
Variable modifications: Oxidation (M), Phospho (ST), Phospho (Y)

Protein sequence coverage: 28%

Matched peptides shown in ***bold red***.

```
  1 TMWGTKWCGS GNKAINYTDL GYFSNLDSCC RTHDHCDNIA AGETKYGLTN
 51 EGKYTMMNCK CEATFQQCLR DVHGPLEGKA AFTIRKLYFG LYGNGCFNVQ
101 CPS
```

Unformatted sequence string: 103 residues (for pasting into other applications).

Sort peptides by ◉ Residue Number ○ Increasing Mass ○ Decreasing Mass

Show predicted peptides also

Query	Start – End	Observed	Mr(expt)	Mr(calc)	ppm	M	Score	Expect	Rank	U	Peptide
683	32 – 45	523.5636	1567.6690	1567.6685	0.31	0	43	0.002	1	U	R.THDHCDNIAAGETK.Y
684	32 – 45	523.5645	1567.6716	1567.6685	1.96	0	43	0.00091	1	U	R.THDHCDNIAAGETK.Y
148	46 – 53	441.2226	880.4306	880.4290	1.76	0	43	0.021	1	U	K.YGLTNEGK.Y
149	46 – 53	441.2229	880.4312	880.4290	2.50	0	49	0.0064	1	U	K.YGLTNEGK.Y
215	54 – 60	474.1965	946.3785	946.3711	7.89	0	19	0.017	1	U	K.YTMMNCK.C

PEAK PROTEINS
Peak Proteins
Based at the BioHub, Alderley Park, Cheshire, SK10 4TG
Company Registration 9265797

Cytotoxin 1 OS=Naja naja OX=35670 PE=1 SV=1

Database: SwissProt
Score: 46
Nominal mass (M_r): 7243
Calculated pI: 9.24
Taxonomy: Naja naja

Sequence similarity is available as an NCBI BLAST search of 3SA1_NAJNA against nr.

Search parameters

MS data file: C:\Rachel\031019 Hswa R30 pm.mgf
Enzyme: Trypsin: cuts C-term side of KR unless next residue is P.
Fixed modifications: Carbamidomethyl (C)
Variable modifications: Oxidation (M), Phospho (ST), Phospho (Y)

Protein sequence coverage: 25%

Matched peptides shown in ***bold red***.

```
 1 LKCNKLIPLA YKTCPAGKNL CYKMYMVSNK TVPVKRGCID VCPKNSLVLK
51 YECCNTDRCN
```

Unformatted sequence string: 60 residues (for pasting into other applications).

Sort peptides by ◉ Residue Number ○ Increasing Mass ○ Decreasing Mass

Show predicted peptides also

Query	Start – End	Observed	Mr(expt)	Mr(calc)	ppm	M	Score	Expect	Rank	U	Peptide
69	6 – 12	409.2624	816.5103	816.5109	-0.72	0	18	0.33	2	U	K.LIPLAYK.T
70	6 – 12	409.2635	816.5124	816.5109	1.79	0	38	0.007	1	U	K.LIPLAYK.T
218	37 – 44	474.7191	947.4236	947.4205	3.27	0	35	0.0056	1	U	R.GCIDVCPK.N

		Score	Mass	Matches	Sequences	emPAI	
2.1	PA2_HETFU	80	11992	5 (5)	3 (3)	1.81	Phospholipase A2 large subunit (Fragment) OS=Heterometrus fulvipes OX=141248

5 peptide matches (3 non-duplicate, 2 duplicate)

Auto-fit to window

Query	Dupes	Observed	Mr(expt)	Mr(calc)	ppm	M	Score	Expect	Rank	U	Peptide
149	1	441.2229	880.4312	880.4290	2.50	0	49	0.0064	1	U	K.YGLTNEGK.Y
215		474.1965	946.3785	946.3711	7.89	0	19	0.017	1	U	K.YTMMNCK.C
683	1	523.5636	1567.6690	1567.6685	0.31	0	43	0.002	1	U	R.THDHCDNIAAGETK.Y

1 subset or intersection (2 subset proteins in total)

		Score	Mass	Matches	Sequences	emPAI	
3	3SA1_NAJNA	46					Cytotoxin 1 OS=Naja naja OX=35670 PE=1 SV=1
3.1	3SA1_NAJNA	46	7243	3 (2)	2 (2)	2.06	Cytotoxin 1 OS=Naja naja OX=35670 PE=1 SV=1
	4 samesets of 3SA1_NAJNA						
	3SA3_NAJNA	46	7197	3 (2)	2 (2)		Cytotoxin 3 OS=Naja naja OX=35670 PE=1 SV=1
	3SA7A_NAJKA	46	7197	3 (2)	2 (2)		Cytotoxin 2 OS=Naja kaouthia OX=8649 PE=1 SV=1
	3SA7_NAJNA	46	7244	3 (2)	2 (2)		Cytotoxin 7 OS=Naja naja OX=35670 PE=1 SV=1
	3SA8_NAJNA	46	7245	3 (2)	2 (2)		Cytotoxin 8 OS=Naja naja OX=35670 PE=1 SV=2

3 peptide matches (2 non-duplicate, 1 duplicate)

Auto-fit to window

Query	Dupes	Observed	Mr(expt)	Mr(calc)	ppm	M	Score	Expect	Rank	U	Peptide
70	1	409.2635	816.5124	816.5109	1.79	0	38	0.007	1	U	K.LIPLAYK.T
218		474.7191	947.4236	947.4205	3.27	0	35	0.0056	1	U	R.GCIDVCPK.N

Appendix XXVIII: Chapter 7: Key of UniProt Aligned Sequences

UniProt Code	Protein Type	Species of Origin
PA2BA_CRODU	Phospholipase A2 crotoxin basic chain CBa2	*Crotalus durissus terrificus*
PA2BA_CRODR	Basic phospholipase A2 A	*Crotalus durissus ruruima*
PA2B1_CROSS	Basic phospholipase A2 Mtx-b	*Crotalus scutulatus scutulatus*
PA2BB_CRODU	Phospholipase A2 crotoxin basic subunit CBb	*Crotalus durissus terrificus*
PA2B6_CRODO	Phospholipase A2 crotoxin basic chain	*Crotalus durissus collilineatus*
PA2BA_CRODM	Basic phospholipase A2 10	*Crotalus durissus cumanensis*
PA2BF_CRODU	Basic phospholipase A2 F16	*Crotalus durissus terrificus*
PA2BE_CRODU	Basic phospholipase A2 F15	*Crotalus durissus terrificus*
PA2B9_CRODM	Basic phospholipase A2 9	*Crotalus durissus cumanensis*
PA2BG_CRODU	Basic phospholipase A2 F17	*Crotalus durissus terrificus*
PA2BC_CRODR	Basic phospholipase A2 Cdr-12	*Crotalus durissus ruruima*
PA2BB_SISTE	Basic phospholipase A2 sistruxin B	*Sistrurus tergeminus*
PA2N_GLOHA	Neutral phospholipase A2 agkistrodotoxin	*Gloydius (Agkistrodon) halys*
PA2B1_CROVE	Basic phospholipase A2 CB1	*Crotalus durissus vegrandis*
PA2_HETFU	Phospholipase A2 large subunit	*Heterometrus fulvipes*
PA2_HOTTA	Phospholipase A2	*Hottentotta tamulus*
PA2_HETLA	Phospholipase A2 heteromtoxin	*Heterometrus laoticus*
IPTXI_PANIM	Phospholipase A2 imperatoxin-1	*Pandinus imperator*
PA2_PANIM	Phospholipase A2 phospholipin	*Pandinus imperator*
PA2_ANUPH	Phospholipase A2 phaiodactylipin	*Anuroctonus phaiodactylus*
PA2_HOFGE	Phospholipase A2	*Hoffmannihadrurus (Hadrurus) gertschi*

Appendix XXIX: Chapter 7: Table of Amino Acid and Single Letter Codes

Name of Amino Acid	One Letter Code
Alanine	A
Arginine	R
Asparagine	N
Aspartic Acid	D
Cysteine	C
Glutamic Acid	E
Glutamine	Q
Glycine	G
Histidine	H
Isoleucine	I
Leucine	L
Lysine	K
Methionine	M
Phenylalanine	F
Proline	P
Serine	S
Threonine	T
Tryptophan	W
Tyrosine	Y
Valine	V